Characterising the role of TssA proteins in the assembly and dynamics of the type VI secretion system

Selina Fecht

Department of Life Sciences

Imperial College London

2023

This thesis is submitted in fulfilment of the requirements for the degree of Doctor of Philosophy

Statement of originality

I declare that the work presented in this thesis is my own and that the contributions of others are duly acknowledged and appropriately referenced.

Copyright Declaration

The copyright of this thesis rests with the author. Unless otherwise indicated, its contents are licensed under a Creative Commons Attribution-Non Commercial 4.0 International Licence (CC BY-NC).

Under this licence, you may copy and redistribute the material in any medium or format. You may also create and distribute modified versions of the work. This is on the condition that: you credit the author and do not use it, or any derivative works, for a commercial purpose.

When reusing or sharing this work, ensure you make the licence terms clear to others by naming the licence and linking to the licence text. Where a work has been adapted, you should indicate that the work has been changed and describe those changes.

Please seek permission from the copyright holder for uses of this work that are not included in this licence or permitted under UK Copyright Law.

Abstract

The gram-negative, opportunistic pathogen *Pseudomonas aeruginosa* encodes many weapons for virulence and interbacterial warfare, including the type VI secretion system (T6SS), a contractile nanomachine delivering effector proteins and antibacterial toxins either into the extracellular environment or directly into neighbouring cells. The T6SS component TssA is variable in size, domain organisation, symmetry and structure. Some TssA proteins are proposed to coordinate the assembly of the T6SS contractile sheath, but the exact role of TssA proteins remains unclear, and understanding is complicated by this relatively low level of conservation of TssA proteins. This project aimed to characterise the three TssA proteins of *P. aeruginosa* to assess their contribution to, and positioning within, their respective T6SSs and determine whether these were influenced by TssA variation. To achieve this, functional assays were optimised to monitor the activity of the three *P. aeruginosa* T6SSs and assess the requirement for TssA proteins. Interactions of both full length TssA proteins and individual domains with other T6SS proteins were also characterised and *in silico* approaches allowed the position of TssA proteins within the T6SS to be modelled. It was identified that each *P. aeruginosa* TssA protein was specifically required for the activity of its respective T6SS. Interactions of these TssA proteins with T6SS components were identified including specific interactions with the cognate contractile sheath, where this specificity could be altered by the exchange of domains. This work conclusively demonstrated specificity determinants for TssA proteins, which allowed the generation of functional chimeric TssA proteins, even with components from different TssA sub-groups. From this work a new docking has been proposed for TssA proteins with the contractile sheath and a model has been developed for how sheath assembly is coordinated by TssA proteins from this position.

Acknowledgements

Firstly, I would like to thank my supervisor Professor Alain Filloux for his support and guidance throughout my PhD. His belief in me when I was struggling to make progress, helped me to persevere and ultimately build my project in new ways. The independence I was allowed enabled me to grow as a scientist.

I am very grateful to all the members of the Filloux lab who I have worked with during my time in the group. This includes those who were there at the beginning of this journey, Laura Nolan and Sara Kisakye, who welcomed me into the lab, and Luke Allsopp for sharing your wealth of expertise. Special thanks must go to Patricia Bernal, who supervised me first as an undergraduate and then early in my PhD, whose training and guidance gave me such strong foundations. I am also grateful to those who I have spent the last few years with: Marta Rudzite, Patricia Paracuellos-Torrecilla, Thomas Clamens and Richard Morton, for their commitment to organising group social events and the time spent doing puzzles, and particularly to Marta for our many discussions and her companionship as the group shrank around us. I would especially like to thank Sophie Howard and Kira Eilers, who have been ever present during my PhD for their friendship and always being on hand to offer support and advice.

The structural aspects of this project would not have progressed without the work of Patricia Paracuellos-Torrecilla and latterly Tiago Costa, whose efforts and advice I very much appreciate. I would like to acknowledge the contribution of the students who I have worked with, Diane Letourneur, Genevieve Butt and Yu Zhai. I am also grateful to Despoina Mavridou and Tiago Costa and the members of their groups, including Chris Furniss, who have provided advice, feedback and support that have helped in the progression of this project.

I would like to thank the CMBI and the people who made it a great place to work. Most notably this includes Krista Grimes, who has been on this journey with me since our first day as undergraduates and has been a constant support and a fantastic friend throughout. Special mentions also go to Will Pearson and Josh McQuail for always providing opportunities to blow off steam. Outside of the CMBI, I am also very grateful to Filip Aniés for his friendship during my time at Imperial.

I have been very fortunate in the support I have received from friends and family. I would particularly like to thank my parents for always being there for me and supporting me through every stage of this journey. Finally, I am incredibly grateful to my partner Michael without whom this would have all been much more difficult, for providing emotional support, organising our social life and helping me disconnect from work.

Contents

Statement of originality 2

Copyright declaration 3

Abstract 4

Acknowledgements 5

Contents 6

List of figures 14

List of tables 18

Abbreviations 19

1. Introduction 22

1.1 *Pseudomonas aeruginosa* 22

1.1.1 *P. aeruginosa* is an opportunistic human pathogen 22

1.1.2 *P. aeruginosa* lifestyles 24

1.1.3 *P. aeruginosa* antibiotic resistance 26

1.2 *P. aeruginosa* virulence factors 28

1.2.1 Lipopolysaccahride 28

1.2.2 Biofilm formation 29

1.2.3 Motility 30

1.2.3.1 Flagella 30

1.2.3.2 Type IV pili 32

1.2.3.3 Rhamnolipids 33

1.2.4 Iron acquisition systems 34

1.2.5 Pyocyanin 34

1.2.6 Secretion systems 35

1.2.6.1 Type I secretion system 35

1.2.6.2 Type II secretion system 36

1.2.6.3 Type III secretion system 37

1.2.6.4 Type V secretion system 39

1.2.6.5 Secretion systems with roles in interbacterial competition 42

1.3 Type VI secretion system 43

1.3.1 Distribution of the T6SS in gram-negative bacteria 43

1.3.2 Structure and assembly of the T6SS 44
1.3.2.1 T6SSs of *P. aeruginosa* 45
1.3.2.2 The membrane complex 46
1.3.2.3 The baseplate complex 48
1.3.2.4 The tail complex 50
1.3.3 Similarity to contractile injection systems 52
1.3.4 Function of the T6SS 55
1.3.4.1 Modes of effector delivery 55
1.3.4.2 Anti-bacterial effectors 56
1.3.4.3 Anti-eukaryotic effectors 58
1.3.4.4 Effectors involved in common goods acquisition 59
1.3.4.5 Immunity-independent protection from the T6SS 59
1.3.4.6 The role of the T6SS 60
1.3.5 Regulation of the *P. aeruginosa* T6SSs 62
1.3.5.1 Gac-Rsm pathway 62
1.3.5.2 Threonine phosphorylation pathway 64
1.3.5.3 Quorum sensing 65
1.3.5.4 Sigma factor 54: RpoN 66
1.3.5.5 Environmental conditions 66
1.4 T6SS component TssA 68
1.4.1 TssA structure and organisation 68
1.4.1.1 TssA Nt1 domain 69
1.4.1.2 Structural features of short TssA proteins ($TssA_S$) 70
1.4.1.3 Structural features of long TssA proteins ($TssA_L$) 71
1.4.2 TssA within the T6SS 75
1.4.2.1 Interactions of TssA with T6SS components 75
1.4.2.2 Role of TssA within the T6SS 76
1.4.3 TssA-associated sheath regulators 77
1.4.3.1 $TssA_L$ and TagA 78
1.4.3.2 $TssA_S$ and TagB 78
1.4.3.3 $TssA_S$ and TagJ 79

1.4.3.4 Link between T6SS kinetics and TssA 79
1.4.3.5 T6SS clusters lacking TssA-associated accessory proteins 80
1.5 Aims of this project 81
2. Experimental procedures 82
2.1 Bacterial strains and growth conditions 82
2.2 Molecular biology techniques 86
2.2.1 Genomic DNA and plasmid extraction 86
2.2.2 KOD PCR 96
2.2.3 Restriction enzyme digestion and ligation 108
2.2.4 Production of chemically competent cells 109
2.2.5 Transformation of plasmids into competent cells 109
2.2.6 Colony PCR 110
2.2.7 Site-directed mutagenesis: alanine substitution 110
2.2.8 Three-partner conjugation to introduce plasmids into *P. aeruginosa* 111
2.2.9 *P. aeruginosa* mutagenesis 111
2.3 Protein analysis 113
2.3.1 SDS-PAGE 113
2.3.2 Coomassie staining 113
2.3.3 Western blot 113
2.3.4 Secretion assays 114
2.3.5 Protein purification 115
2.3.6 Size exclusion chromatography 116
2.3.7 Transmission electron microscopy: negative stain 116
2.4 Interbacterial competition assays 117
2.4.1 Interbacterial competition assay: double incubation 117
2.4.2 Interbacterial competition assay: single incubation 118
2.4.3 Interbacterial competition assay: competitive index 118
2.5 Protein-protein interaction analysis 119
2.5.1 Bacterial two-hybrid spotting assay 119
2.5.2 Bacterial two-hybrid microplate reader β-galactosidase assay 119
2.5.3 Pull-down screen in *P. aeruginosa* 120

2.5.3.1 Pull-down with growth in liquid culture 120
2.5.3.2 Pull-down with growth on solid media 121
2.5.3.3 Cross-linking and pull-down 121
2.5.4 Mass spectrometry analysis 122
2.5.4.1 MaxQuant analysis 122
2.5.4.2 Perseus analysis 122
2.6 Fluorescence microscopy 124
2.6.1 Microscopy analysis of bacterial cells grown in liquid culture 124
2.6.2 Microscopy analysis of bacterial cells grown on solid media 124
2.7 Transcriptional reporter fusion 126
2.8 *In silico* methods 127
2.8.1 Sequence analysis 127
2.8.2 Data presentation and statistical analysis 127
2.8.3 Figure construction 127
2.8.4 Microscopy image analysis 127
2.8.5 Protein homology molecular modelling and protein structural analysis 128
3. Results: Functional characterisation of TssA proteins 129
3.1 Introduction 129
3.1.1 Approaches to study T6SS functionality 129
3.1.2 Functionality of short TssA proteins 129
3.1.3 Functionality of long TssA proteins 130
3.1.4 Theories on functionality of long and short TssA proteins 131
3.2 Aims of this study 132
3.3 Functional characterisation of TssA1 133
3.3.1 H1-T6SS expression and secretion are low in the *rsmA* background 133
3.3.2 TssA1 is required for H1-T6SS activity in the *retS* background 134
3.3.3 TssA1 is required for H1-T6SS activity in the *rsmArsmN* background 138
3.3.4 H1-T6SS expression is elevated in a *rsmArsmN* double mutant compared to a *retS* mutant 141
3.3.5 Elevated H1-T6SS expression in a *tssA1* mutant is independent of the loss of TssA1 142
3.3.6 The position of TssA1 within the H1-T6SS could not be conclusively assessed 143

3.4 Functional characterisation of TssA2 145

3.4.1 TssA2 is required for H2-T6SS secretion and prey killing in the *rsmA* background 145

3.4.2 H2-T6SS sheath structures can form in the absence of TssA2 146

3.5 Functional characterisation of TssA3 149

3.5.1 Interbacterial killing activity of the H3-T6SS activity could not be demonstrated 149

3.5.2 Secretion by the H3-T6SS could not be demonstrated 151

3.5.3 TssA3 is required for the formation of H3-T6SS sheath structures 152

3.6 Discussion 154

3.6.1 Requirement for TssA proteins for T6SS activity 154

3.6.2 Localisation of TssA proteins in the T6SS 156

3.6.3 Functional relevance of different TssA groups: accessory proteins 157

3.6.4 Functional relevance of different TssA groups: T6SS functional diversity 159

3.6.5 Regulation of the H1-T6SS by the Gac-Rsm pathway 160

3.7 Summary 166

4. Results: Positioning and interactions of TssA proteins within the T6SS 167

4.1 Introduction 167

4.1.1 Interactions of TssA proteins with the membrane complex 167

4.1.2 Interactions of TssA proteins with the baseplate complex 168

4.1.3 Interactions of TssA proteins with the tail complex 169

4.2 Aims of this study 170

4.3 Positioning TssA within the T6SS: Interactions of TssA proteins with cognate T6SS components 171

4.3.1 Designing appropriate bacterial two-hybrid combinations and tag position 172

4.3.1.1 C-terminally tagged TssA does not yield productive interactions in the bacterial two-hybrid approach 172

4.3.1.2 Bacterial two-hybrid screen using N-terminal tagged TssA yields productive interactions 173

4.3.2 TssA proteins self-interact 175

4.3.3 TssA interacts with sheath components and Hcp 175

4.3.4 TssA proteins interact with baseplate components, notably TssK 177

4.3.5 Interaction between TssA proteins and VgrG proteins 178

4.3.6 Some TssA proteins interact with ClpV 180

4.3.7 TssA interaction with membrane complex components could not be conclusively identified 181

4.3.8 Interactions of TssA3 appear weaker than those of TssA1 and TssA2 182

4.3.9 Quantification of β-galactosidase activity did not produce consistent data 184

4.4 Site-directed mutagenesis to target interactions of TssA1 187

4.4.1 TssA1 Nt1 and C-terminal domain point mutants lose interaction with known partners non-specifically 187

4.4.1.1 Analysis of Tss1 Nt1 domain mutants 187

4.4.1.2 Analysis of TssA1 C-terminal domain point mutants 189

4.4.2 Substitution of TssA1 residues predicted to be involved in oligomerisation have variable effects on interactions 191

4.4.3 Analysis of TssA1 point mutant interactions 193

4.5 Splitting TssA proteins into domains to assess interaction with cognate T6SS components 194

4.5.1 TssA Nt1 domains interact with their respective sheath components 195

4.5.2 TssA C-terminal domains self-interact 197

4.5.3 A TssA2 protein lacking the C-terminal domain is not functional 199

4.6 Interactions of TssA proteins with non-cognate T6SS components 202

4.6.1 TssA proteins from different P. aeruginosa T6SSs cross-interact 202

4.6.2 TssA proteins interact with components from non-cognate P. aeruginosa T6SSs 204

4.6.3 Heterologous complementation of *tssA* deletion is not observed 205

4.6.4 Non-cognate TssA proteins do not interfere with T6SS activity in the absence of their cognate T6SS cluster 209

4.7 Discussion 211

4.7.1 Interactions involving *P. aeruginosa* long and short proteins 211

4.7.2 Accommodation of TssA symmetry variations and symmetry mismatches in the T6SSs 212

4.7.3 Positioning of TssA at the distal end of the sheath 214

4.7.4 Insights into TssA-sheath interactions 217

4.7.5 Interaction of TssA proteins with T6SS components 220

4.8 Summary 223

5. Results: Characterisation of TssA domains and role in TssA specificity 224

5.1 Introduction 224

5.1.1 The TssA Nt1 domain 224

5.1.2 TssA C-terminal regions 224

5.1.3 TssA proteins are functionally specific 226

5.2 Aims of this study 227

5.3 Functional characterisation of chimeric TssA proteins 228

5.3.1 Chimeric TssA proteins are stable in bacterial two-hybrid experiments 228

5.3.2 The chimeric $TssA1_{Nt1}TssA3_{CTD}$ is functional in the H1-T6SS 230

5.3.3 The chimeric $TssA3_{Nt1}TssA1_{CTD}$ is functional in the H3-T6SS 232

5.3.4 Chimeric TssA proteins with the TssA2 Nt1 domain restore some function to the H2-T6SS 234

5.3.5 Chimeric TssA proteins with P. putida TssA domains are not functional in the H2-T6SS 236

5.4 Characterising interaction specificity of TssA protein domains 239

5.4.1 Nt1 domains interact specifically with their respective sheath components 239

5.4.2 C-terminal domains specifically self-interact 240

5.4.3 T6SS activity is unaffected by the expression of Nt1 domains 241

5.5 Structural characterisation of TssA protein C-terminal domains 243

5.5.1 TssA C-terminal domains can be stably produced 243

5.5.2 $TssA_S$ C-terminal domains form rings with large internal lumens 244

5.5.3 The TssA2 C-terminal domain could not be purified with confidence 247

5.6 Identifying specificity determinants of the interaction between the Nt1 domain and the sheath 249

5.6.1 Point mutants in the TssA1 Nt1 domain do not disrupt interaction with the sheath 249

5.6.2 The structural differences between TssA1 and TssA3 Nt1 domain models arise in two regions 250

5.6.3 Introducing the TssA3 hairpin or loop regions into TssA1 impairs sheath interaction and secretion 251

5.6.4 Introducing the TssA1 hairpin or loop regions into TssA3 impairs sheath interaction and polymerisation 255

5.6.5 Exchange of hairpin and loop regions does not lead to gain of function 256

5.6.6 The TssA1 Nt1 domain model can be docked to the sheath 258

5.7 Discussion 262

5.7.1 Significance of chimeric TssA protein functionality 262

5.7.2 Interaction of TssA Nt1 domains at the distal end of the sheath 265

5.7.3 Implications of Nt1 domain-sheath interactions on TagA accessory protein interactions 272

5.7.4 Proposed mechanism for tail polymerisation with TssA bound to the distal end 273

5.8 Summary 280

6. Discussion 281

6.1 TssA proteins are required for T6SS activity 282

6.1.1 Future perspectives: TssA functionality and T6SS regulation 283

6.2 TssA proteins are sequentially positioned at the membrane complex, baseplate complex and tail complex distal end 285

6.2.1 Future perspectives: TssA positioning and role 288

6.2.2 Future perspectives: Validation of TssA-sheath docking hypothesis 289

6.3 TssA proteins remain functional with exchange of C-terminal regions 291

6.3.1 Future perspectives: Functionality of chimeric TssA proteins 291

6.4 Conclusion 294

7. Bibliography 295

8. Appendices 335

8.1 Image permissions 344

List of figures

Figure 1.1 Schematic of the lifestyle switch model in *P. aeruginosa*.

Figure 1.2 Schematic of the bacterial flagellum structure.

Figure 1.3 Schematic of the type I secretion system structure.

Figure 1.4 Schematic of the type II secretion system structure.

Figure 1.5 Schematic of the type III secretion system structure.

Figure 1.6 Schematic of the type V secretion system autotransporter structure.

Figure 1.7 Schematic of the type Vb two-partner secretion system structure.

Figure 1.8 Schematic of the type VI secretion system structure in extended and contracted conformations.

Figure 1.9 Schematic of the *P. aeruginosa* strain PAO1 T6SS gene clusters.

Figure 1.10 Structure of the enteroaggregative *E. coli* membrane core complex.

Figure 1.11 Structure of the baseplate complex.

Figure 1.12 Structure of the tail complex.

Figure 1.13 Structural comparison of contractile injection systems.

Figure 1.14 Structural comparison of contractile injection system tail complex components.

Figure 1.15 Schematic of the Gac-Rsm pathway in *P. aeruginosa*.

Figure 1.16 Schematic of TssA classification.

Figure 1.17 Structure of $TssA^{BC}$ Nt1 domain.

Figure 1.18 Negative stain electron microscopy images of $TssA_S$ proteins.

Figure 1.19 Structure of $TssA^{BC}$ C-terminal domain ring.

Figure 1.20 Structure of $TssA^{AH}$ Nt2 domain dimers.

Figure 1.21 Dimer interfaces of $TssA_L$ proteins.

Figure 1.22 Structure of $TssA^{AH}$ C-terminal domain ring.

Figure 1.23 Structure of $TssA^{EC}$ C-terminal domain ring.

Figure 1.24 Model of long and short TssA complex domain architecture.

Figure 1.25 Association between T6SS phylogenetic groups, TssA and accessory proteins.

Figure 3.1 Assessment of H1-T6SS activity in a PAO1Δ*rsmA* background.

Figure 3.2 Assessment of H1-T6SS secretion in a PAKΔ*retS* background.

Figure 3.3 Assessment of H1-T6SS secretion in a PAO1Δ*retS* background.

Figure 3.4 Assessment of H1-T6SS prey killing in a PAO1Δ*retS* background.

Figure 3.5 Assessment of H1-T6SS sheath formation in a PAO1Δ*retS* background.

Figure 3.6 Assessment of H1-T6SS activity in a PAO1Δ*rsmA*Δ*rsmN* background.

Figure 3.7 Assessment of H1-T6SS protein expression and secretion in various mutants of the Gac-Rsm pathway: *rsmN, rsmA, retS* and *rsmArsmN*.

Figure 3.8 Expression from the *tssA1* promoter with a transcriptional reporter fusion.

Figure 3.9 Assessing TssB1 and TssA1 co-localisation by fluorescence microscopy.

Figure 3.10 Assessment of H2-T6SS activity in a PAO1Δ*rsmA* background.

Figure 3.11 Assessment of H2-T6SS sheath formation by fluorescence microscopy.

Figure 3.12 Screen for H3-T6SS killing of *P. putida* KT2440R.

Figure 3.13 Assessment of H3-T6SS secretion in various backgrounds.

Figure 3.14 Assessment of H3-T6SS sheath formation.

Figure 3.15 Additional regulation of components of the Gac-Rsm pathway in *P. aeruginosa*.

Figure 3.16 Structures of *P. aeruginosa* Csr family members.

Figure 4.1 Schematic of the bacterial two-hybrid approach.

Figure 4.2 Interactions of C-terminal tagged TssA1 with H1-T6SS components.

Figure 4.3 Interactions of N-terminal tagged TssA1 with H1-T6SS components.

Figure 4.4 Self-interactions of N-terminal tagged TssA proteins.

Figure 4.5 Interactions of TssA proteins with tail complex components.

Figure 4.6 Interactions of TssA proteins with baseplate complex components.

Figure 4.7 Interactions of TssA proteins with VgrG spike proteins.

Figure 4.8 Self-interactions of H1-T6SS VgrG proteins.

Figure 4.9 Interactions of TssA proteins with ClpV proteins.

Figure 4.10 Interactions of TssA proteins with membrane complex components.

Figure 4.11 β-galactosidase assay quantification of TssA1 and TssA2 interactions with their cognate T6SS components.

Figure 4.12 Position of selected TssA1 Nt1 domain residues.

Figure 4.13 Interactions of TssA1 Nt1 domain mutants with known H1-T6SS partners.

Figure 4.14 Interactions of TssA1 C-terminal domain mutants with known H1-T6SS partners.

Figure 4.15 Oligomerisation interface of $TssA^{BC}$.

Figure 4.16 Interactions of proposed TssA1 oligomerisation mutants with known H1-T6SS partners.

Figure 4.17 Solvent accessibility of TssA1 Nt1 and C-terminal domain residues.

Figure 4.18 Domain organisation of *P. aeruginosa* TssA proteins.

Figure 4.19 Protein-protein interaction network of $TssA^{EC}$ and $TssA^{BC}$ domains.

Figure 4.20 Interactions of *P. aeruginosa* TssA Nt1 domains with known T6SS partners and TssA domains.

Figure 4.21 Interactions of *P. aeruginosa* TssA C-terminal domains with known T6SS partners and TssA domains.

Figure 4.22 Functionality of TssA2 lacking the C-terminal domain.

Figure 4.23 Cross-interaction of *P. aeruginosa* TssA proteins.

Figure 4.24 Interaction of TssA proteins with previously identified TssA partners.

Figure 4.25 Assessment of heterologous complementation of H1-T6SS activity by TssA2 and TssA3.

Figure 4.26 Assessment of heterologous complementation of H2-T6SS activity by TssA1 and TssA3.

Figure 4.27 Assessment of heterologous complementation of H3-T6SS activity by TssA1 and TssA2.

Figure 4.28 Assessment of H2-T6SS activity and TssA interference in the absence of H1- and H3-T6SS clusters.

Figure 4.29 Protein-protein interaction networks of *P. aeruginosa* TssA proteins.

Figure 4.30 Models of TssA complexes docked to sheath structures.

Figure 4.31 Superimposition of $TssA^{BC}$ Nt1 and Nt2 domains.

Figure 4.32 Flexibility of $TssA^{AH}$ Nt2 domains.

Figure 4.33 Structures of gp6 C-terminal region and $TssA^{BC}$ C-terminal domain.

Figure 4.34 Identified domain interactions of TssA proteins.

Figure 5.1 Structure of the TssAVC C-terminal domain and Nt2 domain position.

Figure 5.2 Schematic of chimeric TssA proteins engineered.

Figure 5.3 Interactions of chimeric TssA proteins with their component TssA proteins and sheath components.

Figure 5.4 Assessment of H1-T6SS activity with chimeric TssA proteins.

Figure 5.5 Assessment of H3-T6SS sheath formation with chimeric TssA proteins.

Figure 5.6 Assessment of H2-T6SS activity with chimeric TssA proteins.

Figure 5.7 Schematic of chimeric *P. putida* TssA proteins engineered.

Figure 5.8 Assessment of H2-T6SS activity with chimeric TssA proteins with *P. putida* sub-domains.

Figure 5.9 Interactions of TssA domains with sheath components.

Figure 5.10 Interactions between TssA domains.

Figure 5.11 Assessment of T6SS activity with overproduction of Nt1 domains.

Figure 5.12 Production of TssA C-terminal domains.

Figure 5.13 Gel filtration of TssA1 and TssA3 C-terminal domains.

Figure 5.14 Negative stain electron microscopy grids of TssA1 and TssA3 C-terminal domains.

Figure 5.15 2D class averages of TssA1 and TssA3 C-terminal domains.

Figure 5.16 Gel filtration of TssA2 C-terminal domain.

Figure 5.17 Negative stain electron microscopy grid of TssA2 C-terminal domain.

Figure 5.18 Identification and screening of candidate TssA1 Nt1 domain residues for sheath interaction.

Figure 5.19 Structural alignment of TssA1 and TssA3 Nt1 domain models.

Figure 5.20 Interactions of TssA1 proteins with TssA3 hairpin or loop regions introduced.

Figure 5.21 Assessment of H1-T6SS activity with TssA1 with TssA3 hairpin or loop regions introduced.

Figure 5.22 Interactions of TssA3 proteins with TssA1 hairpin or loop regions introduced.

Figure 5.23 Assessment of H3-T6SS sheath formation with TssA3 with TssA1 hairpin or loop regions introduced.

Figure 5.24 Assessment of the H1-T6SS association of TssA3 with TssA1 hairpin or loop regions introduced.

Figure 5.25 *P. aeruginosa* TssB-TssC sheath in extended and contracted conformations.

Figure 5.26 TssA1 Nt1 domain models docked at the distal end of the extended sheath model.

Figure 5.27 TssA1 Nt1 domain hairpin and loop regions at the interface with the extended sheath model.

Figure 5.28 Schematic of predicted structures of chimeric TssA protein complexes.

Figure 5.29 Structural similarities between *P. aeruginosa* TssA ImpA_N regions.

Figure 5.30 TssA1 ImpA_N region model docked at the distal end of the sheath in the contracted conformation.

Figure 5.31 Structural differences between *P. aeruginosa* TssA Nt1 domains.

Figure 5.32 Comparison of TssA1 and TssA2 Nt1 domain models.

Figure 5.33 Structural models of TssA1 and TssA3 Nt1 domains docked to the H1-T6SS contracted sheath structure.

Figure 5.34 Schematics for the association with TssA complexes at the distal end of the sheath.

Figure 5.35 Schematics for an updated cap model for sheath polymerisation with TssA at the distal end of the sheath.

Figure 5.36 Schematics for sheath subunit recruitment by the TssA Nt1 domain.

Figure 5.37 Schematics for a TssA complex bound at the distal end of the tail complex including Hcp.

List of tables

Table 1.1 TssA structural variation

Table 1.2 TssA interactions in the T6SS

Table 2.1 Bacterial strains used in this study

Table 2.2 Media supplements used in this work

Table 2.3 Plasmid vectors used in this study

Table 2.4 Primers used in this study

Table 2.5 Antibodies used in this study

Table 4.1 TssA1 mutants losing interaction by BTH

Table 4.2 Pairwise sequence comparison of baseplate components

Table 5.1 Pairwise comparison of sheath components between *P. aeruginosa* T6SS clusters

Table 8.1 TssA2 pulldown 1: 37 °C liquid culture

Table 8.2 TssA2 pulldown 2: 25 °C solid media

Table 8.3 TssA3 pulldown 1: 37 °C liquid culture

Table 8.4 TssA3 pulldown 2: 30 °C solid media

Table 8.5 PA2372 pull down 1: 37 °C liquid culture

Table 8.6 PA2372 pulldown 2: 30 °C solid media

Abbreviations

ABC	ATP-binding cassette
BSA	Bovine serum albumin
BTH	Bacterial two-hybrid
C-ring	Cytoplasmic ring
CDI	Contact-dependent growth inhibition
CFTR	Cystic fibrosis transmembrane conductance receptor
CIS	Contractile injection system
CPA	Common polysaccharide antigen
Cryo-EM	Cryogenic electron microscopy
CTD	C-terminal domain
ddH_2O	Double distilled water
DMF	Dimethylformamide
DTBP	Dimethyl 3,3'-dithiobispropionimidate
EM	Electron microscopy
EV	Empty vector
FDR	False discovery rate
Fur	Ferric uptake regulator
HEPES	N-2-hydroxyethylpiperazine-N-2-ethane sulfonic acid
HRP	Horse radish peroxidase
HSL	Homoserine lactone
IPTG	Isopropyl ß-D-1-thiogalactopyranoside
IQS	Integrated quorum sensing system
kDa	Kilodalton
L-ring	Lipopolysaccharide ring
LB	Lysogeny broth
LPS	Lipopolysaccharide
MAC arrays	Metamorphosis-associated contractile arrays
MCS	Multiple cloning site
MS-ring	Membrane-supramembrane ring
MW	Molecular weight
OMV	Outer membrane vesicle
OPNG	O-nitrophenyl-beta-D-galactopyranoside
OSA	O-specific antigen

P-ring	Peptidoglycan ring
PBS	Phosphate-buffered saline
PIA	*Pseudomonas* isolation agar
PMSF	Phenylmethylsulfonyl fluoride
PQS	*Pseudomonas* quinolone signal
RMSD	Root mean square deviation
ROS	Reactive oxygen species
RpoB	RNA polymerase β
Sfa	Sigma factor activator
T1SS	Type I secretion system
T2SS	Type II secretion system
T3SS	Type III secretion system
T4SS	Type IV secretion system
T5SS	Type V secretion system
T6SS	Type VI secretion system
T7SS	Type VII secretion system
Tae	Type VI amidase effector
TAE	Tris-acetate-EDTA
$TagA^{EC}$	TagA of enteroaggregative *Escherichia coli*
$TagA^{VC}$	TagA of *Vibrio cholerae*
TBS-T	Tris-buffered saline
TCA	Trichloroacetic acid
Tde	Type VI DNase effector
Tfe	Type VI anti-fungal effector
Tge	Type VI glycoside hydrolase effector
TGS	Tris-glycine-SDS
Tle	Type VI lipase effector
TLR4	Toll-like receptor 4
TLR5	Toll-like receptor 5
Tne	Type VI NADase effector
TNF-α	Tumour necrosis factor α
TPP	Threonine phosphorylation pathway
TSB	Tryptic soy broth
$TssA1^{PP}$	TssA1 of *Pseudomonas putida*

$TssA2^{PP}$	TssA2 of *Pseudomonas putida*
$TssA3^{PP}$	TssA3 of *Pseudomonas putida*
$TssA^{AB}$	TssA of *Acenitobacter baylyi*
$TssA^{AH}$	TssA of *Aeromonas hydrophila*
$TssA^{BC}$	TssA of *Burkholderia cenocepacia*
$TssA^{EC}$	TssA of enteroaggregative *Escherichia coli*
$TssA_L$	Long TssA protein
$TssA_S$	Short TssA protein
$TssA^{VC}$	TssA of *Vibrio cholerae*
VBM	Vogel-Bonner medium
Vfr	Virulence factor regulator
X-Gal	5-bromo-4-chloro-3-indolyl-β-D-galacto-pyranoside

1. Introduction

1.1 *Pseudomonas aeruginosa*

The gram-negative, rod-shaped gamma-proteobacterium *Pseudomonas aeruginosa* is an opportunistic pathogen, ubiquitous in a wide range of ecological niches, such as aquatic and soil ecosystems, and able to colonise numerous host organisms, including plants, insects and animals such as humans (1–4). The ability of *P. aeruginosa* to colonise and proliferate in such varied environments, including those poor in nutrients, has been attributed to its metabolic versatility (5,6). The reference strain PAO1, isolated from an infected wound in 1954 and sequenced in 2000, has a 6.3 Mb genome containing 5570 open reading frames (5,7). It is estimated that almost 10 % of these genes have regulatory roles, underpinning the adaptability of this organism (5,6). This adaptability has been demonstrated by the identification of phenotypic differences between distinct PAO1 laboratory strains, for example in secretion profiles, despite limited genomic alterations, suggesting that microevolution in isolated sublines can contribute to regulatory differences (8). Variation also exists between strains, a core genome has been identified with conservation between *P. aeruginosa* strains, but more variable regions, termed the accessory genome, contribute to strain-specific differences (9).

1.1.1 *P. aeruginosa* is an opportunistic human pathogen

Human hosts can be colonised by *P. aeruginosa,* but it rarely has a pathogenic effect on healthy individuals, while it is strongly associated with nosocomial infections and infections of immunocompromised individuals (10). An estimated 7 % of healthcare-associated infections are suggested to involve *P. aeruginosa* (11). As a metabolically versatile opportunistic pathogen, *P. aeruginosa* can colonise a range of niches within human hosts. *P. aeruginosa* is, for example, the most common gram-negative bacterium associated with infections of burn wounds (12). Infection with *P. aeruginosa* is also a common complication following surgery, accounting for around 5 % of surgical site infections (13) and correlating with an increased mortality risk (14). Medical devices can also be associated with *P. aeruginosa* infection in the form of catheter-associated urinary tract infections or ventilator-associated pneumonia (15,16). *P. aeruginosa* is estimated to be the most common cause of ventilator-associated pneumonia, which can have a mortality rate of up to 30 % (17,18). Cancer patients and organ transplant recipients whose immune systems may be compromised are also vulnerable to such infections (19–21). In healthy individuals, *P. aeruginosa* is a leading cause of microbial keratitis associated with contact lens use (22).

Infection with *P. aeruginosa* is also very commonly found in the lungs of patients with cystic fibrosis. Such infections commonly occur in the first few years of life, and while some can be cleared naturally others need to be targeted with robust antibiotic treatment (23,24). By adulthood, recurring infection commonly develops into chronic infection which cannot be cleared by antibiotic treatment. Data indicates that 60 % of adult cystic fibrosis patients were chronically infected with *P. aeruginosa* in the UK in 2013, with *P. aeruginosa* one of the predominant pathogens in this context along with *Staphylococcus aureus* (25). This chronic infection correlates with poorer clinical outcomes, such as a decline in lung function, higher incidence of pulmonary exacerbations and increased mortality (26–30).

The high prevalence of bacterial infections in the lungs of cystic fibrosis patients is proposed to be linked to impaired mucociliary clearance. Cystic fibrosis is caused by mutations to the cystic fibrosis transmembrane conductance receptor (CFTR), a chloride ion channel regulating ion and water transport in epithelial cells (31). Loss of or mutation to *CFTR* which cause cystic fibrosis, leads to impaired ion transport and fluid homeostasis, particularly affecting lung epithelial cells, causing an increased viscosity of mucus which has been proposed to contribute to the impaired mucociliary clearance, promoting bacterial colonisation and tissue damage caused by subsequent inflammation (32,33). It is not known specifically what causes *P. aeruginosa* to predominate in this niche, although it has been suggested that direct interbacterial competition to eliminate competitors through the delivery of anti-bacterial proteins may play a role (34).

P. aeruginosa isolates from the lungs of chronically infected cystic fibrosis patients display convergent expression profiles and phenotypes through the accumulation of pathoadaptive mutations that are selected for in the cystic fibrosis lung environment (35). A classic example of a pathoadaptive mutation is the development of a mucoid phenotype, linked to mutations in the anti-sigma factor *mucA* and genes involved in production of alginate a key biofilm component, which provides protection against host immune responses (see section 1.2.2) (36,37). Mutations are also accumulated to decrease motility and virulence, which further reduce detection by host immune pathways (38,39). Increased antibiotic resistance is also a common feature of these isolates, through mechanisms that will be described in section 1.1.3. Metabolic adaptation to this environment involves a switch to iron uptake from host haem, via upregulation of the Phu system, while the siderophore pyoverdine is downregulated (see section 1.2.5) (40). The overall effect of these mutations produces strains that have low virulence and motility and are difficult to eradicate.

The presence of other organisms within the cystic fibrosis lung can influence clinical outcomes. It has been suggested that early infection with *S. aureus* may give some protection against subsequent *P.*

aeruginosa infection (41). Antagonistic behaviour is commonly demonstrated between *P. aeruginosa* and *S. aureus* under laboratory conditions, however in the environment of the cystic fibrosis lung these bacteria have been demonstrated to co-exist, which has been linked to adaptive mutations and environmental conditions (69). *P. aeruginosa* can use the protease LasA to lyse *S. aureus* for iron uptake (70), however a pathoadaptive mutation to the cystic fibrosis lung decreases LasA production reducing this antagonism (71,72). Environmental factors, such as oxygen limitation, associated with the cystic fibrosis lung have also been identified to reduce the production of virulence factors linked to competition with *S. aureus* (73). Coinfection with some organisms can have detrimental effects: it has been demonstrated that cystic fibrosis patients coinfected with *P. aeruginosa* and *Burkholderia cepacia* have an accelerated decline in lung function (42). Interbacterial interactions therefore provide an additional level of complexity to bacterial infection.

P. aeruginosa pathogenicity is mediated by a large arsenal of virulence factors which will be discussed in section 1.2.

1.1.2 *P. aeruginosa* lifestyles

P. aeruginosa is associated with different infection types, termed acute and chronic (Figure 1.1), which have quite different clinical profiles. Acute infections are generally more aggressive infections that are acquired by immunocompromised patients, as described above. These infections are classically associated with motile, planktonic bacteria, which attach to the epithelial mucosa using flagella and pili (43–45). Bacteria can then secrete a range of virulence factors either into the extracellular milieu or directly into host cells, causing cell damage, allowing proliferation of the bacterial population and modulating host inflammatory immune responses (46). In contrast, chronic infections are associated with sessile bacteria found in biofilm structures, such as in the lungs of cystic fibrosis patients, which are less virulent, motile and immunogenic.

The regulation of these lifestyles is partly linked to the Gac-Rsm pathway, which will be discussed in more detail in section 1.3.5.1. In brief, the pathway regulates the expression of the small non-coding RNAs RsmY and RsmZ, that sequester post-transcriptional regulators of the Rsm family. Rsm proteins positively regulate factors associated with acute infection, such as expression of the type III secretion system and type IV pili, and negatively regulate factors associated with chronic infection, such as production of biofilm-associated Pel and Psl polysaccharides and the type VI secretion system (Figure

1.1) (47–49). This pathway is therefore a key regulator of this lifestyle switch, influencing the outcome of infection (50).

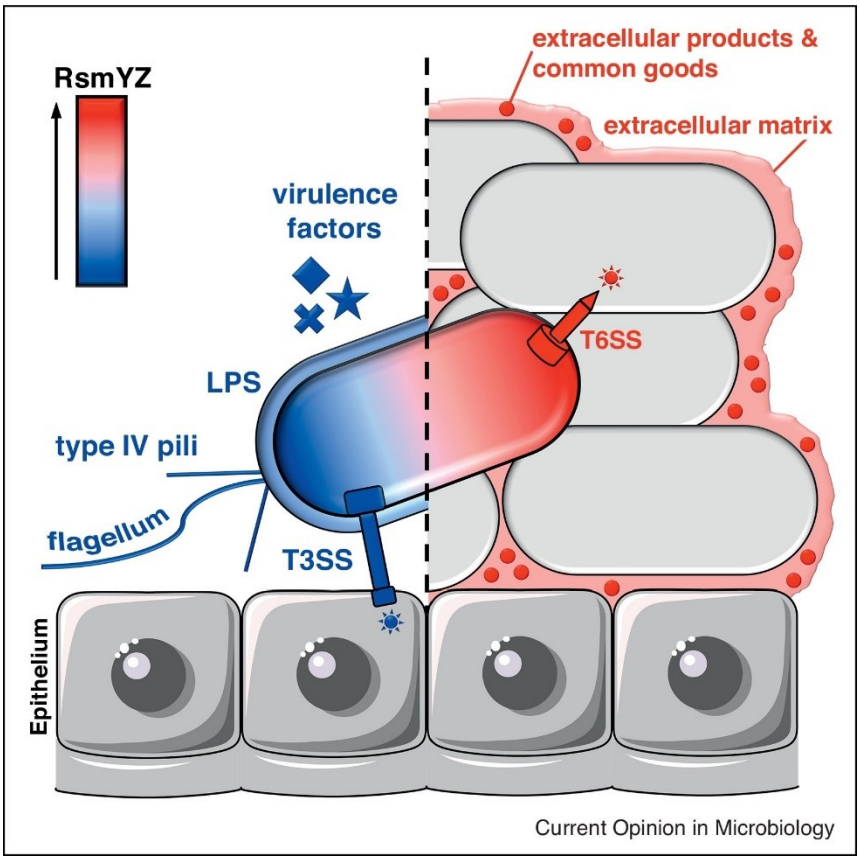


Figure 1.1 Schematic of the lifestyle switch model in *P. aeruginosa*. Low levels of RsmY and RsmZ are associated with a motile, planktonic *P. aeruginosa* lifestyle and acute infection (blue). High levels of RsmY and RsmZ are associated with a sessile *P. aeruginosa* lifestyle in biofilm and chronic infection (red). The type III and type VI secretion systems (T3SS and T6SS) are antagonistically regulated. Figure reproduced from Valentini *et al.* (2018) with permission from Elsevier.

More recently it has become apparent that there is a progressive transition between motile and sessile lifestyles, rather than a binary switch. There are several stages of biofilm formation, with specific gene expression profiles associated with these stages (51–54). Further complexity arises in observations of overlap between factors associated with these different lifestyles, for example factors associated with chronic infection were found to be upregulated in an acute mouse respiratory infection (55). Similarly, biofilm formation was key in an acute mouse burn model (56).

1.1.3 *P. aeruginosa* antibiotic resistance

P. aeruginosa is a highly prevalent nosocomial pathogen, but treatment of these infections is complicated by high rates of antibiotic resistance. Indeed, the WHO has designated *P. aeruginosa* into a 'critical' priority group of pathogens, for whom research targeted at the development of novel antibiotic treatments is urgently needed (57). Additionally, *P. aeruginosa* is one of the ESKAPE pathogens (*Enterococcus faecium, S. aureus, Klebsiella pneumoniae, Acinetobacter baumannii, P. aeruginosa, and Enterobacter spp.*) identified as relevant in healthcare settings and more complex to treat due to multidrug resistance and virulence (58).

Eight categories of antibiotics can be used to treat infections with *P. aeruginosa*, including those targeting peptidoglycan synthesis: carbapenems (i.e. imipenem and meropenem), cephalosporins (i.e. ceftazidime and cefepime), penicillins with β-lactamase inhibitors (i.e. ticarcillin-clavulanic acid and piperacillin-tazobactam), monobactams (i.e. aztreonam) and phosphonic acids (i.e. fosfomycin), as well as aminoglycosides which target protein synthesis (i.e. gentamicin and tobramycin), fluoroquinolones which target DNA synthesis (i.e. ciprofloxacin) and polymyxins which target the cell membrane (i.e. colistin and polymyxin B) (59). Antibiotic resistant strains of *P. aeruginosa* can be designated as either multidrug resistant, extensively drug resistant or pandrug resistant (60,61). A strain which is not susceptible to ≥ 1 agent in ≥ 3 of these antimicrobial categories is classed as multidrug resistant. A strain not susceptible to ≥ 1 agent in all but ≤ 2 antimicrobial categories is classed as extensively drug resistant. While a strain which is not susceptible to all antimicrobial agents is classed as pandrug resistant. In 2016 it was reported that 34 % of *P. aeruginosa* strains screened in Europe demonstrated resistance to at least one of the antimicrobial categories tested (62).

Resistance of bacteria to antibiotics can arise through a range of intrinsic, acquired and adaptive mechanisms. An intrinsic feature which contributes to *P. aeruginosa* antibiotic resistance is the low outer membrane permeability, which is up to 100-fold lower than that of *Escherichia coli* (63). This low intrinsic outer membrane permeability can be further decreased by modulation of porins. Structural changes or reduced expression of the porin OprD can reduce the internalisation of carbapenems (64). Alternatively, OprH overexpression enhances membrane stability and is thus associated with increased resistance to polymyxin B and gentamicin (65,66).

Antibiotics which do enter the bacterium may then be expelled from the cell due to the activity of efflux pumps. Four major multidrug efflux systems of the RND family have been described to contribute to *P. aeruginosa* antibiotic resistance: MexAB-OprM, MexCD-OprJ, MexEF-OprN and MexXY-OprM (67). In each of these efflux systems, one Mex protein is an efflux pump protein anchored within the inner membrane, with the other Mex protein spanning the periplasm to the outer

membrane pore formed by the Opr protein (68). While MexAB-OprM and MexXY-OprM contribute to intrinsic antibiotic resistance, mutations driving overexpression of MexCD-OprJ and MexXY-OprM contribute to acquired antibiotic resistance (68). Expression of these efflux pumps can be induced by exposure to antimicrobial agents (69).

Specific antibiotic resistance genes can modify internalised antibiotics to inactivate them. The core *P. aeruginosa* genome encodes a gene for the cephalosporinase AmpC, which although typically expressed at a low level, can be overproduced due to either induction or point mutation (70). The presence of other β-lactamases in the core genome has also been described in *P. aeruginosa*, including an imipenemase and an oxacillinase (71,72). Various horizontally acquired β-lactamases and other antibiotic resistance genes such as aminoglycoside-modifying enzymes are also common (73–75).

To evade the action of internalised antibiotics, *P. aeruginosa* can also modify the associated antibiotic targets. Resistance to aminoglycosides can be achieved through the acquisition of enzymes which methylate the 16S rRNA antibiotic target (76). Resistance to β-lactam and fluoroquinolone antibiotics can involve the modification of the respective penicillin binding protein (77) or DNA gyrase (78) targets. Modifications to alter the charge of the lipid A moiety of membrane lipopolysaccharide can also reduce the binding of polymyxins (79).

A further strategy used by *P. aeruginosa* to evade the activity of antibiotics is the formation of biofilm structures, where communities of bacteria encased in a polysaccharide matrix are more resistant to killing by antibiotic treatment (see section 1.2.2). This increased resistance has been linked to a reduced diffusion of antibiotics within the biofilm matrix (80) and the reduced metabolic rate of bacteria within the biofilm (81). The rate of horizontal gene transfer is often higher in biofilm communities than planktonic cells, which may facilitate transfer of mobile genetic elements associated with antibiotic resistance (82). Furthermore, the rate of mutation has been found to be higher in biofilm-associated *P. aeruginosa*, which may also promote the emergence of antibiotic resistance (83).

Infections caused by antibiotic resistant *P. aeruginosa* strains are associated with worse clinical outcomes, including increased mortality (84,85). There is also an elevated financial cost associated with the treatment of infections caused by antibiotic resistant bacteria (86).

1.2 *P. aeruginosa* virulence factors

P. aeruginosa produces a large range of virulence factors which contribute to colonisation of the host and establishment of infection. These virulence factors can be cell-associated or secreted into the extracellular environment and may contribute to bacterial adhesion, invasion, nutrient acquisition or evasion and modulation of host immune responses.

1.2.1 Lipopolysaccharide

The cell envelope of gram-negative bacteria is comprised of an inner membrane encased by a thin layer of peptidoglycan which is then surrounded by an asymmetric outer membrane comprised of an inner leaflet of phospholipids and an outer leaflet of glycolipids, primarily lipopolysaccharide (LPS) (87). This extracellularly exposed LPS is formed of three structural domains: the lipid A, the core region and the O-antigen. The lipid A moiety is an acylated glucosamine disaccharide that forms the outer leaflet of the outer membrane via the six or seven acyl chains (88). The core region consists of an oligosaccharide linked to the lipid A, while the O-antigen is the outermost region of the molecule and consists of an extended polysaccharide chain with variable composition (88). LPS molecules present in the outer membrane can either contain an O-antigen, termed capped, or lack an O-antigen, termed uncapped (89). There are two types of O-antigen associated with *P. aeruginosa*: the common polysaccharide antigen (CPA) and the O-specific antigen (OSA) (89).

As the moiety present at the external surface of the bacterium, LPS provides not only a physical barrier, important for structural integrity and influencing membrane permeability, but can also interact with host receptors (90). The detection of LPS by a host organism can trigger immune responses, for example the lipid A acyl chains activate the toll-like receptor 4 (TLR4) activating downstream pro-inflammatory pathways including the production of cytokines (91). Pulmonary inflammation triggered by LPS is also linked to the activation of tumour necrosis factor-α (TNF-α), Interleukin-1, Interleukin-6 and Interferon-γ (92). This pulmonary inflammation correlates with an increase in airway epithelial barrier permeability (93).

LPS also has a role to play in biofilm formation and surface attachment of bacteria, with mutants in LPS biosynthesis genes defective in attachment to airway epithelial cells and with reduced biofilm formation (94). Specific profiles of CPA and OSA O-antigens have been associated with certain stages of biofilm development, while O-antigens also influence the characteristics of outer membrane vesicles (OMVs) (95). CPA O-antigen is linked with chronic infection, promoting immune evasion and biofilm development (95,96). In these chronic infections *P. aeruginosa* LPS has been demonstrated to

induce production of reactive oxygen species (ROSs), driving an increased production of mucin characteristic of these chronic infections and associated with poor clinical outcomes (97,98).

As previously stated, LPS is a target for polymyxin antibiotics, and modifications to LPS can increase resistance to treatment with these agents (79).

1.2.2 Biofilm formation

P. aeruginosa chronic infections are associated with biofilm formation (see section 1.1.2). In biofilms, communities of bacteria are encased in a matrix formed primarily from three exopolysaccharides: alginate and the two aggregative polysaccharides Pel and Psl, in addition to extracellular DNA, lipids and proteins (99). This matrix provides structural support for biofilm assembly and attachment to surfaces, as well as protecting bacteria from damaging agents including antibiotics as previously described (see section 1.1.3) but also host immune defences and disinfectants.

Biofilm development takes place in stages, beginning with an initial reversible attachment to a surface (100). This attachment then becomes irreversible, with growth into more structured microcolonies, which eventually mature into the classical mushroom-shaped biofilm structures (101). Mature biofilm structures contain networks of channels involved in distribution of nutrients and disposal of waste products (99). Dispersal of bacteria from the mature biofilm releases planktonic cells which can adhere to different surfaces to seed new biofilm or contribute to acute virulence. Degradation of extracellular DNA in the matrix is a requirement for this dispersal step (102). Glycoside hydrolases encoded within *pel* and *psl* synthesis operons have also been described to hydrolyse their respective polysaccharides and contribute to biofilm dispersal (103).

A key regulator of chronic infection lifestyles, as previously outlined is the Gac-Rsm pathway (see section 1.1.2), however other regulatory pathways also play a role. Biofilm formation requires collective behaviour from a population, quorum sensing pathways therefore have a role to play in coordinating responses, such as the production of rhamnolipids and polysaccharides (104,105). Quorum sensing pathways also upregulate the production of lectins, whose polysaccharide binding is important for stabilising the exopolysaccharide containing matrix (106,107). Quorum sensing networks also influence motility and the secretion of extracellular enzymes which influence matrix composition (108). The formation of biofilm is also correlated with the level of the secondary messenger c-di-GMP, where elevated c-di-GMP levels drive the production of exopolysaccharides and adhesins (109).

1.2.3 Motility

P. aeruginosa can navigate its environment using different mechanisms of motility, such as swimming, swarming, twitching, sliding and surfing. These allow *P. aeruginosa* to approach surfaces and contribute to attachment and colonisation.

1.2.3.1 Flagella

P. aeruginosa rotates a single, polar flagellum for motility by swimming in liquid environments or swarming and surfing over solid surfaces (110,111). The flagellar structure can be split into three substructures: the basal body, the hook and the helical filament (Figure 1.2) (112). The basal body is comprised of four major ring structures that span the cell envelope, the cytoplasmic (C)-ring, the membrane-supramembrane (MS)-ring, the peptidoglycan (P)-ring and the LPS (L)-ring (113). The C-ring is the rotor unit of the flagellum, and is coupled to ion-conducting stator units of MotAB that are also embedded in the cytoplasmic membrane surrounding the C-ring (114–117). These stator units provide energy for flagellar rotation through the passage of protons through the peptidoglycan-anchored MotB, causing a conformational change in MotA that interacts with FliG of the C-ring, generating torque (118,119).

An export apparatus is connected to the basal body MS- and C-rings and is used to transport flagellar components across the cytoplasmic membrane for assembly, via a similar mechanism to that used by the type III secretion system (see section 1.2.6.3). A central channel formed in this export apparatus by FliOPQR aligns with the MS-ring channel (120). The associated FlhA powers secretion by generating proton-motive force and interacting with the cytoplasmic ATPase complex (121). FlhA and FlhB provide a platform to dock substrates and regulate export specificity (122,123). The cytoplasmic ATPase complex is formed from the ATPase FliI which is associated with substrate unfolding and export, its negative regulator FliH, and FliJ which mediates interaction with FlhA (124,125). Flagellar components, such as those comprising the rod, hook and filament, are sequentially transported through this export apparatus in an unfolded or partially unfolded state, before being incorporated into the growing flagellum structure (123).

Attached to this export apparatus and connecting the MS-ring, the P-ring and the L-ring is the hollow rod, which can be split into the proximal rod, linked to the MS-ring, and the distal rod that links to the hook (126). The hook is a curved tube formed from 11 FlgE protofilaments that extends from the rod out of the cell and connects to the filament (127). The filament is formed from polymerisation of up to 20,000 flagellin (FliC) subunits at a constant rate to a length of approximately 15 µm (128). This

filament is generally comprised of 11 flagellin protofilaments, where new protofilaments are transported through the filament to be incorporated at the distal end (129). Transport of subunits to the tip of the flagellum involves individual subunits being linked to form a chain, where the incorporation of the distal subunit into the tip of the flagellum provides the energy to pull the attached chain further through the channel (130). This distal end is capped with the FliD complex, which forms a cap plate structure from which leg domains extend below to contact the flagellar filament (129,131,132). FliD is associated with the folding and polymerisation of newly secreted FliC subunits at the flagellar tip, rotating as new subunits are incorporated (131).

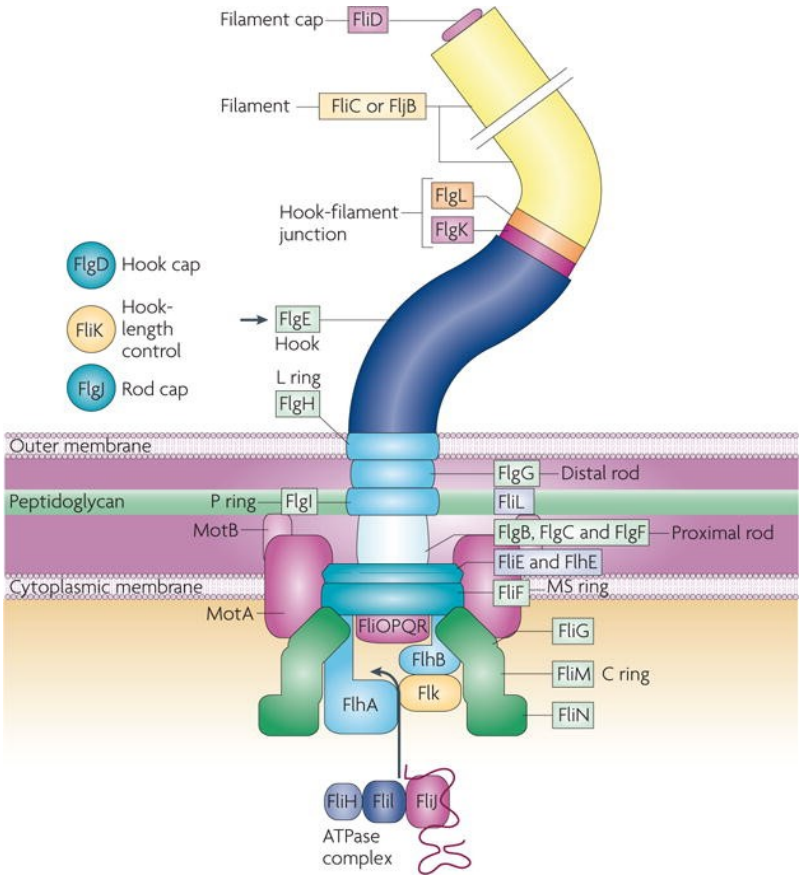


Figure 1.2 Schematic of the bacterial flagellum structure. The flagellar basal body contains four rings, the C-ring, the MS-ring the P-ring and the L-ring. The C-ring motor is surrounded by stator units of MotAB and is connected to the export apparatus of FliOPQR, FlhA and FlhB and the cytoplasmic ATPase. The rings of the basal body are connected by a hollow rod, which links to a curved hook structure, formed of FlgE. The hook is extended by the helical filament of FliC which is capped at its distal end by FliD. Figure reproduced from Chevance *et al.* (2008) with permission from Springer Nature.

Rotation of this filament, transmitted through the hook, propels the bacterium forward. Through switching the direction of flagellar rotation while swimming, bacteria tumble and are then

reorientated allowing navigation in specific directions, particularly in response to chemical signals by chemotaxis (117,133).

P. aeruginosa can use chemoreceptors to detect wound-associated amino acids and use chemotaxis and flagella-driven swimming to navigate to airway epithelial cells (134). Flagellin has also been identified to bind to asialo-GM1, an important glycolipid receptor for *P. aeruginosa* adherence to airway epithelial cells that is more abundant in cystic fibrosis patients (135–137), and heparan sulphate proteoglycans at the basolateral surface of airway epithelial cells (45). Flagella are therefore crucial to *P. aeruginosa* localisation to and binding to host cells.

Flagella are important for pathogenesis in acute *P. aeruginosa* infection. In a mouse pneumonia model, there was reduced mortality caused by bacteria lacking flagella, and inflammation was highly localised, rather than spreading through the lung (135). In contrast, in chronic infections flagella can be mechanically inhibited from rotating through FliD-mediated adhesion to host mucin (138). Additionally, mutation to the anti-sigma factor *mucA* associated with chronic infections drives repression of *fleQ*, the flagellar master regulator, reducing expression of flagellar synthesis genes (139). Reduction in motility is required for the establishment of biofilm, while loss of flagella also acts to prevent immune stimulation (140,141). The host immune system recognises flagellin through toll-like receptor-5 (TLR5), activating NF-KB and stimulating TNF-α production to promote pro-inflammatory responses (142).

1.2.3.2 Type IV pili

Type IV pili are filamentous appendages of polymerised pilin proteins, whose extension and retraction are responsible for twitching motility over surfaces (143,144). Type IV pili also contribute to swarming motility on solid surfaces in conjunction with flagella (145). These helical filaments are several micrometres long and approximately 8 nm in diameter, but able to withstand pulling forces exceeding 100 pN (146,147). The major pilin (PilA) forms most of the filament, which is capped with minor pilins at the distal tip (FimU-PilVWXY1) (148,149). A subset of core minor pilins contribute to pili formation and tip stabilisation, while non-core minor pilins contribute to aggregation, adhesion and DNA binding (150).

Twitching motility requires the activity of two ATPases, an assembly ATPase and a retraction ATPase, which associate with the platform protein from which the pilus is assembled (151). Extension of the pilus involves major pilin polymerisation, powered by the assembly ATPase, and is followed by

adhesion of the pilus tip to a surface (146,152). The pilus is then retracted, via depolymerisation of the major pilin powered by the retraction ATPase.

In addition to motility, type IV pili contribute to attachment and pathogenesis. Type IV pili are required for full virulence in Drosophila infection models (153). The minor pilin protein, PilY1, is required for attachment to basolateral airway epithelial cell surfaces (154). PilY1 contains a mechano-sensor domain, hence this attachment provides a mechanical signal which has been linked to induction of virulence pathways upon attachment to epithelial cells (53,155). The type IV pilus is also able to bind DNA and has thus been suggested to contribute to DNA uptake by natural transformation and biofilm formation by binding extracellular DNA (156). Surface adhesion by type IV pili is enhanced in the presence of the exopolysaccharide Pel, further indicating a role for type IV pili in biofilm formation (157). This enhanced interaction has also been suggested to contribute to a phenomenon, where secretion of polymeric substances from motile bacteria forms trails, which guide the movement of sister cells and can promote microcolony formation (158).

As with other *P. aeruginosa* virulence factors, type IV pili are recognised by the host immune system, with the major pilin subunit activating the inflammasome (159).

1.2.3.3 Rhamnolipids

Rhamnolipids are glycolipids with a rhamnose mono- or disaccharide moiety as the head group connected to a fatty acid tail (160). Rhamnolipids are biosurfactants due to their amphiphilic nature, lowering surface tension at the interface between liquids and other phases. Various types of *P. aeruginosa* motility are therefore facilitated by rhamnolipids, such as sliding motility, in the absence of flagella and type IV pili, and swarming motility (145,161,162). Biofilm formation is also associated with rhamnolipids, which contribute to initial attachment (163) and architecture, where they are involved in maintaining channel structure within the mature biofilm (164).

Rhamnolipids also contribute to pathogenesis, where they have been identified to disrupt airway epithelial junctions (165). The presence of rhamnolipids can also modulate host immune responses, by subverting immune signalling pathways (166) and inducing necrosis of polymorphonuclear leukocytes, which is elevated in the cystic fibrosis lung environment (167,168). *P. aeruginosa* rhamnolipids also have a role to play in interbacterial competition, delivering rhamnolipid micelles containing anti-bacterial toxins into competitors such as *S. aureus* (169).

1.2.4 Iron acquisition systems

Iron uptake is required for bacterial growth and virulence, with this resource being limited in host environments as a defence mechanism against pathogens (170).

P. aeruginosa secretes the siderophores pyoverdine and pyochelin into the extracellular environment to facilitate iron uptake. Pyoverdine has a peptide chain and a dihydroxyquinoline chromophore responsible for binding iron, where the three *P. aeruginosa* pyoverdine classes differ in their peptide chain composition (171,172). These pyoverdines can bind free iron in the extracellular environment in addition to scavenging iron from host proteins (173). Iron-bound complexes are then transported across the outer membrane by TonB-dependent transporters (174,175). Production of pyoverdines is required both for full virulence in acute mouse infection models (176), and for the formation of biofilms associated with chronic infections (177). In addition to its role in iron acquisition, pyoverdine is also a signalling molecule which drives the production of two key virulence factors exotoxin A and the protease PrpL (178).

The siderophore pyochelin has a lower affinity for iron when compared to pyoverdine (179). Pyochelin also contributes to virulence, as iron bound to pyochelin can promote the production of ROS, which cause tissue damage (180).

In addition to the secretion and uptake of chromosomally-encoded siderophores, *P. aeruginosa* can also hijack siderophores produced by other organisms such as *E. coli* enterobactin (181). Iron from host haem and haemoglobin is also targeted by *P. aeruginosa* HasAp (see section 1.2.6.1) and Phu systems (182).

1.2.5 Pyocyanin

Pyocyanin is a tricyclic zwitterionic phenazine responsible for the blue-green colour of *P. aeruginosa.* Pyocyanin production is associated with disease severity and a decline in lung function (183,184). Pyocyanin is pro-inflammatory, stimulating the production of cytokines and attraction of neutrophils (185). Additionally, pyocyanin is redox active and contributes to the generation of ROS, causing tissue damage (186,187). Pyocyanin production has additionally been linked to cell lysis and the release of extracellular DNA, which contributes to biofilm formation (188).

1.2.6 Secretion systems

The export of proteins produced by gram-negative bacteria across their cell envelope is achieved through macromolecular complexes termed protein secretion systems. These complexes use various mechanisms to span the cell envelope and deliver proteins either into the extracellular environment or directly into neighbouring cells. These pathways can secrete proteins across the cell envelope in a single step, or via a two-step process with transport across each membrane achieved by separate components.

1.2.6.1 Type I secretion system

The type I secretion system (T1SS) is comprised of an ATP-binding cassette (ABC) transporter in the inner membrane which is linked via the membrane fusion protein to a channel formed by the outer membrane protein TolC (Figure 1.3) (189–191). There is structural similarity between the T1SS and the RND family of efflux pumps (see section 1.1.3) (192). The ABC transporter couples protein transport across the inner membrane to ATP hydrolysis, and forms a complex in the inner membrane with the membrane fusion protein that has a large periplasmic domain (193,194). The TolC protein forms a β-barrel structure in the outer membrane with a periplasmic extension formed by α-helices that gate this channel, rearrangement of these helices via a twisting motion opens to channel to allow protein secretion (195,196). Substrate binding to the inner membrane components triggers recruitment of TolC to form the transmembrane channel for transport of unfolded substrates into the extracellular medium (191,197).

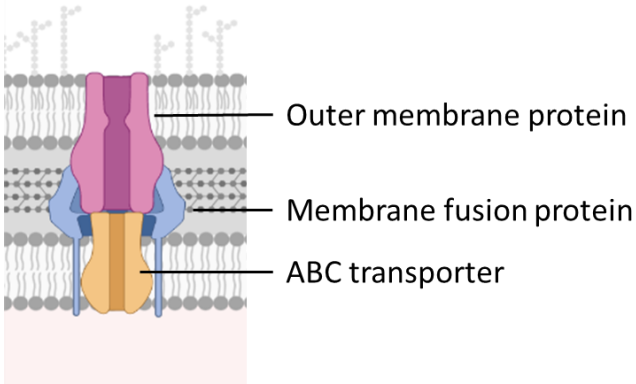


Figure 1.3 Schematic of the type I secretion system structure. A channel is formed between the inner membrane associated ABC transporter and membrane fusion protein with the outer membrane protein, through which proteins are secreted. Figure created with Biorender.com.

The *P. aeruginosa* T1SS is responsible for the secretion of the alkaline protease AprA (198), the haemophore HasAp (199), the host immunomodulator TesG (200) and AprX of unknown function (201). AprA can impair the host immune response by cleavage of components of the immune response

such as complement proteins and cytokines (198,202,203), in addition to degrading extracellular flagellin to prevent its recognition by TLR5 (204). AprA can also block the phagocytosis and subsequent killing of *P. aeruginosa* by neutrophils (203). The production of AprA has been identified in *P. aeruginosa* isolates associated with cystic fibrosis patients (205). It is suggested that the proteolytic activation of a sodium channel in airway epithelial cells by AprA contributes to an increased viscosity of mucus and impaired mucociliary clearance (206).

TesG similarly has roles in suppressing host inflammatory responses by targeting host Rho GTPases, suppressing neutrophil influx and secretion of pro-inflammatory cytokines, thereby contributing to the establishment of chronic infections (200). Secreted HasAp can bind host haem, which it then delivers to the HasR receptor located at the cell surface to facilitate iron uptake (199).

1.2.6.2 Type II secretion system

The type II secretion system (T2SS) is comprised of 12-15 proteins which form a platform associated with the inner membrane, a cytoplasmic ATPase, a periplasmic fibrillar structure called the pseudopilus and a secretin channel in the outer membrane (Figure 1.4) (207–209). Multiple components of this assembly have structural similarities to type IV pili, although this pseudopilus is confined to the periplasm rather than extending out into the extracellular environment (210). The cytoplasmic ATPase powers assembly of the pseudopilus and effector secretion via ATP hydrolysis (211). The pseudopilin is comprised of a major pilin and capped at the tip with minor pilins (212,213). The outer membrane channel is formed from the dodecameric assembly of the secretin protein which contains a closed periplasmic gate (214,215).

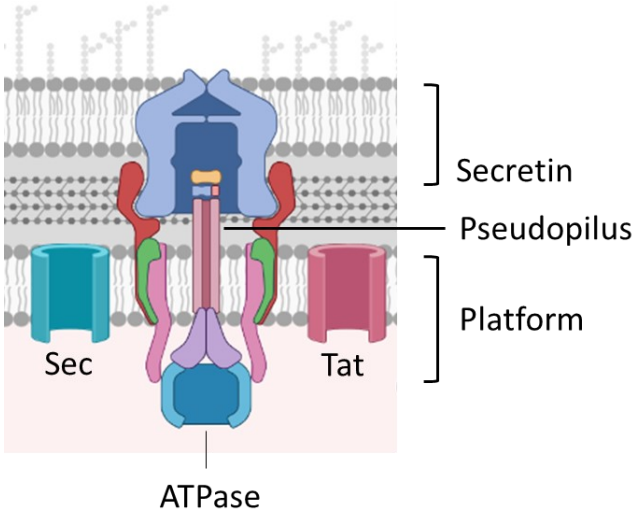


Figure 1.4 Schematic of the type II secretion system structure. Effectors are transported into the periplasm through Sec or Tat export pathways, before being recruited into the T2SS channel. Effectors are pushed out of the cell through the secretin by the ATPase-powered polymerisation of the pseudopilus. Figure created with Biorender.com.

T2SS-associated effectors are targeted for transport across the inner membrane and into the periplasm by N-terminal signal sequences for either the Tat export pathway if they have been folded in the cytoplasm, or via the Sec export pathway if they are unfolded (216,217). From the periplasm effectors are then inserted into the secretin channel through interaction with components of the inner membrane platform and the outer membrane secretin (218), before ATPase-powered pseudopilus polymerisation pushes the proteins through the secretin and out of the cell in a piston-like mechanism (219).

P. aeruginosa has been identified to encode three T2SS machineries: a Xcp system (220), a Hxc system (221) and a Txc system, which is found exclusively in the PA7 strain (222). These T2SSs transport a wide variety of protein effectors into the extracellular environment, including elastases (i.e. LasA and LasB) (223), lipases (i.e. LipA and LipC) (224,225), phospholipases (i.e. PlcB, PlcH and PlcN) (216,226), alkaline phosphatases (i.e. PhoA and LapA) (221,227), the aminopeptidase PaAP (223) and the lipoxygenase LoxA (228). These secreted effectors have broad impacts on pathogenicity and host immune responses. The elastase LasB, for example, can disrupt airway epithelial junctions, degrade components used in the host immune response and degrade exogenous flagellin to prevent its recognition by TLR5 (229–232).

A very potent *P. aeruginosa* virulence factor secreted in a T2SS-dependent manner is the ADP-ribosyl transferase, exotoxin A, one of the virulence factors previously described to be upregulated by pyoverdine signalling (see section 1.2.5) (178,233). Secreted exotoxin A can bind to CD91 on the host cell surface and be internalised through either clathrin-coated pits or caveolin-mediated internalisation (234). In endosomes, exotoxin A is cleaved to an active form before being transported to the cytosol (235,236). One target for ADP-ribosylation by exotoxin A is eukaryotic elongation factor-2, causing impaired host protein synthesis (237). Exotoxin A is also proposed to cause cell cycle arrest and induce apoptosis (238,239). While it can also modulate host inflammatory responses, by decreasing cytokine production and secretion (92,240,241).

1.2.6.3 Type III secretion system

The type III secretion system (T3SS) is described as an injectisome, which delivers effector proteins directly into the cytosol of eukaryotic cells (242,243). Genes encoding *P. aeruginosa* T3SS structural and regulatory components are organised in operons, while genes associated with effector proteins are present at distinct chromosomal loci (244–246). The structural components are assembled into a cytoplasmic ATPase and sorting platform, a basal body that spans the cell envelope, a hollow needle

that extends into the extracellular environment and translocator proteins that form a pore in eukaryotic cell membranes (Figure 1.5) (247,248). There are structural similarities between the T3SS and the flagellum (see section 1.2.3.1), with homologous proteins forming the export apparatuses associated with each of these systems (249,250), and sorting platforms coordinating the hierarchical secretion of substrates (251).

The T3SS needle is formed from the secretion and polymerisation of a single needle protein (PscF) which in *P. aeruginosa* extends to 60-80 nm (247). Three *P. aeruginosa* proteins, PopB, PopD and PcrV, are then transported through the needle, with PopB and PopD inserting into the eukaryotic cell membrane to form the translocon pore (252–254). PcrV is proposed to form a scaffold at the tip of the needle whose interaction with PopB is required for formation of the translocon pore, with antibodies against PcrV inhibiting effector delivery (255,256).

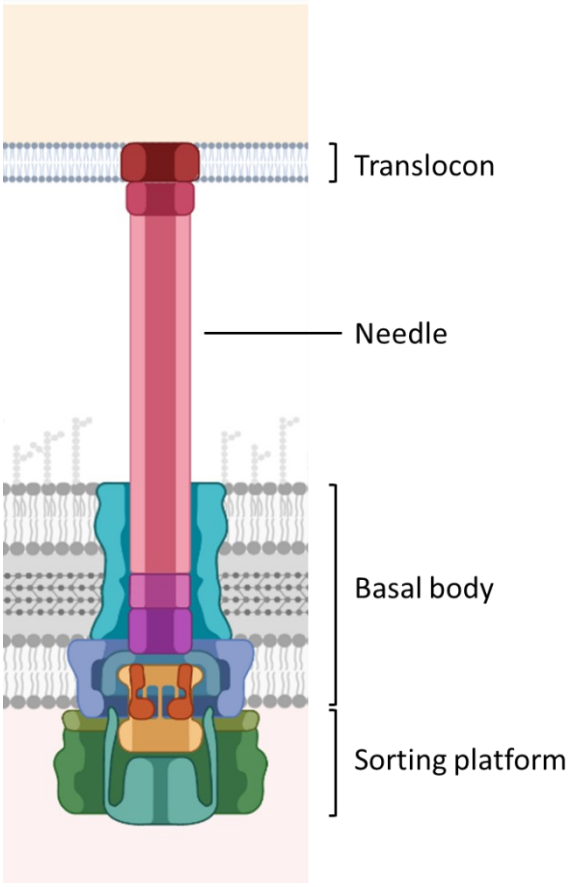


Figure 1.5 Schematic of the type III secretion system structure. Effectors are delivered to the cytoplasmic sorting platform at the base of the cell envelope-spanning basal body. Effectors are then transported through a hollow needle structure, which forms a bridge to the eukaryotic cell cytosol and is capped with a translocon pore in the membrane of a eukaryotic cell. Figure created with Biorender.com.

Following the translocation and assembly of the translocon pore, unfolded effectors are delivered to the cytoplasmic sorting platform by chaperones, before being transported through the needle and the translocon into the eukaryotic cell (257). Targeting of effectors to the T3SS involves the presence of N-terminal secretion signals (258). Four main effectors have been identified associated with the *P. aeruginosa* T3SS, ExoS, ExoT, ExoU and ExoY, although strains commonly encode only a subset of these

effectors (259). ExoS and ExoT are very similar proteins, with N-terminal RhoGAP domains and C-terminal ADP-ribosylation domains, which affect host cytoskeleton and functions such as migration, adhesion and phagocytosis (260). ExoU has phospholipase activity, triggering host cell lysis and pro-inflammatory pathways (261–263). ExoY is an adenylate cyclase, which disrupts cAMP associated signalling pathways, affecting host cytoskeleton, bacterial uptake into host cells and epithelial cell junctions (244,264,265).

P. aeruginosa strains generally encode either ExoS or ExoU, where ExoU-encoding strains are impaired in internalisation and associated with rapid cell lysis, while ExoS-encoding strains are associated with more efficient internalisation and slower cell death (266,267). Isolates from cystic fibrosis patients are more commonly associated with ExoS when compared to other isolates (259).

Additional *P. aeruginosa* T3SS effectors, PemA and PemB, have been identified using a machine-learning approach (268). These effectors have been demonstrated to be translocated by the T3SS into eukaryotic cells but are yet to be functionally characterised.

The T3SS is an important *P. aeruginosa* virulence factor associated with acute infections, influencing tissue damage and mortality (269,270). The master regulator of T3SS expression is ExsA and the ExsADCE cascade, which is induced by signals such as low levels of extracellular calcium ions and host cell contact (271). As with many other *P. aeruginosa* virulence factors, including exotoxin A and type IV pili, the T3SS is regulated by the transcriptional regulator virulence factor regulator (Vfr) (272). The Rsm family of post-transcriptional regulators also promote expression of T3SS genes, through positive regulation of ExsA via an unknown mechanism (49,273). In contrast, expression of the T3SS is typically lost in chronic infections, such as those found in the lungs of cystic fibrosis patients (259,274). Loss of T3SS gene expression in this environment has been linked to mutation of the anti-sigma factor *mucA*, which drives downregulation of *vfr* expression through the alternate sigma factor AlgU, where the *mucA* mutation also contributes to the increased alginate production and mucoid phenotype associated with chronic infections (see section 1.2.2) (275,276).

1.2.6.4 Type V secretion system

Type V secretion system (T5SS) components are transported to the periplasm via the Sec export pathway, using an N-terminal signal sequence, followed by the insertion of the translocation domain into the outer membrane forming a β-barrel structure, through which the passenger domain is secreted (277). Five different types of T5SS have been described, type Va-Ve, where so called autotransporters, Va, Vc, Vd and Ve, contain both translocation domain and passenger domain within

a single polypeptide (Figure 1.6) while Vb T5SSs have separate polypeptides encoding translocation and passenger domains, known as two-partner secretion systems (278).

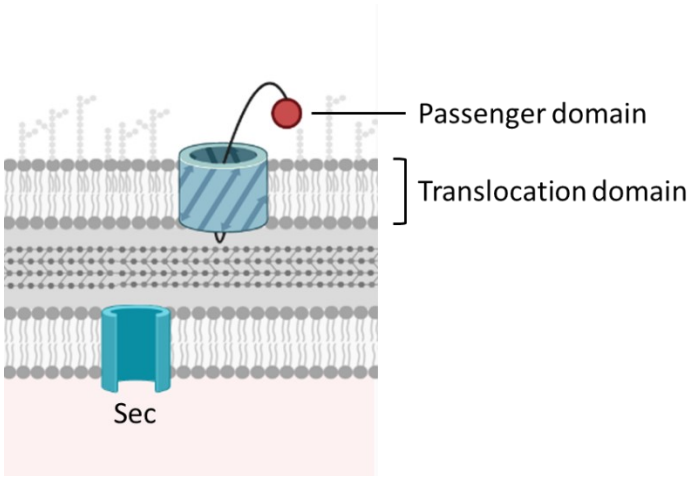


Figure 1.6 Schematic of the type V secretion system autotransporter structure. T5SS components are transported into the periplasm through the Sec export pathway, before folding of the translocation domain into a β-barrel structure which is inserted into the outer membrane. The passenger domain is then transported through this pore and either tethered to the cell surface, as shown, or secreted into the extracellular environment. Figure created with Biorender.com.

P. aeruginosa encodes three of these T5SS autotransporters: EstA, EprS and AaaA (279–281). EstA is transported out of the pore in an unfolded state and remains tethered to the pore and displayed at the bacterial cell surface (282). This surface-associated passenger domain is an esterase, which is required to produce rhamnolipids and is consequently important for motility and biofilm formation (283). Additionally, binding of EstA to laminin contributes to adhesion in respiratory infections (284). The EprS passenger domain, which is secreted through the pore and released into the extracellular environment, has serine protease activity and induces pro-inflammatory host responses (280). The AaaA aminopeptidase passenger domain is tethered to the cell surface where it can cleave N-terminal arginine residues, which can then be used for growth, providing a fitness advantage in certain environments including chronic wound infection (281). A type Vd T5SS, PlpD, is also encoded by *P. aeruginosa* (285). The PlpD passenger domain, which is secreted through the pore and released into the extracellular environment, has lipase activity.

P. aeruginosa encodes multiple type Vb two-partner secretion systems, including LepA-LepB and CdrA-CdrB (286,287). The passenger protein, LepA, contains an RGD motif, which may contribute to adhesion to the extracellular matrix, and a serine protease motif which contributes to the activation pro-inflammatory host responses (286). CdrA is an adhesin which is associated with the biofilm matrix, where it contributes to biofilm stability, through both cross linking Psl polymers and tethering Psl to cells (287).

The CdiA-CdiB sub-family of type Vb two-partner secretion systems mediates contact-dependent growth inhibition (CDI), through toxin delivery to a neighbouring bacterium. The CdiA passenger protein is displayed on the cell surface, through a conserved β-helix filament that extends through the CdiB β-barrel and presents a receptor binding domain the distal end of the filament, which specifically binds targets on the surface of neighbouring bacteria (Figure 1.7) (288–290). A tyrosine and proline rich region, called the YP domain, then extends back through the CdiB β-barrel to the periplasm where the C-terminal toxin domain is sequestered until receptor binding initiates its transport for toxin delivery (289). In *E. coli* it was demonstrated that an FHA2 domain upstream of the toxin domain facilitates transport of the C-terminal toxin across the outer membrane of the target cell and into the periplasm, where pore forming toxins can destabilise the inner membrane (291). Alternatively, many characterised CdiA proteins carry nuclease toxins, which are targeted to the cytoplasm by binding inner membrane proteins (292). CdiA proteins are modular with the conserved N-terminal region followed by more variable receptor binding and C-terminal toxin domains, as such different strains commonly encode distinct CdiA toxin domains (290,293). These anti-bacterial toxins require co-regulated immunity proteins to prevent self-intoxication and intoxication by sister cells (294).

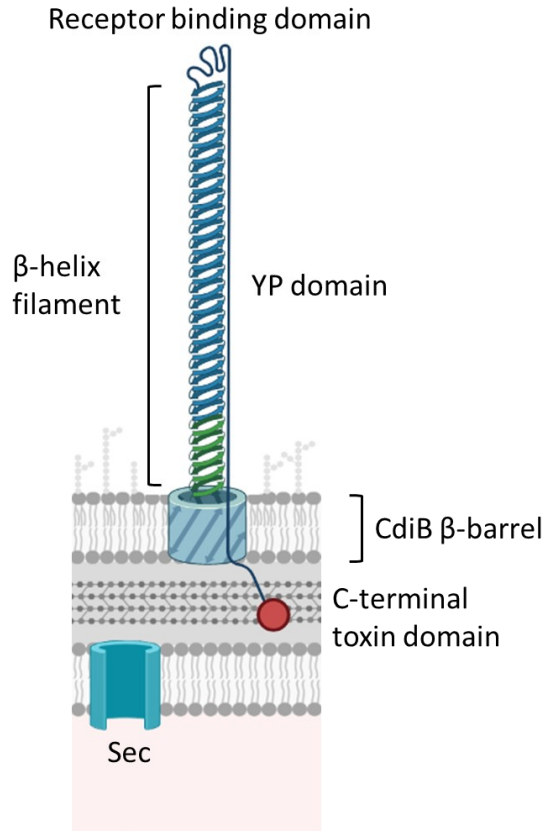


Figure 1.7 Schematic of the type Vb two-partner secretion system structure. T5SS components are transported into the periplasm through the Sec export pathway, before folding of CdiB into a β-barrel structure which is inserted into the outer membrane. The CdiA protein is then presented on the cell surface through this pore, with a β-helix filament presenting a distal receptor binding domain. A YP domain extends into the periplasm where the C-terminal toxin domain is sequestered until contact is made with a target cell and the toxin is then delivered into the neighbouring bacterial cell. Figure created with Biorender.com.

To date, *cdi* loci have been identified in all sequenced *P. aeruginosa* isolates, with 80 % of genomes encoding two loci (295). Five classes of CdiA proteins have been proposed in *P. aeruginosa* based on variable pre-toxin motifs (296). Two such loci are present in the lab strain PAO1, where each was

predicted to have a nuclease domain, and identified to contribute to bacterial killing (296). The clinical isolate PABL017 was identified to have a CDI system which contributed to bacterial killing as well as host virulence in a mouse infection model, through the activity of a CdiA protein with tRNase activity (297). While it remains unclear how this toxin domain is transported into eukaryotic cells, transport into the cytoplasm of bacterial cells was identified to involve the inner membrane receptors DppB and DppC (298).

1.2.6.5 Secretion systems with roles in interbacterial competition

Like the CDI system, other secretion systems with roles in interbacterial competition have been identified, including the type VI secretion system, which will be discussed in more detail in section 1.3. While *P. aeruginosa* does not encode a type IV secretion system (T4SS), those of *Xanthomonas citri* and *Stenotrophomonas maltophilia* have been identified to deliver toxic effectors into prey bacterial cells (299,300). T4SSs can also have roles in pathogenesis in both plant and animal hosts (301,302) and horizontal gene transfer including conjugation (303) and transformation (304). Additionally, the type VII secretion system (T7SS), produced by gram-positive bacteria, secretes effectors with roles in virulence and interbacterial competition (305,306).

1.3 Type VI Secretion System

The type VI secretion system (T6SS) is a contractile nanomachine involved in the delivery of effector proteins across the cell envelope of gram-negative bacteria. These effector proteins can be delivered directly into neighbouring cells, including both prokaryotes and eukaryotes, as well as into the extracellular medium. The T6SS is a key mediator of interbacterial competition through the delivery of toxin effectors to kill or inhibit the growth of neighbouring bacteria (307) and can also target fungi (308). Anti-bacterial effector genes are encoded with cognate immunity genes to prevent self-intoxication or intoxication by sister cells. Additionally, effector delivery can be used to manipulate host eukaryotic cells (309) and for the uptake of extracellular common goods (310,311).

The T6SS shares an evolutionary origin with bacteriophage contractile tails, which are similarly involved in the transport of cargo across bacterial membranes, though the transport of DNA into bacterial cells, rather than export of proteins as is the case for the T6SS (312,313). The bacteriophage and the T6SS share similarity in their baseplate and tail complexes, while the T6SS also contains a membrane complex (314).

1.3.1 Distribution of the T6SS in gram-negative bacteria

The T6SS is found in more than 25 % of all gram-negative bacterial genomes (315). Functional T6SSs have been demonstrated in members of Proteobacteria (316) and Bacteroidetes (317), while bioinformatic data indicates their more widespread presence in other phyla (317). There are four sub-types of T6SS whose distribution varies across phyla, that are classified based on the presence of the 13 T6SS core components, sequence homology and distribution. The archetypal T6SS^{i} is present in a range of Proteobacteria including *Pseudomonas* and *Vibrio*, and is the subject of this study (34,316). The T6SS^{ii} is encoded the *Francisella* pathogenicity island and thus limited to *Francisella* (318,319), while the T6SS^{iii} is found exclusively in Bacteroidetes (318,320). The distribution of the newly characterised T6SS^{iv} is more diverse (312). Both the T6SS^{iii} and the T6SS^{iv} lack the membrane complex components present in the archetypal T6SS^{i}, although the T6SS^{iv} of *Amoebophilus asiaticus* is observed to be connected to the inner membrane via a distinct anchoring platform and a similar functional substitution is suggested for the T6SS^{iii} (312,317). The T6SS component TssA, which is the primary focus of this work, is found in T6SS^{i}, but absent in T6SS^{iii} and some T6SS^{ii} (317,318).

Bacteria encoding T6SSs are associated with a range of ecosystems, both environmental and host associated. Active T6SSs, contributing to interbacterial competition in environmental populations through the killing of neighbouring bacteria, have been identified in several aquatic *Vibrio* species, as

well as the soil bacterium *Pseudomonas putida* (321–324). Host-associated T6SS-encoding bacteria include commensal strains, such as the plant commensal bacterium *Pseudomonas protegens* (325) or the squid symbiont *Vibrio fischeri* (326,327). T6SSs are also encoded in host-associated pathogenic bacteria, including each of the gram-negative ESKAPE pathogens, *K. pneumoniae* (328), *A. baumanii* (329), *P. aeruginosa* (307) and *Enterobacter cloacae* (330), which are leading causes of nosocomial infections.

Many T6SS gene clusters are chromosomally encoded within genomic islands, as described for the *Francisella* and *Salmonella* pathogenicity islands (319,331,332). These T6SS gene clusters are suggested to have been horizontally acquired, which is supported by observations of variable GC content between T6SS genes and the genome as a whole (333,334). Horizontal gene transfer is also involved in the transfer of plasmid-encoded T6SSs, such as pCJDM202 of *Campylobacter jejuni* (335). Integrative and conjugative elements are implicated in the transfer of T6SS genes in Bacteroidetes, which is proposed to be a common mechanism of T6SS acquisition in the gut microbiome (336).

T6SS-positive bacteria may encode a single T6SS gene cluster, as found in *Vibrio cholerae* (316) or *Agrobacterium tumefaciens* (337), or multiple, such as the three found in *P. aeruginosa* (34,338) or the six found in *Burkholderia pseudomallei* (339). Within a species there can be strain-specific differences, commonly in effector proteins which can drive intraspecies competition. One such example is the *P. aeruginosa* effector Tse7, where diversity in this effector between strains is mirrored by immunity protein diversity to provide strain-specific protection (340). Interestingly the presence of immunity genes is not always accompanied by the gene encoding the cognate effector, some bacteria encode gene clusters containing arrays of immunity genes to protect against T6SS attack (341). In *V. cholerae* there is effector gene diversity between strains, while multiple immunity proteins can also be encoded to protect against these diverse effectors encoded by other strains, this is predicted to give an advantage in intraspecies competition allowing certain strains to co-exist (334).

1.3.2 Structure and assembly of the T6SS

The T6SS structural machinery comprises 13 core components, which can be sub-divided into the membrane complex, baseplate complex and tail complex (314). The baseplate complex is anchored to the membrane complex, providing a platform for the assembly of the tail complex, comprising a contractile sheath structure around a rigid inner tube capped at the baseplate with a spike (Figure 1.8). Sheath contraction propels the inner tube and spike, which carry associated effector proteins, out of the cell and either into a neighbouring cell or into the extracellular medium.

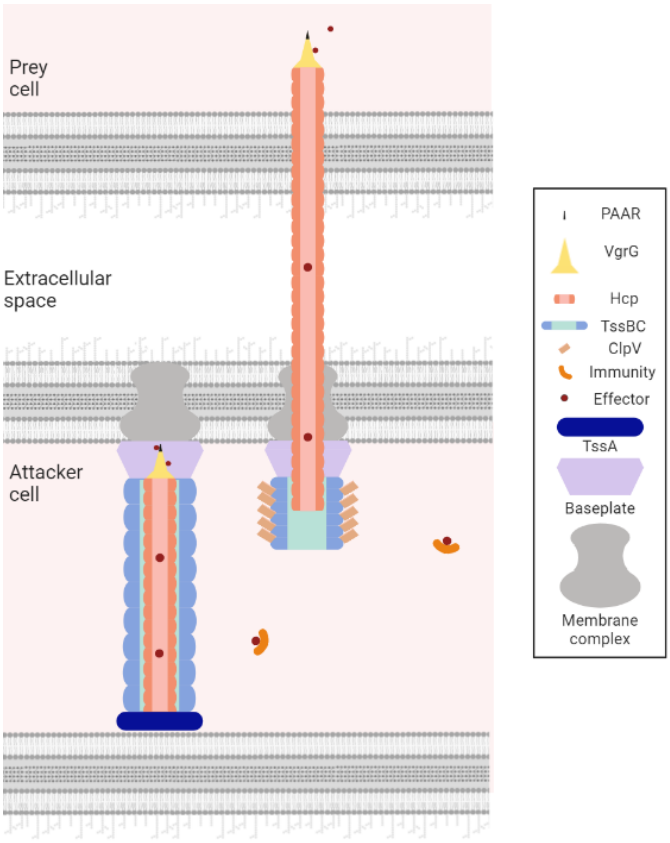


Figure 1.8 Schematic of the type VI secretion system structure in extended and contracted conformations. The assembled extended T6SS is indicated on the left, and contraction of the sheath to propel the inner tube and spike is indicated on the right. Figure created with Biorender.com.

1.3.2.1 T6SSs of *P. aeruginosa*

As previously detailed, three T6SS gene clusters are encoded in the *P. aeruginosa* genome, termed the H1-, H2- and H3-T6SSs (Figure 1.9). Five phylogenetic groups of T6SS^{i} clusters have been described, based on charaterising co-evolution of core components and comparing the presence of conserved accessory proteins (342). The three clusters of *P. aeruginosa* fall into separate groups: H1-T6SS in phylogenetic group 3, H2-T6SS in phylogenetic group 1 and H3-T6SS in phylogenetic group 4A. Each *P. aeruginosa* T6SS cluster encodes a *tssA*, the characterisation of which is the aim of this project.

T6SS clusters encode genes for each of the structural components required to assemble the T6SS as well as regulatory genes. Additionally, islands of T6SS-associated genes are present at distinct chromosomal loci, often encoding effector and immunity genes (343). The contribution of these components to the assembly and dynamics of the T6SS will be discussed in detail.

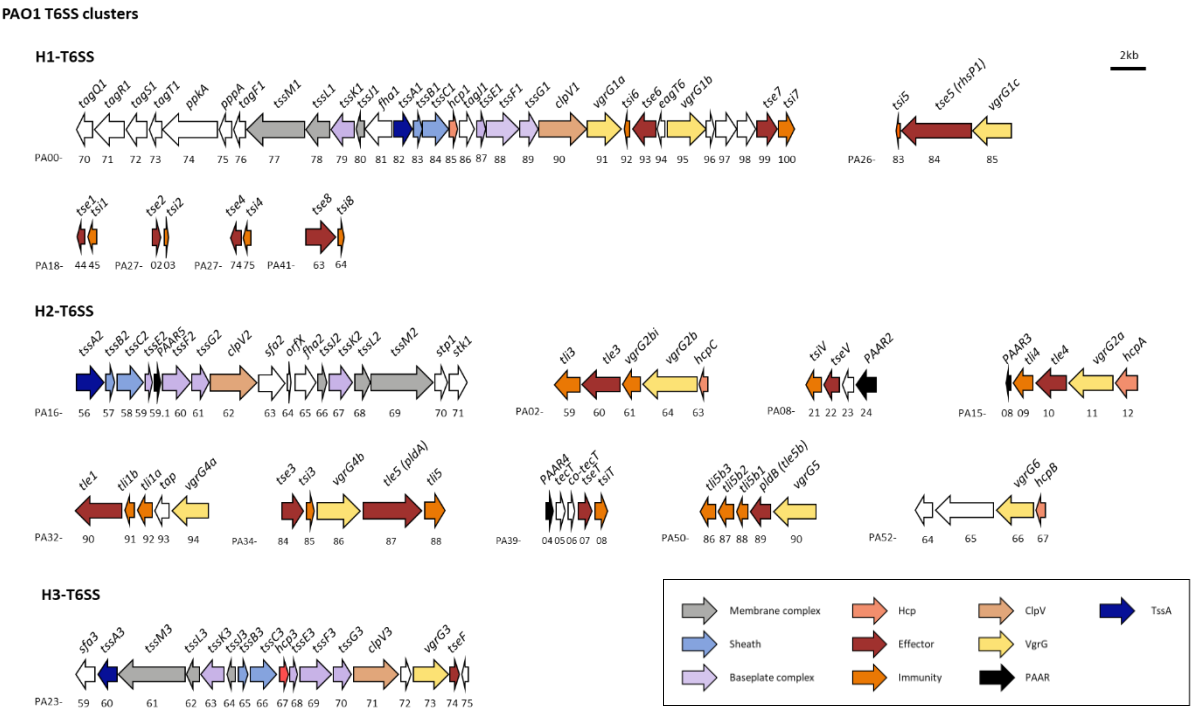


Figure 1.9 Schematic of the *P. aeruginosa* strain PAO1 T6SS gene clusters. PAO1 encodes the H1-, H2- and H3-T6SS clusters, each containing the genes required to form a membrane complex, baseplate complex and tail complex, with associated effector and immunity genes. Genes in white encode for non-structural components, for example regulatory components or are yet to be characterised.

1.3.2.2 The membrane complex

A key difference in the structures of the bacteriophage tail and the T6SS, is the presence of a membrane complex which anchors the T6SS machinery within the gram-negative cell envelope. The membrane complex is formed from the outer membrane lipoprotein TssJ and the inner membrane proteins TssM and TssL, where the inner membrane components were initially identified to resemble the DotU and IcmF components of the type IVb secretion system (344,345). The assembly of the T6SS begins with the insertion of TssJ in the inner leaflet of the outer membrane through an N-terminal acyl group (346). The protein region of TssJ extends into the periplasm and, through a loop region, forms contacts with the C-terminal periplasmic region of TssM (347,348). Anchoring of TssM in the inner membrane is achieved by three transmembrane helices, between which a cytoplasmic domain is displayed that has been demonstrated to have NTPase activity in *A. tumefaciens*, with other putative NTPase domains identified in other organisms (349–351). Mutations to disrupt this NTPase activity in *A. tumefaciens* were found to inactivate the T6SS (349,352).

TssL has a single transmembrane region, through which it interacts with TssM (353), and a cytoplasmic domain which, along with TssM cytoplasmic regions, interacts with the baseplate (344,354). A lack of conservation has been identified in these baseplate-interacting regions, which has been proposed to contribute to binding specificity in organisms when multiple T6SSs are present (344). In some cases, TssL proteins have an additional periplasmic domain for binding to the peptidoglycan, although this can alternatively be achieved by TagL, TagN, TagW or TagP proteins (355). This anchoring to the peptidoglycan is proposed to be required to resist the forces generated by contraction of the sheath.

Structures of the membrane complex of enteroaggregative *E. coli* identify the formation of a 1.7 mDa bell-shaped structure with five-fold symmetry (Figure 1.10) (347,356). The periplasm is bridged by 10 pillars formed of TssJ and TssM, while five TssL dimers are presented to the cytoplasm. The central channel within the membrane complex is constricted within the periplasm by a TssM loop (356). The tip of the bell-shaped structure is positioned within, but not crossing the outer membrane. In other protein secretion systems, the formation of a channel that spans the outer membrane to facilitate protein export is well described (see section 1.2.6) (192). Of course, during T6SS firing, the inner tube and associated spike do cross this outer membrane, but the mechanism by which this occurs is not entirely clear. Interestingly it has been observed that the TssM C-terminus, that has been identified within the periplasm in resolved structures, can cross the outer membrane, with an extracellular cap region, presumed to be comprised of this TssM C-terminus also identified in electron cryotomography (347,357). It has therefore been proposed that this structure represents a closed conformation of the membrane complex, with secretion suggested to be accompanied by a conformational change to release constriction of the lumen and allow release of the spiked inner tube, which could expose membrane complex components to the extracellular medium. This opening of the membrane complex has been proposed to be triggered either by a conformational change in the baseplate, or the physical force of the expulsion of the spiked inner tube (347,356).

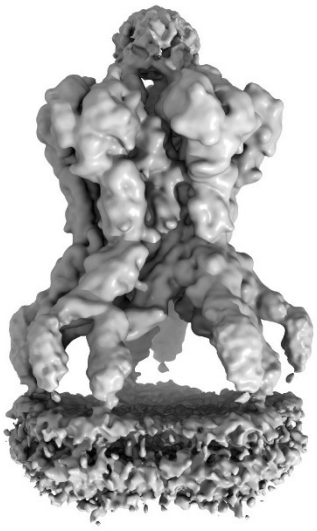


Figure 1.10 Structure of the enteroaggregative *E. coli* membrane complex. Cryo-electron microscopy density of the membrane complex (EMD-0265). Figure reproduced from Rapisarda *et al.* (2019) under the terms of the Creative Commons CC BY license, https://creativecommons.org/licenses/by/4.0/legalcode.

The insertion of the T6SS membrane complex into the cell envelope is proposed to require localised rearrangement of the peptidoglycan. This peptidoglycan rearrangement can be carried out by a T6SS-associated peptidoglycan hydrolase encoded in *Acinetobacter* species (358), while *E. coli* can utilise the housekeeping transglycosylase, MltE (358,359).

The five-fold symmetry observed for the membrane complex contrasts with the six-fold symmetry described for the baseplate complex, that will be discussed in the proceeding section. It is suggested that a high degree of flexibility in TssM and TssL cytoplasmic regions could allow this symmetry mismatch to be overcome (347,356). Alternatively, it has been suggested that a chaperone protein might facilitate the formation of a six-fold symmetry membrane complex structure, where one such proposed chaperone is TssA, which has been identified to bind the cytoplasmic face of the enteroaggregative *E. coli* membrane complex (356,360–362).

1.3.2.3 The baseplate complex

The baseplate complex is recruited to the membrane complex and provides a platform for the assembly of the tail complex. The T6SS baseplate complex resembles that of the bacteriophage, with a central hub surrounded by six wedges (Figure 1.11) (363). In the T6SS, the central hub comprises the trimeric VgrG spike complex which is found at the proximal end of the tail complex inner tube (364,365). The tip of this VgrG trimer is crowned with a small protein containing a characteristic proline-alanine-alanine-arginine sequence, known as a PAAR protein, to sharpen this puncturing device (Figure 1.11B) (366). Several different VgrG proteins can be associated with a single T6SS, such as VgrG1a, VgrG1b and VgrG1c of the H1-T6SS (Figure 1.9) (367). Effector proteins can be associated with both VgrG and PAAR components to target their delivery into neighbouring cells. There can be additional effector domains as part of these components, such as the actin cross-linking domain of *V. cholerae* VgrG-1 (309), or effectors can be bound to them by protein-protein interaction such as *P. aeruginosa* PldA which is delivered by VgrG4b (368).

Around this central hub, baseplate wedges formed of TssE, TssF, TssG and TssK are bound. Within a wedge, these components assemble with a $TssE_1$-$TssF_2$-$TssG_1$-$TssK_6$ stoichiometry (365,369). A single TssG is bound by two TssF monomers forming a triangular trifurcation unit, with TssG loop regions forming contacts with two TssK trimers which are more flexibly associated with the wedge (Figure 1.11A) (365,369).

The polymerisation of six wedge units around the VgrG central hub forms a 2.7 mDa ring structure, with contacts between wedges facilitated by interactions between TssF monomers (Figure 1.11B)

(365,370). A cavity is present between the central hub and the polymerised wedges, which has been proposed to accommodate effector proteins associated with either VgrG or PAAR proteins (364).

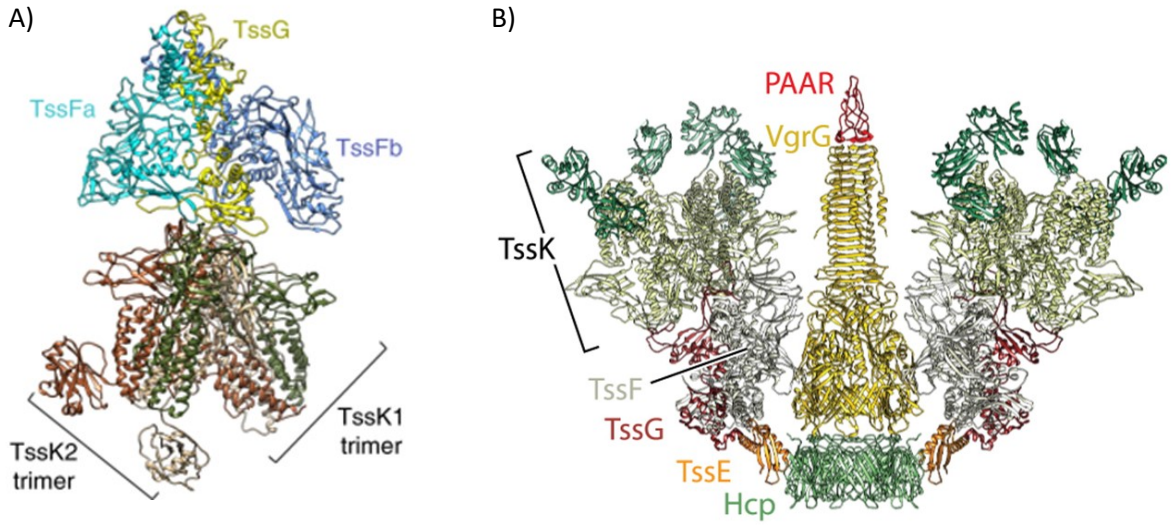


Figure 1.11 Structure of the baseplate complex. A) Structure of the enteroaggregative *E. coli* baseplate complex wedge comprising TssF, TssG and TssK. Figure reproduced from Cherrak *et al.* (2018) with permission from Springer Nature. B) Model of the T6SS baseplate, including the baseplate wedge components, the VgrG central hub and the first layer of the Hcp inner tube. Figure reproduced from Wang *et al.* (2019) with permission from Annual Reviews, Inc.

The baseplate complex serves as an adaptor between the membrane complex and the tail complex. In the *V. cholerae* baseplate, TssK has been identified to form a connector region at the interface between the baseplate and the membrane complex (364). Contacts between TssK and the cytoplasmic regions of both TssL and TssM have been described (354,371,372). Flexibility in the C-terminal domain of TssK, which contacts the membrane complex, is proposed to be key to facilitating this interaction due to the symmetry mismatch at this interface (365). In terms of contacts with the tail complex, the N-terminal base of the VgrG trimer shares structural similarity with the tail complex inner tube, which is polymerised from this hub (313,373). Additionally, structural similarity has been identified between TssE and the sheath, which implicates TssE as the wedge component forming contacts with the sheath to initiate sheath polymerisation (374,375). Remarkably, it has been proposed that certain groups of TssA protein are additional baseplate components, that are found at the interface with the sheath (376,377).

The signal for sheath contraction is currently unknown, however, by comparison to the mechanism for bacteriophage tail contraction it is proposed that a conformational change in the baseplate, from dome- to star-shaped, may trigger contraction by altering contacts at the interface with the sheath (364,365,369,374).

1.3.2.4 The tail complex

The tail complex is polymerised from the T6SS assembly initiation site comprised of the membrane complex and anchored baseplate complex. This tail complex consists of a contractile sheath structure, which surrounds a rigid inner tube. This hollow inner tube is formed from rings of Hcp hexamers stacked in a head-to-tail orientation, which polymerises from the base of the trimeric VgrG spike complex (313,378,379). This tube has a diameter in the region of 80-90 Å and a lumen of approximately 40 Å (34). Effector proteins can be carried in this Hcp ring lumen, where following tube expulsion the Hcp tube breaks down into individual Hcp rings (380).

The Hcp tube is surrounded by a contractile sheath, formed from polymerisation of the sheath protomer, a dimer of TssB and TssC (Figure 1.12) (381–383). Each protomer can be subdivided into three domains, where domains 1 and 2 resemble the classical fold of sheath proteins associated with contractile injection systems (CISs) (see section 1.3.3), while domain 3 contains the TssC N-terminus which forms a ClpV-binding site (384,385). Sheath polymerisation forms a helix with six protomers per layer, where contacts between neighbouring protomers form a four β-strand handshake domain that stabilises a high energy extended sheath conformation (Figure 1.12A) (386). It is suggested that initiation of sheath polymerisation at the baseplate involves TssE donating two β-strands to form a handshake domain with a sheath protomer (374,375,385). The tail complex polymerises from the baseplate to the opposite cell membrane to form a structure in the region of 0.5-1 μm, where length is limited by the dimensions of the cell (387). This contrasts with other CISs, such as the bacteriophage tails, where tape measure proteins control the length of the sheath (388). Within the extended sheath structure, it has been observed that the Hcp tube follows the helical symmetry of the sheath (386).

TssA proteins are implicated both in the initiation of sheath polymerisation and the coordination of sheath and Hcp tube assembly, which will be discussed in more detail in section 1.4.

Contraction of the sheath structure, which can take less than 2 ms and leads to a halving in sheath length (387,389), has been calculated to release energy equivalent to the hydrolysis of 1000 ATP molecules (386). In this contraction, rearrangement of sheath subunits, proposed to be propagated from the baseplate, generates a contracted sheath structure in which the sheath is both compressed towards the baseplate and expanded radially, with additional rotation of the sheath (Figure 1.12) (386). Upon radial expansion interactions with the Hcp tube are lost, commencing near the baseplate. With the sheath attached to the baseplate at the proximal end and Hcp at the distal end, it is therefore suggested that sheath compression beginning at the proximal end propels the Hcp tube and associated spike out of the cell in a drill-like mechanism, where the tube is expelled and rotated (386). It is projected that the contraction of a 1 μm long sheath would eject the Hcp tube 420 nm forward

and rotate it by just over four turns (385–387). This force is predicted to provide the energy for the spike to puncture the membrane of a neighbouring cell to deliver associated effector proteins.

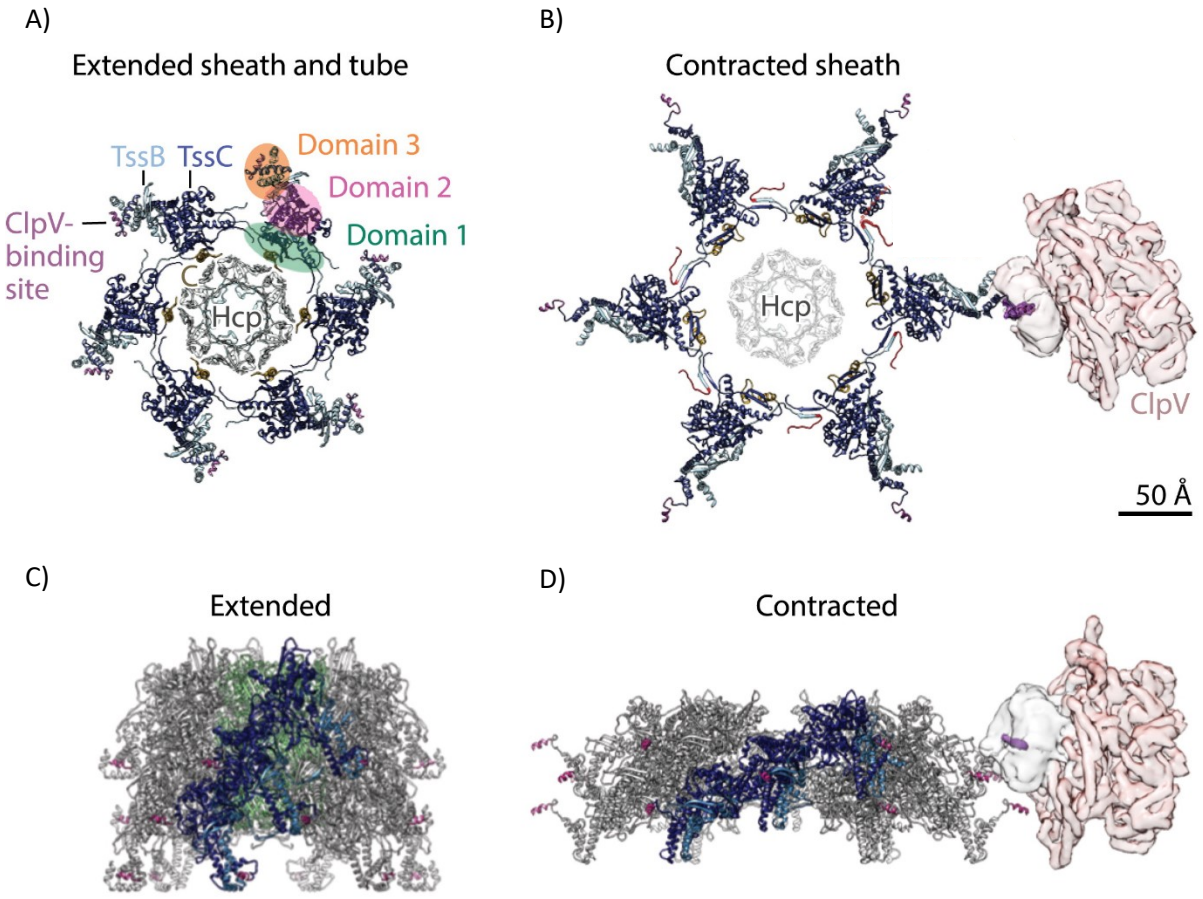


Figure 1.12 Structure of the tail complex. A) Top view of the Hcp tube (grey) and sheath (blue) in the extended conformation with sheath domains highlighted. B) Top view of the Hcp tube and sheath in the contracted conformation with ClpV (pink) bound. C) Side view of the sheath in the extended conformation, one protofilament is highlighted. D) Side view of the sheath in the contracted conformation, one protofilament is highlighted. The ClpV binding site of TssC (purple) is bound by ClpV. Figure adapted from Wang *et al.* (2019) with permission from Annual Reviews, Inc.

The ClpV-binding site at the N-terminus of TssC, is inaccessible in the extended sheath conformation, but can be bound by ClpV upon sheath contraction (Figure 1.12) (386,390,391). ClpV is a hexameric AAA+ ATPase, that can bind along the length of a contracted sheath to recycle sheath subunits, enabling multiple rounds of firing from the same T6SS assembly initiation site (392,393). The T6SS is therefore able to fire in the absence of ClpV, however in the absence of sheath recycling, this is more inefficient as each system assembled can fire only once with components unable to be reused

(389,394). ClpV has also been identified to have a role in preventing the formation of aberrant sheath structures not associated with a baseplate complex (392).

It is projected that for a single T6SS contraction event, approximately 1500 TssB and TssC components must be recycled, which in addition to the approximately 700 expelled Hcp proteins, makes T6SS firing a very energetically costly process (395). Interestingly, it has been identified that *V. cholerae* cells can utilise T6SS components delivered by the firing between sister cells, including Hcp and VgrG proteins as well as effectors (396).

1.3.3 Similarity to contractile injection systems

The T6SS is a well described example of a CIS, which shares similarities with other CISs, such as the bacteriophage tail (374), R-type pyocins (397) and anti-feeding prophages (398). The characteristic feature of CISs is a contractile sheath surrounding a spiked inner tube that extends from a baseplate structure, where sheath contraction is used to propel the inner tube across cell membranes (312).

As described in detail here, the contraction of the cytoplasmic T6SS is used to deliver effector proteins into neighbouring cells as well as the extracellular environment (307–311). Other CISs are produced in bacterial cells and released by cell lysis, to act outside of cells (384). Some of these CISs are exclusively used for penetrating the membranes of bacterial cells, this includes the bacteriophage tail which is used to transport DNA into bacterial cells (374), or R-type pyocins which create a channel in this membrane to disrupt the membrane potential (397,399). CISs are also used to penetrate eukaryotic cell membranes to deliver effector proteins: the *Photorhabdus* virulence cassette and anti-feeding prophages deliver anti-insect effectors (398,400), while metamorphosis-associated contractile (MAC) arrays of *Pseudoalteromonas luteoviolacea* formed of about 100 contractile sheaths deliver a metamorphosis-inducing effector into tubeworm larvae (401).

The most striking difference between the T6SS and other CISs is its cytoplasmic localisation and anchoring in the gram-negative bacterial membrane (Figure 1.13A) (347). The bacteriophage tail, for example, is found in the extracellular medium, with a contractile tail extending from the bacteriophage head to a baseplate (Figure 1.13B) (402). The attachment of this structure to the target cell involves irreversible attachment of baseplate-associated tail fibres to LPS on the bacterial cell membrane (403). Pyocins similarly use tail fibres to attach to their targets (Figure 1.13C) (404). The attachment of these fibres to their targets leads to a structural rearrangement of the baseplate from a dome-shaped structure to a six-pointed star structure, altering the contacts to the sheath and thus triggering sheath contraction (405). As previously detailed, in the absence of comparable tail fibres,

the signals triggering the contraction of the T6SS are currently unknown, but it is suggested to be accompanied by a similar rearrangement of the baseplate.

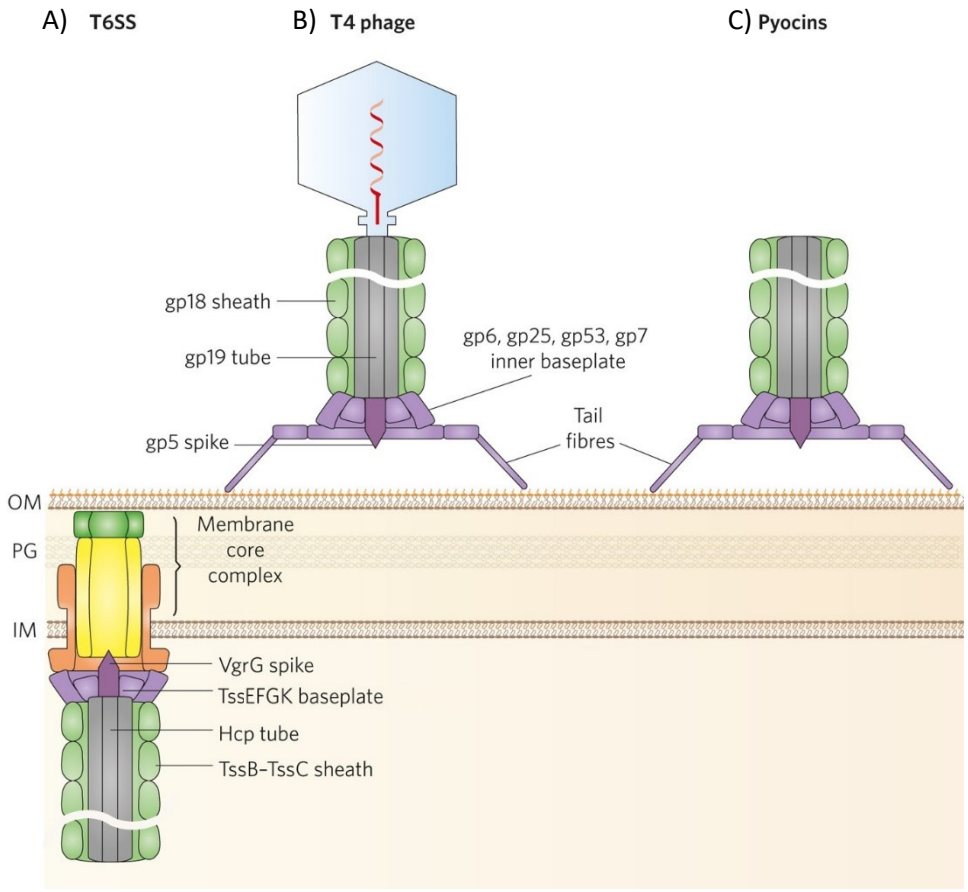


Figure 1.13 Structural comparison of contractile injection systems. A) Schematic of the T6SS structure. B) Schematic of the bacteriophage T4 contractile tail structure. C) Schematic of the R-type pyocin structure. Figure adapted from Filloux *et al.* (2016) with permission from Springer Nature.

The structure of the T6SS baseplate has been described in section 1.3.2.3. While the baseplate structure can be quite variable between CISs, comparable features have been described between them (384). This includes the central hub containing at least two components forming a spike, around which the baseplate wedges assemble. For the bacteriophage T4, the spike is formed from two proteins, gp27 and gp5, and is capped with a sharpening tip gp5.4 (406). Similar to effector domains of T6SS spike components, gp5 has a lysozyme domain (313,407). In comparison, the T6SS spike is formed solely from VgrG, but is also sharpened with a PAAR protein (364–366). For R-type pyocin a gp27 equivalent, PA0628, is topped with a sharpened spike consisting of PA0616 (397). Some equivalence has also been drawn between baseplate components, notably TssE and the bacteriophage T4 component gp25, which mediate contact to the sheath structure (313,375).

Additionally, the wedge components $TssF_2$-TssG are compared to the trifurcation unit of bacteriophage T4 of $gp6_2$-gp7 (406).

Compared to the baseplate complexes, the structures of tail complex components are much more conserved between CISs. Despite low levels of sequence identity, inner tube proteins have very similar folds (Figure 1.14A) and multimerise into hexameric rings which stack in a head-to-tail arrangement (34,313,397,408). The core sheath structure comprising Domain 1 and 2, which forms the inner layers of the sheath, is also well conserved between CISs (Figure 1.14B) (385,386,398,409). These regions drive the polymerisation of the sheath into a helical tube formed of hexameric rings, though the parameters of these helices are variable (384). As detailed, the length of the T6SS sheath is dictated by the cell dimensions, with sheaths polymerising across the cell (387), however tape measure proteins that regulate the length of the tail complex are commonly associated with other CISs (388,410). For example, the bacteriophage T4 sheath polymerises 23 sheath rings (411), while the *P. aeruginosa* R-type pyocin polymerises 27 sheath rings (397).

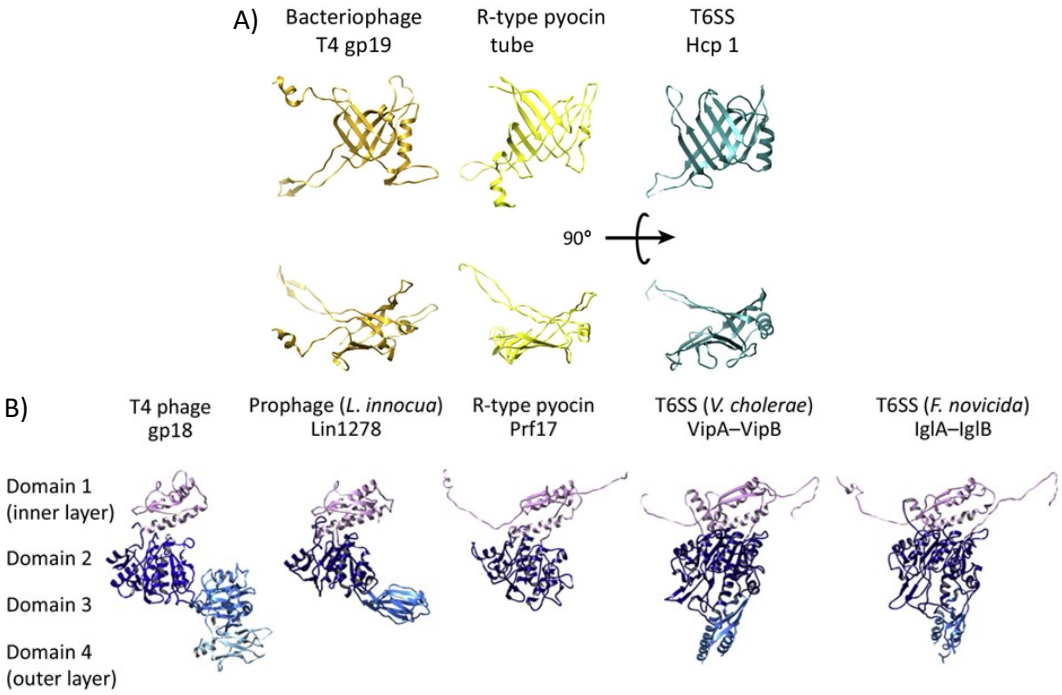


Figure 1.14 Structural comparison of contractile injection system tail complex components. A) Structures of inner tube components of CISs: gp19 of bacteriophage T4 (PDB: 5iv5), R-type pyocin (PDB: 3j9q), and T6SS Hcp1 from *P. aeruginosa* (PDB: 1Y12). B) Structures of sheath components of CISs: T4 phage gp18 model (PDB: 3J2 M), Lin1278 of prophage from *Listeria innocua* (PDB: 3LML), R-type pyocin sheath (PDB: 3J9Q), T6SS sheath from *V. cholerae* (PDB: 3J9G), T6SS sheath from *Francisella novicida* (PDB: 3J9O). Figures adapted from Brackmann *et al.* (2017) with permission from Elsevier.

A further unique feature of the T6SS in comparison to other CISs is the recycling of sheath subunits following contraction by ClpV (392,393). Unlike the T6SS, other CISs contract only once. These CISs are released extracellularly and thus any cargo delivered into target cells cannot be replenished, and no energy source is available to disassemble the sheath in the extracellular environment.

1.3.4 Function of the T6SS

Contraction of the T6SS sheath drives the expulsion of a spiked inner tube loaded with effector proteins out of the cell. These effectors can have eukaryotic or prokaryotic targets, in some cases both, while they may also be involved in uptake of common goods from the extracellular environment. The T6SS therefore influences interactions between microorganisms as well as interactions with a host, which can affect colonisation and competition.

1.3.4.1 Modes of effector delivery

Each of the components of the spiked inner tube, the Hcp tube, the VgrG spike and the PAAR tip, can be used to carry effector proteins into new environments. Hcp-associated effectors are proposed to be found in the Hcp lumen and transported through interaction with Hcp ring units (380). The size of effectors transported in this manner is limited, and increasing effector size through the addition of domains has been shown to block sheath polymerisation (412). Effectors associated with either VgrG or PAAR spike components, are displayed on the outside of the spike complex. The hub of VgrG and PAAR is central to the baseplate structure during assembly and a cavity has been identified between this hub and the surrounding wedges which is proposed to house these effectors (364). A size limit also applies to effectors transported in this manner, with this cavity suggested to accommodate three copies of up to a ~150-kDa protein, which could allow for docking of one effector associated with each VgrG monomer (364).

Effector proteins can be non-covalently associated with these components, known as cargo effectors, or specialised effectors, that are covalently linked as an additional domain. Generally, Hcp-associated effectors are cargo effectors, such as *P. aeruginosa* Tse2 (380,412). In addition to transporting effectors, binding to Hcp has been demonstrated to protect cargo effectors from proteolysis (380). Cargo effectors are also associated with both VgrG proteins, i.e. enteroaggregative *E. coli* Tle1 (413), and less frequently with PAAR proteins, i.e. *P. aeruginosa* TseT (414). PAAR-associated effectors are more commonly specialised effectors, such as *P. aeruginosa* Tse6 and Tse7 which each encode a PAAR domain (340,415). Specialised effectors are also well described for VgrG proteins, such as the actin

crosslinking domain of *V. cholerae* VgrG-1 (309). Furthermore, some specialised Hcp effectors have been identified in *Enterobacteriaceae* with C-terminal toxin domains (416). The loading of both cargo and specialised effectors into the T6SS can involve adaptor proteins, for example the loading of the *P. aeruginosa* specialised PAAR domain-containing Tse6 onto the tip of the VgrG spike requires the adaptor EagT6 (417). The *Aeromonas dhakensis* specialised effector TseI can self-cleave at two sites to separate the effector domain from suspected intramolecular chaperone domains which are required for secretion (418).

A novel mode of effector delivery was recently described for *Yersinia pseudotuberculosis* Tce1, which in addition to being directly injected into neighbouring cells, can also enter prey cells in a contact-independent manner from the extracellular environment in an uncharacterised mechanism involving the outer membrane proteins OmpF and BtuB (419).

Through a combination of these delivery modes, a diverse effector payload can be delivered in a single contraction event. A T6SS can be associated with a variety of Hcp, VgrG and PAAR components, such as the six VgrGs associated with the *P. aeruginosa* H2-T6SS (Figure 1.9), where different combinations of these components and their associated effectors further increases this diversity (420,421). Interestingly, it has been shown that certain combinations of effectors can function synergistically when present together (422). The diverse effector repertoire may also maximise the range of different competitors that can be successfully targeted by the T6SS, where certain competitors may be more sensitive to certain effectors.

Unlike the T3SS, where effector proteins are associated with an N-terminal secretion signal which can allow prediction of novel effectors (268,423), there is no characteristic feature of T6SS effectors. However, conserved motifs have been identified in certain effectors, the MIX motif (424) and the FIX motif (425), which can help guide the identification of new effectors. In the absence of a secretion signal it is also not entirely clear how effectors are targeted to the T6SS machinery, although chaperones are proposed to play a role. As effectors are commonly co-translated with the Hcp, VgrG or PAAR responsible for their transport, the formation of protein-protein interactions between effectors and these structural components may circumvent the need for targeting.

1.3.4.2 Anti-bacterial effectors

The T6SS can be used to deliver anti-bacterial effectors targeting essential cellular features into neighbouring bacteria. Such effectors are produced in tandem with cognate immunity proteins to prevent self-intoxication and intoxication by sister cells, with immunity genes generally encoded

adjacent to the effector in the genome (Figure 1.9). Immunity proteins generally function by binding to and obstructing the active site of their effector, such as the binding of the *P. aeruginosa* Tsi3 immunity to the Tse3 effector and occlusion of the enzymatic pocket (426). Although immunities which can actively reverse the catalytic activity of their effector have also been identified, such as the *Serratia proteamaculans* Tri1 which can act both by binding the Tre1 effector but also by cleaving ADP-ribose groups which are added by Tre1 (427). While the protection conferred by most immunity proteins is highly specific to the cognate effector, owing to its ADP-ribosylhydrolase activity, Tri1 can also provide non-specific protection against other ADP-ribosylating toxins. To protect against intoxication from sister cells immunities are present in the cellular compartment targeted by their cognate effector, for example signal peptides can drive translocation of immunity proteins into the periplasm (428). Protection against effectors delivered by sister cells requires expression of immunity genes, in nutrient limiting conditions bacteria can be vulnerable to T6SS attack despite encoding immunity genes due to low levels of expression (429).

One frequent target of anti-bacterial effectors is the cell envelope. The peptidoglycan can be targeted either through the activity of type VI amidase effectors (Tae) or type VI glycoside hydrolase effectors (Tge) (430,431). The amidase activity of these effectors is directed towards specific peptide bonds either within or between peptide chains crosslinking the peptidoglycan, such as Tse1 (also known as Tae1) of *P. aeruginosa* (428). Glycoside hydrolase activity is directed at the glycosidic bonds between sugar units of the glycan backbone, such as VgrG-3 of *V. cholerae* (432) or *P. aeruginosa* Tse3 (428). Alternatively, phospholipids in the cell membrane can be targeted by type VI lipase effectors (Tle), for example the *P. aeruginosa* phospholipases PldA and PldB (also known as Tle5a and Tle5b) (368). Additionally, T6SS effectors with similarities to pore-forming colicins have also been identified, such as *V. cholerae* VasX, which increases membrane permeability causing a loss of membrane potential (433), while *P. aeruginosa* Tse4 is linked to the formation of ion-selective pores to disrupt the membrane potential (422).

A common cytoplasmic target of anti-bacterial effectors is nucleic acids, targeted by nucleases such as *P. aeruginosa* Tse7 (340). Two type VI DNase effectors (Tde), Tde1 and Tde2, have also been identified in *A. tumefaciens* (434). A diverse range of other cytoplasmic targets have also been described. One such target is the cofactor NAD, which is degraded by type VI NADase effectors (Tne), such as *P. aeruginosa* Tse6 (also known as Tne1) whose hydrolase activity depletes cellular NAD+ and NAD(P)+ (417). In place of *tse6* in the PA14 strain, is *tas1*. Tas1 can deplete cellular ATP by pyrophosphorylating adenosine nucleotides to produce (p)ppApp at a very high rate (435). A further target is FtsZ, which is required for bacterial cell division, which can be ADP-ribosylated by Tre1 of *S. proteamaculans* (427). *P. aeruginosa* Tse8 has been identified to target the transamidosome complex,

which is required for charging tRNAs with asparagine or glutamine in certain organisms, and thus disrupts protein synthesis (436). Effector characterisation can identify novel anti-bacterial targets, which may be useful for the design of new antibiotic agents.

The presence of anti-bacterial effectors is required for T6SS-dependent bacterial killing, indicating that T6SS membrane puncturing alone does not cause significant damage to prey cells (437–439). In *V. cholerae* an 'onboard checking mechanism' has been identified that ensures effectors are loaded onto the T6SS to prevent ineffective firing (439). The presence of several effectors was demonstrated to be required for T6SS assembly regardless of their catalytic activity. Similarly, the *A. tumefaciens* T6SS is only assembled when at least one Tde effector is loaded onto their respective VgrG (440).

1.3.4.3 Anti-eukaryotic effectors

The T6SS can also be used to deliver anti-eukaryotic effectors into neighbouring cells, including host and fungal cells. One target of such effectors is actin from the host cytoskeleton, which can be targeted by the actin cross-linking domain of *V. cholerae* VgrG-1 to modify the actin network and inhibit cytoskeletal rearrangement (309). Alternatively, the *Aeromonas hydrophila* VgrG1 has actin ADP-ribosyl transferase activity causing cell rounding and apoptosis (441).

Anti-eukaryotic effectors can also facilitate bacterial colonisation. Delivery of the *P. aeruginosa* VgrG2b effector domain into epithelial cells facilitates microtubule-dependent internalisation of the bacterium through interaction with microtubule components (442). Cell invasion has been identified to be triggered by the fusion of membranes, for example the *Burkholderia pseudomallei* VgrG5 mediates membrane fusion to form multi-nucleated giant cells (443). Colonisation can also be aided by T6SS effectors subverting host immune responses, such as by *Edwardsiella tarda* EvpP inhibition of the NLRP3 inflammasome, promoting bacterial colonisation (444).

Two anti-fungal T6SS effectors have been identified in *Serratia marcescens*, type VI anti-fungal effector 1 and 2 (Tfe1 and Tfe2) (308). Tfe1 causes a loss of membrane potential, while Tfe2 affects nutrient transport and amino acid metabolism (308). *K. pneumoniae* VgrG4 is also implicated in anti-fungal activity via an unknown mechanism (328).

Some effectors can have both anti-bacterial and anti-eukaryotic activities, termed trans-kingdom effectors, including the *K. pneumoniae* VgrG4, which contributes to both anti-fungal and anti-bacterial activities (328). A number of trans-kingdom effectors have been identified associated with the *P. aeruginosa* H2-T6SS. One such example is the metallopeptidase domain-containing VgrG2b, which is involved in epithelial cell invasion (442), but also targets the periplasm and has been linked to a

bacterial cell division defect (445). Such multi-functional effectors are very useful, allowing a single effector to target different competitors, rather than distinct effectors being required.

1.3.4.4 Effectors involved in common goods acquisition

Firing of the T6SS can lead to delivery of effectors into the extracellular environment, where effectors have roles in acquiring extracellular common goods, such as metal ions. In response to low levels of copper, the *P. aeruginosa* H2-T6SS is expressed, and the secreted VgrG2b-associated cargo effector Azu can bind copper, which is taken up by the cell using the outer membrane transporter OprC (310). Similarly, during oxidative stress *Burkholderia thailandensis* can take up extracellular manganese or zinc using TseM or TseZ and their respective outer membrane transporters MnoT or HmuR (446,447). Acquisition of metal ions can also involve slightly more complex pathways, the secreted *P. aeruginosa* H3-T6SS effector TseF is incorporated into OMVs through interaction with the iron-binding *Pseudomonas* quinolone signal (311). TseF recruits these OMVs to the outer membrane receptor FptA and the porin OprF to facilitate the import of the associated iron (311). Via a similar mechanism, the *Cupriavidus necator* TeoL interacts with LPS in OMVs from diverse species, recruiting them to outer membrane receptors CubA and CstR, to facilitate the delivery of cargo including iron, via an unknown mechanism (448).

1.3.4.5 Immunity-independent protection from the T6SS

In a polymicrobial community, T6SS attack provides a selective pressure on prey cells to acquire protective mechanisms. As identified previously, this can include the acquisition of immunity genes (341), but some T6SS protection mechanisms independent of immunity proteins have also been described.

It has been identified that peptidoglycan modification by *A. baumannii* can provide protection against peptidoglycan-targeting effectors. The modification of L-lysine to the non-canonical D-lysine, and subsequent incorporation into the peptidoglycan confers an advantage in interbacterial competition, through the modification of a T6SS amidase effector target (449). The modification of an effector target could help provide protection against an effector in a similar way to mutations that confer resistance to the activity of antibiotics. Although as with the use of antibiotics in combinations, this would not protect against delivery of multiple effectors with distinct targets.

Other protection mechanisms can be less specific. In response to damage caused by the *V. cholerae* peptidoglycan hydrolase TseH, *E. coli* can activate envelope stress responses to induce capsule synthesis, which is proposed to provide a physical barrier to incoming T6SS attacks (450). The same study also identified that the *V. cholerae* WigKR two-component system, which is a stress response pathway activated by cell wall damage, was required to protect against attack from both the cognate and non-cognate T6SSs despite the presence of cognate immunity genes (450). This indicates that immunity genes alone may not be sufficient to protect from T6SS attack. Several stress response pathways were similarly identified to provide protection to *E. coli* and *P. aeruginosa* against the *V. cholerae* effector TseL (451).

Recipient factors can also increase the vulnerability of a prey cell to T6SS killing. The *E. coli* ClpP protease and its associated ClpA ATPase have been identified as susceptibility factors, responsible for an increased prey susceptibility to the *A. tumefaciens* T6SS (10). Loss of these factors can therefore provide protection.

1.3.4.6 The role of the T6SS

The delivery of T6SS effectors has an important role to play in both interbacterial interactions and interactions with a host. The range of effector activities outlined above identify the T6SS as being able to either kill or inhibit the growth of bacteria and other microbes which can affect the composition of polymicrobial communities. Furthermore, bacteria can use the T6SS to manipulate host cells through cell invasion or host immune modulation to further their colonisation. Finally, the uptake of extracellular goods using the T6SS allows resources to be scavenged and reduces the nutrient pool available to competitors.

The presence of the T6SS has been identified as a key factor in niche colonisation by various bacteria. The T6SS2 of *Pseudomonas syringae* pv. tomato DC3000 can suppress the growth of competing microbes including both bacteria and eukaryotes such as yeast (452). Interestingly, the T6SS can also play a role in intraspecies competition. In the colonisation of squid light organ crypts by the symbiont *V. fischeri* T6SS-encoding strains dominate by outcompete strains lacking a T6SS (327). These crypts can also be colonised by a pair of T6SS encoding strains, which form spatially segregated populations in this niche. As discussed in the previous sections, T6SS effectors can aid colonisation of a eukaryotic host by inducing cell invasion by bacteria, including by stimulating cytoskeletal rearrangements to drive internalisation or by initiating the fusion of cell membranes (442,443).

Numerous human pathogens have been identified to use the T6SS during colonisation to outcompete commensal strains. *Salmonella enterica* Typhimurium was identified to kill specific members of the gut microbiota, such as *Klebsiella oxytoca*, in a T6SS-dependent manner (453). Furthermore, colonisation of the mouse gut by *Salmonella* required anti-bacterial activity of the T6SS encoded in *Salmonella* pathogenicity island 6 (453). Similarly, *Shigella sonnei* uses its T6SS to outcompete commensal strains and establish host colonisation (454). As discussed, *P. aeruginosa* comes to dominate the lungs of in cystic fibrosis patients over time. The identification of Hcp1 in the sputum of cystic fibrosis patients and antibodies directed against Hcp1 in their sera, indicates that the H1-T6SS is active in this environment and may contribute to the effective colonisation of this niche (34). Colonisation can also be aided by manipulation of host physiology. In a zebrafish model, *V. cholerae* can drive the displacement of a symbiotic bacterium in a mechanism dependent on the T6SS, but independent of the anti-bacterial activity. In this case, the actin crosslinking domain of VgrG-1 enhanced host intestinal movements causing the resident bacteria to be expelled and allowing *V. cholerae* colonisation (455).

The host response to interbacterial competition may also increase pathogenicity. Killing of commensal bacteria by the T6SS of *V. cholerae* in both Drosophila and mouse infection models was linked to a stronger host immune response, including intestinal damage and diarrhoea (456,457). This elevated pathogenicity induced by T6SS-dependent killing was thus suggested to contribute to increased transmission.

The T6SS can also play a role in protecting a host organism. A key component of the human gut microbiota are Bacteroidetes, where more than half of Bacteroidetes in this environment have been identified to encode T6SSs (336). The presence of a T6SS allows the commensal *Bacteroides fragilis* to outcompete another commensal, *Bacteroides thetaiotaomicron*, which does not encode a T6SS (317). Further to this, T6SS-dependent pathogen exclusion by a non-toxigenic *B. fragilis* in a mouse model of infection prevented colonisation by a pathogenic enterotoxigenic *B. fragilis* (458). The use of T6SS-encoding bacteria as biocontrol agents to protect against plant pathogens also has been proposed. The soil bacterium *P. putida* can outcompete a range of relevant plant pathogens in both *in vitro* and *in planta* competition settings, protecting the plant from disease (324). Likewise, *Pseudomonas fluorescens* has been shown to have T6SS-dependent anti-bacterial activity to protect potato tubers against rot caused by *Pectobacterium atrosepticum* (459).

Several T6SS effectors induce lysis of competitor bacteria. Efficient prey lysis has been identified to prevent so called corpse barriers, that block the cell-cell contact required to eliminate further prey cells using the T6SS (460). Induction of cell lysis has an additional advantage in that it leads to the

release of a range of useful resources, including DNA which can be taken up by nearby bacteria. In *V. cholerae* it was identified that the T6SS gene cluster and competence genes were co-regulated by quorum sensing pathways, and prey cell lysis led to DNA uptake including the acquisition of new effector genes (461,462). Similarly, the activity of *Acenitobacter baylii* T6SS lytic toxins is correlated with the rate of horizontal gene transfer (438). Horizontal gene transfer is implicated in the acquisition of gene clusters encoding arrays of immunity genes, which are present on mobile genetic elements, by Bacteroidetes (341). T6SS genes clusters of *V. cholerae* also commonly encode arrays of immunity genes without cognate effectors, which are suggested to have been acquired through horizontal gene transfer from other strains, providing protection against intraspecies T6SS attack (463). Regulatory elements can also be acquired by horizontal gene transfer. It has been observed in *A. baumannii* that a plasmid encoding antibiotic resistance genes also carried repressors for the T6SS, where this plasmid could readily be lost to activate T6SS activity but at the cost of the loss of antibiotic resistance genes (33).

1.3.5 Regulation of the *P. aeruginosa* T6SSs

Regulation of T6SS activity takes place at transcriptional, post-transcriptional and post-translational levels. The three T6SSs of *P. aeruginosa* are suggested to have functional specificity, with activity influenced by environmental conditions via regulatory pathways that require further study. Additionally, the delivery of effector proteins through the assembly and firing of the T6SS is an energetically costly process. While it has been described that some T6SS components can be reused for multiple rounds of T6SS firing from the same site (464), contracted sheath protomers must be recycled and new secreted components, including spike, inner tube and effectors, must be produced. Regulation therefore ensures the targeted and efficient activity of each of these T6SSs.

1.3.5.1 Gac-Rsm pathway

The Gac-Rsm pathway is a two-component system implicated in regulation of the *P. aeruginosa* switch between motile and sessile lifestyles through the sensor kinase GacS and its response regulator GacA (see section 1.1.2) (49,465). The activity of GacS is modulated by other sensor kinases (Figure 1.15): RetS inhibits GacS through the formation of a heterodimer (466), while LadS stimulates GacS by direct phosphorelay (467). RetS can itself be inhibited by the binding of the sensor kinase PA1611, which impairs RetS interaction with GacS (468,469). Some signals regulating this pathway have been identified. RetS can be activated by binding of mucins to the sensor domain (470), while *retS*

expression is repressed under magnesium limitation (471). LadS can be activated by the binding of calcium to the periplasmic sensor domain (472), while a periplasmic sensor domain of GacS has been identified to be key for downstream signal transduction, however the nature of the ligand is yet to be determined (473).

Upon activation, GacS can phosphorylate the response regulator GacA which in turn activates the transcription of the small non-coding RNAs, RsmY and RsmZ (Figure 1.15) (49,474). These RNAs can sequester the post-transcriptional regulators RsmA and RsmN which positively regulate factors associated with an acute infection lifestyle, including the T3SS (see section 1.2.6.3), and negatively regulate factors associated with a chronic infection lifestyle, including the T6SS (47–49). RsmA has been identified to repress each of the three *P. aeruginosa* T6SS clusters as well as isolated loci associated with genes encoding VgrG proteins or toxin-immunity pairs (338). In the absence of RsmA, for example upon GacA activation and sequestration by RsmY and RsmZ or upon deletion of *rsmA*, the expression of each *P. aeruginosa* T6SS is upregulated.

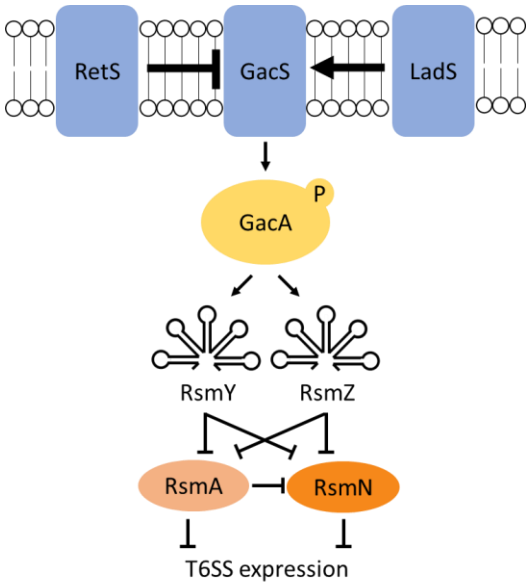


Figure 1.15 Schematic of the Gac-Rsm pathway in *P. aeruginosa*. The sensor kinase GacS is activated by the sensor kinase LadS and repressed by the sensor kinase RetS. Active GacS can phosphorylate its downstream response regulator GacA, driving the production of the small regulatory RNAs RsmY and RsmZ. These small regulatory RNAs can sequester the RNA-binding proteins RsmA and RsmN inhibiting their activity and leading to a protein expression profile linked to a sessile, biofilm lifestyle associated with chronic infection, including T6SS activity. When GacS is repressed, RsmA and RsmN can bind to target RNA sequences leading to a protein expression profile linked to a motile, virulent lifestyle associated with acute infection, where T6SS expression is repressed.

1.3.5.2 Threonine phosphorylation pathway

The threonine phosphorylation pathway (TPP) is a regulatory pathway involving components encoded in the H1-T6SS cluster, which controls the activity of the H1-T6SS at a post-translational level. This pathway is linked to the phosphorylation status of the regulatory protein Fha1, which is reciprocally controlled by the inner membrane anchored protein kinase PpkA and the cytoplasmic phosphatase PppA (475). Homodimerization leads to autophosphorylation and activation of PpkA, possibly through the interaction with a periplasmic protein such as TagR (476), and the recruitment and subsequent phosphorylation of Fha1, which is required for T6SS firing. The activation of PpkA is controlled upstream by TagQRST, where a phosphorelay is proposed to transmit a signal from the outer membrane lipoprotein TagQ, associated with the periplasmic TagR, to an ABC transporter-like complex, TagTS, in the inner membrane, where TagT has ATPase activity (476,477). The role of the TPP in T6SS activity has been linked both to activation of the assembly of the T6SS, with the assembly of TssK structures in response to contact with competing bacteria dependent on TagQ and TagR (478), and to disassembly of the sheath with co-localisation experiments indicating a link to the activity of ClpV1 (475). Dephosphorylation of Fha1 by PppA is linked to a deactivation of T6SS activity. As expected, deletion of *pppA* therefore results in increased T6SS-dependent secretion, however this elevated firing rate occurs with repeated firing from the same T6SS assembly initiation site, indicating a role for PppA in T6SS disassembly, allowing spatial reorientation of the T6SS, which would allow firing in response to a specific stimulus or contact at a distinct position in the cell (479,480). Components of the TPP can also be regulated independently, such as the sequestration of Fha1 by TagF, which represses T6SS activity (481). The signalling and regulation behind this repression is not well understood.

TagQRST has been described as a sensor module, as it is linked to coordinating T6SS responses to a range of envelope disrupting stimuli, including incoming T6SS attacks in what is termed the tit-for-tat response (391,479). Incoming T6SS attacks can be from sister cells, in what is termed duelling (389), or from neighbouring competitor bacteria (479). The tit-for-tat response allows for multiple targeted counter-strikes in response to detected T6SS attack, which generates an effective retaliation whereby the initial aggressor is often outcompeted (479,482). Fha1 is phosphorylated at a greater rate upon incubation on solid surfaces, indicating that cell-cell interactions, which take place at a higher rate on solid surfaces, contribute to activation of the TPP (477). Similarly, cell envelope disruption caused either by the conjugative T4SS of plasmid RP4 or polymyxins are also proposed to be sensed by TagQRST which induces a T6SS attack in response (483). Interestingly, the *P. aeruginosa* tit-for-tat response involving the H1-T6SS can be initiated specifically by the *V. cholerae* lipase TseL, independent of puncturing by an aggressor T6SS, indicating that the lipase activity and localised membrane damage

may be sufficient to induce activation of TagQRST (451). Using a CRISPR interference approach it was subsequently identified that knock down of essential genes involved in outer membrane biogenesis, such as *bamA* and *tolB*, triggered T6SS activation, which was dependent on the TagQRST sensor module (484).

The H1-T6SS can also be activated in response to extracellular DNA and chelation of ions through TagQRST (485). This activation led to a more indiscriminate T6SS-mediated attack on neighbouring cells.

1.3.5.3 Quorum sensing

Quorum sensing is a communication system utilised by bacteria to sense population density through the release and detection of auto-inducer molecules, whose environmental abundance is linked to cell density. Once the auto-inducer concentration exceeds a threshold for detection, appropriate transcriptional responses are coordinated, which may relate to virulence (486), bioluminescence (487) and the development and maturation of biofilm (488).

Four quorum sensing pathways have been described in *P. aeruginosa*, the Las and Rhl pathways which use homoserine lactone (HSL) auto-inducers (489), the *Pseudomonas* quinolone signal (PQS) used by the PQS pathway (490) and the integrated quorum sensing system (IQS) (491). There is a lot of interplay between these pathways, for example with the Las pathway positively regulating each of the other pathways (491,492). This quorum sensing network is also linked to the post-transcriptional regulator RsmA (section 1.3.5.1), which negatively regulates the production of HSL autoinducers associated with Las and Rhl pathways, as well as PqsR which regulates autoinducer PQS production (492,493).

In *P. aeruginosa* it has been identified that quorum sensing pathways have a role in regulating expression of each of the three T6SSs. Expression of the H1-T6SS is repressed by both Las and PQS pathways (494). Conversely, expression of the H2- and H3-T6SSs are positively regulated by these pathways (494) as well as the Rhl pathway (495). A further link between the T6SS and quorum sensing has been identified in the association of the H3-T6SS effector TseF with the auto-inducer PQS in OMVs which is involved in iron uptake as previously described (see section 1.3.4.4) (311).

1.3.5.4 Sigma factor 54: RpoN

RpoN is a sigma factor 54 (σ^{54}) protein, required for the recruitment of RNA polymerase to characteristic -24/-12 promoter sequences to direct specific transcriptomic responses (496,497). RpoN also requires the ATPase activity of sigma factor activator (Sfa) proteins, to remodel the RNA polymerase and activate transcription (498). Typically associated with nitrogen assimilation, RpoN has recently been described to regulate numerous components expressed on the cell surface, thereby influencing the interaction with the environment (499).

In *P. aeruginosa* the H2- and H3-T6SS clusters each encode a Sfa protein, Sfa2 and Sfa3 respectively, and RpoN has been identified to regulate T6SS cluster expression (495,500,501). In a Sfa2-dependent manner, RpoN activates transcription of components of the H2-T6SS, both those found within the primary H2-T6SS gene cluster but also components encoded at isolated chromosomal loci that are associated with genes for VgrG, PAAR and effector-immunity pairs (501). Conversely, RpoN was found to repress transcription of components of the H1- and H3-T6SSs (501). No role has to date been identified for Sfa3.

1.3.5.5 Environmental conditions

Differential expression and activity of the *P. aeruginosa* T6SSs has been linked to temperature (338,502). Specifically, the H3-T6SS is only expressed at lower temperatures, e.g. 25 °C vs 37 °C, while the H1- and H2-T6SS are expressed at both temperatures, although with H2-T6SS better expressed at lower temperatures (338). Interestingly, RsmA-associated repression was overcome for both H1- and H2-T6SSs at lower temperatures. Furthermore, T6SS expression is also influenced by growth phases, expression of the H2- and H3-T6SSs has been found to be induced at the transition between exponential and stationary phases (495). In contrast, H1-T6SS activity can be detected at earlier phases (503). Under laboratory conditions, specific incubation temperatures and times are therefore used to optimise the detection of T6SS activity.

Nutrient availability is a further factor that influences T6SS expression. As previously identified, the H2-T6SS effector Azu is involved in the acquisition of copper from the environment (310). Under copper rich conditions, the cytoplasmic copper ion-sensing transcriptional regulator CueR represses the expression from the H2-T6SS locus and of the effector *azu*. This repression was relieved in response to low levels of copper, allowing H2-T6SS-dependent Azu secretion and copper scavenging from the environment. The expression of the H2-T6SS has also been shown to be negatively regulated in the presence of iron by the ferric uptake regulator (Fur) (504). The only described H3-T6SS effector

to date is involved in iron uptake, and H3-T6SS promoters, including that regulating effector *tseF* expression, have been identified to be negatively regulated by Fur (311). Components associated with all three *P. aeruginosa* T6SSs have additionally been identified to be upregulated under low phosphate conditions (505).

T6SS expression can further be affected by host-associated environmental conditions. Bile in the form of gastro-oesophageal reflux is common in cystic fibrosis patients, and exposure to bile was found to promote expression of both the H1- and H2-T6SSs (506,507). Bile exposure was additionally linked to a range of phenotypes associated with chronic bacterial lifestyles, such as biofilm formation and antibiotic resistance.

1.4 T6SS component TssA

As previously described, the position of most T6SS core components in specific sub-assemblies, and the contribution of these sub-assemblies to the assembly and activity of the T6SS are generally well understood. Only in recent years have roles of TssA been described and many key questions remain about the contribution of TssA to T6SS activity, its positioning within the T6SS and how TssA associates with other T6SS components. TssA proteins have been described as regulators of sheath polymerisation (360,377,508). However, different sub-groups of TssA proteins vary substantially raising questions about whether functionality is conserved, and how similar functions might be achieved by relatively distinct TssA variants (360,376,377,509).

1.4.1 TssA structure and organisation

TssA proteins are the most poorly conserved of the 13 core T6SS components, exhibiting variability in their length, domain organisation, symmetry and structure (360,376,377,509). The differences between TssA proteins have been classified previously into two groups, which are most simply defined by a difference in TssA length (Figure 1.16) (377,508,509). Short TssA proteins ($TssA_S$), previously also known as TssA1 or TsaB, are 340-380 aa or ~40 kDa in length (377,508,509). While long TssA proteins ($TssA_L$), previously also known as TssA2 or TsaC, are 470-540 aa or 55-60 kDa in length (377,508,509). A final group which has been described within the TssA family, also known as TsmA, comprises the accessory protein, TagA, which will be discussed in section 1.4.3.1 (377,510).

We have recently identified that the grouping of TssA proteins by length corresponds with the phylogenetic grouping of T6SS clusters, with phylogenetic groups 1 and 2 encoding T6SS clusters associated with a $TssA_L$, while phylogenetic groups 3-5 encode T6SS clusters associated with a $TssA_S$ (508). Furthermore, TssA length corresponds with domain organisation, $TssA_S$ contain two domains, while $TssA_L$ contain three domains (Figure 1.16) (360,509). All TssA proteins contain a Nt1 domain with the characteristic ImpA_N region, but vary in subsequent domains, with $TssA_L$ proteins containing an Nt2 domain. Long and short TssA proteins encode distinct C-terminal domains, which despite variations in sequence and structure, are each responsible for self-interaction, driving oligomerisation into ring-shaped structures (360,376,377,509).

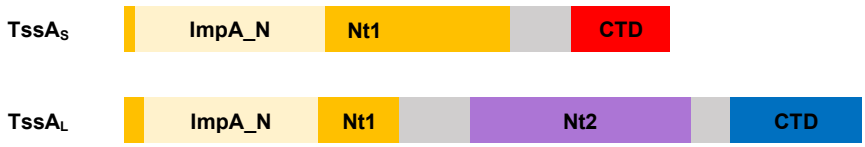


Figure 1.16 Schematic of TssA classification. The ImpA_N region (light yellow) is conserved in all TssA proteins within the Nt1 domain (yellow). In TssA$_S$ proteins, a flexible linker connects the Nt1 domain to the C-terminal domain (CTD) (red). In TssA$_L$ proteins, a flexible linker connects the Nt1 domain to the Nt2 domain (purple). The Nt2 domain is then connected by a flexible linker to a distinct TssA$_L$ CTD (blue).

1.4.1.1 TssA Nt1 domain

The characteristic feature of all TssA proteins is the presence of a ~120 aa ImpA_N (PF06812) region of unknown function within the Nt1 domain (509,511). The ImpA_N region contains 3 blocks of high sequence conservation, referred to previously as ImpA_N1-3, which are expected to give rise to a similar fold in the N-terminus of all TssA proteins (509). Variation between TssA proteins arises downstream of this ImpA_N region, including in the size of the Nt1 domain. The Nt1 domain of TssA$_S$ proteins is slightly longer than that of TssA$_L$ proteins, at ~250 aa compared to ~190 aa, the functional significance of which is unclear (509).

The only available Nt1 domain structure, that of the TssA$_S$ of *Burkholderia cenocepacia* (I35_RS01755) (TssA^{BC}), forms an 11 α-helix monomer, where the sequences comprising the ImpA_N region are found from α1 to the N-terminus of α6 (Figure 1.17) (509). High-resolution structures of full length TssA proteins have not been solved due to the flexibility between domains, however Nt1 domains are predicted to be present at the periphery of TssA ring-shaped structures with significant flexibility relative to the inner ring (360,376,377,509).

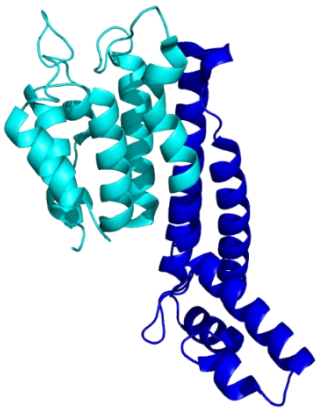


Figure 1.17 Structure of TssA^{BC} Nt1 domain. The TssA^{BC} Nt1 domain (PDB: 6HS5) with conserved ImpA_N region highlighted in light blue.

1.4.1.2 Structural features of short TssA proteins ($TssA_S$)

The $TssA_S$ Nt1 domain is connected via a 40-60 aa flexible linker to a 60-75 aa C-terminal domain, which is required for oligomerisation (376,509). Negative stain electron microscopy (EM) analysis of $TssA^{BC}$ and TssA1 of *P. aeruginosa* (PA0082) ($TssA1^{PA}$) identified the formation of rings with lumenal diameters of 110 Å and 100 Å respectively (Figure 1.18) (376,509). Based on an estimated ~30 subunit oligomer, a double-layered $TssA^{BC}$ C-terminal domain ring of 32 monomers with D16 symmetry was assembled, with a 110 Å lumenal diameter, 200 Å external diameter and a thickness of 25 Å (Figure 1.19) (509). The oligomeric state of $TssA1^{PA}$ is less clear, forming both dodecameric and double-dodecameric oligomers (376).

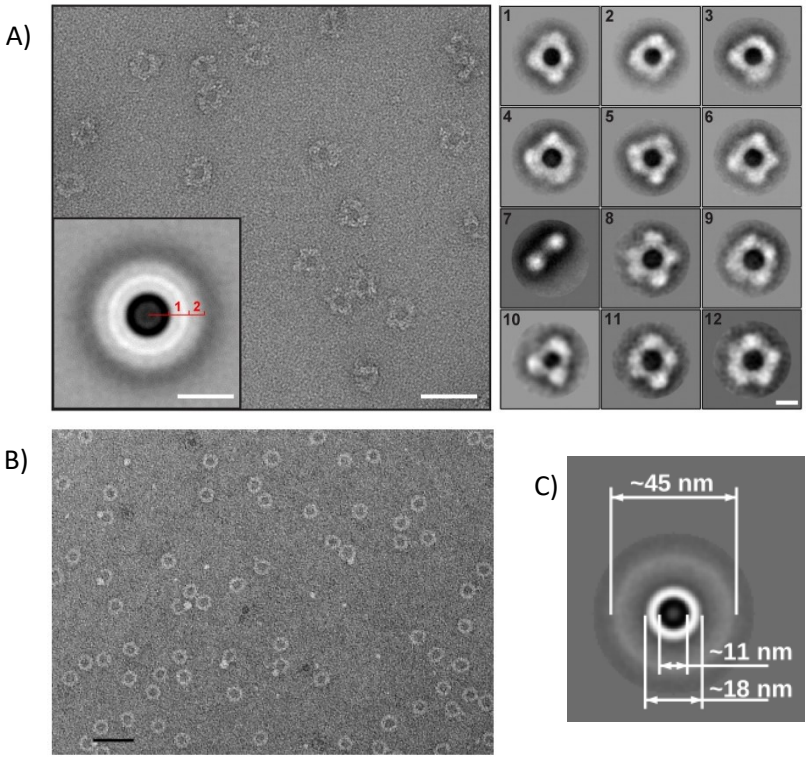


Figure 1.18 Negative stain electron microscopy images of $TssA_S$ proteins. A) Representative micrograph of full length $TssA1^{PA}$ (left), scale bar is 500 Å. The rotationally symmetrised average of the dataset, identifying two layers to the ring (inset), 1 and 2, scale bar is 130 Å. Representative class averages of the $TssA1^{PA}$ ring (right), scale bar is 100 Å. The rings have an average lumenal diameter of ~100 Å, with a ~260 Å diameter of the two layers. Figure reproduced from Planamente *et al.* (2016) under the terms of the Creative Commons CC BY license, https://creativecommons.org/licenses/by/4.0/legalcode. B) Representative micrograph of the $TssA1^{BC}$ C-terminal domain, scale bar is 50 nm. C) The rotationally symmetrised average of full length $TssA1^{BC}$, with a lumenal diameter of 110 Å, a C-terminal domain outer diameter of 180 Å and whole particle diameter of 450 Å. Figure reproduced from Dix *et al.* (2018) under the terms of the Creative Commons CC BY license, https://creativecommons.org/licenses/by/4.0/legalcode.

The TssA^{BC} C-terminal domain contains four α-helices (α12-α15) arranged as two anti-parallel pairs (Figure 1.19C) (509). In the ring structure, each monomer contacts two other monomers in the alternate layer of the ring, where α12 and α13 contribute to a stacking interaction to form dimers, while α15 is required for oligomerisation of these dimers into a ring structure (Figure 1.19) A conserved motif in TssA$_S$ C-terminal domains, the EPxxP motif, is found in the loop connecting α12 and α13 and is predicted to contribute to the stacking interaction (509).

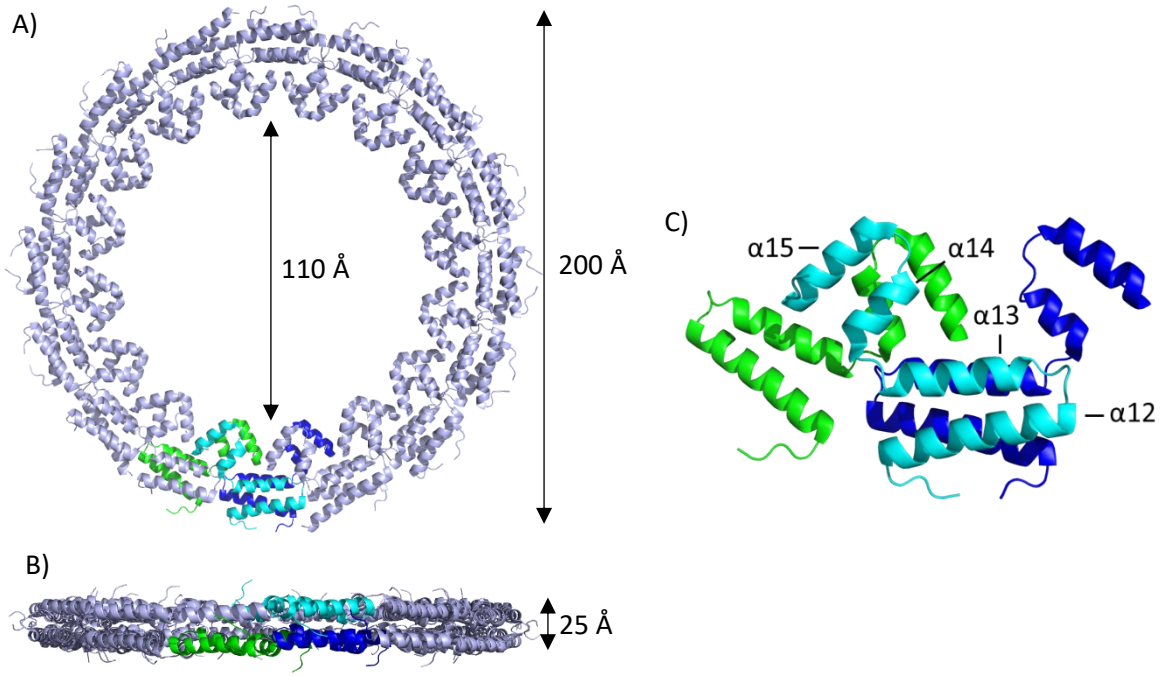


Figure 1.19 Structure of TssA^{BC} C-terminal domain ring. A) Top view of the TssA^{BC} C-terminal domain ring (PDB: 6HS6), with three monomers highlighted in light blue, blue and green. The ring has a lumenal diameter of 110 Å and an outer diameter of 200 Å. B) Side view of the TssA^{BC} C-terminal domain ring, which is 25 Å thick. C) Interactions between three TssA^{BC} C-terminal domain monomers. The α-helices of the light blue monomer are labelled. Helices α12 and α13 contribute to a stacking interaction with the blue monomer, while α15 contributes to an interaction with the green monomer that oligomerises these stacked dimers into rings.

1.4.1.3 Structural features of long TssA proteins (TssA$_L$)

The TssA$_L$ Nt1 domain is connected via a flexible linker to a ~150 aa Nt2 domain, which is connected further by a flexible linker to a distinct C-terminal domain, whose length can vary with the presence of a C-terminal extension (509). The Nt2 domain is formed of seven α-helices (α1-α7), which dimerise (Figure 1.20) (360,377,509). Despite limited sequence similarity, structural similarity has been

reported between the N-terminal five helices of TssA^{BC} Nt1 domain and the Nt2 domains of TssA from enteroaggregative *E. coli* (EC042_4540) (TssA^{EC}) and *A. hydrophila* (AHA1844) (TssA^{AH}) (509). As such, it is proposed that a duplication event may have given rise to Nt2 domains.

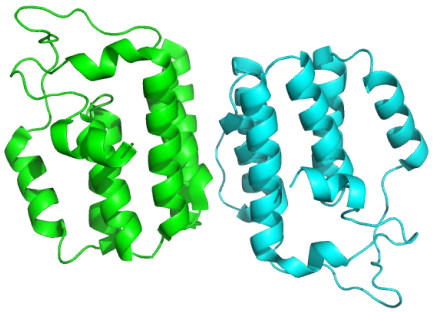


Figure 1.20 Structure of TssA^{AH} Nt2 domain dimers (PDB: 6G7C). Each monomer is comprised of seven α-helices.

The length of the TssA$_L$ C-terminal domains can vary based on the presence or absence of a 20-40 aa extension onto the minimal and conserved ~85 aa C-terminal domain, which introduces variation into TssA$_L$ proteins (509). In the absence of the C-terminal extension, the TssA^{AH} and *V. cholerae* TssA (VCA0119) (TssA^{VC}) C-terminal domains consist of five α-helices (α8-α12), while in the presence of the C-terminal extension, the TssA^{EC} C-terminal domain contains two additional α-helices (α8-α14) (360,377,509). The monomeric units of these C-terminal domains have similar folds, and in both cases one of the interaction interfaces of the C-terminal domain involves dimerisation via a conserved WEP motif in the loop connecting α11 and α12 (Figure 1.21) (377,509).

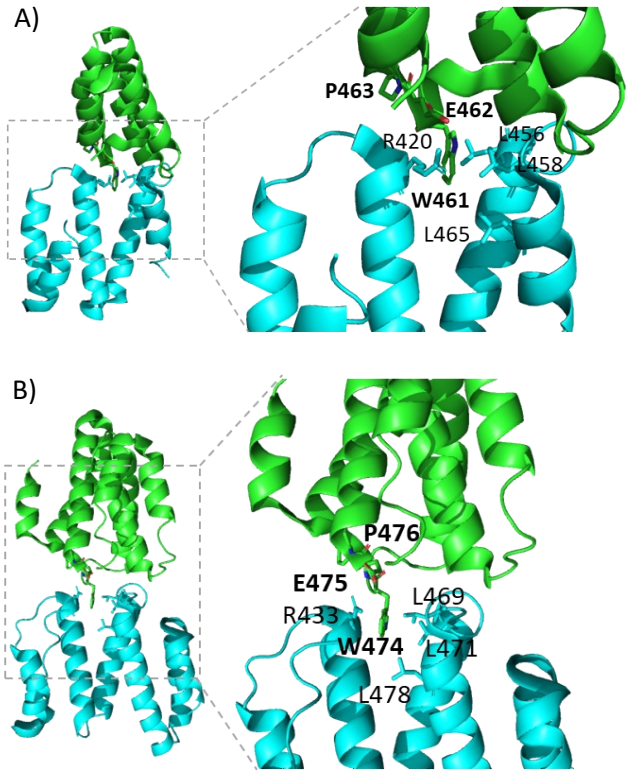


Figure 1.21 Dimer interfaces of TssA$_L$ proteins. The WEP residues (**bold**) of one monomer (green) interact with a hydrophobic pocket formed by another monomer (light blue). A) TssA^{AH} C-terminal domain (PDB: 6G7C) WEP-mediated dimer. **W461** is found within a hydrophobic pocket formed by L456, L458 and L465, with **E462** forming a salt bridge with R420. B) TssA^{EC} C-terminal domain (PDB: 4YO5) WEP-mediated dimer. **W474** is found within a hydrophobic pocket formed by L469, L471 and L478, with **E475** forming a salt bridge with R433.

The way in which these dimers assemble into a ring is influenced by the presence or absence of the C-terminal extension. In the absence of the C-terminal extension, interaction between the surfaces of α9, α10 and α11 of neighbouring subunits stabilises the formation of a thin (30-40 Å) star-shaped structure formed of two interpenetrating rings (Figure 1.22) (377,509). The monomeric units of the WEP-mediated dimers in this structure are almost adjacent to each other. The symmetry of this structure can vary, the decameric $TssA^{AH}$ forming a five-pointed star and the dodecameric $TssA^{VC}$, forming a six-pointed star (377,509).

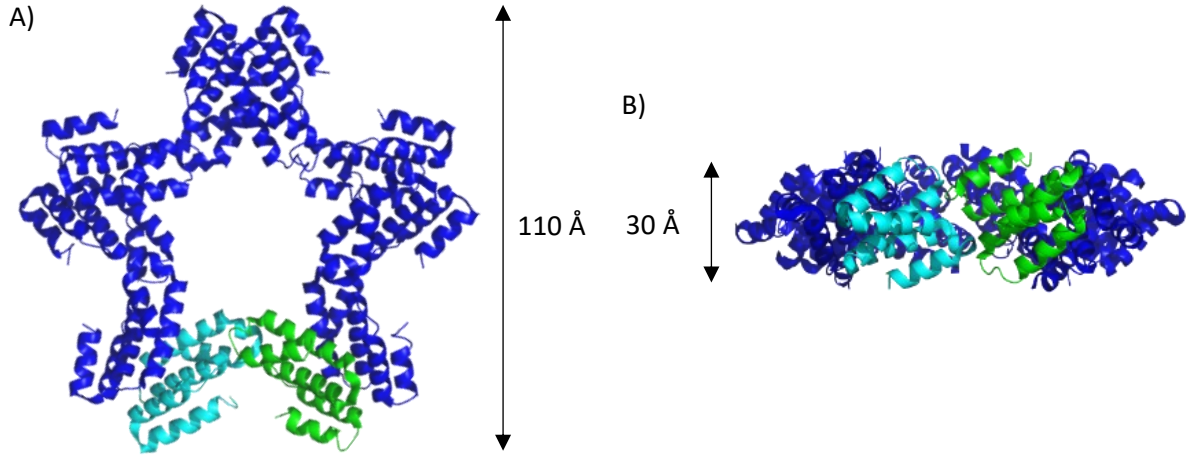


Figure 1.22 Structure of $TssA^{AH}$ C-terminal domain ring. A) Top view of $TssA^{AH}$ C-terminal domain ring (PDB: 6G7C) with monomers of a WEP-mediated dimer highlighted in light blue and green. The ring has a diameter of 110 Å. B) Side view of $TssA^{AH}$ C-terminal domain ring. The ring has a thickness of 30 Å.

In the presence of the C-terminal extension, the two additional α-helices are found at the dimerisation interface with α9, α10 and α11, altering the angle of the WEP-mediated dimer relative to the plane of the ring and causing the monomers of the dimers to stack on top of each other (Figure 1.23) (509). As such, $TssA^{EC}$ forms a thick (~80 Å) dodecamer made of a double-layered ring (360).

The C-terminal extension which is present in some $TssA_L$ C-terminal domains therefore influences whether C-terminal domain rings are formed by two thin interpenetrating rings in the absence of the extension, as seen for $TssA^{AH}$ and $TssA^{VC}$, or a thick double-layered ring in the presence of the extension, as seen for $TssA^{EC}$ (360,377,509). In both cases, the position of Nt2 dimers at the outer edge of the ring is highly flexible and does not follow the symmetry of the respective C-terminal domain ring (377,509).

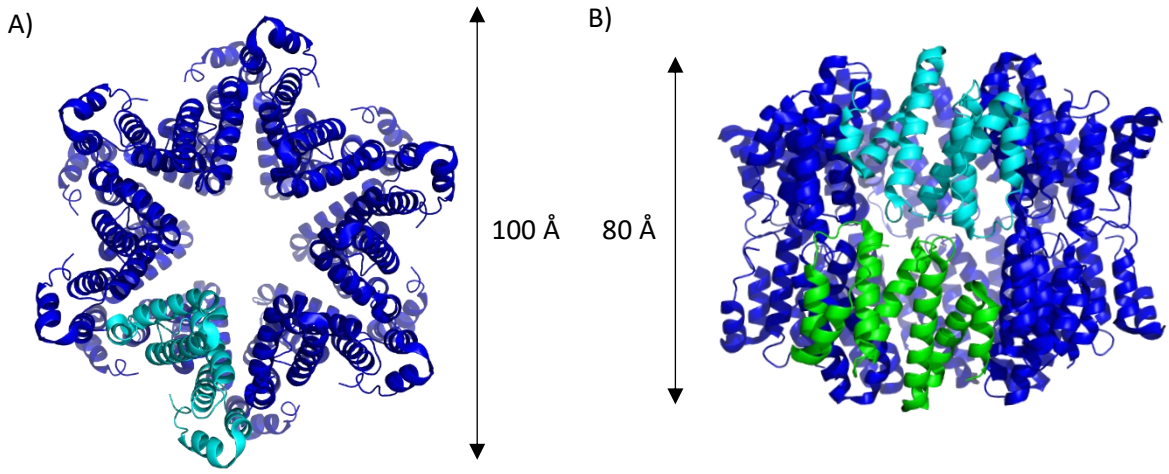


Figure 1.23 Structure of TssA^{EC} C-terminal domain ring. A) Top view of TssA^{EC} C-terminal domain ring (PDB: 4YO5) with monomer highlighted in light blue. The ring has a diameter of 100 Å. B) Side view of TssA^{EC} C-terminal domain ring with monomers of a WEP-mediated dimer highlighted in light blue and green. The ring has a thickness of 80 Å.

Despite variation in symmetry and thickness of TssA$_L$ C-terminal domain rings, their lumenal (25-53 Å) and outer diameters (100-132 Å) have similar dimensions (Table 1.1) (360,377,509). These contrast with the dimensions of TssA$_S$ C-terminal domain ring lumenal (100-110 Å) and outer diameters (200 Å) (376,509). Despite this variation, it has been proposed that the position of the peripheral Nt1 domains relative to the centre of the ring may be approximately equivalent in all TssA proteins (Figure 1.24) (509).

Table 1.1 TssA structural variation

	Organism	Length (aa)	Ring symmetry	Lumenal diameter (Å)	C-terminal domain ring diameter (Å)	Reference
TssA$_L$	**TssA^{EC}**	532	6	30	100	(360)
	TssA^{VC}	469	6	53	132	(377)
	TssA^{AH}	478	5	25	110	(509)
TssA$_S$	**TssA1^{PA}**	344	-	100	-	(376)
	TssA^{BC}	373	16	110	200	(509)

- data inconclusive

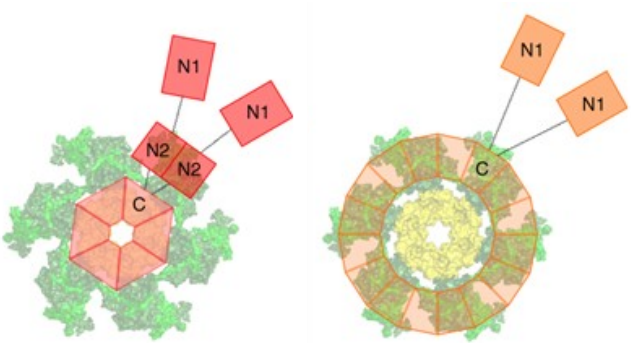


Figure 1.24 Model of long and short TssA complex domain architecture. Representation of a $TssA_L$ ring complex (left) and a $TssA_S$ ring complex at the distal end of the tail complex. Nt1 domains are positioned at a similar distance relative to the centre of each of these rings. Figure adapted from Dix *et al.* (2018) under the terms of the Creative Commons CC BY license, https://creativecommons.org/licenses/by/4.0/legalcode.

1.4.2 TssA within the T6SS

The T6SS is a complex multi-protein nanomachine, whose activity requires the coordinated assembly and interactions of many structural and accessory components (see section 1.3.2). The details of how the diversity of TssA proteins might be accommodated within this framework remain unknown. Indeed, it is unclear whether such diversity might introduce subtle differences in the molecular mechanisms underlying assembly and firing, and whether these might result in functional diversity or specificity in various biological contexts.

1.4.2.1 Interactions of TssA with T6SS components

Despite their differences, both long and short TssA proteins interact with components of each of the T6SS sub-complexes: membrane complex, baseplate complex and tail complex (Table 1.2). $TssA^{EC}$ has been co-purified with the membrane complex (360), while $TssA^{BC}$ and $TssA^{AH}$ interactions with membrane complex components have also been demonstrated (509). Interactions with baseplate components including TssK and VrgG, tail components including Hcp and sheath proteins, as well as the ATPase ClpV have been observed for both TssA groups (360,371,376,377,509).

Table 1.2 TssA interactions in the T6SS

		$TssA_S$		$TssA_L$	
T6SS sub-complex	**T6SS protein**	**$TssA1^{PA}$**	**$TssA^{BC}$**	**$TssA^{EC}$**	**$TssA^{VC}$**
Membrane complex	**TssJ**			(360)	
	TssL		(509)		(512)
	TssM		(509)		(512)
Baseplate complex	**TssE**		(509)	(360)	(512)
	TssF	(376)	(509)		(512)
	TssG				
	TssK	(376)	(509)	(360,371)	(512)
	VgrG	(376)	(509)	(360)	(512)
Tail complex	**Hcp**	(376)	(509)	(360)	(512)
	TssB	(376)			(512)
	TssC		(509)	(360)	(377,512)
ATPase	**ClpV**	(376)			(377)

The interaction with the sheath has been further characterised for $TssA^{EC}$, where an N-terminal region comprising Nt1+Nt2 domains has been demonstrated to interact with the sheath (360). Based on this, Nt2 domains of $TssA^{EC}$ and $TssA^{VC}$ have been modelled to interdigitate with the distal end of the sheath (360,377).

Overall TssA appears as a very ubiquitous T6SS component in terms of positioning within the T6SS machinery, which may relate to a dynamic localisation as the T6SS assembles and fires, as will be discussed later.

1.4.2.2 Role of TssA within the T6SS

The deletion of *tssA* leads to a complete loss or large reduction in the abundance of extending and contracting sheath structures, as well as loss of Hcp secretion and reduced T6SS-dependent prey killing (324,360,376,377,394,508,509,512). This indicates a role for TssA proteins in the assembly of the tail complex and thus T6SS activity.

Interaction of TssA proteins with components of each of the T6SS sub-complexes suggests a dynamic role for TssA during T6SS activity. The positioning of TssA within the T6SS has been studied through fluorescence microscopy experiments, with T6SS components, such as sheath proteins, linked to fluorophores to allowing visualisation of T6SS dynamics over time. TssA interactions with sub-complexes have been shown to be sequential, with TssA successively interacting with components of the membrane complex, baseplate complex and then tail complex (510). Static TssA, associated with the site of the membrane complex and baseplate complex, becomes dynamic upon polymerisation of the tail complex, where it is bound at the growing distal end of the sheath as it extends across the cell to the opposite membrane (360,377,508,513). From this position, TssA is suggested to coordinate the polymerisation of the growing tail complex (360,361). The same TssA complex is suggested to remain associated with the distal end of the sheath, from which the sheath polymerises (360,377,387). The mechanism by which the tail complex polymerises at its distal end with TssA attached remains unclear.

Both long and short TssA proteins have been observed to localise with the distal end of the sheath, however distinct mechanisms for the different TssA groups have also been suggested to explain their structural differences (376,377). The short TssA1^{PA} has been suggested to be a static baseplate component, mediating attachment to the sheath, but this is yet to be conclusively demonstrated (376,377). That both long and short TssA proteins show a similar network of interaction partners and have been shown to be associated with the distal end of the sheath suggests functional conservation, though it cannot be excluded that some TssAs may have distinct roles.

1.4.3 TssA-associated sheath regulators

In addition to core T6SS components, T6SS clusters can encode accessory proteins with roles including aiding T6SS assembly (345) and regulation (479), whose distribution varies between clusters (342). Our recent analysis has identified that not only is there an association between the length of TssA protein and T6SS phylogenetic group, but certain accessory proteins are also associated with these groups (Figure 1.25) (342,508). In general, TssA$_L$ proteins found in groups 1 and 2 co-occur with the TssA-family accessory protein, TagA, while TssA$_S$ proteins found in groups 3-5 co-occur with either a TagJ or a TagB accessory protein (508). An exception to this is the TssA$_S$-encoding group 4A, where no TssA-associated accessory protein has been identified.

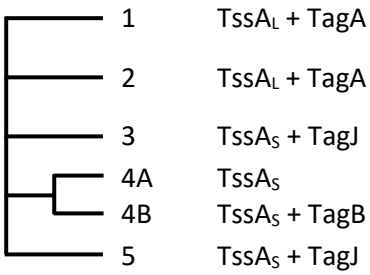


Figure 1.25 Association between T6SS phylogenetic groups, TssA and accessory proteins. T6SS clusters belonging to phylogenetic groups 1 and 2 encode TssA$_L$ proteins, while clusters of groups 3-5 encode TssA$_S$ proteins. Groups encoding TssA$_L$ proteins also generally encode a TagA protein, while groups encoding TssA$_S$ proteins generally also encode a TagJ or TagB protein. Group 4A clusters do not encode an associated accessory protein.

1.4.3.1 TssA$_L$ and TagA

TagA proteins, including those of *E. coli* (EC042_4550) (TagA^{EC}) and *V. cholerae* (VCA0121) (TagA^{VC}), contain the conserved N-terminal ImpA_N region characteristic of TssA proteins and a variable C-terminal region (377,510). TagA proteins interact with their cognate TssA$_L$ and peripherally associate with the membrane at the site where the sheath distal end completes its extension (377,510). Deletion of *tagA* results in both sheaths that contract immediately after extension, without a stable residence stage, and sheaths which continue polymerising after reaching the opposite side of the cell, causing sheaths to bend, and even become detached in some way from the membrane complex at the proximal end (377,510). As these detached sheaths remain in an extended conformation, it is suggested that they are still in contact with the baseplate complex (377). T6SS-dependent killing of prey is still possible in the absence of TagA, though with much reduced effectiveness (377,510). TagA is proposed to capture the extended sheath and anchor it to the membrane at the opposite side of the cell, terminating sheath extension and regulating residence of elongated sheaths before firing (377,510).

1.4.3.2 TssA$_S$ and TagB

We have recently demonstrated that the TagB accessory protein associated with TssA$_S$-encoding T6SS clusters of group 4B also regulates sheath extension, though by a distinct mechanism (508). The *P. putida* TagB1 protein interacts with its cognate TssA (PP3088) (TssA1^{PP}), which recruits TagB1 to the baseplate complex (508). However, while TssA1^{PP} subsequently migrates at the distal end of the

sheath, TagB1 accumulates at the baseplate complex after sheath initiation with TagB1 dissociation coinciding with sheath contraction (508). Deletion of *tagB1* does not affect TssA1^{PP} localisation or sheath abundance, but results in shorter sheaths with less efficient T6SS activity (508). It is proposed that the baseplate complex is stabilised through interaction with TagB1, allowing sheath polymerisation to be completed before contraction is triggered by TagB1 dissociation and a conformational change in the baseplate complex (see section 1.3.2.3) (508).

1.4.3.3 TssA$_S$ and TagJ

It has been suggested that TagJ accessory proteins associated with TssA$_S$-encoding T6SS clusters of groups 3 and 5, may act in a similar way due to similar dynamics being observed in T6SS assembly and their interaction with their respective TssA, but this is yet to be conclusively demonstrated (508). However, TagJ and TagB proteins share no sequence similarity, and thus may have distinct roles. In contrast to *tagB1*, deletion of the *P. aeruginosa tagJ1* (PA0086) caused no detectable effect on T6SS activity (514). Due to interaction with TssB and ClpV, TagJ1 has alternatively been suggested to be involved in coordinating the disassembly of the contracted sheath (514,515).

1.4.3.4 Link between T6SS kinetics and TssA

The diversity in TssA proteins and their associated accessory proteins, and the implications this has on T6SS activity is yet to be understood. One way in which TssA variation has been suggested to influence T6SS activity is in T6SS firing kinetics. Following polymerisation of the sheath, T6SSs associated with a TssA$_S$ contract immediately, while T6SSs associated with a TssA$_L$ can maintain an extended sheath in a resident state for more than 5 minutes (508). The functional significance of these differences in T6SS kinetics is yet to be fully elucidated but could represent a diversity in firing strategies required to optimise T6SS activity in specific environments or in response to particular stimuli. For example, tit-for-tat retaliation by *P. aeruginosa* requires a rapid and spatially oriented counterstrike and is carried out by the TssA$_S$-associated H1-T6SS (see section 1.3.5.2).

1.4.3.5 T6SS clusters lacking TssA-associated accessory proteins

The TssA-associated accessory proteins TagA and TagB are both involved in regulating the extension of the T6SS sheath, for $TssA_L$ and $TssA_S$ proteins respectively (377,508,510). However, for both long and short TssA proteins there are examples of T6SS clusters lacking genes encoding a TssA-associated accessory protein. The $TssA_L$-encoding H2-T6SS cluster of *P. aeruginosa* forms a functional T6SS, but no associated TagA protein has been identified (377,508). In addition, T6SS clusters in group 4A, including the H3-T6SS cluster of *P. aeruginosa,* encode a $TssA_S$ but no associated accessory protein has been identified (508). No differences were identified when comparing the C-terminal domain sequences of $TssA_S$ proteins with and without an associated accessory protein, although those with accessory proteins clustered together in phylogenetic analysis (508). It is not clear how, if at all, T6SSs lacking a TssA-associated accessory protein compensate for this absence.

1.5 Aims of this project

This project involved the characterisation of the three TssA proteins of *P. aeruginosa*. These TssA proteins are representative of the diversity of TssA proteins that have been characterised to date: encoding both long (TssA2) and short (TssA1 and TssA3) TssA proteins. The presence of three independent T6SS machineries in the *P. aeruginosa* genome allowed for the first time the functionality, positioning and specificity of long and short TssA proteins to be characterised in a single organism. To elucidate the role of these TssA proteins relative to their respective T6SSs, functional assays to assess T6SS-dependent secretion and prey killing, as well as fluorescence microscopy to visualise T6SS components, were used. Additionally, this project aimed to characterise the interactions of these TssA proteins, to understand their positioning within their respective T6SSs and to unpick some of the molecular details behind these interactions. To identify interaction partners of each TssA protein, comprehensive bacterial two-hybrid screens were carried out, and the relevance of these was assessed with functional assays. In an organism encoding multiple T6SS machineries, the specificity of these TssA proteins was also investigated. To identify the determinants of TssA functional specificity, the interactions of TssA domains were characterised and the functionality of chimeric TssA proteins assessed.

2. Experimental procedures

2.1 Bacterial strains and growth conditions

This study primarily involved the analysis of *P. aeruginosa* strain PAO1, some additional strains including various *E. coli* strains were also used. A complete list of all bacterial strains used in this study is presented in Table 2.1.

When grown in liquid culture, *Pseudomonas* strains were cultivated either in lysogeny broth (LB) (Miller, Millipore) or tryptic soy broth (TSB) (Sigma) in Erlenmeyer flasks with 150 rpm orbital shaking. *E. coli* strains were cultivated in LB, primarily in universal containers (Starlab) or falcon tubes (VWR). For culture on solid media, bacteria were typically grown on LB agar (Miller), but Vogel-Bonner medium (VBM) agar (100 ml 10x stock: 200 mM magnesium sulfate heptahydrate, 2 g anhydrous citric acid, 10 g potassium phosphate dibasic and 3.5 g ammonium sodium phosphate dibasic tetrahydrate) and *Pseudomonas* isolation agar (PIA) (Millipore) were also occasionally used to grow *P. aeruginosa*.

For routine culture, *P. aeruginosa* and *E. coli* strains were grown at 37 °C. However, they were also grown at other temperatures, such as 20, 25 and 30 °C, for certain experiments including interbacterial competition assays, protein secretion assays and protein purification. Where used, *P. putida* strains were grown at 30 °C. For long term storage, strains were stored in 40 % (v/v) glycerol at -80 °C.

Table 2.1 Bacterial strains used in this study

Strain	Features	Source
P. aeruginosa strains		
PAO1	Wild-type *P. aeruginosa* strain, Lausanne subline	Laboratory collection.
PAO1 Δ*rsmA*	PAO1 with deletion in *rsmA* (PA0905).	Laboratory collection, Luke Allsopp.
PAO1 Δ*rsmN*	PAO1 with deletion in *rsmN* (PA5183.1).	This study.
PAO1 Δ*retS*	PAO1 with deletion in *retS* (PA4856).	This study.
PAO1 Δ*rsmA ΔrsmN*	PAO1 with deletion in *rsmA* (PA0905) and *rsmN* (PA5183.1).	This study.
PAO1 Δ*rsmA ΔtssA1*	PAO1 with deletion in *rsmA* (PA0905) and *tssA1* (PA0082).	This study.
PAO1 Δ*retS* Δ*tssA1*	PAO1 with deletion in *retS* (PA4856) and *tssA1* (PA0082).	This study.
PAO1 Δ*rsmA ΔrsmN* Δ*tssA1*	PAO1 with deletion in *rsmA* (PA0905), *rsmN* (PA5183.1) and *tssA1* (PA0082).	This study.

PAO1 Δ*rsmA ΔtssB1*	PAO1 with deletion in *rsmA* (PA0905) and *tssB1* (PA0083).	This study.
PAO1 Δ*retS* Δ*tssB1*	PAO1 with deletion in *retS* (PA4856) and *tssB1* (PA0083).	This study.
PAO1 Δ*rsmA ΔrsmN* Δ*tssB1*	PAO1 with deletion in *rsmA* (PA0905), *rsmN* (PA5183.1) and *tssB1* (PA0083).	This study.
PAO1 Δ*rsmA ΔtssA2*	PAO1 with deletion in *rsmA* (PA0905) and *tssA2* (PA1656).	This study.
PAO1 Δ*rsmA ΔtssB2*	PAO1 with deletion in *rsmA* (PA0905) and *tssB2* (PA1657).	Laboratory collection, Sophie Howard.
PAO1 Δ*rsmA ΔtssA3*	PAO1 with deletion in *rsmA* (PA0905) and *tssA3* (PA2360).	This study.
PAO1 Δ*rsmA ΔtssB3*	PAO1 with deletion in *rsmA* (PA0905) and *tssB3* (PA2365).	Laboratory collection, Sophie Howard.
PAO1 Δ*rsmA tssB1-GFP*	PAO1 with deletion in *rsmA* (PA0905) with chromosomal fusion of *sfGFP* at the C-terminus of *tssB1* (PA0083).	(508)
PAO1 ΔrsmA Δ*tssA1 tssB1-GFP*	PAO1 with deletion in *rsmA* (PA0905) and *tssA1* (PA0082), with chromosomal fusion of *sfGFP* at the C-terminus of *tssB1* (PA0083).	This study.
PAO1 Δ*retS tssB1-mScarlet-I*	PAO1 with deletion in *retS* (PA4856) with chromosomal fusion of *mScarlet-I* at the C-terminus of *tssB1* (PA0083).	This study.
PAO1 Δ*retS* Δ*tssA1 tssB1-mScarlet-I*	PAO1 with deletion in *retS* (PA4856) and *tssA1* (PA0082), with chromosomal fusion of *mScarlet-I* at the C-terminus of *tssB1* (PA0083).	This study.
PAO1 Δ*rsmA ΔrsmN tssB1-mScarlet-I*	PAO1 with deletion in *rsmA* (PA0905) and *rsmN* (PA5183.1) with chromosomal fusion of *mScarlet-I* at the C-terminus of *tssB1* (PA0083).	This study.
PAO1 Δ*rsmA* Δ*rsmN* Δ*tssA1 tssB1-mScarlet-I*	PAO1 with deletion in *in rsmA (PA0905), rsmN* (PA5183.1) and *tssA1* (PA0082), with chromosomal fusion of *mScarlet-I* at the C-terminus of *tssB1* (PA0083).	This study.
PAO1 Δ*rsmA tssB2-GFP*	PAO1 with deletion in *rsmA* (PA0905) with chromosomal fusion of *sfGFP* at the C-terminus of *tssB2* (PA1657).	(508)
PAO1 Δ*rsmA* Δ*tssA2 tssB2-GFP*	PAO1 with deletion in *rsmA* (PA0905) and *tssA2* (PA1656) with chromosomal fusion of *sfGFP* at the C-terminus of *tssB2* (PA1657).	This study.
PAO1 Δ*rsmA tssB2-mScarlet-I*	PAO1 with deletion in *rsmA* (PA0905) with chromosomal fusion of *mScarlet-I* at the C-terminus of *tssB2* (PA1657).	This study.
PAO1 Δ*rsmA* Δ*tssA2 tssB2-mScarlet-I*	PAO1 with deletion in *rsmA* (PA0905) and *tssA2* (PA1656) with chromosomal fusion of *mScarlet-I* at the C-terminus of *tssB2* (PA1657).	This study.
PAO1 Δ*rsmA tssB3-mScarlet-I*	PAO1 with deletion in *rsmA* (PA0905) with chromosomal fusion of *mScarlet-I* at the C-terminus of *tssB3* (PA2365).	This study.
PAO1 Δ*rsmA* Δ*tssA3 tssB3-mScarlet-I*	PAO1 with deletion in *rsmA* (PA0905) and *tssA3* (PA2360) with chromosomal fusion of *mScarlet-I* at the C-terminus of *tssB3* (PA2365).	This study.

PAO1 Δ*rsmA tssB1-GFP mScarlet-I-tssA1*	PAO1 with deletion in *rsmA* (PA0905) with chromosomal fusion of *sfGFP* at the C-terminus of *tssB1* (PA0083) and *mScarlet-I* at the N-terminus of *tssA1* (PA0082).	This study.
PAO1 Δ*rsmA tssB1-mScarlet-I GFP-tssA1*	PAO1 with deletion in *rsmA* (PA0905) with chromosomal fusion of *mScarlet-I* at the C-terminus of *tssB1* (PA0083) and *sfGFP* at the N-terminus of *tssA1* (PA0082).	This study.
PAO1 *ΔtssB1 ΔtssB2*	PAO1 with deletion in *tssB1* (PA0083) and *tssB2* (PA1657).	This study.
PAO1 Δ*tssB1 ΔtssB2 ΔtssB3*	PAO1 with deletion in *tssB1* (PA0083), *tssB2* (PA1657) and *tssB3* (PA2365).	This study.
PAO1 *ΔrsmA ΔtssB1 ΔtssB2*	PAO1 with deletion in *rsmA* (PA0905), *tssB1* (PA0083) and *tssB2* (PA1657).	Laboratory collection, Sophie Howard.
PAO1 Δ*rsmA* Δ*tssB1* Δ*tssB2* Δ*tssB3*	PAO1 with deletion in *rsmA* (PA0905), *tssB1* (PA0083), *tssB2* (PA1657) and *tssB3* (PA2365).	Laboratory collection, Sophie Howard.
PAO1 Δ*retS* Δ*tssB1* Δ*tssB2* *ΔtssB3*	PAO1 with deletion in *retS* (PA4856), *tssB1* (PA0083), *tssB2* (PA1657) and *tssB3* (PA2365).	Laboratory collection, Marta Rudzite.
PAO1 Δ*rsmA* $tssA2_{1\text{-}391}$	PAO1 with deletion of *rsmA* (PA0905) and chromosomal truncation of *tssA2* (PA1656) to leave residues 1-391.	This study.
PAO1 Δ*rsmA* Δ*H1-T6SS* ΔH*3-T6SS*	PAO1 with deletion in *rsmA* (PA0905), *H1-T6SS* cluster between *tagQ1* and *vgrG1b* (PA0070-PA0095) and *H3-T6SS* cluster between *tssB3* and *clpV3* (PA2365-PA2371)	This study.
PAO1 Δ*rsmA* Δ*H1-T6SS* Δ*tssB2* ΔH*3-T6SS*	PAO1 with deletion in *rsmA* (PA0905), *H1-T6SS* cluster between *tagQ1* and *vgrG1b* (PA0070-PA0095), *tssB2* (PA1657) and *H3-T6SS* cluster between *tssB3* and *clpV3* (PA2365-PA2371).	This study.
PAK Δ*retS*	*P. aeruginosa* PAK strain with deletion in *retS* (PA4856).	Laboratory collection, Abdou Hachani.
PAK Δ*retS* Δ*tssA1*	*P. aeruginosa* PAK strain with deletion in *retS* (PA4856) and *tssA1* (PA0082).	Laboratory collection, Nadine Lossi.
PAK Δ*retS* Δ*tssB1*	*P. aeruginosa* PAK strain with deletion in *retS* (PA4856) and *tssB1* (PA0083).	Laboratory collection, Nadine Lossi.
PA14 Δ*rsmA*	*P. aeruginosa* PA14 strain with deletion in *rsmA* (PA14_52570).	(338)
PA14 Δ*rsmA hcp3-V5*	*P. aeruginosa* PA14 strain with deletion in *rsmA* (PA14_52570) and C-terminal V5 tag attached to *hcp3* (PA14_34030).	(338)
PA14 Δ*rsmA tssB3tl hcp3-V5*	*P. aeruginosa* PA14 strain with deletion in *rsmA* (PA14_52570), *tssB3-lacZ* translational fusion (PA14_34070) and C-terminal *V5* tag attached to *hcp3* (PA14_34030).	(338)
***E. coli* strains**		
DH5α omnimax	Strain used for cloning, F′ {*pro*AB *lac*I_q *lac*ZΔM15 *Tn*10 (Tet_R) Δ(*ccdA*B)} *mcr*A Δ(*mrr hsd*RMS-*mcr*BC) Φ 80(*lac*Z)ΔM15	Invitrogen

	Δ(*lac*ZYA-*arg*F)U169 *end*A1 *rec*A1 *sup*E44 *thi*-1 *gryA96 relA1 tonA panD*.	
DHM1	Strain used for bacterial two-hybrid, F^-, *cya-854, recA1, endA1, gyrA96* (Nal^R), *thi1, hsdR17, spoT1, rfbD1, glnV44(AS)*.	(516)
CC118λ*pir*	Host strain for pKNG101, Δ(ara-leu) *araDΔlacX74 galE galK-phoA20 thi-1 rpsE rpoB argE* (Amp^R) *recA1 Rfrλpir*.	(517)
BL21 (λDE3)	Strain used for protein expression, F^- *dcm lon ompT hsdS*(r_B – m_B –) *gal* λ(DE3 [*lacI lacUV5-T7p07 ind1 sam7 nin5*]).	Stratagene
1047	Helper strain for three-partner conjugation, *oriColE1 RK2-Mob+RK2-Tra+,* Km^R,	(518)
***P. putida* strains**		
KT2440R	Wildtype *P. putida* strain, Rif^R.	Laboratory collection.

Antibiotics and other supplements added to media and their working concentrations are outlined in Table 2.2. All supplements dissolved in sterile double distilled water (ddH_2O) were sterile filtered and all except 20 % (w/v) sucrose were stored at -20 °C long term, or 4 °C while in use. The 20 % (w/v) sucrose was stored at room temperature. Supplements dissolved in ethanol, methanol or dimethylformamide (DMF) were stored at -20 °C.

Table 2.2 Media supplements used in this work

Supplement	**Solvent**	**Final concentration**		
		P. aeruginosa	*E. coli*	*P. putida*
Ampicillin (Amp)	ddH_2O		100 µg/ml	
Carbenicillin (Carb)	ddH_2O	250 µg/ml		
Gentamicin (Gm)	ddH_2O		50 µg/ml	
IPTG	ddH_2O	250 µM	Various, as stated	
Kanamycin (Km)	ddH_2O		50 µg/ml	
Rifampicin (Rif)	Methanol			40 µg/ml
Streptomycin (Sm)	ddH_2O	1000 -2000 µg/ml	100 µg/ml	
Sucrose	ddH_2O	20 % (w/v)		
Tetracyclin (Tet)	Ethanol	150 µg/ml	15 µg/ml	
X-Gal	DMF		100 µg/ml	

2.2 Molecular biology techniques

2.2.1 Genomic DNA and plasmid extraction

All the plasmid vectors generated in this work were generated using genes from *P. aeruginosa* strain PAO1. This PAO1 genomic DNA was extracted using the Purelink™ Genomic DNA Mini Kit (Thermo Fisher Scientific) following the manufacturer's instructions. Plasmid DNA was extracted from cells using the QIAprep Spin Miniprep Kit (Qiagen). Following purification, all DNA was eluted with ddH_2O, DNA concentration was measured with the Nanodrop™ spectrophotometer and solubilised DNA was stored at -20 °C. Genomic and plasmid DNA were used for the construction of novel plasmids for this work, see Table 2.3.

Table 2.3 Plasmid vectors used in this study

Plasmid	Characteristics	Source
Cloning vector		
pCR®-Blunt II-TOPO®	Sub-cloning vector for blunt end ligation, Km^R.	Invitrogen
***P. aeruginosa* chromosomal mutagenesis vectors**		
pRK2013	Self-transmissible helper plasmid for mobilisation of non-self-transmissible plasmids, Km^R.	(518)
pKNG101	Non-replicative suicide vector to alter *P. aeruginosa* chromosome, *ori6K, mobRK2, sacB*, Sm^R.	(519)
pKNG101-Δ*tssA1*	pKNG101 suicide plasmid to delete *tssA1* (PA0082), Sm^R.	This study.
pKNG101-Δ*tssA2*	pKNG101 suicide plasmid to delete *tssA2* (PA1656), Sm^R.	This study.
pKNG101-Δ*tssA3*	pKNG101 suicide plasmid to delete *tssA3* (PA2360), Sm^R.	This study.
pKNG101-Δ*tssB1*	pKNG101 suicide plasmid to delete *tssB1* (PA0083), Sm^R.	(514)
pKNG101-Δ*tssB2*	pKNG101 suicide plasmid to delete *tssB2* (PA1657), Sm^R.	(338)
pKNG101-Δ*tssB3*	pKNG101 suicide plasmid to delete *tssB3* (PA2365), Sm^R.	Laboratory collection, Thomas Wood.
pKNG101-*GFP-tssA1*	pKNG101 suicide plasmid to introduce *sfGFP* at the N-terminus of the *tssA1* gene (PA0082), Sm^R.	This study.
pKNG101-*tagJ1-GFP*	pKNG101 suicide plasmid to introduce *sfGFP* at the C-terminus of the *tagJ1* gene (PA0086), Sm^R.	This study.
pKNG101-$tssA2_{1\text{-}391}$	pKNG101 suicide plasmid to C-terminally truncate *tssA2* (PA1656), leaving residues 1-391, Sm^R.	This study.
pKNG101-*tssB1-mScarlet-I*	pKNG101 suicide plasmid to introduce *mScarlet-I* at the C-terminus of the *tssB1* gene (PA0083), Sm^R.	This study.

pKNG101-*tssB2-mScarlet-I*	pKNG101 suicide plasmid to introduce *mScarlet-I* at the C-terminus of the *tssB2* gene (PA1657), Sm^R.	This study.
pKNG101-*tssB3-mScarlet-I*	pKNG101 suicide plasmid to introduce *mScarlet-I* at the C-terminus of the *tssB3* gene (PA2365), Sm^R.	This study.
pKNG101-Δ*H1-T6SS*	pKNG101 suicide plasmid to delete the *H1-T6SS* cluster between *tagQ1* and *vgrG1b* (PA0070-PA0095), Sm^R.	This study.
pKNG101-Δ*H3-T6SS*	pKNG101 suicide plasmid to delete the *H3-T6SS* cluster between *tssB3* and *clpV3* (PA2365-PA2371), Sm^R.	(338)
pKNG101-Δ*retS*	pKNG101 suicide plasmid to delete *retS* (PA4856), Sm^R.	Laboratory collection, Luke Allsopp.
pKNG101-Δ$tagJ1_{50-230}$	pKNG101 suicide plasmid to delete the central region, residues 50-230, of *tagJ1* (PA0086), Sm^R.	This study.
pKNG101-Δ*rsmN*	pKNG101 suicide plasmid to delete *rsmN* (PA5183.1) made in PAO1, Sm^R.	This study, with Marta Rudzite.
Bacterial two-hybrid vectors		
pKT25	Bacterial two-hybrid vector, encoding the T25 fragment of *B. pertussis cyaA,* with the MCS at the C-terminal end of T25, Km^R.	(516)
pKNT25	Bacterial two-hybrid vector, encoding the T25 fragment of *B. pertussis cyaA,* with the MCS at the N-terminal end of T25, Km^R.	(516)
pUT18	Bacterial two-hybrid vector, encoding T18 fragment of *B. pertussis cyaA*, with the MCS at the N-terminal end of T18, Amp^R.	(516)
pUT18C	Bacterial two-hybrid vector, encoding T18 fragment of *B. pertussis cyaA*, with the MCS at the C-terminal end of T18, Amp^R.	(516)
pKT25-*zip*	pKT25 encoding the leucine zipper region of yeast protein GCN4, Km^R.	(516)
pUT18C-*zip*	pUT18C encoding the leucine zipper region of yeast protein GCN4, Amp^R.	(516)
pKT25-*tssA1*	pKT25 encoding *tssA1* (PA0082), Km^R.	(376)
pKT25-*tssA1* K69A	pKT25 encoding *tssA1* (PA0082) with K69A substitution, Km^R.	This study, with Genevieve Butt.
pKT25-*tssA1* G86A	pKT25 encoding *tssA1* (PA0082) with G86A substitution, Km^R.	This study, with Genevieve Butt.
pKT25-*tssA1* L94A	pKT25 encoding *tssA1* (PA0082) with L94A substitution, Km^R.	This study, with Genevieve Butt.
pKT25-*tssA1* R282A	pKT25 encoding *tssA1* (PA0082) with R282A substitution, Km^R.	This study, with Genevieve Butt.
pKT25-*tssA1* L286A	pKT25 encoding *tssA1* (PA0082) with L286A substitution, Km^R.	This study.
pKT25-*tssA1* L289A	pKT25 encoding *tssA1* (PA0082) with L289A substitution, Km^R.	This study.
pKT25-*tssA1* E300A	pKT25 encoding *tssA1* (PA0082) with E300A substitution, Km^R.	This study, with Genevieve Butt.
pKT25-*tssA1* L309A	pKT25 encoding *tssA1* (PA0082) with L309A substitution, Km^R.	This study.

pKT25-*tssA1* D14A	pKT25 encoding *tssA1* (PA0082) with D14A substitution, Km^R.	This study.
pKT25-*tssA1* Q41A	pKT25 encoding *tssA1* (PA0082) with Q41A substitution, Km^R.	This study.
pKT25-*tssA1* D44A	pKT25 encoding *tssA1* (PA0082) with D44A substitution, Km^R.	This study.
pKT25-*tssA1* D116A	pKT25 encoding *tssA1* (PA0082) with D116A substitution, Km^R.	This study.
pKT25-*tssA1* R146A	pKT25 encoding *tssA1* (PA0082) with R146A substitution, Km^R.	This study.
pKT25-*tssA1* R148A	pKT25 encoding *tssA1* (PA0082) with R148A substitution, Km^R.	This study.
pKT25-*tssA1* S169A	pKT25 encoding *tssA1* (PA0082) with S169A substitution, Km^R.	This study.
pKT25-*tssA1* E170A	pKT25 encoding *tssA1* (PA0082) with E170A substitution, Km^R.	This study.
pKT25-*tssA1* L238A	pKT25 encoding *tssA1* (PA0082) with L238A substitution, Km^R.	This study.
pKT25-$tssA1_{Nt1}$	pKT25 encoding *tssA1* (PA0082) Nt1 domain residues 1-240, Km^R.	This study.
pKT25-$tssA1_{CTD}$	pKT25 encoding *tssA1* (PA0082) CTD residues 275-344, Km^R.	This study.
pKT25-*tssB1*	pKT25 encoding *tssB1* (PA0083), Km^R.	Laboratory collection, Heather Coombe.
pKT25-*tssC1*	pKT25 encoding *tssC1* (PA0084), Km^R.	Laboratory collection, Nadine Lossi.
pKT25-*tssB1tssC1*	pKT25 encoding *tssB1* and *tssC1* (PA0083-84), Km^R.	This study.
pKT25-*tssE1*	pKT25 encoding *tssE1* (PA0087), Km^R.	Laboratory collection, Nadine Lossi.
pKT25-*tssF1*	pKT25 encoding *tssF1* (PA0088), Km^R.	Laboratory collection, Nadine Lossi.
pKT25-*tssG1*	pKT25 encoding *tssG1* (PA0089), Km^R.	Laboratory collection, Nadine Lossi.
pKT25-*tssK1*	pKT25 encoding *tssK1* (PA0079), Km^R.	Laboratory collection, Sara Planamente.
pKT25-*hcp1*	pKT25 encoding *hcp1* (PA0085), Km^R.	Laboratory collection, Sara Planamente.
pKT25-*tagJ1*	pKT25 encoding *tagJ1* (PA0086), Km^R	Laboratory collection, Nadine Lossi.
pKT25-*clpV1*	pKT25 encoding *clpV1* (PA0090), Km^R.	Laboratory collection, Nadine Lossi.

pKT25-*vgrG1a*	pKT25 encoding *vgrG1a* (PA0091), Km^R.	Laboratory collection, Luke Allsopp.
pKT25-*vgrG1b*	pKT25 encoding *vgrG1b* (PA0095), Km^R.	Laboratory collection, Panayiota Pissaridou.
pKT25-*vgrG1c*	pKT25 encoding *vgrG1c* (PA2685), Km^R.	Laboratory collection, Luke Allsopp.
pKT25-*tssA2*	pKT25 encoding *tssA2* (PA1656), Km^R.	This study.
pKT25-$tssA2_{Nt1}$	pKT25 encoding *tssA2* (PA2360) Nt1 domain residues 1-190, Km^R.	This study.
pKT25-$tssA2_{Nt2+CTD}$	pKT25 encoding *tssA2* (PA1656) Nt2+CTD residues 222-528, Km^R.	This study.
pKT25-*tssA3*	pKT25 encoding *tssA3* (PA2360), Km^R.	This study.
pKT25-$tssA3_{Nt1}$	pKT25 encoding *tssA3* (PA2360) Nt1 domain residues 1- 260, Km^R.	This study.
pKT25-$tssA3_{CTD}$	pKT25 encoding *tssA3* (PA2360) CTD residues 296-366, Km^R.	This study.
pKT25-*PA2372*	pKT25 encoding *PA2372*, Km^R.	This study.
pKT25-$tssA1_{Nt1}$-$tssA2_{CTD}$	pKT25 encoding $tssA1_{Nt1}$ (PA0082) (residues 1-275) $tssA2_{CTD}$ (PA1656) (residues 388-518) chimera, Km^R.	This study.
pKT25-$tssA1_{Nt1}$-$tssA2_{Nt2+CTD}$	pKT25 encoding $tssA1_{Nt1}$ (PA0082) (residues 1-275) $tssA2_{Nt2+CTD}$ (PA1656) (residues 222-518) chimera, Km^R.	This study.
pKT25-$tssA1_{Nt1}$-$tssA3_{CTD}$	pKT25 encoding $tssA1_{Nt1}$ (PA0082) (residues 1-275) $tssA3_{CTD}$ (PA2360) (residues 296-366) chimera, Km^R.	This study.
pKT25-$tssA2_{Nt1}$-$tssA1_{CTD}$	pKT25 encoding $tssA2_{Nt1}$ (PA1656) (residues 1-192) $tssA1_{CTD}$ (PA0082) (residues 246-344) chimera, Km^R.	This study.
pKT25-$tssA2_{Nt1}$-$tssA3_{CTD}$	pKT25 encoding $tssA2_{Nt1}$ (PA1656) (residues 1-222) $tssA3_{CTD}$ (PA2360) (residues 296-366) chimera, Km^R.	This study.
pKT25-$tssA3_{Nt1}$-$tssA1_{CTD}$	pKT25 encoding $tssA3_{Nt1}$ (PA2360) (residues 1-262) $tssA1_{CTD}$ (PA0082) (residues 246-344) chimera, Km^R.	This study.
pKT25-$tssA3_{Nt1}$-$tssA2_{CTD}$	pKT25 encoding $tssA3_{Nt1}$ (PA2360) (residues 1-262) $tssA2_{CTD}$ (PA1656) (residues 375-518) chimera, Km^R.	This study.
pKT25-$tssA3_{Nt1}$-$tssA2_{Nt2+CTD}$	pKT25 encoding $tssA3_{Nt1}$ (PA2360) (residues 1-262) $tssA2_{Nt2+CTD}$ (PA1656) (residues 192-518) chimera, Km^R.	This study.
pKT25-*tssA1 with tssA3 loop*	pKT25 encoding *tssA1* (PA0082) with loop region (Q37-E53) replaced with *tssA3* (PA2360) loop region (D46-D62), Km^R.	This study.
pKT25-*tssA1 with tssA3 hairpin*	pKT25 encoding *tssA1* (PA0082) with hairpin region (F169-L172) replaced with *tssA3* (PA2360) hairpin region (A174-Q191), Km^R.	This study.
pKT25-*tssA1 with tssA3 hairpin and loop*	pKT25 encoding *tssA1* (PA0082) with hairpin (F169-L172) and loop (Q37-E53) regions replaced with *tssA3* (PA2360) hairpin (A174-Q191) and loop (D46-D62) regions, Km^R.	This study.
pKT25-*tssA3 with tssA1 loop*	pKT25 encoding *tssA3* (PA2360) with loop region (D46-D62) replaced with *tssA1* (PA0082) loop region (Q37-E53), Km^R.	This study.

pKT25-*tssA3 with tssA1 hairpin*	pKT25 encoding *tssA3* (PA2360) with hairpin region (A174-Q191) replaced with *tssA1* (PA0082) hairpin region (F169-L172), Km^R.	This study.
pKT25-*tssA3 with tssA1 hairpin and loop*	pKT25 encoding *tssA3* (PA2360) with hairpin (A174-Q191) and loop (D46-D62) regions replaced with tssA1 (PA0082) hairpin (F169-L172) and loop (Q37-E53) regions, Km^R.	This study.
pKNT25-*tssA1*	pKNT25 encoding *tssA1* (PA0082), Km^R.	This study.
pKNT25-*tssB1*	pKNT25 encoding *tssB1* (PA0083), Km^R.	This study.
pKNT25-*tssC1*	pKNT25 encoding *tssC1* (PA0084), Km^R.	This study.
pKNT25-*tssB1tssC1*	pKNT25 encoding *tssB1* and *tssC1* (PA0083-84), Km^R.	This study.
pKNT25-*tssE1*	pKNT25 encoding *tssE1* (PA0087), Km^R.	This study.
pKNT25-*tssF1*	pKNT25 encoding *tssF1* (PA0088), Km^R.	This study.
pKNT25-*tssG1*	pKNT25 encoding *tssG1* (PA0089), Km^R.	This study.
pKNT25-*tssK1*	pKNT25 encoding *tssK1* (PA0079), Km^R.	This study.
pKNT25-*hcp1*	pKNT25 encoding *hcp1* (PA0085), Km^R.	Laboratory collection, Sarah Wettstadt.
pKNT25-*tagJ1*	pKNT25 encoding *tagJ1* (PA0086), Km^R.	Laboratory collection, Diane Letourneur.
pKNT25-*clpV1*	pKNT25 encoding *clpV1* (PA0090), Km^R.	Laboratory collection, Thomas Clamens.
pKNT25-*vgrG1a*	pKNT25 encoding *vgrG1a* (PA0091), Km^R.	Laboratory collection, Sarah Wettstadt.
pKNT25-*PA2372*	pKNT25 encoding *PA2372*, Km^R.	This study.
pUT18-*tssA1*	pUT18 encoding *tssA1* (PA0082), Amp^R.	This study.
pUT18-*tssB1*	pUT18 encoding *tssB1* (PA0083), Amp^R.	This study.
pUT18-*tssC1*	pUT18 encoding *tssC1* (PA0084), Amp^R.	This study.
pUT18-*tssB1tssC1*	pUT18 encoding *tssB1* and *tssC1* (PA0083-84), Amp^R.	This study.
pUT18-*tssE1*	pUT18 encoding *tssE1* (PA0087), Amp^R.	This study.
pUT18-*tssF1*	pUT18 encoding *tssF1* (PA0088), Amp^R.	This study.
pUT18-*tssG1*	pUT18 encoding *tssG1* (PA0089), Amp^R.	This study.
pUT18-*tssK1*	pUT18 encoding *tssK1* (PA0079), Amp^R.	This study.
pUT18-*hcp1*	pUT18 encoding *hcp1* (PA0085), Amp^R.	Laboratory collection, Sarah Wettstadt.
pUT18-*tagJ1*	pUT18 encoding *tagJ1* (PA0086), Amp^R.	Laboratory collection, Diane Letourneur.
pUT18-*clpV1*	pUT18 encoding *clpV1* (PA0090), Amp^R.	Laboratory collection, Thomas Clamens.
pUT18-*vgrG1a*	pUT18 encoding *vgrG1a* (PA0091), Amp^R.	Laboratory collection, Sarah Wettstadt.
pUT18-*PA2372*	pUT18 encoding *PA2372*, Amp^R.	This study.

pUT18C-*tssA1*	pUT18C encoding *tssA1* (PA0082), Amp^R.	(376)
pUT18C-*tssA1* K69A	pUT18C encoding *tssA1* (PA0082) with K69A substitution, Amp^R.	This study.
pUT18C-*tssA1* G86A	pUT18C encoding *tssA1* (PA0082) with G86A substitution, Amp^R.	This study.
pUT18C-*tssA1* L94A	pUT18C encoding *tssA1* (PA0082) with L94A substitution, Amp^R.	This study.
pUT18C-*tssA1* R282A	pUT18C encoding *tssA1* (PA0082) with R282A substitution, Amp^R.	This study.
pUT18C-*tssA1* L286A	pUT18C encoding *tssA1* (PA0082) with L286A substitution, Amp^R.	This study.
pUT18C-*tssA1* L289A	pUT18C encoding *tssA1* (PA0082) with L289A substitution, Amp^R.	This study.
pUT18C-*tssA1* E300A	pUT18C encoding *tssA1* (PA0082) with E300A substitution, Amp^R.	This study.
pUT18C-*tssA1* L309A	pUT18C encoding *tssA1* (PA0082) with L309A substitution, Amp^R.	This study.
pUT18C-$tssA1_{Nt1}$	pUT18C encoding $tssA1_{Nt1}$ (PA0082) residues 1-240, Amp^R.	This study.
pUT18C-$tssA1_{CTD}$	pUT18C encoding $tssA1_{CTD}$ (PA0082) residues 275-344, Amp^R.	This study.
pUT18C-*tssB1*	pUT18C encoding *tssB1* (PA0083), Amp^R.	Laboratory collection, Heather Coombe.
pUT18C-*tssC1*	pUT18C encoding *tssC1* (PA0084), Amp^R.	Laboratory collection, Nadine Lossi.
pUT18C-*tssB1tssC1*	pUT18C encoding *tssB1* and *tssC1* (PA0083-84), Amp^R.	This study.
pUT18C-*tssE1*	pUT18C encoding *tssE1* (PA0087), Amp^R.	Laboratory collection, Nadine Lossi.
pUT18C-*tssF1*	pUT18C encoding *tssF1* (PA0088), Amp^R.	Laboratory collection, Nadine Lossi.
pUT18C-*tssG1*	pUT18C encoding *tssG1* (PA0089), Amp^R.	Laboratory collection, Nadine Lossi.
pUT18C-*tssK1*	pUT18C encoding *tssK1* (PA0079), Amp^R.	Laboratory collection, Sara Planamente.
pUT18C-*hcp1*	pUT18C encoding *hcp1* (PA0085), Amp^R.	Laboratory collection, Sara Planamente.
pUT18C-*tagJ1*	pUT18C encoding *tagJ1* (PA0086), Amp^R.	Laboratory collection, Nadine Lossi.
pUT18C-*clpV1*	pUT18C encoding *clpV1* (PA0090), Amp^R.	Laboratory collection, Nadine Lossi.

pUT18C-*vgrG1a*	pUT18C encoding *vgrG1a* (PA0091), Amp^R.	Laboratory collection, Laura Nolan.
pUT18C-*vgrG1b*	pUT18C encoding *vgrG1b* (PA0095), Amp^R.	Laboratory collection, Laura Nolan.
pUT18C-*vgrG1c*	pUT18C encoding *vgrG1c* (PA2685), Amp^R.	Laboratory collection, Laura Nolan.
pUT18C-*tssL1*	pUT18C encoding *tssL1* (PA0078), Amp^R.	This study.
pUT18C-$tssM1_{cyt}$	pUT18C encoding *tssM1* (PA0077) cytoplasmic region residues 1-369, Amp^R.	This study.
pUT18C-*tssA2*	pUT18C encoding *tssA2* (PA1656), Amp^R.	This study.
pUT18C-$tssA2_{Nt1}$	pUT18C encoding $tssA2_{Nt1}$ (PA1656) residues 1- 190, Amp^R.	This study.
pUT18C-$tssA2_{Nt2+CTD}$	pUT18C encoding $tssA2_{Nt2+CTD}$ (PA1656) residues 222-528, Amp^R.	This study.
pUT18C-*tssB2*	pUT18C encoding *tssB2* (PA1657), Amp^R.	Laboratory collection, Nadine Lossi.
pUT18C-*tssC2*	pUT18C encoding *tssC2* (PA1658), Amp^R.	Laboratory collection, Nadine Lossi.
pUT18C-*tssB2tssC2*	pUT18C encoding *tssB2* and *tssC2* (PA1657-1658), Amp^R.	This study.
pUT18C-*tssE2*	pUT18C encoding *tssE2* (PA1659), Amp^R.	This study.
pUT18C-*tssF2*	pUT18C encoding *tssF2* (PA1660), Amp^R.	This study.
pUT18C-*tssG2*	pUT18C encoding *tssG2* (PA1661), Amp^R.	This study.
pUT18C-*tssK2*	pUT18C encoding *tssK2* (PA1667), Amp^R.	This study.
pUT18C-*hcp2*	pUT18C encoding *hcp2* (PA1512/PA5267/PA0263), Amp^R.	Laboratory collection, Abderrahman Hachani.
pUT18C-*clpV2*	pUT18C encoding *clpV2* (PA1662), Amp^R.	Laboratory collection, Sara Planamente.
pUT18C-*vgrG2a*	pUT18C encoding *vgrG2a* (PA1511), Amp^R.	This study.
pUT18C-*vgrG2b*	pUT18C encoding *vgrG2b* (PA0264), Amp^R.	This study.
pUT18C-*vgrG4a*	pUT18C encoding *vgrG4a* (PA3294), Amp^R.	This study.
pUT18C-*vgrG4b*	pUT18C encoding *vgrG4b* (PA3486), Amp^R.	This study.
pUT18C-*vgrG5*	pUT18C encoding *vgrG5* (PA5090), Amp^R.	Laboratory collection, Laura Nolan.
pUT18C-*vgrG6*	pUT18C encoding *vgrG6* (PA5266), Amp^R.	Laboratory collection, Laura Nolan.
pUT18C-*tssL2*	pUT18C encoding *tssL2* (PA1668), Amp^R.	This study.
pUT18C-$tssM2_{cyt}$	pUT18C encoding *tssM2* (PA1669) cytoplasmic region residues 1-447, Amp^R.	This study.

pUT18C-*tssA3*	pUT18C encoding *tssA3* (PA2360), Amp^R.	This study.
pUT18C-$tssA3_{Nt1}$	pUT18C encoding $tssA3_{Nt1}$ (PA2360) residues 1-260, Amp^R.	This study.
pUT18C-$tssA3_{CTD}$	pUT18C encoding $tssA3_{CTD}$ (PA2360) residues 296-366, Amp^R.	This study.
pUT18C-*tssB3*	pUT18C encoding *tssB3* (PA2365), Amp^R.	This study.
pUT18C-*tssC3*	pUT18C encoding *tssC3* (PA2366), Amp^R.	This study.
pUT18C-*tssB3tssC3*	pUT18C encoding *tssB3* and *tssC3* (PA2365-2366), Amp^R.	This study.
pUT18C-*tssE3*	pUT18C encoding *tssE3* (PA2668), Amp^R.	This study.
pUT18C-*tssF3*	pUT18C encoding *tssF3* (PA2369), Amp^R.	This study.
pUT18C-*tssG3*	pUT18C encoding *tssG3* (PA2670), Amp^R.	This study.
pUT18C-*tssK3*	pUT18C encoding *tssK3* (PA2363), Amp^R.	This study.
pUT18C-*hcp3*	pUT18C encoding *hcp3* (PA2367), Amp^R.	Laboratory collection, Sophie Howard.
pUT18C-*clpV3*	pUT18C encoding *clpV3* (PA2371), Amp^R.	Laboratory collection, Thomas Clamens.
pUT18C-*vgrG3*	pUT18C encoding *vgrG3* (PA2373), Amp^R.	Laboratory collection, Laura Nolan.
pUT18C-*tssL3*	pUT18C encoding *tssL3* (PA2362), Amp^R.	This study.
pUT18C-$tssM3_{cyt}$	pUT18C encoding *tssM3* (PA2361) cytoplasmic region residues 1-348, Amp^R.	This study.
pUT18C-*PA2372*	pUT18C encoding *PA2372*, Amp^R.	This study.
***Pseudomonas* expression vectors**		
pBBR1MCS4	Broad host range vector, with constitutive P_{LAC} promoter, Amp^R/$Carb^R$.	(520)
pBBR1MCS4-*tssA1*	pBBR1MCS4 encoding *tssA1* (PA0082), Amp^R/$Carb^R$.	This study.
pBBR1MCS4-*tssA2*	pBBR1MCS4 encoding *tssA2* (PA1656), Amp^R/$Carb^R$.	This study.
pBBR1MCS4-*tssA3*	pBBR1MCS4 encoding *tssA3* (PA2360), Amp^R/$Carb^R$.	This study.
pBBR1MCS4-$tssA1_{Nt1}$-$tssA2_{CTD}$	pBBR1MCS4 encoding $tssA1_{Nt1}$ (PA0082) (residues 1-275) $tssA2_{CTD}$ (PA1656) (residues 388-518) chimera, Amp^R/$Carb^R$.	This study.
pBBR1MCS4-$tssA1_{Nt1}$-$tssA2_{Nt2+CTD}$	pBBR1MCS4 encoding $tssA1_{Nt1}$ (PA0082) (residues 1-275) $tssA2_{Nt2+CTD}$ (PA1656) (residues 222-518) chimera, Amp^R/$Carb^R$.	This study.
pBBR1MCS4-$tssA1_{Nt1}$-$tssA3_{CTD}$	pBBR1MCS4 encoding $tssA1_{Nt1}$ (PA0082) (residues 1-275) $tssA3_{CTD}$ (PA2360) (residues 296-366) chimera, Amp^R/$Carb^R$.	This study.
pBBR1MCS4-$tssA2_{Nt1}$-$tssA1_{CTD}$	pBBR1MCS4 encoding $tssA2_{Nt1}$ (PA1656) (residues 1-192) $tssA1_{CTD}$ (PA0082) (residues 246-344) chimera, Amp^R/$Carb^R$.	This study.
pBBR1MCS4-$tssA2_{Nt1}$-$tssA3_{CTD}$	pBBR1MCS4 encoding $tssA2_{Nt1}$ (PA1656) (residues 1-222) $tssA3_{CTD}$ (PA2360) (residues 296-366) chimera, Amp^R/$Carb^R$.	This study.

pBBR1MCS4-*tssA3*$_{Nt1}$-*tssA1*$_{CTD}$	pBBR1MCS4 encoding *tssA3*$_{Nt1}$ (residues 1-262) *tssA1*$_{CTD}$ (PA0082) (residues 246-344) chimera, Amp^R/Carb^R.	This study.
pBBR1MCS4-*tssA3*$_{Nt1}$-*tssA2*$_{CTD}$	pBBR1MCS4 encoding *tssA3*$_{Nt1}$ (PA2360) (residues 1-262) *tssA2*$_{CTD}$ (PA1656) (residues 375-518) chimera, Amp^R/Carb^R.	This study.
pBBR1MCS4-*tssA3*$_{Nt1}$-*tssA2*$_{Nt2+CTD}$	pBBR1MCS4 encoding *tssA3*$_{Nt1}$ (PA2360) (residues 1-262) *tssA2*$_{Nt2+CTD}$ (PA1656) (residues 192-518) chimera, Amp^R/Carb^R.	This study.
pBBR1MCS4-*tssA1*$_{Nt1}$	pBBR1MCS4 encoding *tssA1*$_{Nt1}$ (PA0082) residues 1-240, Amp^R/Carb^R.	This study.
pBBR1MCS4-*tssA2*$_{Nt1}$	pBBR1MCS4 encoding *tssA2*$_{Nt1}$ (PA1656) residues 1-190, Amp^R/Carb^R.	This study.
pBBR1MCS4-*tssA1 with tssA3 hairpin*	pBBR1MCS4 encoding *tssA1* (PA0082) with hairpin region (F169-L172) replaced with *tssA3* (PA2360) hairpin region (A174-Q191), Amp^R/Carb^R.	This study.
pBBR1MCS4-*tssA1 with tssA3 hairpin and loop*	pBBR1MCS4 encoding *tssA1* (PA0082) with hairpin (F169-L172) and loop (Q37-E53) regions replaced with *tssA3* (PA2360) hairpin (A174-Q191) and loop (D46-D62) regions, Amp^R/Carb^R.	This study.
pBBR1MCS4-*tssA1 with tssA3 loop*	pBBR1MCS4 encoding *tssA1* (PA0082) with loop region (Q37-E53) replaced with *tssA3* (PA2360) loop region (D46-D62), Amp^R/Carb^R.	This study.
pBBR1MCS4-*tssA3 with tssA1 hairpin*	pBBR1MCS4 encoding *tssA3* (PA2360) with hairpin region (A174-Q191) replaced with *tssA1* (PA0082) hairpin region (F169-L172), Amp^R/Carb^R.	This study.
pBBR1MCS4-*tssA3 with tssA1 hairpin and loop*	pBBR1MCS4 encoding *tssA3* (PA2360) with hairpin (A174-Q191) and loop (D46-D62) regions replaced with *tssA1* (PA0082) hairpin (F169-L172) and loop (Q37-E53) regions, Amp^R/Carb^R.	This study.
pBBR1MCS4-*tssA3 with tssA1 loop*	pBBR1MCS4 encoding *tssA3* (PA2360) with loop region (D46-D62) replaced with *tssA1* (PA0082) loop region (Q37-E53), Amp^R/Carb^R.	This study.
pBBR1MCS4-*tssA2*^{PP}	pBBR1MCS4 encoding *tssA2* (PP4072) of *P. putida,* Amp^R/Carb^R.	This study.
pBBR1MCS4-*tssA3*^{PP}	pBBR1MCS4 encoding *tssA3* (PP2626) of *P. putida*, Amp^R/Carb^R.	This study.
pBBR1MCS4-tssA2$_{Nt1}$-tssA2$^{PP}{}_{Nt2+CTD}$	pBBR1MCS4 encoding *tssA2*$_{Nt1}$ (PA1656) (residues 1-222) *tssA2*$_{Nt2+CTD}$ of *P. putida* (PP4072) (residues 220-488) chimera, Amp^R/Carb^R.	This study.
pBBR1MCS4-tssA2$_{Nt1}$-tssA3$^{PP}{}_{Nt2+CTD}$	pBBR1MCS4 encoding *tssA2*$_{Nt1}$ (PA1656) (residues 1-222) *tssA3*$_{Nt2+CTD}$ of *P. putida* (PP2626) (residues 220-487) chimera, Amp^R/Carb^R.	This study.
pMMB67HE	Broad host range vector, with IPTG inducible P$_{TAC}$ promoter, RSF1010 ori, Amp^R/Carb^R.	(521)
pMMB67HE-*tagJ1*	pMMB67HE encoding *tagJ1* (PA0086), Amp^R/Carb^R.	This study.
pMMB67HE-*amrZ-V5*	pMMB67HE encoding *amrZ* (PA3385) with a C-terminal *V5* tag, Amp^R/Carb^R.	(338)
pME6032	Broad host range vector with IPTG inducible P$_{TAC}$ promoter, P15A ori, Tet^R.	(522)

pME6032-*tssA2*	pME6032 encoding *tssA2* (PA1656), Tet^R.	This study.
pME6032-*FLAG-tssA2*	pME6032 encoding *tssA2* (PA1656) with N-terminal *FLAG* tag, Tet^R.	This study.
pME6032-*tssA3*	pME6032 encoding *tssA3* (PA2360), Tet^R.	This study.
pME6032-*FLAG-tssA3*	pME6032 encoding *tssA3* (PA2360) with N-terminal *FLAG* tag, Tet^R.	This study.
pME6032-*PA2372*	pME6032 encoding *PA2372*, Tet^R.	This study.
pME6032-*FLAG-PA2372*	pME6032 encoding *PA2372* with N-terminal *FLAG* tag, Tet^R.	This study.
pRL662-*GFP*	Broad host range vector producing GFP under a constitutive P_{LAC} promoter, pBBR1 ori, Gm^R.	Laboratory collection, Thomas Wood.
pUCP22-*tssA1promoter-GFPmut3b*	Broad host range vector producing GFPmut3b under the *tssA1* promoter, Gm^R.	Laboratory collection, Marta Rudzite.
***E. coli* expression vectors**		
pET28a	High expression vector with IPTG inducible T7 promoter, pBR322 ori, Km^R.	Novagen
pET28a-*his6-tssA2*	pET28a encoding *his6* tagged *tssA2* (PA1656), Km^R.	This study.
pET28a-*his6-tssA2*$_{1-391}$	Overexpression of *his6* tagged truncated *tssA2* (PA1656) residues 1-391, Km^R.	This study.
pETDuet-1	High expression vector with two multiple cloning sites, both with IPTG inducible T7 promoter, pBR322 ori, Amp^R.	EMD Biosciences
pETDuet-1-*his6-tssA1*	pETDuet-1 encoding full length, N-terminal *his6* tagged *tssA1* (PA0082), Amp^R.	This study.
pETDuet-1-*his6-tssA2*	pETDuet-1 encoding full length, N-terminal *his6* tagged *tssA2* (PA1656), Amp^R.	This study.
pETDuet-1-*his6-tssA3*	pETDuet-1 encoding full length, N-terminal *his6* tagged *tssA3* (PA2360), Amp^R.	This study.
pETDuet-*Strep-tssA1*	pETDuet-1 encoding N-terminal *Strep* tagged *tssA1* (PA0082), Amp^R.	This study.
pETDuet-*Strep-tssA2*	pETDuet-1 encoding N-terminal *Strep* tagged *tssA2* (PA1656), Amp^R.	This study.
pETDuet-*Strep-tssA3*	pETDuet-1 encoding N-terminal *Strep* tagged *tssA3* (PA2360), Amp^R.	This study.
pETDuet-1-*Strep-tssA1*$_{CTD}$	pETDuet-1 encoding N-terminal *Strep* tagged *tssA1*$_{CTD}$ (PA0082) residues 275-344, Amp^R.	This study.
pETDuet-1-*Strep-tssA2*$_{Nt2+CTD}$	pETDuet-1 encoding N-terminal *Strep* tagged *tssA2*$_{Nt2+CTD}$ (PA1656) residues 223-518, Amp^R.	This study.
pETDuet-1-*Strep-tssA2*$_{CTD}$	pETDuet-1 encoding N-terminal *Strep* tagged *tssA2*$_{CTD}$ (PA1656) residues 386-518, Amp^R.	This study.
pETDuet-1-*Strep-tssA3*$_{CTD}$	pETDuet-1 encoding N-terminal *Strep* tagged *tssA3*$_{CTD}$ (PA2360) residues 296-366, Amp^R.	This study.

2.2.2 KOD PCR

For the construction of plasmids, PAO1 genomic DNA was amplified by PCR using the KOD Hot Start polymerase (Merck). The 50 µl reaction mix contained 60 ng of genomic DNA as the template with 1 µl KOD polymerase, 5 µl 10x KOD Hot Start buffer (Merck), 2 µl of each primer, 10 µl betaine solution (Sigma Aldrich), 100 µM of dNTP mix (Merck), 1.5 mM magnesium sulfate and ddH_2O. The primers used for this work were manufactured by Sigma Aldrich and are presented in Table 2.4. Primers typically contained restriction enzyme recognition sites at the 5' end, to allow for subsequent restriction enzyme digestion and ligation of purified PCR products. The annealing temperature of primers was typically designed to be between 55-64 °C, and the PCR cycling conditions followed the manufacturers specifications for optimal KOD polymerase activity.

Following the PCR, the reaction mix was analysed by electrophoresis on 1% (w/v) Tris-acetate-EDTA (TAE) agarose gel with the Quick-Load® Purple 1 kb Plus DNA Ladder (NEB) as a molecular weight marker. 2 % (w/v) TAE agarose gels were occasionally used for the resolution of DNA fragments smaller than 500 bp. The gel was imaged using the Bio-Rad ChemiDoc XRS+.

DNA fragments of the correct size were purified either directly from the reaction mix using the QIAquick® PCR Purification Kit (QIAgen) or via a band excised from a TAE agarose gel using the QIAquick® Gel Extraction Kit (QIAgen). Purified DNA fragments were either used for blunt-end ligation into the pCR®-Blunt II-TOPO® (Invitrogen) cloning vector following the manufacturers protocol, or subject to restriction enzyme digestion and sticky-end ligation.

Table 2.4 Primers used in this study

Construct	Code	Primer name	Sequence
Vector screening primers			
pBBR1MCS4 and pCR®-Blunt II-TOPO®	OAL684	M13F	TGTAAAACGACGGCCAGT
	OAL685	M13R	CAGGAAACAGCTATGACC
pKT25	OAL193	T25F	GTGACCAGCGGCGATTCGGTGACCGATTAC
	OAL192	T25R	TGGCGAAAGGGGGATGTGCTGCAAGGCGAT
pKNT25	OAL1567	NT25F	TGTGGAATTGTGAGCGGATA
	OAL1568	NT25R	GTAACCAGCCTGATGCGATT
pUT18	OAL1876	T18F	ATGCTTCCGGCTCGTATGTTGTG
	OAL1877	T18R	TTTCCACAACAAGTCGATGCGTT
pUT18C	OAL190	T18CF	GAAGTTCTCGCCGGATGTACTGGAAACGGT
	OAL191	T18CR	TTGGCGGGTGTCGGGGCTGGCTTAACTATG
pMMB67HE	OAL2452	MMB67F	TGGTATGGCTGTGCAGGTCGTAA
	OAL2453	MMB67R	TCAGACCGCTTCTGCGTTCTGAT
pKNG101	OAL682	Rpkn	CATATCACAACGTGCGTGGA

	OAL683	Upkn	CCCTGGATTTCACTGATGAG
pET28a	OAL517	T7 promoter	TAATACGACTCACTATAGGG
	OAL518	T7 terminator	GCTAGTTATTGCTCAGCGG
pETDuet-1 (MCS1)	OAL1279	DuetUP1	GGATCTCGACGCTCTCCCT
	OAL1280	DuetDOWN1	GATTATGCGGCCGTGTACAA
pME6032	OAL4786	pME6032F	GCGCACTCCCGTTCTGGATAATG
	OAL4787	pME6032R	GCTCTCGGGTAACATCAAGGCC
***P. aeruginosa* mutator construction primers**			
pKNG101-Δ*tssA1*	OAL4929	Δ*tssA1* P1	ATATTTCTAGAGTTGGTGCTGGTGTCGGTGAGGTAGTAC
	OAL4930	Δ*tssA1* P2	TTACTCGCTATCCAGCACGGTGACGATCTCCC
	OAL4931	Δ*tssA1* P3	GTGCTGGAAAGCGAGTAACGCCTAGCGG
	OAL4932	Δ*tssA1* P4	AATAAGGATCCTTGCCGTCCATGTAGGTCAGCAGG
pKNG101-Δ*tssA2*	OAL5442	Δ*tssA2* P1	TGCCTTCTAGAAACAAGTGAATTGAGCAAGAAGTTGCGCA
	OAL5443	Δ*tssA2* P2	CTATTCGAGATAGGTCATCCTAACCCTTCAATGCACACC
	OAL5444	Δ*tssA2* P3	ATGACCTATCTCGAATAGGGCTTCGCGCCC
	OAL5198	*tssA2* truncation P4	ATATAGGATCCCCCAGCTCGCCCAGCACACG
pKNG101-Δ*tssA3*	OAL5445	Δ*tssA3* P1	ATATGTCTAGAAGCCGCACCACCTCGCGTTCCTGC
	OAL5446	Δ*tssA3* P2	ATGACCCTGCTGCCCTAGGAGGCGTGGCTATATCTTT
	OAL5447	Δ*tssA3* P3	CTAGGGCAGCAGGGTCATGGGGTACCTCCGGTGC
	OAL5448	Δ*tssA3* P4	TATTAGGATCCCTGCTCGGCGTCGCCCTGGACATCG
pKNG101-*GFP-tssA1*	OAL4896	*GFP-tssA1* P1	TATATTCTAGATGGCGGCTGGAGACCAGG
	OAL4897	*GFP-tssA1* P2	TTTACGCATGGTGACGATCTCCCTATCATC
	OAL4898	*GFP-tssA1* P3	ATCGTCACCATGCGTAAAGGCGAAGAACTGTTCACGG
	OAL4767	*GFP-tssA1* P4	TCCTCCTCCTGCTGCTGCCTTATACAGCTCGTCCAT
	OAL4899	*GFP-tssA1* P5	GCAGCAGCAGGAGGAGGACTGGATGTACCCGTTTTGCTGGC
	OAL4900	*GFP-tssA1* P6	TTATAGGATCCATCTGCTCGGGACTCAGGGTC
pKNG101-*tagJ1-GFP*	OAL4921	*tagJ1-GFP* P1	AAAAATCTAGAGCCGATGGTACAGACCTACTCCACCG
	OAL4922	*tagJ1-GFP* P2	TGCTGCTGCGGCGTCCGTCGGCTCGAAGTCC
	OAL4923	*tagJ1-GFP* P3	CCGACGGACGCCGCAGCAGCAGGAGGAGGA
	OAL4924	*tagJ1-GFP* P4	CGCAGGTCGAACTTACTTATACAGCTCGTCCATACCG
	OAL4925	*tagJ1-GFP* P5	TATAAGTAAGTTCGACCTGCGTGAACTGGACTTCGAGC
	OAL4926	*tagJ1-GFP* P6	TATAAGGATCCGCCGGTCTCCAGGTCCAGGTTG
pKNG101-$tssA2_{1-391}$	OAL5195	*tssA2* truncation P1	ATAAATCTAGACCATCGACAACGAGCGCGACGCC
	OAL5196	*tssA2* truncation P2	GAAGCCCTACACGGTCTCGACCTTGCGCGGC
	OAL5197	*tssA2* truncation P3	GAGACCGTGTAGGGCTTCGCGCCCTCAATTCTC

	OAL5198	*tssA2* truncation P4	ATATAGGATCCCCCAGCTCGCCCAGCACACG
pKNG101-*tssB1-mScarlet-I*	OAL5339	*tssB1-mScarlet-I* P1	TAATAAGGATCCAGGGAGAAACAAGATGGGAAGCA
	OAL5340	*tssB1-mScarlet-I* P2	TGCTGCTGCCGCCTGCGGCTCGTCGTCTTT
	OAL5341	*tssB1-mScarlet-I* P3	CCGCAGGCGGCAGCAGCAGGAGGAGGA
	OAL5342	*tssB1-mScarlet-I* P4	GGAATCCTCTTACGAACCCTTATACAGTTCGTCCAT
	OAL5343	*tssB1-mScarlet-I* P5	GGTTCGTAAGAGGATTCCAGCATGGCCGA
	OAL5344	*tssB1-mScarlet-I* P6	TAATAAGGGCCCGCCGAACTGGCCGTATTCCTCTTC
pKNG101-*tssB2-mScarlet-I*	OAL5197	tssA2 truncation P3	GAGACCGTGTAGGGCTTCGCGCCCTCAATTCTC
	OAL6424	*tssB2-mScarlet-I* P2	TGCTGCTGCGGCGTCCTGGGAGGGGGCGGC
	OAL6425	*tssB2-mScarlet-I* P3	CAGGACGCCGCAGCAGCAGGAGGAGGA
	OAL6426	*tssB2-mScarlet-I* P4	GGGGGTGGCTCACGAACCCTTATACAGTTCGTCCATGCCGC
	OAL6427	*tssB2-mScarlet-I* P5	GGTTCGTGAGCCACCCCCTAGCCAAGGAAG
	OAL6428	*tssB2-mScarlet-I* P6	TAATTCGATGATGGCGCCGACCGGCTG
pKNG101-*tssB3-mScarlet-I*	OAL6429	*tssB3-mScarlet-I* P1	ATATTCATTGCATCGGAGTCAGCCGCCATGGCCGAG
	OAL6430	*tssB3-mScarlet-I* P2	TGCTGCTGCGGCCGGCTGGTCGGCCGGGGG
	OAL5273	*tssB3-mScarlet-I* P3	CAGCCGGCCGCAGCAGCAGGAGGAGGA
	OAL6431	*tssB3-mScarlet-I* P4	GAAGAGGGTCACGAACCCTTATACAGTTCGTCCATGCCGCC
	OAL6432	*tssB3-mScarlet-I* P5	GGTTCGTGACCCTCTTCCCGGAGAAGCCG
	OAL6433	*tssB3-mScarlet-I* P6	TATATAGGCCGATGTCCTGCGGATGGCGACCG
pKNG101-*tssB1-GFP*	OAL4283	*tssB1-GFP* P1	GGGAAGCACTACCAGCAGTCAGAAGTTCAT
	OAL4296	*tssB1-GFP* P2	CCTGCTGCTGCCGCCTGCGG
	OAL1686	*tssB1-GFP* P3	GCAGCAGCAGGAGGAGGAATGCGTAAAGGCGAAGAA
	OAL4294	*tssB1-GFP* P4	ATCCTCTCATTACTTATACAGCTCGTCCAT
	OAL4293	*tssB1-GFP* P5	TAATGAGAGGATTCCAGCATGGCCGAATTGAG
	OAL4288	*tssB1-GFP* P6	GTAGTAGTCGCCGACCAGGCAGCC
pKNG101-*mScarlet-I-tssA1*	OAL4896	*GFP-tssA1* P1	TATATTCTAGATGGCGGCTGGAGACCAGG
	OAL6731	*mScarlet-I-tssA1* P2	GCTAACCATGGCAGCCAGCAAAACGGGTAC
	OAL6732	*mScarlet-I-tssA1* P3	CTGGCTGCCATGGTTAGCAAAGGCGAGGCG

	OAL6733	*mScarlet-I-tssA1* P4	ATCCAGCACTCCTCCTCCTGCTGCTGCGGATCCCTTATACAGTTCGTCCATGCC
	OAL6734	*mScarlet-I-tssA1* P5	GGAGGAGGAGTGCTGGATGTACCCGTTTTGCTG
	OAL4900	*GFP-tssA1* P6	TTATAGGATCCATCTGCTCGGGACTCAGGGTC
pKNG101-*GFP-tssA1*	OAL4896	*GFP-tssA1* P1	TATATTCTAGATGGCGGCTGGAGACCAGG
	OAL4897	*GFP-tssA1* P2	TTTACGCATGGTGACGATCTCCCTATCATC
	OAL4898	*GFP-tssA1* P3	ATCGTCACCATGCGTAAAGGCGAAGAACTGTTCACGG
	OAL4767	*GFP-tssA1* P4	TCCTCCTCCTGCTGCTGCCTTATACAGCTCGTCCAT
	OAL4899	*GFP-tssA1* P5	GCAGCAGCAGGAGGAGGACTGGATGTACCCGTTTTGCTGGC
	OAL4900	*GFP-tssA1* P6	TTATAGGATCCATCTGCTCGGGACTCAGGGTC
pKNG101-Δ*tagJ1*$_{50-230}$	OAL6289	*tagJ1* Δ51-229 P1	ACTGTGGATCCGAGTACCTGATCATCACCCTGAAGGAAGTCC
	OAL6290	*tagJ1* Δ51-229 P2	GACGGTTTCAGCGTTCGACGGCTGGCTGCGCACC
	OAL6291	*tagJ1* Δ51-229 P3	CGAACGCTGAAACCGTCGAGCACGGCGACGAC
	OAL6292	*tagJ1* Δ51-229 P4	GCGGTTCTAGAGTCTCCAGGTCCAGGTTGGTGGTCAGC
pKNG101-Δ*H1-T6SS*	OAL862	Δ*H1-T6SS* P1	ATGGTCAACGACATGGAGCTGGAG
	OAL863	Δ*H1-T6SS* P2	TCAGTTCTGAAGGCCTGATCGGCCTCG
	OAL864	Δ*H1-T6SS* P3	TCAGGCCTTCAGAACTGAAGCGGCGCA
	OAL865	Δ*H1-T6SS* P4	GGTGGCGTTCAACAGTTCCATGTC
pKNG101-Δ*rsmN*	OAL3239	Δ*rsmN* P1	ATGATGGGCCCGCTCCAGGTTGAGCTGATTGAGGC
	OAL3240	Δ*rsmN* P2	CAACTCGTCGAAACCCATGTTCCGCGT
	OAL3241	Δ*rsmN* P3	ATGGGTTTCGACGAGTTGAAGACGGCACCG
	OAL3242	Δ*rsmN* P4	ATCATGGATCCTAATCGCGTTCGGCCTGCTG
***P. aeruginosa* chromosomal mutagenesis screening primers**			
tssA1	OAL872	*tssA1* exF	AAGTCGAACAGGTCGGGCTTGGTGT
	OAL873	*tssA1* exR	ATCGACTTGATCGCGTCGTTGGAGAT
tssA2	OAL3437	*tssA2* exF	TCTCTGTCGTCGCCGTACGC
	OAL3438	*tssA2* exR	AGCGCCTGGAAATCGGGATG
tssA3	OAL5514	*tssA3* exF	GGCTCGCGCTGGTGTAGC
	OAL5515	*tssA3* exR	CCAGGACAGTGCCGAGCTG
tssB1	OAL4289	*tssB1* exF	CGCCAACCGCGAAGACGTCCT
	OAL4290	*tssB1* exR	CTTCCTTCAGGGTGATGATCAGGTACT
tssB2	OAL1594	*tssB2* exF	CAGGCGATGCGGGAAGTCGAAA
	OAL1595	*tssB2* exR	TCTGCCACTTGGCGAACTGC
tssB3	OAL5277	*tssB3* exF	TCCGTGCTTCATGGGAGTCC
	OAL5278	*tssB3* exR	TCGAACAGGCGTGGGCTG
tagJ1	242	*tagJ1* exF	CCTGAGGCATTCAACGACAG
	243	*tagJ1* exR	ACAGGTTGTGGGTGAAGGTC
H1-T6SS	OAL866	*H1-T6SS* exF	ATCAGCCTGACCACCCTCGACGAC
	OAL867	*H1-T6SS* exR	AGAACGGCTTGAAGGGAACGAACT
rsmN	OAL3243	*rsmN* exF	CGGCCCAGTGACAGAGATCG

	OAL3244	*rsmN* exR	TGATGGTCCGGCCTTTGTGC
retS	OAL1897	*retS* exF	GAGGAGGCCAGCTTCATCGTCATG
	OAL1898	*retS* exR	TGCTGCACGTTGTCGCTCTG
H3-T6SS	OAL1006	*H3-T6SS* exF	AACTGCTGCCGGTAGTCGCGGCGGTAC
	OAL1007	*H3-T6SS* exR	CTGACAGTTCCCCTGCCGTTAACGCCG
Bacterial two-hybrid primers			
pKT25 and pUT18C-*tssA1*$_{Nt1}$	OAL839	PA0082 BTH F	GCTCTAGAGGTGCTGGATGTACCCGTT
	OAL6544	*tssA1* Nt1 BTH R	ATATAGGATCCTTAGCCGTACAGGTCGAACAC
pKT25 and pUT18C-*tssA1*$_{CTD}$	OAL6545	*tssA1* CTD BTH F	TATTATCTAGAGATCGCCAACCGCGAAG
	OAL840	PA0082 BTH R	GGGGTACCTTACTCGCTTTCCGGGCC
pKT25 and pUT18C-*tssB1tssC1*	194	BTH *tssB1* F	GCTCTAGAGATGGGAAGCACTACCAGCAGTCAG
	197	BTH *tssC1* R	GGGGTACCGCTGTCGTTGAATGCCTCAGGCCTC
pKT25 and pUT18C-*tssA2*	OAL5524	BTH *tssA2* F	TAAATTCTAGAGATGACCTATTCGAGCAAGCTCTCC
	OAL5525	BTH *tssA2* R	TATAAGGATCCCCCTATTCGAGCACCACCTCG
pKT25 and pUT18C-*tssA2*$_{Nt1}$	OAL5524	BTH *tssA2* F	TAAATTCTAGAGATGACCTATTCGAGCAAGCTCTCC
	OAL6537	BTH *tssA2* Nt1 R	TATATGGATCCTTACTGGTTGTCGGCGGCGCG
pKT25 and pUT18C-*tssA2*$_{Nt2+CTD}$	OAL6538	BTH *tssA2* Nt2+CTD F	TTAATTCTAGACGCCCACAAGGCCATG
	OAL5525	BTH *tssA2* R	TATAAGGATCCCCCTATTCGAGCACCACCTCG
pKT25 and pUT18C-*tssA3*	OAL5526	BTH *tssA3* F	ATTTATCTAGAGATGACCCTGCCTCTTTCCGG
	OAL5527	BTH *tssA3* R	TATAAGGATCCTCCTAGGGCAGTACGCC
pKT25 and pUT18C-*tssA3*$_{Nt1}$	OAL5526	BTH *tssA3* F	ATTTATCTAGAGATGACCCTGCCTCTTTCCGG
	OAL6539	BTH *tssA3* Nt1 R	TTATAGGATCCTTAGTGCATGGCGATGAACTCCTTG
pKT25 and pUT18C-*tssA3*$_{CTD}$	OAL6540	BTH *tssA3* CTD F	ATATATCTAGAGCCGGCTGGCGCGCCGAC
	OAL5527	BTH *tssA3* R	TATAAGGATCCTCCTAGGGCAGTACGCC
pKT25 and pUT18C-*PA2372*	OAL6191	BTH *PA2372* F	GGGCCTCTAGAGAACTATTTATTCGTGCCATTCACAAG
	OAL6192	BTH *PA2372* R	ACTAAGAATTCTAAGGTACTCTCTGTCTTGCTTCC
pKT25-*tssA1*$_{Nt1}$-*tssA2*$_{CTD}$	OAL839	PA0082 BTH F	GCTCTAGAGGTGCTGGATGTACCCGTT
	OAL6703	*A1* Nt1 - *A2* CTD *A1* R	GGTCTCGACGGCTCGCGGTGCCGGCGC
	OAL6704	*A1* Nt1 - *A2* CTD *A2* F	CCGCGAGCCGTCGAGACCGTGGCCCTG
	OAL5525	BTH *tssA2* R	TATAAGGATCCCCCTATTCGAGCACCACCTCG
pKT25-*tssA1*$_{Nt1}$-*tssA2*$_{Nt2+CTD}$	OAL839	PA0082 BTH F	GCTCTAGAGGTGCTGGATGTACCCGTT
	OAL6807	*A1* Nt1 - *A2* Nt2+CTD *A1* R 2	CATGGCCTTGTGGGCGTCGGCTCGCGGTGCCGGCGC
	OAL6808	*A1* Nt1 - *A2* Nt2+CTD *A2* F 2	GCGCCGGCACCGCGAGCCGACGCCCACAAGGCCATG
	OAL5525	BTH *tssA2* R	TATAAGGATCCCCCTATTCGAGCACCACCTCG
pKT25-*tssA1*$_{Nt1}$-*tssA3*$_{CTD}$	OAL839	PA0082 BTH F	GCTCTAGAGGTGCTGGATGTACCCGTT
	OAL6648	*A1* Nt1 - *A3* CTD *A1* R	GCCAGCCGGGGCTCGCGGTGCCGGCGC

	OAL6649	*A1* Nt1 - *A3* CTD *A3* F	CCGCGAGCCCCGGCTGGCGCGCCGACC
	OAL5527	BTH *tssA3* R	TATAAGGATCCTCCTAGGGCAGTACGCC
pKT25-*tssA2*$_{Nt1}$-*tssA1*$_{CTD}$	OAL5524	BTH *tssA2* F	TAAATTCTAGAGATGACCTATTCGAGCAAGCTCTCC
	OAL6652	*A2* Nt1 - *A1* CTD *A2* R	CAAGGACTCTTCGGGCTGGTTGTCGGC
	OAL6653	*A2* Nt1 - *A1* CTD *A1* F	CAGCCCGAAGAGTCCTTGGCGCCGGGTGCC
	OAL840	PA0082 BTH R	GGGGTACCTTACTCGCTTTCCGGGCC
pKT25-*tssA2*$_{Nt1}$-*tssA3*$_{CTD}$	OAL5524	BTH *tssA2* F	TAAATTCTAGAGATGACCTATTCGAGCAAGCTCTCC
	OAL6707	*A2* Nt1 - *A3* CTD *A2* R	GCCAGCCGGGTCGCGCTCGTTGTCGAT
	OAL6708	*A2* Nt1 - *A3* CTD A3 F	GAGCGCGACCCGGCTGGCGCGCCGACC
	OAL5527	BTH *tssA3* R	TATAAGGATCCTCCTAGGGCAGTACGCC
pKT25-*tssA3*$_{Nt1}$-*tssA1*$_{CTD}$	OAL5526	BTH *tssA3* F	ATTTATCTAGAGATGACCCTGCCTCTTTCCGG
	OAL6849	*A3* Nt1 - *A1* CTD *A3* R 2	GCTGGCTCGCCCGCTCGGCGCGCTCG
	OAL6850	*A3* Nt1 - *A1* CTD *A1* F 2	GCCGAGCGGGCGAGCCAGCGGCGAGATCGCC
	OAL840	PA0082 BTH R	GGGGTACCTTACTCGCTTTCCGGGCC
pKT25-*tssA3*$_{Nt1}$-*tssA2*$_{CTD}$	OAL5526	BTH *tssA3* F	ATTTATCTAGAGATGACCCTGCCTCTTTCCGG
	OAL6709	*A3* Nt1 - *A2* CTD *A3* R	GGGCATGACTTGCGGGTGCATGGCGAT
	OAL6710	*A3* Nt1 - *A2* CTD *A2* F	CACCCGCAAGTCATGCCCCATCTCCAG
	OAL5525	BTH *tssA2* R	TATAAGGATCCCCCTATTCGAGCACCACCTCG
pKT25-*tssA3*$_{Nt1}$-*tssA2*$_{Nt2+CTD}$	OAL5526	BTH *tssA3* F	ATTTATCTAGAGATGACCCTGCCTCTTTCCGG
	OAL6711	*A3* Nt1 - *A2* Nt2+CTD *A3* R	GCCAGGTTCTTGCGGGTGCATGGCGAT
	OAL6712	*A3* Nt1 - *A2* Nt2+CTD *A2* F	CACCCGCAAGAACCTGGCGTGGTCGGC
	OAL5525	BTH *tssA2* R	TATAAGGATCCCCCTATTCGAGCACCACCTCG
pKT25-*tssA1 with tssA3 loop*	OAL839	PA0082 BTH F	GCTCTAGAGGTGCTGGATGTACCCGTT
	OAL6819	*A1* with *A3* hairpin R	GGGACTCTGAAGTTGCGCCGCTTCCAGCGCCGCCT TGGCGCTCTTGCTGTCGCCGCTGGCGCGTTGCAGC CCGGCGGCGTTC
	OAL6823	*A1* with *A3* hairpin F 2	GAAGCGGCGCAACTTCAGAGTCCCGAGCAGATCGC CGGCG
	OAL840	PA0082 BTH R	GGGGTACCTTACTCGCTTTCCGGGCC
pKT25-*tssA1 with tssA3 hairpin*	OAL839	PA0082 BTH F	GCTCTAGAGGTGCTGGATGTACCCGTT
	OAL6821	*A1* with *A3* loop R	CGGCCAGTCGGCGCGCTTGGCCTCCGCTTGCCAGA CGCCGGTCGGCAGGCTGCTGTCGCCCTGGGCGATG CGTTCGAGTTCGAG
	OAL6822	*A1* with *A3* loop F	AAGCGCGCCGACTGGCCGCGCGTACGCGCGCTG
	OAL840	PA0082 BTH R	GGGGTACCTTACTCGCTTTCCGGGCC
	OAL5526	BTH *tssA3* F	ATTTATCTAGAGATGACCCTGCCTCTTTCCGG

pKT25-*tssA3 with tssA1 loop*	OAL6847	*A3* with *A1* loop R	GCAGCACGGCATCGCCCATCTGGCGCTCGGGTTGGTCCTCCCGGCGCAACTCGCG
	OAL6848	*A3* with *A1* loop F	CAGATGGGCGATGCCGTGCTGCCCGCCGAGCCGCCGGAGTGGGCCGCGGTGGAGCAGTTG
	OAL5527	BTH *tssA3* R	TATAAGGATCCTCCTAGGGCAGTACGCC
pKT25-*tssA3 with tssA1 hairpin*	OAL5526	BTH *tssA3* F	ATTTATCTAGAGATGACCCTGCCTCTTTCCGG
	OAL6845	*A3* with *A1* hairpin R	CAGGGTCTCGCTGGCGAAGACCTGCTGGCGCTGCAACCTCTG
	OAL6846	*A3* with *A1* hairpin F	CAGGTCTTCGCCAGCGAGACCCTGCAGAAGAAGCTAGACGAAGCGTTGCGCG
	OAL5527	BTH *tssA3* R	TATAAGGATCCTCCTAGGGCAGTACGCC
pKNT25 and pUT18-*tssA1*	OAL6337	BTH *tssA1* C-tag F	ATATATCTAGAGCGTGCTGGATGTACCCGTT
	OAL6338	BTH *tssA1* C-tag R	AATTAGGATCCTCCTCGCTTTCCGGGC
pKNT25 and pUT18-*tssB1*	OAL6339	BTH *tssB1* C-tag F	TATATTCTAGAAGATGGGAAGCACTACCAGCAGTCAG
	OAL6340	BTH *tssB1* C-tag R	ATTAAGGATCCTCCGCCTGCGGCTCGTCG
pKNT25 and pUT18-*tssC1*	OAL6341	BTH *tssC1* C-tag F	ATATTTCTAGAAGGCGTAAGAGGATTCCAGCATGGCC
	OAL6342	BTH *tssC1* C-tag R	TAATTGGTACCCGGGCCTCTTTGGCCGAAGGCAG
pKNT25 and pUT18-*tssB1tssC1*	OAL6339	BTH *tssB1* C-tag F	TATATTCTAGAAGATGGGAAGCACTACCAGCAGTCAG
	OAL6342	BTH *tssC1* C-tag R	TAATTGGTACCCGGGCCTCTTTGGCCGAAGGCAG
pKNT25 and pUT18-*tssE1*	OAL6343	BTH *tssE1* C-tag F	ATATATCTAGAACATGGCCGAACTGACCCTCCAG
	OAL6344	BTH *tssE1* C-tag R	ATATAGGATCCTCTGTACGCCTCCGCTCGCC
pKNT25 and pUT18-*tssF1*	OAL6345	BTH *tssF1* C-tag F	TTATATCTAGAACATGAACCCGCGCCTGCTC
	OAL6346	BTH *tssF1* C-tag R	ATATAGGATCCTCGAGGTTCGGACGGCTGCCC
pKNT25 and pUT18-*tssG1*	OAL6347	BTH *tssG1* C-tag F	ATATATCTAGAAGATGGCAGGCGAAGCCGGG
	OAL6348	BTH *tssG1* C-tag R	ATATAGGATCCTCCTCATGTTCCTTCTCCTTGTGCTCGTGCG
pKNT25 and pUT18-*tssK1*	OAL6349	BTH *tssK1* C-tag F	TAATATCTAGACTATGTCCTGGAATAACCGCG
	OAL6350	BTH *tssK1* C-tag R	ATTAAGGATCCTCTCCTCGAATGGCCCAGAAG
pKNT25 and pUT18-*PA2372*	OAL6623	BTH *PA2372* C-tag F	ATATTTCTAGAATGAACTATTTATTCGTGCCATTCACA
	OAL6624	BTH *PA2372* C-tag R	ATTTAGAATTCGAAGGTACTCTCTGTCTTGCTTCC
pUT18C-*tssL1*	OAL6353	BTH *tssL1* F	ATTTATCTAGAGCCTCCCATCGACGATCCCTT
	OAL6355	BTH *tssL1* R	TAATTGGATCCTCTTGCGCGCCCTCCGCGAAT
	OAL6356	BTH *tssM1* F	ATATTTCTAGAGCAGAGTCTCGCCGAGGTCAG

pUT18C-*tssM1*$_{cyt}$	OAL6554	BTH *tssM1*$_{cyt}$ R	ATATAGGATCCTCACTTGCGGCGGCGCTCG
pUT18C-*tssB2tssC2*	OAL655	PKT25 B2 F	GCTCTAGAGATGGCCAAAGAAGGCTCG
	OAL658	PKT25 C2 R	CGGAATTCTTACTCTTTGTCCAGCTT
pUT18C-*tssE2*	OAL6469	BTH *tssE*2 F	TTAAATCTAGAGACTGGATACGGCAGCCTGTTC
	OAL6470	BTH *tssE2* R	AATTTGGATCCCCTCCTTAGCTGACCTTCACCTG
pUT18C-*tssF2*	OAL6471	BTH *tssF2* F	TTATTTCTAGAGATGCACCTGCTGTGGCC
	OAL6472	BTH *tssF2* R	ATATAGGATCCGCGCTTACAGCAGGGGC
pUT18C-*tssG2*	OAL6473	BTH *tssG2* F	ATATATCTAGAGGAAACCGCGCATGGGTTTG
	OAL6474	BTH *tssG2* R	ATAAAGGATCCCCTTAATGAATCTTGCTGCCCAGC
pUT18C-*tssK2*	OAL6069	BTH *tssK2* F	AGAGATCTAGAGATGAACGTGCACAAGATCGTCTGG
	OAL6070	BTH *tssK2* R	GAGAGGAATTCGTTCAGTTCCTGATGGCCCAG
pUT18C-*vgrG2a*	OAL6475	BTH *vgrG2a* F	ATATAGGATCCTCGCTGCTCATGTGTTGGAC
	OAL6476	BTH *vgrG2a* R	TATTTATCTAGAGCGTCAAAGGGACCTGAAATTC
pUT18C-*vgrG2b*	OAL6477	BTH *vgrG2b* F	TATATTCTAGACGTGAGCAGCGGGTCTACC
	OAL6478	BTH *vgrG2b* R	ATAAAGGATCCGGTGGCCCTAGGATTCGTTTGAG
pUT18C-*vgrG4a*	OAL6479	BTH *vgrG4a* F	ATTATTCTAGAGTTCAACCCGGCCAACCAG
	OAL6480	BTH *vgrG4a* R	ATATAGGATCCGCGGTTCCTCAGCGCTC
pUT18C-*vgrG4b*	OAL6481	BTH *vgrG4b* F	ATTTTTCTAGAGTTCAACCCGGCCAACCAG
	OAL6482	BTH *vgrG4b* R	ATTAAGGATCCCAACATGGATCAGTCCTTGGCC
pUT18C-*tssL2*	OAL6559	BTH *tssL2* F	ATTTATCTAGAGATCAAGGAAAGGGAATACCACGAG
	OAL6560	BTH *tssL2* R	ATATAGGATCCTTACGAACCGGGCTGTCCTG
pUT18C-*tssM2*$_{cyt}$	OAL6555	BTH *tssM2* F	ATTTATCTAGAGAAAAACTTCTTCAAGAAAGTCGGCG
	OAL6556	BTH *tssM2*$_{cyt}$ R	ATATAGGATCCTCAGCGCTGGCCCCAGTGGATG
pUT18C-*tssB3*	OAL6295	BTH *tssB3* F	ATTATTCTAGACATGGCCGAGAGTACGCAG
	OAL6296	BTH *tssB3* R	ATTAAGGATCCGAAGAGGGTCAGGCCGGC
pUT18C-*tssC3*	OAL6483	BTH *tssC3* F	ATTTATCTAGAGCCCAAGTCATCCGCCGC
	OAL6484	BTH *tssC3* R	ATAATGGATCCCGGACTCACGCCGCTACC
pUT18C-*tssB3tssC3*	OAL6295	BTH *tssB3* F	ATTATTCTAGACATGGCCGAGAGTACGCAG
	OAL6484	BTH *tssC3* R	ATAATGGATCCCGGACTCACGCCGCTACC
pUT18C-*tssE3*	OAL6485	BTH *tssE3* F	ATATATCTAGAGTCCGGAGCCCTGCCGCC
	OAL6486	BTH *tssE3* R	ATTTAGGATCCAGGTCGGCATCAATCGAATCGCTC
pUT18C-*tssF3*	OAL6487	BTH *tssF3* F	TTAAATCTAGAGAGCGATTCGATTGATGCCGAC
	OAL6488	BTH *tssF3* R	AAATAGGATCCCCGCTGACTCAGAGGGAGAG
pUT18C-*tssG3*	OAL6489	BTH *tssG3* F	ATATTTCTAGAGGCAACCCCAGGCCGGCTC
	OAL6490	BTH *tssG3* R	ATATAGGATCCTCCATTTCAGGCTACCTCCGGCTG
pUT18C-*tssK3*	OAL6297	BTH *tssK3* F	TTATATCTAGATATGAGTGTTCTGCCTGACGCG
	OAL6298	BTH *tssK3* R	ATATAGGATCCTGTCTAGGTGTTGTCGCTG
pUT18C-*tssL3*	OAL6561	BTH *tssL3* F	ATATATCTAGAGCCCGAAGGGAGTGCAGGG
	OAL6562	BTH *tssL3* R	ATATAGGATCCTCATGGCGCCTGCTCCGC
pUT18C-*tssM3*$_{cyt}$	OAL6557	BTH *tssM3* F	ATTTATCTAGAGAGCGGCGCGACGCTGTTC
	OAL6558	BTH *tssM3*$_{cyt}$ R	ATATACCCGGGTCACCCGCGCTGCCAGCGCTG

***P. aeruginosa* expression construct primers**			
pBBR1MCS4-*tssA1*	OAL5546	pBBR-*tssA1* F	TAATAGTCGACAGGTGAGGGCCGCGCAGCGG
	OAL5548	pBBR-*tssA1* R	ATAATGGATCCTTACTCGCTTTCCGGGCCTCGCAG
pBBR1MCS4-*tssA2*	OAL5549	pBBR-*tssA2* F	ATTAAGTCGACGTTAAGATATTCATTGGCGCACATGGTG
	OAL5551	pBBR-*tssA2* R	ATATAGGATCCCTATTCGAGCACCACCTCGAGATC
pBBR1MCS4-*tssA3*	OAL5552	pBBR-*tssA3* F	ATTATGTCGACCGCGACGCTGTTGCCGGCCAC
	OAL5554	pBBR-*tssA3* R	TTAATGGATCCCTAGGGCAGTACGCCAAGCAGCGA
pBBR1MCS4-$tssA1_{Nt1}$-$tssA2_{CTD}$	OAL5546	pBBR-*tssA1* F	TAATAGTCGACAGGTGAGGGCCGCGCAGCGG
	OAL6703	*A1* Nt1 - *A2* CTD *A1* R	GGTCTCGACGGCTCGCGGTGCCGGCGC
	OAL6704	*A1* Nt1 - *A2* CTD *A2* F	CCGCGAGCCGTCGAGACCGTGGCCCTG
	OAL5551	pBBR-*tssA2* R	ATATAGGATCCCTATTCGAGCACCACCTCGAGATC
pBBR1MCS4-$tssA1_{Nt1}$-$tssA2_{Nt2+CTD}$	OAL5546	pBBR-*tssA1* F	TAATAGTCGACAGGTGAGGGCCGCGCAGCGG
	OAL6807	*A1* Nt1 - *A2* Nt2+CTD *A1* R 2	CATGGCCTTGTGGGCGTCGGCTCGCGGTGCCGGCGC
	OAL6808	*A1* Nt1 - *A2* Nt2+CTD *A2* F 2	GCGCCGGCACCGCGAGCCGACGCCCACAAGGCCATG
	OAL5551	pBBR-*tssA2* R	ATATAGGATCCCTATTCGAGCACCACCTCGAGATC
pBBR1MCS4-$tssA1_{Nt1}$-$tssA3_{CTD}$	OAL5546	pBBR-*tssA1* F	TAATAGTCGACAGGTGAGGGCCGCGCAGCGG
	OAL6648	*A1* Nt1 - *A3* CTD *A1* R	GCCAGCCGGGGCTCGCGGTGCCGGCGC
	OAL6649	*A1* Nt1 - *A3* CTD *A3* F	CCGCGAGCCCCGGCTGGCGCGCCGACC
	OAL5554	pBBR-*tssA3* R	TTAATGGATCCCTAGGGCAGTACGCCAAGCAGCGA
pBBR1MCS4-$tssA2_{Nt1}$-$tssA1_{CTD}$	OAL5549	pBBR-*tssA2* F	ATTAAGTCGACGTTAAGATATTCATTGGCGCACATGGTG
	OAL6652	*A2* Nt1 - *A1* CTD *A2* R	CAAGGACTCTTCGGGCTGGTTGTCGGC
	OAL6653	*A2* Nt1 - *A1* CTD *A1* F	CAGCCCGAAGAGTCCTTGGCGCCGGGTGCC
	OAL5548	pBBR-*tssA1* R	ATAATGGATCCTTACTCGCTTTCCGGGCCTCGCAG
pBBR1MCS4-$tssA2_{Nt1}$-$tssA3_{CTD}$	OAL5549	pBBR-*tssA2* F	ATTAAGTCGACGTTAAGATATTCATTGGCGCACATGGTG
	OAL6707	*A2* Nt1 - *A3* CTD *A2* R	GCCAGCCGGGTCGCGCTCGTTGTCGAT
	OAL6708	*A2* Nt1 - *A3* CTD *A3* F	GAGCGCGACCCGGCTGGCGCGCCGACC
	OAL5554	pBBR-*tssA3* R	TTAATGGATCCCTAGGGCAGTACGCCAAGCAGCGA
pBBR1MCS4-$tssA3_{Nt1}$-$tssA1_{CTD}$	OAL5552	pBBR-*tssA3* F	ATTATGTCGACCGCGACGCTGTTGCCGGCCAC
	OAL6849	*A3* Nt1 - *A1* CTD *A3* R 2	GCTGGCTCGCCCGCTCGGCGCGCTCG
	OAL6850	*A3* Nt1 - *A1* CTD *A1* F 2	GCCGAGCGGGCGAGCCAGCGGCGAGATCGCC
	OAL5548	pBBR-*tssA1* R	ATAATGGATCCTTACTCGCTTTCCGGGCCTCGCAG
pBBR1MCS4-$tssA3_{Nt1}$-$tssA2_{CTD}$	OAL5552	pBBR-*tssA3* F	ATTATGTCGACCGCGACGCTGTTGCCGGCCAC
	OAL6709	*A3* Nt1 - *A2* CTD *A3* R	GGGCATGACTTGCGGGTGCATGGCGAT

	OAL6710	*A3* Nt1 - *A2* CTD *A2* F	CACCCGCAAGTCATGCCCCATCTCCAG
	OAL5551	pBBR-*tssA2* R	ATATAGGATCCCTATTCGAGCACCACCTCGAGATC
pBBR1MCS4-*tssA3*$_{Nt1}$-*tssA2*$_{Nt2+CTD}$	OAL5552	pBBR-*tssA3* F	ATTATGTCGACCGCGACGCTGTTGCCGGCCAC
	OAL6711	*A3* Nt1 - *A2* Nt2+CTD *A3* R	GCCAGGTTCTTGCGGGTGCATGGCGAT
	OAL6712	*A3* Nt1 - *A2* Nt2+CTD *A2* F	CACCCGCAAGAACCTGGCGTGGTCGGC
	OAL5551	pBBR-*tssA2* R	ATATAGGATCCCTATTCGAGCACCACCTCGAGATC
pBBR1MCS4-*tssA1*$_{Nt1}$	OAL5546	pBBR-*tssA1* F	TAATAGTCGACAGGTGAGGGCCGCGCAGCGG
	OAL6544	BTH *tssA1* Nt1 R	ATATAGGATCCTTAGCCGTACAGGTCGAACAC
pBBR1MCS4-*tssA2*$_{Nt1}$	OAL5549	pBBR-*tssA2* F	ATTAAGTCGACGTTAAGATATTCATTGGCGCACATGGTG
	OAL6537	BTH *tssA2* Nt1 R	TATATGGATCCTTACTGGTTGTCGGCGGCGCG
pBBR1MCS4-*tssA1 with tssA3 hairpin*	OAL5546	pBBR-*tssA1* F	TAATAGTCGACAGGTGAGGGCCGCGCAGCGG
	OAL6819	*A1* with *A3* hairpin R	GGGACTCTGAAGTTGCGCCGCTTCCAGCGCCGCCTTGGCGCTCTTGCTGTCGCCGCTGGCGCGTTGCAGCCCGGCGGCGTTC
	OAL6823	*A1* with *A3* hairpin F 2	GAAGCGGCGCAACTTCAGAGTCCCGAGCAGATCGCCGGCG
	OAL5548	pBBR-*tssA1* R	ATAATGGATCCTTACTCGCTTTCCGGGCCTCGCAG
pBBR1MCS4-*tssA1 with tssA3 loop*	OAL5546	pBBR-*tssA1* F	TAATAGTCGACAGGTGAGGGCCGCGCAGCGG
	OAL6821	*A1* with *A3* loop R	CGGCCAGTCGGCGCGCTTGGCCTCCGCTTGCCAGACGCCGGTCGGCAGGCTGCTGTCGCCCTGGGCGATGCGTTCGAGTTCGAG
	OAL6822	*A1* with *A3* loop F	AAGCGCGCCGACTGGCCGCGCGTACGCGCGCTG
	OAL5548	pBBR-*tssA1* R	ATAATGGATCCTTACTCGCTTTCCGGGCCTCGCAG
pBBR1MCS4-*tssA3 with tssA1 hairpin*	OAL5552	pBBR-*tssA3* F	ATTATGTCGACCGCGACGCTGTTGCCGGCCAC
	OAL6845	*A3* with *A1* hairpin R	CAGGGTCTCGCTGGCGAAGACCTGCTGGCGCTGCAACCTCTG
	OAL6846	*A3* with *A1* hairpin F	CAGGTCTTCGCCAGCGAGACCCTGCAGAAGAAGCTAGACGAAGCGTTGCGCG
	OAL5554	pBBR-*tssA3* R	TTAATGGATCCCTAGGGCAGTACGCCAAGCAGCGA
pBBR1MCS4-*tssA3 with tssA1 loop*	OAL5552	pBBR-*tssA3* F	ATTATGTCGACCGCGACGCTGTTGCCGGCCAC
	OAL6847	*A3* with *A1* loop R	GCAGCACGGCATCGCCCATCTGGCGCTCGGGTTGGTCCTCCCGGCGCAACTCGCG
	OAL6848	A3 with *A1* loop F	CAGATGGGCGATGCCGTGCTGCCCGCCGAGCCGCCGGAGTGGGCCGCGGTGGAGCAGTTG
	OAL5554	pBBR-*tssA3* R	TTAATGGATCCCTAGGGCAGTACGCCAAGCAGCGA
pBBR1MCS4-*tssA2*^{PP}	OAL6834	*tssA2*$_{PP}$ F	ATATAGAATTCTTTTGACGCTCAGGGGCTGGACC
	OAL6835	*tssA2*$_{PP}$ R	AATTTGGATCCTCATCGAGGCTCCTGCTCCTTGTTCC
pBBR1MCS4-*tssA3*^{PP}	OAL6836	*tssA3*$_{PP}$ F	ATAATGAATTCGATGCGCAAGGCCTGGC
	OAL6837	*tssA3*$_{PP}$ R	ATTATGGATCCTCATCGAGGCTCCTGATCCTTGTCTTGAAC
pBBR1MCS4-*tssA2*$_{Nt1}$-*tssA2*$^{PP}{}_{Nt2+CTD}$	OAL6838	*tssA2* F with EcoRI	AATTAGAATTCTGTTAAGATATTCATTGGCGCACATGGTG
	OAL6839	*tssA2-A2PP* R	GTTACCGCCCGACAAGTCGCGCTCGTTGTCGATGG

	OAL6840	*tssA2-A2PP* F	AGCGCGACTTGTCGGGCGGTAACGAGCG
	OAL6835	*tssA2PP* R	AATTTGGATCCTCATCGAGGCTCCTGCTCCTTGTTCC
pBBR1MCS4-*tssA2*$_{Nt1}$-*tssA3*$^{PP}_{Nt2+CTD}$	OAL6838	*tssA2* F with EcoRI	AATTAGAATTCTGTTAAGATATTCATTGGCGCACATGGTG
	OAL6841	*tssA2-A3PP* R	CATTGCCCATCGAGTCGCGCTCGTTGTCGATGG
	OAL6842	*tssA2-A3PP* F	GAGCGCGACTCGATGGGCAATGAGCGTGAGACAC
	OAL6837	*tssA3PP* R	ATTATGGATCCTCATCGAGGCTCCTGATCCTTGTCTTGAAC
pMMB67HE-*tagJ1*	OAL6748	pMMB67HE-*tagJ* F	ATATAGGTACCCGCCATGGCCGACCCTTC
	OAL6749	pMMB67HE-*tagJ* R	ATATAGAATTCTCAGGCGTCCGTCGGCTCGAA
pME6032-*tssA2*	OAL6359	*tssA2* pull-down F	ATTTAGAATTCATGACCTATTCGAGCAAGCTCTCC
	OAL6361	*tssA2* pull-down R	ATATTGGTACCGCCCTATTCGAGCACCACC
pME6032-*FLAG-tssA2*	OAL6360	*tssA2* FLAG pull-down F	ATTAAGAATTCATGGACTACAAAGATGACGACGATAAAACCTATTCGAGCAAGCTCTCCTC
	OAL6361	*tssA2* pull-down R	ATATTGGTACCGCCCTATTCGAGCACCACC
pME6032-*tssA3*	OAL6362	*tssA3* pull-down F	AATTTGAATTCATGACCCTGCCTCTTTCCGG
	OAL6364	*tssA3* pull-down R	TTAATGGTACCCTAGGGCAGTACGCCAAGC
pME6032-*FLAG-tssA3*	OAL6363	*tssA3* FLAG pull-down F	AATTAGAATTCATGGACTACAAAGATGACGACGATAAAACCCTGCCTCTTTCCGGC
	OAL6364	*tssA3* pull-down R	TTAATGGTACCCTAGGGCAGTACGCCAAGC
pME6032-*PA2372*	OAL6193	*PA2372* pull-down F	GGCGCGAATTCATGAACTATTTATTCGTGCCATTCACAAG
	OAL6195	*PA2372* pull-down R	TGACCCTCGAGTTAAGGTACTCTCTGTCTTGCTTCCG
pME6032-*FLAG-PA2372*	OAL6194	*PA2372* pull-down FLAG R	ATGCTCTCGAGCTATTTATCGTCGTCATCTTTGTAGTCAGGTACTCTCTGTCTTGCTTCCG
	OAL6195	*PA2372* pull-down R	TGACCCTCGAGTTAAGGTACTCTCTGTCTTGCTTCCG
***E. coli* expression construct primers**			
pET28a-*his6-tssA2*	OAL4870	pET28a-*tssA2* F	ATTGGCATATGACCTATTCGAGCAAGCTCTCCTC
	OAL4871	pET28a-*tssA2* R	CCTGAGAATTCAAGCCCTATTCGAGCACC
pET28a-*his6-tssA2*$_{1-391}$	OAL4870	pET28a-*tssA2* F	ATTGGCATATGACCTATTCGAGCAAGCTCTCCTC
	OAL4872	pET28a-*tssA2*_1-391 R	ATCAGGAATTCTCACACGGTCTCGACCTTGCG
pETDuet-1-*his6-tssA1*	OAL4866	Duet-*tssA1* F	ATCGAGAATTCCGTGCTGGATGTACCCG
	OAL4867	Duet-*tssA1* R	TGGCCAAGCTTCCGCTAGGCGTTACTCG
pETDuet-1-*his6-tssA2*	OAL5520	Duet-*tssA2* F	ATTTAGAATTCGATGACCTATTCGAGCAAGCTCTC
	OAL5521	Duet-*tssA2* R	ATATTAAGCTTGCGCGAAGCCCTATTCGAG
pETDuet-1-*his6-tssA3*	OAL5522	Duet-*tssA3* F	ATTTAGAATTCCATGACCCTGCCTCTTTCCGG
	OAL5523	Duet-*tssA3* R	ATTTTAAGCTTGCCACGCCTCCTAGGGC

pETDuet-*Strep-tssA1*	OAL6286	New *Strep-tssA1* F	TAATACCATGGGCAGCAGCTGGAGCCACCCGCAGTTCGAAAAGAGCCAGGATCCGAATTCCGTGCTGGATGTACCCG
	OAL4867	Duet-*tssA1* R	TGGCCAAGCTTCCGCTAGGCGTTACTCG
pETDuet-*Strep-tssA2*	OAL5520	Duet-*tssA2* F	ATTTAGAATTCGATGACCTATTCGAGCAAGCTCTC
	OAL5521	Duet-*tssA2* R	ATATTAAGCTTGCGCGAAGCCCTATTCGAG
pETDuet-*Strep-tssA3*	OAL5522	Duet-*tssA3* F	ATTTAGAATTCCATGACCCTGCCTCTTTCCGG
	OAL5523	Duet-*tssA3* R	ATTTTAAGCTTGCCACGCCTCCTAGGGC
pETDuet-1-*Strep-tssA1 CTD*	OAL6421	*tssA1* CTD F	ATATTGAATTCAGCCAGCGGCGAGATC
	OAL4867	Duet-*tssA1* R	TGGCCAAGCTTCCGCTAGGCGTTACTCG
pETDuet-1-*Strep-tssA2 Nt2+CTD*	OAL6422	*tssA2* Nt2+CTD F	ATTATGAATTCCGCCCACAAGGCCATGC
	OAL5521	Duet-*tssA2* R	ATATTAAGCTTGCGCGAAGCCCTATTCGAG
pETDuet-1-*Strep-tssA2*$_{CTD}$	OAL6543	Duet *tssA2* CTD F	TAATTGAATTCGCGCAAGGTCGAGACCGT
	OAL5521	Duet-*tssA2* R	ATATTAAGCTTGCGCGAAGCCCTATTCGAG
pETDuet-1-*Strep-tssA3 CTD*	OAL6423	*tssA3* CTD F	ATTTAGAATTCGCCGGCTGGCGCGCCGA
	OAL5523	Duet-*tssA3* R	ATTTTAAGCTTGCCACGCCTCCTAGGGC
Site-directed mutagenesis primers			
tssA1 K69A	OAL6087	*tssA1* K69A F	CGAACTGTTCGGCCGTAGCGCCGACCTGCGGGTAGCCAACCTGC
	OAL6088	*tssA1* K69A R	GCAGGTTGGCTACCCGCAGGTCGGCGCTACGGCCGAACAGTTCG
tssA1 G86A	OAL6089	*tssA1* G86A F	CAACGTCGCCCTCGACGCCCTGGACGGGCTCGC
	OAL6090	*tssA1* G86A R	GCGAGCCCGTCCAGGGCGTCGAGGGCGACGTTG
tssA1 L94A	OAL6091	*tssA1* L94A	GCTCGCCGACGGCGCCCTGCTGGTCCGCGAGC
	OAL6092	*tssA1* L94A	GCTCGCGGACCAGCAGGGCGCCGTCGGCGAGC
tssA1 R282A	OAL6093	*tssA1* R282A F	GCGGCGAGATCGCCAACGCCGAAGACGTCCTGCGCC
	OAL6094	*tssA1* R282A R	GGCGCAGGACGTCTTCGGCGTTGGCGATCTCGCCGC
tssA1 L286A	OAL5925	*tssA1* L286A F	AACCGCGAAGACGTCGCCCGCCAGCTCGATCGC
	OAL5926	*tssA1* L286A R	GCGATCGAGCTGGCGGGCGACGTCTTCGCGGTT
tssA1 L289A	OAL6006	*tssA1* L289A F	CCGCGAAGACGTCCTGCGCCAGGCCGATCGCCTGCTCGAG
	OAL6007	*tssA1* L289A R	CTCGAGCAGGCGATCGGCCTGGCGCAGGACGTCTTCGCGG
tssA1 E300A	OAL6097	*tssA1* E300A F	CGAGTATTACGTTCGCCACGCCCCGTCGAGTCCGGTGCCGG
	OAL6098	*tssA1* E300A R	CCGGCACCGGACTCGACGGGGCGTGGCGAACGTAATACTCG
tssA1 L309A	OAL6293	*tssA1* L309A F	CCGGTGCCGGTGCTGGCCAAGCGCGCCAAGACACTGG
	OAL6294	*tssA1* L309A R	CCAGTGTCTTGGCGCGCTTGGCCAGCACCGGCACCGG
tssA1 D14A	OAL6713	*tssA1* D14A F	GCTGCCGTATCCCCGGCTTCGCCCTGTGGCGACG
	OAL6714	*tssA1* D14A R	CGTCGCCACAGGGCGAAGCCGGGGATACGGCAGC

tssA1 Q41A	OAL6715	*tssA1* Q41A F	CCAACCCGAGCGCGCTATGGGCGATGCCGTGC
	OAL6716	*tssA1* Q41A R	GCACGGCATCGCCCATAGCGCGCTCGGGTTGG
tssA1 D44A	OAL6717	*tssA1* D44A F	CGCCAGATGGGCGCTGCCGTGCTGCCCGCC
	OAL6718	*tssA1* D44A R	GGCGGGCAGCACGGCAGCGCCCATCTGGCG
tssA1 D116A	OAL6719	*tssA1* D116A F	CTATCCGTTGCTCGACGCCGATGCTGACAACGACCC CACCTTCCG
	OAL6720	*tssA1* D116A R	CGGAAGGTGGGGTCGTTGTCAGCATCGGCGTCGA GCAACGGATAG
tssA1 R146A	OAL6721	*tssA1* R146A F	GATCCCGCTGGTGGCTTCGCGGGCGTTCGG
	OAL6722	*tssA1* R146A R	CCGAACGCCCGCGAAGCCACCAGCGGGATC
tssA1 R148A	OAL6723	*tssA1* R148A F	CTGGTGCGCTCGGCTGCGTTCGGCCCG
	OAL6724	*tssA1* R148A R	CGGGCCGAACGCAGCCGAGCGCACCAG
tssA1 S169A	OAL6725	*tssA1* S169A F	GGCTGCAACGCTTCGCCGCTGAGACCCTGAGTCCC G
	OAL6726	*tssA1* S169A R	CGGGACTCAGGGTCTCAGCGGCGAAGCGTTGCAG CC
tssA1 E170A	OAL6727	*tssA1* E170A F	CTGCAACGCTTCGCCAGCGCTACCCTGAGTCCCGA GCAG
	OAL6728	*tssA1* E170A R	CTGCTCGGGACTCAGGGTAGCGCTGGCGAAGCGTT GCAG
tssA1 L238A	OAL6729	*tssA1* L238A F	CCTCCAGGTGTTCGACGCTTACGGCCCGCAGGGCG
	OAL6730	*tssA1* L238A R	CGCCCTGCGGGCCGTAAGCGTCGAACACCTGGAGG

2.2.3 Restriction enzyme digestion and ligation

To ligate desired DNA fragments into target plasmids, both fragment and plasmid were digested with restriction enzymes to generate compatible sticky ends. Plasmids were digested in a 50 µl reaction mix containing 2500 ng of DNA, 2 µl of each restriction enzyme (NEB) and 5 µl of 10x digest buffer (NEB), while purified DNA fragments were digested in a 25 µl reaction mix containing 21.5 µl of purified DNA, 1 µl of each restriction enzyme (NEB) and 2.5 µl of 10x digest buffer (NEB). Restriction digests were incubated at 37 °C for upwards of 2 hours before purification. Digested plasmids were purified via a band excised from a TAE agarose gel using the QIAquick® Gel Extraction Kit, while digested DNA fragments were purified using the QIAquick® PCR Purification Kit.

Purified digested plasmid and DNA fragment were mixed at a 3:1 insert to vector ratio and ligated using 1 µl T4 DNA ligase (NEB) and 1 µl T4 DNA ligase buffer (NEB) for either 30 minutes at room temperature or at 16 °C overnight.

2.2.4 Production of chemically competent cells

Following either blunt- or sticky-end ligation, plasmids were transformed into chemically competent *E. coli* cells. Briefly, to generate chemically competent cells, the desired *E. coli* strain was grown in LB broth overnight at 37 °C, before being sub-cultured to OD_{600} 0.1 in 50 ml LB broth. This culture was grown at 37 °C to an OD_{600} between 0.4-0.6, when cells were harvested by centrifugation at 4 °C at 4000 rpm for 10 minutes. The pellet was resuspended in 25 ml cold and sterile 50 mM $CaCl_2$ with 15 % glycerol, before being incubated on ice for 30 minutes and then centrifuged again. The pellet was then resuspended in 2.5 ml of cold and sterile 50 mM $CaCl_2$ with 15 % glycerol, aliquoted into appropriate volumes and stored at -80°C.

2.2.5 Transformation of plasmids into competent cells

Transformation protocols differed slightly depending on the *E. coli* strain used. In general, 50-100 µl of thawed competent cells was mixed with up to 20 µl of the ligation mix or 2 µl of purified plasmid. This mixture was incubated on ice for 30 minutes, before heat shock at 42 °C for 30 seconds and then being returned to ice for 2 minutes. LB broth was added to the transformation mixture up to 1 ml, followed by incubation at 37 °C for 45 minutes. The transformation mix was then plated onto LB agar plates supplemented with appropriate antibiotics to select transformants. LB agar plates were incubated at 37 °C overnight to isolate single colonies.

For transformation into DHM1 competent cells, 2 µl of pUT18/pUT18C plasmid and 4 µl of pKT25/pKNT25 plasmid were mixed with 30 µl of competent cells. This transformation mix followed the general protocol, until the heat shock stage, where the transformation mix was heated to 42 °C for 2 minutes and then incubated on ice for 10 minutes. Following the addition of 250 µl of LB broth, this mix was incubated at 37 °C for 1 hour before plating on LB agar plates supplemented with both 50 µg/ml kanamycin and 100 µg/ml ampicillin. DHM1 co-transformant LB agar plates were incubated at 30 °C overnight.

For transformation of pKNG101 plasmids into CC118λpir competent cells, the transformation mixture was heat shocked for 2 minutes at 42 °C, before incubation on ice for 1 minute. Following the addition of 500 µl of LB broth, this mix was incubated at 37 °C for 1 hour before plating on LB agar plates supplemented with 100 µg/ml streptomycin.

2.2.6 Colony PCR

Transformant colonies containing either blunt- or sticky-end ligated plasmids and selected for on antibiotic-supplemented LB agar plates, were screened for the presence of the desired plasmid using colony PCR. Bacteria recovered from individual colonies were replica plated and then resuspended in 100 µl ddH_2O and vortexed, with 1 µl of this comprising the template DNA in the PCR mix. The remaining PCR mix comprised of 2 µl 10x Taq buffer [750 mM Tris pH 9, 200mM $(NH_4)_2SO_4$, 0.1 % Tween® 20 detergent, 15 mM $MgCl_2$], 1 µl of each primer, 1 µl dimethyl sulfoxide (DMSO), 0.4 µl 20 mM dNTP mix and 0.4 µl Taq polymerase made up to 20 µl with ddH_2O. The PCR involved heating to 95 °C for 10 minutes, followed by 30 cycles of 95 °C for 30 seconds, 55 °C or specific annealing temperature for 30 seconds and 72 °C for 1 minute/kb, followed by a final 10 minutes at 72 °C.

Following the PCR, the reaction mix was analysed by electrophoresis on 1% (w/v) TAE agarose gel and imaged using the Bio-Rad ChemiDoc XRS+. Transformants containing plasmids with the correct sized insert were grown in LB broth at 37 °C overnight. Subsequently the plasmid was purified using the QIAprep Spin Miniprep Kit (QIAgen) and sequenced using GATC at Eurofins Supreme Sanger Sequencing.

DNA fragments blunt-end ligated into the pCR®-Blunt II-TOPO® (Invitrogen) cloning vector could then be sub-cloned into the desired vector using restriction enzyme recognition sites within the cloning vector multiple cloning site (MCS). This involved restriction enzyme digestion and ligation, transformation and colony PCR as described in sections 2.2.3, 2.2.4 and 2.2.5.

2.2.7 Site-directed mutagenesis: alanine substitution

Site-directed mutagenesis was used to introduce targeted alanine substitutions at specific residues. This involved the design of a pair of specialised primers, between 25-45 bases in length and with an annealing temperature of at least 75 °C, with the mutated residues found centrally within the primer sequences. The PCR mix comprised of 70 ng of template plasmid, 5 µl 10x KOD Hot Start buffer (Merck), 1.5 µl of each primer, 10 µl betaine (Sigma Aldrich), 500 mM dNTP mix (Merck), 1.5 mM magnesium sulfate and ddH_2O to 50 µl. The PCR involved heating to 95 °C for 2 minutes, followed by 18 cycles of 95 °C for 20 seconds, 55 °C for 10 seconds and 70 °C for 25 seconds/kb, followed by a final 5 minutes at 70 °C.

To confirm plasmid amplification, the reaction mix was analysed by electrophoresis on 1% (w/v) TAE agarose gel and imaged using the Bio-Rad ChemiDoc XRS+. The reaction mix was then purified using the QIAquick® PCR Purification Kit (QIAgen). To remove the methylated template DNA, the purified

sample was digested with DpnI (NEB) in a 40 µl reaction overnight at 37 °C. This reaction mix containing the intact mutated DNA was then transformed into DH5α competent cells as described in section 2.2.5. Bacteria from individual colonies were grown in LB broth overnight at 37 °C, plasmid was purified using the QIAprep Spin Miniprep Kit (QIAgen) and sequencing was performed using GATC at Eurofins Supreme Sanger Sequencing to confirm mutagenesis.

2.2.8 Three-partner conjugation to introduce plasmids into *P. aeruginosa*

The introduction of plasmids into *P. aeruginosa* involved three strains: an *E. coli* plasmid-encoding donor strain, a helper *E. coli* 1047 strain with the self-transmissible helper plasmid pRK2013 and the receiver *P. aeruginosa* strain. Each of these strains were grown in liquid culture overnight at 37 °C with appropriate antibiotics, *E. coli* in LB broth and *P. aeruginosa* in TSB. On an LB agar plate, a spot containing 20 µl of the donor strain and 20 µl of the helper strain was dried and the plate incubated at 37 °C for 2 hours. In parallel, an aliquot of the receiver strain was incubated at 43 °C for 2 hours to inactivate the restriction modification system. Following this incubation, 40 µl of the receiver strain was spotted on top of the donor and helper strains and once dried, the plate was incubated at 37 °C for at least 4 hours. The three mixed strains were then recovered with a 10 µl inoculation loop (VWR) and resuspended in 1 ml LB broth. This mix was plated on VBM agar with appropriate antibiotics to select for conjugants and incubated overnight at 37 °C.

2.2.9 *P. aeruginosa* mutagenesis

Modifications to the *P. aeruginosa* genome involved using three-partner conjugation as described in section 2.2.8 to introduce the suicide vector pKNG101 into *P. aeruginosa* receiver strains. The non-replicative pKNG101 containing a mutator fragment was transformed into the replication-permissive CC118λpir strain. The mutator fragment could undergo homologous recombination with the *P. aeruginosa* genome, due to the presence of two regions of at least 500 bp of sequence homologous to that of the *P. aeruginosa* genome, found upstream and downstream of the region to be altered in the chromosome. Between the sequences of these two homologous regions any desired changes were introduced to generate the mutated locus, i.e. the loss of a region of coding sequence or the introduction of a fluorophore gene. In general, upon gene deletions three codons at the start and the end of the open reading frame remained.

Chromosomal mutation involved two homologous recombination events. Firstly, upon mobilisation of pKNG101 into *P. aeruginosa*, conjugants were selected by plating on VBM agar supplemented with

1000 µg/ml streptomycin, due to the presence of a streptomycin resistance gene encoded on pKNG101. With the plasmid unable to replicate in *P. aeruginosa,* maintenance of this streptomycin resistance gene required plasmid integration into the chromosome at one of the homologous regions. Following the identification of conjugant colonies, the *sacB Bacillus subtilis* gene encoded on pKNG101, which confers sucrose sensitivity, was used to select for the second recombination event. Conjugant colonies were streaked on LB agar plates containing 20 % (w/v) sucrose and grown at room temperature until the appearance of isolated colonies. This counterselection produced colonies having undergone a second recombination to excise the plasmid, leaving the chromosomal sequence either wildtype or mutated. Colonies were replica plated onto LB agar supplemented with 2000 µg/ml streptomycin, PIA and LB agar, to confirm that colonies were *Pseudomonas* that had excised the plasmid. Streptomycin sensitive strains able to grow on PIA and LB agar were screened by colony PCR using primers external to the homologous regions, to distinguish between wildtype or mutant genotypes. Identified mutants were streaked onto LB agar alone and LB agar supplemented with 2000 µg/ml streptomycin. Single colonies from LB agar were screened by colony PCR to confirm the mutant genotype. Bacteria from these single colonies were then inoculated into TSB and grown at 37 °C overnight and an aliquot stored in 40 % (v/v) glycerol at -80 °C.

2.3 Protein analysis

2.3.1 SDS-PAGE

Protein samples were analysed by SDS-PAGE, Coomassie staining and western blotting to assess the presence and abundance of proteins of interest. Cells grown in liquid culture were pelleted by centrifugation at 8000 rpm for 3 minutes before removal of the culture supernatant and resuspension in Laemmli buffer [0.0625 M Tris-HCl pH 6.8, 2 % (w/v) SDS, 4 % (v/v) glycerol, 5 % (v/v) β-mercaptoethanol, 0.002 % (w/v) bromphenol blue]. Samples in Laemmli buffer were denatured by boiling at 95 °C for 10 minutes before loading onto polyacrylamide gels for SDS-PAGE. The percentage of polyacrylamide in these gels was variable (10, 12 or 15 %) depending on the target protein size, with 15 % gels used to resolve small proteins such as Hcp or TssA C-terminal truncations, while 10 % gels were used to resolve larger proteins such as RNA polymerase β (RpoB) and 12 % gels used for intermediate sized proteins. Polyacrylamide gels were run at 80 V for the samples to pass through the stacking gel and then 100 V in Tris-glycine-SDS (TGS) buffer [0.3 % (w/v) Tris, 1.44 % (w/v) glycine, 0.01 % SDS]. The Precision Plus Protein™ Kaleidoscope™ Prestained Protein Standards (Bio-Rad) was used as a molecular weight marker. Following SDS-PAGE, resolved proteins were visualised using either Coomassie staining or western blotting of polyacrylamide gels.

2.3.2 Coomassie stain

Coomassie stain [0.5 % (w/v) Coomassie Brilliant Blue R250 dye (Sigma Aldrich), 50 % ddH_2O, 40 % methanol, 10 % acetic acid] was added to polyacrylamide gels for 1 hour on a rocking shaker. Gels were then incubated with Coomassie destain [50 % ddH_2O, 40 % methanol, 10 % acetic acid] on a rocking shaker to remove excess Coomassie stain before imaging.

2.3.3 Western blot

For western blotting, resolved proteins were transferred from polyacrylamide gels to nitrocellulose membranes (Amersham). The acrylamide gel was placed on top of the nitrocellulose membrane and this was sandwiched between two stacks of three sheets of damp filter paper (Whatman). The filter paper was dampened in transfer buffer [10 % (v/v) TGS buffer, 20 % (v/v) ethanol, 70 % (v/v) ddH_2O], and the transfer took place using a Trans-Blot SD Semi-Dry Transfer Cell (Bio-Rad).

Following transfer, membranes were blocked for 1 hour with either milk in Tris-buffered saline with tween (milk in TBS-T) [5 % (w/v) skimmed milk powder (Sigma Aldrich), 50 mM Tris-HCl pH 9.0, 150 mM NaCl, 0.1 % (v/v) Tween® 20 detergent] or bovine serum albumin (BSA) (Sigma Aldrich) in phosphate-buffered saline with tween (BSA in PBS-T) (3% BSA, 137 mM NaCl, 2.7 mM KCl, 10 mM Na_2HPO_4, 1.8 mM KH_2PO_4, 0.1 % (v/v) Tween® 20 detergent).

Primary antibodies were then added to 10 ml of the appropriate blocking buffer at the correct dilution and incubated with the membrane for at least 1 hour. All antibodies used in this work are presented in Table 2.5. Following three 10-minute washes of the membrane with either TBS-T or PBS-T, the secondary antibody conjugated to horse-radish peroxidase (HRP) at the appropriate dilution in blocking buffer was incubated with the membrane for 45 minutes. The HRP-conjugated anti-Strep antibody required only a single 1-hour incubation as no secondary antibody was required. After a further three 10-minute washes, the membrane was developed with the Novex™ ECL Chemiluminescent Substrate Reagent Kit (Invitrogen) and imaged with the Bio-Rad ChemiDoc XRS+.

Table 2.5 Antibodies used in this study

Antibody	Host	Sera	Dilution	Source
anti-Hcp1	Rabbit	Polyclonal	1:500	(523)
anti-Hcp2	Rabbit	Polyclonal	1:500	(524)
anti-Hcp3	Rabbit	Polyclonal	1:500	(338)
anti-TssB1	Rabbit	Polyclonal	1:1000	(514)
anti-VgrG1a	Rabbit	Polyclonal	1:1000	(523)
anti-TagJ	Rabbit	Polyclonal	1:1000	(514)
anti-RpoB	Mouse	Monoclonal	1:1000	Neoclone
anti-His	Mouse	Monoclonal	1:1000	Sigma Aldrich
anti-Strep (HRP conjugate)	-	Monoclonal	3:1000	IBA
anti-V5	Mouse	Monoclonal	1:5000	Invitrogen
HRP-conjugated anti-Mouse	Rabbit	Polyclonal	1:5000	Sigma Aldrich
HRP-conjugated anti-Rabbit	Goat	Polyclonal	1:5000	Sigma Aldrich

2.3.4 Secretion assays

Secretion assays were used to assess the presence of proteins in the whole cell extract and extracellular fraction. *P. aeruginosa* strains were grown overnight at 37 °C in TSB supplemented with antibiotics where appropriate. Bacteria were then sub-cultured to an OD_{600} 0.1 in 20 ml TSB. Culture conditions varied depending on the T6SS studied. For the H1-T6SS, cultures were grown at 37 °C for

at least 5 hours, for the H2-T6SS cultures were grown at 25 °C for 18-24 hours, and for the H3-T6SS cultures were grown at 25 °C for 24 hours. Following this incubation an OD_{600} equivalent of 1.0 was centrifuged at 8000 rpm for 3 minutes to generate a cellular pellet. The supernatant was removed and the pellet resuspended in 100 µl Laemmli buffer, to a concentration of 0.1 OD_{600} equivalent per 10 µl.

To isolate an extracellular supernatant fraction, the remaining culture was centrifuged at 4 °C, 4000 rpm for 10 minutes, the uppermost 15 ml was removed and centrifuged under identical conditions for a further 20 minutes. This was repeated with 12 ml, 10 ml and then 7 ml to separate the supernatant from any remaining cells. Following the 7 ml spin, the uppermost 1.8 ml were recovered, 200 µl of trichloroacetic acid (TCA) (Sigma Aldrich) was added to this and the sample was incubated at 4 °C overnight to precipitate proteins.

Precipitated proteins were pelleted by centrifugation at 4 °C, 16000 g for 30 minutes before being washed with 1 ml cold 90 % (v/v) acetone (VWR) followed by centrifugation with identical conditions. The supernatant was removed, and the pellet air-dried before addition of Laemmli buffer to resuspend the pellet to a concentration of 1.0 OD_{600} equivalent per 10 µl. Whole cell and supernatant samples were then resolved by SDS-PAGE before being visualised by western blot to identify the presence of at least RpoB and the relevant Hcp.

2.3.5 Protein purification

Protein purification was carried out by Patricia Paracuellos. Either pETDuet-1 or pET28a plasmids encoding tagged forms of full length or truncated *tssA* genes were transformed into BL21 (λDE3) competent cells as outlined in section 2.2.5. After overnight incubation of agar plates at 37 °C, all colonies were harvested by resuspension in LB broth using and L-shaped spreader (VWR), before transfer to a flask containing 100 ml of LB supplemented with appropriate antibiotics. This culture was grown at 37 °C for 2 hours with agitation, before 20 ml was transferred into four flasks each containing 1 L of LB broth supplemented with appropriate antibiotics. This flask was grown at 37 °C until reaching an OD_{600} 0.6, whereupon 0.5 mM Isopropyl ß-D-1-thiogalactopyranoside (IPTG) (Melford) was added. The culture was then incubated at 20 °C with agitation overnight.

The following day the cultures were centrifuged at 4200 rpm for 20 minutes at 4 °C. The supernatant was removed, and the cell pellet was resuspended in 30 ml lysis buffer per 1 L of culture [20 mM N-2-hydroxyethylpiperazine-N-2-ethane sulfonic acid (HEPES) pH 7.5, 250 mM NaCl, 100 µl/100 ml Triton x100, 0.5 mM phenylmethylsulfonyl fluoride (PMSF), 1 mg/ml lysozyme]. Cells were lysed using the Fisherbrand™ with Q500 Sonicator probe (Thermo Fisher Scientific) at 60 % amplitude with a process

time of 2 minutes and 20 seconds. Lysed cells were then centrifuged at 41000 rpm at 4 °C for 45 minutes to clarify the cellular lysate. The supernatant was passed through a 0.45 µm syringe filter (Sartorious).

The supernatant was passed through a Strep-trap HP 1 ml column (Sigma Aldrich), which had been washed with two column volumes of ddH_2O and equilibrated with four column volumes of PBS using an ÄKTA purifier (GE Healthcare). After passing the supernatant through the column, the column was washed with 20 column volumes of PBS. Bound proteins were then eluted using elution buffer (PBS, 2.5 mM desthiobiotin). The eluted sample was dialysed overnight at 4 °C in 4 L of dialysis buffer (20 mM HEPES pH 7.5, 150 mM NaCl).

2.3.6 Size exclusion chromatography

Size exclusion chromatography, also known as gel filtration, was performed using an ÄKTA purifier (GE Healthcare) with Superose 6 10/300 GL column (GE Healthcare), which had been washed with two column volumes of ddH_2O and equilibrated with two column volumes of dialysis buffer (20 mM HEPES pH 7.5, 150 mM NaCl). The dialysed sample was centrifuged to remove any aggregates before 500 µl was used for size exclusion chromatography using running buffer (20 mM HEPES pH 7.5, 150 mM NaCl). SDS-PAGE was used to assess the purity of eluted fractions.

2.3.7 Transmission electron microscopy: negative stain

Purified protein samples were diluted to 0.003 mg/ml with dialysis buffer (20 mM HEPES pH 7.5, 150 mM NaCl). Copper electron microscopy 400 mesh grids were coated with a thin layer of carbon using glow discharger Turbo Carbon Coater (Agar Scientific). 10 µl of sample was place onto the grids and incubated for 2 minutes. Grids were then held with clamping forceps and washed with water twice for 10 seconds. Excess water was blotted off onto filter paper (Whatman). Grids were then stained with 2 % (w/v) uranyl acetate for 20 seconds. The excess uranyl acetate was blotted off and grids were allowed to air dry for 2 minutes. Grids were then stored in a grid box prior to visualisation. General purpose high-resolution FEI Tecnai G2 Spirit Twin Transmission electron microscope (Field Electron and Ion Company) was used to visualise the negative stained grids.

2.4 Interbacterial competition assays

All interbacterial competition assays were carried out on solid media to facilitate contact and thus contact-dependent killing by the T6SS. LB agar plates upon which interbacterial competition spots were incubated were well dried, for at least 2 hours, prior to plating.

To assess T6SS-dependent killing by each of the H1- and H2-T6SSs, the ability to kill an *E. coli* prey strain harbouring the pRL662-*GFP* plasmid was investigated with various *P. aeruginosa* attacker strains. To assess T6SS-dependent killing by the H3-T6SSs, the ability to kill a *P. putida* prey strain was investigated with various *P. aeruginosa* attacker strains. All strains were grown in LB supplemented with appropriate antibiotics overnight before harvesting cells by centrifuging 1.5 ml at 8000 rpm for 3 minutes. Under the growth conditions specified, the *P. aeruginosa* strains used produced extracellular biofilm. The bacteria and the biofilm were separated by varying densities during centrifugation, and the biofilm layer on top of the cellular pellet could therefore be removed before washing the pellet in 1 ml sterile PBS. The OD_{600} was then adjusted to 3.0 with PBS, and equal volumes of attacker and prey were mixed. In some cases where described the ratio of attacker to prey was altered, in these cases a greater volume of attacker was added to the mix. The attacker-prey mix was centrifuged at 8000 rpm for 3 minutes, half the supernatant was removed, and the pellet resuspended in the remaining volume. In triplicate, 5 µl of each competition mix was spotted onto well dried LB agar plates and spots were dried before incubation. The temperature and length of incubation varied depending on the T6SS.

The input attacker-prey mix was serially diluted to 10^{-7} and plated in duplicate to be grown under conditions to select either for growth of the prey or the attacker strain. In *P. aeruginosa* competitions with *E. coli*, the input was plated on LB agar supplemented with either 50 µg/ml gentamycin to select for *E. coli* or 100 µg/ml ampicillin to select for *P. aeruginosa*. In *P. aeruginosa* competitions with *P. putida*, the input was plated on LB agar supplemented with 40 µg/ml rifampicin to select for *P. putida* (grown at 30 °C as is standard for *P. putida*) and LB agar grown at 42 °C to select for *P. aeruginosa*. This confirmed the ratio of prey and attacker strains within the mix.

2.4.1 Interbacterial competition assay- double incubation

A H1-T6SS competition assay was carried out with two incubation steps. The competition mixes were incubated at 37 °C for 5 hours before being recovered with a 10 µl inoculation loop (VWR) and resuspended in 1 ml sterile PBS. These mixes were then serially diluted to 10^{-2} and 20 µl of each diluted competition mix was spotted onto LB agar plates and incubated at 37 °C for 17 hours. It is suggested

that this second incubation step re-establishes contact between remaining prey and attacker cells. Competition mixes were then similarly recovered into 1 ml sterile PBS. Following 30 minutes of agitation in a vortex mixer, 200 µl of each competition mix was transferred into a 96-well microplate (Falcon 96 Well Black with Clear Flat Bottom TC-Treated Microplate) (SLS). The GFP fluorescence intensity associated with each competition mix was then measured in a microplate reader (BMG Labtech), with an excitation filter of 485 nm and emission filter of 250 nm.

2.4.2 Interbacterial competition assay- single incubation

Both H1- and H2-T6SS interbacterial competition assays were also carried out with a single incubation step. For H1-T6SS competitions, competition mixes were incubated at 37 °C for 24 hours before recovery into sterile PBS as described in section 2.4.1. For H2-T6SS competitions, competition mixes were incubated at 25 °C for 24 hours before recovery. Following recovery into 1 ml sterile PBS, competition mixes were agitated for 30 minutes in a vortex mixer before 200 µl was transferred into a 96-well microplate (SLS) and GFP fluorescence intensity was assessed as described in section 2.4.1.

2.4.3 Interbacterial competition assay- competitive index

H3-T6SS interbacterial competitions were carried out assessing competition with *P. putida* prey. A range of competition conditions were screened to probe H3-T6SS killing activity: temperatures ranging from 20-30 °C and incubation times ranging from 6-30 hours. Following incubation, competition mixes were recovered into 1 ml sterile PBS as described in section 2.4.1. Resuspended competition mixes were agitated for 30 minutes in a vortex mixer, before being serially diluted to 10^{-7} and plated in duplicate as described for the input: on LB agar for incubation at 42 °C and LB agar supplemented with 40 µg/ml rifampicin. Selective growth allowed the colony forming units of attacker and prey strains to be enumerated in both the input and output. The competitive index was calculated using the following formula:

$$competitive\ index\ = \frac{(output\ attacker/output\ prey)}{(input\ attacker/input\ prey)}$$

2.5 Protein-protein interaction analysis

2.5.1 Bacterial two-hybrid spotting assay

To investigate interactions between proteins of interest a bacterial two-hybrid approach was used. To expand upon the existing collection of bacterial two-hybrid constructs new constructs were generated, briefly, genes of interest were cloned in frame into some or all the bacterial two-hybrid vectors (pKT25, pKNT25, pUT18, pUT18C), giving rise to either N- or C-terminal fusions to the T18 or T25 subunits of the catalytic domain of *Bordetella pertussis* adenylate cyclase, CyaA. As described in section 2.2.5, one T18 and one T25 encoding plasmid were co-transformed into DHM1 competent cells lacking an endogenous adenylate cyclase. Co-transformants were selected on LB agar plates supplemented with 50 µg/ml kanamycin and 100 µg/ml ampicillin during incubation at 30 °C until the appearance of isolated colonies.

In triplicate, single colonies were inoculated into LB broth supplemented with 50 µg/ml kanamycin, 100 µg/ml ampicillin and 0.5 mM IPTG (Melford) and grown at 30 °C overnight. 10 µl of culture was spotted onto LB agar supplemented with 50 µg/ml kanamycin, 100 µg/ml ampicillin, 1 mM IPTG (Melford) and 100 µg/ml 5-Bromo-4-chloro-3-indolyl beta-D-galactopyranoside (X-Gal) (Melford) and incubated at 30 °C for 24 or 40 hours. Hydrolysis of X-Gal in the media to produce a blue colour indicated an interaction of the protein fusions and reconstitution of the adenylate cyclase domain. The positive control for bacterial two-hybrid interactions was the homodimerisation of the leucine zipper region of the yeast protein GCN4 (516). Interactions with empty vector partners were used as a negative control.

2.5.2 Bacterial two-hybrid microplate reader β-galactosidase assay

Bacterial two-hybrid interactions were more quantitatively assessed with a microplate reader β-galactosidase assay. Co-transformation and overnight growth of single colonies in liquid culture were performed as described in section 2.5.1. Following growth at 30 °C, bacteria were sub-cultured to OD_{600} 0.1 and incubated under identical conditions overnight.

In a 96-well microplate (SLS), 80 µl of culture, either neat or diluted 1 in 10 in LB broth for strong interactions, was added to each well. The OD_{600} was then measured against an LB broth blank of equivalent volume in a microplate reader (BMG Labtech). To each well, 120 µl aliquots of Z-buffer (60 mM Na_2HPO_4, 40 mM NaH_2PO_4, 10 mM KCl, 1 mM $MgSO_4$) containing additional 35 mM β-

mercaptoethanol, 166 mg/ml T7 lysozyme, 1.1 mg/ml o-nitrophenyl-β-D-galactopyranoside (ONPG) and 6.7 % PopCulture® Reagent (Merck) were added. The microplate was then quickly transferred back to the microplate reader (BMG Labtech) set to 30 °C, and the OD_{420} was measured every minute for up to 4 hours depending on the strength of interaction. This captured the colorimetric change upon hydrolysis of ONPG by β-galactosidase to produce a yellow colour.

The OD_{420} for each well was plotted against time, to give a slope representing β-galactosidase activity per minute. The gradient of the slope over time was calculated in sub-sections of 5 timepoints and from this the maximum rate of β-galactosidase activity was estimated. This OD_{420}/minute and the initial culture OD_{600}, were used to calculate β-galactosidase activity in Miller units using the following equation:

$$Miller\ Units = \frac{1000 * (\mathrm{OD420/min})}{\text{Initial culture OD600} * \text{volume used (ml)}}$$

2.5.3 Pull-down screen in *P. aeruginosa*

Pull-down experiments used pME6032 vectors producing proteins of interest fused to a FLAG tag. For each protein of interest, three constructs were required: the FLAG-tagged protein of interest, an untagged version of the same protein and an unrelated FLAG-tagged protein. These plasmids were conjugated into *P. aeruginosa* strains as outlined in section 2.2.8. Two different methods of bacterial growth were carried out.

2.5.3.1 Pull-down with growth in liquid culture

For growth in liquid media, strains were grown in TSB at 37 °C overnight before being sub-cultured to OD_{600} 0.1 in 50 ml TSB with appropriate antibiotics. Cultures were grown at 37 °C until reaching an OD_{600} 0.3 before induction of protein production with 250 µM IPTG (Melford). Cultures were then grown for a further 5.5 hours at 37 °C, before an OD_{600} equivalent of 200 was centrifuged at 4000 rpm at 4 °C for 20 minutes and the supernatant discarded. The recovered pellet was resuspended in 50 ml sterile-filtered PBS (Dulbecco's Phosphate Buffered Saline with $MgCl_2$ and $CaCl_2$, sterile-filtered) (Sigma Aldrich) to a final OD_{600} 4.0.

2.5.3.2 Pull-down with growth on solid media

For growth on solid media, strains were streaked onto LB agar plates and incubated at 37 °C overnight. From this plate, a single colony was recovered and resuspended in 300 µl LB broth. On three LB agar plates supplemented with appropriate antibiotics and 100 µM IPTG (Melford), 100 µl aliquots of resuspended culture were spread and incubated overnight at 25 °C for studying the H2-T6SS or 30 °C for studying the H3-T6SS. Bacteria were then harvested using L-shaped spreaders (VWR) and resuspended in sterile-filtered PBS (Sigma Aldrich). The resuspended bacteria were normalised to an OD_{600} 4.0 in 50 ml PBS, as above.

2.5.3.3 Cross-linking and pull-down

Bacteria resuspended in PBS were cross-linked with the addition of 5 mM dimethyl 3,3'-dithiobispropionimidate (DTBP) (Thermo Fisher Scientific). The cross-linking reaction was incubated for 45 minutes at room temperature, with agitation every 10 minutes. 20 mM Tris- HCl pH 7.6 was then added and incubated for 15 minutes at room temperature to quench the remaining DTBP. Cells were then recovered by centrifugation at 4000 rpm at 4 °C for 20 minutes, the supernatant discarded, and cells resuspended in 50 ml sterile-filtered PBS (Sigma Aldrich), before being centrifuged again and resuspended in 35 ml sterile-filtered PBS (Sigma Aldrich). Cells were lysed using the Fisherbrand™ with Q500 Sonicator probe (Thermo Fisher Scientific) at 60 % amplitude with a process time of 2 minutes. Lysed cells were then centrifuged at 18000 *g* at 4 °C for 45 minutes to isolate the cellular lysate.

To avoid contamination, the sample was transferred to a microbiological safety cabinet to carry out the remaining steps. Anti-FLAG® M2 Magnetic Beads (Millipore) were equilibrated by washing three times with 1 ml sterile-filtered PBS (Sigma Aldrich). Each lysate was mixed with 40 µl of beads, and this was mixed on a tube roller at 4 °C overnight. A magnetic rack was used to recover the beads with any bound bait protein and cross-linked partners from the supernatant. The beads were carefully washed eight times with 1 ml sterile-filtered PBS (Sigma Aldrich). The beads were finally resuspended in 20 µl sterile-filtered PBS (Sigma Aldrich) and flash frozen in liquid nitrogen for mass spectrometry analysis.

2.5.4 Mass spectrometry analysis

To identify proteins pulled down on anti-FLAG beads (Millipore), frozen beads with bound bait proteins and cross-linked partners were sent for mass spectrometry analysis at the BBSRC Mass Spectrometry and Proteomics Facility at the University of St Andrews, UK.

Protein samples were resuspended to a concentration of 1 µg/ml in 25 µl of 20 mM ammonium bicarbonate. Proteins were digested overnight at 30 °C with trypsin at a ratio of 20:1 protein mixture:trypsin. The resulting peptide mixture was analysed under trap and elute conditions using an Acclaim™ Pepmap™ 100 Nano-trap column (Thermo Fischer Scientific) on and Eksigent NanoLC-Ultra 2D HPLC System (AB Sciex) coupled to a Triple-TOF 5600+ mass spectrometer (AB Sciex) via a Nanospray III source (AB Sciex). Peptides were loaded in 98 % (v/v) water, 2 % (v/v) acetonitrile, 0.05 % (v/v) trifluoroacetic acid and washed on the trap for 20 minutes. Peptides were then injected onto the column and eluted over 100 minutes with an increasing gradient of acetonitrile. Mass spectra were acquired between 400-1250 *m/z* and the top 20 peptides with a charge between +2 and +5 were selected to proceed to MS/MS.

2.5.4.1 MaxQuant analysis

Data were processed using MaxQuant version 1.5.8.3 (525). Peptides identified in MS/MS spectra were searched against the Uniprot *P. aeruginosa* PAO1 reference proteome (proteome ID: UP000002438) using the Andromeda search engine. Carboamidomethyl was specified as a fixed modification, while methionine oxidation and N-terminal acylation were specified as variable modifications. *In silico* digest of the reference proteome was performed using the Trypsin/P setting with up to two missed cleavages allowed. The false discovery rate (FDR) was set at 0.01 for peptides, proteins and sites. The “match between runs” function was enabled. The sequence decoy mode used was “revert”. Protein quantification was performed using the MaxLFQ algorithm within MaxQuant. Unique and razor peptides were used for quantification. All other parameters were used as pre-set in MaxQuant.

2.5.4.2 Perseus analysis

Data was analysed using Perseus version 1.5.8.5 (526). Proteins present in the “reverse”, “only identified by site” and “potential contaminant” databases were removed, and proteins identified by one or more unique peptides were retained for further analysis. LFQ identities were logarithmised

(log_2) and biological replicates were grouped together. The data was filtered to retain only proteins that appeared in two or more biological replicates from at least one sample. Missing log_2 LFQ values were imputed using a downshifted normal distribution (1.8 downshift, 0.3 width).

Proteins identified as enriched in the sample corresponding to the FLAG-tagged protein of interest were cross-referenced against the untagged control and unrelated FLAG-tagged protein to determine binding specificity. Proteins were ranked according to enrichment compared to the untagged control with a t-test LFQ intensity difference of ≥ +1.5 log_2 as a cut off.

2.6 Fluorescence microscopy

P. aeruginosa strains with fluorophore fusions to T6SS genes at their native loci were imaged using fluorescence microscopy to assess the abundance and dynamics of these components. Samples were prepared through either growth in liquid culture or on solid media.

2.6.1 Microscopy analysis of bacterial cells grown in liquid culture

In some cases, samples were prepared for microscopy imaging by growth in liquid culture as described previously (508). Briefly, strains were grown at 37 °C in TSB supplemented with appropriate antibiotics before being sub-cultured to an OD_{600} of 0.1 in 50 ml TSB without antibiotic. Bacteria were grown with shaking at 200 rpm to an OD_{600} between 3.0-5.0. Conditions for growth varied depending on the T6SS being assessed: for the H1- and H2-T6SS growth at 37 °C for 6-8 hours, for the H3-T6SS growth at 25 °C for 13 hours.

Cells were then imaged using a glass bottomed 35 mm imaging dish (µ-Dish 35 mm, high Glass Bottom) (ibidi). 6 µl of bacterial culture was transferred to the glass base of the dish and a VBM agar pad was placed on top of the culture to sandwich it between the agar and the glass. Samples were imaged using the Axio Observer Z1 (Zeiss) inverted widefield microscope with a 100x/1.4 Oil Ph3 M27 Plan-Apochromat objective (Zeiss), a SpectraX LED light engine (Lumencore) and an ORCA-Flash 4.0 digital CMOS camera (Hamamatsu). An environmental control system was used to regulate the temperature of the sample within the microscope chamber.

Images were captured using phase contrast to assess total bacterial abundance and fluorescence channels to capture signal from sfGFP and mScarlet-I fluorophores either independently or in parallel.

2.6.2 Microscopy analysis of bacterial cells grown on solid media

Alternatively, samples were prepared for microscopy imaging by growth on solid media. Strains were grown at 37 °C in TSB supplemented with appropriate antibiotics before harvesting cells by centrifuging 1.5 ml at 8000 rpm for 3 minutes. The pellet was washed with sterile PBS and the OD_{600} adjusted to 0.05. 6 µl of diluted culture was then spotted onto an LB agar pad and well dried. This agar pad was then inverted and transferred to a glass bottomed 35 mm imaging dish (ibidi), where the dried spot was sandwiched between the agar and the glass. The dish was then incubated under conditions specific to the T6SS being imaged: for the H1-T6SS samples were incubated at 37 °C for 3-

4 hours, for the H2-T6SS samples were incubated at 25 °C for 5-6 hours. Following incubation, samples were imaged as described in section 2.6.1.

2.7 Transcriptional reporter fusion

A transcriptional reporter fusion was used to assess expression from the H1-T6SS *tssA1* promoter in different genetic backgrounds. This involved the introduction of a plasmid encoding a *tssA1* promoter fusion with *sfGFP*. Bacteria were grown overnight at 37 °C in LB supplemented with appropriate antibiotics before harvesting cells by centrifuging 1.5 ml at 8000 rpm for 3 minutes. After washing in 1.5 ml sterile PBS the OD_{600} was adjusted to 1.0. A 1 in 10 dilution was then made to a total volume of 200 µl with LB supplemented with the appropriate antibiotic in a 96-well microplate (SLS). The microplate was transferred to a microplate reader (BMG-Labtech) and bacteria were grown at 37 °C with agitation. sfGFP fluorescence intensity and OD_{600} were measured every 10 minutes. The GFP fluorescence intensity was measured with an excitation filter of 485 nm and emission filter of 250 nm.

2.8 *In silico* methods

2.8.1 Sequence analysis

The *Pseudomonas* genome database version 20.2 (https://pseudomonas.com/) (527) was used as a source of *P.* aeruginosa and *P. putida* DNA and protein sequence information. Pairwise sequence alignments were performed using EMBOSS Needle (EMBL) (528), while multiple sequence alignments were performed using Clustal Omega (EMBL) (529). The prediction of transmembrane helices was performed using the TMHMM server v2.0 (530).

2.8.2 Data presentation and statistical analysis

All quantitative data presented here were analysed in GraphPad Prism version 9.4.0 for Windows (GraphPad Software, San Diego, California USA, www.graphpad.com), including the plotting of graphs and statistical analysis. For the statistical analysis of competition assay data, one-way ANOVA was performed followed by Dunnett's multiple comparisons test.

2.8.3 Figure construction

Figures for qualitative data were assembled in Microsoft PowerPoint. Schematics were created either in Microsoft PowerPoint or using Biorender.com.

2.8.4 Microscopy image analysis

Microscopy images were analysed using ZEISS ZEN 3.4 (blue edition) and FIJI ImageJ version 2.0.0/1.53c (531). ZEISS ZEN software was used to adjust signal brightness and contrast, merge images taken with different channels, crop images, embed scale bars and export image files. FIJI was used to determine cell count: the Threshold tool was used to identify cells relative to the background, the Watershed tool was then used to distinguish individual cells in highly populated regions, then the Analyse Particles tool was used to count the highlighted cells. FIJI was also used to count fluorescent foci using the Multi-point tool.

2.8.5 Protein homology molecular modelling and protein structural analysis

Protein structural models of TssA domains were generated using Robetta protein structure prediction service (532) and SWISS MODEL protein structure homology-modelling server (533). GetArea was used to calculate the solvent accessible surface area of proteins (534). Molecular docking of proteins was performed using the ZDock server (535). Protein structural alignment was carried out using the Dali protein structure comparison server (536). Protein structures were visualised and images exported using PyMOL (The PyMOL Molecular Graphics System, Version 2.0 Schrödinger, LLC).

3. Results: Functional characterisation of TssA proteins

3.1 Introduction

There are three T6SS clusters within the *P. aeruginosa* genome (H1-, H2- and H3-T6SS), each encoding all the core structural components required for assembling a functional T6SS (*tssA-M*). Clusters can also encode accessory components whose roles can include T6SS regulation (i.e. *tagQRST*). The *tssA* genes encode a class of proteins of particular interest due to their variability between different T6SSs. TssA proteins vary in size, domain organisation, symmetry and structure (360,376,377,508,509). One way this variation has been classified is grouping TssA proteins by size, i.e. long ($TssA_L$) and short ($TssA_S$) proteins (see section 1.4.1) (508). *P. aeruginosa* encodes three TssA proteins: the short TssA1 and TssA3 and the long TssA2. The distribution of long and short TssA proteins is consistent with the phylogenetic group to which the corresponding T6SS gene cluster belongs, specific phylogenetic groups are associated with either a $TssA_L$ or a $TssA_S$ (508). The sizes of TssA proteins also corresponds with specific domain organisation and dimensions of quaternary structures formed by these proteins (508).

3.1.1 Approaches to study T6SS functionality

The functionality of the T6SS can be studied through various approaches to assess different aspects of its activity. In protein secretion assays, western blots are used to assess the presence of T6SS secretion markers, such as the Hcp inner tube, VgrG spike or effector proteins (i.e. *P. aeruginosa* Tse proteins), within the whole cell extract and the supernatant. The antibacterial activity can be studied with interbacterial competition assays, where the T6SS-encoding attacker strain is incubated with a T6SS-sensitive prey strain and killing of the prey is quantified. Finally, fluorescence microscopy can monitor the abundance and localisation of T6SS components tagged with a fluorophore such as sfGFP or mScarlet. Each approach elucidates distinct information and their use in combination can help paint a more complete picture of T6SS function.

3.1.2 Functionality of short TssA proteins

The $TssA_S$ proteins whose functional contribution to T6SS activity have been studied to date are those of *P. aeruginosa* (TssA1), *B. cenocepacia* ($TssA^{BC}$), *P. putida* ($TssA1^{PP}$) and *Acinetobacter baylyi* ($TssA^{AB}$) (324,358,376,377,508,509,513). Each of these short TssAs has been shown to be required for

secretion of T6SS-associated secretion markers (324,358,376,508,509). Additionally, TssA1^{PP} is required for T6SS-dependent killing of *E. coli* and relevant plant pathogens, whilst in its absence sheath structures that can be visualised by fluorescence microscopy no longer form (324,508). It is not always the case that TssA$_S$ proteins are essential for sheath formation. Upon deletion of *tssA1,* fluorophore-tagged sheath structures could still be visualised, although at a far reduced abundance and only few showing typical sheath dynamics, i.e. extension and contraction (376,377). Using differential tagging and fluorescence microscopy the relative position of different T6SS components can also be studied. This showed that TssA1 is static at the T6SS assembly initiation site, suggesting it is found at the baseplate (377). However, this localisation could only be visualised in the presence of the wildtype untagged TssA1, indicating that the tagged version was unable to fully complement wildtype *tssA1* deletion and so the full range of TssA1 activity may not be captured (377). In contrast, fluorophore-tagged TssA1^{PP} and TssA^{AB} associate with the T6SS assembly initiation site, but are then displaced by the polymerisation of the sheath and are present at the distal end of the sheath as it extends across the cell before it contracts (508,513). While studies on the contribution of TssA$_S$ proteins to T6SS functionality showed similar trends overall, it is unclear whether they all associate with the T6SS in the exact same way.

3.1.3 Functionality of long TssA proteins

The TssA$_L$ proteins whose functional contribution to T6SS activity have been studied to date are those of enteroaggregative *E. coli* (TssA^{EC}), *P. aeruginosa* (TssA2) and *V. cholerae* (TssA^{VC}) (360,377,394,512,537). The long TssA^{EC} and TssA^{VC} have been shown to be required for secretion of T6SS-associated secretion markers (360,394). Furthermore, T6SS-dependent killing of both *E. coli* and amoeba by *V. cholerae* is much reduced in the absence of TssA^{VC} (377,394,512). When studying sheath formation by fluorescence microscopy, there were no sheath structures formed in the absence of TssA^{EC}, while upon deletion of *tssA^{VC}* or *tssA2* sheath structures could still be visualised, although at a far reduced abundance and with few showing typical sheath dynamics (360,377). The *V. cholerae* sheath structures formed in the absence of TssA^{VC} were polymerised at a slower rate (377). In another study, sheath structures were completely absent upon *tssA^{VC}* deletion, suggesting that experimental set-up may influence the outcome of these approaches (512). Each of the studied TssA$_L$ proteins has been shown to localise with the T6SS assembly initiation site prior to sheath polymerisation and then at the distal end of the polymerising sheath, with dissociation before contraction (360,377). Some diversity has been demonstrated in TssA association with the sheath, with TssA^{VC} and TssA2 on occasion observed to dissociate from either a fully extended sheath or a polymerising sheath, or alternatively remaining associated with the distal end of the sheath following contraction (377).

3.1.4 Theories on functionality of long and short TssA proteins

As said, there is a great variability in TssA proteins, with very different structures containing distinct domains being formed from long and short TssA proteins (see section 1.4.1) (360,376,377,509). This variability in domain organisation and structure is a key factor in the debate about the functional similarities and differences between long and short TssA proteins. There are two prevailing theories about the functionality of TssA proteins. On the one hand it is postulated that the differences between TssA proteins are associated with a functional difference. Specifically, it is suggested that $TssA_S$ proteins are static components associated with the baseplate and involved in the initiation of sheath polymerisation, while $TssA_L$ proteins are dynamic components which act as chaperones at the distal end of the sheath and inner tube, coordinating the co-polymerisation of this structure (376,377). On the other hand, it is postulated that despite their differences, the functionality of all TssA proteins is similar. This theory is based on the similarities in TssA proteins, including similarity in interaction partners, despite structural differences. It is suggested that TssA proteins may share a common function as dynamic components associated with the distal end of the sheath, where this common function is achieved through slightly different mechanisms for long and short TssA proteins (509).

From the available data both long and short TssA proteins are required for secretion of T6SS-associated secretion markers (360,376,377,508,509). While, in the absence of TssA both T6SS-dependent killing and the formation of fluorophore-tagged sheath structures is either completely abolished or drastically reduced (360,376,377,508,509). The requirement for TssA proteins for a fully functional T6SS therefore does not seem to vary between clusters encoding a long or short TssA. Fluorescence microscopy has identified both long and short TssA proteins as dynamic components at the distal end of the sheath, however the short TssA1 has also been identified as a static, baseplate-associated component. Because of this ambiguity, it is therefore not currently clear whether and to what degree different groups of TssA proteins may have distinct functionalities despite all the evidence showing similarities.

3.2 Aims of this study

The aim of this study was to carry out a comprehensive and systematic analysis of the contribution of the *P. aeruginosa* TssA proteins to the functionality of their respective T6SSs. This would provide the basis to compare the role and associated mechanisms of long and short TssA proteins within a single organism.

This analysis involved:

1) Chromosomal in-frame deletion mutants engineered for each of the three *tssA* genes; *tssA1*, *tssA2* and *tssA3*.
2) Phenotypic assays to evaluate T6SS activity, including i) secretion assays, where the presence of T6SS-associated secretion markers in the supernatant is examined by western blot, ii) interbacterial competition assays, where the ability of a T6SS-encoding attacker strain to kill a prey is quantified.
3) Fluorescence microscopy to visualise the T6SS, using fluorescently tagged T6SS components to study the formation and abundance of T6SS structures and their localisation.

The genetic backgrounds and conditions required for these techniques were initially optimised, allowing them to be used to assess the contribution of each TssA protein according to the conditions required for functionality of the associated T6SS.

These techniques measure different outputs so when used together they can provide a comprehensive overview of T6SS behaviours, setting the foundation for further studies, including complementation of *tssA* deletions using various non-cognate *tssA* genes (Chapters 4 and 5).

3.3 Functional characterisation of TssA1

3.3.1 H1-T6SS expression and secretion are low in the *rsmA* background

It has previously been shown that the post-transcriptional regulator RsmA is a repressor of all three of the *P. aeruginosa* T6SSs (338). It is therefore expected that in a genetic background with deletion of *rsmA*, there will be increased expression and activity of each of these T6SSs, including the H1-T6SS. In a PAO1Δ*rsmA* background, a chromosomal in-frame deletion mutant of *tssA1* was engineered, and a secretion assay was used to assess the production and secretion of the H1-T6SS secretion markers, inner tube protein Hcp1 and spike protein VgrG1a. In the parental *rsmA* background, expression of Hcp1 and VgrG1a was detectable, but faint (Figure 3.1A). However, these secretion markers could not be detected in the supernatant fraction, likely due to the low levels of expression detected. In other repeats some low levels of secretion could be detected, but this was not consistent. A difference in H1-T6SS secretion could therefore not be demonstrated between the *rsmA* positive control and the T6SS-negative control with deletion of the gene encoding the sheath component TssB1.

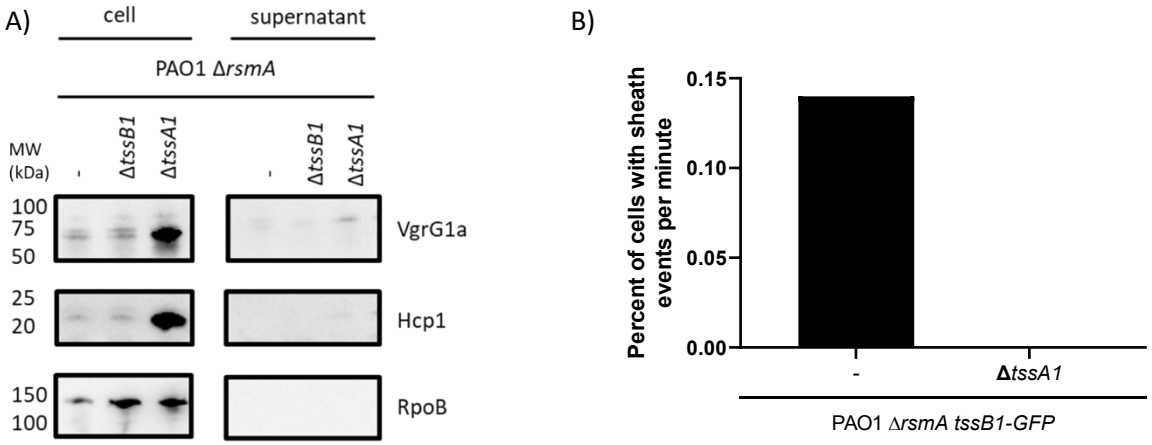


Figure 3.1 Assessment of H1-T6SS activity in a PAO1Δ*rsmA* background. A) Western blot of a H1-T6SS secretion assay in the *rsmA* background, to assess the levels of secretion markers Hcp1 and VgrG1a in the supernatant sample. Cell and supernatant samples were harvested after 5-7 hours growth at 37 °C. Proteins detected in the western blot are indicated to the right. Molecular weight (MW) markers (left) are in kilodaltons (kDa). RpoB was used as a loading and bacterial lysis control. B) Quantification of the percent of cells with TssB1-GFP sheath events per minute in the *rsmA* background by fluorescence microscopy. Strains were grown in liquid culture at 37 °C for 6 hours before imaging. The percent of cells with sheath events per minute fell from 0.14 % (n=8829) to 0 % (n=7086) upon deletion of *tssA1*. Data were taken from three fields of view for one experiment.

To assess the activity and abundance of the H1-T6SS *in vivo*, fluorescence microscopy was used to visualise sheath structures. Strains were engineered to produce TssB1-GFP, expressed from the native *tssB1* locus. The formation of H1-T6SS sheaths was infrequent, with 0.14 % of cells forming sheath structures per minute (Figure 3.1B). Upon deletion of *tssA1* this fell to 0 %. Few sheath structures were therefore detected in this background, potentially explaining why limited secretion was identified in secretion assays.

In light of these data, it was concluded that the *rsmA* background was not appropriate for studying H1-T6SS activity. Additionally, upon deletion of *tssA1*, a strong polar effect was observed with the production of Hcp1 and VgrG1a proteins encoded by downstream genes being hugely upregulated (Figure 3.1A). With this polar phenotype and in the absence of detectable secretion, other genetic backgrounds were investigated.

3.3.2 TssA1 is required for H1-T6SS activity in the *retS* background

Previous functional characterisation of TssA1 has taken place in the PAKΔ*retS* and PAO1Δ*retS* backgrounds, where RetS is a sensor acting upstream of RsmA (376,377). RetS inhibits the activity of the sensor kinase GacS, which acts through its downstream response regulator GacA to control the production of the small non-coding RNAs RsmY and RsmZ (see section 1.3.5.1). These RNAs sequester RsmA preventing its binding to, and regulation of, mRNA targets. Thus the *retS* deletion promotes the sequestration of RsmA by the overproduced RsmY and RsmZ (466). A *retS* deletion was shown to increase the abundance of H1-T6SS components by 2-6 fold (538).

In the previously studied PAKΔ*retS* strain, a chromosomal in-frame deletion mutant of *tssA1* was engineered, identical to the *rsmAtssA1* mutant described in section 3.3.1. In this genetic background, production of TssB1 and Hcp1 could be detected, and Hcp1 secretion was unambiguously observed in the parental strain (Figure 3.2). This secretion was abolished upon deletion of either *tssB1* or *tssA1*, corroborating previous data identifying TssA1 as required for the secretion of Hcp1 in this background (376). The deletion of *tssA1* did not lead to a notable upregulated production of TssB1 and Hcp1 (Figure 3.2), suggesting that the upregulation observed in the PAO1Δ*rsmA*Δ*tssA1* strain is either a feature of the PAO1 background or of the *rsmA* deletion (Figure 3.1A).

The PAKΔ*retS* background could thus be used to study secretion by the H1-T6SS, however, the PAK background was previously identified to have lower levels of expression and activity of the H2- and H3-T6SSs. To characterise all three *P. aeruginosa* TssA proteins in a single strain background, the PAO1 strain was preferred, as expression of all three T6SS gene clusters has been demonstrated. A

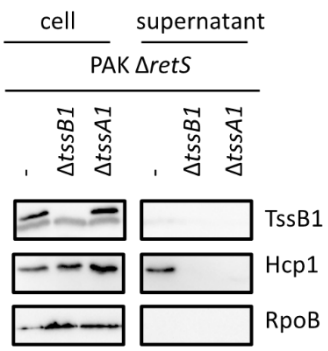


Figure 3.2 Assessment of H1-T6SS secretion in a PAKΔ*retS* background. Western blot of a H1-T6SS secretion assay in the PAKΔ*retS* background, to assess the levels of secretion marker Hcp1 in the supernatant sample. Cell and supernatant samples were harvested after 5-7 hours growth at 37 °C. Proteins detected in the western blot are indicated to the right. RpoB was used as a loading and bacterial lysis control.

chromosomal in-frame deletion of *retS* was engineered in the PAO1 background, with subsequent in-frame deletions of *tssB1* or *tssA1*. In contrast to the PAO1Δ*rsmA* background, a clear Hcp1 secretion phenotype could be observed in the parental strain, and secretion was dependent on the presence of TssB1 and TssA1 (Figure 3.3). The absence of Hcp1 secretion in the *tssA1* background could be complemented with a plasmid constitutively expressing *tssA1*.

Upon deletion of *tssA1* in the PAO1Δ*retS* background, there was upregulated expression of Hcp1, although far less pronounced than in the PAO1Δ*rsmA* background (Figures 3.1A and 3.3). This downstream overexpression phenotype seen in a *tssA1* deletion may be PAO1 specific, as it does not seem to be present in the PAKΔ*retS* background (Figure 3.2). However, these observations are purely based on interpretation of western blot signal intensity, a technique such as RT-PCR would allow for a more quantitative assessment.

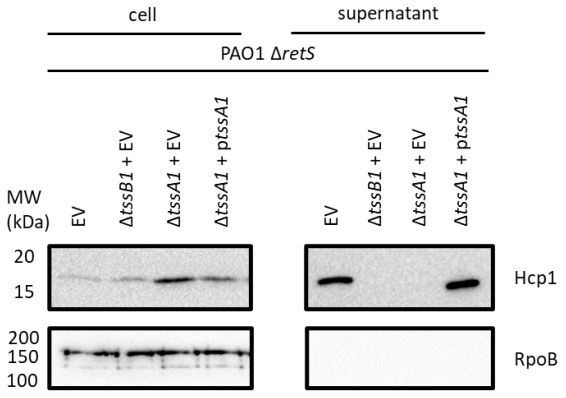


Figure 3.3 Assessment of H1-T6SS secretion in a PAO1Δ*retS* background. Western blot of a H1-T6SS secretion assay in the *retS* background, to assess the levels of secretion marker Hcp1 in the supernatant sample. To assess complementation of the *tssA1* deletion, the pBBR1MCS4 vector was introduced either as empty vector (EV) or encoding *tssA1* (p*tssA1*). Cell and supernatant samples were harvested after 5-7 hours growth at 37 °C. Proteins detected in the western blot are indicated to the right. MW markers (left) are in kDa. RpoB was used as a loading and bacterial lysis control.

Given that a secretion assay in the *retS* background produced a clear T6SS-dependent secretion phenotype, these strains were also used to optimise an interbacterial competition assay to assess H1-T6SS-dependent killing of an *E. coli* prey strain producing GFP. Initially, attacker *P. aeruginosa* strains and prey *E. coli* were mixed at a 1:1 ratio and incubated at 37 °C for 24 hours before being recovered and fluorescence signal intensity quantified. Under these conditions, no significant difference was observed in the fluorescence of recovered competition mixes containing the parental strain and the *tssB1* strain, suggesting no significant prey killing (Figure 3.4A). To increase the amount of T6SS-dependent prey killing, the competition was modified by altering the ratio of attacker to prey to 3:1 (Figure 3.4B) or 5:1 (Figure 3.4C). Each of these competitions was carried out only twice, and while there appeared to be a difference in killing between the parental strain and mutants lacking either *tssB1* or *tssA1*, the fold change was not particularly large, 1.6-fold for the 3:1 competition and 1.4-fold for the 5:1 competition. The competition assay was therefore modified according to previously described protocols, where attacker and prey strains undergo two incubations (412,503). Attacker and prey strains were mixed at a 1:1 ratio at 37 °C for 5 hours, then recovered and serially diluted before incubation at 37 °C overnight. The diluted bacteria were then recovered, and fluorescence signal intensity quantified. Under these conditions, T6SS-dependent killing of the *E. coli* prey by the parental attacker strain could be monitored and was impaired upon deletion of either *tssB1* or *tssA1*, with a 3.5-fold change between positive and negative controls (Figure 3.4D). The deletion of *tssA1* could be complemented by constitutive expression of *tssA1* from a broad host range plasmid.

Some variability was observed in fluorescence signal of the *tssB1* and *tssA1* mutants using this two-incubation method when compared to the 3:1 and 5:1 single incubation method, where repeats were very consistent (Figure 3.4). A protocol with two incubations may give rise to additional variability as bacteria must be plated and recovered twice before signal quantification. In the *retS* background the two-incubation method produced the most conclusive data, however a single incubation method would be preferred although it may require a genetic background with a higher level of H1-T6SS activity.

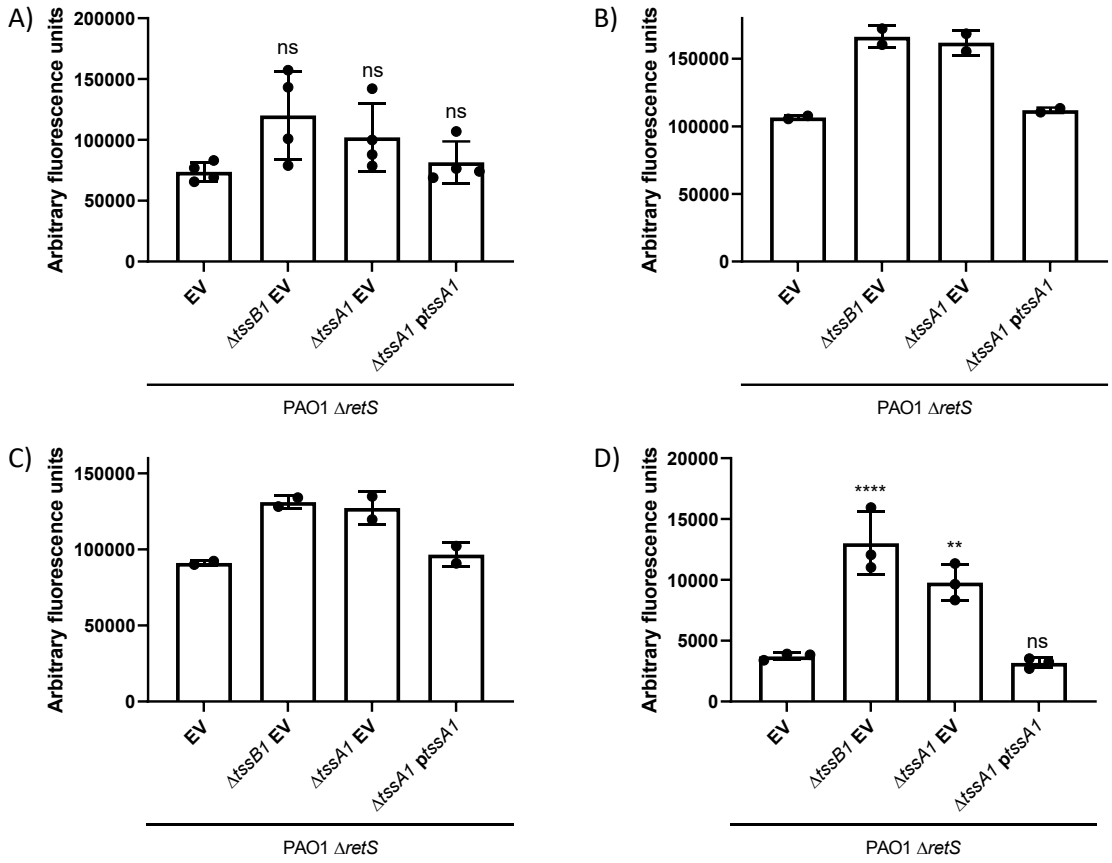


Figure 3.4 Assessment of H1-T6SS prey killing in a PAO1Δ*retS* background. H1-T6SS competition assays in the *retS* background, to assess the T6SS-dependent killing of a GFP-producing *E. coli* prey by *P. aeruginosa* attacker strains carrying the pBBR1MCS4 vector either as empty vector (EV) or encoding *tssA1* (p*tssA1*). Values are presented as means and error bars represent the standard deviation. A) Attacker *P. aeruginosa* and prey *E. coli* were mixed at a 1:1 ratio and incubated at 37 °C for 24 hours, before GFP signal quantification. (n=4). B) Attacker *P. aeruginosa* and prey *E. coli* were mixed at a 3:1 ratio and incubated at 37 °C for 24 hours, before GFP signal quantification. (n=2). C) Attacker *P. aeruginosa* and prey *E. coli* were mixed at a 5:1 ratio and incubated at 37 °C for 24 hours, before GFP signal quantification. (n=2). D) Attacker *P. aeruginosa* and prey *E. coli* were mixed at a 1:1 ratio and incubated at 37 °C for 5 hours, before recovery, dilution, and incubation at 37 °C for 17 hours overnight. GFP signal was then quantified. (n=3). Statistical testing was conducted by one-way ANOVA with Dunnett's multiple comparisons test, each strain was compared to parental PAO1Δ*retS* EV (ns = not significant, ** $p < 0.001$, **** $p < 0.0001$).

To visualise the H1-T6SS *in vivo* by fluorescence microscopy, strains were engineered to produce TssB1 fused to the red fluorescent protein mScarlet from the native *tssB1* locus. In the parental *retS* strain 10.7 % of cells formed sheaths or foci, which fell to 0.26 % upon deletion of *tssA1* (Figures 3.5A and

3.5B). The loss of sheaths upon *tssA1* deletion could be partially complemented upon constitutive expression of *tssA1* where 5.2 % of cells formed sheaths or foci.

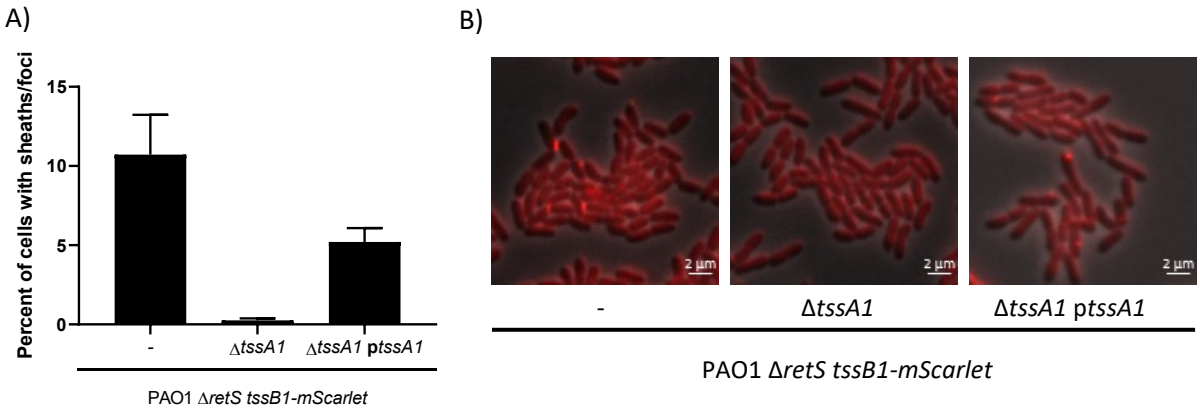


Figure 3.5 Assessment of H1-T6SS sheath formation in a PAO1Δ*retS* background. A) Quantification of the percent of cells with TssB1-mScarlet sheaths or foci in the *retS* background by fluorescence microscopy. Strains were grown on LB agar pads for 3-4 hours at 37 °C before imaging. The percent of cells with sheaths or foci fell from 10.7 % (n=19244) in the parental strain to 0.26 % (n=16387) with *tssA1* deletion, expression of *tssA1* from pBBR1MCS4 recovered this to 5.2 % (n=8117). Data were taken from 2 fields of view for three experiments. Values are presented as means and error bars represent the standard deviation. B) Representative images of TssB1-mScarlet sheath formation in the *retS* background in the presence and absence of *tssA1*. Scale bar represents 2 µm.

In conclusion, the PAO1Δ*retS* background is appropriate to assess the activity of the H1-T6SS, and therefore the role of TssA1, through secretion and competition assays, while fluorophore-tagged H1-T6SS sheath structures could also be visualised by fluorescence microscopy.

3.3.3 TssA1 is required for H1-T6SS activity in the *rsmArsmN* background

In the PAO1Δ*retS* background the activity of the H1-T6SS could be assessed and TssA1 was required for this activity (Figures 3.3, 3.4 and 3.5). In contrast, in the PAO1Δ*rsmA* background the expression of H1-T6SS is too low to conclusively assess its functionality (Figure 3.1). Within the Gac-Rsm pathway, the activity of RetS in modulating GacS influences the downstream activity of the translational repressor RsmA. However, *P. aeruginosa* also encodes the RsmA homologue RsmN, which is also proposed to play a role in the Gac-Rsm pathway. In a *retS* deletion both RsmA and RsmN would be expected to be sequestered by the small non-coding RNAs RsmY and RsmZ, while in an *rsmA* deletion RsmN is still present and may be able to compensate for the absence of RsmA, as they have been shown to bind some overlapping targets (539–541). Both RsmA and RsmN have been identified to

bind to sequences in the *tssA1* and *fha1* promoter regions, so would be expected to affect H1-T6SS production (539,541,542). In fact, a double *rsmArsmN* mutant strain has been shown to have high levels of H1-T6SS activity, both in terms of Hcp1 secretion and prey killing (539). Functional H1-T6SS assays were therefore carried out in a *rsmArsmN* background, to identify whether it may be an appropriate background for studying the contribution of TssA1 to H1-T6SS activity.

A secretion assay demonstrated that the parental *rsmArsmN* strain was able to secrete Hcp1, which was dependent on the presence of TssB1 and TssA1 (Figure 3.6A). Absence of Hcp1 secretion in the *tssA1* background could be complemented with a plasmid constitutively expressing *tssA1*. These strains were also used for an interbacterial competition assay, where attacker *P. aeruginosa* strains and prey *E. coli* were mixed at a 1:1 ratio and incubated at 37 °C for 24 hours. In the *retS* background, a competition assay under these conditions yielded no significant difference in killing between strains with active and inactive T6SS (Figure 3.4A). In contrast, in the *rsmArsmN* background there was a 3-fold change in prey fluorescence signal between the T6SS-positive parental strain and a strain with *tssB1* deletion (Figure 3.6B). A strain with *tssA1* deletion killed prey slightly less than the *tssB1* deletion strain, loss of killing in the *tssA1* background could be complemented with a plasmid constitutively expressing *tssA1*. To visualise the formation of H1-T6SS sheaths *in vivo* using fluorescence microscopy, strains were engineered to produce a TssB1-mScarlet chimeric protein expressed from the native *tssB1* locus. In the parental *rsmArsmN* strain 11.5 % of cells formed sheaths or foci, which fell to 0.62 % upon deletion of *tssA1* (Figures 3.6C and 3.6D).

In conclusion, as in the *retS* background, the *rsmArsmN* background is appropriate to study the activity of the H1-T6SS and the role of TssA1 by secretion assay, interbacterial competition assay and fluorescence microscopy.

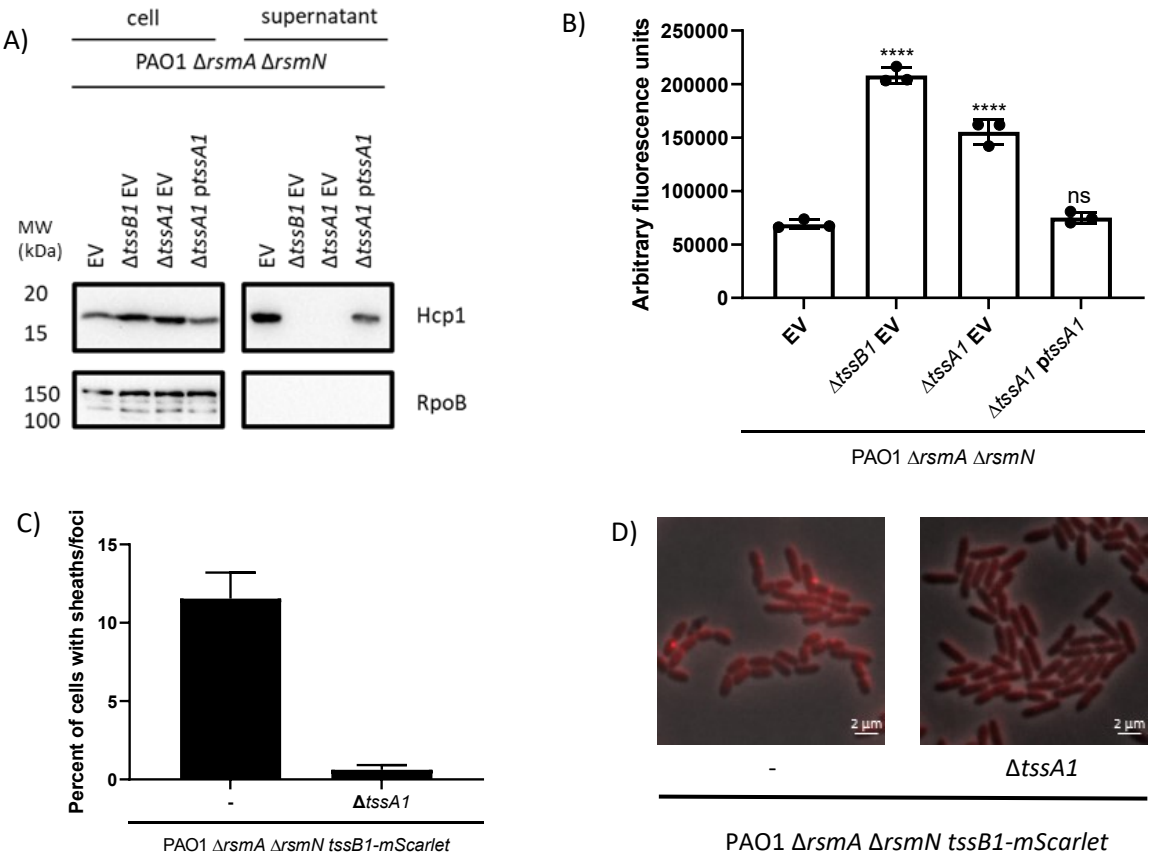


Figure 3.6 Assessment of H1-T6SS activity in a PAO1Δ*rsmA*Δ*rsmN* background. To assess complementation of the *tssA1* deletion, the pBBR1MCS4 vector was introduced either as empty vector (EV) or encoding *tssA1* (p*tssA1*). Values are presented as means and error bars represent the standard deviation. A) Western blot of a H1-T6SS secretion assay in the *rsmArsmN* background, to assess the levels of secretion marker Hcp1 in the supernatant sample. Cell and supernatant samples were harvested after 5-7 hours growth at 37 °C. Proteins detected in the western blot are indicated to the right. MW markers (left) are in kDa. RpoB was used as a loading and bacterial lysis control. B) H1-T6SS competition assays in the *rsmArsmN* background, to assess the T6SS-dependent killing of a GFP-encoding *E. coli* prey by *P. aeruginosa* attacker strains. Attacker *P. aeruginosa* and prey *E. coli* were mixed at a 1:1 ratio and incubated at 37 °C for 24 hours before GFP signal quantification. Statistical testing was conducted by one-way ANOVA with Dunnett's multiple comparisons test, each strain was compared to parental PAO1Δ*rsmA*Δ*rsmN* EV (ns = not significant, **** $p < 0.0001$). (n=3). C) Quantification of the percent of cells with TssB1-mScarlet sheaths or foci by fluorescence microscopy. Strains were grown on LB agar pads for 3-4 hours at 37 °C before imaging. The percent of cells with sheaths or foci fell from 11.5 % (n=11523) in the parental strain to 0.62 % (n=15717) with *tssA1* deletion. Data were taken from 2 fields of view for three experiments. D) Representative images of TssB1-mScarlet sheath formation in the *rsmArsmN* background in the presence and absence of *tssA1*. Scale bar represents 2 µm.

3.3.4 H1-T6SS expression is elevated in a *rsmArsmN* double mutant compared to a *retS* mutant

To characterise the activity of the H1-T6SS and the role of TssA1, components of the Gac-Rsm pathway were deleted to relieve repression on T6SS expression. The *retS* and *rsmArsmN* backgrounds were appropriate for characterisation of H1-T6SS activity, compared to the *rsmA* background. It would be expected that the H1-T6SS activity in *retS* and *rsmArsmN* backgrounds would be similar as the activity of RsmA and RsmN should be lost in both cases, either due to their sequestration or due to their absence. However, a single incubation competition assay could be used to assess T6SS-dependent prey killing in the *rsmArsmN* background, but not the *retS* background, suggesting that the *rsmArsmN* background may have elevated H1-T6SS activity (Figures 3.4A and 3.6B). This could be linked incomplete sequestration of RsmA and RsmN upon *retS* deletion, when compared to their absence upon *rsmArsmN* deletion. To test the relative H1-T6SS expression in these backgrounds, a *rsmN* mutant was added to the panel of Gac-Rsm mutants with additional *tssB1* or *tssA1* deletion and all were screened for production and secretion of Hcp1.

With single deletions of *rsmN* or *rsmA* production of Hcp1 was low and could not be detected without saturating the signal from other backgrounds (Figure 3.7). Secretion of Hcp1 could also therefore not be detected in these backgrounds. In the *retS* and *rsmArsmN* backgrounds, as previously identified, there was detectable Hcp1 production, with secretion dependent on the presence of TssA1 and TssB1. Upon double deletion of *rsmA* and *rsmN*, Hcp1 production appeared elevated when compared to the *retS* background. Despite individual *rsmA* or *rsmN* deletions leading to only minimal Hcp1 production, in combination their deletion had a synergistic effect, leading to high Hcp1 production and secretion. The level of Hcp1 secretion in the *rsmArsmN* background was far greater than that in the *retS* background.

Upon *tssA1* deletion there was increased production of Hcp1 in both *rsmA* and *retS* backgrounds, as was seen previously (Figures 3.1A and 3.3), however in the *rsmArsmN* background there was no detectable increase in Hcp1 production. This suggests that the overproduction of Hcp1 may be linked to the presence of RsmN.

Despite a deletion in *retS* being proposed to lead to the sequestration of RsmA and RsmN, the H1-T6SS activity of a *retS* strain and a *rsmArsmN* strain were different. The production and secretion of Hcp1 by the *rsmArsmN* strain appears higher, and while a *tssA1* deletion leads to increased Hcp1 production in the *retS* strain, this cannot be detected in the *rsmArsmN* strain. This difference may be explained by RsmA and RsmN not being fully sequestered by RsmY and RsmZ, or other differences between these strains may contribute.

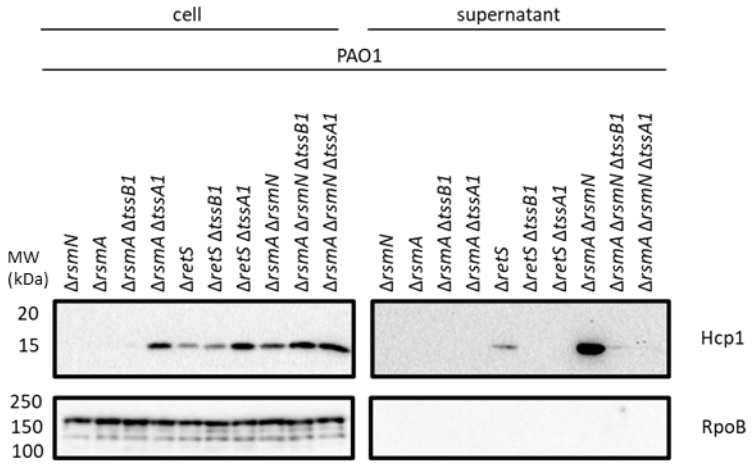


Figure 3.7 Assessment of H1-T6SS protein expression and secretion in various mutants of the Gac-Rsm pathway: *rsmN, rsmA, retS* and *rsmArsmN*. Western blot of a H1-T6SS secretion assay to assess the levels of secretion marker Hcp1 in whole cell extract and supernatant samples. Cell and supernatant samples were harvested after 5-7 hours growth at 37 °C. Proteins detected in the western blot are indicated to the right. MW markers (left) are in kDa. RpoB was used as a loading and bacterial lysis control.

3.3.5 Elevated H1-T6SS expression in a *tssA1* mutant is independent of the loss of TssA1

In both *rsmA* and *retS* strains, upon deletion of *tssA1* downstream gene products such as Hcp1 and VgrG1a were produced at a higher level (Figures 3.1A and 3.3). One way that the *tssA1* deletion could influence production of H1-T6SS components, may be through the absence of the TssA1 protein. It has previously been suggested that TssA of *V. fischeri* has a role in regulating expression of its T6SS cluster, through an unknown mechanism (543). A repressive effect of TssA1 on H1-T6SS expression, likely indirectly as TssA1 is not expected to directly bind DNA, could limit energy expenditure by preventing the production of an excess of T6SS machineries. However, this would also likely limit the effectiveness of T6SS killing in a competition scenario.

Alternatively, the increased production of downstream proteins could be due to a change in regulation of the H1-T6SS cluster at the DNA or RNA level upon deletion of *tssA1*. *tssA1* is the first gene of a polycistronic mRNA transcribed from the H1-T6SS cluster, as such its gene sequence might contain additional regulatory sequences required to fine tune the expression and production of this large multiprotein assembly (Figure 3.8A) (514). Deletion of *tssA1* may also alter the mRNA secondary structure, affecting the binding by regulatory elements. Loss of regulatory sequences or altered mRNA structural features could lead to deregulation of downstream gene expression, including overproduction of T6SS components.

To test whether the absence of TssA1 causes upregulation of H1-T6SS expression, a transcriptional reporter fusion was used with GFP readout under the control of the native *tssA1* promoter. The expression of GFP from the native *tssA1* promoter was identical in the *tssA1* deletion compared to the parental strain and the *tssB1* deletion (Figure 3.8B). This suggests that upregulation of downstream gene expression upon *tssA1* deletion is not due to loss of TssA1, but more likely due to a change in regulation either at transcriptional or post-transcriptional levels.

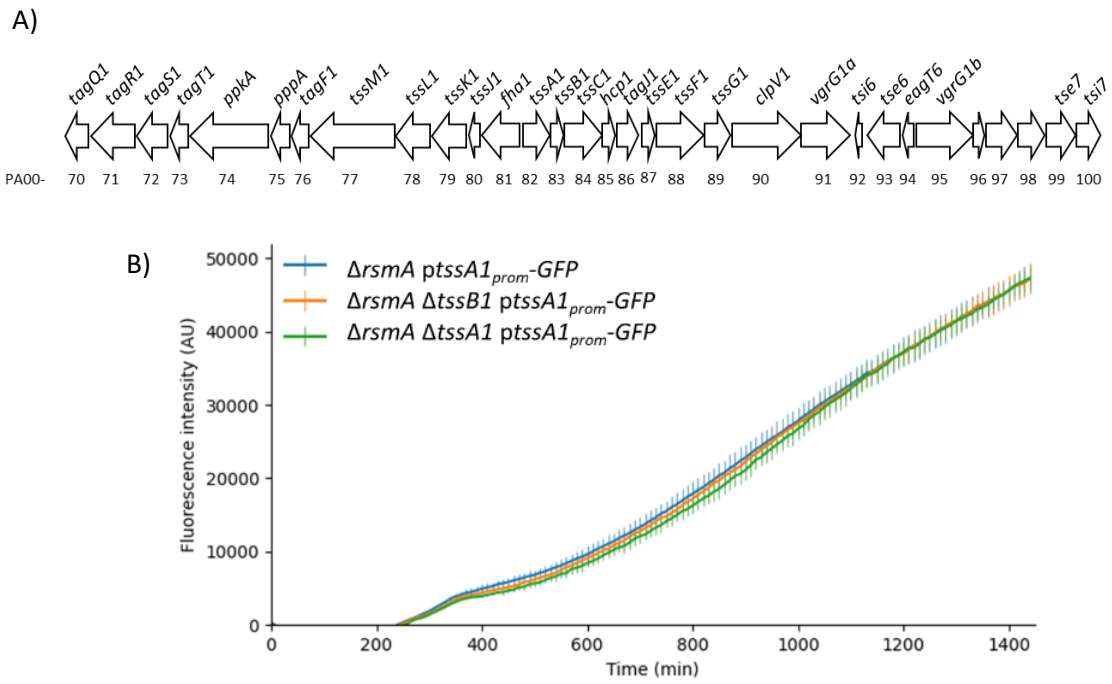


Figure 3.8 Expression from the *tssA1* promoter with a transcriptional reporter fusion. A) Genomic organisation of the H1-T6SS cluster. B) Transcriptional reporter fusion assay, assessing the production of GFP under the control of the native *tssA1* promoter. Strains were grown for 24 hours at 37 °C with agitation.

3.3.6 The position of TssA1 within the H1-T6SS could not be conclusively assessed

Previous time lapse fluorescence microscopy data has been key to characterising the dynamic role of TssA proteins in the assembly of the T6SS (360,377,508). In most cases these data have shown the association of TssA with the T6SS assembly initiation site before association with the distal end of the extending sheath upon its polymerisation to reach the other side of the cell. The outlier to this is TssA1, for whom only a static, baseplate-associated form has been visualised, although only in the presence of native TssA1 (377).

To study TssA1 dynamics, strains were engineered producing fluorophore tagged TssA1 and TssB1 expressed from their chromosomal loci. In a *rsmA* strain producing TssB1-mScarlet and GFP-TssA1 the formation of sheath structures could be identified and some weak TssA1 foci could also be detected

(Figure 3.9A). The low signal strength of the GFP-TssA1 was hypothesised to be linked to background fluorescence due to the production of the green, fluorescent fluorophore pyoverdine by *P. aeruginosa*. A *rsmA* strain was then engineered to produce TssB1-GFP and mScarlet-TssA1. Similarly, in this background the formation of both sheath structures and TssA1 foci could be identified, however, the fluorescent signal of mScarlet-TssA1 was also weak (Figure 3.9B).

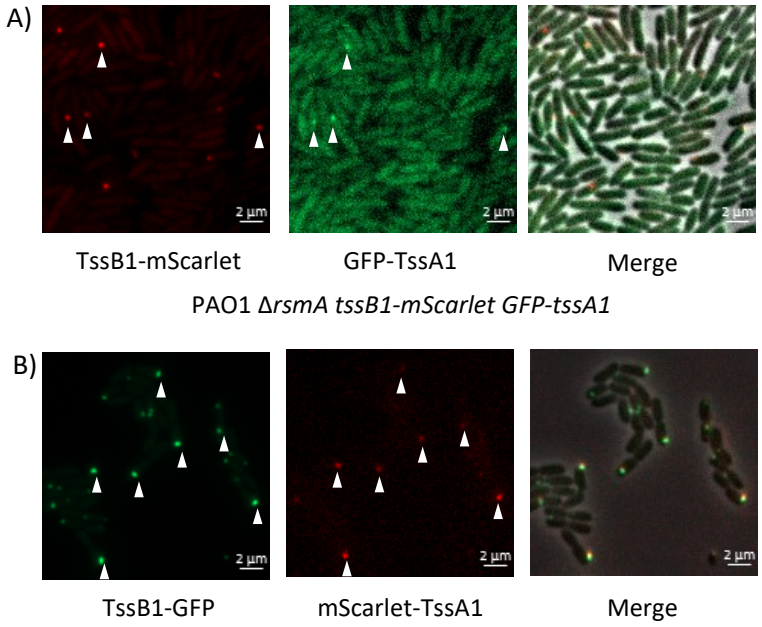


Figure 3.9 Assessment of TssB1 and TssA1 localisation by fluorescence microscopy. Strains were grown on LB agar pads for 3-4 hours at 37 °C before imaging. A) Representative images of mScarlet-tagged TssB1 and GFP-tagged TssA1 in the *rsmA* background. Images to visualise each fluorophore independently and then merged with the phase. B) Representative images of GFP-tagged TssB1 and mScarlet-tagged TssA1 in the *rsmA* background. Images to visualise each fluorophore independently and then merged with the phase. White arrows indicate co-localising foci. Scale bar represents 2 µm.

Some co-localisation of these proteins could be seen (Figure 3.9, white arrows). However, the weak signal of TssA1 with either associated fluorophore did not allow the capture of time lapses, which are required to determine the relative positions of components in a dynamic system. No further details on the positioning of TssA1 within the H1-T6SS could therefore be elucidated.

3.4 Functional characterisation of TssA2

The H2-T6SS is associated with the long TssA2. To assess the contribution of TssA2 to the functionality of the H2-T6SS, functional assays including secretion and competitions assays were carried out as well as fluorescent microscopy to visualise sheath structures. However, and in contrast to the H1-T6SS, most assays presented were performed at 25 °C, unless otherwise stated, which has previously been described to be optimal for expression of the H2-T6SS (338).

3.4.1 TssA2 is required for H2-T6SS secretion and prey killing in the *rsmA* background

Characterisation of the contribution of TssA2 to the activity of the H2-T6SS was carried out in the *rsmA* background, where H2-T6SS expression is derepressed (338). In this background a chromosomal in-frame deletion mutant of *tssA2* was engineered.

The activity of the H2-T6SS was initially assessed by a secretion assay. In the parental *rsmA* strain the production of Hcp2 in the whole cell extract could be identified and the presence of Hcp2 in the supernatant indicates secretion (Figure 3.10A). Hcp2 secretion was dependent on the presence of TssB2 and TssA2, and the absence of Hcp2 secretion in the *tssA2* background could be complemented by constitutive expression of *tssA2* from a broad host range plasmid.

As secretion by the H2-T6SS could be demonstrated in the rsmA background, these strains were also used for an interbacterial competition assay, where attacker *P. aeruginosa* strains and GFP-producing prey *E. coli* were mixed at a 1:1 ratio and incubated at 25 °C for 24 hours. The competition assay yielded a 3.4-fold difference in prey fluorescence between the parental *rsmA* strain and the *tssB2* deletion strain, indicating H2-T6SS-dependent prey killing (Figure 3.10B). The level of prey killing was indistinguishable between a *tssB2* deletion and a *tssA2* deletion, suggesting that both are required for prey killing. The loss of killing upon deletion of *tssA2* could be effectively complemented by constitutive expression of *tssA2* from a broad host range plasmid.

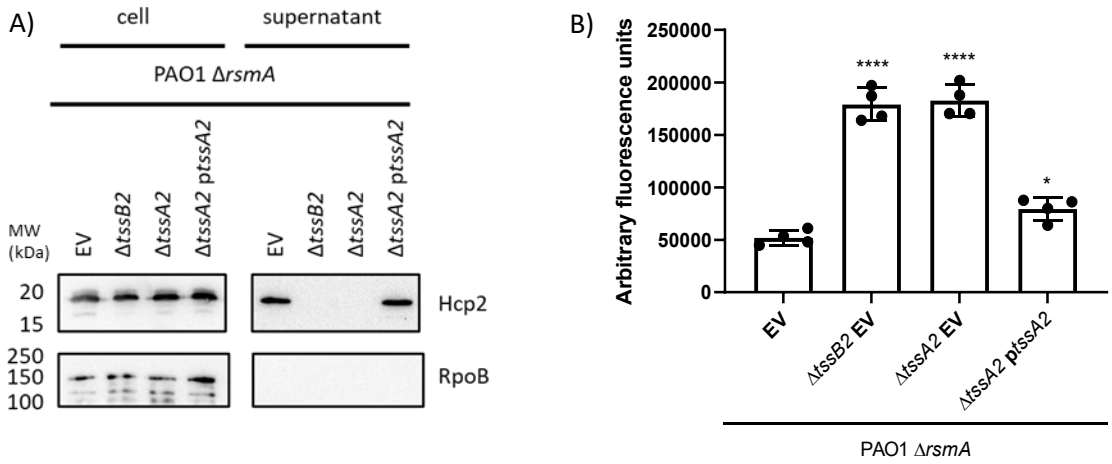


Figure 3.10 Assessment of H2-T6SS activity in a PAO1Δ*rsmA* background. To assess complementation of the *tssA2* deletion, the pBBR1MCS4 vector was introduced either as empty vector (EV) or encoding *tssA2* (p*tssA2*). A) Western blot of a H2-T6SS secretion assay in the *rsmA* background, to assess the levels of secretion marker Hcp2 in the supernatant sample. Cell and supernatant samples were harvested after 18 hours of growth at 25 °C. Proteins detected in the western blot are indicated to the right. MW markers (left) are in kDa. RpoB was used as a loading and bacterial lysis control. B) H2-T6SS competition assay in the *rsmA* background, to assess the T6SS-dependent killing of a GFP-producing *E. coli* prey by *P. aeruginosa* attacker strains. Attacker *P. aeruginosa* and prey *E. coli* were mixed at a 1:1 ratio and incubated at 25 °C for 24 hours before GFP signal quantification. Values are presented as means and error bars represent the standard deviation. Statistical testing was conducted by one-way ANOVA with Dunnett's multiple comparisons test, each strain was compared to parental PAO1Δ*rsmA* EV (ns = not significant,* $p < 0.05$, **** $p < 0.0001$). (n=4).

3.4.2 H2-T6SS sheath structures can form in the absence of TssA2

In the *rsmA* background, TssA2 was required for both secretion and prey killing by the H2-T6SS (Figure 3.10). To visualise H2-T6SS sheaths *in vivo* by fluorescent microscopy, strains were engineered to produce TssB2 fused to a fluorophore and expressed from the native *tssB2* locus. Two approaches were used to prepare cells for imaging: in one approach bacteria were grown in liquid culture and then applied to an agar pad immediately before imaging, in another approach bacteria were grown on agar pads before imaging.

Initially, cells were imaged according to a previously described protocol with growth in liquid culture at 37 °C (508). When prepared under these conditions, the percent of cells with sheath structures was 62.4 %, which fell to 24.6 % upon deletion of *tssA2* (Figures 3.11A and B). The presence of sheath

structures in the absence of a TssA protein has been described previously, including the presence of extended sheath structures which could also be detected here (377). Given that the functional assays indicated a lack of H2-T6SS functionality in the absence of TssA2 (Figure 3.10), the presence of sheath structures upon *tssA2* deletion was unexpected. However, the conditions of this experiment were quite different to those of the H2-T6SS functional assays, indeed at 37 °C secretion by the H2-T6SS is much less effective than at 25 °C (Thomas Clamens, unpublished).

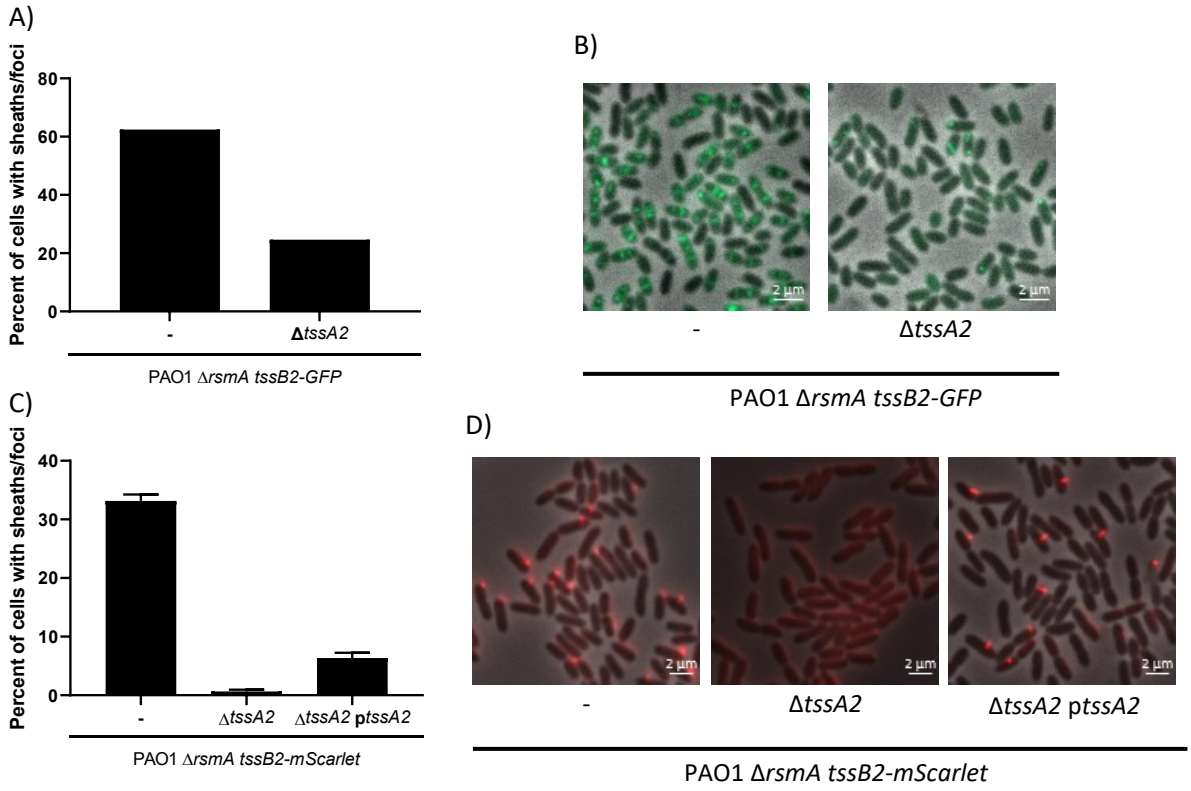


Figure 3.11 Assessment of H2-T6SS sheath formation by fluorescence microscopy. Values are presented as means and error bars represent standard deviation. A) Quantification of the percent of cells with TssB2-GFP sheaths or foci by fluorescence microscopy. Strains were grown in liquid culture at 37 °C for 6 hours before imaging. The percent of cells with sheaths or foci fell from 62.4 % (n=13292) to 24.6 % (n=10627) upon deletion of *tssA2*. B) Representative images of TssB2-GFP sheath formation in the *rsmA* background upon growth in liquid media at 37 °C. C) Quantification of the percent of cells with TssB2-mScarlet sheaths or foci by fluorescence microscopy. Strains were grown on LB agar pads for 5-6 hours at 25 °C before imaging. The percent of cells with sheaths or foci fell from 33.1 % (n=9930) in the parental strain to 0.64 % (n=9920) upon *tssA2* deletion, expression of *tssA2* from pBBR1MCS4 recovered this to 6.3 % (n=5412). Data were taken from 3 fields of view for two experiments. D) Representative images of TssB2-mScarlet sheath formation in the *rsmA* background in the presence and absence of *tssA2* upon growth on solid media at 25 °C. Scale bar represents 2 µm.

Therefore, the fluorescence microscopy experiments were repeated under different conditions, similar to the approach used here to quantify H1-T6SS sheath structures. Bacteria were grown on agar pads at 25 °C for 5-6 hours before imaging. When prepared under these conditions, in the parental *rsmA* strain 33.1 % of cells formed sheaths or foci, which fell to 0.64 % upon deletion of *tssA2* (Figures 3.11C and D). In the *tssA2* background, constitutive expression of *tssA2* from a plasmid led to an increase in sheath and focus formation, present in 6.3 % of cells. These data are more consistent with the results of the functional assays (Figure 3.10). Constitutive expression of *tssA2* from a plasmid only restores about one fifth of H2-T6SS sheaths and foci, which may explain why in the competition assay introduction of *tssA2* from a plasmid in the *tssA2* deletion strain did not restore prey killing to the same level as the parental strain (Figure 3.10B).

It is unexpected that growth at a temperature (37 °C) at which lower levels of H2-T6SS activity have previously been noted would lead to higher levels of sheath formation than growth at 25 °C. However, sheath formation may not necessarily correlate with T6SS activity, as T6SS structures may assemble but not fire. Additionally, a number of factors were altered between these experiments, including the fluorophore fused to TssB2, the incubation time and temperature, as well as growth either in liquid or on solid media prior to imaging. It is therefore not clear which factors were responsible for the variations seen between these experimental set-ups.

In conclusion, the activity of the H2-T6SS can be studied by secretion assay, interbacterial competition assay and fluorescence microscopy in the *rsmA* background, and the data presented suggest that TssA2 is required for secretion of H2-T6SS secretion markers and prey killing. In the absence of TssA2, sheath formation can be detected under certain conditions, but the functionality of these structures has not been determined.

3.5 Functional characterisation of TssA3

The H3-T6SS is associated with another short TssA protein, TssA3. To assess the contribution of TssA3 to the functionality of the H3-T6SS, it was first necessary to identify an appropriate background or technique for studying the activity of this system, since H3-T6SS activity has not been well characterised to date, particularly in the PAO1 background.

3.5.1 Interbacterial killing activity of the H3-T6SS activity could not be demonstrated

The only previous description of a H3-T6SS interbacterial competition assay was carried out between a wildtype PAO1 strain and a prey *P. putida* KT2440 (544). As this prey *P. putida* strain encodes the constitutively active K1-T6SS (324), and the H1-T6SS is known to retaliate to incoming T6SS attack via tit-for-tat (see section 1.3.5.2), it is possible that the H1-T6SS would reduce the *P. putida* prey pool in such a competition. Therefore, to assess H3-T6SS activity in competition between these bacteria, a strain was generated where solely the H3-T6SS could be assembled. In the PAO1 background, strains were generated with chromosomal in-frame deletion of *tssB1* and *tssB2* either with or without deletion of *tssB3*. The previously described competition was carried out at 37 °C for 24 hours, however in attempting to replicate this competition experiment under these conditions, prey *P. putida* KT2440R could not be recovered. This may reflect the variation in temperatures at which these bacteria are most optimally grown, 30 °C for *P. putida* KT2440R and 37 °C for *P. aeruginosa*, which may allow *P. aeruginosa* to dominate under these conditions in a T6SS-independent manner.

A screen of various incubation temperatures (20, 25 and 30 °C) and times (6, 16, 20, 24 and 30 hours) was therefore carried out to identify conditions where wildtype PAO1 could kill *P. putida* KT2440R in a H3-T6SS-dependent manner. At 20 °C for incubation times of up to 24 hours, there was limited competition between attacker and prey, with $\log_{10}$ competitive index values close to 0 indicating no change in the relative abundance of these strains over the course of the incubation (Figure 3.12A). Under the remaining conditions, PAO1 strains were able to effectively outcompete *P. putida* strains, with $\log_{10}$ competitive index values above 0 indicating an attacker outcompeting the prey strain during incubation. However, when comparing the competitive index values in the presence or absence of the H3-T6SS, this competition was independent of the H3-T6SS. This indicates that the *P. aeruginosa* population expanded more than the *P. putida* population during the incubation, but that this did not involve T6SS-dependent prey killing.

As RsmA has been shown to negatively regulate H3-T6SS expression (338), the screen of competition conditions was also carried out in a *rsmA* background in an attempt to increase H3-T6SS activity. As in the wildtype background, in the *rsmA* background none of the screened conditions showed a

difference in competitiveness depending on the presence of the H3-T6SS, so no trend of H3-T6SS-dependent killing could be observed (Figure 3.12B).

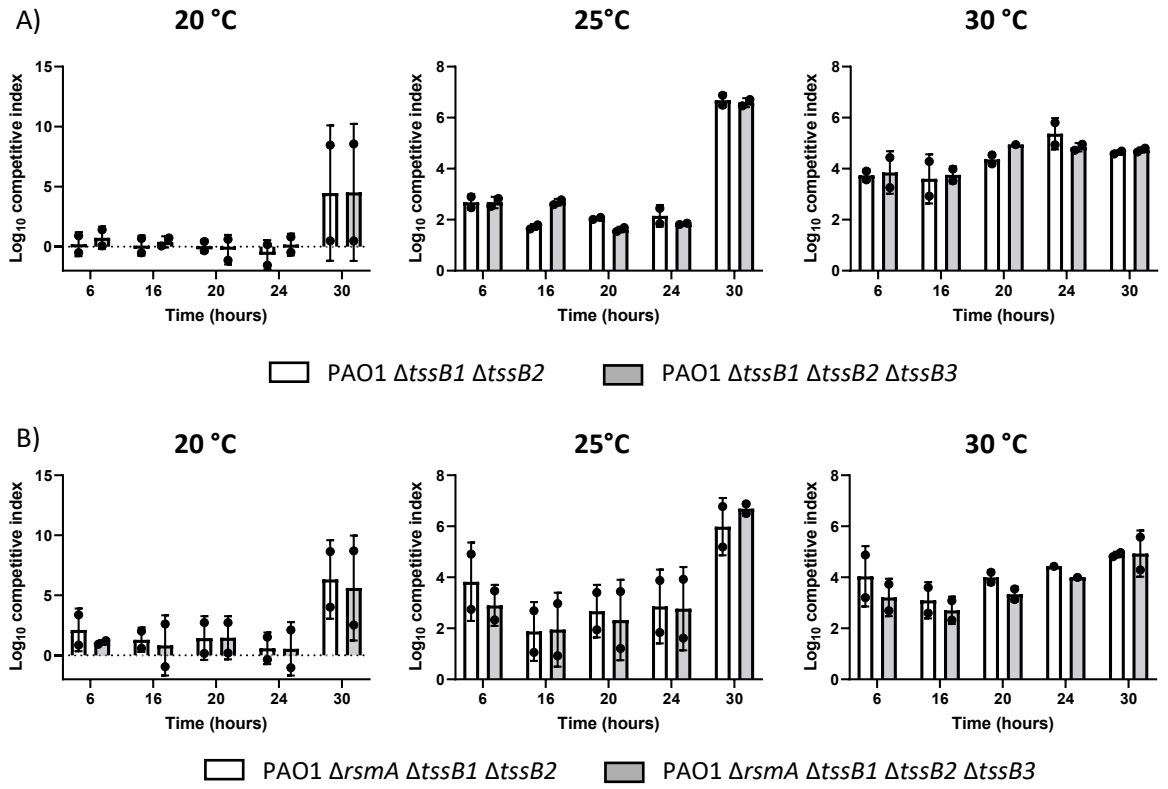


Figure 3.12 Screen for H3-T6SS killing of *P. putida* KT2440R. Attacker *P. aeruginosa* and prey *P. putida* were mixed at a 1:1 ratio and incubated at 20, 25 or 30 °C for 6, 16, 20, 24 or 30 hours before recovery and growth under selective conditions. A $\log_{10}$ competitive index value above 0 indicates an attacker which outcompetes the prey strain. Values are presented as means and error bars represent the standard deviation. A) H3-T6SS competition assay in the PAO1 background, to assess the T6SS-dependent killing of a *P. putida* prey by *P. aeruginosa* attacker strains that either have H3-T6SS (PAO1Δ*tssB1*Δ*tssB2*) or lack H3-T6SS (PAO1Δ*tssB1*Δ*tssB2*Δ*tssB3*). (n=2). B) H3-T6SS competition assay in the PAO1Δ*rsmA* background, to assess the T6SS-dependent killing of a *P. putida* prey by *P. aeruginosa* attacker strains that that either have H3-T6SS (*PAO1ΔrsmAΔtssB1ΔtssB2*) or lack H3-T6SS (PAO1*ΔrsmA*Δ*tssB1*Δ*tssB2*Δ*tssB3*). (n=2). In cases where only one measurement is present, prey could not be recovered following incubation in one repeat.

Under the conditions tested, the H3-T6SS was not effective at killing *P. putida*. This could be due to low levels of H3-T6SS activity in the chosen genetic backgrounds or associated with the experimental set up. Alternatively, it could reflect a lack of H3-T6SS effectors that are toxic for *P. putida*. In any case, the impact of TssA3 on H3-T6SS-dependent prey killing could not be assessed.

3.5.2 Secretion by the H3-T6SS could not be demonstrated

The activity of the H3-T6SS could not be characterised by assessing anti-bacterial activity through interbacterial competition assays. The activity of the T6SS is not exclusively involved in the delivery of anti-bacterial toxins, effectors can also target eukaryotes (316,545), fungi (308,328) or be involved in the capture of extracellular common goods (310,311,342,446,546). For example, the sole H3-T6SS associated effector characterised to date, TseF, is involved in the acquisition of iron (see section 1.3.4.4) (311). Therefore, a more appropriate way to assess H3-T6SS activity may be through studying T6SS-dependent secretion.

Hcp3 secretion dependent on the H3-T6SS of PA14Δ*rsmA* has previously been observed with growth at 25 °C for 24 hours (338), therefore these conditions were used in an attempt to replicate this in the PAO1Δ*rsmA* background. A chromosomal in-frame deletion mutant of *tssA3* was engineered in this background. In the parental *rsmA* strain Hcp3 was produced, but secretion was absent (Figure 3.13A). Secretion of the H3-T6SS, and the contribution of TssA3 to activity could therefore not be characterised under these conditions.

The transcriptional regulator AmrZ has previously been shown to activate H3-T6SS expression by binding to corresponding promoter regions (338). A plasmid carrying an inducible *amrZ* was therefore introduced into the *rsmA* strains. Induction of *amrZ* expression did not lead to a very noticeable increase in Hcp3 production, nor did it lead to the secretion of Hcp3 (Figure 3.13B).

When studying the H1-T6SS, deletions of other components of the Gac-Rsm pathway, such as *retS*, gave rise to a notable increase in production and secretion of H1-T6SS secretion markers (Figure 3.3). To test whether a similar trend could be seen for the H3-T6SS, a secretion assay was carried out in the *retS* background. Although Hcp3 production could be detected in this background, there was no detectable Hcp3 secretion (Figure 3.13C).

In an attempt to replicate the previous findings, a secretion assay was carried out using identical PA14Δ*rsmA* strains. However, the previous results could not be replicated, Hcp3 was produced but not secreted (Figure 3.13D). It is unclear why secretion by the H3-T6SS could not be replicated using identical strains, but there may have been some variation in the experimental set up. The H3-T6SS secretion assay was also attempted at 30 °C at various times of incubation, but this also failed to yield Hcp3 secretion (data not shown). None of the genetic backgrounds or conditions used in this study could demonstrate the secretion of Hcp3 by the H3-T6SS. As such the impact of TssA3 on H3-T6SS secretion could not be assessed.

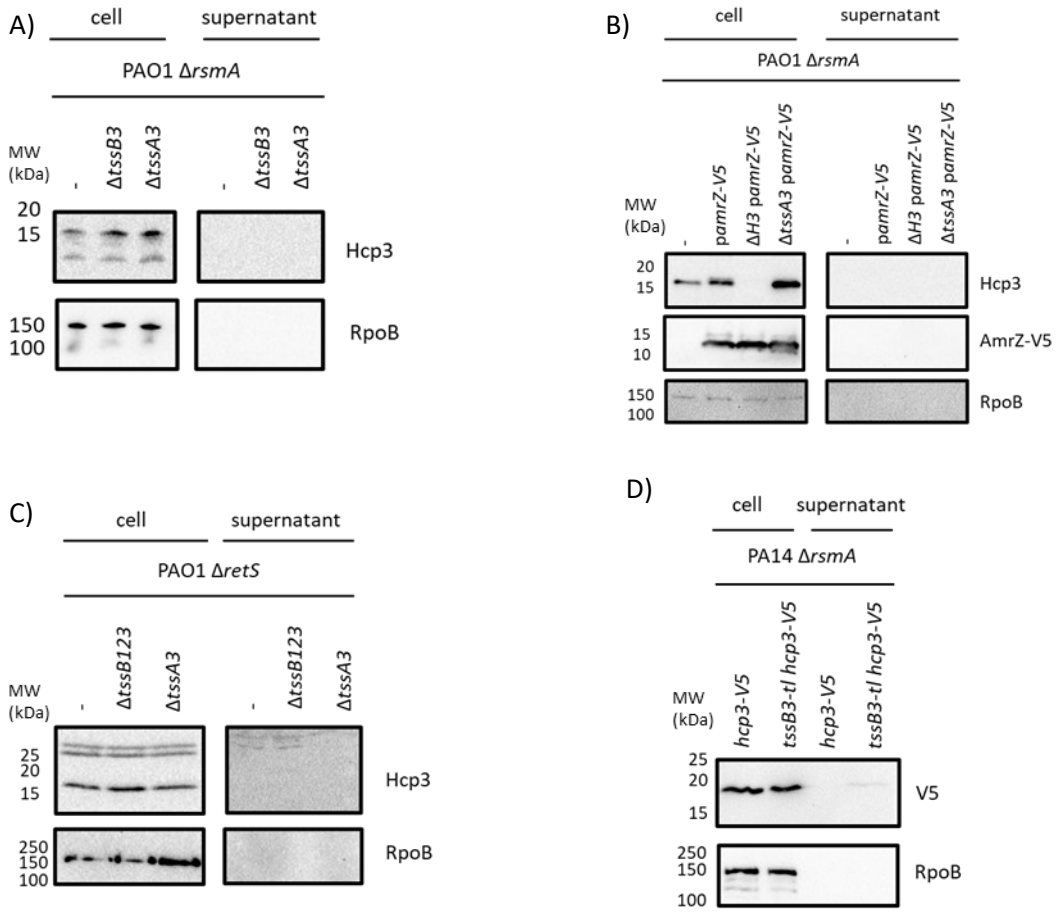


Figure 3.13 Assessment of H3-T6SS secretion in various backgrounds. Cell and supernatant samples were harvested after 24 hours of growth at 25 °C. Proteins detected in the western blot are indicated to the right. MW markers (left) are in kDa. RpoB was used as a loading and bacterial lysis control. A) Western blot of a H3-T6SS secretion assay in the PAO1Δ*rsmA* background, to assess the levels of secretion marker Hcp3 in the supernatant sample. B) Western blot of a H3-T6SS secretion assay in the PAO1Δ*rsmA* background with induced overexpression of the H3-T6SS activator *amrZ*, and deletion of either the H3-T6SS cluster (Δ*H3*) or *tssA3*. C) Western blot of a H3-T6SS secretion assay in the PAO1Δ*retS* background, with deletion of either each TssB encoding gene (Δ*tssB123*) or *tssA3*. D) Western blot of a H3-T6SS secretion assay in the PA14Δ*rsmA* background with V5-tagged Hcp3. The introduction of a *lacZ* translational reporter at the *tssB3* promoter (*tssB3-tl*) inactivated the H3-T6SS.

3.5.3 TssA3 is required for the formation of H3-T6SS sheath structures

Although production of the inner tube protein Hcp3 could be detected by western blot, the activity of the H3-T6SS could not be characterised either through secretion or interbacterial competition assays. The identification of Hcp3 production suggested that there might be assembly of the H3-T6SS, despite

no evidence of phenotypic activity. We have previously engineered GFP-tagged H3-T6SS sheaths for imaging via fluorescence microscopy, and identified assembly of such sheath structures (508). Further strains were engineered producing TssB3 fused to mScarlet and expressed from the native *tssB3* locus. When prepared as described previously, the presence of H3-T6SS sheath structures could be visualised. In the parental *rsmA* strain, 38.9 % of cells formed sheaths or foci, which fell to 0.062 % upon deletion of *tssA3* (Figure 3.14). In the *tssA3* background, upon constitutive expression of *tssA3* from a plasmid there was effective complementation with 27.2 % of cells forming sheaths or foci.

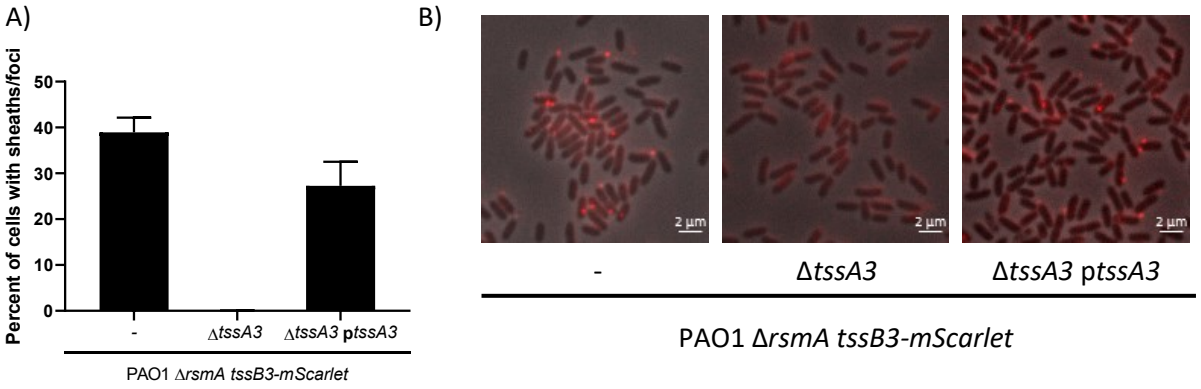


Figure 3.14 Assessment of H3-T6SS sheath formation by fluorescence microscopy. A) Quantification of the percent of cells with TssB3-mScarlet sheaths or foci in the *rsmA* background by fluorescence microscopy. Strains were grown in liquid culture at 25 °C for 13 hours before imaging. The percent of cells with sheaths or foci fell from 38.9 % (n=10582) in the parental strain to 0.062 % (n=12882) upon *tssA3* deletion, expression of *tssA3* from pBBR1MCS4 recovered this to 27.2 % (n=26253). Data were taken from 2 fields of view for three experiments. Values are presented as means and error bars represent the standard deviation. B) Representative images of TssB3-mScarlet sheath formation in the presence and absence of *tssA3*. Scale bar represents 2 µm.

The activity of the H3-T6SS cannot be studied by secretion assay or interbacterial competition assay, however fluorescence microscopy could be a suitable approach to monitor H3-T6SS functionality via assembly of sheath structures in the *rsmA* background. Using this approach, it was demonstrated that assembly of the H3-T6SS sheath was dependent on the presence of TssA3, and this phenotypic defect in the *tssA3* mutant could be complemented by expressing *tssA3* from a broad host range plasmid.

3.6 Discussion

3.6.1 Requirement for TssA proteins for T6SS activity

Previous characterisation of the contribution of TssA proteins to the functionality of the T6SS has generally identified a requirement of TssA proteins for T6SS activity, be that in T6SS-dependent secretion or killing of bacterial competitors, or the formation of T6SS sheath structures (324,360,376,377,394,508,509,512,537). This requirement is independent of whether the TssA in question is a $TssA_L$ or $TssA_S$. In this study, assessing the contributions of the TssA proteins of *P. aeruginosa* to the functionality of their respective T6SSs, both the short TssA1 and the long TssA2 were required for T6SS-dependent secretion and killing activities, and a requirement for sheath formation could also be demonstrated (Figures 3.6 and 3.10). Furthermore, TssA3 was required for the formation of H3-T6SS sheath structures as visualised by fluorescence microscopy (Figure 3.14).

The complete loss of sheath structures has commonly been reported upon deletion of a *tssA*¸ including with loss of the long $TssA^{EC}$ and $TssA^{VC}$, as well as the short $TssA1^{PP}$ (360,508,512). However, it has also been observed that some sheath structures are still able to form, although at a much reduced abundance, upon *tssA* deletion (376,377). This includes the long TssA2 and $TssA^{VC}$, as well as the short TssA1 (376,377). The presence of sheath structures upon deletion of *tssA2* was also identified in this work, although this was dependent on the method of sample preparation for imaging. Sample growth and imaging on agar pads identified a loss of sheath structures upon *tssA2* deletion (Figures 3.10C and D). However, when the sample was grown in liquid culture prior to imaging, the proportion of cells forming sheath structures fell from 62.4 % to 24.6 % upon deletion of *tssA2* (Figures 3.10A and B).

The presence of H1-T6SS sheath structures in the absence of a TssA1 has also been demonstrated previously. The percentage of cells with fluorescent TssB1 foci fell from 79 % to 29 % upon deletion of *tssA1* (376). Notably this experiment only quantified the formation of fluorescent foci, which could represent the recruitment of sheath components to the baseplate regardless of whether these were subsequently able to polymerise into full sheath structures. It was not clear from the data whether extended sheath structures were able to form in the absence of TssA1 (376). In a separate analysis, the dynamics of the T6SS structures formed was considered. It was identified that 50 % of cells formed fluorescent H1-T6SS structures, where around 75 % of these were extending and contracting structures (377). Upon deletion of *tssA1*, 26 % of cells formed T6SS structures, where only around 15 % were extending and contracting structures. A similar observation was made upon deletion of *tssA2*, where the proportion of cells with T6SS structures fell from 99.5 % to 7 %, and the proportion of these that were extending and contracting fell from around 90 % to closer to 15 % (377).

These data identify that sheath structures, including both foci and extending and contracting structures, can be formed in the absence of TssA proteins. This suggests that in the absence of TssA proteins, sheath components can be recruited to the T6SS assembly initiation site and in some cases can even polymerise into what appear to be functional sheaths. For this reason, TssA proteins have been described in some reports as not strictly essential for T6SS activity, and instead characterised as chaperones involved in co-ordinating sheath and inner tube polymerisation (377). While it is likely that a T6SS sheath that is observed to extend and contract in the absence of a TssA protein delivers effector proteins, the functionality of these sheaths is difficult to assess conclusively. This is in part due to their low abundance, meaning a phenotypic effect on T6SS activity would be difficult to detect in secretion and competition assays. Interestingly, it could be identified that prey killing was slightly, but significantly, reduced upon *tssA1* deletion compared to *tssB1* deletion (Figure 3.6B). This was only observed in the *rsmArsmN* strain, which was identified to have a high level of Hcp1 secretion by the H1-T6SS (Figure 3.7). Perhaps a genetic background with a high level of T6SS activity, allowed the effect of this low proportion of functional sheaths to be detected. However, in this background, almost no sheath structures could be visualised in the absence of TssA1 (Figures 3.6C and D), so the difference in killing identified between *tssB1* and *tssA1* strains may not be associated with functional sheath structures in the *tssA1* background.

In the absence of TssA proteins, there is either a complete loss of sheath structures, or a drastically reduced abundance, with a lower proportion of these structures having typical T6SS extension and contraction dynamics. The overall reduced abundance of sheath structures suggests that TssA proteins aid in the recruitment of sheath components to the baseplate complex, for the initiation of sheath and inner tube polymerisation. The reduction in extending and contracting sheath structures suggests that TssA proteins are also involved in co-ordinating the polymerisation of the sheath and inner tube.

Whether TssA proteins can be described as essential components of the T6SS is up for debate. In T6SS functional assays, such as secretion and competition assays, TssA proteins have been found to be required for T6SS activity both in the previous literature and in this study. At the level of a single cell, TssA proteins may not be essential for the assembly and firing of a T6SS. However, the T6SS is an apparatus used in bacterial warfare, manipulating the composition of polymicrobial communities (547). Within these communities the influence of isolated T6SS firing events is limited, a more coordinated activity is required to influence population dynamics. At the population level therefore, the loss of TssA renders the T6SS largely ineffective as an instrument to influence the surrounding community. For the purpose of this study, TssA proteins will thus be described as essential for T6SS activity.

3.6.2 Localisation of TssA proteins in the T6SS

The loss of both long and short TssA proteins has a similar effect on T6SS activity, both are required for a fully functioning T6SS (Figures 3.6, 3.10 and 3.14). This is despite a great deal of variation between long and short TssA proteins. All TssA proteins share a similar Nt1 domain, but the downstream domain organisation differs: $TssA_S$ proteins have a C-terminal domain while $TssA_L$ proteins have a Nt2 domain and a distinct C-terminal domain (360,376,509). The oligomerisation of these distinct C-terminal domains generates ring-shaped structures of very different dimensions and symmetries: $TssA_S$ C-terminal domains form large, high symmetry rings with a large internal lumen, while $TssA_L$ C-terminal domains form smaller, lower symmetry rings with Nt2 domains at the periphery (see section 1.4.1) (360,376,377,509). The variation between the domain organisation and structures formed from long and short TssA proteins has contributed to a discussion about whether all TssA proteins have similar function and whether they associate with the T6SS in the same way.

One theory on the localisation of different TssA proteins within the T6SS is that $TssA_S$ proteins are static baseplate components, while $TssA_L$ proteins are more dynamic components associated with the distal end of the polymerising sheath (376,377). An alternative theory is that despite their differences, all TssA proteins have similar association to the T6SS, equivalent to the association suggested for $TssA_L$ proteins, at the distal end of the sheath (508,509).

One way in which the association of TssA proteins with the T6SS has been studied is using fluorescence microscopy. The fluorescent tagging of both TssA proteins and other T6SS components, such as sheath components, allows the relative position of TssA within the T6SS to be studied. The localisation of TssA proteins within the T6SS was found to be similar for the long $TssA^{EC}$, $TssA^{VC}$ and TssA2 and the short $TssA1^{PP}$ and $TssA^{AB}$, while the localisation of the short TssA1 differed (360,377,508,513). For most of the studied TssA proteins, it was identified that TssA proteins are recruited to the T6SS assembly initiation site, comprising the membrane complex and baseplate complex. Following TssA recruitment, the polymerisation of the sheath is initiated from the baseplate with TssA associated with the distal end of the growing sheath as it extends across the cell (360,377,508). In contrast to this, it has been identified that TssA1 is found static at the T6SS assembly initiation site, prior to and during the extension of the sheath (377).

In this study an attempt was made to study the localisation of TssA proteins relative to the position of their sheath structures. However, in each case the low fluorescence intensity of the TssA-linked fluorophore led to signal bleaching before conclusive time lapse data could be collected (Figure 3.9). Therefore, while some amount of co-localisation could be identified in single images, the relative position of the TssA to the T6SS could not be studied.

From the existing data it has been demonstrated that both long and short TssA proteins can be found as dynamic T6SS components, which associate with the distal end of the T6SS sheath (360,377,508). This contradicts the theory that the different groups of TssA proteins have distinct positioning within the T6SS. There is some evidence that the short TssA1 may be statically associated with the baseplate (377). However, this is not a conserved feature of all $TssA_S$ proteins, as $TssA1^{PP}$ and $TssA^{AB}$ are dynamically associated with the distal end of the sheath (508,513). The two main explanations for this alternative localisation of TssA1 are either that TssA1 has a distinct positioning within the T6SS to all other characterised TssA proteins, or that this experiment was unable to capture the localisation of TssA1. It is worth noting that these TssA1 dynamics could only be visualised in the presence of a native TssA1, suggesting that native TssA1 may perform additional functions that the fluorophore tagged TssA1 cannot. Without additional experimental data, it is difficult to say conclusively whether TssA1 has distinct T6SS localisation to other TssA proteins. However, the data indicate that both long and short TssA proteins can be found at the distal end of the sheath during its polymerisation, which may thus be considered as the most likely functional fate of this family of proteins.

3.6.3 Functional relevance of different TssA groups: accessory proteins

It appears that the variation in TssA proteins does not correlate with a difference in their localisation within the T6SS. The requirement for the diversity in TssA proteins and the implications on T6SS activity are thus not fully understood. However, links have been demonstrated between different groups of TssA proteins and the phylogeny of the T6SS cluster their corresponding genes are encoded within, as well as the presence of specific accessory proteins (see section 1.4.3) and T6SS firing dynamics (see section 3.6.4) (508). Phylogenetic analysis of the distribution of long and short TssA proteins, identified that genes encoding $TssA_L$ proteins are found within T6SS clusters belonging to phylogenetic groups 1 and 2, while genes encoding $TssA_S$ proteins are found within T6SS clusters belonging to phylogenetic groups 3, 4A, 4B and 5 (Figure 1.25) (508). The presence of $TssA_L$ proteins is generally associated with the presence of a TagA accessory protein, which shares the conserved ImpA_N region found in TssA proteins (508,510). An exception to this is TssA2, where no associated TagA protein has been identified. T6SS clusters of phylogenetic groups 3 and 5 are associated with the presence of genes encoding a $TssA_S$ and the accessory protein TagJ, while phylogenetic group 4B clusters are associated with the presence of genes encoding a $TssA_S$ and the accessory protein TagB (508). Interestingly, T6SS clusters of phylogenetic group 4A are associated with the presence of genes encoding a $TssA_S$ but no associated accessory protein has been identified. The H3-T6SS belongs to phylogenetic group 4A.

It has been suggested that both the $TssA_L$-associated TagA and $TssA_S$-associated TagB accessory proteins regulate sheath polymerisation. The membrane-associated TagA accessory protein is proposed to capture the extended sheath structure at the opposite membrane through interaction with the distal $TssA_L$ protein, terminating sheath extension (510). The extended sheath structure is therefore attached to the baseplate at the proximal end and to TagA at the distal end, which is proposed to lock the sheath to a fixed position and maintain the high energy extended sheath structure (510). In contrast, the accessory protein TagB is associated with the baseplate complex (508). TagB proteins associate with the baseplate, accumulating during sheath polymerisation, and allow sheath polymerisation to be completed before firing (508). The interaction with the baseplate is proposed to prevent the dome- to star-shape conformational change in the baseplate which leads to sheath contraction (508).

The role of the accessory protein TagJ is unclear, unlike the other TssA-associated accessory proteins, *tagJ* deletion does not have a detectable effect on T6SS activity (514). It has been proposed that TagJ proteins may act similarly to a TagB accessory protein, in associating with the baseplate (508). Alternatively, it has been suggested that TagJ proteins are involved in coordinating the disassembly of the contracted sheath due to interaction with components of the sheath and the ATPase ClpV (514,515).

Building on our recently published study identifying the role of the TagB accessory protein (508), one avenue that this project explored but was ultimately unable to resolve was whether there are accessory proteins associated with the long TssA2 or the short TssA3. Unlike many $TssA_L$-associated T6SSs, the H2-T6SS does not have an associated TagA accessory, while no similar accessory proteins have been identified to date associated with the T6SS phylogenetic group 4A, which includes the H3-T6SS (Figure 1.25). One candidate that was proposed within the H3-T6SS cluster was the uncharacterised PA2372. This PA2372 was previously identified in a pulldown using Hcp3, and had thus been proposed to be a H3-T6SS effector protein, although this has not been confirmed (412). To identify possible accessory proteins and further characterise PA2372, pulldown experiments were carried out using TssA2, TssA3 and PA2372 as baits, where nearby proteins were crosslinked, pulled down and identified by mass spectrometry. Unfortunately, among the many proteins identified to be pulled down by TssA2 or TssA3, very few T6SS components were present (Appendix I: Table 8.1, 8.2, 8.3 and 8.4). This was similarly the case for PA2372, where the previously identified interaction partner Hcp3 was also not identified (Appendix I: Table 8.5 and 8.6). To identify possible TssA-associated accessory proteins, it would be expected that components of the T6SS should also be strongly pulled down. In the absence of this, and due to time constraints, no in-depth characterisation was performed on these hits.

3.6.4 Functional relevance of different TssA groups: T6SS functional diversity

Multiple T6SS clusters may be encoded within a genome, such as the three T6SS clusters of *P. aeruginosa* or the six T6SS clusters of *Burkholderia pseudomallei* (548). The three T6SSs clusters of *P. aeruginosa* belong to different phylogenetic groups, H1-T6SS in group 3, H2-T6SS in group 1 and H3-T6SS in group 4A, and are therefore likely to have been acquired through horizontal gene transfer rather than through duplications (315). The maintenance of multiple functional T6SS clusters within a genome, suggests these clusters are functionally distinct rather than acting redundantly. There are many ways in which distinct function of T6SS can be achieved including the association of specific effectors, independent regulation and diverse firing strategies.

The different types of TssA protein have been proposed to introduce such functional diversity to T6SSs through different firing dynamics between T6SSs that are associated with a long or short TssA protein (508). $TssA_S$-associated T6SSs, such as the H1-T6SS of *P. aeruginosa*, the K1-T6SS of *P. putida* and that of *A. baylyi*, have a short residence time, firing very rapidly after assembling (438,508). For the H1-T6SS there can be less than 30 seconds between the initiation of T6SS assembly and contraction of the sheath (508). In contrast, $TssA_L$-associated T6SSs, such as those associated with TssA2, $TssA^{EC}$ and $TssA^{VC}$, have a much longer residence time, where assembled sheath structures are maintained in the extended conformation for a prolonged period of time before firing (377,508,510). For example, the T6SSs associated with TssA2 or $TssA^{EC}$ can remain extended for more than 10 minutes before firing (508,510). The presence of TagA, anchoring the extended sheath structure, may contribute to this long term T6SS stability, while the presence of TagB accessory proteins may aid the rapid firing of T6SSs associated with $TssA_S$ proteins.

The different firing dynamics of T6SSs associated with long or short TssA proteins may be linked to specific T6SS attack strategies. Upon detection of a T6SS attack by a neighbouring cell, the *P. aeruginosa* H1-T6SS and the T6SS of *A. baylyi* can swiftly retaliate with a T6SS attack of their own, known as the tit-for-tat strategy (see section 1.3.5.2) (479,513). Such a retaliation strategy relies upon the ability to assemble a T6SS at a specific site and fire rapidly, which correlates with the rapid firing behaviours identified for $TssA_S$-associated T6SSs (508). A highly aggressive T6SS attack strategy, such as that employed by the soil bacterium *P. putida* K1-T6SS, may also benefit from rapid firing dynamics to fire indiscriminately at competitors. The K1-T6SS is constitutively active, as such the wildtype strain can very effectively outcompete a variety of ecologically relevant competitors in a T6SS-dependent manner (324). The long residence times of $TssA_L$-associated T6SSs may be linked to the absence of a

stimulus that would be present in the native environment to fire, for example the detection of a specific type of cell.

One outlier to the short residence time and rapid contraction of $TssA_S$-associated T6SSs is the H3-T6SS, which is within a phylogenetic group of T6SS clusters not associated with an accessory protein. Previous visualisation of the H3-T6SS identified the presence of H3-T6SS extended sheath structures but an exceptionally low rate of contraction (508). A similar trend was identified here when characterising the activity of the H3-T6SS. T6SS-dependent *P. putida* prey killing by the H3-T6SS could not be demonstrated in a variety of conditions (Figure 3.12). No anti-bacterial effectors have thus far been identified associated with the H3-T6SS (PldB was previously reported to be H3-T6SS associated but has since been demonstrated as H2-T6SS-associated (368,544)). The only characterised H3-T6SS effector to date, TseF, is involved in iron uptake (311). It is therefore possible that the activity of the H3-T6SS may not be best characterised by studying interbacterial competition if no antibacterial effectors are indeed associated with it.

While the activity of a T6SS might not necessary always be associated with the killing of bacterial prey, it should be associated with the secretion of T6SS-associated secretion markers. However, while components of the H3-T6SS were expressed in a range of genetic backgrounds, conditions could not be found for T6SS-dependent secretion of H3-T6SS secretion markers (Figure 3.13). Despite this, the assembly of H3-T6SS sheath structures could be identified by fluorescence microscopy (Figure 3.14), although the infrequent firing raises questions about why under these conditions there would be T6SS assembly but not firing. It is likely that a separate, currently unknown signal is required to activate H3-T6SS firing, identification of this would enable a more comprehensive assessment of H3-T6SS activity.

3.6.5 Regulation of the H1-T6SS by the Gac-Rsm pathway

This study identified differential expression and secretion of H1-T6SS associated proteins upon deletion of components of the Gac-Rsm pathway (Figure 3.7). The Gac-Rsm pathway of *P. aeruginosa* is a key regulator of the switch between bacterial lifestyles associated with acute and chronic infection (465,549). The activity of the sensor kinase GacS is inversely modulated by the sensors RetS and LadS, to either prevent or enhance activation of GacS respectively (Figure 1.15) (49). Activation of GacS allows the phosphorylation of the response regulator GacA, driving expression of the small regulatory RNAs RsmY and RsmZ, which can sequester post-transcriptional regulators of the Rsm family, which are homologs of Csr proteins of *E. coli* (48,550). Pseudomonads generally encode an RsmA along with either RsmE or RsmN (also known as RsmF) (551). The presence of RsmN is highly conserved in *P. aeruginosa* genomes and also present in other Pseudomonads (551). Rsm proteins negatively regulate

factors linked to a chronic infection lifestyle, such as the T6SS and biofilm components including exopolysaccharide (47,48). While Rsm proteins positively regulate factors linked with an acute infection lifestyle, such as the T3SS, virulence factor regulator (Vfr) and type IV pili (48,49).

In studying T6SS activity, manipulation of the Gac-Rsm pathway is a common strategy to enhance T6SS expression by relieving the repression exerted by Rsm proteins (338,376,377). Previous studies on the activity of the H1-T6SS have primarily involved the deletion of *retS*, however *rsmA* deletion has also been shown to increase H1-T6SS expression (338,376). Data presented here identify that in the PAO1 background the production and secretion of the inner tube protein Hcp1 is elevated in the *retS* background compared to the *rsmA* background (Figure 3.7). While deletion of the other *P. aeruginosa* Rsm protein encoding gene, *rsmN*, in isolation did not lead to detectable levels of Hcp1 production, a double deletion of both *rsmA* and *rsmN* produced a synergistic effect, giving rise to higher levels of Hcp1 production and secretion than the *retS* background. This elevated H1-T6SS expression in the *rsmArsmN* background compared to the *retS* background has been confirmed more quantitatively by both transcriptional and translational fusion experiments (Marta Rudzite, unpublished). It has previously been shown that for phenotypes either activated or repressed by *P. aeruginosa* Rsm proteins, such as biofilm formation or expression of T3SS or T6SS, deletion of *rsmN* or *rsmA* individually has a smaller effect than deletion of both, supporting the synergistic effect seen here (539,541). This is also the case in *Pseudomonas fluorescens*, which encodes a RsmA and RsmE, each Rsm contributes similarly to target gene expression, and loss of both similarly gives a greater effect (552). There is a discrepancy in the effect of deleting a single *rsm* from the wildtype background, where a minimal effect is seen, compared to deleting from a background with a *rsm* already deleted, where a significant effect is seen. The effect of RsmN is likely masked in the presence of RsmA as its transcript has been shown to be a target for repression by RsmA (541). Therefore, upon deletion of *rsmA*, RsmN will be derepressed and is likely able to compensate for the deletion, the full effect of this pathway on regulation is therefore only seen in the absence of both *rsmA* and *rsmN*.

The trend of a much greater effect in a *rsmArsmN* deletion than either a single *rsmA* or *rsmN* deletion is well established (539,541). Expression from a *rsmArsmN* double deletion has not previously been compared to the effect of disrupting the Gac-Rsm pathway further upstream, as investigated here with a *retS* mutation (Figure 3.7). It would be expected that a *retS* mutation, allowing GacS and GacA activation and subsequent Rsm sequestration, would have a similar effect to deleting the genes encoding these Rsm proteins. However, the data indicates that a *rsmArsmN* mutant induces stronger Hcp1 production than a *retS* mutant. Upon *retS* deletion, the activated RsmY and RsmZ might not be able to sequester all RsmA and RsmN when compared to total absence in the *rsm* deletion, however it is also possible that other factors may influence this discrepancy.

It has been demonstrated that the downstream signalling induced by the Gac-Rsm pathway is mediated exclusively through the Rsm-binding RNAs, RsmY and RsmZ (550). However, RsmY and RsmZ are not exclusively regulated by the Gac-Rsm pathway, several pathways modulate the level of these RNAs in terms of their expression and stability (553). Expression can be both repressed, for example mediated by the global anaerobic response regulator Anr (554), or activated, for example mediated by the magnesium transporter MgtE, by other signalling pathways (555). Additionally, the turnover of these RNAs can be influenced my multiple pathways, RsmY is suggested to be stabilised by Hfq (556), while degradation of RsmZ has been linked to the BfiRS two-component system (557). Other regulatory pathways therefore influence the sequestration of RsmA and RsmN independent of the Gac-Rsm pathway by modulating the availability of RsmY and RsmZ (Figure 3.15).

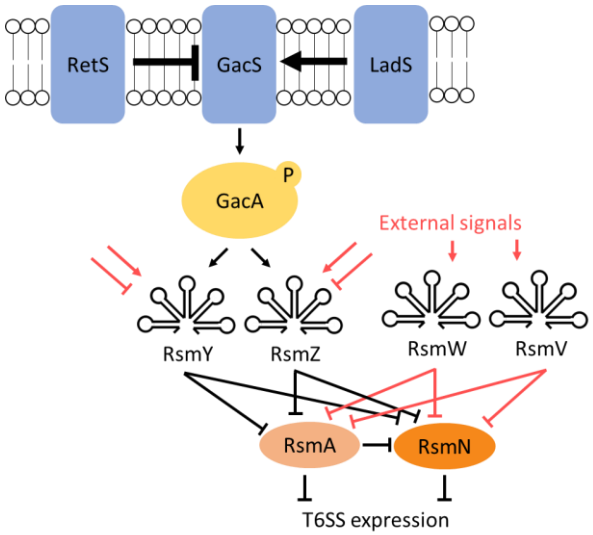


Figure 3.15 Additional regulation of components of the Gac-Rsm pathway in *P. aeruginosa*. The expression and stability of RsmY and RsmZ regulatory RNAs can be influenced by other pathways. RsmW and RsmV are regulated independently of the Gac-Rsm pathway and can sequester Rsm proteins.

In addition to RsmY and RsmZ, two further Rsm-binding RNAs have been identified whose expression is independent of the Gac-Rsm pathway, RsmW and RsmV (558,559). There is evidence of differential expression and stabilities of these Rsm-binding RNAs, linked to specific growth phases, nutrient availability and temperature (553,557–559). The affinities with which these RNAs bind RsmA and RsmN differ, for example RsmV has been identified to bind RsmN with a far greater affinity than RsmA (559). The Gac-Rsm pathway-associated RsmY and RsmZ strongly bind RsmA, but binding of RsmN has been disputed (48,541). In one study RsmN was shown to have far weaker binding and lower binding stoichiometry to RsmY and RsmZ when compared to that of RsmA (541), while in another study only RsmY was identified as binding RsmN (539). Furthermore, the additional deletion of *rsmY* and *rsmZ* from a *rsmA* background did not lead to a significant difference in Rsm regulated phenotypes by RsmN, suggesting that RsmY and RsmZ may not directly regulate RsmN (541). However, a structure has been solved for RsmN bound to a hairpin of RsmZ, where the hairpin interacted with RsmA with equivalent affinity (551). It has been suggested that the regulation of RsmN by the Gac-Rsm pathway may only be indirect, through its repression by RsmA rather than through sequestration by RsmY and RsmZ,

though this is yet to be conclusively demonstrated (541). If this were the case it might explain the difference in H1-T6SS expression between *retS* and *rsmArsmN* backgrounds: in a *retS* background only RsmA would be sequestered and its repression of RsmN relieved allowing it to act on targets, while only in the *rsmArsmN* background would targets not be repressed. In any case, these variable binding affinities between Rsm proteins and the RNAs that sequester them, have been suggested to modulate the availability of Rsm proteins, influencing the regulatory network in response to environmental signals (560). The presence of Rsm-binding RNAs that are independent of the Gac-Rsm pathway further explains how variation may be introduced between *retS* and *rsmArsmN* backgrounds (Figure 3.16).

One reason for the different binding affinities of RsmA and RsmN to regulatory RNAs that have previously been observed may be the structural differences between these proteins. All previously characterised structures of Csr and RsmA/RsmE proteins share a highly conserved structure, comprising five β-strands with a C-terminal α-helix, which form homodimers with the α-helices as 'wings' at opposite sides of the dimer (Figure 3.16A) (561–564). Similarly, RsmN proteins form homodimeric structures comprised of five β-strands and one α-helix, however, the α-helix is repositioned between the second and third β-strands and is found central following the β-strand dimer, contributing to the interaction interface between monomeric units (Figure 3.16B) (541,551). As a result of the altered α-helix position, the dimer interfaces and therefore overall structures differ between the domain swapped structures of classical Csr/Rsm and the monomer docked structure of

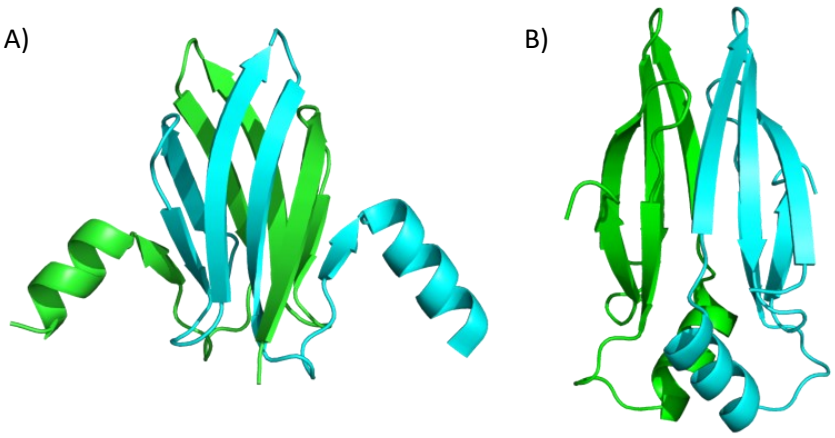


Figure 3.16 Structures of *P. aeruginosa* Csr family members. A) Structure of the RsmA (PDB: 1VPZ) homodimer. The C-terminal α-helix of each monomer form wing-like protrusions. Extensive contacts are formed between β-strands of each monomer. B) Structure of the RsmN (PDB: 4K59) homodimer. The α-helix of each monomer is found between β-strand 2 and 3. Contact between monomers primarily involve the α-helix and the third β-strand.

RsmN (541,551). Despite this, the position of key residues required for RNA binding is conserved, allowing both homodimers to specifically recognise stem loop structures containing exposed GGA motifs (541,551,565,566). The structural differences may confer some specificity to this binding. While RsmA and RsmN have been shown to bind to overlapping targets, they have also been identified to bind to distinct transcripts or motifs in transcripts (539–541). Overlapping but distinct regulons likely contribute to the synergistic effect seen upon *rsmArsmN* deletion.

Both RsmA and RsmN have been identified as able to bind and repress the two H1-T6SS transcripts starting with *fha1* and *tssA1*, the first genes found in H1-T6SS polycistronic mRNAs (48,539,541). It has also been demonstrated, as also shown here (Figure 3.7), that deletion of both *rsmA* and *rsmN* gives rise to high levels of Hcp1 secretion (539,541). Interestingly, the deletion of *tssA1* in the *rsmA* or *retS* background gave rise to elevated Hcp1 production, this effect in the *rsmA* background could no longer be detected upon the subsequent deletion of *rsmN* (Figure 3.7). The increased Hcp1 production was not directly linked to the presence or absence of TssA1 (Figure 3.8B). Instead, it appears that regulation of the H1-T6SS upon *tssA1* deletion is influenced by the presence of RsmN. Both RsmA and RsmN can specifically bind a GGA-containing stem loop structure which overlaps with the *tssA1* Shine-Dalgarno sequence, although RsmN binds with lower affinity (48,541). The deletion of *tssA1* does not remove any residues predicted to be involved in the formation of this stem loop structure, however it cannot be discounted that removal of downstream residues alters the stability and secondary structures formed by the transcript, impairing binding and repression by RsmN. Alternatively, as several stem loop structures containing GGA motifs are typically present in a Csr/Rsm regulated transcript (48,567,568), including within the coding sequence (569), it is possible that *tssA1* deletion may remove residues involved in a downstream stem loop structure, impairing binding and repression by RsmN. A further distinction between RsmA and RsmN is that RsmN requires the presence of two consensus motifs for binding, while RsmA requires only one, which may influence regulation upon alteration of the transcript (540,542). It is not clear why this effect is not seen upon *tssA1* deletion in the PAK strain (Figure 3.2), no sequence difference is present in the upstream GGA stem loop region though some SNPs are present in the coding sequence. The regulation of this transcript may differ somewhat between PAO1 and PAK strains.

In this study, the complex regulation of the H1-T6SS by components of the Gac-Rsm pathway has been explored. Less work has been done to characterise the effect of these components on the regulation of H2- and H3-T6SSs. RsmA is known to negatively regulate all three *P. aeruginosa* T6SSs (338), while RsmN has been shown to bind transcripts belonging to both H2- and H3-T6SS components, in addition to the better characterised binding to H1-T6SS transcripts (539). This suggests that similar regulation

may be involved in the expression of each of the three T6SSs. While this has not been characterised here, this work is ongoing in a separate study from the laboratory (Marta Rudzite, unpublished).

3.7 Summary

Overall, this chapter presented a characterisation of how the Gac-Rsm pathway influences expression of all *P. aeruginosa* T6SSs, revealing a complex network and a strain-specific variation in the Gac-Rsm response. This allowed the selection of conditions and genetic backgrounds which are optimal to individually study each T6SS and evaluate the importance of the TssA components associated with each system. This led to the conclusion that despite some subtle variation, TssA proteins, long or short, are key for the functionality of these systems. Further details on TssA activity and contributions are studied in subsequent chapters.

4. Results: Positioning and interactions of TssA proteins within the T6SS

4.1 Introduction

Each of the three *P. aeruginosa* TssA proteins are required for the activity of their respective T6SS, including in the assembly of the contractile sheath required for effector transport across the cell envelope (Figures 3.6, 3.10, 3.11 and 3.14) (Chapter 3). This effect is seen for both types of TssA proteins referred to as long (TssA2) and short (TssA1 and TssA3). It has been demonstrated that both long and short TssA proteins have similar dynamics during T6SS assembly: fluorescently-tagged TssA proteins associate with the T6SS assembly initiation site, then upon the initiation of sheath polymerisation from this site, TssA proteins are displaced to the distal end of the polymerising sheath as it extends across the cell (360,377,508,513). These dynamics suggest association of TssA proteins with multiple T6SS sub-assemblies. Due to the positioning of TssA proteins at the distal end of the sheath, and a decrease or complete loss in sheath assembly upon *tssA* gene deletion, it is proposed that TssA proteins are primarily involved in the initiation and coordination of the assembly of the sheath (360,376,377,508).

To date, the TssA proteins whose interactions with T6SS components have been studied are the short TssA proteins of *P. aeruginosa* (TssA1) and *B. cenocepacia* ($TssA^{BC}$) and the long TssA proteins of enteroaggregative *E. coli* ($TssA^{EC}$) and *V. cholerae* ($TssA^{VC}$) (360,376,377,509,512). The data to date do not suggest a difference in the interactions of long and short TssA proteins, which have each been shown to associate with components of the membrane complex, baseplate complex and tail complex (Table 1.2) (360,376,377,509,512). There are some variations in the individual components that specific TssA proteins have been observed to bind, which may be due to other differences between TssA proteins.

4.1.1 Interactions of TssA proteins with the membrane complex

The membrane complex is comprised of the outer membrane lipoprotein TssJ and the inner membrane proteins TssL and TssM, which assemble to form a large bell-shaped structure that is anchored in the outer membrane and spans the periplasm and inner membrane (see section 1.3.2.2) (346,347,356). The base of this bell-shaped structure, comprised of TssL and TssM, is exposed to the cytoplasm (347,356). The construction of the membrane complex is the first step in the assembly of the T6SS, providing a platform on which other components dock (345). Both the long $TssA^{EC}$ and $TssA^{VC}$ and the short $TssA^{BC}$ have been shown to interact with the inner membrane components of the

membrane complex, presumably via regions exposed at the cytoplasmic face (Table 1.2) (360,509,512). The most thorough characterisation of this association has taken place using $TssA^{EC}$ (360). Using a fluorescently tagged $TssA^{EC}$, the formation of TssA foci was dependent on the presence of the membrane complex protein TssM, but independent of the presence of any baseplate components, suggesting the recruitment of TssA to the T6SS assembly initiation site is dependent solely on the membrane complex (360). A direct binding was subsequently shown in a co-purification of the complete TssJLM membrane complex with $TssA^{EC}$ (360). Imaging of this complex by negative stain EM identified the presence of an additional density at the cytoplasmic face of the membrane complex, when compared to the membrane complex alone, which was suggested to be $TssA^{EC}$ (360). However, in the absence of high-resolution structural data, the details of this interaction are unclear including how a symmetry mismatch between the five-fold membrane complex symmetry and the six-fold $TssA^{EC}$ symmetry might be accommodated.

4.1.2 Interactions of TssA proteins with the baseplate complex

The baseplate complex components TssE, TssF, TssG and TssK polymerise around a central hub formed of the trimeric VgrG spike which is found at the tip of the Hcp inner tube (see section 1.3.2.3) (365). The baseplate complex docks to the membrane complex, providing a platform for the assembly of the tail complex (365,370). Both the long $TssA^{EC}$ and $TssA^{VC}$ and the short TssA1 and $TssA^{BC}$ have been shown to interact with components of the baseplate complex (Table 1.2) (360,376,377,509,512). The specific interaction partners vary between different TssA proteins, but in all cases, TssK and VgrG have been reported (360,371,376,509,512). In a subset of studies, contacts with other baseplate components including TssE and TssF have also been reported for both long and short TssA proteins (360,376,509,512).

In functional characterisation of $TssA^{EC}$, association with baseplate complex components is dependent on the presence of the membrane complex, but recruitment of the baseplate complex to the membrane complex does not require $TssA^{EC}$ (365,510). The baseplate complex is required for the polymerisation of the sheath and the displacement of TssA to the sheath distal end (360). TssA therefore associates with components of both the membrane complex and the baseplate complex once it is docked at the T6SS assembly initiation site. The details of these interactions are unknown, whether TssA binds both sub-complexes simultaneously, or whether there is some sequential binding. The presence of TssA is not required for the assembly of either sub-complex but may be required to stabilise their docking or for the recruitment of tail components to initiate tail complex assembly.

4.1.3 Interactions of TssA proteins with the tail complex

The tail complex is comprised of the TssB-TssC contractile sheath, which forms around an inner tube of stacked Hcp hexameric rings (see section 1.3.2.4) (378,379,570). In most of the studied systems, TssA is associated with the distal end of this tail complex as it polymerises from the baseplate complex (360,377,508,513). All studied TssA proteins have been shown to interact both with the inner tube component Hcp and components of the contractile TssB-TssC sheath (Table 1.2) (360,376,377,509,512). The $TssA^{EC}$ contact with the sheath is mediated specifically through the N-terminal region comprising the Nt1 and Nt2 domains (360). Using available structures for the Nt2 domain, this region has been modelled to dock to the distal end of the sheath for the long TssA proteins $TssA^{EC}$ and $TssA^{VC}$, whereby the TssA ring aligns to cap the lumen of sheath structure (360,377). However, the short $TssA1^{PP}$ and $TssA^{AB}$, which lack the Nt2 domain found in $TssA_L$ proteins, have also been found at the distal end of the sheath (508,513). The existing model therefore does not explain how, in the absence of a Nt2 domain, a $TssA_S$ protein might dock to the distal end of the sheath. It has been shown that a single TssA complex that initially associates with the T6SS, remains attached to the distal end of the sheath as it polymerises (360,377), however it is unclear how new sheath and inner tube subunits might be incorporated at this growing distal end with this complex bound.

The distinct C-terminal domains of both the long $TssA^{EC}$ and the short $TssA^{BC}$ have been shown to interact with Hcp (360,509). The Hcp tube assembles in a head-to-tail conformation of stacked hexameric rings (379). It has been identified that $TssA^{EC}$ binds the distal tail side of a Hcp ring, while the baseplate associated VgrG spike binds the proximal head side of the Hcp ring (373). How new Hcp subunits are incorporated into the inner tube when the sheath that surrounds it is capped at its distal end is unclear. It has been proposed that the ~100 Å lumen of a $TssA_S$ C-terminal domain ring capping the distal end of the sheath would be large enough to accommodate the passage of a hexameric Hcp ring of ~ 90 Å diameter (see section 1.4.1.2), however, the 25 - 50 Å lumen in the $TssA_L$ C-terminal domain ring would not allow the passage of a Hcp ring (see section 1.4.1.3) (360,376,377,509).

In addition to associating with the T6SS sub-complexes, TssA proteins can also interact with other T6SS components. Both long and short TssA proteins can bind with the ATPase ClpV, which is involved in the disassembly of the contracted sheath (376,377,392,393). Additionally, TssA proteins can interact with their cognate accessory proteins, as described in section 1.4.3 (376,377,508,510).

4.2 Aims of this study

The aim of this study was to identify and characterise the interactions of the three *P. aeruginosa* TssA proteins with other components of the T6SS, so that the overall architecture of the system, and notably the positioning of TssA, could be further clarified.

This analysis involved:

1) Protein-protein interaction assays, using the bacterial two-hybrid (BTH) approach, to identify binding partners of *P. aeruginosa* TssA proteins. An existing collection of BTH constructs was expanded upon to allow a comprehensive screening for partners of all three *P. aeruginosa* TssA proteins among the three T6SS clusters.
2) Alignments and structural comparisons to identify and characterise the role of specific residues in known interactions.
3) Truncations of TssA proteins to characterise roles of TssA domains.
4) Functional characterisation of TssA interactions, applying the techniques previously optimised to probe T6SS functionality as described in Chapter 3.

This aimed to provide insights both into how individual TssA proteins associate with the different T6SS sub-complexes, but also how TssA proteins varying in domain organisation, symmetry and structure interact with these different T6SS components to contribute to similar functional outcomes.

4.3 Positioning TssA within the T6SS: Interactions of TssA proteins with cognate T6SS components

To assess the interactions of TssA proteins with components of their respective T6SSs, the BTH approach was used. This involves engineering protein fusion constructs, where proteins of interest are tagged with either the T25 or T18 fragments of the *Bordetella pertussis* adenylate cyclase catalytic domain (516). Interaction of TssA with the protein of interest brings the attached fusion proteins into proximity to associate and reconstitute their adenylate cyclase activity, leading to the production of cAMP in a strain otherwise lacking an adenylate cyclase enzyme (Figure 4.1). The generated cAMP binds the catabolite activator protein (CAP), forming a complex which can bind DNA and regulate gene expression, including of the *lacZ* gene (571). Production of cAMP therefore corresponds with the expression of *lacZ* and β-galactosidase activity. Contact between proteins of interest can thus be measured by assessing level of the β-galactosidase activity, both quantitatively and qualitatively, by monitoring the hydrolysis of lactose analogues, which give rise to a colorimetric output.

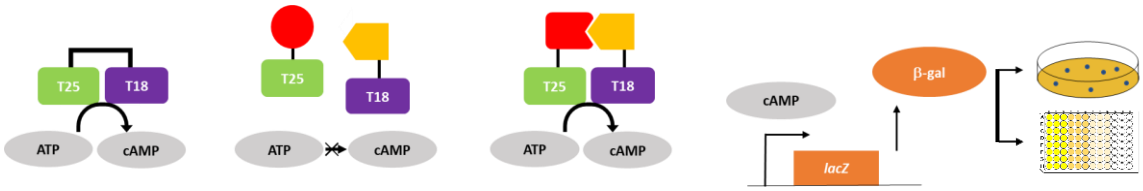


Figure 4.1 Schematic of the BTH approach. Proteins of interest are fused to T18 and T25 catalytic subunits of the *B. pertussis* adenylate cyclase domain. Interaction reconstitutes the adenylate cyclase activity, leading to production of cAMP which can drive production of β-galactosidase. The hydrolysis of substrate analogues by β-galactosidase generates a colorimetric output, for example blue colonies on a plate or yellow in liquid suspension.

To date, of the *P. aeruginosa* TssA proteins, only the interactions of TssA1 have been characterised using pulldown and subsequent mass spectrometry, BTH experiments with only a subset of H1-T6SS proteins and dot blot assays to confirm suspected interactions (376,508). The main outputs of these approaches were that TssA1 associates with itself, with the baseplate components TssK1 and TssF1, the tail complex components TssB1 and Hcp1, the spike protein VgrG1a, the ATPase ClpV1 and the accessory protein TagJ1. The details and functional contributions of many of these interactions are not currently understood.

Although this reveals an already broad network, here the approach was revisited with a more comprehensive and systematic methodology. The aim was to assess interactions between each TssA protein and all components of their cognate T6SS machinery. The existing collection of BTH constructs

was thus dramatically expanded. Identification of TssA partners using this approach provides insight into how TssA proteins are incorporated into the T6SS and whether this is influenced by TssA diversity. This would provide the foundations for hypotheses based on a consistent and global insight into the TssA interaction network and positioning within the T6SS.

4.3.1 Designing appropriate BTH combinations and tag position

An initial consideration was the position of the BTH tag components, T18 or T25, either at the N- or C-terminus. In previous $TssA^{EC}$ BTH data the output was affected depending on whether the T18 or T25 tag was used and whether the tag was present at the N- or C-terminus (360). Each protein can be tagged with each of the two fragments at two different sites: tagging with T25 at the N- (pKT25) or C-terminus (pKNT25) or tagging with T18 at the N- (pUT18C) or C-terminus (pUT18). To comprehensively assess a single interaction, each of the two genes must be cloned into these four vectors, giving rise to eight possible combinations of constructs to screen. Here, the interactions of TssA1 with a subset of H1-T6SS components were systematically tested in all eight combinations to identify which, if any, vector combination/s may be most suitable for further study.

4.3.1.1 C-terminal tagged TssA does not yield productive interactions in the BTH approach

Previous BTH with TssA1 was carried out exclusively with an N-terminal T25 tag (376). Here, the interactions of TssA1 with C-terminal T25 or T18 tags were initially screened, to assess if these or other interactions were identified by altering tag position. In both cases with a C-terminal tag, TssA1 could not be identified to interact with any H1-T6SS components, including itself (Figure 4.2).

In a previous BTH screen with $TssA^{BC}$, constructs with a C-terminal tag were also unable to bind any components in their respective T6SS (509). The oligomerisation of TssA proteins is driven by C-terminal domains (see section 1.4.1) (360,376,377,509), therefore the presence of large C-terminal T25 and T18 tags may sterically hinder this oligomerisation. These constructs not binding any other H1-T6SS components also suggests that C-terminal tagged TssA1 constructs are not appropriate. These interactions may require the formation of a higher order TssA1 complex, which may be blocked by the C-terminal tag. It is also possible that these constructs do not form a stable, folded TssA1 protein. Alternatively, the tagged TssA1 may be able to interact with these proteins, but the position of the tag might not permit reconstitution of the catalytic domain. Yet, in the case of $TssA^{EC}$, the use of a C-terminal tagged BTH construct did not affect the partners identified (360). This could be linked to the fact that $TssA^{EC}$ is a $TssA_L$, while TssA1 and $TssA^{BC}$ are both $TssA_S$ proteins. The C-terminal tag position

may not prevent the oligomerisation of a $TssA_L$, or this C-terminal tag may have better relative positioning to be reconstituted when compared to a $TssA_S$. As such the BTH screen may have to be adapted to every individual TssA protein.

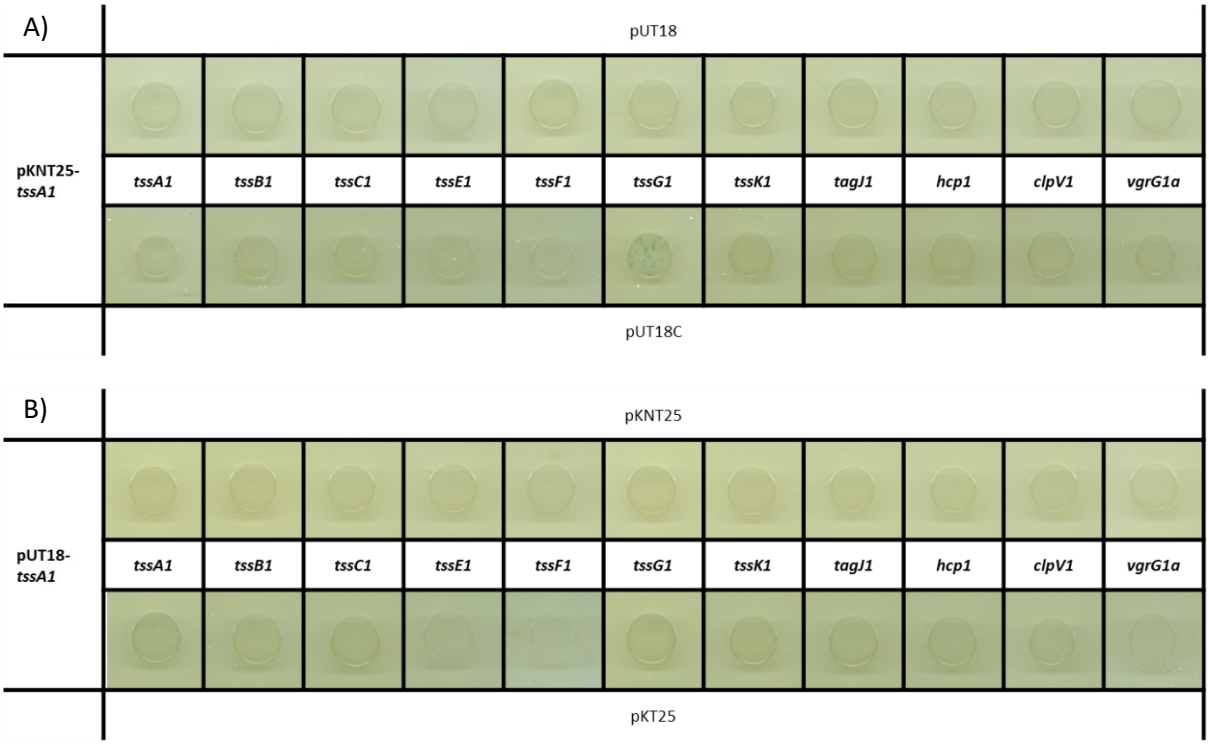


Figure 4.2. Interactions of C-terminal tagged TssA1 with H1-T6SS components. BTH with C-terminal T25 (pKNT25) or T18 (pUT18) linked TssA1 and either N- terminal T25 (pKT25) or T18 (pUT18C) or C-terminal T25 (pKNT25) or T18 (pUT18) linked H1-T6SS proteins produced in DHM1 cells. Representative spots after 24 hours growth on 5-bromo-4-chloro-3-indolyl-β-D-galacto-pyranoside (X-Gal) containing LB agar are shown. Blue spots indicate protein-protein interaction, spots are white in the absence of interaction. A) Interactions of C-terminal T25 (pKNT25) tagged TssA1 with C- (pUT18) or N-terminal (pUT18C) T18 tagged H1-T6SS proteins. B) Interactions of C-terminal T18 (pUT18) tagged TssA1 with C- (pKNT25) or N-terminal (pKT25) T25 tagged H1-T6SS proteins.

4.3.1.2 BTH screen using N-terminal tagged TssA yields productive interactions

As BTH with C-terminal tagged TssA1 was unsuccessful, N-terminal tagged TssA1 proteins were screened. When tagged at the N-terminus TssA1 was able to interact with T6SS components (Figure 4.3). With an N-terminal T25 tag, TssA1 bound TssK1 independent of the position of its T18 tag, as well as N-terminal T18 tagged TssA1, Hcp1, ClpV1 and VgrG1a (Figure 4.3A). With an N-terminal T18 tag, TssA1 bound a C-terminal T25 tagged TssK1 and a N-terminal T25 tagged TssA1 (Figure 4.3B).

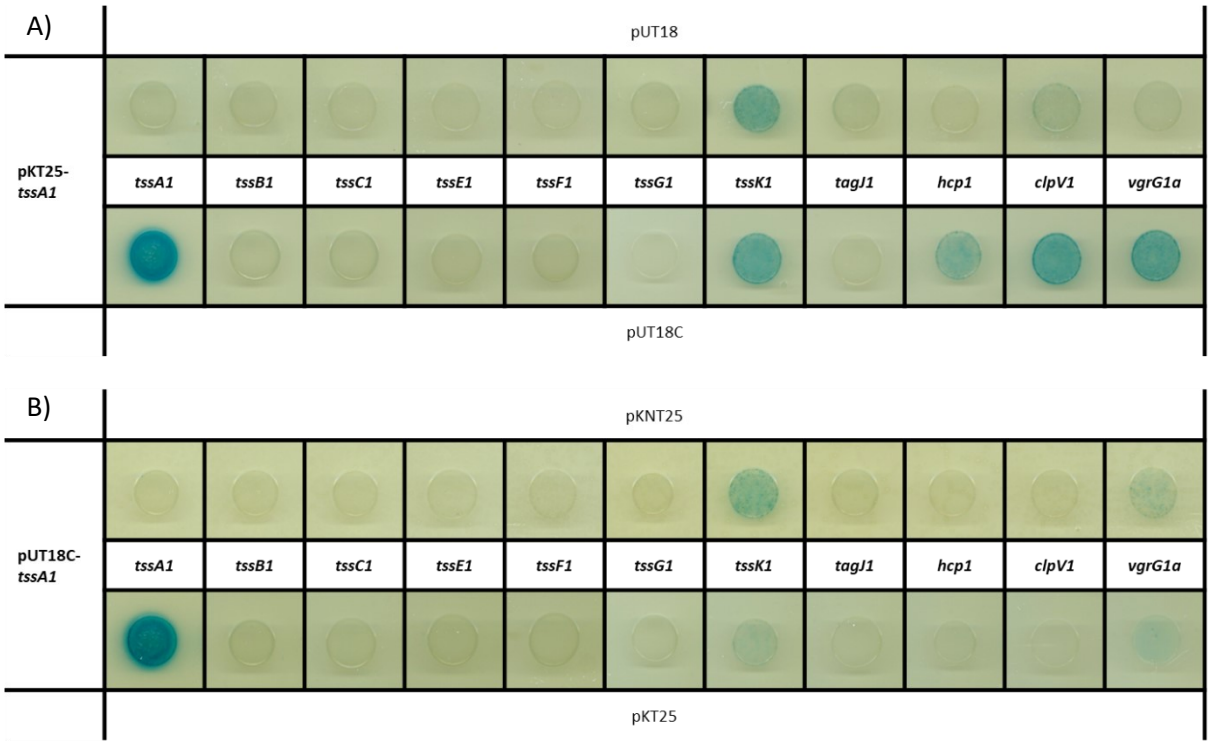


Figure 4.3 Interactions of N-terminal tagged TssA1 with H1-T6SS components. BTH with N-terminal T25 (pKT25) or T18 (pUT18C) linked TssA1 and either N- terminal T25 (pKT25) or T18 (pUT18C) or C-terminal T25 (pKNT25) or T18 (pUT18) linked H1-T6SS proteins produced in DHM1 cells. Representative spots after 24 hours growth on X-Gal LB agar are shown. Blue spots indicate protein-protein interaction, spots are white in the absence of interaction. A) Interactions of N-terminal T25 (pKT25) tagged TssA1 with C- (pUT18) or N-terminal (pUT18C) T18 tagged H1-T6SS proteins. B) Interactions of N-terminal T18 (pUT18C) tagged TssA1 C- (pKNT25) or N-terminal (pKT25) T25 tagged H1-T6SS proteins.

N-terminal tagged TssA1 proteins were therefore able to self-interact, although only when both TssA1 components were tagged at the N-terminus, as well as binding other H1-T6SS components (Figure 4.3). This overall confirmed previously reported data, where TssA1 interacts with itself, components of the baseplate component, notably TssK1, the inner tube protein Hcp1, the spike protein VgrG1a and the ATPase ClpV1 (376).

In conclusion, all identified TssA1 partners were identified when both components were tagged at the N-terminus. However, there were differences in the interactions identified based on what tag was present: more partners were identified with TssA1 tagged with T25 (Figure 4.3A) than with T18 (Figure 4.3B). All of the TssA1 partners identified were present when screening N-terminal T25 tagged TssA1 (pKT25) with N-terminal T18 tagged H1-T6SS components (pUT18C), so going forward this

combination of constructs was used to systematically assess interactions of *P. aeruginosa* TssA proteins with all components of their T6SS.

4.3.2 TssA proteins self-interact

Firstly, the self-association of each of the *P. aeruginosa* TssA proteins with N-terminal tags was assessed. This self-association is well characterised in the literature, with oligomerisation shown to give rise to the formation of higher order TssA complexes (360,376,377,509,512). As expected, each of the TssA proteins were identified to self-interact using a BTH approach (Figure 4.4).

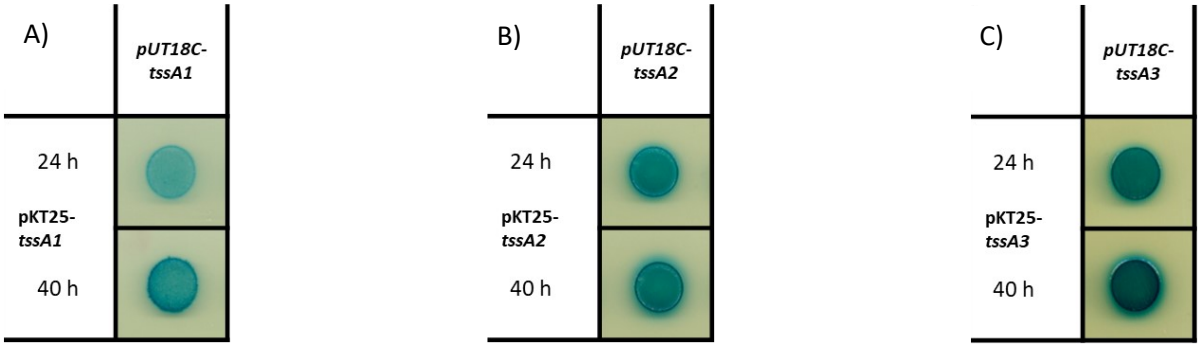


Figure 4.4 Self-interactions of N-terminal tagged TssA proteins. BTH with N-terminal T25 (pKT25) and T18 (pUT18C) linked TssA proteins produced in DHM1 cells. Representative spots imaged after 24 and 40 hours growth on X-Gal LB agar are shown. Blue spots indicate protein-protein interaction, spots are white in the absence of interaction. A) Self-interaction of TssA1. B) Self-interaction of TssA2. A) Self-interaction of TssA3.

These spots were incubated for 40 hours as well as the initial 24 hours to reveal weaker interactions. However, in this case, self-interaction could clearly be demonstrated after 24 hours for each TssA.

4.3.3 TssA interacts with sheath components and Hcp

Contacts between TssA1 and the sheath component TssB1 has previously been identified in pulldown data, however this had not previously been demonstrated in BTH experiments (376). The association between TssA proteins and their respective sheath is well established, with previous BTH and pulldown data for $TssA^{EC}$, $TssA^{VC}$ and $TssA^{BC}$ proteins demonstrating interaction with one or both of TssB and TssC (360,376,377,509,512). Additionally, the association of TssA complexes with the distal end of the polymerising sheath has been demonstrated by fluorescence microscopy

(360,377,508,513). To further characterise the details of this key interaction using the BTH approach, it was first necessary to identify conditions giving a clear colorimetric output.

In the initial BTH screen, TssA1 could not be observed to interact with either TssB1 or TssC1 in isolation, regardless of tag position (Figures 4.2 and 4.3). There was a similar outcome for TssA2 and TssA3 with their respective sheath components (Figure 4.5).

As such, a three-component BTH approach was designed (23). In this approach, in addition to the two T18 and T25 tagged proteins being produced, a third protein is also produced which may either promote or interfere with contact between the tagged proteins. Constructs were thus engineered where the coding sequence for the sequential *tssB* and *tssC* genes was introduced into pUT18C, where TssB was tagged at the N-terminus and native TssC was also produced. The theory being that with both TssB and TssC present, a higher order sheath structure may form, which may be more likely to provide an appropriate interface to bind the respective TssA protein compared to these proteins in isolation.

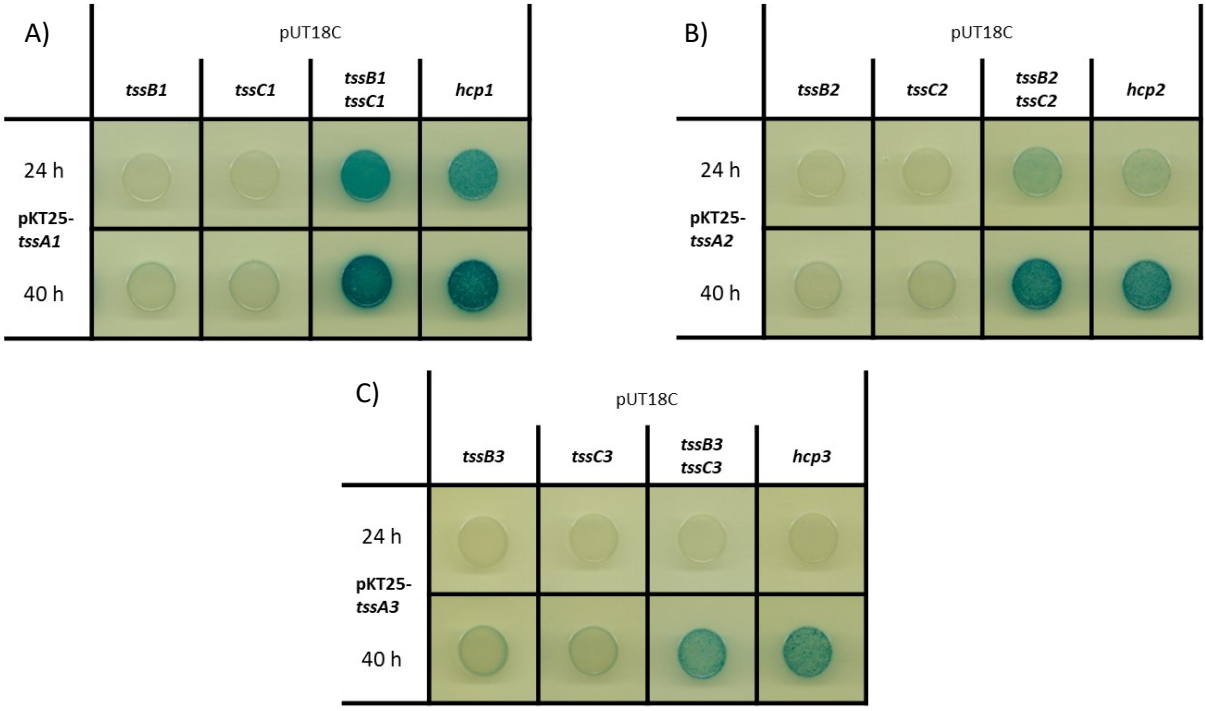


Figure 4.5 Interactions of TssA proteins with tail complex components. BTH with N-terminal T25 (pKT25) linked TssA proteins and N-terminal T18 (pUT18C) linked sheath components (TssB and TssC) and Hcp proteins produced in DHM1 cells. Representative spots imaged after 24 and 40 hours growth on X-Gal LB agar are shown. Blue spots indicate protein-protein interaction, spots are white in the absence of interaction. A) Interaction of TssA1 with H1-T6SS sheath and inner tube proteins. B) Interaction of TssA2 with H2-T6SS sheath and inner tube proteins A) Interaction of TssA3 with H3-T6SS sheath and inner tube proteins.

For each of the *P. aeruginosa* TssA proteins, interaction with sheath components could be demonstrated when both TssB and TssC were present (Figure 4.5). Interestingly, the interactions with sheath components appeared strongest for the H1-T6SS, while that for the H3-T6SS only became clear after 40 hours of incubation.

This is the first time a BTH approach has demonstrated interaction between a *P. aeruginosa* TssA protein and sheath components, allowing this technique to be used for future more detailed assessment of this interaction. This association of TssA with the sheath is proposed to be key for sheath initiation and polymerisation, therefore further characterisation is crucial to understanding the role and positioning of TssA in the T6SS.

Each *P. aeruginosa* TssA protein was also identified to bind the other component of the tail complex: the inner tube protein Hcp (Figure 4.5). This had already been described within the H1-T6SS (376), as well as for $TssA^{EC}$, $TssA^{BC}$ and $TssA^{VC}$ (360,509,512), but this is the first description of an interaction with Hcp for TssA2 and TssA3.

Overall, these data suggest that the association of *P. aeruginosa* TssA proteins with their respective tail complexes, including the sheath and the inner tube, is similar between each of the three T6SSs and similar to that of other studied TssA proteins.

4.3.4 TssA proteins interact with baseplate components, notably TssK

TssA proteins, such as $TssA^{EC}$, $TssA^{BC}$ and $TssA^{VC}$, have previously been identified to interact with components of the baseplate complex including TssE, TssF and TssK via a combination of BTH and pulldown experiments (360,371,509,512). Likewise, TssA1 binding to TssK1 and TssF1 has been identified by BTH and pulldown experiments (376). Here, the interaction of each *P. aeruginosa* TssA protein with their respective baseplate complex components, TssE, TssF, TssG and TssK, was systematically screened.

Each *P. aeruginosa* TssA protein was shown to bind its respective TssK (Figure 4.6). The previously identified interaction between TssA1 and TssF1 could not be conclusively demonstrated, with only a very weak blue signal present after 40 hours of incubation. A more conclusive signal was present for TssF3, which was the only other baseplate complex component identified to form contacts with a TssA protein in this screen (Figure 4.6C). As for tail complex components, signal for TssA3 and other H3-T6SS components was weaker than the other two T6SSs, only becoming detectable after 40 hours of incubation.

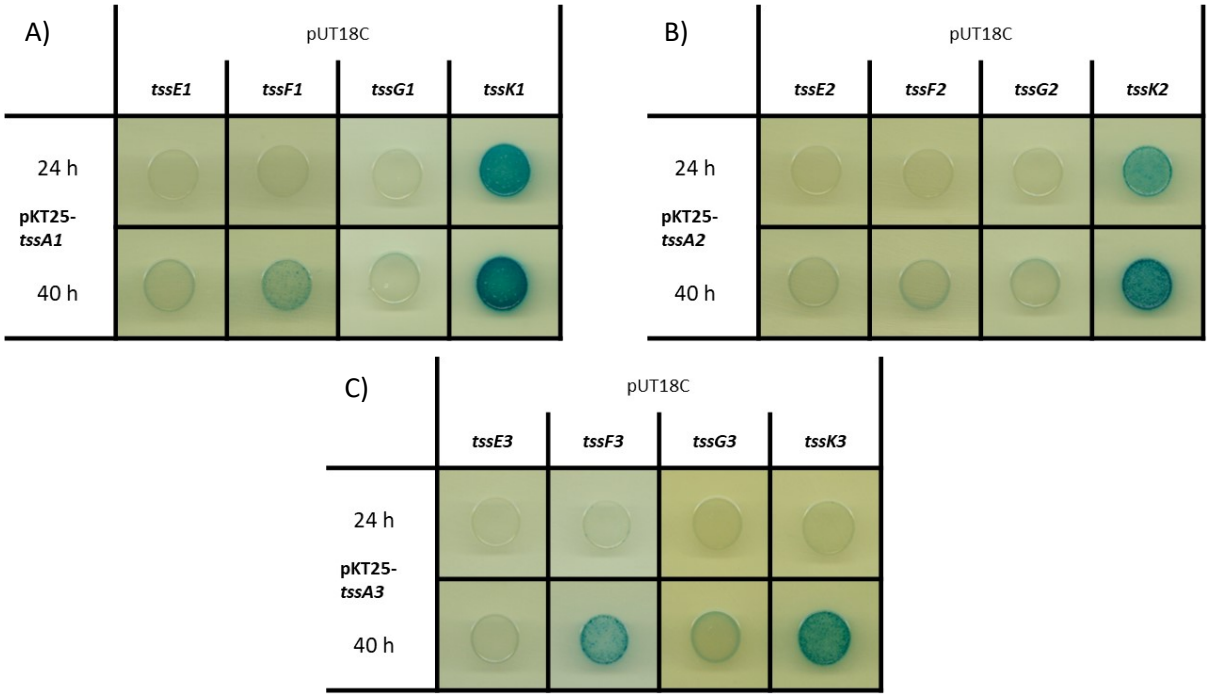


Figure 4.6 Interactions of TssA proteins with baseplate complex components. BTH with N-terminal T25 (pKT25) linked TssA proteins and N-terminal T18 (pUT18C) linked baseplate complex components (TssE, TssF, TssG and TssK) produced in DHM1 cells. Representative spots imaged after 24 and 40 hours growth on X-Gal LB agar are shown. Blue spots indicate protein-protein interaction, spots are white in the absence of interaction. A) Interaction of TssA1 with H1-T6SS baseplate complex components. B) Interaction of TssA2 with H2-T6SS baseplate complex components. C) Interaction of TssA3 with H3-T6SS baseplate complex components.

In light of these results, TssK appears to be a very important partner for TssA proteins, with consistent interactions detected for every T6SS studied to date (360,371,376,509,512). Other partners identified in the baseplate, TssE and TssF, are more variable, which may reflect subtle differences in TssA association with these components. Alternatively, there may be limitations in the BTH approach for identifying these interactions.

4.3.5 Interaction between TssA proteins and VgrG proteins

The interaction of TssA proteins with their associated VgrG spike protein has been demonstrated for $TssA^{EC}$, $TssA^{BC}$, $TssA^{VC}$ and TssA1 (360,376,509,512). Here, TssA1 was identified to bind VgrG1a and more weakly VgrG1b, but not the other H1-T6SS-associated VgrG1c (Figure 4.7A). TssA2 was also identified to weakly interact with VgrG2a, but not with any other H2-T6SS-associated VgrG proteins (Figure 4.7B), while TssA3 was not identified to interact with the single H3-T6SS-associated VgrG3 (Figure 4.7C).

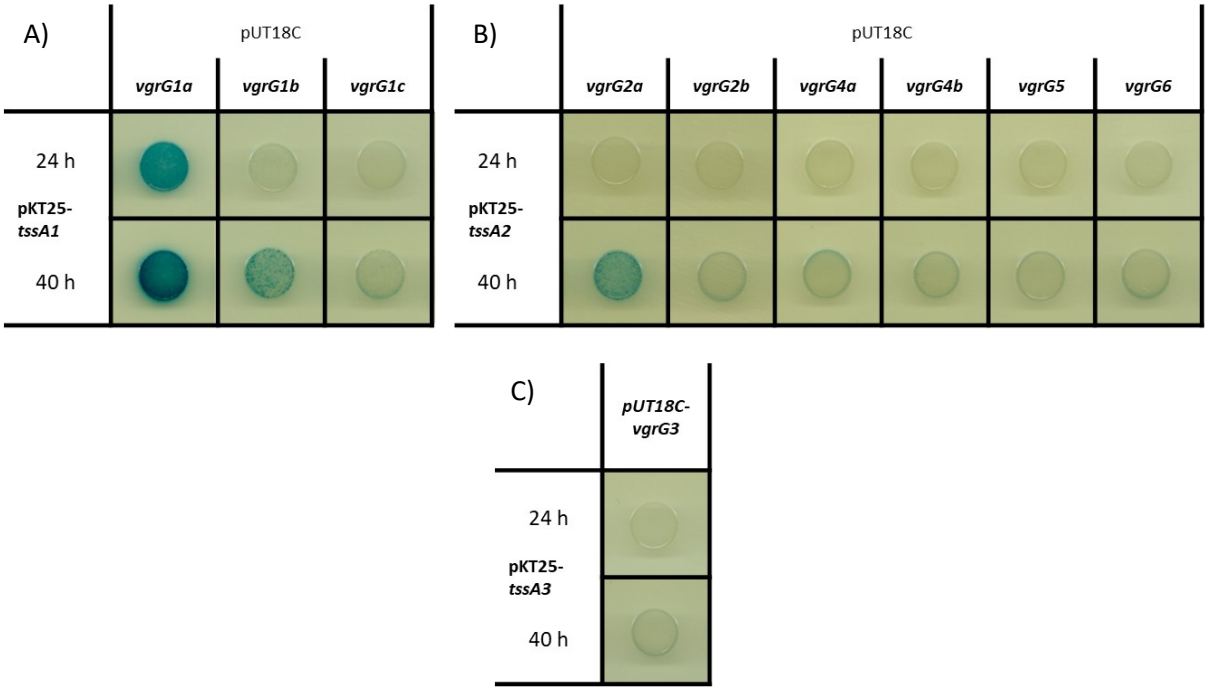


Figure 4.7 Interactions of TssA proteins with VgrG spike proteins. BTH with N-terminal T25 (pKT25) linked TssA proteins and N-terminal T18 (pUT18C) linked VgrG proteins produced in DHM1 cells. Representative spots imaged after 24 and 40 hours growth on X-Gal LB agar are shown. Blue spots indicate protein-protein interaction, spots are white in the absence of interaction. A) Interaction of TssA1 with H1-T6SS VgrG proteins (VgrG1a, VgrG1b and VgrG1c). B) Interaction of TssA2 with H2-T6SS VgrG proteins (VgrG2a, VgrG2b, VgrG4a, VgrG4b, VgrG5 and VgrG6). C) Interaction of TssA3 with VgrG3.

It is unexpected that a TssA protein would form different contacts with their respective VgrG spike proteins as seen here (Figure 4.7). Each spike component would be expected to dock in the baseplate during T6SS assembly to form a trimer, with both homo- and heterotrimeric assemblies being observed for the H1-T6SS (523). It may therefore be that oligomerisation of a VgrG trimer is required to associate with TssA proteins. Only VgrG1a was identified to self-interact after 24 hours of incubation, mirroring the observed interaction with TssA1 after the same period of incubation (Figures 4.7A and 4.8). The lack of strong self-interaction of the VgrG1b and VgrG1c BTH constructs could reflect an inability of these constructs to form a homo-trimeric VgrG structure. If a trimeric VgrG is required to associate with a TssA protein, the lack of self-interaction could then prevent this association. This could have functional implications, identifying certain combinations of VgrG proteins as required for trimer formation. One way this could be assessed is with a three-component BTH approach, assessing these interactions in the presence of different combinations of VgrG proteins.

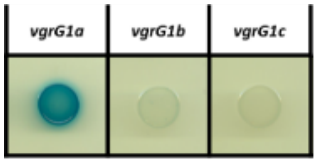


Figure 4.8 Self-interactions of H1-T6SS VgrG proteins. Bacterial two- hybrid with N-terminal T25 (pKT25) and T18 (pUT18C) linked H1-associated VgrG proteins produced in DHM1 cells. Representative spots imaged after 24 hours growth on X-Gal LB agar are shown. Blue spots indicate protein-protein interaction, spots are white in the absence of interaction.

Interaction has previously been consistently detected between TssA proteins and an associated VgrG whenever tested (360,376,509,512). The absence of detected contacts could be linked to the BTH approach or the constructs used, these data should therefore be supplemented with additional techniques, such as pulldown or dot blot assays. A more comprehensive BTH screen, varying the tag type and location might also provide new insights. Indeed, in previous BTH experiments between TssA proteins and VgrG proteins, interactions have not always been apparent depending on the position of the tag. While BTH tag position did not affect the association between $TssA^{BC}$ and its VgrG protein, for $TssA^{EC}$, interaction was only identified with the VgrG tagged at the C-terminus (360,509). Integrating a few approaches may give a clearer picture of the conservation of the interaction between TssA and VgrG proteins.

4.3.6 Some TssA proteins interact with ClpV

The association of TssA proteins and the ATPase ClpV has previously only been described for TssA1 and $TssA^{VC}$, although this reflects an absence of testing for other TssA proteins (376,377). To test the conservation of this interaction, all three *P. aeruginosa* TssA proteins were screened for interaction with their respective ClpV proteins by BTH.

Only TssA1 was identified to interact with its associated ClpV, but not TssA2 or TssA3 (Figure 4.9). As with the VgrG BTH constructs, some differences have been identified in the self-interaction of ClpV constructs, with only ClpV1 able to self-interact. ClpV proteins form hexamers, so self-interaction is expected (393,572). If this oligomerisation is required for association with TssA proteins, these BTH constructs may not be appropriate.

However, a phylogenetic grouping of ClpV proteins has been described that corresponds with distinct modes of interaction with TssC proteins, where ClpV1 is found in a different phylogenetic group to

ClpV2 and ClpV3 (515). These differences between these ClpV proteins may also affect their association with their respective TssA proteins.

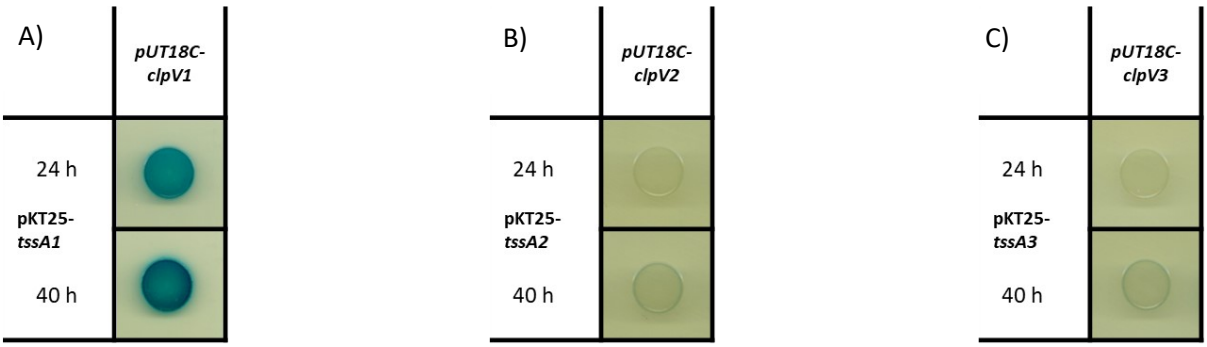


Figure 4.9 Interactions of TssA proteins with ClpV proteins. BTH with N-terminal T25 (pKT25) linked TssA proteins and N-terminal T18 (pUT18C) linked ClpV proteins produced in DHM1 cells. Representative spots imaged after 24 and 40 hours growth on X-Gal LB agar are shown. Blue spots indicate protein-protein interaction, spots are white in the absence of interaction. A) Interaction of TssA1 with ClpV1. B) Interaction of TssA2 with ClpV2. C) Interaction of TssA3 with ClpV3.

Unlike TssA interactions with other components where functional roles have been proposed, i.e. contributing to initiation of sheath assembly at the baseplate complex and coordination of tail complex polymerisation (360), the role of TssA association with the ATPase involved in disassembling the contracted sheath is less clear. It has been suggested that ClpV proteins may have roles in recycling the TssA ring (376), although it has not been described that TssA proteins would require active recycling, unlike the sheath which undergoes a significant conformational change upon contraction. Alternatively, the ClpV1-associated phylogenetic group has been linked to T6SS clusters encoding a $TssA_S$ protein and their associated TagJ accessory protein, with interactions have been demonstrated between each of TssA1, ClpV1 and TagJ1 (376,508,515). The association of ClpV and TssA has therefore been suggested to be linked to the, as yet uncharacterised, activity of the accessory protein TagJ.

The role of interactions between TssA and ClpV proteins is not yet clear, further work is required to confirm how widespread these interactions are, and to further characterise them.

4.3.7 TssA interaction with membrane complex components could not be conclusively identified

Interaction between TssA proteins and the inner membrane proteins of the membrane complex, TssL and TssM, has been identified for $TssA^{EC}$, $TssA^{BC}$ and $TssA^{VC}$ (360,509,512), but this has not been studied for any *P. aeruginosa* TssA to date.

As inner membrane proteins, care was taken in the design of BTH constructs for TssL and TssM to ensure tags would be present in the cytoplasm. In previous work, TssL interactions have been identified with either the full length protein or truncations leaving N-terminal cytoplasmic regions (509,512). BTH constructs were generated with full-length TssL proteins with the tag at the cytoplasmic N-terminus. Previously described TssM constructs all involved truncation of TssM and tagging of the cytoplasmic N-terminal domain (509,512), therefore constructs were designed based on the predicted position of transmembrane helices, using TMHMM (530).

In BTH analyses, only a weak binding to TssM1 could be identified (Figure 4.10). As previously suggested, a more comprehensive BTH screen with membrane complex components, including altering the truncation site, coupled with complementary techniques would help give a more conclusive characterisation.

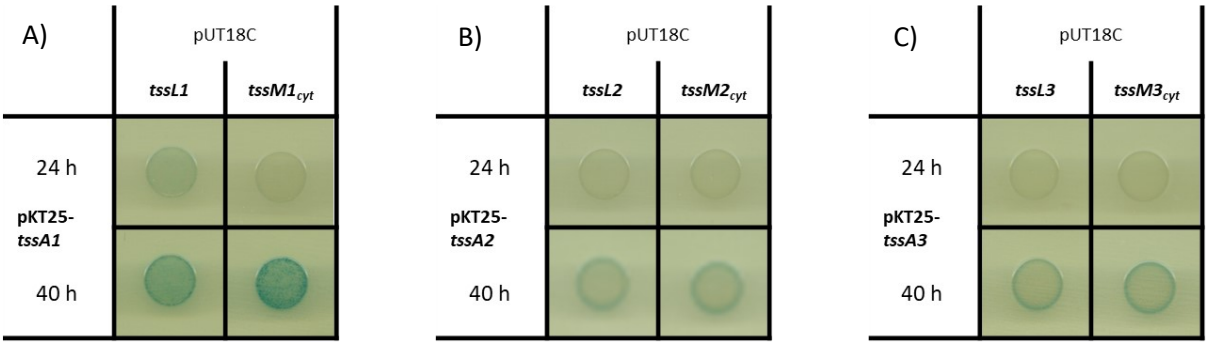


Figure 4.10 Interactions of TssA proteins with membrane complex components. BTH with N-terminal T25 (pKT25) linked TssA proteins and N-terminal T18 (pUT18C) linked membrane complex components (TssL and TssM cytoplasmic region) produced in DHM1 cells. Representative spots imaged after 24 and 40 hours growth on X-Gal LB agar are shown. Blue spots indicate protein-protein interaction, spots are white in the absence of interaction. A) Interaction of TssA1 with H1-T6SS-associated membrane complex components. B) Interaction of TssA2 with H2-T6SS-associated membrane complex components. C) Interaction of TssA3 with ClpV H3-T6SS-associated membrane complex components.

4.3.8 Interactions of TssA3 appear weaker than TssA1 and TssA2 interactions

A trend that emerged in this BTH screen was the relative weakness of TssA3 interactions when compared to those of TssA1 or TssA2. After 24 hours of incubation, only TssA3 self-interaction could be identified, but no interactions with other H3-T6SS components (Figures 4.4, 4.5, 4.6, 4.7, 4.9 and 4.10). In comparison, numerous TssA1 and TssA2 interactions could be identified at 24 hours of

incubation, although more pronounced for TssA1. The varying strength of these contacts is quite remarkable and may suggest that the assembly and stability of the H3-T6SS differs from that of the H1- and H2-T6SSs. It would be interesting to test whether this relative weakness of interactions is present between different H3-T6SS components or reflects solely on the association of TssA3 to the H3-T6SS.

Overall, all three *P. aeruginosa* TssA proteins behave quite similarly: self-interacting as well as interacting with components of their respective sheaths, the baseplate protein TssK and the inner tube protein Hcp (Figures 4.4, 4.5, 4.6, 4.7, 4.9 and 4.10). These interactions are generally comparable to previously reported data for TssA proteins, however there are subtle differences and some associations could not be consistently confirmed, such as with membrane complex components and VgrG proteins (360,376,377,509,512).

Ultimately, while the BTH approach allows for systematic screening of interaction partners, it has limitations with outcomes affected by tag positioning and the large size of the tag possibly obscuring binding. To be done in the most comprehensive way, all vector combinations should be assessed, which is quite an undertaking with such a large panel of proteins to screen. This BTH data provides a platform from which a more robust understanding of the interactions of *P. aeruginosa* TssA proteins can be built. A range of approaches should be integrated to both validate this data and investigate further partners that were absent in this screen.

It is important to bear in mind that associations between proteins are not binary, particularly in such a complex, multiprotein machinery as the T6SS. Interactions may not become entirely apparent in the absence of other components of the T6SS, as demonstrated here for interactions with the sheath, which could only be observed in the presence of both components (Figure 4.5). The T6SS is also a dynamic machinery that undergoes structural changes. It is proposed that both the baseplate and sheath complexes are assembled in high energy conformations, where the structures and associations of component proteins may differ at various stages of T6SS activity. This diversity in conformations is difficult to capture when assessing the interactions of individual proteins in a non-native setting. Additionally, the variable strengths of contacts can make it difficult to conclusively assess interactions that may be weaker or more transient. Variations in interaction strength between components in different T6SSs may reflect subtle mechanistic differences which affect overall T6SS behaviour.

4.3.9 Quantification of β-galactosidase activity did not produce consistent data

While strong interactions could be identified with confidence by spotting BTH cultures on X-Gal containing media, weaker interactions were more difficult to conclusively assess. An alternative, and more quantitative approach for assessing β-galactosidase activity, involves measuring the rate with which O-nitrophenyl-beta-D-galactopyranoside (ONPG) is metabolised by β-galactosidase to produce a yellow colorimetric output. For this approach, cells carrying complementary BTH vectors were grown in liquid culture and subsequently lysed to release the produced β-galactosidase, with the rate of colour change due to ONPG hydrolysis measured in a microplate reader. This protocol was adapted based on a previously reported single step β-galactosidase assay (573).

For very strong interactions, such as that of the leucine zipper positive control or TssA1 self-interaction, the bacterial suspension was diluted to avoid signal saturation and allow the rate of colour change to be accurately assessed (Figure 4.11A). These interactions were far stronger than the background level obtained when the vector encoding TssA1 was combined with an empty vector negative control. For screening other H1-T6SS components, the bacterial suspension was not diluted, and interactions were identified with TssB1 in the presence of TssC1, TssK1, ClpV1 and VgrG1a in general agreement with the spotting assay (Figures 4.5, 4.6, 4.7, 4.9 and 4.11B). Somewhat surprisingly, the binding of TssA1 to Hcp1 that could be demonstrated in the spotting assay (Figure 4.5), could not be distinguished from the negative control in the microplate reader assay. In any case, this method did not confirm any additional partners as compared to the spotting assay. At most it differentiated ClpV1 and VgrG1a as being stronger partners, as compared to TssB1 and TssK1, which was unexpected and may require further statistical assessment.

The microplate reader assay was also used to assess the interactions of TssA2 with H2-T6SS components. TssA2 self-interaction, interaction with sheath components and baseplate components TssE2 and TssK2 were demonstrated (Figures 4.11C and D). Here again, the Hcp2 binding was not detected, as was the case for Hcp1, while the weak interaction with VgrG2a identified in the spotting assay was also absent (Figure 4.7). As with TssA1, a clear statement could not be made about the quantitative level of interaction between the various hits, although TssK2 appeared to be the strongest binding partner.

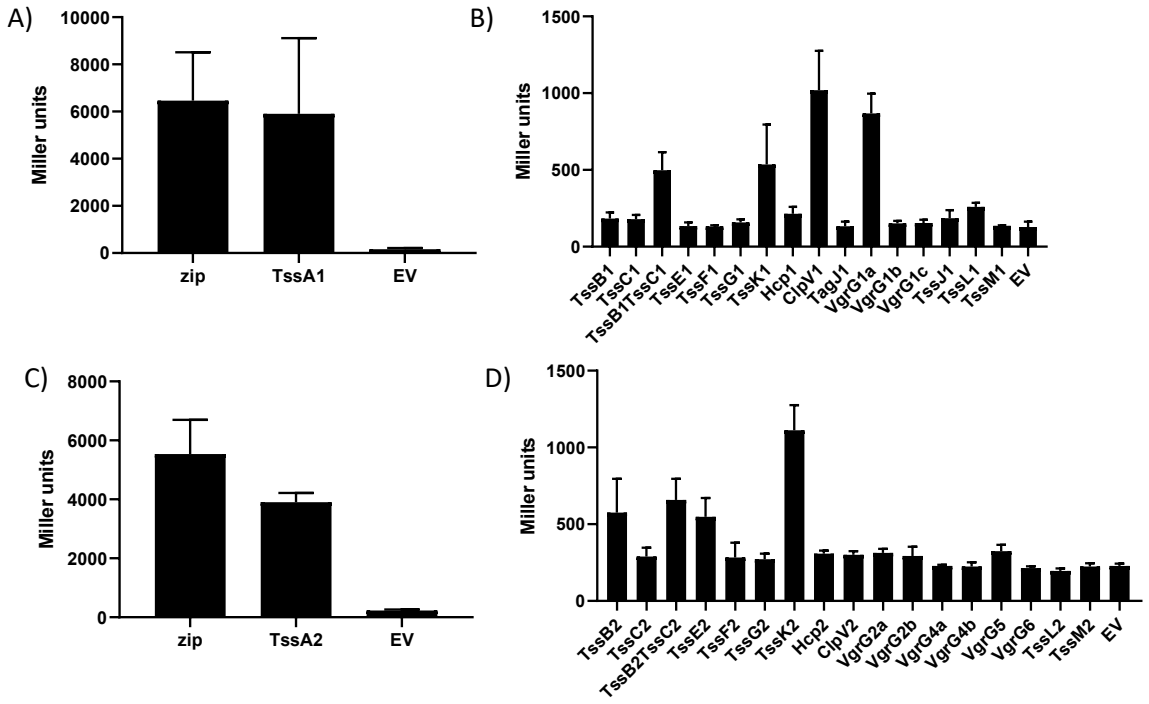


Figure 4.11 β-galactosidase assay quantification of TssA1 and TssA2 interactions with their cognate T6SS components. BTH with N-terminal T25 (pKT25) linked TssA1 and TssA2 and N-terminal T18 (pUT18C) linked H1-and H2-T6SS components produced in DHM1 cells. The activity of β-galactosidase is given in Miller units. Interaction with the pUT18C empty vector (EV) provides a negative control, self-interaction of the leucine zipper (zip) provides a positive control. All data are from 3 biological replicates. Values are presented as means and error bars represent standard deviation. A) Self-interaction of TssA1 and the leucine zipper. B) Interaction of TssA1 with H1-T6SS components. C) Self-interaction of TssA2 and the leucine zipper. B) Interaction of TssA2 with H2-T6SS components.

The overall approach is thus not particularly conclusive, and unexpectedly, the data sets produced for BTH with TssA1 and TssA2 varied between the qualitative spotting assay and quantitative microplate reader approaches (Figures 4.4, 4.5, 4.6, 4.7, 4.9, 4.10 and 4.11). In both cases weaker interactions, such as between TssA1 and Hcp1 or VgrG1b which could be identified in the spotting assay, were absent in the microplate reader assay. For TssA2 some partners, i.e. TssB2 alone and TssE2, were identified that were not present in the spotting assay (Figures 4.5, 4.6 and 4.11D).

One explanation for the slightly different partners identified with these two approaches may be linked to the level of induction. For both approaches, cells were grown in liquid culture with 0.5 mM IPTG before either lysis or spotting on agar. However, the agar plate on which the spotting experiment was carried out contained 1 mM IPTG, for optimal induction of BTH constructs. It may be that at the lower

IPTG concentration in the liquid culture, BTH constructs were not as strongly produced as on agar in the spotting assay and therefore only stronger contacts producing large amounts of β-galactosidase could be detected.

In conclusion, the microplate reader assay did not help in identifying weaker partners. The more transient nature of these weaker contacts may introduce a level of variability into the data. The level of sensitivity of this approach was thus too low to identify new partners or draw conclusions about the relative strength of different interactions.

4.4 Site-directed mutagenesis to target interactions of TssA1

Having comprehensively assessed the interactions of TssA proteins, the molecular details contributing to these interfaces could be probed, notably the identification of key residues and regions. To date, this is generally poorly characterised, although where TssA structural data is available, key residues involved in oligomerisation have been suggested (see section 1.4.1) (360,377,509).

High-resolution structural data was not available for $TssA_S$ proteins at the beginning of this project. To screen TssA1 residues for their contribution to interactions with T6SS proteins, candidate residues were thus initially selected based on previous studies. This began with a library of *tssA1* mutants generated using error prone PCR and subsequently screened using the BTH assay for loss of binding to the known partners TssA1 and TssK1 (Table 4.1) (Josh McQuail, unpublished). Mutants that lost these interactions were sequenced and generally harboured a combination of mutations. Residues were thus selected from this panel to be studied in isolation. The selection was based on the frequency with which the mutation was identified, the residue position in TssA1 domains and the level of conservation in TssA sequences based on previously published multiple sequence alignment data (509).

Table 4.1 TssA1 mutants losing interaction by BTH

Mutants losing TssA1-TssA1 interaction			
A1	G129S	L289P	
A2	L136P	L309P	
A3	P250L	A280S	L289P
A4	G86E	L286P	
A5	L90P	L159P	
Mutants losing TssA1-TssK1 interaction			
K1	L94P		
K2	E170K	A232V	
K3	L136P	L309P	

4.4.1 TssA1 Nt1 and C-terminal domain point mutants lose interaction with known partners non-specifically

4.4.1.1 Analysis of Tss1 Nt1 domain mutants

TssA1 is comprised of Nt1 and a C-terminal domains connected by a flexible linker (see section 1.4.1) (Figure 4.12A). Based on data described in the previous section, residues in the TssA1 Nt1 domain were selected for site-directed mutagenesis to alanine and BTH screening with previously identified TssA1 H1-T6SS partners; i.e. TssA1, TssB1 in the presence of TssC1, TssK1, Hcp1, ClpV1 and VgrG1a.

Residues G86, for self-interaction, and L94, for interaction with TssK1, were identified in the BTH mutant library screen, and were also identified as highly conserved within TssA sequences (Table 4.1) (509). Residue K69 was also selected as a conserved residue with charge, as it was hypothesised that the charge may be involved in stabilising contact via ionic interactions. Based on the resolved $TssA^{BC}$ Nt1 domain structure, a model was generated of the TssA1 Nt1 domain using the Robetta protein structure prediction service (532). The position of the candidate residues in the TssA1 Nt1 domain primary sequence and predicted tertiary structure is shown in Figures 4.12B and C.

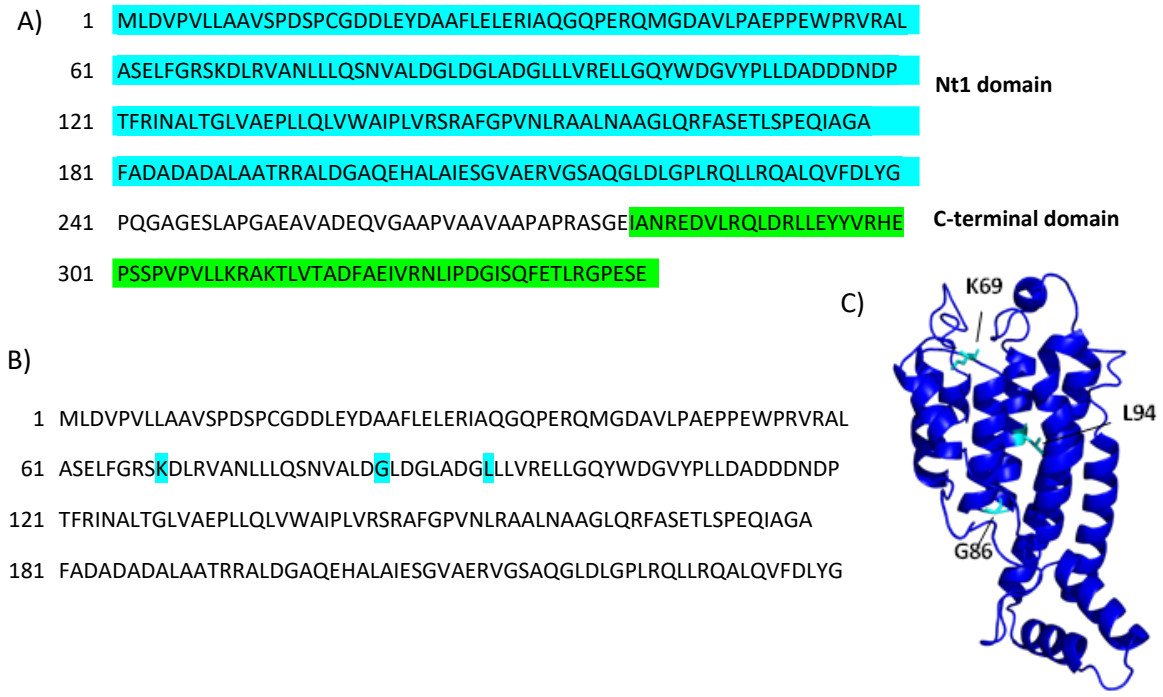


Figure 4.12 Position of selected TssA1 Nt1 domain residues. A) Position of TssA1 Nt1 and C-terminal domains. B) Position of K69, G86 and L94 (light blue) in the TssA1 Nt1 domain sequence. C) Position of K69, G86 and L94 (light blue) in a predicted model of the TssA1 Nt1 domain structure.

Upon substitution of each of the above-described residues into alanine, the TssA1 point mutants were all able to associate with wildtype TssA1, suggesting that each variant was stable and the C-terminal domains folded properly (Figure 4.13). While K69A and L94A mutants were able to self-interact, the G86A mutant was not. Self-interaction has previously been shown to involve oligomerisation of the C-terminal regions for both long and short TssA proteins (see section 1.4.1), so it is unlikely that G86A is directly involved in self-interaction. It is surprising that this mutant could interact with wildtype TssA1 but not self-interact. Otherwise, all TssA1 Nt1 domain mutants were unable to bind other TssA1 partners. This widespread effect on TssA1 interactions might suggest that these substitutions may

affect the overall fold of the Nt1 domain rather than specifically contributing to the binding of TssA1 to a partner.

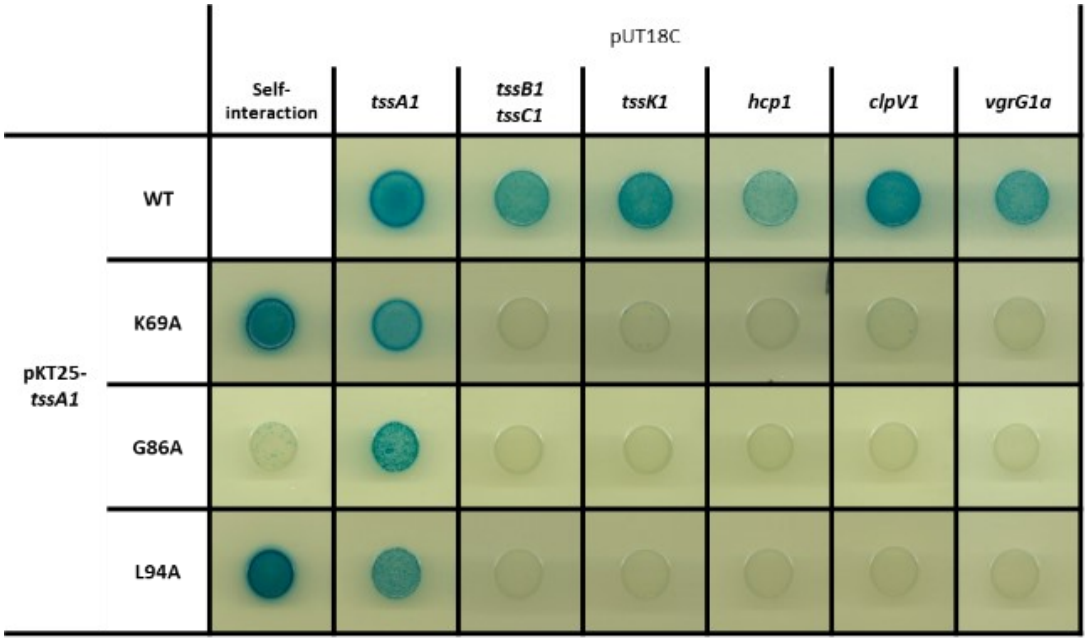


Figure 4.13 Interactions of TssA1 Nt1 domain mutants with known H1-T6SS partners. BTH with N-terminal T25 (pKT25) linked TssA1 mutants and N-terminal T18 (pUT18C) linked H1-T6SS partners produced in DHM1 cells. Representative spots imaged after 24 hours growth on X-Gal LB agar are shown. Blue spots indicate protein-protein interaction, spots are white in the absence of interaction. Data generated with Yu Zhai.

4.4.1.2 Analysis of TssA1 C-terminal domain point mutants

The effect of introducing mutations into the TssA1 C-terminal domain was subsequently assessed. Residues L286, L289 and L309 were identified in the initial BTH mutant library screen. L289 was also identified as highly conserved, with L286 and L309 frequently conserved, within TssA sequences (509). The position of these residues in the TssA1 C-terminal domain primary sequence and predicted tertiary structure is shown in Figures 4.14A and B. These residues were substituted into alanine and their interactions with known TssA1 partners were assessed.

Upon mutation of each residue to alanine, the TssA1 point mutants were all able to associate with wildtype TssA1, suggesting that a folded protein is formed in all cases (Figure 4.14C). Mutation of L286A had no effect on binding to any of the known partners, possibly because it is not highly conserved. It should be noted that the initial BTH mutant library screen recorded this mutation only in combination with another mutation (Table 4.1), and the substitution identified in the screen was for a proline residue rather than an alanine substitution, which would be expected to introduce more

significant structural changes. The functionality of the L286A variant was further tested in an interbacterial competition assay, and the outcome was equivalent to a wildtype TssA1 protein, though this was only performed with two replicates (Yu Zhai, unpublished).

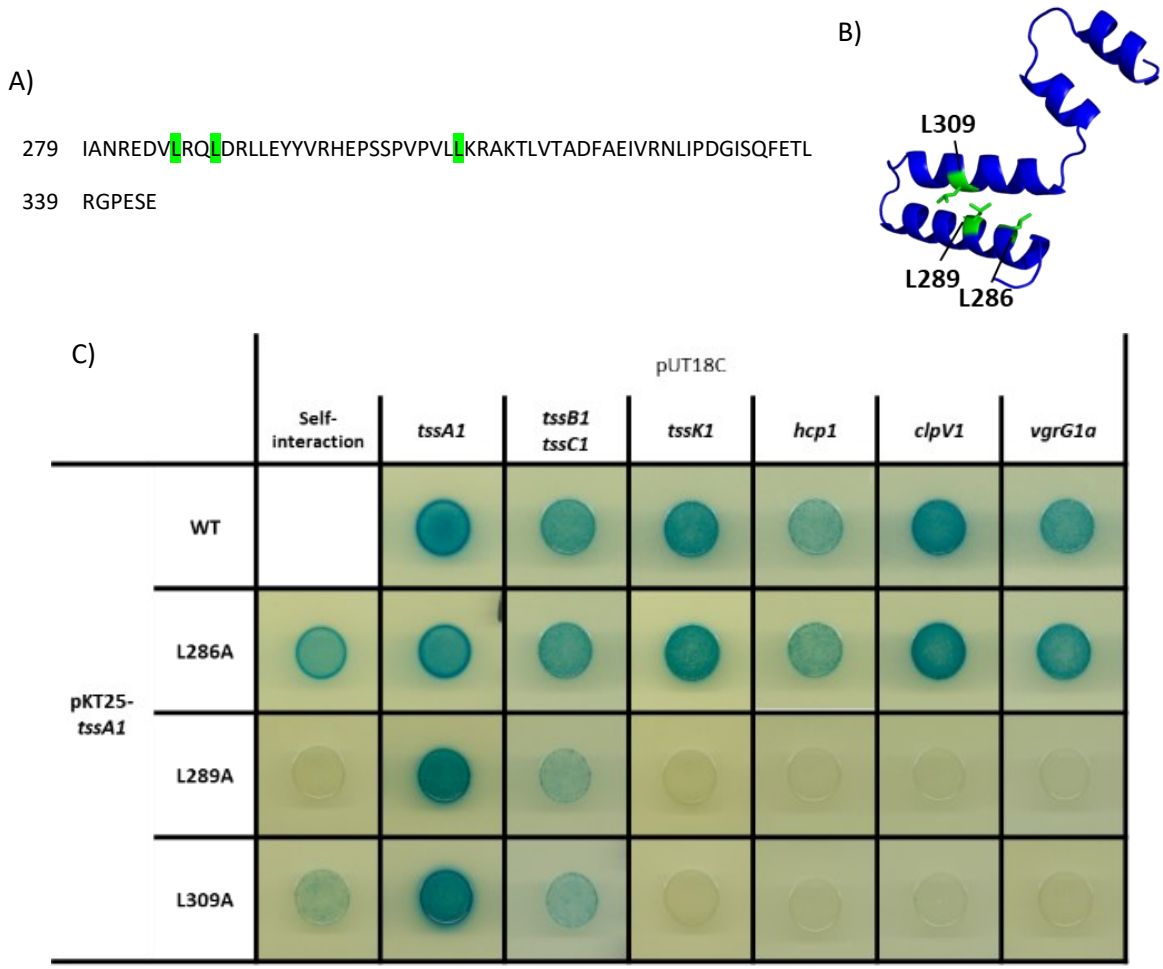


Figure 4.14 Interactions of TssA1 C-terminal domain mutants with known H1-T6SS partners. A) Position of L286, L289 and L309 (green) in the TssA1 C-terminal domain sequence. B) Position of L286, L289 and L309 (green) in a predicted model of the TssA1 C-terminal domain structure. C) BTH with N-terminal T25 (pKT25) linked TssA1 mutants and N-terminal T18 (pUT18C) linked H1-T6SS partners produced in DHM1 cells. Representative spots imaged after 24 hours growth on X-Gal LB agar are shown. Blue spots indicate protein-protein interaction, spots are white in the absence of interaction. Data generated with Yu Zhai.

For the other two mutants tested here, the results were more pronounced. In particular, the L309A mutant was only very weakly able to self-interact, while the L289A mutant was unable to self-interact (Figure 4.14C). Furthermore, both L289A and L309A mutants retained a weak association with the sheath but were unable to bind the other known TssA1 partners, i.e. TssK1, Hcp1, ClpV1 and VgrG1a.

It is interesting here that TssA contacts with the sheath were not abrogated with these mutations, suggesting that the C-terminus may not be crucial for binding the sheath. This supports previous data identifying that N-terminal regions of the long TssA^{EC} interact with the sheath (360). On the other hand, interactions with other partners might require an intact C-terminus or the formation of TssA oligomers.

4.4.2 Substitution of TssA1 residues predicted to be involved in oligomerisation have variable effects on interactions

To more specifically probe the oligomerisation of TssA1, residues were selected based on their suggested role in the oligomerisation of the short TssA^{BC} C-terminal domain once this structure was reported (509). As outlined in section 1.4.1.2, an oligomerisation interface of TssA^{BC} monomers involves the α12 and α13 region, where the connecting loop contains the TssA$_S$ conserved EPxxP motif (509). It is predicted that a salt bridge formed between the glutamic acid residue of this motif and an arginine residue of another monomer is involved in stabilising the stacking of two monomers (Figure 4.15) (509). To probe whether the equivalent TssA1 residues, R282 and E300 (Figures 4.16A and B), might stabilise a stacking interaction, these residues were substituted into alanine and their interactions with known partners tested.



Figure 4.15 Oligomerisation interface of TssA^{BC}. The predicted salt bridge between E324 of one TssA^{BC} C-terminal domain (PDB: 6HS6) monomer (green) and R306 of another monomer (light blue) involved in a stacking interaction.

Mutation of R282A had no effect on the binding to any of the known partners (Figure 4.16C). Upon mutation of E300A, the TssA1 variant was still able to self-interact and interact with wildtype TssA1 and the sheath, but not with other partners. It was unexpected that self-interaction and interaction with wildtype TssA1 were retained. In TssA^{BC}, a further region in α15 also separately contributes to oligomerisation, therefore mutation of these residues may disrupt a single binding interface but may

not be sufficient to prevent self-interaction (509). It was shown that while deletion of α15 prevented ring formation, dimers were still able to form through the α12 and α13 region, the inverse may be true in this case (509).

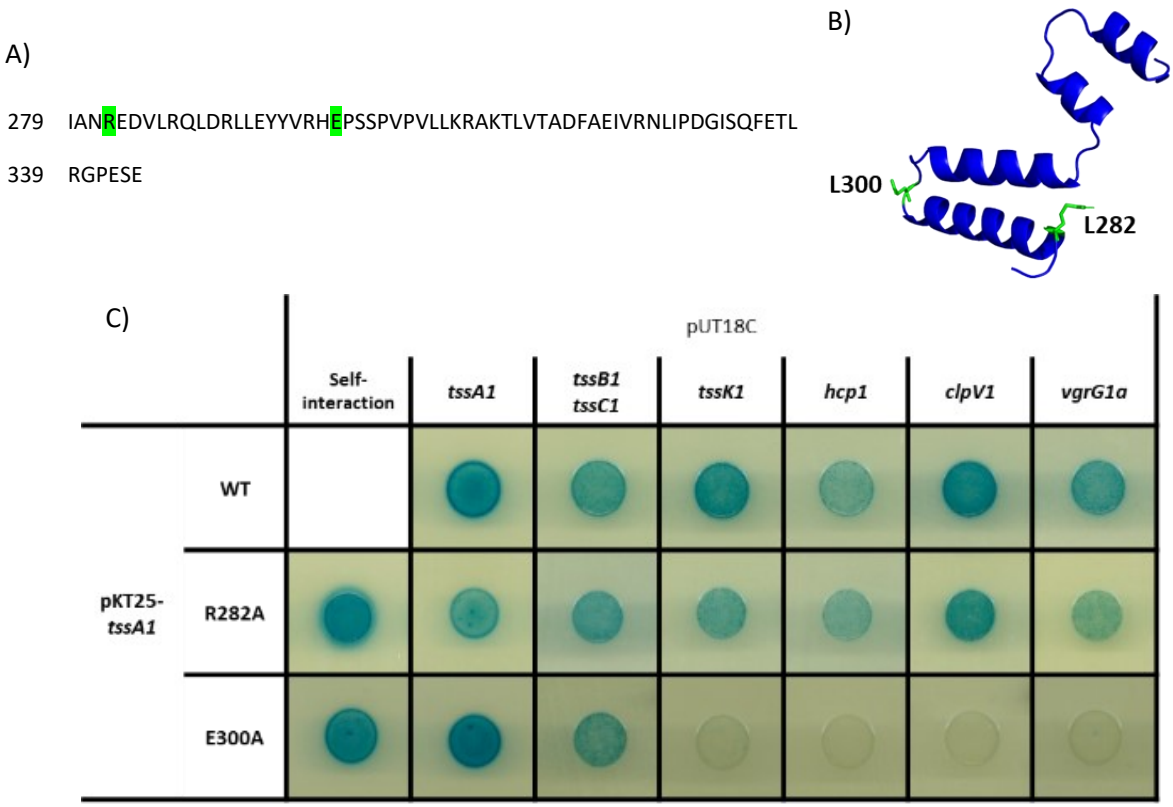


Figure 4.16 Interactions of proposed TssA1 oligomerisation mutants with known H1-T6SS partners. A) Position of R282 and E300 (green) in the TssA1 C-terminal domain sequence. B) Position of R282 and E300 (green) in a predicted model of the TssA1 C-terminal domain structure. C) BTH with N-terminal T15 (pKT25) linked TssA1 mutants and N-terminal T18 (pUT18C) linked H1-T6SS partners produced in DHM1 cells. Representative spots imaged after 24 hours growth on X-Gal LB agar are shown. Blue spots indicate protein-protein interaction, spots are white in the absence of interaction. Data generated with Yu Zhai.

For the E300A variant, as in the case for L289A and L309A variants, interaction with the sheath was maintained while other interactions were lost (Figures 4.14C and 4.16C). Loss of these interactions may be due to failure of these variants to oligomerise into higher order structures. While individual TssA1 variants may be able to self-interact, this interaction may not lead to formation of native TssA complexes if certain interaction interfaces are disrupted.

4.4.3 Analysis of TssA1 point mutant interactions

Interestingly, when TssA1 point mutants were screened for interactions with known partners, interactions of mutants with TssK1, Hcp1, ClpV1 and VgrG1a were all lost concurrently, with all Nt1 domain mutants and some C-terminal domain mutants (L289A, L309A and E300A). It is not clear why this happened and with such a range of diverse mutations.

The structural models generated for the TssA1 Nt1 and C-terminal domains were analysed to estimate solvent accessible surface area (534). The selected residues mutated in the TssA1 Nt1 domain (Figure 4.17A) and C-terminal domain (Figure 4.17B), highlighted in red, were generally predicted to be buried within the structures (solvent exposure <80 %) as opposed to solvent accessible (solvent exposure >80 %). It may be that these conserved residues are important for protein folding rather than for interaction with specific partners. Mutating residues that affect protein folding may explain why in many cases mutants were unable to interact with multiple partners.

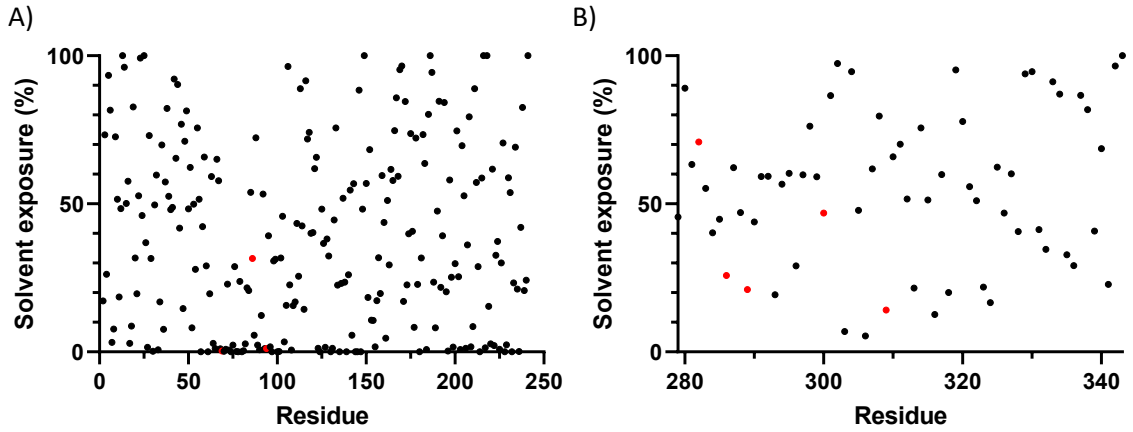


Figure 4.17 Solvent accessibility of TssA1 Nt1 and C-terminal domain residues. Using GetArea, the solvent accessible surface area of TssA1 domain structural models were estimated. The solvent exposure gives the likelihood of a residue being accessible to the solvent. A) Solvent accessibility of TssA1 Nt1 domain residues. The residues mutated here (K69, G86 and L94) are highlighted in red. B) Solvent accessibility of TssA1 C-terminal domain residues. The residues mutated here (R282, L286, L289, E300 and L309) are highlighted in red.

4.5 Splitting TssA proteins into domains to assess interaction with cognate T6SS components

Introducing point mutations to TssA1 conserved residues not provide much insight into the molecular details of interactions with identified partners. As an alternative strategy the interactions of individual domains of TssA proteins with identified partners was assessed using BTH. Long and short TssA proteins share a conserved sequence in their Nt1 domains, but have distinct C-terminal domains, and long TssAs have an additional intervening Nt2 domain (see section 1.4.1) (Figure 4.18). It was thus of particular interest to understand whether and how the varying domain organisation of long and short TssA proteins might influence interactions.

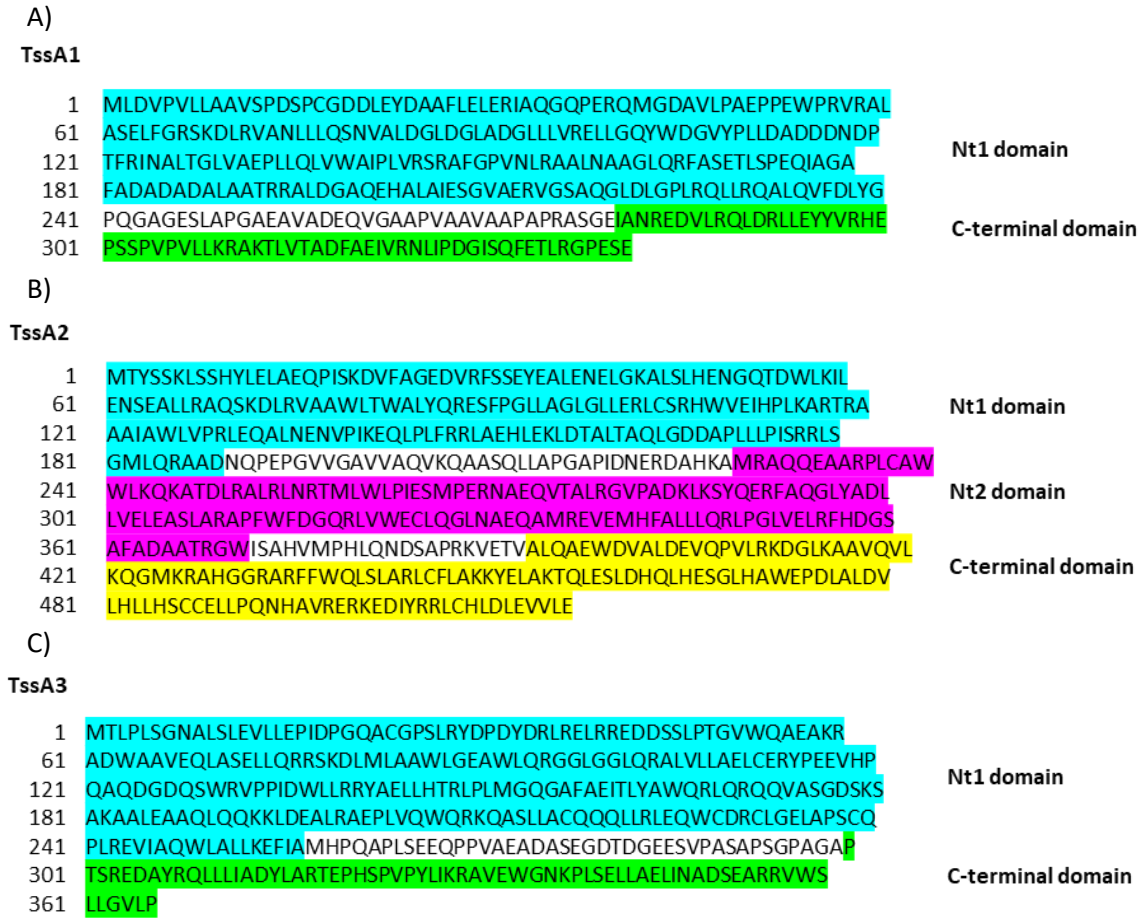


Figure 4.18 Domain organisation of *P. aeruginosa* TssA proteins. A) Annotation of the Nt1 (light blue) and C-terminal domain (green) in the TssA1 primary sequence. B) Annotation of the Nt1 (light blue), Nt2 (purple) and C-terminal domain (yellow) in the TssA2 primary sequence. A) Annotation of the Nt1 (light blue) and C-terminal domain (green) in the TssA3 primary sequence.

Some interactions of TssA sub-domains have previously been studied (360,509,512). This has for example identified that an N-terminal region of the long TssA^{EC}, comprising both Nt1 and Nt2 domains

binds sheath components and TssE (Figure 4.19A) (360). Furthermore, both the long TssA^{EC} and the short TssA^{BC} associate with Hcp and VgrG via their C-terminal domains (Figure 4.19), while the long TssA^{VC} interacts with VgrG via both N- and C-terminal domains (360,509,512). The TssA^{BC} C-terminal domain has also been shown to interact with TssF (509). To date, using *P. aeruginosa* TssA proteins, only the C-terminal domain-dependent formation of higher order TssA1 oligomers has been identified (376). The role of TssA C-terminal domains in oligomerisation is also supported with structural data (360,377,509).

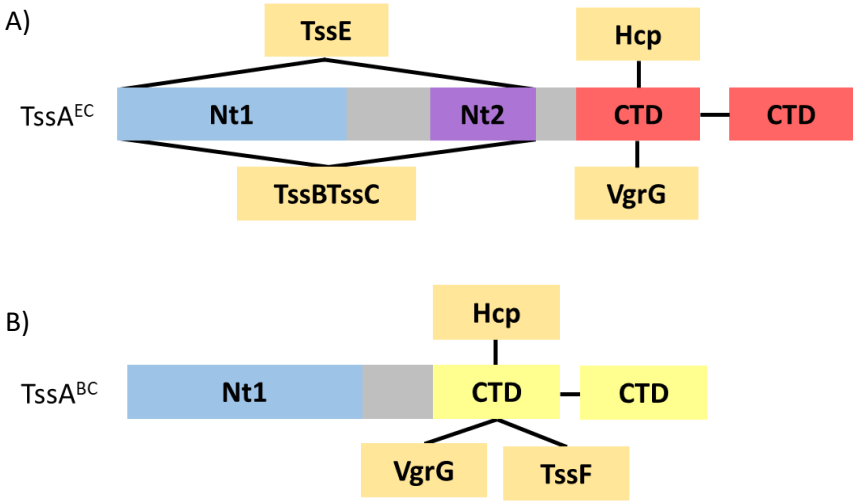


Figure 4.19 Protein-protein interaction network of TssA^{EC} and TssA^{BC} domains. A) Protein-protein interaction network of TssA^{EC} domains. B) Protein-protein interaction network of TssA^{BC} domains.

As the interactions and roles of *P. aeruginosa* TssA protein domains had not been previously studied, a comprehensive screen of TssA domain interactions with known partners was carried out.

4.5.1 TssA Nt1 domains interact with their respective sheath components

Interaction of each TssA Nt1 domain was assessed with partners identified in section 4.3. Each Nt1 domain was identified as interacting with their respective sheath components (Figure 4.20). The Nt1 domains of the short TssA1 and TssA3 were able to interact with the cognate full length TssA but the Nt1 domains in isolation did not self-interact (Figures 4.20A and C). The TssA2 Nt1 domain did not interact with full length TssA2 (Figure 4.20B). This difference may be due to TssA2 being a TssA$_L$ while the other two are TssA$_S$ proteins.

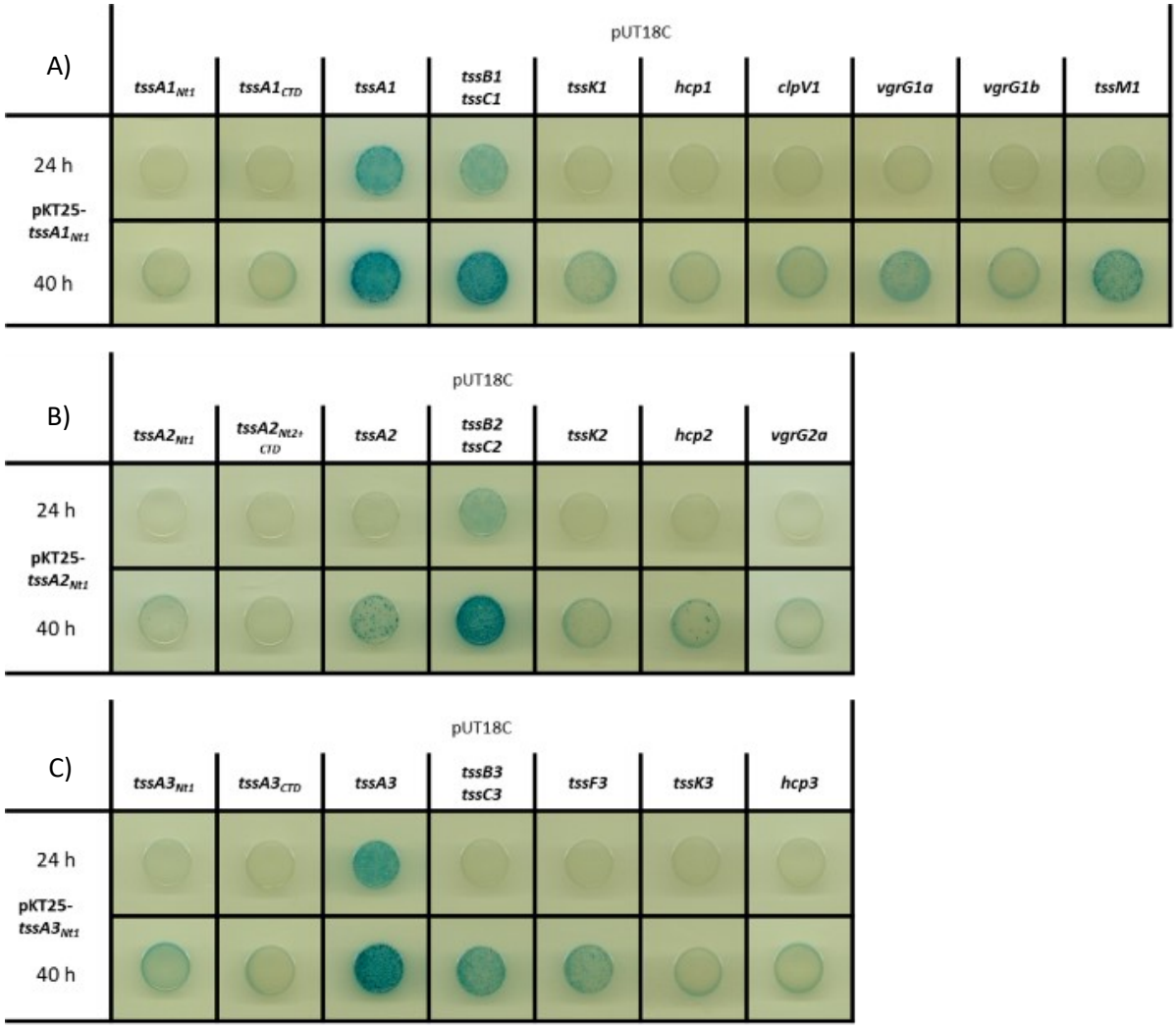


Figure 4.20 Interactions of *P. aeruginosa* TssA Nt1 domains with known T6SS partners and TssA domains. BTH with N-terminal T25 (pKT25) linked TssA Nt1 domains and N-terminal T18 (pUT18C) linked T6SS partners and TssA domains produced in DHM1 cells. Representative spots imaged after 24 and 40 hours growth on X-Gal LB agar are shown. Blue spots indicate protein-protein interaction, spots are white in the absence of interaction. A) Interactions of TssA1 Nt1 domain with TssA1 partners. B) Interactions of TssA2 Nt1 domain with TssA2 partners. C) Interactions of TssA3 Nt1 domain with TssA3 partners.

Other weaker interactions could be detected with the Nt1 domains, but these were also not conserved across the different TssA proteins. For example, specific to TssA1 Nt1 domain, additional weak interactions with TssM1 and VgrG1a were detected, while the TssA3 Nt1 domain interacted with TssF3 after 40 hours of incubation (Figures 4.20A and C). The significance of these non-conserved interactions cannot conclusively be determined at this stage.

The characterisation of the association between these Nt1 domains and their respective sheath components is a key finding (Figure 4.20). It has previously been identified for the long $TssA^{EC}$ that the N-terminal region comprising Nt1 and Nt2 domains interacts with the sheath (Figure 4.19) (360). This has been modelled as the docking of Nt2 domains to the distal end of the sheath (360,377), but this has not been experimentally demonstrated, and would not explain how $TssA_S$ proteins lacking an Nt2 would interact with the sheath as demonstrated here (Figure 4.5). In constrast, the data presented here suggest that the conserved Nt1 domain is responsible for interaction with the sheath, which for the first time demonstrates how both long and short TssA proteins interact with the sheath through a similar mechanism.

4.5.2 TssA C-terminal domains self-interact

In contrast to the conserved Nt1 domains, the C-terminal regions of TssA proteins are much more variable (509). Slightly different constructs were therefore engineered for the long TssA2 and the short TssA1 and TssA3. The C-terminal domains of the short TssA proteins, TssA1 and TssA3, were engineered with N-terminal T25 tags. In previous structural work on the long $TssA^{EC}$, $TssA^{AH}$ and $TssA^{VC}$, fragments comprising Nt2 and C-terminal domains could be stably purified and structures solved, while the flexibility of the Nt1 domain relative to this structure always prevented the relative position of this domain being determined (360,377,509). This suggested that the Nt2 domain is more closely associated with the C-terminal domain, therefore a TssA2 C-terminal region of the combined Nt2 and C-terminal domains was engineered with a N-terminal T25 tag.

Using the bacterial two hybrid spotting assay, interaction of each TssA C-terminal region was assessed with partners identified in section 4.3. In brief, each C-terminal region was able to self-interact and interact with the cognate full length TssA (Figure 4.21). Weaker interaction of the TssA1 C-terminal domain with ClpV1 and VgrG1a could be identified after 40 hours of incubation (Figure 4.21A). Weak interaction of the TssA2 C-terminal region with TssK2 could be identified after 40 hours of incubation (Figure 4.21B). The significance of these weaker interactions is yet to be confirmed.

As anticipated, the self-interaction of the TssA C-terminal regions observed here is consistent with previously reported literature on the role of these C-terminal domains in oligomerisation (see section 1.4.1) (360,376,377,509).

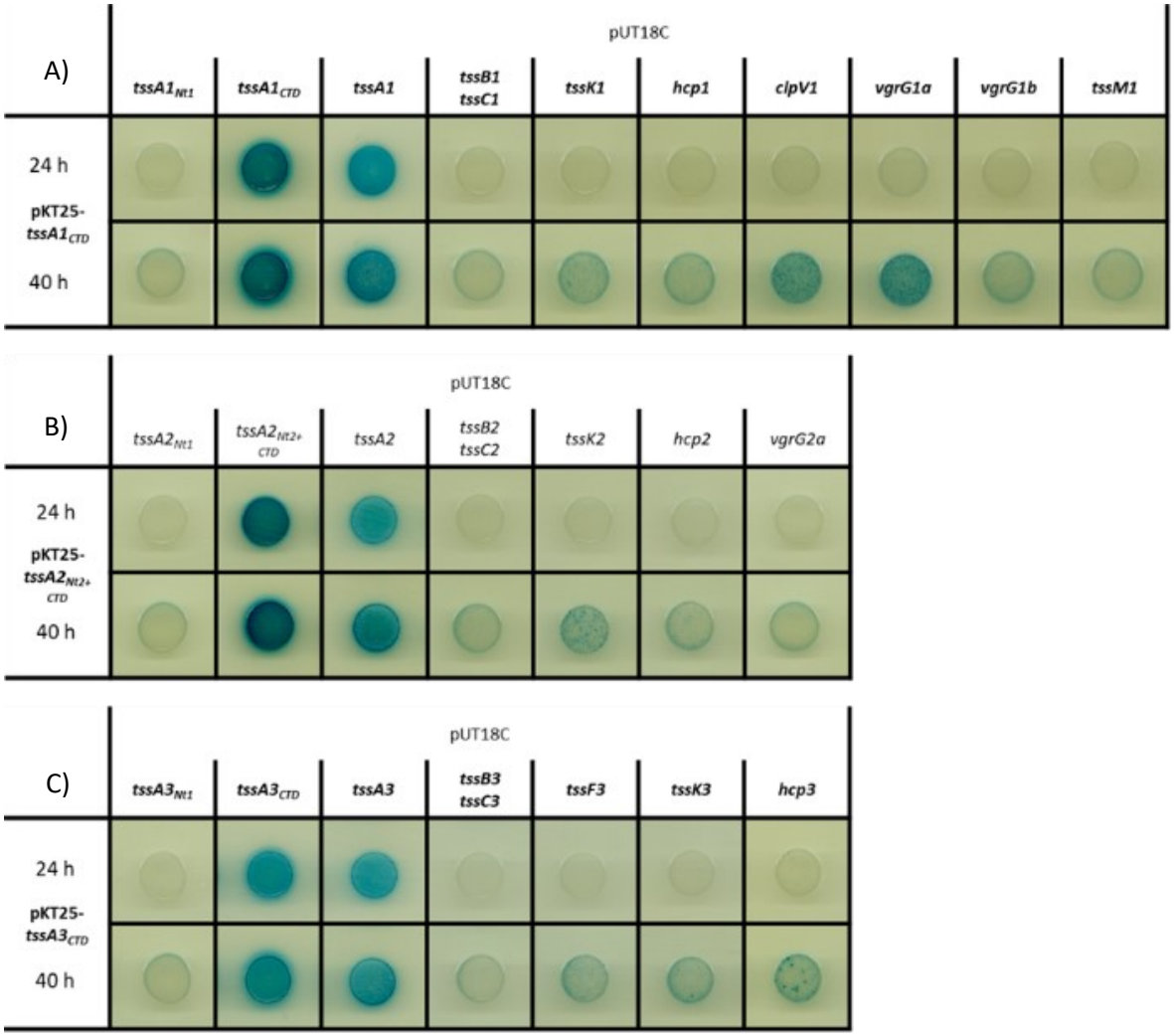


Figure 4.21 Interactions of *P. aeruginosa* TssA C-terminal domains with known T6SS partners and TssA domains. BTH with N-terminal T25 (pKT25) linked TssA C-terminal domains (CTDs) and N-terminal T18 (pUT18C) linked T6SS partners and TssA domains produced in DHM1 cells. Representative spots imaged after 24 and 40 hours growth on X-Gal LB agar are shown. Blue spots indicate protein-protein interaction, spots are white in the absence of interaction. A) Interactions of TssA1 C-terminal domain with TssA1 partners. B) Interactions of TssA2 C-terminal domain with TssA2 partners. C) Interactions of TssA3 C-terminal domain with TssA3 partners.

In conclusion, for all three *P. aeruginosa* TssA proteins the Nt1 domain is involved in interaction with the respective sheath proteins, while the C-terminal region contributes to oligomerisation. This is true for both long and short TssA proteins, suggesting that despite their differences these core interactions are similar. Some other weaker interactions were identified for specific TssA domains but would need to be confirmed. Components of the T6SS that can interact with the full-length TssA protein but not with sub-domains may interact with multiple regions of TssA proteins or require oligomerisation to form multiple stabilising contacts. Alternatively, the positioning of the BTH tags at the N-terminus of

individual domains may not be optimal for identifying all interactions, for example a tag at the N-terminus of the TssA2 Nt2 domain may not be optimally positioned to reconstitute with a protein interacting with the C-terminal domain.

4.5.3 A TssA2 protein lacking the C-terminal domain is not functional

TssA C-terminal domains have been identified here (Figure 4.21), and previously in the literature (360,376,377,509), as required for TssA oligomerisation, thus, it would be expected that this domain is essential for TssA function. However, it has previously been reported that a long $TssA^{EC}$ lacking the C-terminal domain is able to complement the deletion of the full-length protein and restore sheath formation in this background (537). This is remarkable given that TssA rings would not be expected to properly oligomerise in the absence of these C-terminal domains. Regardless, the sheaths formed in this background did not resemble wildtype sheaths, with sheath extension either not terminating upon reaching the opposite side of the cell and extending sheaths sliding along the membrane, or sheaths contracting rapidly after assembly rather than remaining assembled for a long period of time, as is characteristic of systems encoding a $TssA_L$ (508,537). To assess the functionality of the long TssA2 in the absence of its C-terminal domain, a chromosomal truncation was engineered to remove the C-terminal domain.

The secretion of the inner tube protein Hcp2 was lost upon chromosomal truncation removing the corresponding TssA2 C-terminal domain, although Hcp2 was still produced (Figure 4.22A). Similarly, in an interbacterial competition assay, the killing of the prey *E. coli* was significantly reduced upon deletion of *tssA2* or, and at a comparable level, upon truncation to remove the corresponding TssA2 C-terminal domain (Figure 4.22B). This data indicates that the TssA2 C-terminal domain is required for TssA2 functionality. Remarkably, introduction of full length TssA2 on a plasmid in this background did not restore either secretion or prey killing, suggesting that the remaining N-terminal regions of the truncated protein may interact with the H2-T6SS in a way that interferes with the activity of the wildtype protein, for example by competing for binding partners.

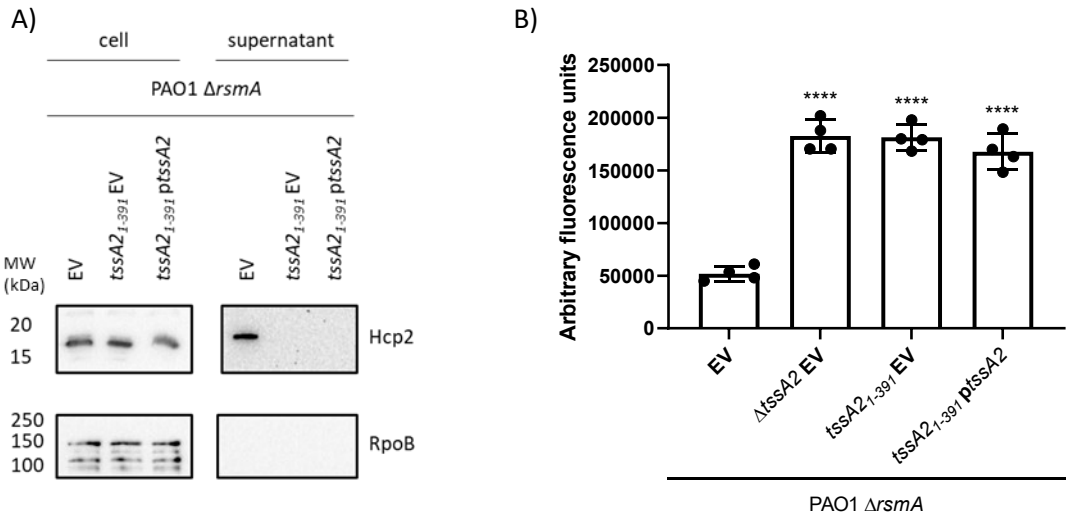


Figure 4.22 Functionality of TssA2 lacking the C-terminal domain. To assess complementation of the TssA2 truncation, the pBBR1MCS4 vector was introduced either as empty vector (EV) or encoding *tssA2* (p*tssA2*). A) Western blot of a H2-T6SS secretion assay, to assess the levels of secretion marker Hcp2 in the supernatant sample. Cell and supernatant samples were harvested after 18 hours growth at 25 °C. Proteins detected in the western blot are indicated to the right. MW markers (left) are in kDa. RpoB was used as a loading and bacterial lysis control. B) H2-T6SS competition assay to assess the T6SS-dependent killing of a GFP-encoding *E. coli* prey by *P. aeruginosa* attacker strains. Attacker *P. aeruginosa* and prey *E. coli* were mixed and incubated at 25 °C for 24 hours before GFP signal quantification. Values are presented as means and error bars represent the standard deviation. Statistical testing was conducted by one-way ANOVA with Dunnett's multiple comparisons test, each strain was compared to parental PAO1Δ*rsmA*Δ*rsmN* EV (ns = not significant, **** $p < 0.0001$). (n=4).

These data differ somewhat from what was found upon removal of the TssA^{EC} C-terminal domain, although different assays were used (537). Firstly, the previous work with TssA^{EC} involved the complementation of a *tssA* deletion with a truncated TssA^{EC}, while this work involved chromosomal truncation which may have had some downstream effects on T6SS expression. Furthermore, previous work assessed the assembly and dynamics of sheath structures, while this assay assessed the functionality of the H2-T6SS in secretion and competition assays. Contraction of assembled sheaths could be observed in the previous work, which indicates that the sheaths formed should be capable of delivering effectors into prey. However, sheaths did not behave entirely like wildtype sheaths and their degree of functionality is unknown. It is unclear why there seems to be a difference between the results obtained with TssA^{EC} C-terminal domain and TssA2 C-terminal domains. One difference between these two T6SSs is the presence of a TagA accessory protein encoded in the *E. coli* T6SS

cluster, that is absent from the H2-T6SS cluster. Genes encoding TagA proteins are often found in T6SS clusters which are associated with genes encoding $TssA_L$ proteins (see section 1.4.3.1). TagA proteins share N-terminal sequence similarity with TssA proteins and associate through C-terminal regions with the cytoplasmic membrane where they bind the distal end of the polymerising sheath (377,510). It has been proposed that TagA may have roles not only in the termination of sheath extension, but also in initiation, which may support the formation of these structures in the presence of a truncated $TssA^{EC}$ (512).

Introduction of the full length TssA2 protein was unable to restore the secretion and killing activities of the H2-T6SS in the presence of a chromosomally encoded C-terminally truncated TssA2 (Figure 4.15). This may be due to a competition for binding partners between these two forms of TssA2. The chromosomally encoded truncated form could benefit from co-translation with the other H2-T6SS components and therefore interact with these nearby proteins before the plasmid encoded wildtype protein. Binding of this truncated TssA2 to sheath subunits via its Nt1 domain, or to the T6SS assembly initiation site, could block the binding of wildtype TssA2 and therefore disrupt H2-T6SS activity. Alternatively, the chromosomal truncation could cause downstream effects that disrupt H2-T6SS expression or assembly in a way that prevents activity, even in the presence of the wildtype TssA2. This would be simple to assess with a western blot monitoring the production of downstream components such as TssB2 for which antibodies are available.

4.6 Interactions of TssA proteins with non-cognate T6SS components

The diversity in TssA proteins has raised questions about variations in TssA function and interactions (see section 1.4.2.2). The variations in TssA size and domain organisation contribute to structural differences including in the symmetries and dimensions of the ring-shaped oligomers formed (see section 1.4.1). The oligomerisation of $TssA_S$ C-terminal domains forms a large ring predicted to be made of up to 32 monomers, with an internal 100 Å lumen (Figure 1.19), while the oligomerisation of $TssA_L$ C-terminal domains forms a smaller ring of 10-12 monomers and an external diameter in the region of 100 Å (Figures 1.22 and 1.23) (360,376,377,509).

It might be expected that these differences would have a large impact on the way that different TssA proteins interact with their respective T6SS. However, when assessing their interactions by BTH, each *P. aeruginosa* TssA associated with a similar subset of T6SS components, including self-interaction, interaction with components of the sheath, the inner tube protein Hcp and the baseplate component TssK (see section 4.3) (Figures 4.4, 4.5, 4.6, 4.7, 4.9 and 4.10). By splitting TssA proteins into their domains, it was possible to identify regions contributing to distinct interactions, the most variable region, the C-terminal regions, responsible for self-interaction (Figure 4.21), while the most conserved region, the Nt1 domain, was responsible for interaction with components of the sheath (Figure 4.20).

It would also be expected that these interactions are specific within each T6SS and not promiscuous, for example it has been shown that *E. coli* Hcp and TssB proteins interact specifically with proteins encoded from their cognate T6SS and not across systems (379). Given the observed similarities in the interaction networks of TssA proteins, it was assessed whether any cross-functionality could be observed in *P. aeruginosa* T6SSs.

Owing to the library of *P. aeruginosa* T6SS component BTH constructs generated here, the specificity of the interactions of TssA proteins could be tested, and interactions between non-cognate T6SS components was investigated.

4.6.1 TssA proteins from different *P. aeruginosa* T6SSs cross-interact

The BTH screen with TssA proteins consistently and strongly identified self-interaction (Figure 4.5). Cross-interaction between TssA proteins encoded by each of the three T6SS clusters was therefore tested. In the data reported in previous sections it was confirmed that C-terminal regions, which are distinct between long and short TssA proteins, are responsible for self-interaction (Figure 4.14) and therefore it might not be expected that cross-interactions be observed between these.

However, following 24 hours of incubation, all TssA proteins could be identified as both self- and cross-interacting with each other (Figure 4.23). Intriguingly there also does not seem to be any large differences in the strength of these interactions.

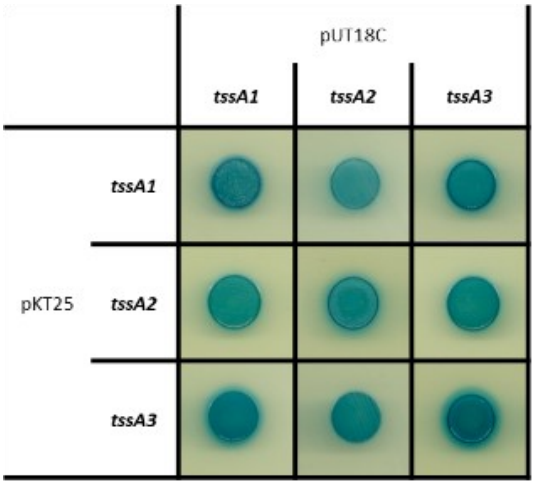


Figure 4.23 Cross-interaction of *P. aeruginosa* TssA proteins. BTH with N-terminal T25 (pKT25) and T18 (pUT18C) linked TssA1, TssA2 and TssA3 produced in DHM1 cells. Representative spots imaged after 24 hours growth on X-Gal LB agar are shown. Blue spots indicate protein-protein interaction, spots are white in the absence of interaction.

The cross interaction of all three TssA proteins was somewhat unexpected, particularly interactions between long and short TssA proteins whose C-terminal regions, are clearly distinct. It is possible that these heterologous interactions might not ultimately result in the formation of higher order mixed ring structures, and whether such a mixed ring structure would have any functionality is also unclear. While a low number of non-cognate subunits could potentially be tolerated within an oligomeric ring structure, it seems more likely that these interactions represent smaller oligomeric units or monomers associating in a way that less closely represents the native ring structure.

The functional significance of these TssA cross interactions is thus unclear. It may be that these interactions are an artefact of the experimental technique, identifying interactions that may not take place under native conditions. It seems unlikely in an optimally functioning T6SS that a heteromeric TssA would be required or beneficial. It has previously been observed that *P. aeruginosa* Hcp proteins encoded in different clusters can also cross-interact in BTH experiments (Tom Snelling, unpublished). However, these heterologous interactions were not subsequently identified in pulldown assays performed under native conditions in *P. aeruginosa*, although conditions were used to optimally express each T6SS independently which may limit co-expression of different T6SSs (412). To study these systems under laboratory conditions, growth at specific temperatures and incubation times is required for optimal expression and activity of each T6SS (see section 1.3.5.5), the expression of the

different T6SS clusters is therefore independently regulated, which may minimise the simultaneous expression of components from different clusters. Despite this it cannot be ruled out that there could be some crosstalk between T6SSs, and the concurrent presence of multiple different T6SSs has been observed in fluorescence microscopy experiments (Marta Rudzite, unpublished).

One thing these heterologous interactions indicate is a slightly higher level of interaction promiscuity than might have been expected between such different components. This raises questions about the specificity of TssA proteins within their T6SSs, and whether they can influence activity of non-cognate T6SSs. These will be addressed at a later point.

4.6.2 TssA proteins interact with components from non-cognate *P. aeruginosa* T6SSs

To test whether non-cognate interactions extended beyond just interactions between different TssA proteins (Figure 4.23), interactions between the TssA proteins and components of other, non-cognate T6SSs were studied.

The interactions of the three distinct TssA proteins with H1-T6SS partners were probed. Following 24 hours of incubation, some weak signal involving non-cognate interactions between TssK1 and TssA3, or ClpV1 with TssA2 and TssA3 was identified (Figure 4.24Ai). Non-cognate interactions were also detectable for components of the H2-T6SS, and surprisingly TssA1 appeared to interact more strongly with some H2-T6SS components than TssA2, including the sheath components, the baseplate component TssK2 and the inner tube protein Hcp2, while TssA3 was also able to interact with TssK2 (Figure 4.24Aii). For interactions with H3-T6SS components, as previously observed, cognate interactions with TssA3 were not present at 24 hours, but again TssA1 could interact with TssK3 and Hcp3, which represented a stronger interaction than that with the cognate TssA3 (Figure 4.17Aiii).

Overall, for various components of each T6SS there were non-cognate interactions involving TssA proteins after 24 hours of incubation. It is worth noting the promiscuity of TssA1, interacting with most components independent of their T6SS origin. By 40 hours of incubation, there were non-cognate interactions with almost all the partners screened (Figure 4.17B).

The identification of these non-cognate interactions between components from different T6SSs challenges the current understanding of specificity within each T6SS. The extent of these non-cognate interactions was unexpected, particularly given the diversity of TssA proteins. Furthermore, some components were able to interact more strongly with a non-cognate TssA than their cognate protein. As with the heterologous interactions between TssA proteins (Figure 4.23), it is unclear the extent to which these interactions may play a role in a native environment, whether they are due to the non-

native conditions involved, and whether they would result in the assembly of a functional T6SS machinery.

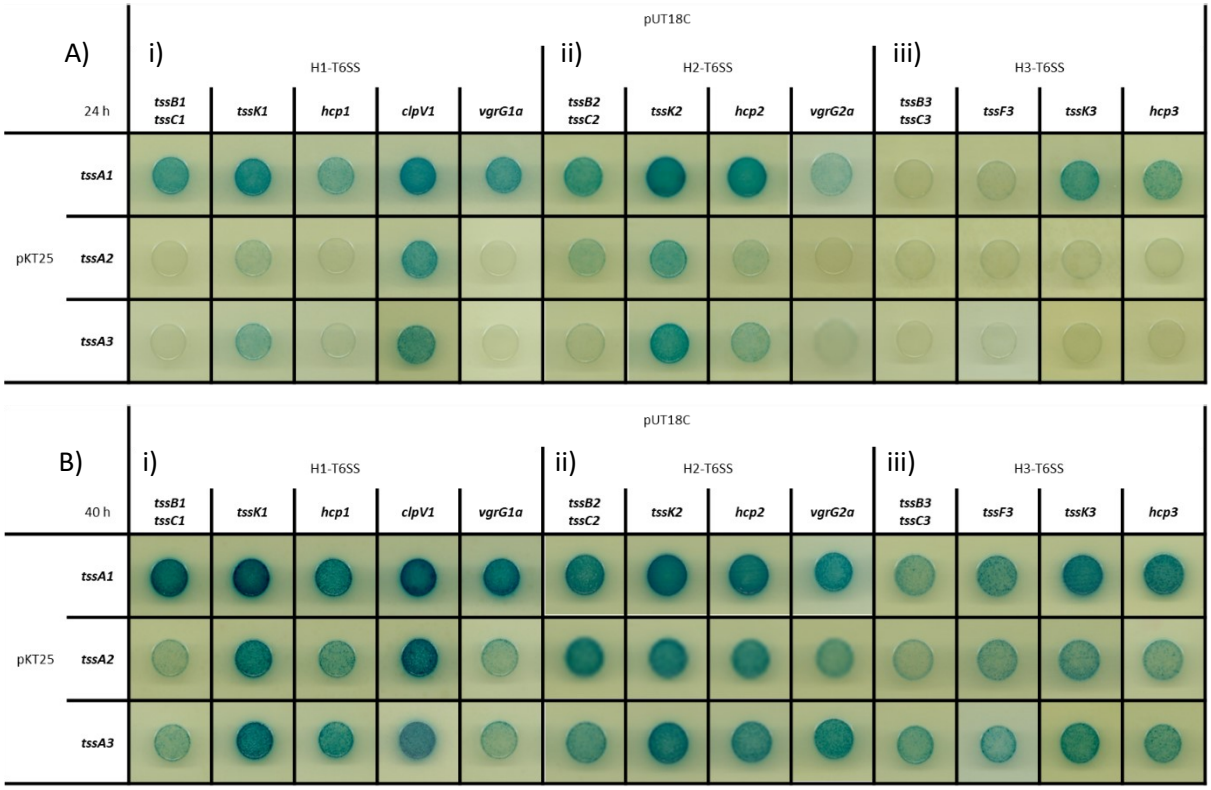


Figure 4.24 Interaction of TssA proteins with previously identified TssA partners. BTH with N-terminal T25 (pKT25) linked TssA1, TssA2 and TssA3 and N-terminalT18 (pUT18C) linked H1-, H2- and H3-T6SS interaction produced in DHM1 cells. Representative spots imaged after 24 (A) and 40 (B) hours growth on X-Gal LB agar are shown. Blue spots indicate protein-protein interaction, spots are white in the absence of interaction. A) i) Interactions of TssA proteins with TssA1 partners after 24 hours of incubation. ii) Interactions of TssA proteins with TssA2 partners after 24 hours of incubation. iii) Interactions of TssA proteins with TssA3 partners after 24 hours of incubation. B) i) Interactions of TssA proteins with TssA1 partners after 40 hours of incubation. ii) Interactions of TssA proteins with TssA2 partners after 40 hours of incubation. iii) Interactions of TssA proteins with TssA3 partners after 40 hours of incubation.

4.6.3 Heterologous complementation of *tssA* deletion is not observed

The identification of non-cognate interactions between TssA proteins and components encoded in different T6SS clusters raised questions about whether a TssA protein could be functionally inserted into a non-cognate T6SS. To assess the functional specificity of TssA proteins, the assays optimised in Chapter 3 were used to probe T6SS activity.

The activity of the H1-T6SS secretion system was found to be exclusively dependent on the presence of *tssA1*. Hcp1 secretion or prey killing were only possible in the presence either of chromosomal *tssA1* or with a *tssA1* mutant complemented by *tssA1* expressed from a plasmid *in trans* (Figure 4.25). Neither *tssA2* nor *tssA3* expression from a plasmid could restore these H1-T6SS secretion or killing phenotypes.

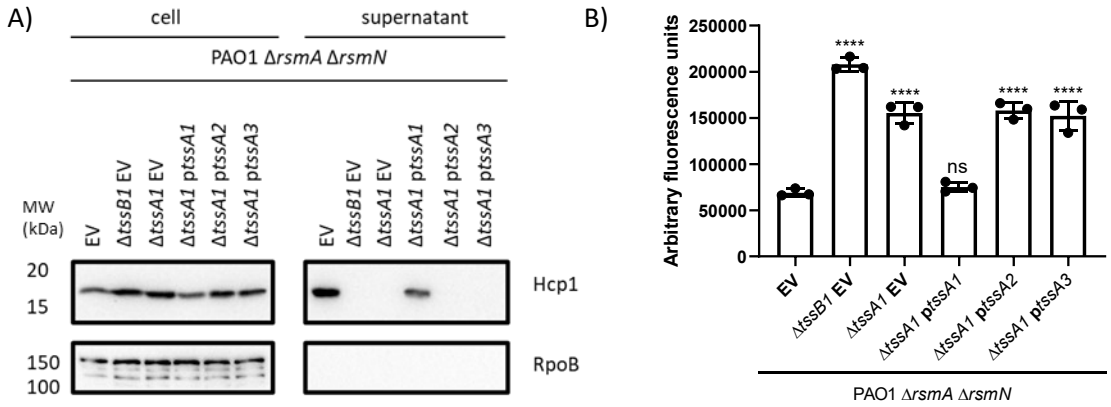


Figure 4.25 Assessment of heterologous complementation of H1-T6SS activity by TssA2 and TssA3. To assess complementation of the *tssA1* deletion, the pBBR1MCS4 vector was introduced either as empty vector (EV) or encoding *tssA1, tssA2* or *tssA3* (p*tssA1/2/3*). A) Western blot of a H1-T6SS secretion assay to assess the levels of the secretion marker Hcp1 in the supernatant sample. Cell and supernatant samples were harvested after 5-7 hours growth at 37 °C. Proteins detected in the western blot are indicated to the right. MW markers (left) are in kDa. RpoB was used as a loading and bacterial lysis control. B) H1-T6SS competition assay to assess the T6SS-dependent killing of a GFP-encoding *E. coli* prey by *P. aeruginosa* attacker strains. Attacker *P. aeruginosa* and prey *E. coli* were mixed and incubated at 37 °C for 24 hours, before quantification of GFP signal. Values are presented as means and error bars represent the standard deviation. Statistical testing was conducted by one-way ANOVA with Dunnett's multiple comparisons test, each strain was compared to parental EV strains (ns = not significant, **** $p < 0.0001$). (n=3).

The non-cognate interactions of TssA proteins with H1-T6SS components did not translate into a functional heterologous complementation of *tssA1* deletion (Figure 4.25). This may be because only a subset of H1-T6SS components, i.e. TssK1 and ClpV1, were able to efficiently interact with TssA2 and TssA3 (Figures 4.24Ai and Bi). However, all H2-T6SS components that interact with TssA2 were also able to interact with TssA1 and TssA3, with some interactions even stronger with a non-cognate TssA than TssA2 (Figures 4.24Aii and Bii). The ability of TssA1 and TssA3 to complement the deletion of *tssA2* was therefore studied by assessing the activity of the H2-T6SS.

The H2-T6SS-dependent secretion of Hcp2 was abrogated in the *tssA2* background but could be specifically complemented by the constitutive expression of *tssA2 fr*om a plasmid, while neither the expression of *tssA1* or *tssA3* could complement the *tssA2* deletion (Figure 4.26A). Similar was observed in the interbacterial competition assay, where killing of the prey strain was exclusively dependent on the presence of *tssA2*, and not restored *in trans* by the expression of *tssA1* or *tssA3* (Figure 4.26B). There was therefore no heterologous complementation of *tssA2* deletion despite TssA1 and TssA3 interacting with all previously identified H2-T6SS partners (Figures 4.24Aii and 4.26).

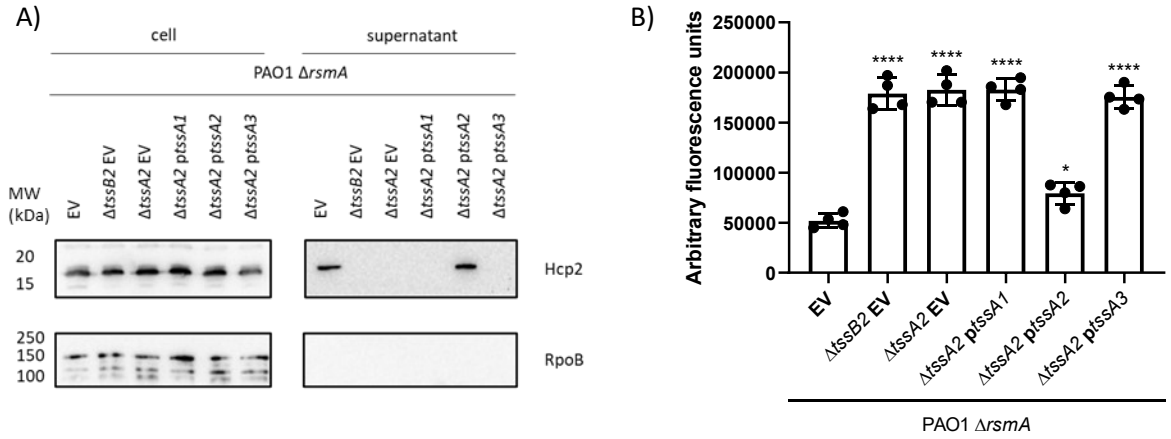


Figure 4.26 Assessment of heterologous complementation of H2-T6SS activity by TssA1 and TssA3. To assess complementation of the *tssA2* deletion, the pBBR1MCS4 vector was introduced either as empty vector (EV) or encoding *tssA1, tssA2* or *tssA3* (p*tssA1/2/3*). A) Western blot of a H2-T6SS secretion assay to assess the levels of the secretion marker Hcp2 in the supernatant sample. Cell and supernatant samples were harvested after 18 hours growth at 25 °C. Proteins detected in the western blot are indicated to the right. MW markers (left) are in kDa. RpoB was used as a loading and bacterial lysis control. B) H2-T6SS competition assay to assess the T6SS-dependent killing of a GFP-encoding *E. coli* prey by *P. aeruginosa* attacker strains. Attacker *P. aeruginosa* and prey *E. coli* were mixed and incubated at 25 °C for 24 hours, before quantification of GFP signal. Values are presented as means and error bars represent the standard deviation. Statistical testing was conducted by one-way ANOVA with Dunnett's multiple comparisons test, each strain was compared to parental EV strains (ns = not significant, * $p < 0.05$, **** $p < 0.0001$). (n=3).

Finally, the possibility of heterologous complementation was studied using the H3-T6SS. Since there are no functional assays in place to assess H3-T6SS activity, the ability of *tssA1* and *tssA2* to complement the deletion of *tssA3* was studied by assessing sheath and focus formation by a fluorophore tagged TssB3 using fluorescence microscopy. When wildtype *tssA3* was present on the chromosome, 38.9 % of cells formed sheaths or foci, which fell to 0.036 % upon *tssA3* deletion and in the presence of an empty cloning vector (Figure 4.27). The constitutive expression of *tssA1* or *tssA2*

from this vector did not lead to an increase in the abundance of H3-T6SS sheath structures, while expression of *tssA3* restored sheath and focus formation to 27.2 % of cells.

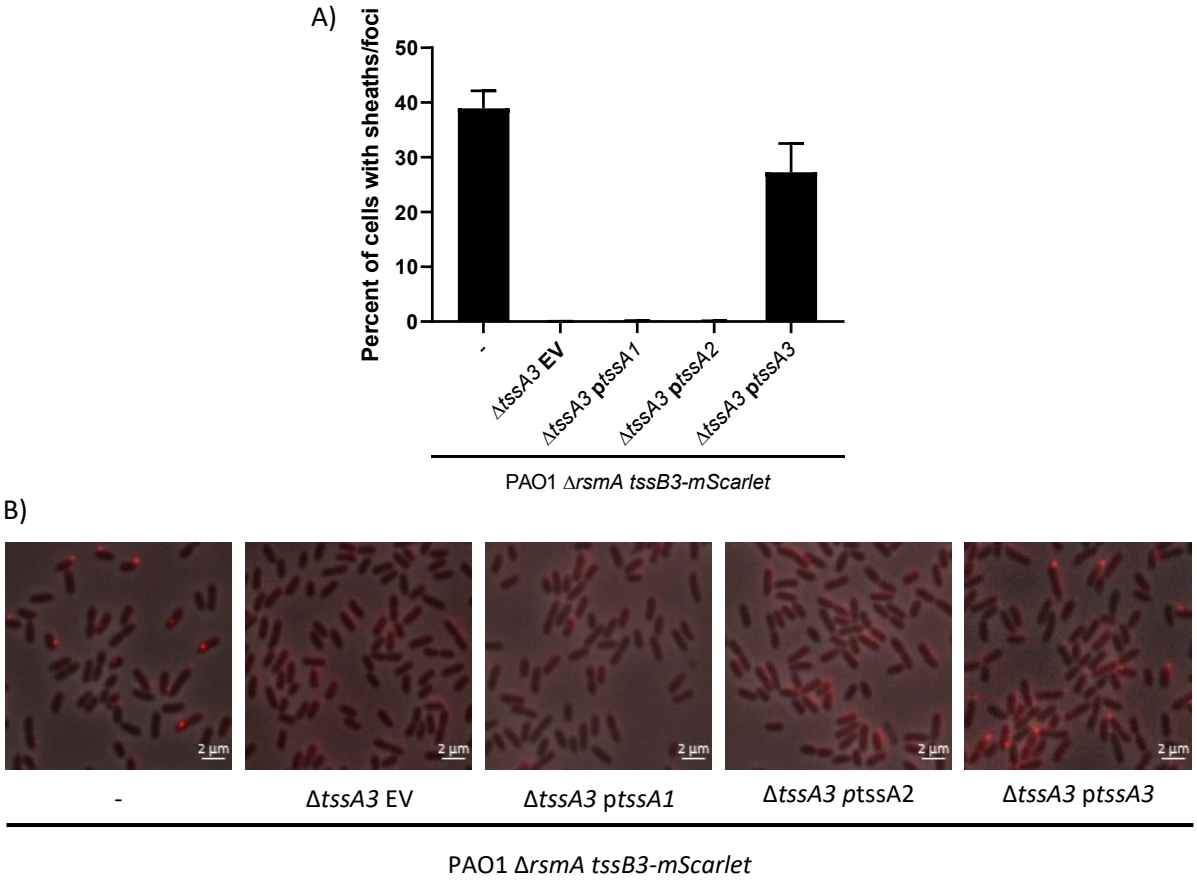


Figure 4.27 Assessment of heterologous complementation of H3-T6SS activity by TssA1 and TssA2. To assess complementation of the tssA3 deletion, the pBBR1MCS4 vector was introduced either as empty vector (EV) or encoding *tssA1*, *tssA2* or *tssA3* (p*tssA1/2/3*). A) Quantification of the percent of cells with TssB3-mScarlet sheaths or foci by fluorescence microscopy. Strains were grown in liquid culture at 25 °C for 13 hours before imaging. In the parental strain, sheaths or foci were formed in 38.9 % of cells (n=10582), upon deletion of *tssA3* with the empty vector present this fell to 0.036 % (n=16822), upon introduction of TssA1 0.14 % of cells formed sheaths or foci (n=11205) and with TssA2 this was 0.082 % (n=8500). Upon introduction of TssA3 27.2 % of cells formed sheaths or foci (n=16253). Data were taken from 2 fields of view for three experiments (n=3). Values are presented as means and error bars represent the standard deviation. B) Representative images of TssB3-mScarlet sheath formation in cells expressing either wildtype *tssA3*, or with *tssA3* deletion and either EV or *tssA1*, *tssA2* or *tssA3* expressed from pBBR1MCS4. Scale bar represents 2 µm.

Therefore, the non-cognate interactions identified for *P. aeruginosa* TssA proteins with components of different T6SSs are insufficient to reconstitute the function of a missing endogenous TssA (Figures 4.24, 4.25, 4.26 and 4.27). This may be because these interactions do not take place under native conditions. Cognate interactions are likely facilitated within the cell by the localised translation of T6SS components from polycistronic mRNAs. However, as *tssA* deletion can be complemented *in trans* by a cognate *tssA*, this is likely not the sole explanation. Alternatively, if interactions between TssA proteins and non-cognate T6SS components do take place under native conditions they may not result in a properly assembled complex and may have regulatory roles, that cannot be captured in these assays.

4.6.4 Non-cognate TssA proteins do not interfere with T6SS activity in the absence of their cognate T6SS cluster

The non-cognate interactions of TssA proteins with T6SS components encoded in different T6SS clusters (Figure 4.24) did not translate into functional heterologous complementation (Figures 4.25, 4.26 and 4.27). However, if these interactions are non-productive, the overproduction of a given TssA may interfere with the functionality of a heterologous T6SS by competing with the cognate TssA.

Therefore a *P. aeruginosa* strain was engineered with chromosomal deletions of both H1- and H3-T6SS clusters in a *rsmA* background where the remaining H2-T6SS was active. In this background, TssA2 is still present and the activity of the H2-T6SS was assessed with the non-cognate *tssA1* or *tssA3* genes overexpressed *in trans* from a plasmid. The overproduction of non-cognate TssA proteins in the absence of their respective partners from the H1- and H3-T6SS might disrupt H2-T6SS activity if non-productive interactions were to occur. In a secretion assay, Hcp2 secretion was unaffected by the overproduction of any of the TssA proteins (Figure 4.28A). Likewise, in an interbacterial competition assay, the level of prey killing by the parental strain was unaffected by overproduction of non-cognate TssA proteins (Figure 4.28B).

In conclusion, the overexpression of *tssA1* and *tssA3* in the absence of H1- and H3-T6SS clusters did not interfere with H2-T6SS function (Figure 4.28). As stated, it might be that the non-cognate interactions are minimal in the cellular context, or that they have a subtle role that cannot be monitored in these functional assays.

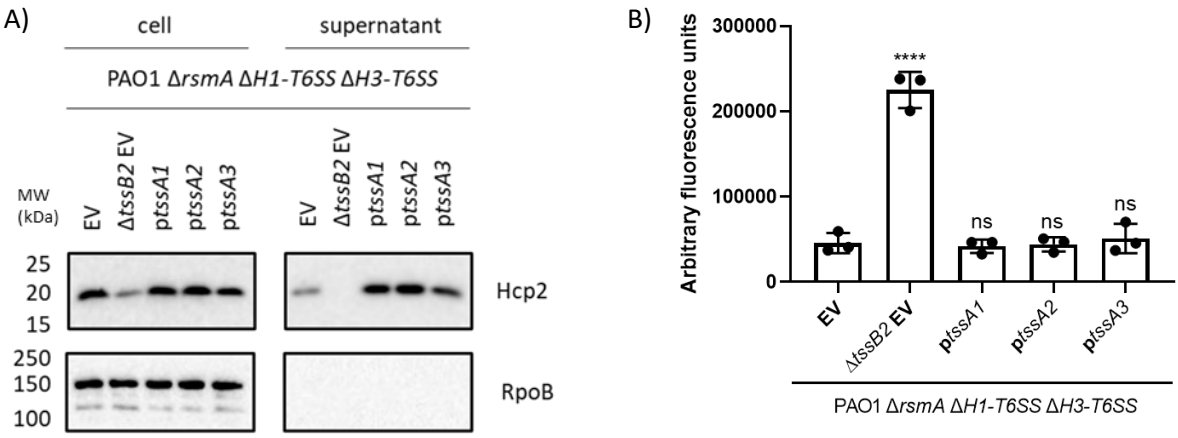


Figure 4.28 Assessment of H2-T6SS activity and TssA interference in the absence of H1- and H3-T6SS clusters. To assess interference in H2-T6SS activity, the pBBR1MCS4 vector was introduced either as empty vector (EV) or encoding *tssA1, tssA2* or *tssA3* (p*tssA1/2/3*). A) Western blot of a H2-T6SS secretion assay to assess the levels of the secretion marker Hcp2 in the supernatant sample. Cell and supernatant samples were harvested after 18 hours growth at 25 °C. Proteins detected in the western blot are indicated to the right. MW markers (left) are in kDa. RpoB was used as a loading and bacterial lysis control. B) H2-T6SS competition assay to assess the T6SS-dependent killing of a GFP-encoding *E. coli* prey by *P. aeruginosa* attacker strains. Attacker *P. aeruginosa* and prey *E. coli* were mixed and incubated at 25 °C for 24 hours, before quantification of GFP signal. Values are presented as means and error bars represent the standard deviation. Statistical testing was conducted by one-way ANOVA with Dunnett's multiple comparisons test, each strain was compared to parental EV strains (ns = not significant, **** $p < 0.0001$). (n=3).

4.7 Discussion

4.7.1 Interactions involving *P. aeruginosa* long and short TssA proteins

Previous characterisation of the interactions of *P. aeruginosa* TssA proteins has solely focussed on TssA1 interactions with H1-T6SS components (376). However, the interactions of TssA proteins from other organisms, such as $TssA^{BC}$, $TssA^{EC}$ and $TssA^{VC}$, have been more extensively studied (360,377,509,512). The specific partners can vary between each TssA, but generally TssA proteins have been described to self-interact as well as interacting with components of the sheath, the inner tube, the spike, the baseplate complex and the membrane complex (360,376,377,509,512). This broad range of interactions indicates a central role for TssA proteins in T6SS assembly and activity. This correlates with the dynamics observed for TssA proteins in T6SS assembly and firing: the TssA complex associates with the T6SS assembly initiation site comprising the membrane complex and baseplate, once the extension of the sheath begins from this site, TssA is present at the distal end of the polymerising sheath structure as it extends across the cell to the opposite membrane (360,377,508,513).

The interactions of all three *P. aeruginosa* TssA proteins were studied with components of their respective T6SSs. The TssA partners identified here follow some trends of previously reported data, with interactions identified between each TssA and respective sheath components, baseplate components and inner tube components (Figures 4.4, 4.5, 4.6, 4.7, 4.9 and 4.10). One main outcome of this study is thus that despite differences in domain organisation, symmetry and structure of long and short TssA proteins, the interaction networks they are involved in are similar, raising questions about what kind of specificity or variation in function these quite distinct protein structures are contributing to (Figure 4.29).

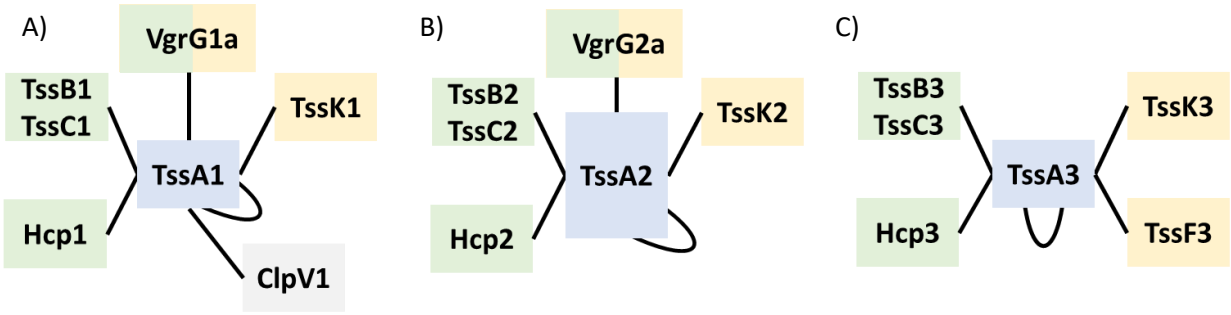


Figure 4.29 Protein-protein interaction networks of *P. aeruginosa* TssA proteins. Interactions of TssA proteins (blue) with their respective tail complex components (green), baseplate complex components (yellow) and ClpV (grey). A) Protein-protein interaction network for TssA1. A) Protein-protein interaction network for TssA2. A) Protein-protein interaction network for TssA3.

4.7.2 Accommodation of TssA symmetry variations and symmetry mismatches in the T6SSs

The different TssA sub-groups share a common Nt1 domain, which is followed by distinct C-terminal domains, which share no similarity in either the amino acid sequences or in structural features, with the addition of an Nt2 domain in $TssA_L$ proteins (see section 1.4.1) (360,376,377,509). Functionally, however, there is similarity in these C-terminal domains, which are required for the oligomerisation of their respective proteins into ring-shaped structures (360,376,377,509). This role was confirmed here, with self-interaction for the C-terminal domains of the short TssA1 and TssA3, and the Nt2 and C-terminal domains of the long TssA2, which is likely driven by the C-terminal domain (Figure 4.21). Using their distinct C-terminal domains, these different TssA subgroups achieve a similar outcome in oligomerisation into a ring-shaped structure.

However, this oligomerisation also introduces variation into TssA proteins. With distinct folds, the way in which these C-terminal domains oligomerise generates quite different ring-shaped structures which vary in their symmetries and dimensions (see section 1.4.1) (360,376,377,509). The oligomerisation of the C-terminal domain of the short $TssA^{BC}$ is expected to involve 32 monomers, forming a large ring with 16-fold symmetry and an internal lumen of ~100 Å (509). In contrast, the oligomerisation of the C-terminal domain of $TssA_L$ proteins involves 10 or 12 subunits forming a much smaller ring with five- or six-fold symmetry and an external diameter in the region of 100-130 Å, with dimeric Nt2 domains flexibly associated with the periphery (Table 1.1) (360,377,509). While no high-resolution structures of any full-length TssA protein has been determined, in all cases the Nt1 domains are predicted to be peripherally associated relative to the oligomeric ring structure through flexible linkers (360,376,377,509).

The conservation of TssA interaction partners, despite little sequence or structural conservation, suggests that these interactions are very important for TssA activity. One way in which such different TssA structures might interact with a similar subset of components could be that the structures of these components vary in conjunction with the TssA variation. However, the general structure of T6SS components is very similar across systems and organisms. The structures of numerous Hcp complexes associated with both long and short TssA proteins have been solved to date, and while amino acid sequence identity between Hcp proteins can vary, there is structural similarity in both the symmetry and dimensions of the rings formed: conserved Hcp hexameric ring structures with an outer diameter of 80-90 Å and a lumenal diameter of 40 Å (34,574–578). Most of the variability in Hcp sequence involves residues found lining the inner lumen, which likely reflects a variation and specificity relating to effectors carried within the lumen of a Hcp ring, while residues exposed on external regions that are more likely to contact other T6SS proteins have higher conservation (380,574). Similarly, the available structures of contracted T6SS sheaths each form a helical tube with six-fold symmetry, which

have similar dimensions: an outer diameter of 240-290 Å and an inner diameter of 110-120 Å (385,579,580). Less structural data exists on the sheath in the extended conformation, as this is a high energy state that does not form *in vitro*, but the six-fold symmetry is conserved in a narrower helical tube with an internal lumen of closer to 80 Å (357,386). It is therefore clear that while T6SS clusters encode TssA proteins that vary in their symmetry and dimensions, components of the T6SS that these varied TssA proteins interact with, have conserved structural features. Interestingly, some differences have been observed between ClpV proteins, as previously described (see section 4.3.6). The current BTH data indicate that differences between ClpV1 compared to ClpV2 and ClpV3 may contribute to variable interactions with TssA (Figure 4.9), however further work is required to validate these interactions.

Generally, it therefore seems that for TssA proteins of very variable symmetries to form similar interactions with quite conserved T6SS components, some symmetry mismatches would have to be tolerated. As described above, the Hcp tube and both extended and contracted sheath structures have six-fold symmetry, while the membrane complex has five-fold symmetry and the baseplate six-fold symmetry (34,347,357,364,385,574–580). The six-fold symmetries reported for $TssA^{EC}$ and $TssA^{VC}$ matches the symmetries of many of the T6SS sub-complexes (360,377). In contrast, five-fold and 16-fold symmetries reported for $TssA^{AH}$ and $TssA^{BC}$ respectively, clash with the symmetries of other sub-complexes, raising questions about how these interactions may be mediated (509). However, mismatches in the symmetries of complexes at the site of their interaction are well described (581). In tailed DNA bacteriophages, a mismatch exists at the interface between the five-fold symmetry of the capsid vertex and the 12-fold symmetry of the portal complex (582–584). Symmetry mismatches are also well described in T4SSs. This includes symmetry mismatches between different sub-complexes of the *Legionella pneumophila* T4SS, where the outer membrane cap displays 13-fold symmetry while the periplasmic ring displays 18-fold symmetry (585). A symmetry mismatch has even been reported between the two concentric rings comprising the outer membrane core complex of the F-plasmid T4SS, with an inner ring of 17-fold symmetry and an outer ring of 13-fold symmetry (586).

The FliD protein that caps the bacterial flagellum bears similarity to TssA proteins in terms of both accommodating a symmetry mismatch and variation in oligomeric states (132,509). Oligomerisation of FliD D2 and D3 domains generates a hexameric structure in *E. coli* and *P. aeruginosa* while forming a pentameric structure in *Salmonella typhimurium*, tetrameric arrangements have also been described (131,132,587–589). These FliD complexes cap the distal, growing end of the flagellar filament which has 11-fold symmetry (see section 1.2.3.1) (590–592). In this cap structure, the oligomerised D2 and D3 domains form a cap plate structure on top of the flagellar filament, while the D1 domains extend vertically down from this plate as legs (132). Both FliD and TssA proteins are found as capping

structures at the growing distal end of a helical structure. Additionally, the symmetries of these capping structures are not conserved between different organisms and can vary from that of the structure they are capping. Interestingly, it was observed that FliD cap proteins could be functionally exchanged between flagella from different families (593). This varies from the functional specificity that was identified here for TssA proteins (Figures 4.25, 4.26 and 4.27), which may relate to additional TssA roles, for example linked to interactions with other T6SS sub-complexes. Alternatively, this functional specificity may also relate to the presence of distinct T6SS machineries within an organism, where this type of variation is not present for flagella.

The mismatch in symmetries between TssA proteins and sub-complexes of the T6SS that they have been shown to interact with somewhat complicates the understanding of these interactions, as they cannot intuitively be pieced together. However, symmetry mismatches in interacting complexes are not uncommon, and high-resolution structural data and targeted biochemistry can be used to elucidate and then refine these molecular details.

4.7.3 Positioning of TssA at the distal end of the sheath

The existing hypothesis for the interaction between TssA proteins and the sheath is based on previous BTH data identifying that a Nt1 and Nt2 domain region of $TssA^{EC}$ was able to interact with components of the sheath (360). With the available Nt2 structure, modelling allowed the docking of the Nt2 domains to the distal end of the sheath, interdigitating with sheath subunits in the extended but not contracted conformation (Figures 4.30A and B) (360). The dodecameric $TssA^{EC}$ and $TssA^{VC}$ each have six Nt2 domain dimers, which could each be modelled to bind in one of six grooves on the distal end of the extended sheath (Figure 4.30) (360,377). These tight contacts were suggested to stabilise the extended, high-energy conformation of the sheath during its polymerisation (360). Based on this model, the decameric $TssA^{AH}$ with only five Nt2 domain dimers might only fill five of the six sites. While this symmetry mismatch could possibly be tolerated with the flexibility of the Nt2 domain dimers relative to the C-terminal domain ring, it is unclear whether the proposed effect on sheath stability would be comparable to the six-fold symmetry $TssA_L$ proteins.

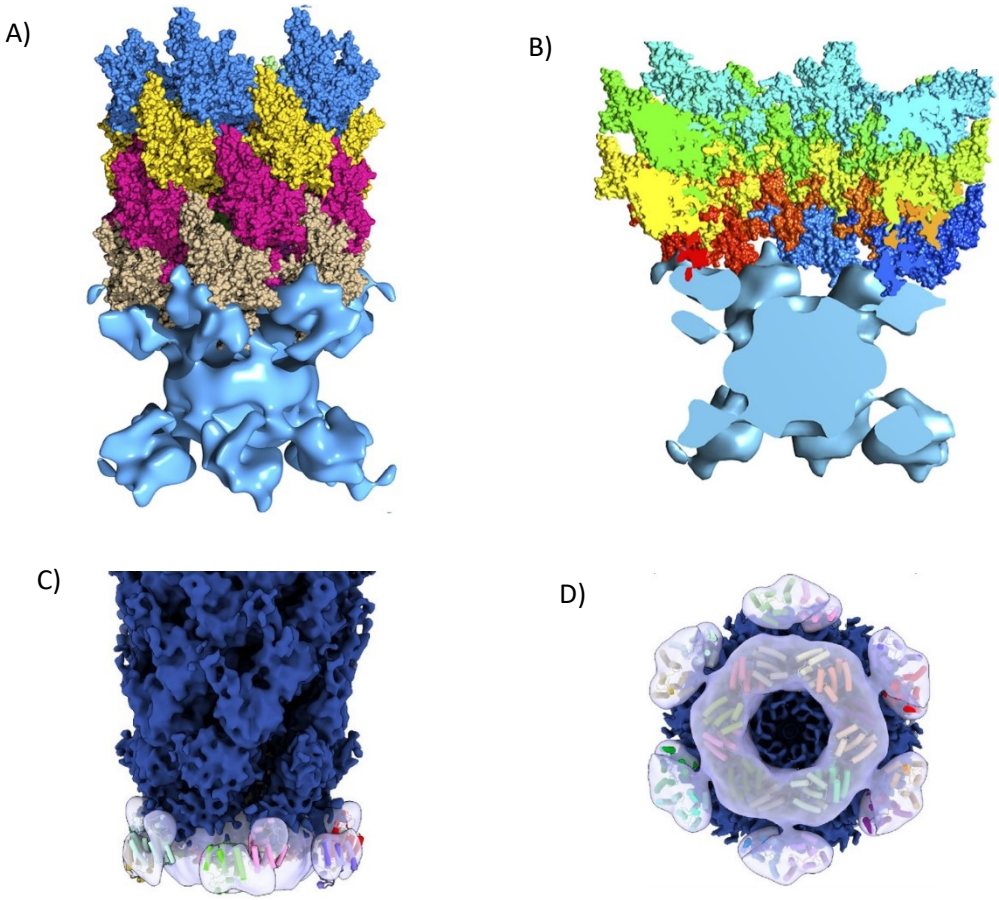


Figure 4.30 Models of TssA complexes docked to sheath structures. A) $TssA^{EC}$ docked to the distal end of the associated extended sheath structure. B) $TssA^{EC}$ docked to the distal end of the associated contracted sheath structure. Figures A and B reproduced from Zoued *et al.* (2016) with permission from Springer Nature. C) Side view of $TssA^{VC}$ docked to the distal end of the associated extended sheath structure. C) Top view of $TssA^{VC}$ docked to the distal end of the associated extended sheath structure. Figure reproduced from Schneider *et al.* (2019) under the terms of the Creative Commons CC BY license, https://creativecommons.org/licenses/by/4.0/legalcode.

This model only accounts for interactions of $TssA_L$ proteins containing an Nt2 domain with the sheath. As demonstrated here and elsewhere, $TssA_S$ proteins also interact with sheath components despite lacking an Nt2 domain (Figure 4.5) (376,509). These interactions may be distinct, with $TssA_L$ proteins interacting with the sheath via their Nt2 domains, and $TssA_S$ proteins forming a similar interaction with a separate component. When point mutations were introduced at conserved TssA1 Nt1 domain residues (K69, G86 and L94), interactions with the sheath were abolished, while interaction with the sheath were maintained upon introduction of point mutations at conserved TssA1 C-terminal domain residues (L286, L289, L309, R282 and E300), suggesting the Nt1 domain may be involved in the sheath interaction (Figures 4.13, 4.14 and 4.16). In separating TssA proteins into component domains, it was identified that the Nt1 domains of both long and short TssA proteins were involved in interaction with

their respective sheath proteins (Figure 4.20). Sheath binding through the conserved Nt1 domains, suggests that the interaction between TssA proteins and their respective sheath occurs by similar mechanisms in both long and short TssA proteins. Remarkably, it has been identified that despite a lack of sequence similarity, the structure of the first seven α-helices of the Nt1 domain resembles that of the Nt2 domain (Figure 4.31) (509). These first seven α-helices of the Nt1 domain represent the majority of the highly conserved and characteristic TssA feature, the ImpA_N region (509). It has been suggested that a duplication event may have been involved in the evolution of Nt1 and Nt2 domains in $TssA_L$ proteins (509). This structural similarity may explain why the Nt2 domain could be docked to the sheath structure when it appears that Nt1 domains are involved in this interaction.

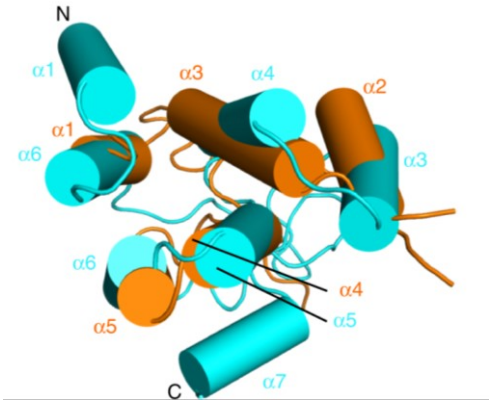


Figure 4.31 Superimposition of $TssA^{BC}$ Nt1 and Nt2 domains. The first 7 α-helices of the $TssA^{BC}$ Nt1 domain (PDB: 6HS5) superimposed with the $TssA^{BC}$ Nt2 domain (PDB: 6G7B) Figure reproduced from Dix *et al.* (2018) under the terms of the Creative Commons CC BY license, https://creativecommons.org/licenses/by/4.0/legalcode.

No full length TssA structure has been solved at a high resolution to date. At most, the region corresponding to $TssA_L$ Nt2 and C-terminal domains have been resolved together, but the structure of an Nt1 domain connected to another domain has been elusive (377,509). The structures of the Nt2 and C-terminal domains of $TssA^{AH}$ and $TssA^{VC}$ have identified that the Nt2 domain dimers formed at the outer edge of the C-terminal domain ring do not follow the symmetry of the ring (Figure 4.32A) (377,509). Instead, the linker region between these domains confers flexibility to these Nt2 domains which can be found up to 60° either above or below the plane of the ring as well as being able to rotate around horizontal and torsional axes (Figure 4.32) (377,509).

A high degree of flexibility in the linker connecting the Nt1 domain to the ring structure, either Nt2 and C-terminal domain for $TssA_L$ or just C-terminal domain for $TssA_S$, is expected to account for the absence of an Nt1 domain density when studying either full length or Nt1 and Nt2 structures by EM (360,376,377). Nt1 domains are therefore predicted to be flexibly associated at the periphery of TssA ring-shaped structures. As with Nt2 domains, these highly flexible Nt1 domains are not constrained by the symmetries of their associated ring-shaped C-terminal domains. In theory this allows Nt1 domains to interact with their respective sheaths of six-fold symmetry independent of the variable symmetries of their C-terminal domain rings. In this manner, the interaction of TssA proteins that have variable

domain organisation, symmetries and structures with their respective sheaths seems to be maintained through the conserved Nt1 domains which are flexibly associated with oligomerised ring structures. This model is further expanded upon in Chapter 5.

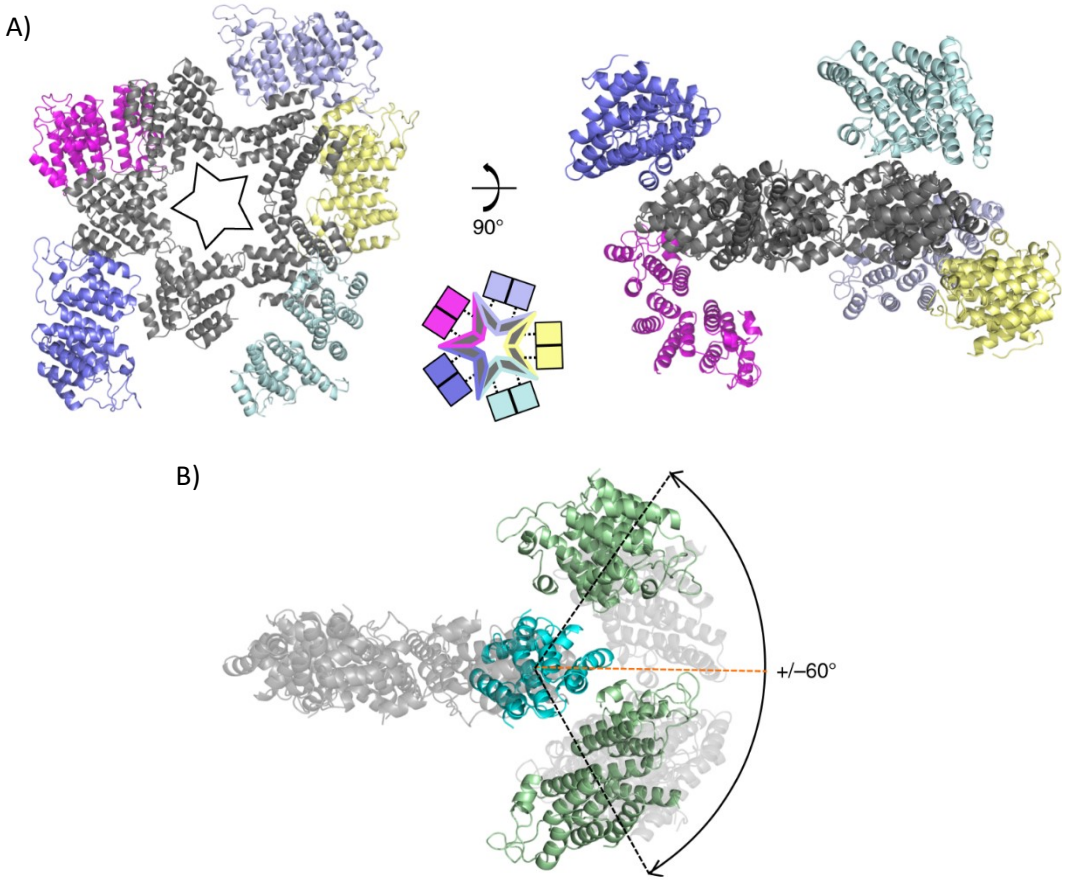


Figure 4.32 Flexibility of TssA^{AH} Nt2 domains. A) Positioning of TssA^{AH} Nt2 domain dimers (various colours) around the C-terminal domain ring (grey), as viewed from the top (left) and the side (right). B) Displacement of TssA^{AH} Nt2 domains (green) by up to 60° above and below the plane (orange line) of the C-terminal domain ring (grey and light blue monomer). Figure reproduced from Dix *et al.* (2018) under the terms of the Creative Commons CC BY license, https://creativecommons.org/licenses/by/4.0/legalcode.

4.7.4 Insights into TssA functionality: sheath interactions

It has been suggested that the variation in the size, domain organisation and structure of TssA proteins may be linked to a functional difference, with TssA$_S$ proteins as static, baseplate-associated components, while TssA$_L$ proteins are dynamic, associated first with the baseplate and then at the distal end of the polymerising sheath (376,377). As previously described, this hypothesis arises from

observations of static TssA1 foci at the base of the sheath structure in fluorescence microscopy experiments, while $TssA_L$ proteins form dynamic foci that localise at the distal end of the sheath (360,377). However, the short $TssA1^{PP}$ and $TssA^{AB}$ have also been identified as having similar dynamics to those previously described for $TssA_L$ proteins, suggesting that both long and short TssA proteins can associate with the distal end of the sheath structure (see section 3.6.2) (508,513). Nevertheless, a question therefore remains about the localisation of TssA1, and whether it has different position in the T6SS compared to all other studied TssA proteins.

In the model of TssA1 as a static, baseplate-associated component, TssA1 has been compared to the bacteriophage T4 baseplate component gp6 (376). A ring formed of the gp6 C-terminal region is found around the central hub of the baseplate and is required for the assembly of baseplate wedges into the final baseplate complex (363,594). This gp6 protein contributes to contacts between the baseplate complex and the sheath, and this structure helps maintain the stability of the baseplate complex during the structural rearrangement that triggers sheath contraction (594). The gp6 C-terminal region forms a dodecameric ring-shaped structure with external diameter of 240 Å, internal lumen of ~100 Å and width of ~80 Å, which is comparable to the identified dimensions of the TssA1 ring, with external diameter of 260 Å, internal lumen of ~100 Å and width of ~95 Å (376,594). Sequence similarity was also identified between the C-terminal regions of gp6 and TssA1, including in regions identified to be involved in the oligomerisation of the gp6 ring (376,594).

However, these comparisons between gp6 and TssA1 were made in the absence of high-resolution structural data for a $TssA_S$ protein. Now, with a better understanding of TssA domain organisation and structure, differences between these proteins are more apparent. Firstly, the C-terminal region of gp6 involved in ring formation comprises the terminal 326 aa, while $TssA_S$ C-terminal domains are far smaller, in the region of 70 aa (509,594). Therefore unsurprisingly, the structure formed by the gp6 C-terminal region is very different to that of the $TssA^{BC}$ C-terminal domain (Figure 4.33).

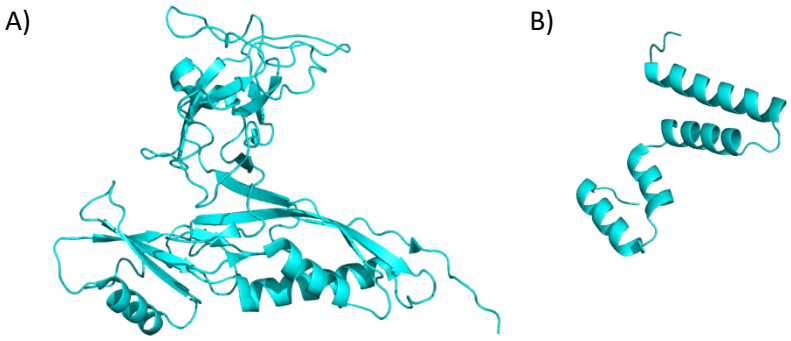


Figure 4.33 Structures of gp6 C-terminal region and $TssA^{BC}$ C-terminal domain. A) Structure of the gp6 C-terminal region monomer (PDB: 3H2T). This structure is formed of 3 domains. B) Structure of $TssA^{BC}$ C-terminal domain monomer (PDB: 6HS6). This structure is comprised of 4 α-helices.

The C-terminal domains of TssA1 and TssA^{BC} share 24 % sequence identity and based on this are predicted to share structural similarity. TssA1 is therefore likely to have a similar fold and oligomerise similarly to TssA^{BC}. However, having a distinct fold from gp6 does not exclude TssA1 from being localised with the baseplate complex during sheath polymerisation.

There are several ways in which the static localisation of TssA1 at the baseplate during sheath polymerisation, as was identified by fluorescence microscopy (377), could come about. TssA1 could associate, as previously suggested, at the interface between the baseplate and the sheath, with the lumen of the C-terminal ring aligning with that of the sheath at its proximal end. Alternatively, TssA1 could interact with the surface of the baseplate complex, exposed to the cytoplasm. It has been identified here that all *P. aeruginosa* TssA proteins interact with sheath components through their Nt1 domains (Figure 4.20). At the interface between the baseplate and the sheath a TssA protein would therefore interact with the sheath through these Nt1 domains at one face and then with the baseplate at the other face either through Nt1 domains at the other face of the double-layered ring, or directly through the C-terminal domain.

Imaging of an extended *V. cholerae* sheath structure by cryo-EM provided some low-resolution structural data of the interface between the baseplate complex and the sheath (364). In this structure, no TssA-like density was present at the interface between the baseplate complex and the sheath, however a density was present at the distal end of the sheath which was proposed to be TssA. Of course, the *V. cholerae* T6SS is associated with a TssA$_L$, which has been shown to associate with the distal end of the sheath by fluorescence microscopy, but this data indicates a direct interaction between components of the baseplate complex and the sheath (364,377). It is unexpected that such a key interaction interface would vary between T6SSs, though this theory cannot be totally disregarded at this stage.

The short TssA1^{PP} of the *P. putida* K1-T6SS localises first with the baseplate and then at the distal end of the sheath during its polymerisation (508), in contrast to the static localisation observed for TssA1 of the *P. aeruginosa* H1-T6SS (376). For TssA1 to localise at the interface between the baseplate and sheath, structural differences might be expected between H1-T6SS and K1-T6SS baseplate components. However, pairwise sequence comparisons of baseplate components from the H1- and K1-T6SS clusters identified a high level of sequence identity between proteins encoded in these clusters (Table 4.2). It is therefore unlikely that very different baseplate structures are formed between these T6SSs that would necessitate the presence of TssA1 as a static baseplate component in the H1-T6SS.

Table 4.2 Pairwise sequence comparison of baseplate components

	TssE	TssF	TssG	TssK
(%) sequence identity H1-T6SS vs K1-T6SS	31.8	34.1	30.1	30.9

Alternatively, TssA1 could be identified as a static baseplate component through association with the external surface of the baseplate complex exposed to the cytoplasm. This may mirror the association of TssA proteins with the T6SS assembly initiation site comprising the membrane and baseplate complexes, that has been identified prior to sheath polymerisation (360,377,508,513). In fluorescence microscopy experiments identifying TssA1 as a static baseplate-associated component, TssA1 fluorescent foci could only be visualised with an active sheath structure in the presence of the wildtype TssA1 protein (377). This indicates that the fluorophore tagged TssA1 is not entirely functional. Authors hypothesised that mixed wildtype and fluorophore tagged TssA1 structures form and so the fluorescent foci visualised represent all TssA1 structures. However, this may not necessarily be the case, wildtype TssA1 may function independently from the fluorophore tagged form, and for example be present at the distal end of the sheath, though undetectable in this assay.

Given that all three *P. aeruginosa* TssA proteins interact with their respective sheath components via their Nt1 domains, the interactions of these domains with the sheath are likely similar. This suggests that each of these TssA proteins have a similar position in the T6SS relative to the sheath. There is an abundance of evidence identifying TssA proteins, including TssA2 and TssA1^{PP}, as dynamic T6SS components present at the distal end of the polymerising sheath (360,377,508,513). For the purpose of this work, it will therefore be assumed that all TssA proteins localise at the distal end of the sheath.

4.7.5 Interaction of TssA proteins with T6SS components

It is tempting to propose that all interactions of TssA proteins with T6SS components are mediated through the Nt1 domains, both because these domains are highly conserved across TssA proteins and because their flexibility relieves them of the symmetry constraints associated with the ring structure. Additionally, if these interactions involve the Nt1 domain, but require proper positioning/orientation by the C-terminal domain ring, this could explain why they were not identified as interacting in the BTH experiments with Nt1 domains alone. This theory would involve the spider-like positioning of TssA proteins at the site of interaction, Nt1 domains interacting with components of the membrane and baseplate complexes, with the associated ring-shaped structure holding these flexible ‘legs’ together.

However, the data suggests that this is not necessarily the case and there is likely to be more complexity.

While the data presented here identified for each TssA the interaction of Nt1 domains with the sheath and self-interaction via C-terminal domains, specific interactions of TssA domains with other components were less clear (Figures 4.20 and 4.21). There were weak interactions of some TssA domains, which are summarised, along with the previous domain interaction data in Figure 4.34. There is evidence of both long, TssA^{EC} and TssA^{VC}, and short, TssA1 and TssA^{BC}, TssA proteins interacting with VgrG proteins through C-terminal domains (360,509,512). It is interesting that such distinct C-terminal domains should interact with the conserved, trimeric VgrG spike structure. Similar has been reported for interaction with Hcp proteins, which interact with the C-terminal domains of both long TssA^{EC} and short TssA^{BC} (360,509). It seems therefore that while interaction with the sheath occurs via a both highly conserved and flexibly associated Nt1 domain, interactions with some other T6SS components occur through the very distinct and structurally rigid C-terminal domains.

	N-terminal domain/s						C-terminal region					
	$TssA_S$			$TssA_L$			$TssA_S$			$TssA_L$		
	TssA1	TssA3	TssA^{BC}	TssA2	TssA^{EC}	TssA^{VC}	TssA1	TssA3	TssA^{BC}	TssA2	TssA^{EC}	TssA^{VC}
TssA	■	■					■	■		■		
TssBTssC	■	■		■	■							
Hcp									■		■	
TssE					■							
TssF									■			
TssK										■		
VgrG	■					■	■				■	■
ClpV							■					
TssM	■											

Figure 4.34 Identified domain interactions of TssA proteins. Summary of previously reported TssA domain interactions, combined with those identified here. Interactions of TssA N-terminal domains represent Nt1 domain interactions except in the case of TssA^{EC} which represents Nt1 and Nt2 domains. Interactions of C-terminal regions represent interactions of $TssA_S$ C-terminal domains, TssA^{EC} C-terminal domain and TssA2 and TssA^{VC} Nt2 and C-terminal domains. Identified interactions are highlighted in green.

The interaction of both VgrG and Hcp proteins with a similar region of TssA proteins is not surprising. The N-terminal gp27-like domain of VgrG which is found at the base of the trimeric spike has a similar fold to the Hcp hexamer that binds to it forming the inner tube (313). The head side of a Hcp ring interacts with this gp27-like domain akin to the head-to-tail stacking of Hcp hexamers, leaving the tail side to polymerise further Hcp hexamers (373). Therefore, the gp27-like base of VgrG resembles the tail side of the Hcp ring, which has been shown to be the side of the Hcp ring that interacts with TssA (373). This identifies TssA as binding to Hcp at the distal end of the Hcp tube, as would be expected given the association of TssA with the distal end of the polymerising tail complex. While the C-terminal domains of long and short TssA proteins are distinct and will interact differently with VgrG and Hcp proteins, each C-terminal domain is likely to interact via a similar mechanism with both VgrG and Hcp.

The TssA domains contributing to interactions with other T6SS components could not be determined here. Both the N-terminal (Nt1 and Nt2) region of the long $TssA^{EC}$ and the C-terminal domain of the short $TssA^{BC}$ have been previously identified to interact with components of the baseplate complex (Figure 4.34) (360,509). This suggests that interactions with baseplate components are either achieved by different domains in long and short TssA proteins, or that both N- and C-terminal domains may contribute to interactions with baseplate components.

4.8 Summary

This chapter presented a comprehensive and systematic characterisation of the interactions of *P. aeruginosa* TssA proteins, uncovering interaction networks. This allowed further details to be elucidated, including the discovery of key conserved interactions that may facilitate functional similarities despite structural diversity. This led to the conclusion that TssA proteins, long and short, are positioned similarly in their respective T6SS. Further details on the association of TssA proteins with T6SS components, and the specificity of these interactions are studied in Chapter 5.

5. Results: Characterisation of TssA domains and role in TssA specificity

5.1 Introduction

TssA proteins are formed of discrete domains connected by flexible linkers, where the domains present differ between long and short TssA proteins (360,376,509). All TssA proteins have an N-terminal ImpA_N containing Nt1 domain. In $TssA_S$ proteins this is linked to a C-terminal domain, while in $TssA_L$ proteins this is linked to a Nt2 domain connected to a distinct C-terminal domain (Figure 1.16) (360,376,509). These domains have distinct contributions to TssA interactions as outlined in Chapter 4.

5.1.1 The TssA Nt1 domain

The Nt1 domains of TssA proteins share the conserved ImpA_N region at the N-terminus, which is suggested to introduce structural homology in this region between all TssA proteins (509). There is some variation in the size of Nt1 domains, with those of $TssA_S$ proteins being larger than those of $TssA_L$ proteins, i.e. ~250 aa compared to ~190 aa respectively (509). The only resolved Nt1 domain structure is that of the short $TssA^{BC}$, which is comprised of 11 α-helices (see section 1.4.1.1) (509). The Nt1 domains of both long and short TssA proteins are predicted to be flexibly associated at the periphery of ring-shaped structures whose dimensions and symmetries vary hugely between long and short TssA proteins (360,376,377,509). These ring-shaped structures are formed through the oligomerisation of distinct C-terminal domains (360,376,377,509). A functional role of the Nt1 domain has not previously been described.

The association of TssA proteins with components of their respective sheath is well described, both through direct interaction data and visualisation of this association through fluorescence microscopy (360,376,377,508). In this study it has been identified that the TssA domain responsible for the interaction with the sheath is the Nt1 domain for both long and short TssA proteins (Figure 4.20).

5.1.2 TssA C-terminal regions

The C-terminal regions of TssA proteins are variable, particularly between long and short TssA proteins, but variations in symmetry and structure are also apparent between members of these groups (360,377,509). Despite this variation, it has been suggested that the distinct C-terminal regions

of long and short TssA proteins have a common function: in mediating the oligomerisation of a ring-shaped structure where a similar positioning of Nt1 domains is maintained at the periphery (Figure 1.24) (509). TssA C-terminal domains have also been identified to interact with T6SS components, such as VgrG and Hcp (360,509,512). The contribution of the distinct C-terminal domains in the oligomerisation of both long and short TssA proteins is clear from previous structural work (360,377,509), and was also demonstrated here through consistent self-interaction in BTH experiments (Figure 4.21).

The ring structures formed through this oligomerisation are very different between long and short TssA proteins. The rings formed from the C-terminal domains of long TssA proteins result from 10-12 monomers assembling into a double layered ring of five- or six-fold symmetry with an external diameter in the region of 100-130 Å (Figures 1.22 and 1.23) (360,377,509). At the outer edge of this ring, flexible linkers connect to dimeric Nt2 domains that are flexibly associated with the inner ring (360,377,509). The diameter of the ring structure is increased by the presence of these Nt2 domains; the $TssA^{VC}$ C-terminal ring diameter of 130 Å is increased to 190 Å with the addition of the Nt2 domains (Figure 5.1), similarly the 100 Å C-terminal ring diameter of the $TssA^{EC}$ is increased to 200 Å with the outer Nt2 domains (360,377). These outer ring dimensions for the Nt2 and C-terminal domain structures closely resemble the outer ring dimensions of the C-terminal domain ring of the short $TssA^{BC}$. The $TssA^{BC}$ C-terminal domain ring is predicted to be formed from 32 monomers assembling into a double layered ring of 16-fold symmetry with an external diameter of 200 Å and an internal lumen of 110 Å (Figure 1.19) (509). Therefore, both the thick ring formed by $TssA_L$ proteins comprised of the C-terminal and Nt2 domains and the thinner ring formed by $TssA_S$ proteins comprised of just

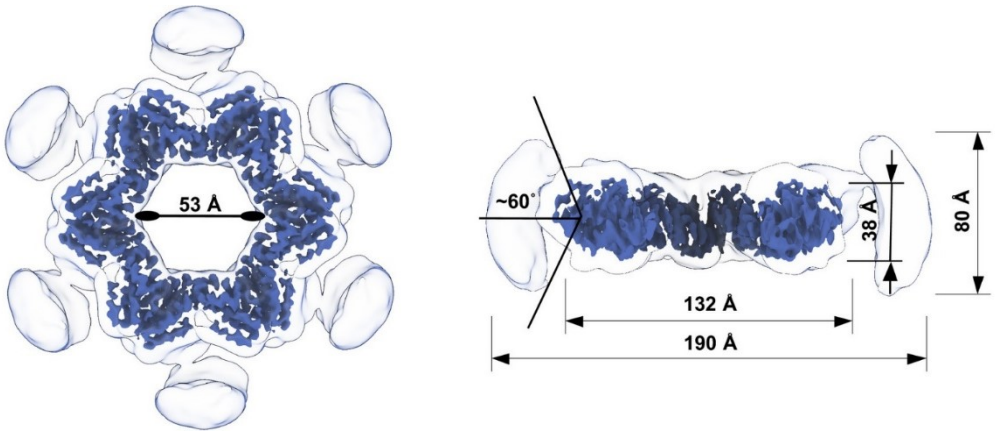


Figure 5.1 Structure of the $TssA^{VC}$ C-terminal domain and Nt2 domain position. Top and side view of the $TssA^{VC}$ C-terminal domain ring, with additional white densities corresponding to the Nt2 domains. The flexibly associated Nt2 domains increase the external diameter of the ring structure to 190 Å. Figure reproduced from Schneider *et al.* (2019) under the terms of the Creative Commons CC BY license, https://creativecommons.org/licenses/by/4.0/legalcode.

the C-terminal domain, have an external diameter in the region of 200 Å from which the flexible linkers connecting to Nt1 domains extend. In contrast, the internal lumens of these structures do differ (Table 1.1).

5.1.3 TssA proteins are functionally specific

TssA proteins interact with a similar subset of components of their respective T6SSs (Figures 4.4, 4.5, and 4.6) (360,376,377,509,512), and the TssA proteins of *P. aeruginosa* were identified to interact promiscuously with T6SS components encoded in different T6SS gene clusters in BTH experiments (Figure 4.24). However, these non-cognate interactions did not translate to either heterologous complementation of *tssA* mutants or a dominant negative effect on the activity of a different T6SS (Figures 4.25, 4.26, 4.27 and 4.28).

The TssA proteins of *P. aeruginosa* therefore seem to be functionally specific to their associated T6SS machinery. This is not necessarily surprising given the structural differences identified between different TssA proteins, despite their conserved features in forming ring shaped structures with similar positioning of Nt1 domains. However, it does raise questions about what the determinants of specificity are in TssA activity, including whether and which of the different domains contribute both to the specificity and activity of TssA proteins.

5.2 Aims of this study

The aim of this study was to investigate the specificity and activity of TssA domains relative to their respective T6SSs. This would provide novel insights into the determinants of functionality and specificity of TssA proteins in a context where three T6SSs are at play in *P. aeruginosa*.

This analysis involved:

1) Chimeric TssA proteins engineered, with domains of both long and short TssA proteins exchanged, and functionality assessed in the associated T6SSs, to determine if these domains confer any specificity.
2) Protein-protein interaction assays to assess domain interaction specificity.
3) Structural analysis of TssA domains, to determine the dimensions and symmetries of TssA C-terminal domains.
4) Modelling and alignments to predict determinants of TssA specificity, which were tested by functional and protein-protein interaction assays.

This study expands upon the insights previously gained on the functionality, interactions and specificity of *P. aeruginosa* TssA proteins (Chapters 3 and 4) and investigates more thoroughly the contributions of TssA domains.

5.3 Functional characterisation of chimeric TssA proteins

To better characterise the contribution of the TssA domains to T6SS activity, chimeric TssA proteins were engineered with mixed domains originating from distinct TssA proteins. In total eight chimeric TssA constructs were generated (Figure 5.2). The Nt1 domain of each TssA was combined with the C-terminal regions of each of the other two TssA proteins. In the case of TssA2, both the C-terminal domain alone and in combination with the Nt2 domain were combined with TssA1 and TssA3 Nt1 domains. It is proposed that exchanging the Nt2 and C-terminal domains of TssA2 with the C-terminal domains of the short TssA1 and TssA3 may lead to similar positioning of the Nt1 domains in the ring shaped-structures generated.

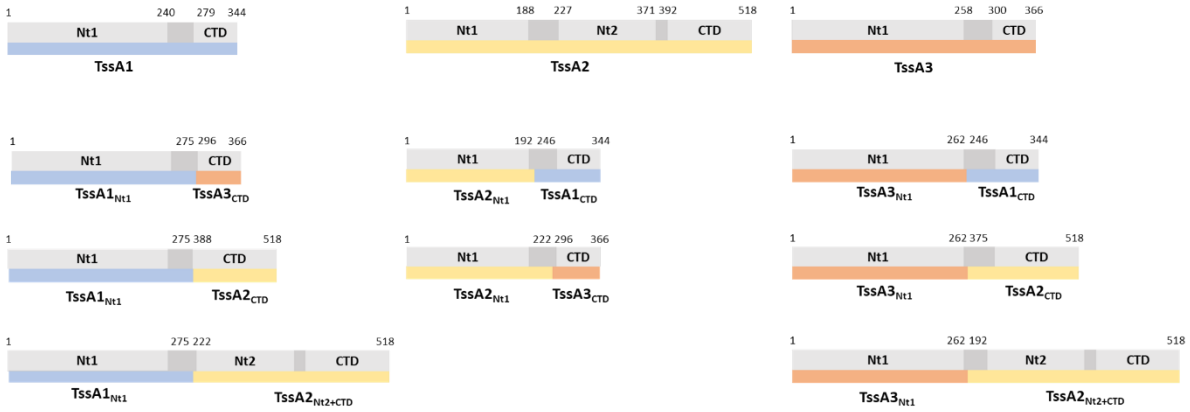


Figure 5.2 Schematic of chimeric TssA proteins engineered. The Nt1, Nt2 and C-terminal domains (CTDs) of the *P. aeruginosa* TssA1 (blue), TssA2 (yellow) and TssA3 (red) were exchanged to generate eight chimeric TssA proteins with mixed domains. The TssA2 C-terminal regions used in generating these chimeric proteins were both the C-terminal domain alone and the Nt2 and C-terminal domains jointly. Residues taken from each component protein are given.

5.3.1 Chimeric TssA proteins are stable in BTH experiments

To ascertain if the engineered chimeric TssA proteins were stable and able to fold correctly, they were introduced into BTH vectors. Interactions were then screened with various TssA proteins or sheath components. Each chimeric protein was able to interact with each TssA protein (Figure 5.3), similar to the cross-interactions between TssA proteins identified previously (Figure 4.23). This indicated that each chimera was forming a stable, folded protein. TssA1 could interact most strongly with chimeric proteins possessing the TssA1 C-terminal domain, however such a trend was not apparent for the other TssA proteins.

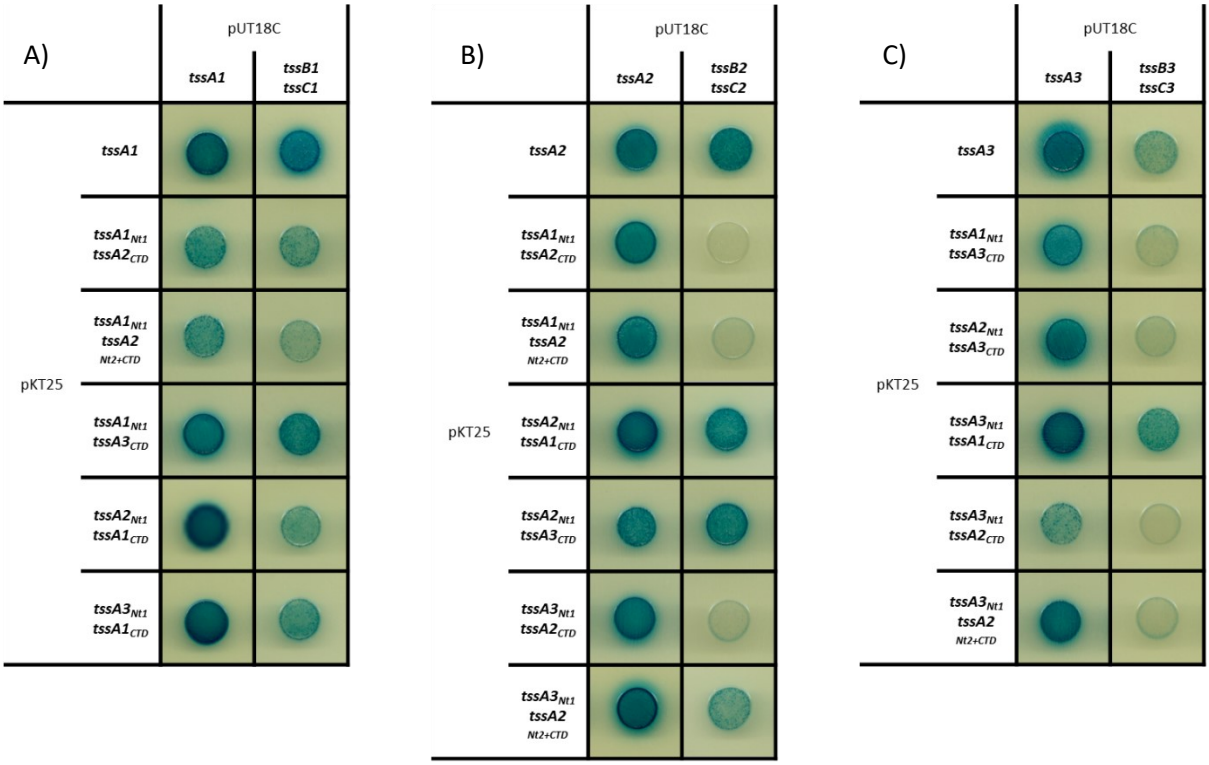


Figure 5.3 Interactions of chimeric TssA proteins with their component TssA proteins and sheath components. BTH with N-terminal T25 (pKT25) linked chimeric proteins and N-terminal T18 (pUT18C) associated TssA proteins and sheath components produced in DHM1 cells. Representative spots grown for 40 hours on X-Gal LB agar are shown. Blue spots indicate protein-protein interaction, spots are white in the absence of interaction. A) Interactions of chimeric proteins containing TssA1 domains with TssA1 and H1-T6SS sheath components. B) Interactions of chimeric proteins containing TssA2 domains with TssA2 and H2-T6SS sheath components. C) Interactions of chimeric proteins containing TssA3 domains with TssA3 and H3-T6SS sheath components.

Chimeric proteins with TssA1 domains were able to interact to some degree with the H1-T6SS sheath components, most clearly seen for $TssA1_{Nt1}TssA3_{CTD}$ (Figure 5.3A). For TssA2 domain-containing chimeras, $TssA2_{Nt1}TssA1_{CTD}$ and $TssA2_{Nt1}TssA3_{CTD}$ were able to interact with the H2-T6SS sheath components, in addition to $TssA3_{Nt1}TssA2_{Nt2+CTD}$ which interacted more weakly (Figure 5.3B). The $TssA3_{Nt1}TssA1_{CTD}$ chimeric protein was the only TssA3 domain containing chimera to interact with the H3-T6SS sheath components (Figure 5.3C).

Interestingly, this BTH data indicated a preference for sheath interaction linked to the presence of the Nt1 domain from the cognate TssA (Figure 5.3), confirming what was previously shown that the Nt1 domain is the domain responsible for interaction with the cognate sheath (Figure 4.20). This suggests the possibility of chimeric TssA proteins being incorporated into a functional T6SS.

5.3.2 The chimeric TssA1$_{Nt1}$TssA3$_{CTD}$ is functional in the H1-T6SS

To assess the functionality of chimeric TssA proteins, beginning with assessing the contribution to H1-T6SS activity, each of the five chimeric proteins containing TssA1 domains were introduced into a background with deletion of *tssA1*. H1-T6SS activity was then assessed to identify whether function could be restored by chimeric proteins.

In a secretion assay, the loss of Hcp1 secretion in the absence of *tssA1* was restored with the constitutive expression of either wildtype *tssA1* or *tssA1$_{Nt1}$tssA3$_{CTD}$* on a plasmid (Figure 5.4A). It is remarkable that a chimeric TssA protein with the C-terminal region exchanged for a non-cognate domain had similar function compared to the native TssA. Similar was demonstrated in an interbacterial competition assay, where prey killing was increased to a similar level with constitutive expression of either wildtype *tssA1* or *tssA1$_{Nt1}$tssA3$_{CTD}$* (Figure 5.4B). Production of mScarlet-TssB1 expressed from the *tssB1* chromosomal locus allowed the visualisation of H1-T6SS sheaths *in vivo*. In the absence of *tssA1* 0.37 % of cells formed sheaths or foci, which rose to 4.95 % and 5.26 % respectively upon introduction of *tssA1* or *tssA1$_{Nt1}$tssA3$_{CTD}$* (Figure 5.4C and D).

The C-terminal domain of the short TssA1 could therefore be exchanged for that of the short TssA3 without a significant difference in H1-T6SS activity in terms of secretion, prey killing or sheath assembly (Figure 5.4). Such an outcome is novel, as a chimeric protein being functional in a T6SS has never been described to date, let alone one that is functionally equivalent. This suggests that the TssA1 Nt1 domain confers the specificity of TssA1 to the H1-T6SS, potentially through its interaction with the sheath as described previously (Figure 4.20). Chimeric proteins where the TssA1 Nt1 domain was fused to C-terminal regions from the long TssA2 were not functional in the H1-T6SS, potentially due to differences in C-terminal regions which are proposed to form very different ring-shaped structures between long and short TssA proteins.

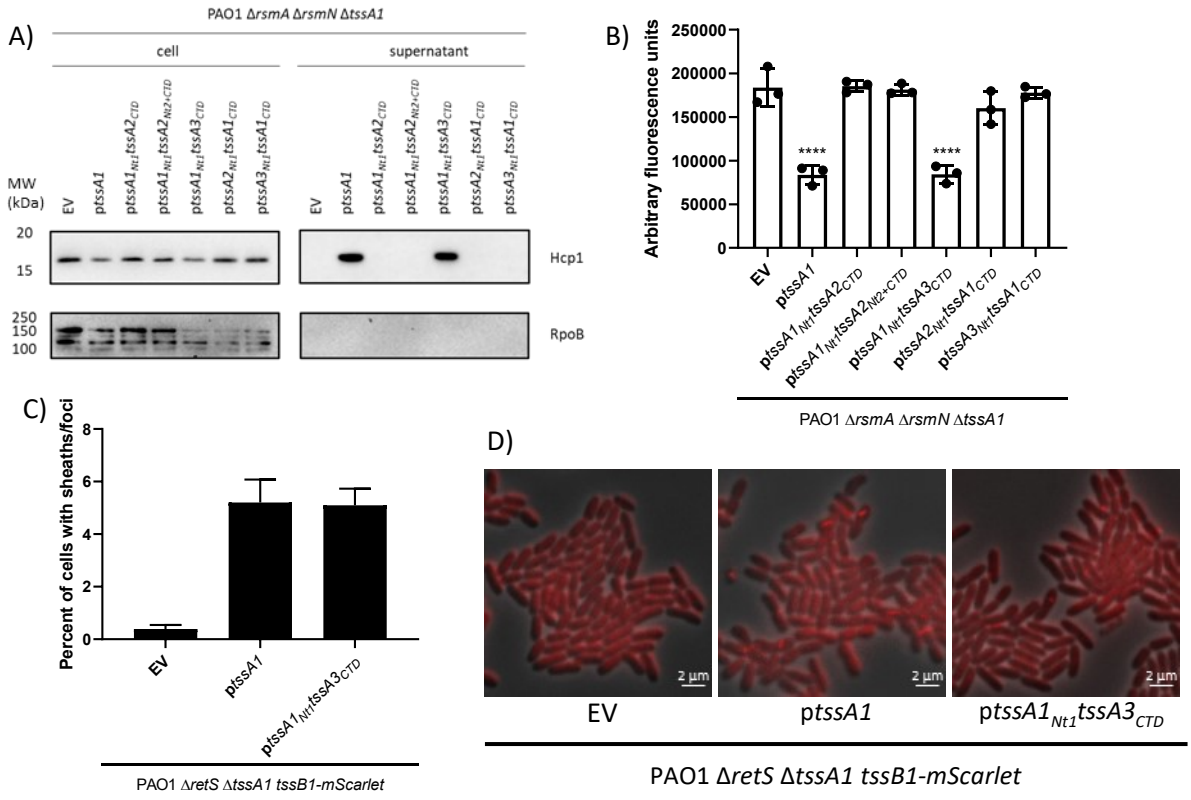


Figure 5.4 Assessment of H1-T6SS activity with chimeric TssA proteins. To assess complementation of the *tssA1* deletion, the pBBR1MCS4 vector was introduced either as empty vector (EV), encoding *tssA1* (ptssA1) or chimeric *tssAs*. Values are presented as means and error bars represent the standard deviation. A) Western blot of a H1-T6SS secretion assay, to assess the levels of secretion marker Hcp1 in the supernatant sample. Cell and supernatant samples were harvested after 5-7 hours growth at 37 °C. Proteins detected in the western blot are indicated to the right. MW markers (left) are in kDa. RpoB was used as a loading and bacterial lysis control. B) H1-T6SS competition assay to assess the T6SS-dependent killing of a GFP-encoding *E. coli* prey by *P. aeruginosa* attacker strains. Attacker *P. aeruginosa* and prey *E. coli* were incubated at 37 °C for 24 hours before GFP signal quantification. Statistical testing was conducted by one-way ANOVA with Dunnett's multiple comparisons test, each strain was compared to parental *tssA1* strain (**** $p < 0.0001$). (n=3). C) Quantification of the percent of cells with TssB1-mScarlet sheaths or foci by fluorescence microscopy. Strains were grown on LB agar pads for 3-4 hours at 37 °C before imaging. The percent of cells with sheaths or foci was 0.37 % (n=10017) with *tssA1* deletion, upon introduction of *tssA1* or $tssA1_{Nt1}tssA3_{CTD}$ on a plasmid this rose to 4.95 % (n=8117) and 5.26 % (n=10553) respectively. Data were taken from 2 fields of view for three experiments. D) Representative images of TssB1-mScarlet sheath formation. Scale bar represents 2 µm.

5.3.3 The chimeric $TssA3_{Nt1}TssA1_{CTD}$ is functional in the H3-T6SS

A chimeric TssA protein formed from the two $TssA_S$ proteins was functional in the H1-T6SS when the TssA1 Nt1 domain was present. To establish whether any of the three chimeric TssA proteins with the TssA3 Nt1 domain were functional in the H3-T6SS, fluorescence microscopy was used to visualise the formation of fluorophore tagged H3-T6SS sheath structures.

The formation of sheath structures was barely detectable in the absence of *tssA3*. Upon introduction of a constitutively expressed *tssA3* sheath formation was restored to 27.2 % of cells, and a comparable 28.1 % of cells formed sheaths upon the introduction of the chimeric $tssA3_{Nt1}tssA1_{CTD}$ (Figure 5.5). Sheath structures were barely detectable upon introduction of either of the two chimeric proteins with TssA2 C-terminal regions.

The C-terminal domain of TssA3 could therefore be switched with that of TssA1 without altering the abundance of H3-T6SS sheath structures formed. For both the H1- and H3-T6SS, a chimeric TssA protein formed of domains of the two short TssA proteins was functional with the T6SS associated with the Nt1 domain, while chimeric proteins formed with the C-terminal regions from the long TssA2 were not functional. The BTH data do not indicate any issue with the stability of chimeric TssA proteins with TssA2 C-terminal regions (Figure 5.3), indicating that other factors, such as fusing domains from long and short TssA proteins, may influence T6SS functionality.

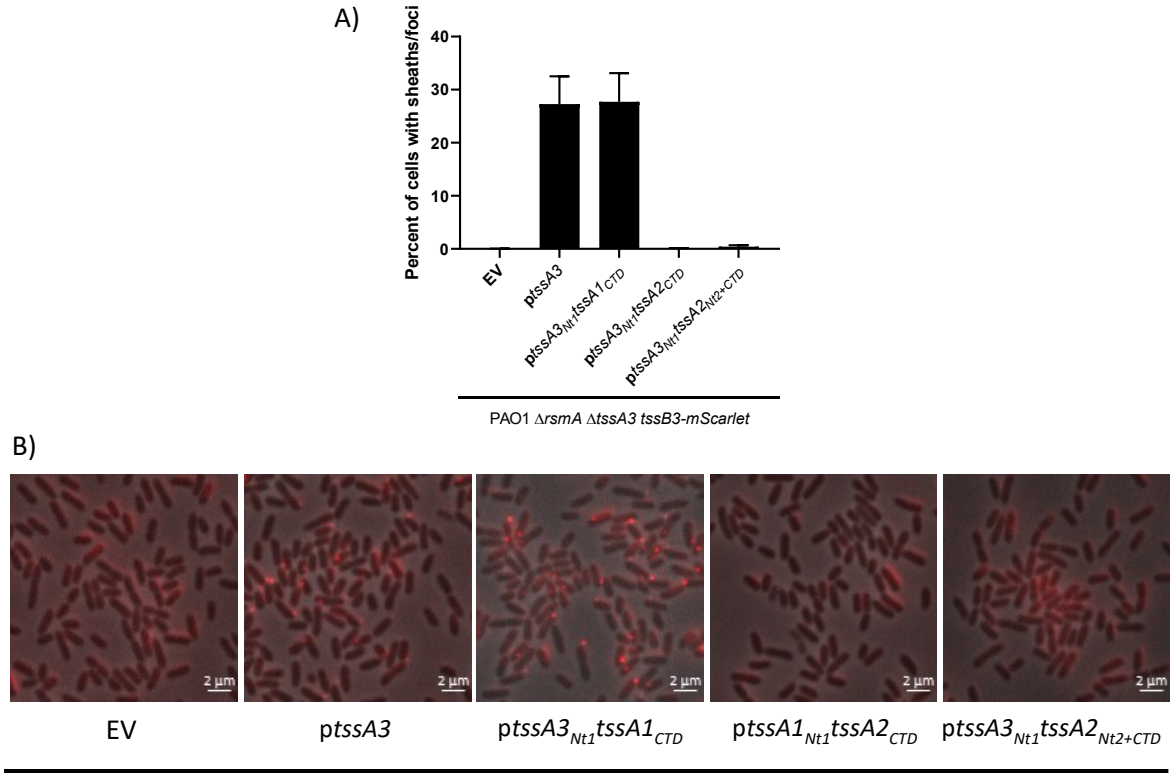


Figure 5.5 Assessment of H3-T6SS sheath formation with chimeric TssA proteins. A) Quantification of the percent of cells with TssB3-mScarlet sheaths or foci by fluorescence microscopy. Strains were grown in liquid culture at 25 °C for 13 hours before imaging. To assess complementation of the *tssA3* deletion, the pBBR1MCS4 vector was introduced either as empty vector (EV), encoding *tssA3* (ptssA3) or chimeric *tssAs*. The percent of cells with sheaths or foci was 0.036 % (n=16822) in the absence of *tssA3*, this rose to 27.2 % (n=16253) with expression of *tssA3* on a plasmid and 28.1 % (n=10456) with *tssA3*$_{Nt1}$*tssA1*$_{CTD}$ on a plasmid. With expression of *tssA3*$_{Nt1}$*tssA2*$_{CTD}$ or *tssA3*$_{Nt1}$*tssA2*$_{Nt2+CTD}$ from a plasmid, 0.076 % (n=8751) and 0.41 % (n=9472) of cells had sheaths or foci respectively. Data were taken from 2 fields of view for three experiments. Values are presented as means and error bars represent the standard deviation. B) Representative images of TssB3-mScarlet sheath formation. Scale bar represents 2 µm.

5.3.4 Chimeric TssA proteins with the TssA2 Nt1 domain restore some function to the H2-T6SS

In assessing the functionality of chimeric TssA proteins with the $TssA_S$-associated H1- and H3-T6SSs, only chimeric proteins comprised solely of the domains of $TssA_S$ proteins were functional. In no case was a chimeric protein containing a TssA2 domain functional within the H1- or H3-T6SS. It might therefore be expected that domains can only be functionally switched between TssA proteins of the same long or short subgroup. To test whether any of the chimeric TssA proteins were functional within the H2-T6SS, each of the six chimeric proteins containing TssA2 domains were introduced into a *tssA2* background and H2-T6SS activity was assessed.

The lack of Hcp2 secretion in the absence of *tssA2* was restored with the constitutive expression of wildtype *tssA2* (Figure 5.6A). Hcp2 was also secreted, although at a lower level, with the constitutive expression of the two fusion constructs encoding the TssA2 Nt1 domain, $tssA2_{Nt1}tssA1_{CTD}$ or $tssA2_{Nt1}tssA3_{CTD}$. Similar was demonstrated in the interbacterial competition assay, where prey killing was restored with constitutive expression of wildtype *tssA2,* and partially restored with expression of $tssA2_{Nt1}tssA1_{CTD}$ or $tssA2_{Nt1}tssA3_{CTD}$ (Figure 5.6B). The visualisation of TssB2 sheaths through chromosomal fusion to mScarlet identified a barely detectable number of sheath structures in the absence of *tssA2*, this rose to 6.3 % upon introduction of *tssA2* and 4.4 % and 7.7 % upon introduction of $tssA2_{Nt1}tssA1_{CTD}$ and $tssA2_{Nt1}tssA3_{CTD}$ respectively (Figures 5.6C and D).

The H1- and H3-T6SS functional assays with chimeric TssA proteins identified that functionality with a specific T6SS required the Nt1 domain of the cognate TssA, but chimeric proteins were only functional with the exchange of domains between $TssA_S$ proteins (Figures 5.4 and 5.5). However, chimeric TssA proteins with the TssA2 Nt1 domain and C-terminal regions of $TssA_S$ proteins could restore some function in the H2-T6SS (Figure 5.6). This data suggests that the TssA2 Nt1 domains have a similar position when connected to a ring formed by the C-terminal domain of a $TssA_S$ protein compared to a ring formed by the Nt2 and C-terminal domains of a $TssA_L$ protein, which allows H2-T6SS activity to be maintained.

The functionality of chimeric TssA proteins indicates that TssA functionality depends on the oligomerisation of a ring structure, with Nt1 domains conferring specificity to the T6SS.

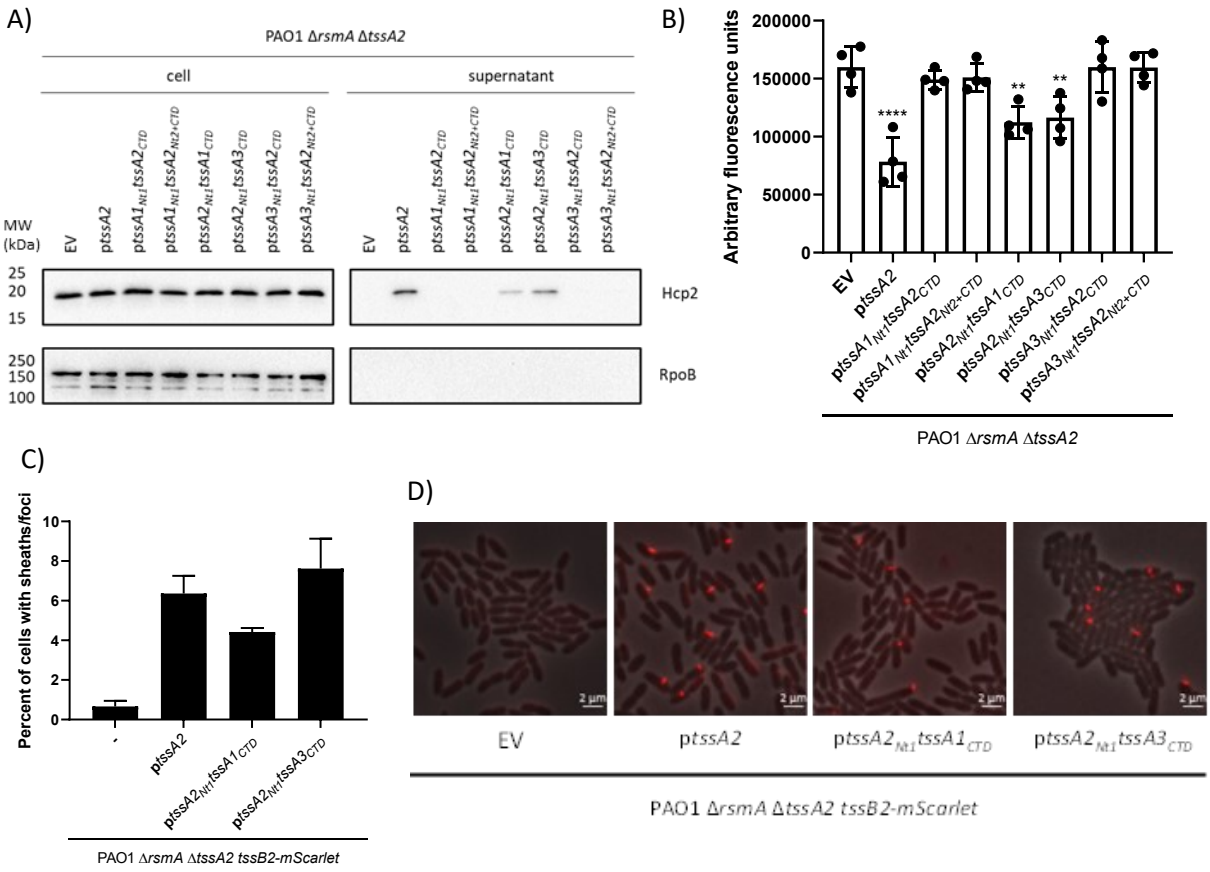


Figure 5.6 Assessment of H2-T6SS activity with chimeric TssA proteins. To assess complementation of the *tssA2* deletion, the pBBR1MCS4 vector was introduced either as empty vector (EV), encoding *tssA2* (ptssA2) or chimeric *tssAs*. Values are presented as means and error bars represent the standard deviation. A) Western blot of a H2-T6SS secretion assay to assess the levels of secretion marker Hcp2 in the supernatant sample. Cell and supernatant samples were harvested after 18 hours growth at 25 °C. Proteins detected in the western blot are indicated to the right. MW markers (left) are in kDa. RpoB was used as a loading and bacterial lysis control. B) H2-T6SS competition assay to assess the T6SS-dependent killing of a GFP-encoding *E. coli* prey by *P. aeruginosa* attacker strains. Attacker *P. aeruginosa* and prey *E. coli* were incubated at 25 °C for 24 hours before GFP signal quantification. Statistical testing was conducted by one-way ANOVA with Dunnett's multiple comparisons test, each strain was compared to parental *tssA2* strain (** $p < 0.01$, **** $p < 0.0001$). (n=4). C) Quantification of the percent of cells with TssB2-mScarlet sheaths or foci seen by fluorescence microscopy. Strains were grown on LB agar pads for 5-6 hours at 25 °C before imaging. The percent of cells with sheaths or foci was 0.64 % (n=9920) in the absence of *tssA2*, upon introduction of *tssA2* on a plasmid this rose to 6.3 % (n=5412). Upon introduction of chimeric $tssA2_{Nt1}tssA1_{CTD}$ or $tssA2_{Nt1}tssA3_{CTD}$, 4.4 % (n=4687) and 7.7 % (n=5387) of cells had sheaths or foci respectively. Data were taken from 3 fields of view for two experiments. D) Representative images of TssB2-mScarlet sheath formation. Scale bar represents 2 µm.

5.3.5 Chimeric TssA proteins with *P. putida* TssA domains are not functional in the H2-T6SS

The activity of the H1- and H3-T6SSs could be fully restored with chimeric TssA proteins where the C-terminal domain was exchanged for that of another $TssA_S$ protein (Figures 5.4 and 5.5). In comparison the H2-T6SS was functional, although only partially, with chimeric TssA proteins, however these chimeric proteins involved the exchange of the long TssA2 Nt2 and C-terminal domains for the C-terminal domains of $TssA_S$ proteins (Figure 5.6).

To assess whether exchange of domains with another $TssA_L$ protein would allow full restoration of H2-T6SS activity, $TssA_L$ proteins from *P. putida* were used to generate chimeras. *P. putida* contains three T6SS gene clusters (K1- to K3-T6SS), where only the K1-T6SS machinery has been demonstrated to be active (324). This K1-T6SS machinery is associated with a $TssA_S$, while the K2- and K3-T6SS are associated with $TssA_L$ proteins. These *P. putida* TssA2 ($TssA2^{PP}$) and TssA3 ($TssA3^{PP}$) proteins have 77 % sequence identity and were both used to generate chimeric TssA proteins with TssA2 (324). To generate these cross-species chimeric TssA proteins, the TssA2 Nt1 domain was linked to the Nt2 and C-terminal domains of either $TssA2^{PP}$ or $TssA3^{PP}$, producing chimeric TssA proteins with exclusively $TssA_L$ domains (Figure 5.7).

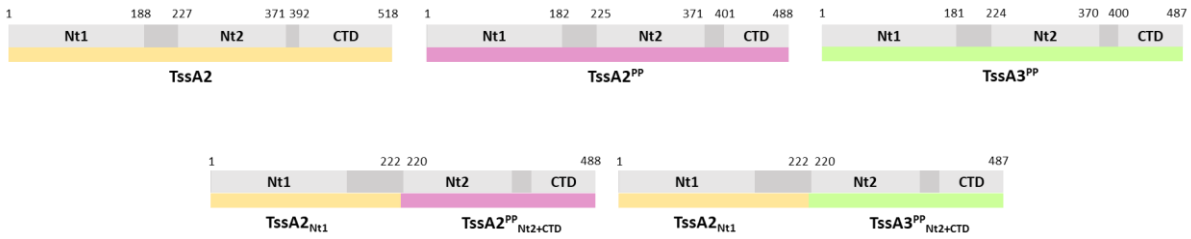


Figure 5.7 Schematic of chimeric *P. putida* TssA proteins engineered. The Nt2 and C-terminal domains (CTDs) of the long *P. putida* TssA proteins, $TssA2^{PP}$ and $TssA3^{PP}$, were exchanged with those of TssA2 to generate two chimeric TssA proteins comprised of solely $TssA_L$ domains.

It was then tested whether these cross-species chimeric TssA proteins were functional in the H2-T6SS. The functionality of the full-length *P. putida* proteins was also tested. In a secretion assay, only the constitutive expression of *tssA2* could restore the secretion of Hcp2 (Figure 5.8A). Neither the native *P. putida* $TssA_L$ proteins, or the chimeric TssA proteins with the TssA2 Nt1 domain were functional in the H2-T6SS. Similar was demonstrated in the interbacterial competition assay where prey killing was restored with constitutive expression of *tssA2,* but not with expression of either *P. putida* $TssA_L$ proteins or the chimeric TssA proteins (Figure 5.8B).

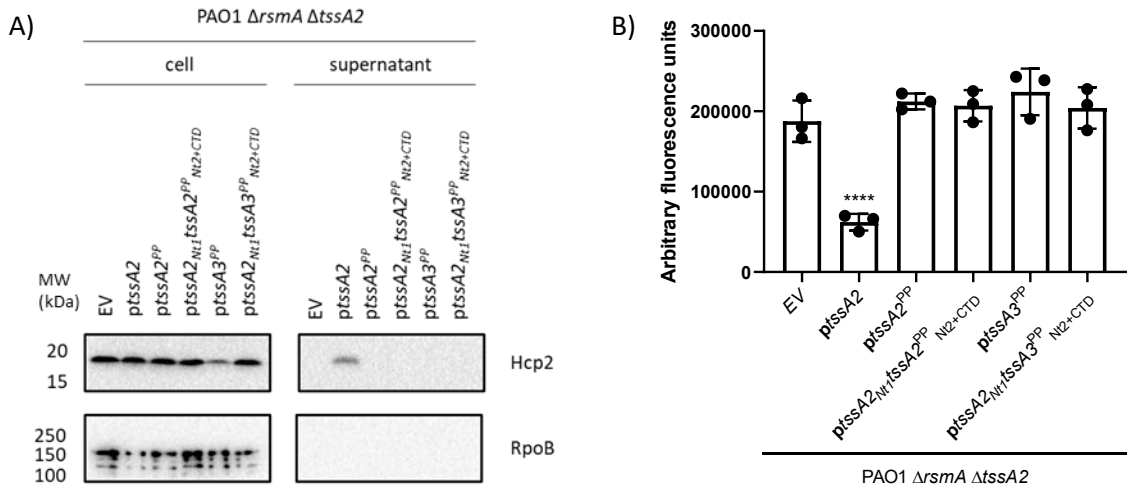


Figure 5.8 Assessment of H2-T6SS activity with chimeric TssA proteins with *P. putida* domains. To assess complementation of the *tssA2* deletion, the pBBR1MCS4 vector was introduced either as empty vector (EV), encoding *tssA2* (ptssA2) or chimeric *tssAs*. A) Western blot of a H2-T6SS secretion assay to assess the levels of secretion marker Hcp2 in the supernatant sample. Cell and supernatant samples were harvested after 18 hours growth at 25 °C. Proteins detected in the western blot are indicated to the right. MW markers (left) are in kDa. RpoB was used as a loading and bacterial lysis control. B) H2-T6SS competition assay to assess the T6SS-dependent killing of a GFP-encoding *E. coli* prey by *P. aeruginosa* attacker strains. Attacker *P. aeruginosa* and prey *E. coli* were incubated at 25 °C for 24 hours before recovery and GFP signal quantification. Values are presented as means and error bars represent the standard deviation. Statistical testing was conducted by one-way ANOVA with Dunnett's multiple comparisons test, each strain was compared to parental *tssA2* strain (**** $p < 0.0001$). (n=3).

Chimeric TssA proteins formed solely from $TssA_L$ sub-domains with exchanged C-terminal regions taken from *P. putida* TssA proteins were not functional in the H2-T6SS (Figure 5.8). The T6SS gene clusters that these TssA proteins are encoded in have not been demonstrated to have any T6SS activity. Indeed, two genes in the K2-T6SS cluster encoding essential structural proteins, TssC2 and VgrG2, have premature stop codons, suggesting that this T6SS is not functional (324). It is possible that neither of these gene clusters encode a functional T6SS and therefore the *tssA* genes used to generate these chimeric proteins may not be functional or even form properly folded proteins. The fold and stability of these proteins could be validated in the future by using a BTH approach. If $TssA2^{PP}$ and $TssA3^{PP}$ are indeed non-functional, this could explain why these cross-species chimeric TssA proteins failed to contribute to H2-T6SS activity. A long TssA protein from an organism where T6SS activity has been demonstrated, i.e. $TssA^{EC}$ or $TssA^{VC}$, may be more appropriate to conclusively answer

this question. Alternatively, these chimeric proteins may not be functional because they are taken from another organism. If the non-cognate interactions of TssA proteins previously identified (Figure 4.24) do play a role in the functionality of these chimeric TssA proteins, domains from another organism may not interact with the *P. aeruginosa* T6SSs.

5.4 Characterising interaction specificity of TssA protein domains

Specific contributions of TssA domains to interactions were previously identified: the C-terminal domains are involved in self-interaction, driving oligomerisation into ring-shaped structures, while Nt1 domains interact with sheath components (Figures 4.20 and 4.21). Interactions between the different TssA proteins, and with components associated to different T6SSs have also been demonstrated (Figures 4.23 and 4.24), however, the activity of each TssA protein is specific to the cognate T6SS (Figures 4.25, 4.26, 4.27). Remarkably, in switching the Nt1 domain, the T6SS specificity of a TssA protein can be altered (Figures 5.4, 5.5 and 5.6). To better understand how the specificity of TssA proteins is achieved, the interactions of TssA domains with components from different T6SSs were characterised in more detail.

5.4.1 Nt1 domains interact specifically with their respective sheath components

A BTH approach was used to investigate the specificity of the interactions between TssA Nt1 domains and sheath components encoded in different T6SS clusters. This identified that despite full length TssA proteins being able to interact with non-cognate sheath components (Figure 4.24), the interactions of the Nt1 domains in isolation was very specific. Each Nt1 domain interacted exclusively with its respective sheath components, while TssA C-terminal regions did not interact with sheath components (Figure 5.9).

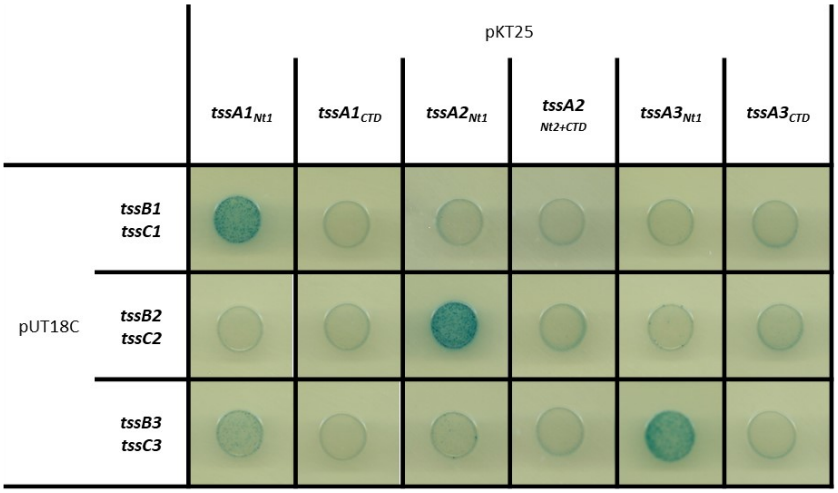


Figure 5.9 Interactions of TssA domains with sheath components. BTH with N-terminal T25 (pKT25) linked TssA domains and N-terminal T18 (pUT18C) linked sheath components produced in DHM1 cells. Representative spots grown for 40 hours on X-Gal LB agar are shown. Blue spots indicate protein-protein interaction, spots are white in the absence of interaction.

This supports functional characterisation of chimeric proteins, in implicating Nt1 domains in the specific interaction with the sheath.

5.4.2 C-terminal domains specifically self-interact

The other TssA interaction that was previously linked to a specific domain was self-interaction, which was shown to be mediated by C-terminal regions (Figure 4.21). Interactions between full length TssA proteins belonging to different T6SSs were also demonstrated (Figure 4.23).

The interactions between different TssA domains were investigated using BTH. This identified that despite cross-interactions being identified between full length TssA proteins (Figure 4.23), interactions of individual C-terminal regions were very specific. There was self-interaction of TssA C-terminal regions, but no other interactions between TssA domains (Figure 5.10).

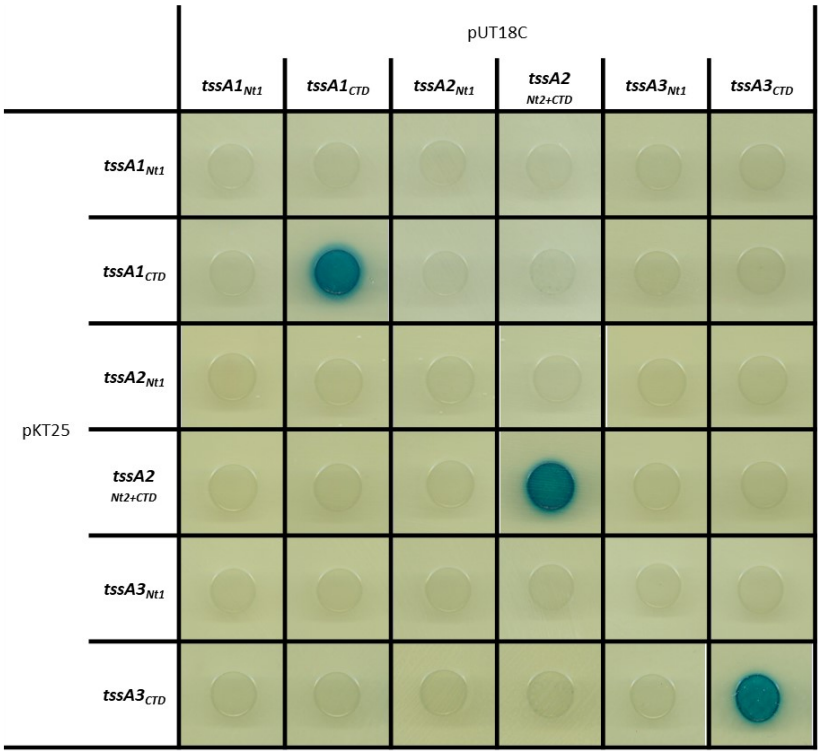


Figure 5.10 Interactions between TssA domains. BTH with N-terminal T25 (pKT25) and T18 (pUT18C) linked TssA domains produced in DHM1 cells. Representative spots grown for 40 hours on X-Gal LB agar are shown. Blue spots indicate protein-protein interaction, spots are white in the absence of interaction.

For both interactions between TssA proteins and interactions with sheath components, specific cognate interactions were demonstrated for TssA domains (Figures 5.9 and 5.10). However, this

contrasted with a lack of specificity previously identified in the interactions of the full-length TssA proteins (Figure 4.23 and 5.24). While full length TssA proteins were able to interact with components encoded in different T6SS clusters, TssA domains interacted very specifically with components from their own T6SS cluster. This suggests that the interactions of TssA proteins with components encoded in different T6SS clusters are not analogous to the interactions with cognate T6SS components, which may explain why there is no functional heterologous complementation between TssA proteins (Figures 4.25, 4.26, 4.27). The interaction specificity observed in these BTH experiments appears to have functional significance, given that exchanging the Nt1 domain of a short TssA protein alters the functional specificity of the chimeric TssA to the T6SS associated with the Nt1 domain. It is unclear why full length TssA proteins could be identified to interact with non-cognate TssA and sheath components when interactions of the domains in isolation are very specific.

5.4.3 T6SS activity is unaffected by the expression of Nt1 domains

The TssA Nt1 domains interact very specifically with their respective sheath components (Figure 5.9). To test whether the interactions of Nt1 domains in isolation might impair the activity of the T6SS through competitive binding to the sheath, interbacterial competition experiments were carried out with the overexpression of Nt1 domains on plasmids. For both the H1- and H2-T6SS, the overexpression of the respective TssA Nt1 domain did not have any effect on the ability to kill prey (Figure 5.11). This suggests that these domains were not outcompeting full length, chromosomally encoded TssA proteins for binding to the sheath. However, chromosomally encoded proteins may preferentially interact with other components of their T6SS due to their co-translation from polycistronic mRNAs. Alternatively, in the absence of a C-terminal domain ring to coordinate the position of multiple Nt1 domains, a functionally significant interaction of the Nt1 domains with other T6SS components may not be detected.

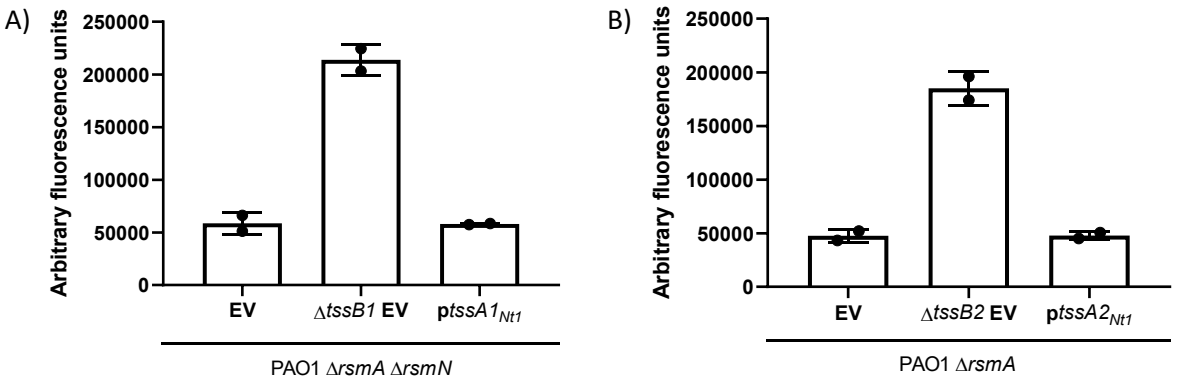


Figure 5.11 Assessment of T6SS activity with overproduction of Nt1 domains. Competition assays to assess the T6SS-dependent killing of a GFP-encoding *E. coli* prey by *P. aeruginosa* attacker strains. To assess T6SS activity in the presence of Nt1 domains, the pBBR1MCS4 vector was introduced either as empty vector (EV) or encoding the respective Nt1 domain. Values are presented as means and error bars represent the standard deviation. A) H1-T6SS competition assay, attacker *P. aeruginosa* and prey *E. coli* were mixed and incubated at 37 °C for 24 hours before GFP signal quantification. (n=2). B) H2-T6SS competition assay, attacker *P. aeruginosa* and prey *E. coli* were incubated at 25 °C for 24 hours before GFP signal quantification. (n=2).

5.5 Structural characterisation of TssA protein C-terminal domains

A key difference in long and short TssA proteins is in the ring-shaped structures that are formed through the oligomerisation of the C-terminal domains (see section 1.4.1). Several high-resolution structures are available for the C-terminal domains of $TssA_L$ proteins (360,377,509), while a single high-resolution structure is available for the C-terminal domain of a $TssA_S$ protein (509). Some structural characterisation was previously carried out on TssA1, allowing the visualisation of the ring structure and estimation of ring dimensions, but no high-resolution data was obtained (Figure 1.18) (376).

It has been demonstrated that these C-terminal domains can be exchanged between *P. aeruginosa* TssA proteins, with chimeric proteins formed retaining functionality (Figures 5.4, 5.5 and 5.6). To understand the variation introduced in chimeric proteins, attempts were made to elucidate the ring structure, dimensions and symmetries generated by each of the TssA C-terminal domains. Overexpression constructs were therefore engineered for protein purification and subsequent structural analysis.

5.5.1 TssA C-terminal domains can be stably produced

Initially full length *tssA* genes were introduced into expression constructs, and while proteins were well produced, there was also degradation into constituent domains. Therefore, subsequent protein production experiments focussed on TssA C-terminal domains, as the main contributor to structural variation between TssA proteins. The production of each of the TssA C-terminal domains with an N-terminal Strep-tag could be induced in *E. coli* (Figure 5.12). Production of the TssA3 C-terminal domain was less abundant than that of the other two constructs, possibly reflecting a reduced stability.

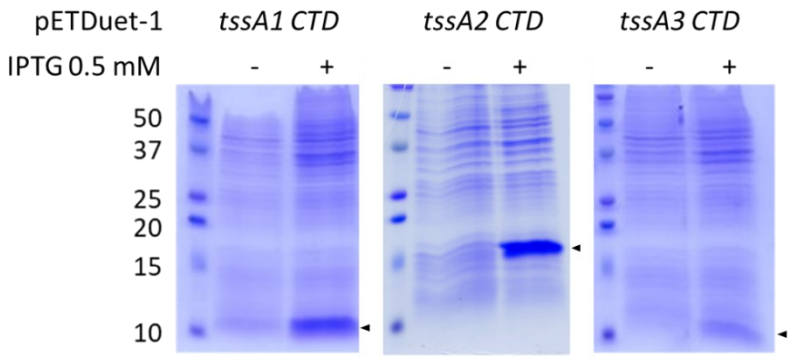


Figure 5.12 Production of TssA C-terminal domains. The production of TssA1 (~10 kDa), TssA2 (~17 kDa) and TssA3 (~10 kDa) C-terminal domains (CTDs) from the pETDuet-1 expression vector and induced with 0.5 mM IPTG. Desired protein bands indicated with black arrows.

5.5.2 TssA$_S$ C-terminal domains form rings with large internal lumens

The C-terminal domain constructs of the two TssA$_S$ proteins, TssA1 and TssA3 were produced and purified with a view to generating high-resolution structural data of oligomeric ring-shaped structures. Strep-tagged TssA$_S$ C-terminal domains were purified by affinity chromatography through specific binding to a Strep-Tactin resin, and then subject to gel filtration chromatography to separate from any impurities based on their size. Gel filtration of each of TssA1 and TssA3 C-terminal domains produced elution of a single peak, which was confirmed to contain high purity protein of the correct size (10 kDa) (Figure 5.13).

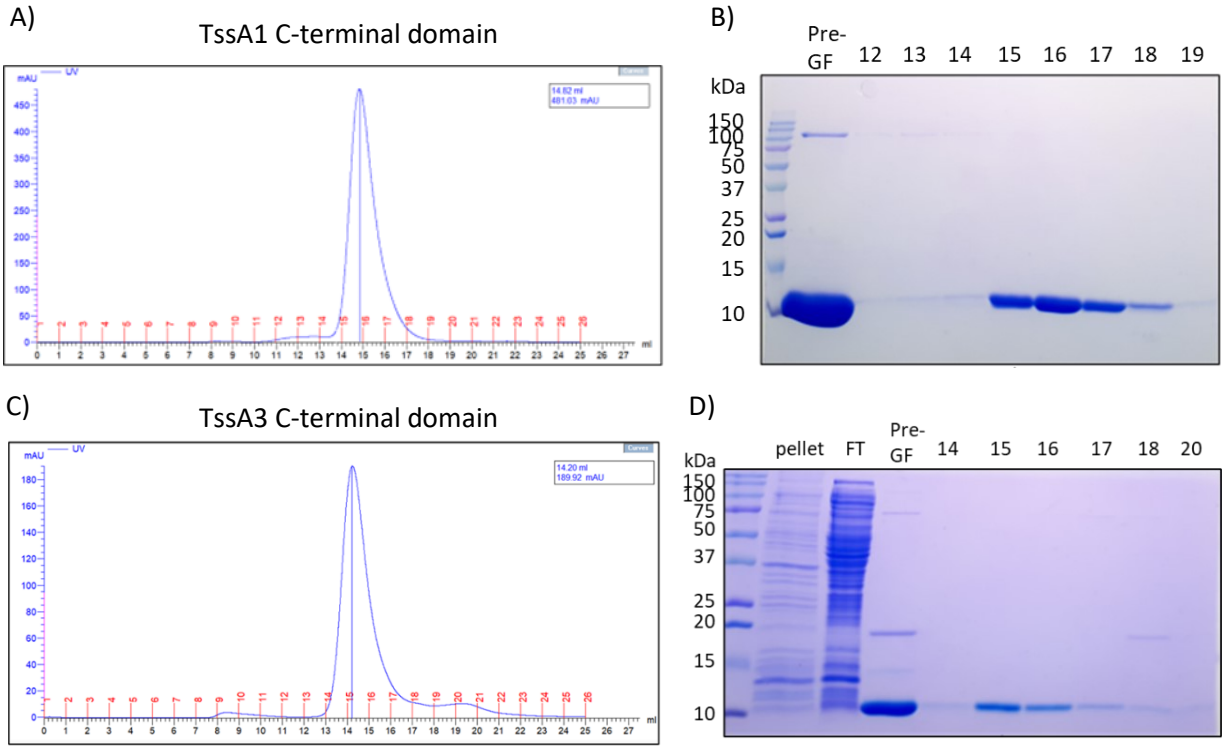


Figure 5.13 Gel filtration of TssA1 and TssA3 C-terminal domains. A) Gel filtration elution profile for TssA1 C-terminal domain. B) SDS-PAGE and Coomassie stain of TssA1 C-terminal domain purification samples, before gel filtration (Pre-GF) and samples from gel filtration elution fractions 12-19. C) Gel filtration elution profile for TssA3 C-terminal domain. D) SDS-PAGE and Coomassie stain of TssA3 C-terminal domain purification samples, from the pellet, the affinity chromatography flow through (FT), before gel filtration (Pre-GF) and samples from gel filtration elution fractions 14-20. Protein purification carried out by Patricia Paracuellos.

The high purity TssA1 and TssA3 C-terminal domain protein samples were then prepared on EM grids for negative stain EM. Both the TssA1 and TssA3 C-terminal domain complexes formed ring-shaped structures with a large internal lumen (Figure 5.14). These structures resemble rings formed by $TssA^{BC}$ that were collected by negative stain EM (Figure 1.18) (509). For TssA1 C-terminal domain rings in particular, a variety of particle orientations were present, including top views and side views, which is promising for future structural analysis.

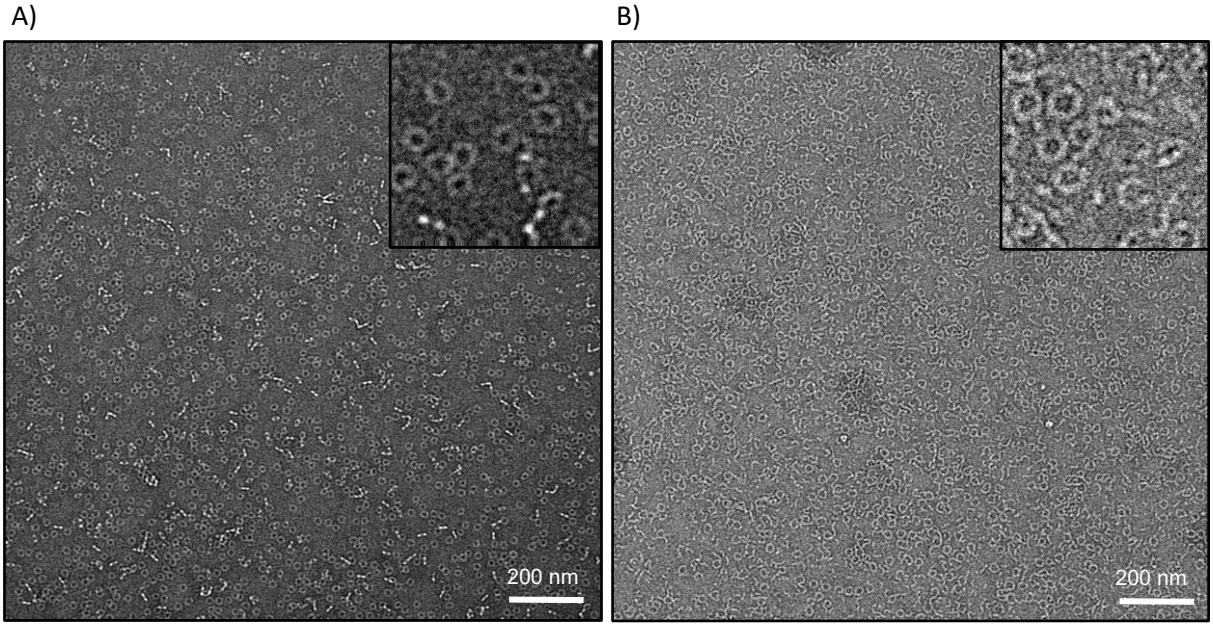


Figure 5.14 Negative stain EM grids of TssA1 and TssA3 C-terminal domains. A) Representative negative stain EM images of TssA1 C-terminal domain single particles. B) Representative negative stain EM images of TssA3 C-terminal domain single particles. Scale bars represent 200 nm. Sample preparation and imaging by Patricia Paracuellos and Tiago Costa.

The TssA1 C-terminal domain was imaged via cryogenic EM (cryo-EM), single particles of were picked and used to generate 2D class averages. From the 2D class averages it can be determined that the TssA1 C-terminal domain forms a very consistent ring structure (Figure 5.15A). At this stage it is not possible to determine the dimensions of this ring, but in previous structural characterisation the lumenal diameter was calculated to be 100 Å (376). From these class averages it is also difficult to estimate the symmetry of the ring, further high-resolution data will be required to resolve this.

To date only negative stain EM has been carried out with the TssA3 C-terminal domain. From this dataset, single particles were picked to generate 2D class averages (Figure 5.15B). Interestingly, these TssA3 C-terminal domain rings display quite a bit of flexibility and are less consistent in their dimensions when compared to the TssA1 C-terminal domain (Figure 5.15A). This maybe an inherent

feature of the TssA3 C-terminal domain ring or it may be linked to the absence of the Nt1 domain, although the Nt1 domain is also absent for the TssA1 C-terminal domain. The TssA3 C-terminal domain 2D class averages allow for an initial estimation of 12-fold symmetry for this ring, which requires future validation. As with the TssA1 C-terminal domain, the dimensions of this ring could not be accurately calculated at this time.

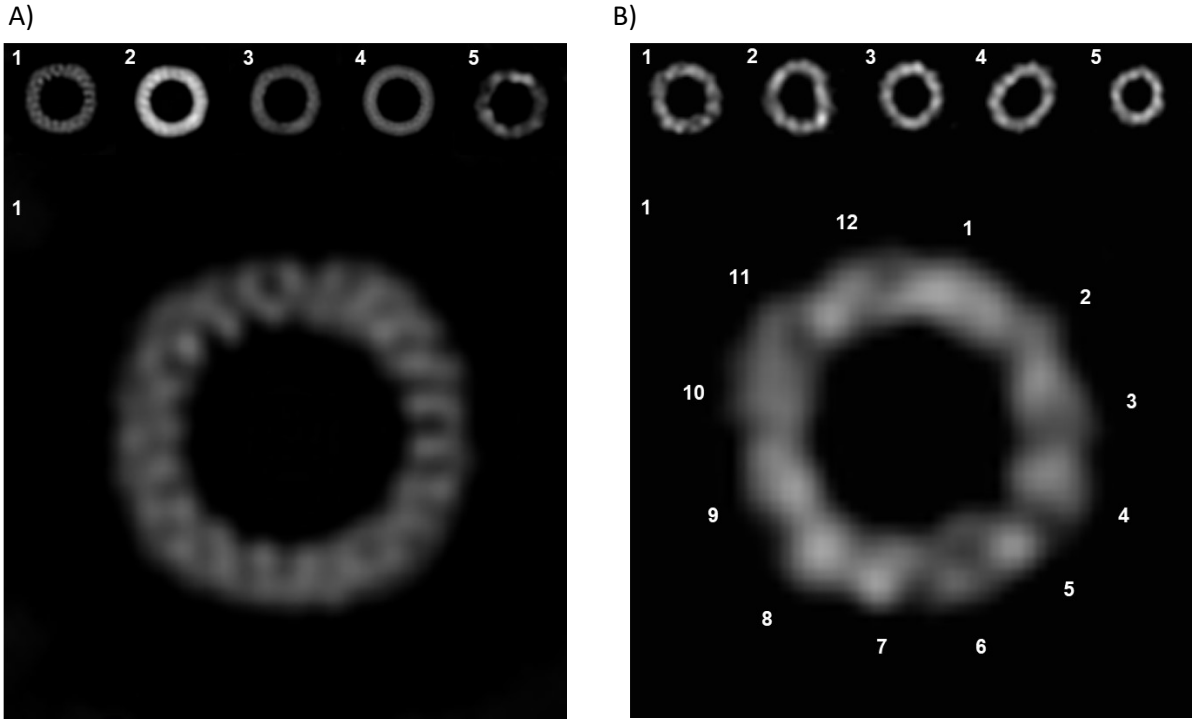


Figure 5.15 2D class averages of TssA1 and TssA3 C-terminal domains. A) Representative 2D class averages of TssA1 C-terminal domain particles picked from cryo-EM images. Class average 1 is enlarged (below). B) Representative 2D class averages of TssA3 C-terminal domain particles picked from negative stain EM images. Class average 1 is enlarged with proposed symmetric units annotated (below). Scale is not comparable between A) and B). Data analysis by Tiago Costa.

Further structural characterisation is ongoing by cryo-EM to generate high-resolution structural data on these C-terminal domain complexes, including conclusive characterisation of ring dimensions and oligomeric state.

These preliminary structural insights suggest that the ring-shaped structures formed by TssA1 and TssA3 C-terminal domain complexes follow the trends previously outlined for the structures of $TssA_S$ proteins, forming rings with a large internal lumen (509). Further high-resolution data is required to determine the degree of similarity between these C-terminal domain complexes, but the fact that they are functionally interchangeable in chimeric TssA proteins suggests there is some structural similarity.

5.5.3 The TssA2 C-terminal domain could not be purified with confidence

The C-terminal domain construct of the $TssA_L$ protein, TssA2 was also produced and purified with a view to generate high-resolution structural data. The purification was carried out as for the $TssA_S$ proteins described above. Affinity chromatography led to the elution of a protein with the correct size of ~17 kDa. Gel filtration of a sample containing this protein produced an elution profile with multiple peaks (Figure 5.16A). Samples of elution fractions representing different peaks were separated by SDS-PAGE, but the protein of interest could not be identified following Coomassie staining (Figure 5.16B).

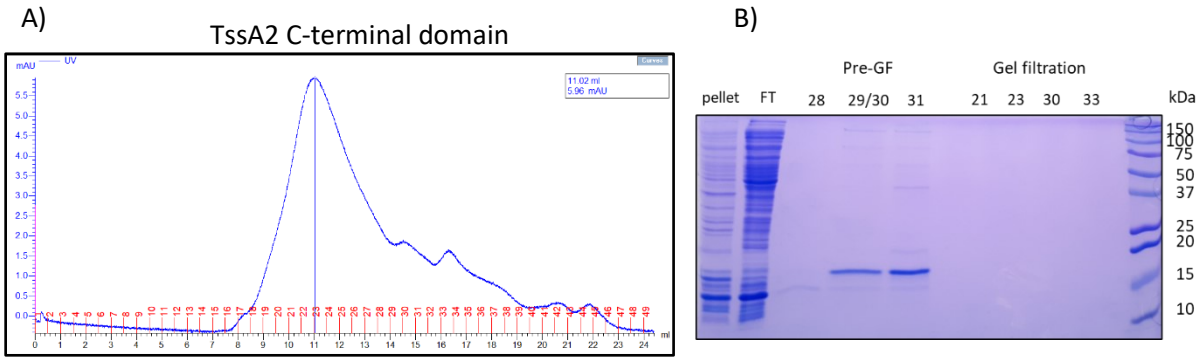


Figure 5.16 Gel filtration of TssA2 C-terminal domain. A) Gel filtration elution profile for TssA2 C-terminal domain. B) SDS-PAGE with Coomassie staining of TssA2 C-terminal domain purification samples, from the pellet, the affinity chromatography flow through (FT), samples from affinity fractions 28-31 before gel filtration (Pre-GF) and samples from gel filtration elution fractions 21, 23, 30 and 33. Protein purification carried out by Patricia Paracuellos.

It was suspected that the TssA2 C-terminal domain may be present in the gel filtration fractions at a low concentration that could not be visualised by Coomassie staining. Samples were therefore prepared on EM grids for negative stain EM. Some spherical densities were identified in the resultant images, however these varied in size (Figure 5.17). Defined ring-shaped structures similar to those previously identified for $TssA_L$ proteins could not be identified (360,377,509).

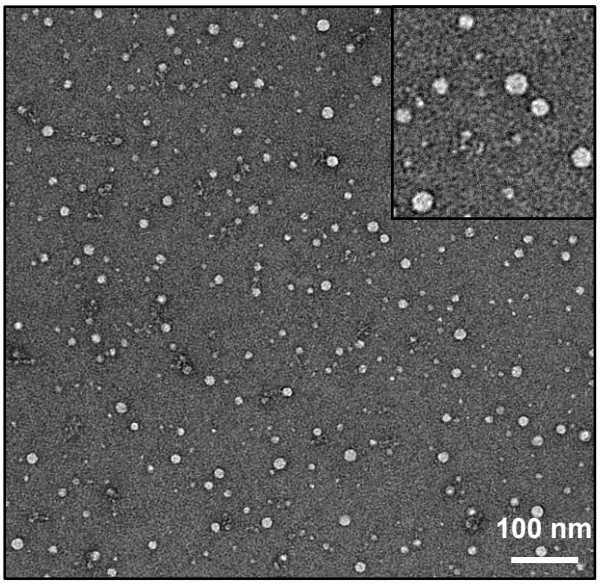


Figure 5.17 Negative stain EM grid of TssA2 C-terminal domain. Representative negative stain EM images. Scale bar represents 100 nm. Sample preparation and imaging by Patricia Paracuellos and Tiago Costa.

It is unclear whether the densities identified in the EM data correspond with TssA2 C-terminal domain, as this protein could not be conclusively identified in sample fractions eluted by gel filtration. Alternatively, they could be negative stain artefacts or non-specific aggregates. The TssA2 C-terminal domain could be produced and purified by affinity chromatography with some contaminants, however in attempting to isolate this from contaminants by gel filtration, the TssA2 C-terminal domain could not be specifically eluted. To generate high-resolution structural data, further optimisation of the purification protocol is thus required.

5.6 Identifying specificity determinants for the interaction between the Nt1 domain and the sheath

It has been identified that the three TssA proteins of *P. aeruginosa* are functionally specific to their cognate T6SS (Figures 4.25, 4.26 and 4.27). Investigating the functionality of chimeric TssA proteins, demonstrated that this specificity is conferred by the Nt1 domain (Figures 5.4, 5.5 and 5.6). Specifically, exchange of the $TssA_S$ Nt1 domains of TssA1 and TssA3 generated chimeric proteins that were fully functional with the T6SS associated with the Nt1 domain. The specificity of TssA proteins through their Nt1 domains was therefore investigated through direct comparison between TssA1 and TssA3 Nt1 domains.

5.6.1 Point mutants in the TssA1 Nt1 domain do not disrupt interaction with the sheath

To identify the differences in the Nt1 domains of TssA1 and TssA3 which may contribute to the specificity of sheath interactions, several approaches were used. It was hypothesised that specificity may be linked to non-conserved residues exposed on the surface.

To identify non-conserved residues, the sequences of the Nt1 domains were aligned using Clustal Omega (Figure 5.18A) (595). Using the model of the TssA1 Nt1 domain structure previously generated (Figure 4.12), the solvent accessible surface area was estimated, using GETAREA, residues assigned a value of over 80 % were considered to be solvent accessible (Figure 5.18B) (534). By cross-referencing these two datasets, 16 residues were identified that were both non-conserved between TssA1 and TssA3 Nt1 domains, and predicted to be surface exposed in the TssA1 Nt1 domain (D14, D19, M42, D44, D113, D116, R146, F167, S169, E170, D185, D187, R194, S216, Q218 and L238) (Figure 5.18C).

An initial seven of these residues were mutated to alanine, and interactions with wildtype TssA1 and the H1-T6SS sheath were assessed by BTH. Each of these TssA1 point mutants were able to interact with both wildtype TssA1 and the sheath components (Figure 5.18D). The interaction of TssA1 D116A with the sheath was possibly weaker than that of the other mutants, but this was not conclusive and lacks a control to compare to the wildtype interaction. This suggests that these mutations did not disrupt the overall fold of the protein, but also that none of these individual residues were essential for interaction with the sheath. It was therefore hypothesised that point mutations might not be sufficient, and that multiple residues may need to be altered to affect this interaction.

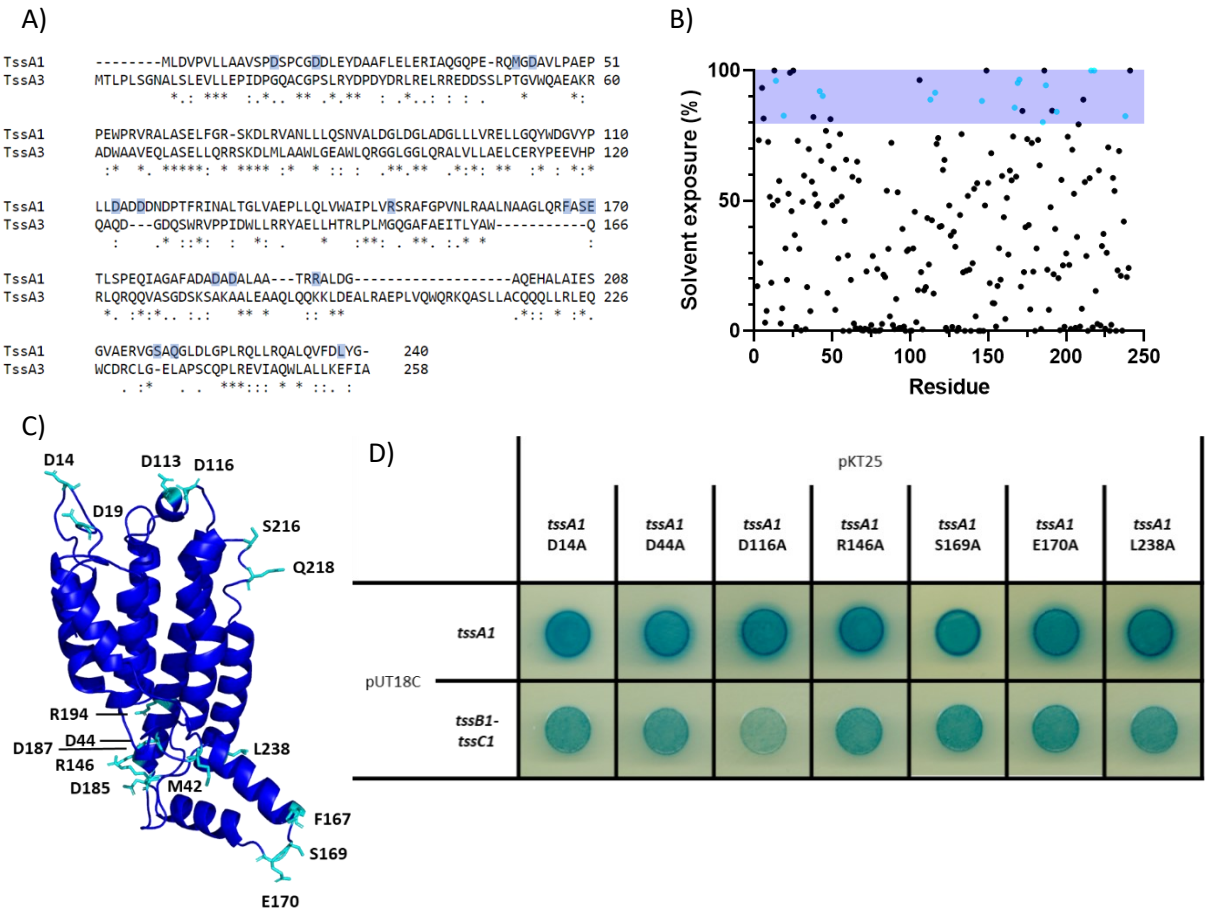


Figure 5.18 Identification and screening of candidate TssA1 Nt1 domain residues for sheath interaction. A) Pairwise sequence alignment between the Nt1 domains of TssA1 and TssA3, generated using Clustal Omega. Non-conserved, surface exposed residues highlighted in light blue. B) Predicted solvent accessibility of TssA1 Nt1 domain residues based on the structural model using GETAREA. A solvent exposure value over 80 %, blue box, was considered surface exposed. Non-conserved, surface exposed residues highlighted in light blue. C) Position of non-conserved, surface exposed residues (light blue) in a predicted model of the TssA1 Nt1 domain structure. D) BTH with N-terminal T25 (pKT25) linked TssA1 point mutants and N-terminal T18 (pUT18C) linked TssA1, and sheath components produced in DHM1 cells. Representative spots grown for 24 hours on X-Gal LB agar are shown. Blue spots indicate protein-protein interaction, spots are white in the absence of interaction.

5.6.2 The structural differences between TssA1 and TssA3 Nt1 domain models arise in two regions

When comparing the structural models generated for the TssA1 and TssA3 Nt1 domains using the Dali structural alignment server, the overall fold is predicted to be very similar with an RMSD of 1.7 Å (536).

This is not particularly surprising, given the high level of sequence identity and that both structural models were generated based on the structure of the TssA^{BC} Nt1 domain (509). The high degree of similarity in the models could be demonstrated in a structural alignment between these two models (Figure 5.19A). However, the alignment also identified two regions of varied structure between the two Nt1 domain models, named the hairpin and the loop (Figure 5.19B).

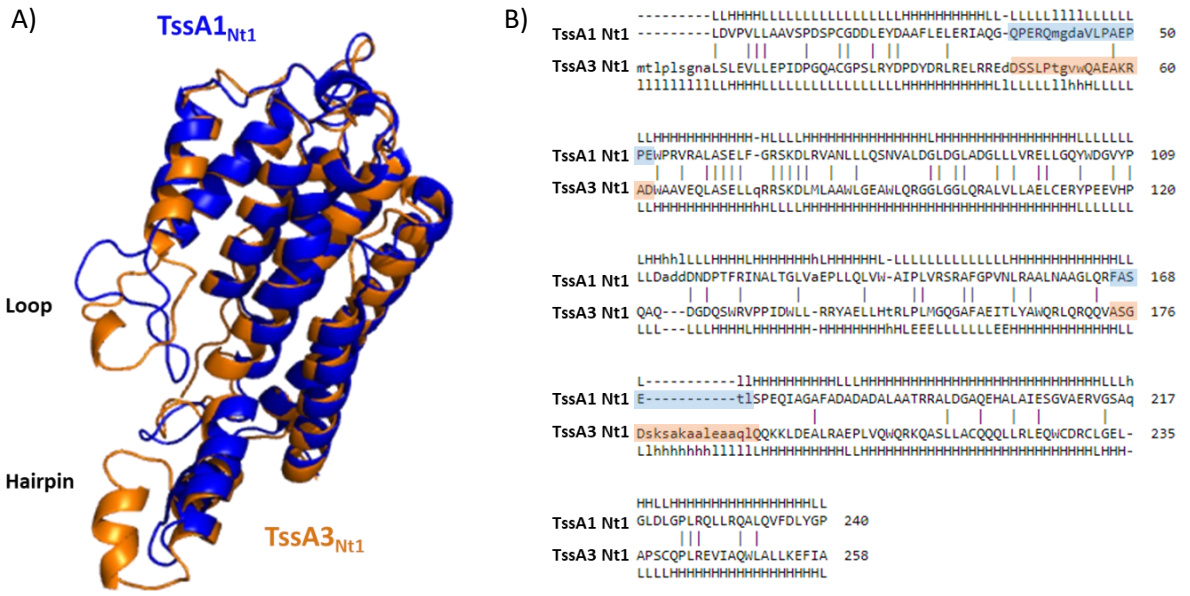


Figure 5.19 TssA1 and TssA3 Nt1 domain models. A) Structural models for the TssA1 Nt1 domain (blue) and TssA3 Nt1 domain (orange) generated using the Robetta protein structural prediction service were aligned based on structural similarity. Structural differences were identified in two regions named the hairpin and the loop region. B) The sequences of TssA1 and TssA3 Nt1 domains were aligned based on structural similarity using the Dali structural alignment server. The loop and hairpin regions that were identified as differing between the structures were highlighted in blue for TssA1 and orange for TssA3.

5.6.3 Introducing the TssA3 hairpin or loop regions into TssA1 impairs sheath interaction and secretion

The hairpin and loop regions were therefore predicted to be responsible for introducing structural variation between the TssA1 and TssA3 Nt1 domains, which was hypothesised to account for the specificity in sheath interaction. To assess if these regions in TssA1 were conferring any specificity to the H1-T6SS, the hairpin and loop sequences of TssA1 were exchanged for those of TssA3 individually and in combination.

Upon the introduction of both hairpin and loop sequences from *tssA3* into *tssA1*, the resultant protein was unable to interact with either TssA1 or the H1-T6SS sheath by BTH, suggesting it did not form a folded protein (Figure 5.20). Individually, the introduction of TssA3 hairpin or loop regions into the TssA1 Nt1 domain disrupted interaction with the H1-T6SS sheath but interaction with TssA1 was unaffected.

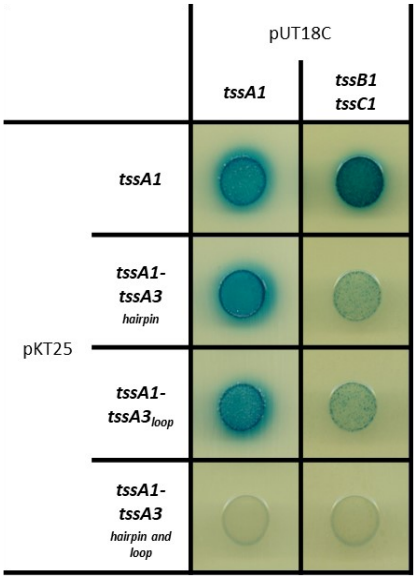


Figure 5.20 Interactions of TssA1 proteins with TssA3 hairpin or loop regions introduced. BTH with N-terminal T25 (pKT25) linked TssA1 with TssA3 hairpin and/or loop regions and N-terminal T18 (pUT18C) linked TssA1 and sheath components produced in DHM1 cells. Representative spots grown for 40 hours on X-Gal LB agar are shown. Blue spots indicate protein-protein interaction, spots are white in the absence of interaction.

These TssA1 proteins with TssA3 hairpin or loop regions were then introduced into a *P. aeruginosa* strain to assess their functional contribution to H1-T6SS activity. In a secretion assay, the secretion of Hcp1 was similar when a *tssA1* deletion was complemented with either *tssA1* or *tssA1-tssA3*$_{hairpin}$, but secretion was much lower with introduction of *tssA1-tssA3*$_{loop}$ (Figure 5.21A). However, in an interbacterial competition assay, the killing of an *E. coli* prey was not significantly different with introduction of either wildtype *tssA1* or *tssA1* with *tssA3* sequences, suggesting that each of these TssA proteins was able to interact functionally with the T6SS leading to T6SS-dependent prey killing (Figure 5.21B). Visualisation of H1-T6SS sheaths with a fluorophore tagged sheath component identified that a similar proportion of cells formed sheath structures when a *tssA1* deletion was complemented with either *tssA1* or *tssA1-tssA3*$_{hairpin}$, but this proportion was lower with introduction of *tssA1-tssA3*$_{loop}$ (Figures 5.21C and D).

Both the introduction of TssA3 hairpin and loop regions into the TssA1 Nt1 domain led to a weaker interaction with H1-T6SS components, but this did not necessary correlate with a reduction in H1-T6SS activity (Figure 5.20). While the introduction of the TssA3 loop region reduced the abundance of H1-T6SS sheath structures and the level of secretion, this did not affect the efficiency of *E. coli* prey killing by the H1-T6SS (Figures 5.21). It is curious that a reduced sheath abundance and level of secretion did not correlate with a reduced killing efficiency. With fewer H1-T6SS sheath structures formed, it would be expected that a reduced effector payload would be delivered to prey cells. However, even with reduced sheath formation and secretion, the effector payload delivered may still be sufficient to kill prey cells, due to the sensitivity of this assay.

The exchange of the loop region of TssA1 for that of TssA3 did therefore lead to a reduced H1-T6SS activity, suggesting that this region may confer some specificity. The hairpin region on the other hand seemed to have less of an effect, although sheath interaction was affected.

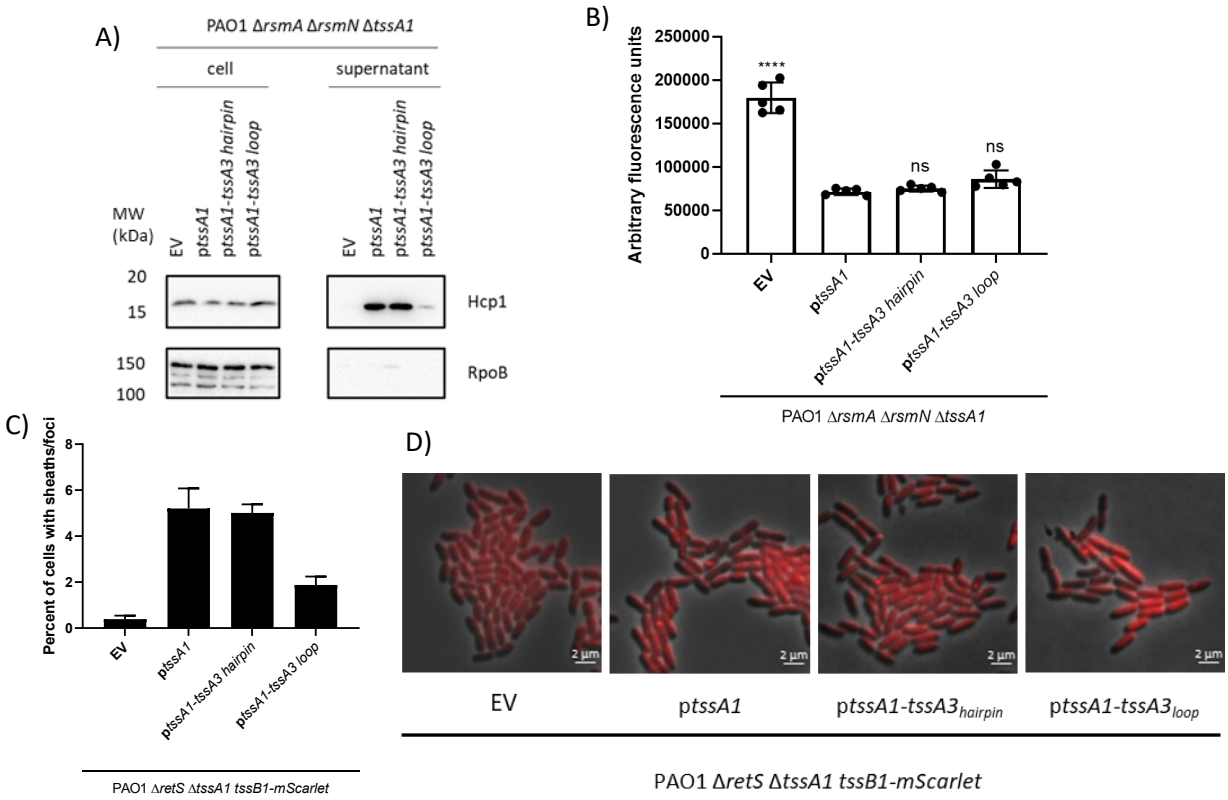


Figure 5.21 Assessment of H1-T6SS activity with TssA1 with TssA3 hairpin or loop regions introduced. To assess complementation of the *tssA1* deletion, the pBBR1MCS4 vector was introduced either as empty vector (EV), encoding *tssA1* (ptssA1) or *tssA1* with *tssA3* sequences. Values are presented as means and error bars represent the standard deviation. A) Western blot of a H1-T6SS secretion assay, to assess the levels of secretion marker Hcp1 in the supernatant sample. Cell and supernatant samples were harvested after 5-7 hours growth at 37 °C. Proteins detected in the western blot are indicated to the right. MW markers (left) are in kDa. RpoB was used as a loading and bacterial lysis control. B) H1-T6SS competition assay to assess the T6SS-dependent killing of a GFP-encoding *E. coli* prey by *P. aeruginosa* attacker strains. Attacker *P. aeruginosa* and prey *E. coli* were mixed and incubated at 37 °C for 24 hours before GFP signal quantification. Statistical testing was conducted by one-way ANOVA with Dunnett's multiple comparisons test, each strain was compared to complemented p*tssA1* strain (ns=not statistically significant, **** $p < 0.0001$). (n=5). C) Quantification of the percent of cells with TssB1-mScarlet sheaths or foci by fluorescence microscopy. Strains were grown on LB agar pads for 3-4 hours at 37 °C before imaging. The percent of cells with sheaths or foci was 0.37 % (n=10017) with *tssA1* deletion, upon introduction of *tssA1* on a plasmid this rose to 4.95 % (n=8117). Upon introduction of *tssA1-tssA3*$_{hairpin}$ 5.02 % (n=10683) of cells formed sheaths or foci, this was 1.87 % (n=9471) for introduction of *tssA1-tssA3*$_{loop}$. Data were taken from 3 fields of view for two experiments. D) Representative images of TssB1-mScarlet sheath formation. Scale bar represents 2 µm.

5.6.4 Introducing the TssA1 hairpin or loop regions into TssA3 impairs sheath interaction and polymerisation

It was also assessed whether H3-T6SS activity was affected by these hairpin and loop sequences. The hairpin and loop sequences of *tssA3* were exchanged for those of *tssA1* both individually and in combination. Upon the introduction of the TssA1 hairpin regions into TssA3, there was weaker interaction with H3-T6SS sheath components, while this interaction was completely lost with introduction of the TssA1 loop region either alone or in combination with the hairpin region (Figure 5.22).

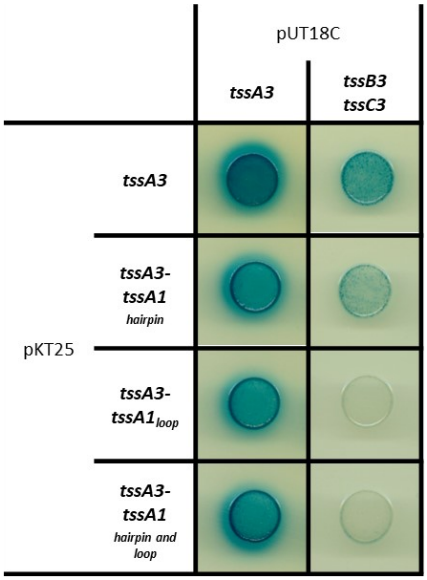


Figure 5.22 Interactions of TssA3 proteins with TssA1 hairpin or loop regions introduced. BTH with N-terminal T25 (pKT25) linked TssA3 with TssA1 hairpin or loop regions and N-terminal T18 (pUT18C) linked TssA3 and H3-T6SS sheath components produced in DHM1 cells. Representative spots grown for 40 hours on X-Gal LB agar are shown. Blue spots indicate protein-protein interaction, spots are white in the absence of interaction.

These TssA3 proteins with TssA1 hairpin and/or loop regions were then introduced into a *P. aeruginosa* strain to assess their functional contribution to H3-T6SS activity. The formation of H3-T6SS sheaths was visualised in the absence of *tssA3* with a fluorophore tagged sheath component. While almost a third of cells formed sheath structures when *tssA3* was introduced, this abundance was much reduced upon introduction of *tssA3* with *tssA1* hairpin or loop sequences and fell to almost no sheath structures when both sequences were replaced (Figure 5.23). Both hairpin and loop regions therefore seem to be required for the activity of TssA3.

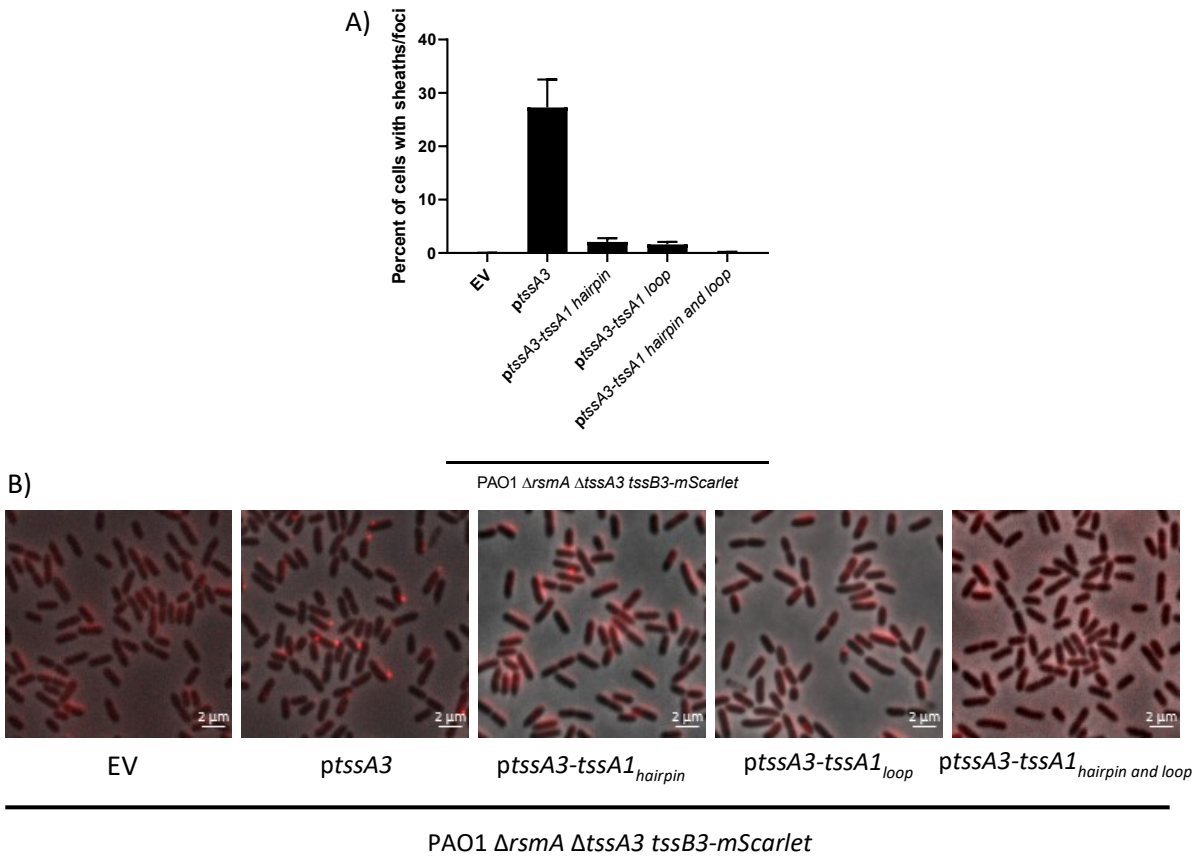


Figure 5.23 Assessment of H3-T6SS sheath formation with TssA3 with TssA1 hairpin or loop regions introduced. To assess complementation of the *tssA3* deletion, the pBBR1MCS4 vector was introduced either as empty vector (EV), encoding *tssA3* or *tssA3* with *tssA1* sequences. A) Quantification of the percent of cells with TssB3-mScarlet sheaths or foci by fluorescence microscopy. Strains were grown in liquid culture at 25 °C for 13 hours before imaging. The percent of cells with sheaths or foci was 0.036 % (n=16822) in the absence of *tssA3*, this rose to 27.2 % (n=16253) with expression of *tssA3* on a plasmid. Upon introduction of *tssA3-tssA1*$_{hairpin}$, *tssA3-tssA1*$_{loop}$ and *tssA3-tssA1*$_{hairpin\ and\ loop}$ sheath structures were detectable in 2.3 % (n=10760), 1.6 % (n=13968) and 0.078 % (n=11530) of cells respectively. Data were taken from 3 fields of view for two experiments. Values are presented as means and error bars represent the standard deviation. B) Representative images of TssB3-mScarlet sheath formation. Scale bar represents 2 µm.

5.6.5 Exchange of hairpin and loop regions does not lead to gain of function

Exchange of TssA3 hairpin and loop regions with those from TssA1 generated TssA proteins that lost interaction with H3-T6SS sheath components and were not functional within the H3-T6SS (Figures 5.22 and 5.23). In theory, the introduction of these regions made the TssA3 Nt1 domain more similar to the TssA1 Nt1 domain. To test whether this TssA might therefore associate with the H1-T6SS rather

than the H3-T6SS, interactions with H1-T6SS components and H1-T6SS functional assays were carried out.

Introduction of *tssA1* hairpin and loop sequences into *tssA3* did not lead to interaction of the generated protein with H1-T6SS sheath components (Figure 5.24A). Interaction was identified with TssA1, which was not surprising given the cross-interaction of TssA proteins previously identified (Figure 4.23). These TssA3 proteins with TssA1 regions were also unable to complement the deletion of *tssA1* in the activity of the H1-T6SS (Figure 5.24B), indicating that introducing TssA1 regions into the TssA3 Nt1 domain was not sufficient for a switch in the specificity of TssA3 to the H1-T6SS.

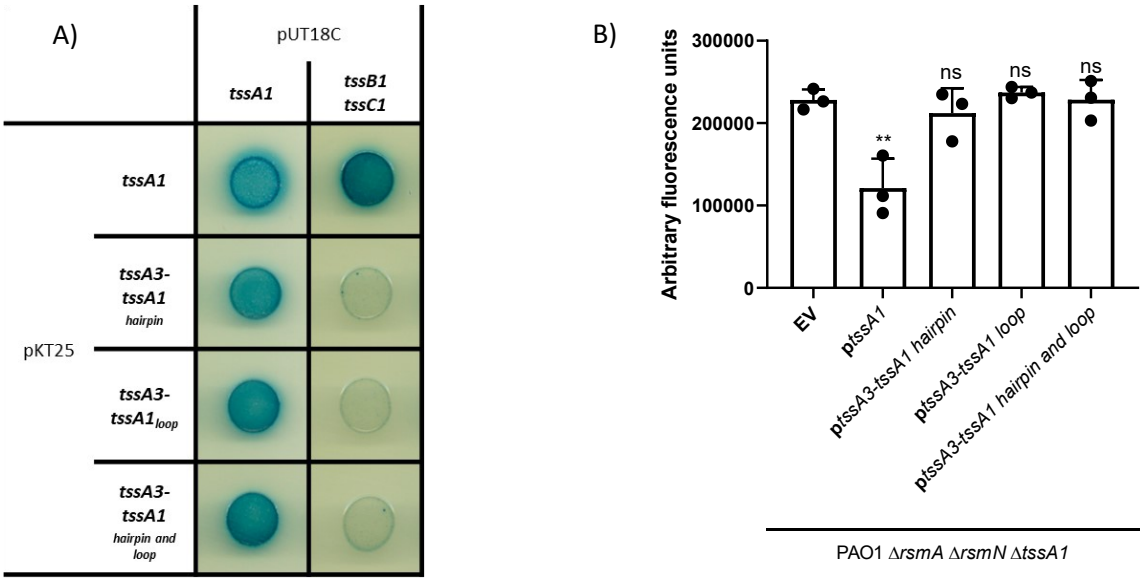


Figure 5.24 Assessment of the H1-T6SS association of TssA3 with TssA1 hairpin or loop regions introduced. A) BTH with N-terminal T25 (pKT25) linked TssA3 with TssA1 hairpin and/or loop regions and N-terminal T18 (pUT18C) linked TssA1 and sheath components produced in DHM1 cells. Representative spots grown for 40 hours on X-Gal LB agar are shown. Blue spots indicate protein-protein interaction, spots are white in the absence of interaction. B) H1-T6SS competition assay to assess the T6SS-dependent killing of a GFP-encoding *E. coli* prey by *P. aeruginosa* attacker strains carrying the pBBR1MCS4 vector, either as empty vector (EV), encoding *tssA3* (ptssA3) or *tssA3* with *tssA1* sequences. Attacker *P. aeruginosa* and prey *E. coli* were mixed and incubated at 37 °C for 24 hours before GFP signal quantification. Values are presented as means and error bars represent the standard deviation. Statistical testing was conducted by one-way ANOVA with Dunnett's multiple comparisons test, each strain was compared to the parental EV strain (ns=not statistically significant, ** $p < 0.01$). (n=3).

5.6.6 The TssA1 Nt1 domain model can be docked to the sheath

In the assembly of the T6SS, TssA proteins have generally been found to be associated with the distal end of the sheath as it polymerises (360,377,508,513). BTH experiments identified that *P. aeruginosa* TssA proteins interact with their respective sheath components specifically via the Nt1 domain (Figures 4.20 and 5.9). The exchange of these Nt1 domains between different TssA proteins generated chimeric TssA proteins that were functional with the T6SS corresponding to the Nt1 domain (Figures 5.4, 5.5 and 5.6). The specificity of TssA proteins to the T6SS therefore appears to be associated with the Nt1 domain, likely through the interaction with the sheath.

To understand how these Nt1 domains may interact with their respective sheaths, models of H1-T6SS components were docked using the ZDock server (535). To date the only *P. aeruginosa* sheath structure that has been resolved is that of the H1-T6SS sheath in the contracted conformation (579). During sheath polymerisation, it would be anticipated that TssA1 would be in contact with the sheath in the extended conformation. Most reported sheath structures are in the contracted conformation due to this representing a lower energy state than the extended conformation in which the sheath is initially assembled. A small number of structures are available of sheaths in the extended conformation, notably in *V. cholerae* (357,386). By comparison to this sheath structure, a model was generated of the H1-T6SS sheath in the extended conformation (Figure 5.25).

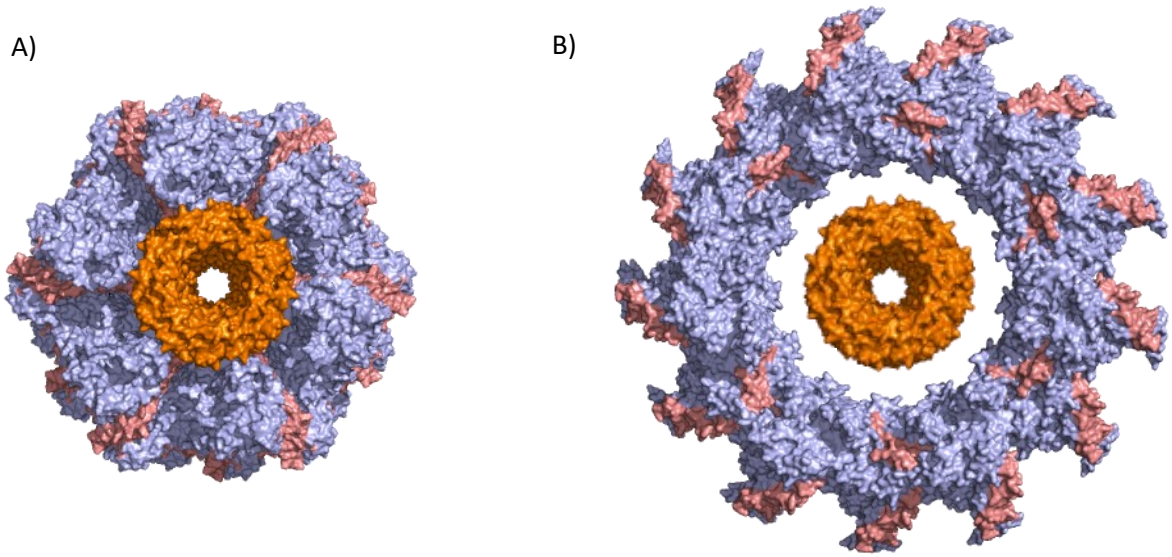


Figure 5.25 *P. aeruginosa* TssB-TssC sheath in extended and contracted conformations. The Hcp inner tube (orange) is positioned within the sheath. A) Model of the *P. aeruginosa* TssB-TssC sheath in the extended conformation with the Hcp inner tube. B) Resolved structure of the *P. aeruginosa* TssB-TssC sheath in the contracted conformation (PDB: 5N8N) with the Hcp inner tube. Extended conformation model generated by Patricia Paracuellos.

Previous attempts to model the interaction between TssA proteins and sheath components has involved the docking of the Nt2 domains of $TssA_L$ proteins to the distal end of the sheath (360,377). These Nt2 domains were modelled to interdigitate with grooves at the distal end of the sheath. With the subsequent characterisation of the Nt1 domain structure of $TssA^{BC}$, some structural similarity was identified between the first 7 α-helices of this Nt1 domain and the structure of Nt2 domains of $TssA^{EC}$ and $TssA^{AH}$ (509). This suggests that the interaction of TssA Nt1 domains to the sheath may resemble the previous model involving Nt2 domains, with Nt1 domains fitting in similar grooves at the sheath distal end to stabilise the higher energy extended conformation.

The TssA1 Nt1 domain structural model was docked to the model of the H1-T6SS extended sheath using the ZDock server (Figures 5.26A and B) (535). The docking of two structural models is not a reliable predictor for the interaction of two proteins, therefore this model is highly speculative of how interaction between the sheath and the Nt1 domain could take place. However, it has also been identified upon co-purification of TssA1 with the H1-T6SS sheath, that TssA1 binds at one end of the sheath in its contracted form (376). Docking of the TssA1 Nt1 domain model to the known structure of the sheath in the contracted conformation yielded a very similar positioning of the Nt1 domain at the distal end of the sheath (Figure 5.26C).

The docking model generated suggests that the binding of the Nt1 domains into grooves on the distal end of the sheath resembles the model previously proposed for Nt2 domains (360,377). However, unlike Nt2 domains, all TssA proteins have an Nt1 domain, and for both long and short TssA proteins interactions with the sheath were shown to be mediated exclusively through the Nt1 domain (Figures 4.20 and 5.9). Unlike the previous model, this new model therefore hypothesises a conserved mechanism by which all TssA proteins interact with their cognate sheath components.

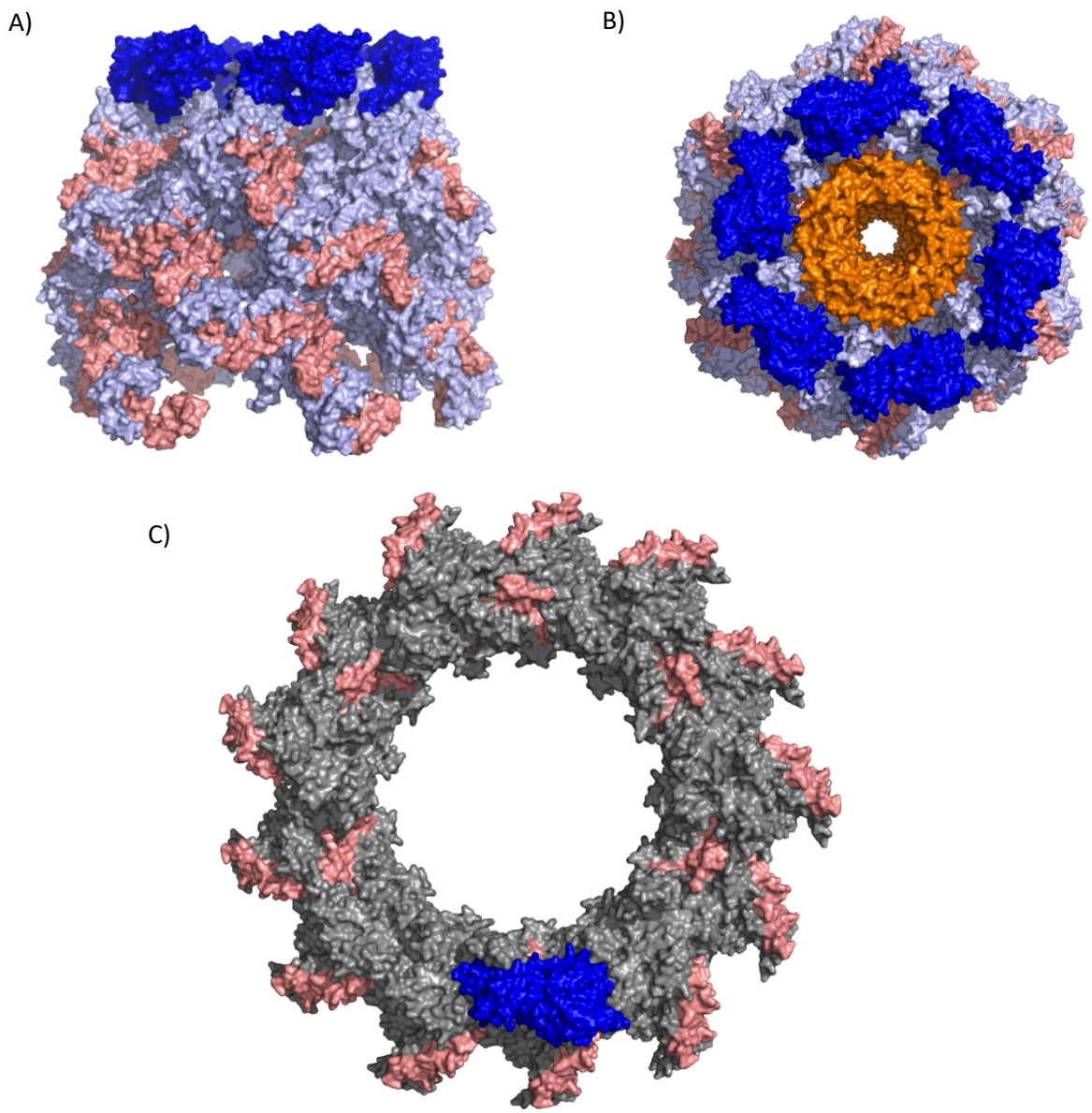


Figure 5.26 TssA1 Nt1 domain models docked at the distal end of the sheath. A) Side view of the docking of the TssA1 Nt1 domain models (blue) to the distal end of the extended sheath model. B) Top view of the docking of the TssA1 Nt1 domain models to the distal end of the extended sheath model. The Hcp inner tube (orange) is positioned within the sheath. C) Docking of the TssA1 Nt1 domain model to the distal end of the contracted sheath structure (PDB:5N8N). Docking carried out with Patricia Paracuellos.

An alignment of structural models of TssA1 and TssA3 Nt1 domains suggested that structural differences primarily arose in regions termed the hairpin and loop. Exchange of these sequences affected both interaction with cognate sheath components and T6SS functionality. In the docking of the TssA1 Nt1 domain model to the extended sheath model, the position of these residues can be identified (Figure 5.27). In this docking these residues are found at the interaction interface, which

would explain why the exchange of sequences between *tssA1* and *tssA3* may affect interaction with the sheath.

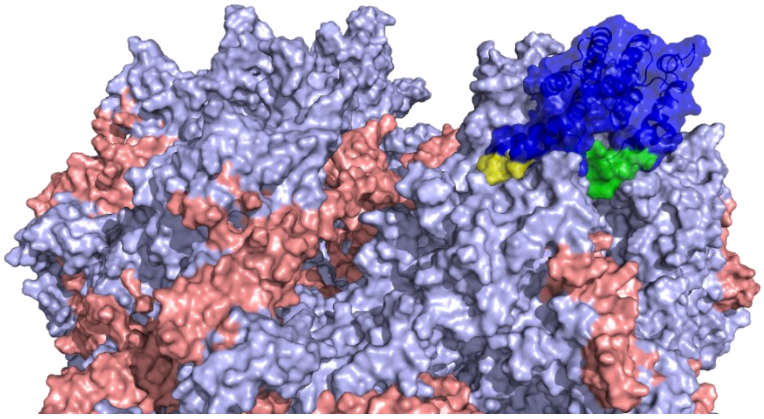


Figure 5.27 TssA1 Nt1 domain hairpin and loop regions at the interface with the extended sheath model. The position of TssA1 Nt1 domain hairpin (yellow) and loop (green) sequences in the docking of a single Nt1 domain model (blue) to the extended sheath model.

5.7 Discussion

5.7.1 Significance of chimeric TssA protein functionality

To account for the variability of TssA proteins, it has been suggested that long and short TssA proteins are functionally distinct within their respective T6SSs (376,377). However, the positioning of both long and short TssA proteins within the T6SS has been observed to be similar: associating with the T6SS assembly initiation site before being displaced to the distal end of the sheath during its polymerisation (360,377,508,513). The exception to this is TssA1, which has only been observed as a static component associated with the baseplate complex (377). A competing hypothesis is that the variability of TssA proteins is not related to distinct functions, but instead a different means to achieve a common function. This proposes that the varying C-terminal regions of TssA proteins achieve the oligomerisation into ring-shaped structures, which are suggested to form a platform that facilitates the proper positioning of the more conserved Nt1 domains at an equivalent radial position from the centre of the ring (Figure 1.24). BTH data and structural work on the C-terminal domains of $TssA_S$ proteins generated here, support a role for TssA C-terminal regions in oligomerisation into ring-shaped structures (Figures 4.21, 5.10, 5.14 and 5.15). Furthermore, Nt1 domains of both long and short TssA proteins have been demonstrated to interact with sheath components (Figure 4.20).

To test the hypothesis that TssA proteins function similarly and that their distinct C-terminal regions are functionally similar, chimeric TssA proteins were generated by the exchange of domains between both long and short TssA proteins. For each *P. aeruginosa* T6SS, at least one chimeric TssA protein could be identified that restored T6SS functionality in the absence of the native TssA (Figures 5.4, 5.5 and 5.6). H1-T6SS activity was fully restored in the presence of $tssA1_{Nt1}tssA3_{CTD}$ and H3-T6SS was fully restored in the presence of $tssA3_{Nt1}tssA1_{CTD}$, while H2-T6SS function was partially restored by either $tssA2_{Nt1}tssA1_{CTD}$ or $tssA2_{Nt1}tssA3_{CTD}$. Each functional chimeric protein contained the Nt1 domain natively associated with the T6SS that it functions with. This suggests that the Nt1 domain is essential for TssA activity and thus activity of the T6SS, while C-terminal regions have likely no specificity and can be switched while maintaining the proper functioning of the T6SS. Given the interaction of TssA Nt1 domains with sheath components, which was shown to be highly specific for the cognate sheath components (Figure 5.9), it is likely that this specific interaction is required for T6SS activity.

A key role of TssA proteins is in coordinating sheath initiation at the baseplate and polymerisation at the distal end of the sheath (360) (see section 3.6.1). The TssA Nt1 domain is therefore implicated in each of these activities, while the C-terminal regions are dispensable. TssA proteins are recruited to

the assembly initiation site comprised of the membrane complex and baseplate complex, and are generally required for efficient sheath initiation (360,377,508). The data indicates that functional chimeric TssA proteins containing the cognate Nt1 domain can be recruited to this assembly initiation site to facilitate sheath initiation, suggesting that Nt1 domains are involved in the recruitment of TssA proteins to the T6SS. The cognate Nt1 domain is then likely essential for the initiation and coordination of sheath polymerisation through interaction with sheath components.

Upon the exchange of very similar C-terminal regions, such as those of the short TssA1 and TssA3, full H1- and H3-T6SS functionality was maintained (Figures 5.4 and 5.5). These C-terminal domains share 34 % sequence identity and are expected to have a similar fold and oligomerise into similar ring-shaped structures (Figure 5.28) (509). Preliminary structural data also indicates that this is the case (Figures 5.14 and 5.15). Therefore, the exchange of these C-terminal domains would not be expected to have a large effect on the overall architecture of the TssA protein. Like the wildtype proteins, each of the functional chimeric proteins would be expected to be a ring-shaped structure of high symmetry and a large internal lumen with peripherally associated Nt1 domains (Figure 5.28). The positioning of the Nt1 domains would be expected to be very conserved upon exchange of $TssA_S$ C-terminal domains. Equivalent T6SS functionality upon exchange of $TssA_S$ C-terminal domains suggests that a crucial role of these C-terminal domains is as a platform to facilitate proper positioning of Nt1 domains.

Exchange of distinct C-terminal domains from long and short TssA proteins did not lead to function with the $TssA_S$-associated H1- and H3-T6SSs, however, there was functionality associated with these chimeric proteins in the $TssA_L$-associated H2-T6SS. Interaction with the H2-T6SS sheath and partial H2-T6SS function were restored by $tssA2_{Nt1}tssA1_{CTD}$ and $tssA2_{Nt1}tssA3_{CTD}$ (Figures 5.3 and 5.6). TssA2 C-terminal regions, including the Nt2 domain that was previously suggested to be responsible for sheath interaction, are therefore not required for interaction of TssA2 Nt1 domains with sheath components and functionality within the H2-T6SS. Instead, it seems that introduction of $TssA_S$ C-terminal domains facilitates a similar positioning of the TssA2 Nt1 domains compared to the native protein (Figure 5.28). The fact that the introduction of a distinct C-terminal domain structure can be tolerated within a functioning T6SS supports the hypothesis that the distinct C-terminal regions of long and short TssA proteins achieve a common function, the proper positioning of Nt1 domains, through distinct means.

The presence of the Nt1 domain alone was not always sufficient for the functionality of a chimeric protein, suggesting that while specific C-terminal regions are not required for T6SS activity, they do have some contribution. Chimeric TssA proteins formed from a mix of domains from long and short TssA proteins were non-functional in the H1- and H3-T6SSs, while only partial functionality was restored with these proteins in the H2-T6SS. The C-terminal regions of long and short TssA proteins

are structurally distinct (Figure 5.28) (see section 1.4.1) (360,377,509). Therefore, exchange of these C-terminal regions would be expected to introduce changes in ring dimensions and symmetry of the complex, which may influence functionality. Exchange of C-terminal regions would involve either loss or gain of the large internal lumen associated with $TssA_S$ proteins (Figure 5.28). It has been suggested that the variation in lumen size may be linked to the varying firing modes of $TssA_S$- and $TssA_L$-associated T6SSs (see section 3.6.4) (508). A $TssA_L$-associated T6SS is linked to slow firing dynamics, remaining extended for longer periods of time after sheath polymerisation before firing (508). Stable residence of the extended sheath may require the distal end of the tail complex to be capped with the narrower $TssA_L$ lumen to prevent the loss of the inner tube. The presence of a wider lumen might be tolerated in a $TssA_S$-associated T6SS, linked to rapid firing dynamics after sheath polymerisation, as stability of the tail complex need not be maintained for a long period of time before firing. Alternatively, it has been suggested that with a $TssA_S$ C-terminal domain, in polymerisation of the inner tube, Hcp hexameric rings would be able to pass through the internal lumen of $TssA_S$ rings to be added to the growing structure, while a distinct mechanism has been suggested for $TssA_L$ C-terminal regions (360). Altered TssA lumenal diameter through C-terminal region exchange may therefore affect T6SS activity through sheath stability or coordination of inner tube polymerisation.

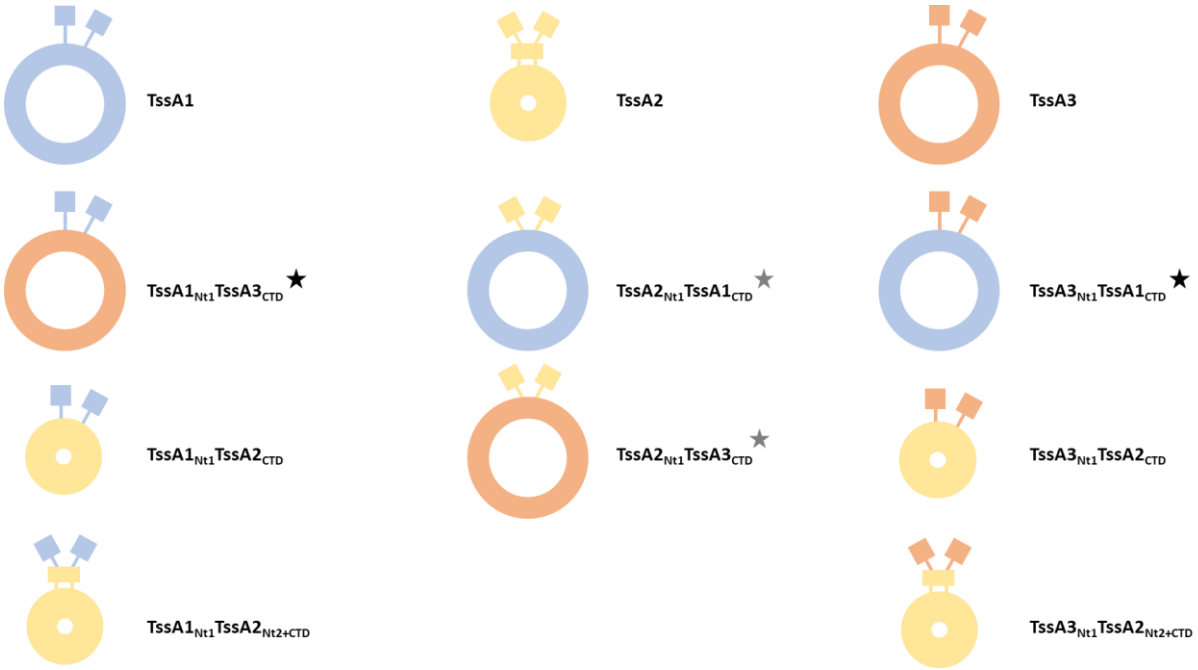


Figure 5.28 Schematic of predicted structures of chimeric TssA protein complexes. Domains of TssA1 (blue), TssA2 (yellow) and TssA3 (red) were exchanged to generate eight chimeric TssA proteins with mixed domains. Chimeric TssA proteins are grouped according to the presence of a specific Nt1 domain. Fully functional chimeric proteins are indicated with a black star, partially functional chimeric proteins are indicated with a grey star.

Exchange of C-terminal regions would also alter the symmetry of the chimeric protein relative to the native TssA. With $TssA_S$ C-terminal domains forming rings with ~16-fold symmetry and $TssA_L$ C-terminal domains forming rings with five- or six-fold symmetry (360,377,509), exchange of these regions would quite dramatically increase or decrease the number of monomeric units in the oligomer and with this the abundance of peripheral Nt1 domains. The abundance of peripheral Nt1 domains may be important for the activity of distinct TssA groups, thus an altered abundance could explain loss of T6SS activity. Further to just providing a platform for the proper positioning of Nt1 domains, TssA C-terminal regions may also be important for determining the oligomeric state of the protein and through this the abundance of Nt1 domains.

A further change in TssA structure resulting from the introduction of the $TssA_S$ C-terminal domain is the absence of the TssA2 Nt2 domain. It has been hypothesised that the Nt2 domain acts as a spacer to ensure proper positioning of Nt1 domains (509), but no other direct function has been linked to this domain. However, these chimeric proteins were not fully functional despite positioning of their Nt1 domains permitting interaction with the sheath (Figures 5.3 and 5.6). This suggests that Nt2 domains may have other contributions to $TssA_L$ functionality.

5.7.2 Interaction of TssA Nt1 domains at the distal end of the sheath

Based on interactions with the sheath being mediated by Nt1 domains (Figures 4.20 and 5.9), and TssA proteins being identified to localise at the distal end of the polymerising sheath (360,377,508,513), it appears that TssA proteins interact specifically via their Nt1 domains with the distal end of the sheath. In previous models it has been suggested that the rings of the sheath and the TssA complex align, with Nt1 domains at the periphery of these rings possibly positioned around the external surface of the sheath (360,509). Given the identification of interaction between Nt1 domains and the sheath, a model of the TssA1 Nt1 domain was docked to the H1-T6SS sheath structure (Figure 5.26). In both extended and contracted sheath conformations, the Nt1 domain was similarly positioned at the tip of the distal end of the sheath within grooves that would be occupied by subsequent sheath subunits upon polymerisation (Figure 5.26). Evidently, as the TssA1 Nt1 domain docked to the sheath structures is just a model based on the $TssA^{BC}$ Nt1 domain structure, such organisation remains speculative. However, this provides a solid hypothesis for the interaction of Nt1 domains within grooves at the tip of the sheath distal end that can be further investigated.

Sequence comparison between different TssA proteins has identified that the Nt1 domains of long and short TssA proteins vary in size, with those of $TssA_S$ proteins being ~250 aa while those of $TssA_L$

proteins being ~190 aa (509). The conserved feature of these Nt1 domains is the N-terminal ImpA_N region of ~120 aa. Given the conservation of both the ImpA_N regions and sheath binding ability for all TssA proteins, it may be that the ImpA_N region confers general sheath binding properties, while specificity for different T6SSs may be introduced in other Nt1 domain regions. The ImpA_N region comprises the first 5 α-helices and the N-terminal portion of the sixth helix of the $TssA^{BC}$ Nt1 domain (509). Within this ImpA_N region of $TssA^{BC}$, most of the conserved residues were involved in packing interactions, suggesting that they likely contribute to a similar fold between different TssA proteins (509).

While overall Nt1 domain sequence and length does vary between long and short TssA proteins, the sequence of the core ImpA_N region is quite conserved between long and short TssA proteins. Based on the known structure of the $TssA^{BC}$ Nt1 domain, structural models were generated for each of the *P. aeruginosa* TssA Nt1 domains. The ImpA_N regions of each of the *P. aeruginosa* TssA proteins are predicted to be formed of five antiparallel α-helices whose arrangement is similar between TssA proteins (Figure 5.29A). In an alignment of these predicted structures, the five helices can be identified in each of the ImpA_N regions, but variations are also present (Figure 5.29B). The TssA1 and TssA3 ImpA_N regions are similar, sharing a RMSD of 1.8 Å, while the TssA2 ImpA_N region is more different sharing an RMSD of 4.0 Å with the TssA1 ImpA_N region (536). This variation may arise from differences in the orientation or length of the ImpA_N helices (Figure 5.29). As previously stated, these are structural models based on a single known Nt1 domain structure, without additional structural data on these ImpA_N regions, is it difficult to ascertain the degree of similarity between different ImpA_N regions.

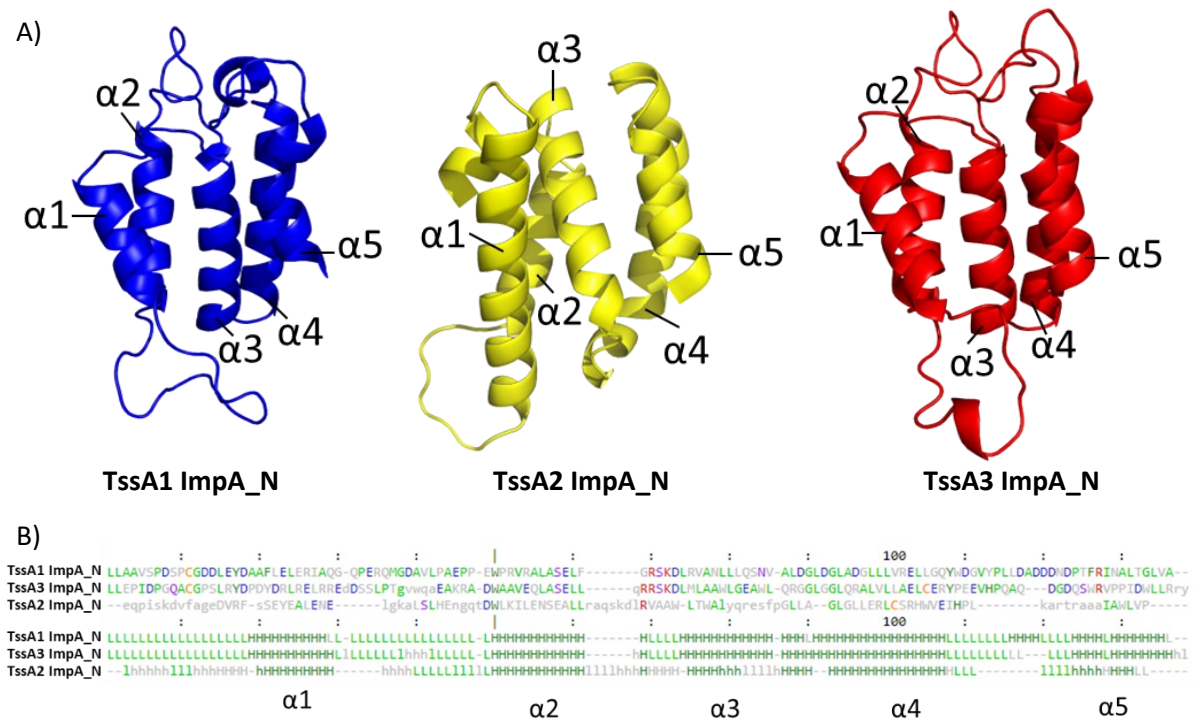


Figure 5.29 Structural similarities between *P. aeruginosa* TssA ImpA_N regions. A) Structural models of the *P. aeruginosa* TssA ImpA_N regions. The TssA1 (blue), TssA2 (yellow) and TssA3 (red) ImpA_N regions. Each ImpA_N region is comprised of five antiparallel α-helices with a similar orientation. B) Sequence and secondary structure alignments of the *P. aeruginosa* TssA ImpA_N regions. Combined pairwise alignments of TssA3 and TssA2 ImpA_N regions to the TssA1 ImpA_N region. Uppercase represents structurally equivalent positions with TssA1 ImpA_N. Lowercase represents insertions relative to TssA1 ImpA_N. H/h: helix, L/l: coil. The consensus regions for the five α-helices are annotated.

There are currently no T6SSs where structures for both the sheath and the TssA Nt1 domain are known, which limits the reliability of models docking TssA proteins onto the sheath. For *P. aeruginosa*, the structure of the H1-T6SS sheath is resolved in its contracted conformation, where TssA1 has been observed to bind to one end of this structure (376,596). A model for the TssA1 Nt1 domain has been docked to the distal end of this sheath structure (Figure 5.26). In this docking, the TssA1 ImpA_N region fits within a groove at the sheath distal end (Figure 5.30). It is possible that such a groove at the distal end of the sheath could be filled by ImpA_N regions in all T6SSs.

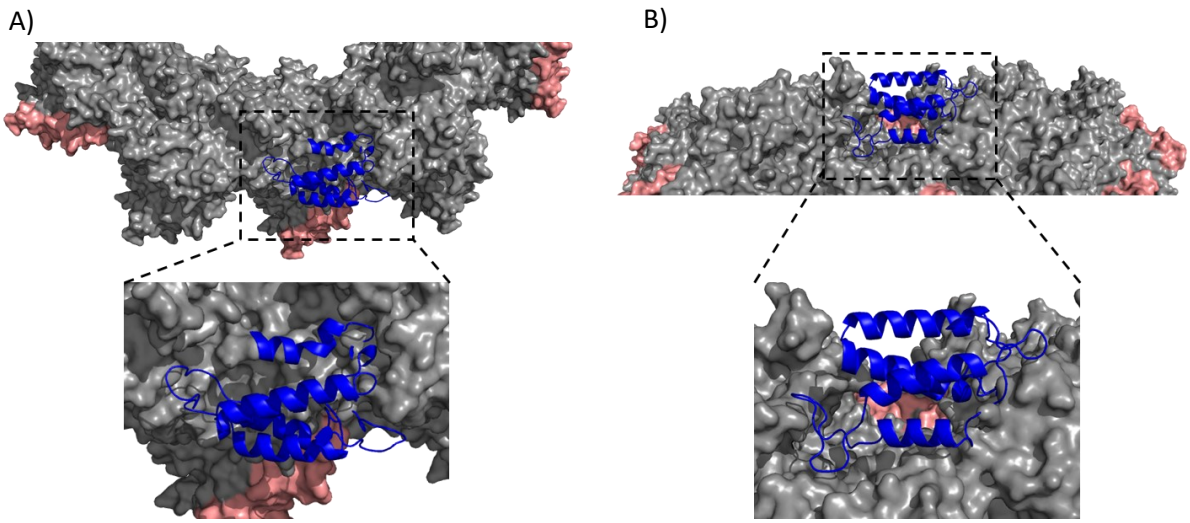
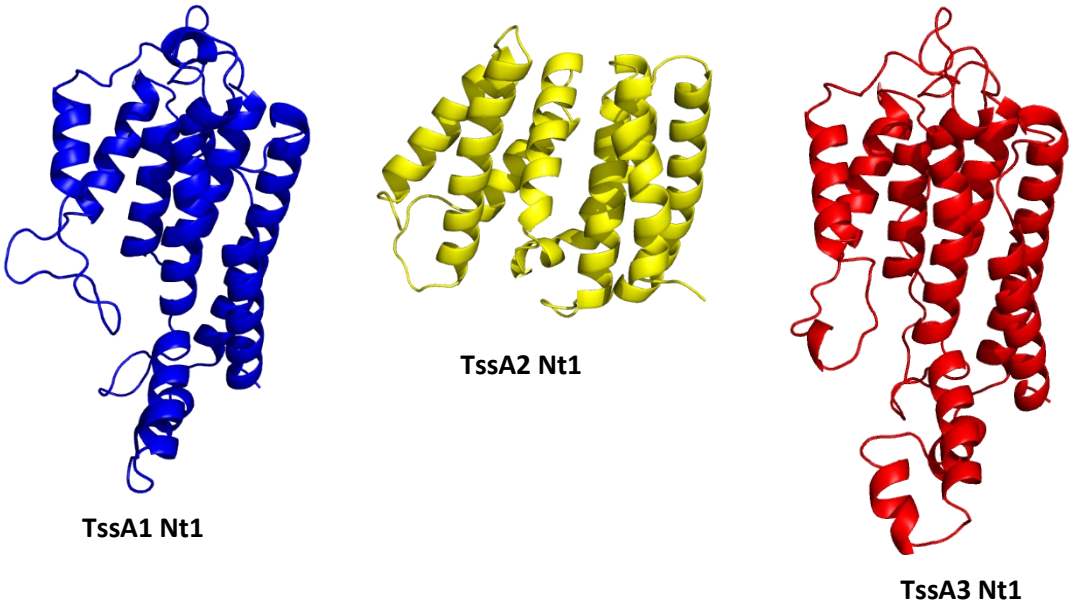


Figure 5.30 TssA1 ImpA_N region model docked at the distal end of the sheath in the contracted conformation. A) Top view of the docking of the TssA1 ImpA_N region model (blue) to the distal end of the contracted sheath structure (PDB: 5N8N). B) Side view of the docking of the TssA1 ImpA_N region model to the distal end of the contracted sheath structure. Docking carried out with Patricia Paracuellos.

P. aeruginosa Nt1 domains interact specifically with their cognate sheath components (Figures 4.20 and 5.9), which likely drives the functional specificity of TssA proteins (Figures 4.25, 4.26 and 4.27). However, this functional specificity can be altered by the exchange of Nt1 domains (Figures 5.4, 5.5 and 5.6). The specific interaction between Nt1 domains and sheath components is therefore crucial for T6SS specificity linked to TssA proteins. It is thus hypothesised that subtle variations in TssA Nt1 domain and sheath tip structures may contribute to TssA system specificity.

Structural models were generated for each of the *P. aeruginosa* TssA Nt1 domains. In each case, the Nt1 domain is formed of a bundle of α-helices (Figure 5.31A). The TssA1 and TssA3 Nt1 domains are predicted to have a core α-helical bundle, containing the ImpA_N region, and an additional extension below this. Alignment of the Nt1 domain regions downstream of the ImpA_N region identifies both sequence and secondary structure variation between the short TssA1 and TssA3 compared to the long TssA2 (Figure 5.31B). The structures of the TssA1 and TssA3 Nt1 domains are predicted to be quite similar: structural alignment of these models yields an RMSD of 1.7 Å (536). The TssA1 and TssA3 Nt1 domains were aligned to reveal two primary regions of variable structure, termed the hairpin and the loop (Figure 5.19).

A)



B)

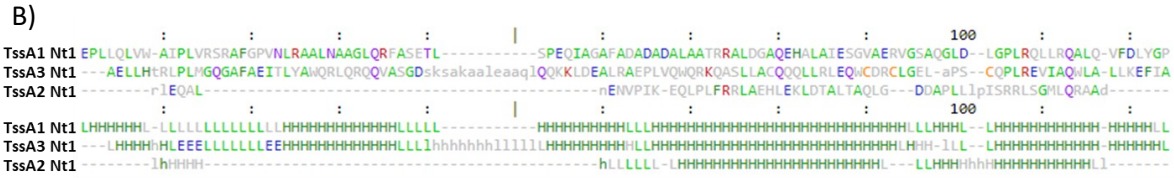


Figure 5.31 Structural differences between *P. aeruginosa* TssA Nt1 domains. A) Structural models of the *P. aeruginosa* TssA1 (blue), TssA2 (yellow) and TssA3 (red) Nt1 domains. B) Sequence and secondary structure alignments of the *P. aeruginosa* TssA Nt1 domains excluding ImpA_N regions. Combined pairwise alignments of TssA3 and TssA2 Nt1 domains excluding ImpA_N regions to that of TssA1. Uppercase represents structurally equivalent positions with TssA1. Lowercase represents insertions relative to TssA1. H/h: helix, L/l: coil.

Meanwhile, structural alignment of TssA1 and TssA3 Nt1 domains models to that of TssA2 yields RMSD values of 4.2 Å and 3.9 Å respectively (536). This indicates that the two Nt1 domains belonging to $TssA_S$ proteins, TssA1 and TssA3, are quite similar but differ to the Nt1 domain of the long TssA2. The variation can be demonstrated in a secondary structure alignment between TssA1 and TssA2 Nt1 domains (Figure 5.32). While some helices do align in the core helical bundle, there are variations in the positioning of helices between the structures, and the TssA1 Nt1 domain has an additional helical extension below the aligned region, which is absent in the TssA2 Nt1 domain. The predicted structural differences between these Nt1 domains may be linked to the difference in size between the Nt1 domains of long and short TssA proteins, with the Nt1 domain of $TssA_S$ proteins being longer. Of course, these structural comparisons are based on structural models, and the structures used may therefore not be entirely accurate.

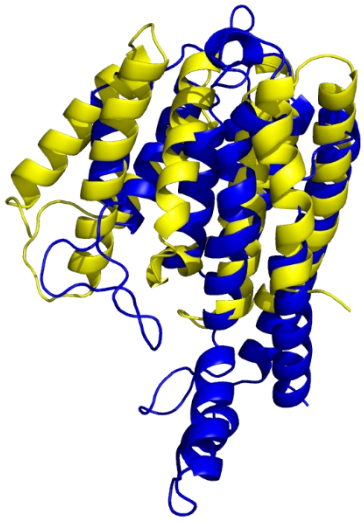


Figure 5.32 Comparison of TssA1 and TssA2 Nt1 domain models. Structural alignment TssA1(blue) and TssA2 (yellow) Nt1 domain models.

The structures of the short TssA1 and TssA3 Nt1 domains are predicted to be more similar when compared to the long TssA2 Nt1 domain structure (Figure 5.31). It is hypothesised that differences in Nt1 domain structure may contribute to the specificity of interaction with sheath components and functional specificity. It would therefore be expected that variation between sheath components of different T6SSs would also contribute to this specificity. In a pairwise comparison of T6SS component sequences encoded in different *P. aeruginosa* T6SS clusters, it was identified that both TssB and TssC proteins were more similar between the $TssA_S$-associated H1- and H3-T6SSs than when compared to the $TssA_L$-associated H2-T6SS (Table 5.1). This association was more pronounced with TssB proteins, perhaps implicating TssB in contributing to the specificity of interactions with TssA proteins.

Table 5.1 Pairwise comparison of sheath components between *P. aeruginosa* T6SS clusters

		TssA	TssB	TssC
% sequence identity	H1-T6SS vs H2-T6SS	14.7	25.1	38.4
	H1-T6SS vs H3-T6SS	28.1	35.3	44.3
	H2-T6SS vs H3-T6SS	17.9	27.6	41.1

Interestingly, the additional extension present below the core helical bundle in $TssA_S$ proteins contains the hairpin region that was identified to be variable between TssA1 and TssA3 Nt1 domains (Figure 5.19). The exchange of the hairpin regions between TssA1 and TssA3 resulted in a reduced interaction strength with the cognate sheath components for both proteins (Figures 5.21 and 5.22), implicating these sequences in the specificity of interaction between these $TssA_S$ proteins and their respective sheath components. In the docking of the TssA1 Nt1 domain to the sheath structure, the hairpin region

is identified to fit within a groove (Figure 5.33A). The TssA3 Nt1 domain has an additional sequence present in the hairpin region, and when aligned with the docked TssA1 Nt1 domain, this additional sequence clashes with the sheath (Figure 5.33B). This clash may explain why neither the TssA3 Nt1 domain or TssA1 with TssA3 hairpin regions interact with H1-T6SS sheath components (Figures 5.9 and 5.20).

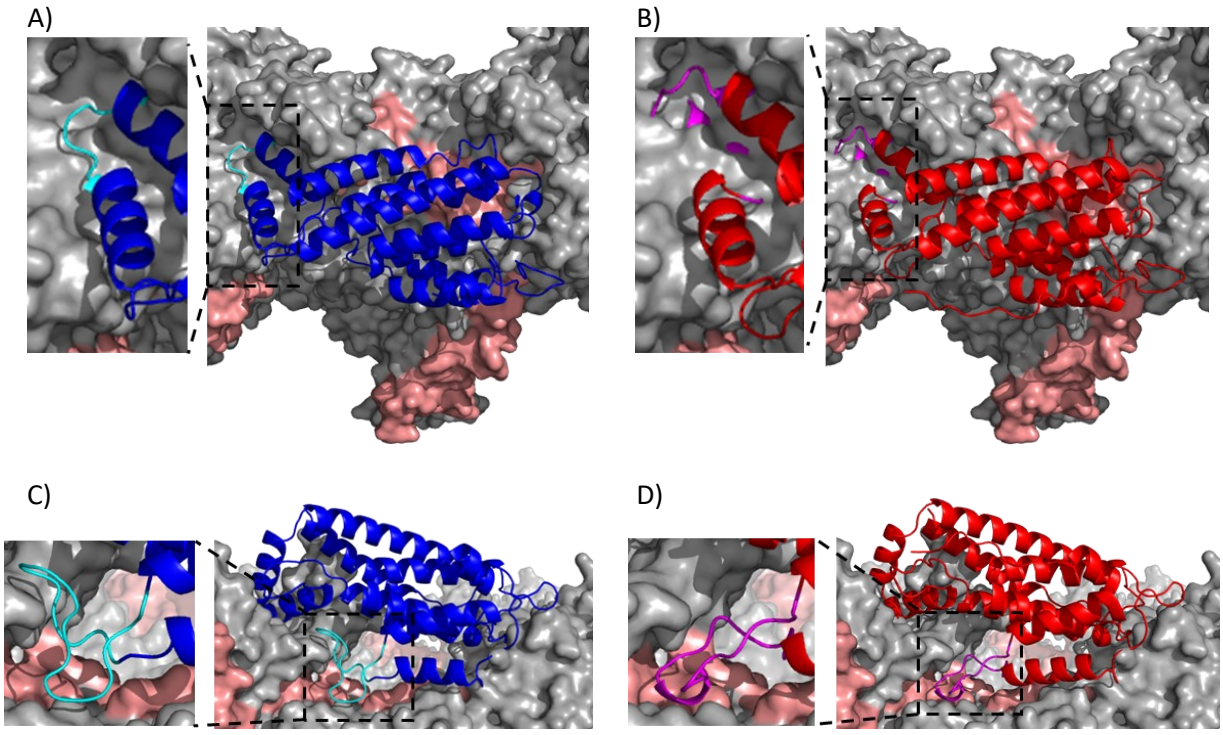


Figure 5.33 Structural models of TssA1 and TssA3 Nt1 domains docked to the H1-T6SS contracted sheath structure. A) Top view of the TssA1 Nt1 domain model (blue) docked to the H1-T6SS contracted sheath structure (PDB: 5N8N). The hairpin region (light blue) fits within a groove. B) Top view of the TssA3 Nt1 domain model (red) with equivalent docking to the H1-T6SS contracted sheath structure. The extension to the hairpin region (magenta) in the TssA3 Nt1 domain clashes with the sheath structure. C) Side view of the TssA1 Nt1 domain model docked to the H1-T6SS contracted sheath structure, with the loop region (light blue) highlighted. B) Side view of the TssA3 Nt1 domain model with equivalent docking to the H1-T6SS contracted sheath structure with the loop region (magenta) highlighted.

The other area that was identified to be variable between TssA1 and TssA3 Nt1 domain models was the loop region, which is found between α1 and α2 of the ImpA_N region (Figure 5.19). The exchange of the loop regions between TssA1 and TssA3 also resulted in a reduced interaction with the cognate sheath components for both proteins, as well as a reduced abundance of sheath structures (Figures 5.21, 5.22 and 5.23). The TssA1 Nt1 domain loop region can be identified in the model docked to the

H1-T6SS sheath structure (Figure 5.33C). When the TssA3 Nt1 domain is aligned to this structure, there is no steric clash with the sheath structure as there was in the case of the hairpin region (Figure 5.33D). It is therefore less clear why exchange of loop regions affected sheath interaction, particularly as introduction of the loop region generally had a greater effect; residues within this region may specifically contribute to interaction with H1-T6SS sheath components.

5.7.3 Implications of Nt1 domain-sheath interactions on TagA accessory protein interactions

This work has identified that TssA Nt1 domains are responsible for binding to the sheath (Figure 4.20). These Nt1 domains contain the conserved feature of TssA proteins, the ImpA_N region. Interestingly, in addition to being present in TssA proteins, this ImpA_N region is also present in the TssA-associated accessory protein TagA (377,510). These TagA proteins are typically associated with T6SSs which have a $TssA_L$ protein and have been implicated in the stabilisation of extended sheath structures by anchoring the distal end of the sheath through association with the membrane (see section 1.4.3.1) (377,508,510). At the distal end of fully extended *E. coli* T6SS sheaths both $TssA^{EC}$ and $TagA^{EC}$ foci have independently been observed to be present up to contraction, suggesting that these proteins form a complex at the distal end of the sheath to stabilise the extended structure (510). In *V. cholerae* $TssA^{VC}$ was generally only present at the distal end of the T6SS sheath during the polymerisation, following the formation of a fully extended structure there was loss of $TssA^{VC}$ association and either sudden contraction or a prolonged stable state in the absence of $TssA^{VC}$ before contraction (377). It was suggested that these outcomes were influenced by $TagA^{VC}$, where upon dissociation of $TssA^{VC}$, sheaths were either stabilised by $TagA^{VC}$ and if not, immediately contracted. $TagA^{VC}$ has been identified to bind several T6SS components, including TssA, ClpV, sheath components, Hcp and baseplate components (512). Given that the interaction of TssA proteins with sheath components involves the ImpA_N-containing Nt1 domains, it is tempting to speculate that TagA proteins may form similar interactions with sheath components through their ImpA_N regions. The ImpA_N regions of $TssA^{EC}$ and $TagA^{EC}$ share 24 % sequence identity, while the ImpA_N region of $TssA^{VC}$ shares 5 % sequence identity with that of $TagA^{VC}$. It may be that TagA proteins completely replace TssA proteins at the distal end of the sheath, as suggested for *V. cholerae*, or that TagA and TssA proteins simultaneously bind the distal end of the sheath, as suggested for *E. coli*.

It has been suggested that the interaction of TssA proteins with their TagA accessory proteins may be mediated through interaction of ImpA_N regions, as previous work identified self-interactions of $TssA^{EC}$ N-terminal regions comprising of Nt1 and Nt2 domains (360,377). However, studying the interactions between the domains of TssA proteins identified that there is no interaction between Nt1

domains (Figures 4.20 and 5.10). The previously reported self-interaction of $TssA^{EC}$ N-terminal regions was likely because of interaction between Nt2 domains, which have been identified to dimerise (377,509). The interaction between TssA and TagA proteins is therefore unlikely to be mediated through interactions between the different ImpA_N regions.

5.7.4 Proposed mechanism for tail polymerisation with TssA bound to the distal end

A single TssA complex is present at the distal end of the sheath as it polymerises across the cell (360,377,508). The mechanism by which new sheath and inner tube subunits are incorporated at the distal end of the tail complex with TssA bound is currently unclear (387). The binding of Nt1 domains to the distal end of the sheath may introduce a physical barrier to the incorporation of new sheath and Hcp subunits. The mechanism by which the Hcp inner tube is extended has been suggested to vary between long and short TssA proteins. With a $TssA_S$ bound at the distal end of the sheath, the approximately 100 Å lumen of the C-terminal domain ring shaped structure could accommodate the passage of a 90 Å diameter Hcp hexameric ring to extend the inner tube (376,509). In contrast, with a $TssA_L$ bound, the lumenal diameter of this C-terminal domain ring shaped structure is around 25-50 Å, which could not accommodate the passage of a Hcp ring (360,377,509). It has been suggested that a conformational change in the $TssA_L$ C-terminal region might open a sufficient lumen for the passage of a Hcp ring (360). In this model it is suggested that the “closed” form of the ring which has been observed would prevent the release of the inner tube through the TssA lumen, however, an “open” form has not been observed and thus far remains an untested hypothesis. It is currently unclear, with the positioning of the TssA complex at the distal end of this tail structure, the mechanism by which both sheath and inner tube undergo polymerisation.

Several hypotheses have been proposed for the mechanism by which both sheath and Hcp subunits might be incorporated with TssA bound at the distal end of the sheath. These hypotheses were suggested based on the previous model where interaction between the sheath and associated TssA proteins was suggested to involve the Nt2 domain (361). Given that it now appears that this interaction instead involves the more flexibly associated Nt1 domain (Figure 4.20), these hypotheses may require re-examination.

In the exchange model, the existing TssA complex is replaced by a new TssA complex carrying sheath subunits and Hcp. However, this contradicts previous data identifying that the same TssA remains associated to the distal end of the sheath (360,377). Furthermore, if as previously suggested, the binding of TssA to the distal end of the sheath is involved in the maintenance of the sheath in the high

energy extended conformation (360), it seems unlikely that this energy would be maintained if the TssA were to dissociate to allow new subunits to be added. Regardless of the role of TssA in maintaining the sheath in an extended conformation, it would appear to be energetically unfavourable to lose the interaction between a TssA complex and the distal end of the sheath, which has been suggested to be one of the strongest interactions formed by TssA (360). The exchange model therefore does not appear to best fit the available data.

The flip model is based on observations that TssA complexes form double-layered ring structures. In this model it is suggested that while one face of the TssA complex associates with the extended sheath structure, the other face can bind free sheath subunits and Hcp (361). The flipping of the TssA complex is proposed to incorporate these new components into the sheath and inner tube. While this model is consistent with a single TssA complex associating with the distal end of the sheath during polymerisation, it again proposes that all contacts between the TssA complex and the extended sheath are lost for polymerisation to occur, which seems unlikely. Furthermore, there are many gaps in the understanding of how this manoeuvre might be coordinated, i.e. the requirement of chaperones to guide such a rearrangement, since no such TssA interaction partners have been identified to date.

Finally in the cap model, it is proposed that contact between the TssA complex and the sheath is maintained during polymerisation of the inner tube and sheath (132). It was suggested in this model that Hcp hexamers could enter either directly through the $TssA_S$ ring lumen or through structural rearrangement of the $TssA_L$ C-terminal domain ring to allow their passage, while sheath subunits would be incorporated like flagellins at the flagellar tip (132).

A model akin to the cap model seems most likely given the data. An update to the cap model should consider that the interaction with the sheath, likely at the distal end as identified in previous fluorescence microscopy data (360,377,508,513), has now been identified to involve TssA Nt1 domains (Figure 4.20). Molecular docking with sheath structures and Nt1 domain models has proposed that this interaction involves Nt1 domains docking into grooves at the surface of the distal end (Figure 5.26). Six such grooves are found at the distal end of the sheath. All TssA complexes described to date are comprised of at least 10 monomers, so a maximum of six Nt1 domains would be expected to form contacts with these grooves, with remaining Nt1 domains being flexible (Figure 5.34). It is predicted that in this spider-like arrangement, the C-terminal domain ring structures will orientate above the distal end of the sheath with Nt1 domains extending below.

In the cap model it is proposed that TssA behaves like the FliD flagellar cap. Some similarities between TssA proteins and FliD proteins have already been highlighted (see section 4.7.2). Both proteins are

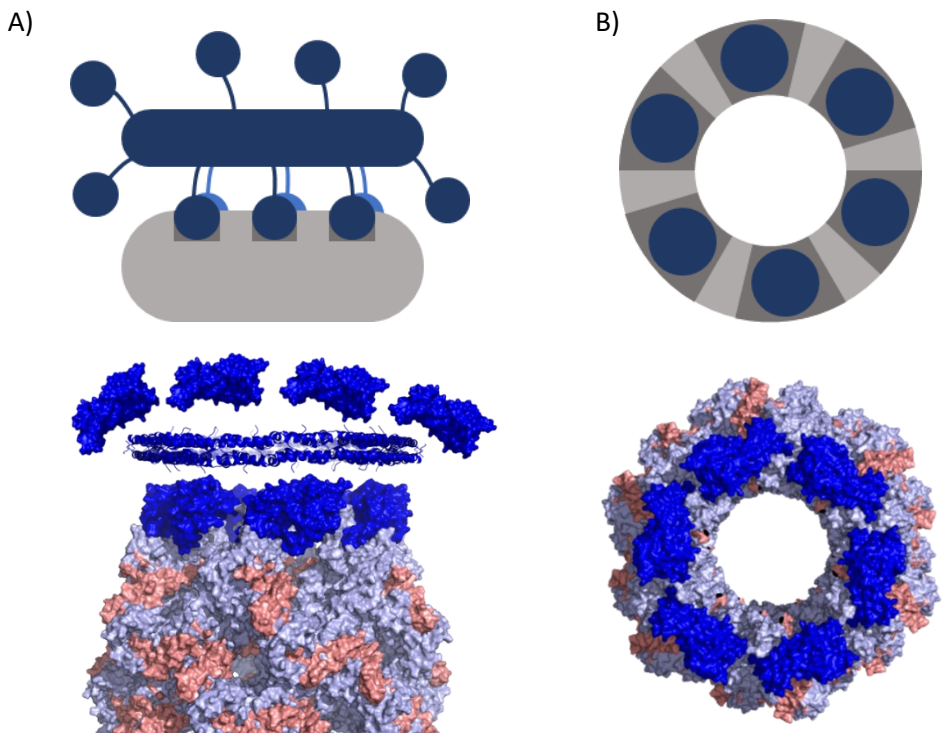


Figure 5.34 Schematics for the association with TssA complexes at the distal end of the sheath. A) Side view of the suggested positioning of the TssA complex (blue) at the distal end of the sheath (light grey) with both schematic and structural models. Nt1 domains are represented by blue circles in the schematic. B) Top view of Nt1 domains within the grooves (dark grey) at the distal end of the sheath with both schematic and structural models. Six grooves would be able to accommodate Nt1 domains.

found at the distal end of a helical structure at a site where further polymerisation takes place, these complexes can vary in their symmetries, which also vary compared to that of the structure that they cap (131,587–589,597). For both FliD and TssA proteins, oligomerisation involves a subset of domains, FliD D2 and D3 domains oligomerise into a star-shaped plate structure while TssA C-terminal domains oligomerise into a ring-shaped structure (132,360,377,509). A further comparison that can be drawn is the association of a more peripherally positioned domain relative to this oligomeric structure, FliD D1 domain and TssA Nt1 domain, where the D1 domain contacts the flagellar filament below the plate structure while the Nt1 domain has been shown to interact with the sheath (Figure 4.20) (132,360,377,509). It has been noted that while the ring-shaped structures formed by the C-terminal domains of $TssA_S$ or the Nt2 and C-terminal domains of $TssA_L$ proteins are very different, the position at which Nt1 domains are found relative to the centre of the rings is similar (Figure 1.24) (509). This comparable positioning is achieved for $TssA_S$ proteins through a large C-terminal domain ring with a large internal lumen and linkers to the peripheral Nt1 domains, while for $TssA_L$ proteins this is achieved

through a smaller C-terminal domain ring that has the addition of dimeric Nt2 domains, which may act as spacers at the outer edge to ensure the proper positioning of Nt1 domains (509). The Nt1 domains contacting the sheath from an oligomeric platform at the distal end of the sheath resembles the oligomeric FliD plate structure that sits atop the flagellar filament with D1 domains extending down and embedding in the filament.

The exact mechanism by which the flagellar filament is extended with FliD at its distal end is not entirely clear. It is known that the legs which extend from the oligomeric plate structure have structural similarities with flagellin and so embed within the growing flagellar filament filling gaps that will sequentially be occupied by new flagellin molecules (132). Unlike in sheath polymerisation, flagellin subunits are transported through the flagellar filament to the capped end, where it is suggested that subunits exit through a cavity (597). Exposure to hydrophobic residues at the filament end is suggested to promote correct folding and thus polymerisation into the filament (597). The incorporation of this new flagellin subunit is suggested to introduce conformational changes which dislodge the FliD leg from an adjacent binding pocket causing the cap complex to rotate and facilitating the incorporation of a further flagellin subunit (132,597).

Drawing from this, an updated cap model is proposed, where Nt1 domains bind to the grooves at the distal end of the sheath. In order to polymerise the sheath, new sheath TssB-TssC protomers must either displace a bound Nt1 domain or bind to an unoccupied groove. It is possible that, as in the proposed model for flagellar polymerisation, the addition of a new sheath subunit introduces a conformational change that displaces a neighbouring Nt1 domain from its groove (Figure 5.35). Such a mechanism with sequential Nt1 domain displacement and polymerisation of sheath subunits, would lead to sheath polymerisation while maintaining Nt1 domain contact with the sheath.

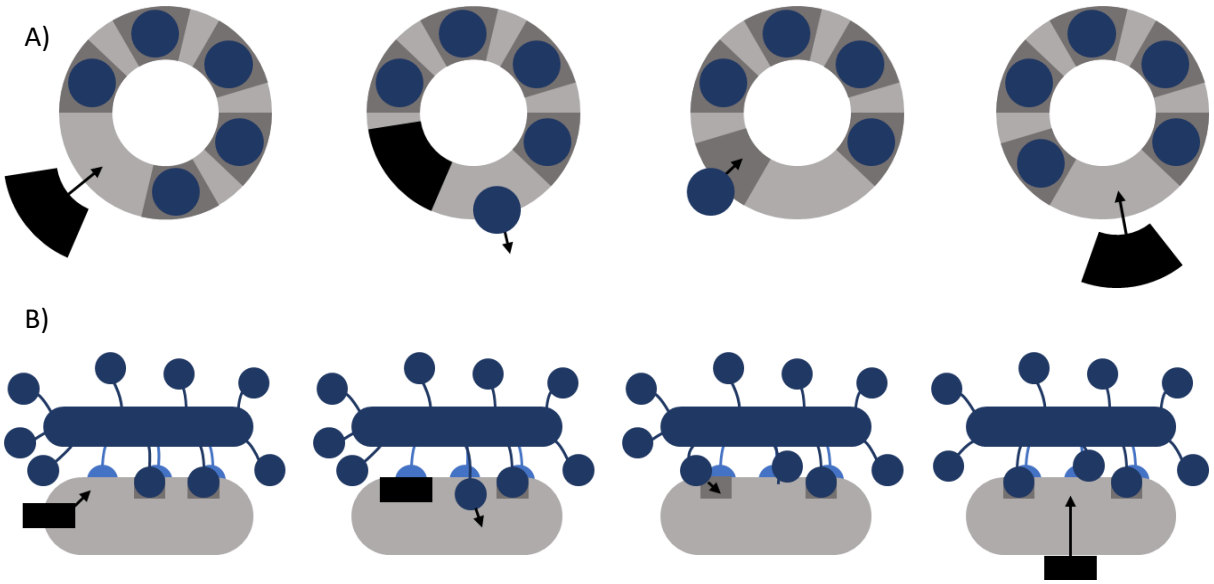


Figure 5.35 Schematics for an updated cap model for sheath polymerisation with TssA at the distal end of the sheath. A) Top view of sheath polymerisation model. B) Side view of sheath polymerisation model. A new sheath subunit (black) is recruited to the distal end of the sheath (light grey). Incorporation of this sheath subunit displaces a neighbouring TssA Nt1 domain subunit (blue circle). A Nt1 domain subunit can bind to the newly incorporated sheath subunit. This cycle would maintain contact between TssA and the distal end of the sheath during polymerisation.

Alternatively, free Nt1 domains could bind TssB-TssC protomers and recruit them to the polymerising sheath, replacing existing contacts between a single Nt1 domain and the sheath with the addition of a new subunit with an already bound Nt1 domain (Figure 5.36).

These updated hypotheses for the cap model are based on advances in our understanding on the interaction between TssA proteins and the sheath. Unfortunately, equivalent developments that would provide insights into how the inner tube is polymerised have not been made to date. It has been identified that a hexameric Hcp ring would be able to pass through the central lumen of $TssA_S$ proteins but not of $TssA_L$ proteins as discussed above. Spaces sufficient for the passage of hexameric Hcp rings could be achieved though the flexibility conferred by the linkers between Nt1 domains and the TssA ring platform. Alternatively, if only a portion of sheath grooves were filled by Nt1 domains, perhaps only on one side of the sheath, this might also allow a Hcp ring to enter and be incorporated. Previous models have generally suggested the polymerisation of the Hcp tube by the incorporation of assembled hexameric Hcp rings onto the existing structure (361). Polymerisation by the addition of single monomers may alternatively be possible to overcome the spatial restrictions imposed by the presence of TssA at the distal end of the tail complex.

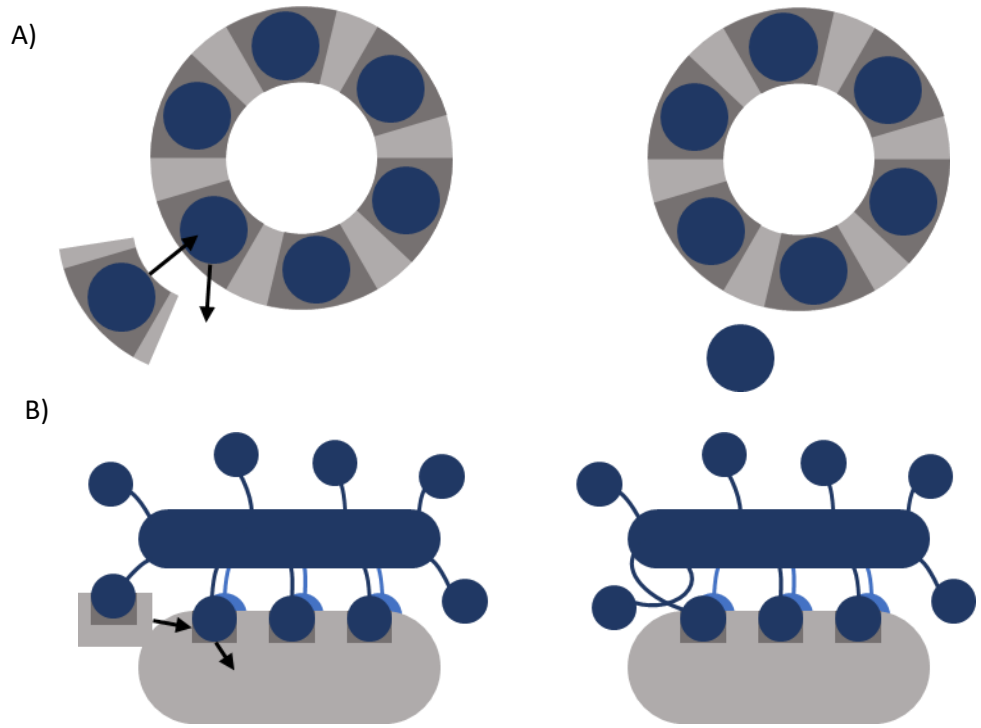


Figure 5.36 Schematics for sheath subunit recruitment by the TssA Nt1 domain. A) Top view of proposed sheath subunit recruitment by the TssA Nt1 domain. B) Side view of proposed sheath subunit recruitment by the TssA Nt1 domain. A free TssA Nt1 domain (blue circle) could bind a sheath subunit and displace an existing Nt1 domain to polymerise the sheath.

Interactions have previously been identified between the distal end of the Hcp tube with the C-terminal regions of both long and short TssA proteins (360,509). It has been suggested that the Hcp tube may act as a framework for the polymerisation of the surrounding sheath, similar to what was suggested for the bacteriophage T4 tail (379,598). If the Hcp tube were to extend beyond the distal end of the sheath, interactions with TssA C-terminal regions may have a role in orientating the TssA ring above the sheath (Figure 5.37). A distal TssA complex may therefore be in contact with the sheath through Nt1 domains and the Hcp inner tube through the C-terminal ring. Polymerisation of the Hcp tube could push the TssA complex further towards the distal end and provide some tension to maintain the polymerisation of the sheath.

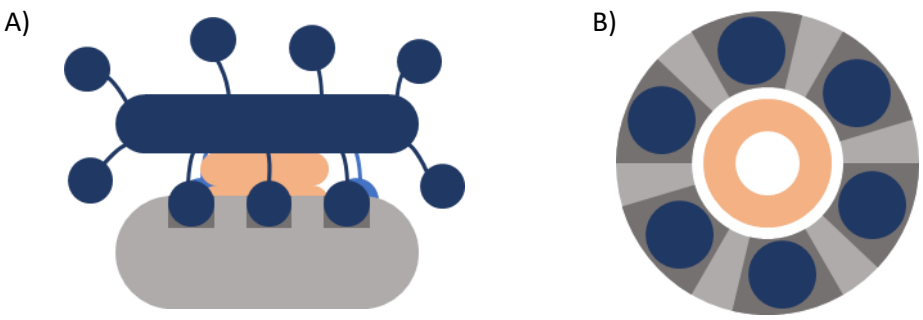


Figure 5.37 Schematics for a TssA complex bound at the distal end of the tail complex including Hcp. A) Side view of the proposed positioning of the TssA complex (blue) at the distal end of the sheath (light grey) with the Hcp tube (orange). Nt1 domains are represented by blue circles. B) Top view of Nt1 domains docked at the distal end of the tail complex containing Hcp.

5.8 Summary

Overall, this chapter presented a novel investigation into the contribution of TssA domains to the functionality of the T6SS, revealing the functionality of chimeric TssA proteins. These data contributed to the development of new hypotheses about the positioning of TssA proteins and their role in the assembly of the T6SS. This work led to the conclusion that functional specificity of TssA proteins is dependent on Nt1 domains, whose positioning is facilitated by C-terminal regions.

6. Discussion

The T6SS is one of many protein secretion systems that assemble complex proteinaceous nanomachines embedded within the bacterial cell envelope of gram-negative bacteria. These systems are highly specific and have very distinct mechanisms to transport proteins across the cell envelope. These secretion systems are assembled from very different proteins, although some elements are conserved between systems, such as the outer membrane secretin associated with the T2SS and T3SS. Despite the conservation of individual components within each of these systems, the level of conservation varies, and some components have quite a low level of similarity. This weaker conservation may reflect specificity towards certain substrates or could indicate subtle mechanistic variation between systems. Here, the most variable component of the T6SS, the TssA protein, notably of the *P. aeruginosa* T6SSs, has been studied. Structural and functional aspects of TssA proteins have been assessed to evaluate possible commonality and differences.

6.1 TssA proteins are required for T6SS activity

The contribution of numerous TssA proteins from different organisms to the activity of their respective T6SSs has been studied to date, including the long $TssA^{EC}$ and $TssA^{VC}$ and the short $TssA1^{PP}$ and $TssA^{BC}$ (360,377,508,509). This work expanded on this characterisation to assess the contribution of each of the TssA proteins of *P. aeruginosa* to the activity of their respective T6SS. In line with previous work, the H1- and H2-T6SSs were non-functional and assembled almost no T6SS sheath structures in the absence of their respective TssA proteins (Figures 3.6, 3.10 and 3.11). Studying the contribution of TssA3 was complicated by the absence of functional assays to assess H3-T6SS activity. While assembly of H3-T6SS sheath structures could be observed by fluorescence microscopy, T6SS firing was not observed, and as such secretion and interbacterial competition assays could not be used to characterise H3-T6SS activity (Figures 3.12, 3.13 and 3.14). However, fluorescence microscopy data did indicate a requirement for TssA3 for the assembly of H3-T6SS sheath structures.

Curiously, it has been demonstrated here and elsewhere that the assembly of the T6SS sheath could still be observed in some cases even in the absence of TssA (Figure 3.11) (376,377,512). Given the overall reduced sheath abundance and the reduced proportion of extending and contracting sheaths in the absence of TssA proteins, it appears that key contributions of TssA proteins are in promoting the initiation and coordination of sheath assembly, without being entirely essential. Potential roles for TssA proteins in the assembly of the T6SS will be discussed in section 6.2, but it is likely that these roles enhance processes that are inefficient in its absence. For example, if TssA has a role in stabilising the membrane and baseplate complexes to allow initiation of sheath assembly, the threshold level of stability may occasionally be met by chance in the absence of TssA allowing sheath initiation.

Considering all the available data, it was determined that TssA proteins are required for the activity of the T6SS. This conclusion was drawn by considering T6SS activity as a population level trait, where despite a low number of sheath structures being assembled in the absence of their cognate TssA protein, functional assays indicate that the bacterial population is unable to effectively use its T6SS.

A notable observation in fluorescent microscopy experiments to visualise T6SS sheath structures was the variation in the localisation, abundance and dynamics of the *P. aeruginosa* T6SSs. While H1- and H2-T6SS sheath structures were randomly assembled throughout the cell, H3-T6SS sheath structures were found to localise at the cell poles (Figures 3.6, 3.11 and 3.14). The abundance of these structures also varied: in a *rsmA* background, when cells were grown in liquid culture prior to imaging H2- and H3-T6SS sheath structures were identified in 62 % and 39 % of cells respectively, while H1-T6SS sheath structures were identified in just 0.14 % of cells per minute (Figures 3.1, 3.11 and 3.14). For the H1-T6SS more sheath structures were observed upon growth on solid media prior to imaging, while for

the H2-T6SS this led to fewer sheaths being present. Additionally, cells grown in liquid culture assembled multiple H2-T6SS sheath structures per cell, sometimes as many as six, while cells generally assembled single H2-T6SS sheaths when grown on solid media. Cells generally produced single H1- and H3-T6SS sheaths regardless of the method of sample preparation. As previously noted, these T6SSs also have varied firing dynamics, with H1-T6SSs firing quickly after sheath assembly, H2-T6SSs remaining stable for a long period of time after assembly and with firing rarely being observed for assembled H3-T6SS sheaths (see section 3.6.4).

6.1.1 Future perspectives: TssA functionality and T6SS regulation

It does remain of interest to better characterise the sheath structures that are formed in the absence of TssA proteins. For example, while a small number of these structures are observed to extend and contract, it has not been conclusively demonstrated that this contraction is functional and paired with the expulsion of T6SS components, including effectors. It could be that these are non-canonical contraction events that do not cause effective secretion, explaining why their effects cannot be demonstrated in functional assays. Alternatively, it may purely be due to a low frequency of T6SS contraction events within the population.

Interestingly, it appears that sample preparation for fluorescent microscopy can influence the abundance of these sheath structures (Figure 3.11) (see section 3.6.1). In optimising these assays, it was observed that H1-T6SS sheath abundance was elevated when cells were grown on solid media prior to imaging as compared to growth in liquid media. This could be explained by increased contact between bacteria on solid media, where the firing of a H1-T6SS at a neighbouring cell would activate T6SS duelling by a tit-for-tat response (479). The opposite was true for the H2-T6SS, where tit-for-tat behaviour is not seen, with sheath abundance elevated with cells grown in liquid culture when compared to solid media. Remarkably, sheath abundance in the absence of *tssA2* also differed between the two approaches, from almost no sheaths on solid media to 23 % in liquid media (Figure 3.11). The reason for this varied sheath abundance is not clear as several factors were altered between these approaches. The production of these T6SSs likely varies depending on the environmental conditions, and this work provides some evidence that certain conditions could potentially also alter the requirement for the TssA protein. Investigating how T6SS abundance and activity are regulated under different conditions could therefore offer new insights into TssA function.

In the absence of functional assays to assess H3-T6SS activity, there are limits to the characterisation of TssA3. Future work should therefore also attempt to better characterise the regulation of the H3-

T6SS, including the conditions or stimuli required to activate firing. One candidate that stands out for future study is the sigma factor activator, *sfa3*, which is encoded in the H3-T6SS cluster. While the H2-T6SS-associated Sfa2 was demonstrated to activate expression of the H2-T6SS, and repress the H1- and H3-T6SS, the activity of Sfa3 remains elusive (501). To date just a single H3-T6SS effector has been identified, TseF involved in iron acquisition, where iron-limiting conditions were demonstrated to induce H3-T6SS expression (311). Identification and characterisation of other effectors associated with this T6SS could provide further clues about the conditions required to activate H3-T6SS firing. Candidates for this have been identified in pulldown experiments using Hcp3 (412).

An interesting feature of H3-T6SS sheath structures was their polar positioning within the cell, as compared to non-polar positioning for H1- and H2-T6SS structures (Figures 3.6, 3.11 and 3.14). Polar localisation of a T6SS apparatus has been identified previously in *F. novicida* and the T6SS-5 of *B. thailandensis* (599,600). Polarly localised H3-T6SS sheaths had two distinct orientations: either extending along the long axis of the cell but terminating before reaching the opposite pole, or extending diagonally from the pole until reaching a membrane (508). In contrast, polar *F. novicida* sheaths were found to span the length of the cell (599). It has been suggested that this longer sheath assembled between the cell poles could allow a greater force to be delivered through sheath contraction, perhaps allowing delivery of effectors over a greater distance. While this would not be the case for the H3-T6SS it does demonstrate how differences in T6SS positioning could contribute to functional diversity. It is also worth noting that the polar *B. thailandensis* sheaths were observed, like H3-T6SS sheaths, to fire quite infrequently (600).

Confining T6SS localisation to the poles may limit the efficiency of T6SS activity if the intended target does not align with this localisation, for example, an antibacterial T6SS would only be able to fire at competitors at cell poles. Likewise, it seems unlikely that the H3-T6SS would be able to effectively respond to T6SS attack by a competitor via tit-for-tat, as spatial re-orientation of the T6SS would not be possible. Both the *F. novicida* T6SS and the *B. thailandensis* T6SS-5 are important in eukaryotic cell manipulation following bacterial internalisation. The *F. novicida* T6SS is important in phagosomal escape, while the *B. thailandensis* T6SS-5 is involved in the formation of multinucleated giant cells (599,600). It has been suggested that within this intracellular environment, polar localisation may be beneficial as the cell poles are likely to be closer to the membranes surrounding the bacteria (599). While commonly considered an extracellular pathogen, *P. aeruginosa* can be taken up by non-phagocytic cells, notably the H2-T6SS evolved effector VgrG2b promotes microtubule-dependent internalisation into epithelial cells (442). It could be that following internalisation the polar H3-T6SS has a role to play in host cell manipulation. As previously outlined, identification and characterisation of H3-T6SS effectors is important to better understanding its functional role.

6.2 TssA proteins are sequentially positioned at the membrane complex, baseplate complex and tail complex distal end

TssA proteins have been identified to interact with components of the T6SS membrane complex, baseplate complex and tail complex (360,376,377,509,512). This indicates a dynamic localisation during T6SS activity, which has been further characterised through fluorescence microscopy experiments, identifying the positioning of TssA proteins over time relative to other T6SS components (360,377,508,513). Interactions with baseplate complex and tail complex components were also identified in this study (Figures 4.5 and 4.6). The current model for the assembly and firing of the T6SS is outlined below, including proposed contributions of TssA proteins.

The assembly of the T6SS begins with the insertion of the lipoprotein TssJ in the inner leaflet of the outer membrane via an N-terminal acyl group (346). The inner membrane proteins TssM and TssL are then sequentially recruited, and these three components polymerise to form the bell-shaped membrane complex, which in enteroaggregative *E. coli* has five-fold symmetry (see section 1.3.2.2) (344,345,347,356). This membrane complex extends into the cytoplasm, with cytoplasmic domains of TssL and TssM forming interactions to dock the baseplate complex to the membrane complex (344,354). A symmetry mismatch, however, exists between the five-fold symmetry of the membrane complex and the six-fold symmetry of the baseplate complex (347,356,365). One suggestion for how this symmetry mismatch is overcome is in flexibility of cytoplasmic domains. Alternatively, as this structural data was generated by overproduction of solely membrane complex components, it has been suggested that in the native context some other protein/s may be involved in generating a six-fold symmetry membrane complex.

Given the interaction that has been demonstrated between TssA proteins and the inner membrane proteins of the T6SS (360,509,512), TssA has been suggested to act as a chaperone to guide the symmetry of the membrane complex (361). The recruitment of TssA to the membrane complex is dependent on TssM, suggesting that TssA could be recruited before TssL (360,537). While TssA is not required for TssL binding, TssA could be recruited during membrane complex assembly and influence polymerisation of the membrane complex (347). Upon co-purification and EM analysis of $TssA^{EC}$ with its respective membrane complex, $TssA^{EC}$ was implicated as binding at the cytoplasmic face of the complex (360). It was proposed that association of the six-fold symmetry $TssA^{EC}$ C-terminal region with the cytoplasmic face during membrane complex assembly may guide the membrane complex into a six-fold symmetric state (361). While this makes sense with the six-fold $TssA^{EC}$ symmetry, the symmetries of TssA proteins are very variable and it is less likely that the 16-fold symmetry $TssA^{BC}$ would similarly guide the formation of a six-fold symmetry membrane complex (509). It therefore

seems more likely that a symmetry mismatch between the T6SS membrane complex and baseplate complex exists but is overcome by the flexibility in interacting regions, although it cannot be ruled out that some other component modifies membrane complex symmetry. The functional contribution of the interaction of TssA proteins with membrane complex components remains unclear. Interestingly, the T6SS^{iv} of *A. asiaticus* lacks the archetypal membrane complex components, but has an apparently functionally similar anchoring platform linked to the inner membrane, which, like its baseplate has six-fold symmetry (312). While this may not have any relevance to the phylogenetically distinct archetypal T6SS^{i} and its associated membrane complex, it is noteworthy that this apparent symmetry mismatch is not present in this machinery.

Following the assembly of the membrane complex, the baseplate complex is recruited. The baseplate complex comprises a central hub formed of the trimeric spike protein VgrG, surrounded by six wedges of $TssE_1$-$TssF_2$-$TssG_1$-$TssK_6$ (see section 1.3.2.3) (365,369). The tip of this VgrG hub is capped with a protein of the PAAR repeat family, which sharpens the tip to contribute to membrane piercing (601). Effector proteins can be associated with both VgrG and PAAR proteins, either as evolved effectors encoded as an extension to the spike component or as cargo effectors that interact with spike components (414,415,434,602,603). The two TssK trimers associated with each wedge are more flexibly associated with the baseplate structure and form the contacts with the membrane complex through cytoplasmic domains of TssL and TssM (371). The trigger for baseplate assembly is unclear, it has been suggested that it may be triggered by contact with the membrane complex or through contact with other proteins such as TssA.

TssA^{EC} associates with the membrane complex prior to the recruitment of the baseplate complex (360). Based on the interaction of TssA proteins with components of both the membrane complex and baseplate complex (360,509,512), it was suggested that TssA may be required for the docking of these complexes (360). However, the recruitment of fluorophore tagged baseplate proteins to the membrane complex was identified independent of TssA^{EC}, suggesting that neither the assembly of the baseplate complex, nor recruitment to the membrane complex requires TssA (365). As outlined previously (see section 3.6.2), it has been suggested that some TssA proteins are static components of the baseplate complex (376,377). While there is some evidence that TssA1 associates statically with the baseplate complex during T6SS assembly and activity, this does not seem to be a general trend as other TssA proteins only transiently associate with the T6SS assembly initiation site prior to the polymerisation of the tail complex (360,377,508,513). The functional contribution of the interaction of TssA proteins with baseplate complex components is therefore also unclear. It may be that TssA stabilises the association of membrane and baseplate complexes or facilitates a particular mode of interaction which is more conducive to assembly of the tail complex. Alternatively, interactions with

the membrane and baseplate complexes may simply serve to recruit TssA proteins to the T6SS assembly initiation site to facilitate downstream activity.

While the role of TssA proteins in their interaction with both membrane and baseplate complexes components is yet to be elucidated, the picture is slightly clearer for the association of TssA proteins with the tail complex.

The baseplate provides a platform for the polymerisation of the tail complex comprising the Hcp inner tube and the surrounding sheath, which assembles in a high energy extended conformation (364,365,369,374). The polymerisation of the Hcp tube is nucleated from the base of the VgrG spike, and Hcp rings can interact with effector proteins to transport them out of the cell (313,373,380). Each sheath subunit is formed of a protomer comprising TssB and TssC which polymerise to form a helical tube around the Hcp inner tube (385,386). Based on comparisons to the phage contractile tail, it is suggested that contraction of the T6SS sheath is initiated by conformational changes in the baseplate (405,411,604). Sequential contraction of sheath rings from the baseplate to the distal end of the sheath involves a radial expansion of the sheath to release contacts with the Hcp inner tube, which is rotated as it is expelled out of the cell (385–387). Roles have been suggested for TssA proteins in the initiation and coordination of sheath polymerisation (360,377).

The interaction of TssA proteins with components of the tail complex, both sheath components and Hcp, has been widely described (360,376,509,512). In general, TssA proteins localise at the T6SS assembly initiation site before being displaced to the distal end of the tail complex where they are pushed towards the opposite side of the cell by tail complex polymerisation (360,377,508,513). In T6SSs containing a $TssA_S$ protein and an associated TagB accessory protein, the TssA recruits TagB to the baseplate complex where it accumulates, stabilising the baseplate to prevent the conformational change associated with T6SS firing until the sheath is fully extended (508). In T6SSs containing a $TssA_L$ and an associated TagA accessory protein, the TagA protein anchors the distal end of the sheath at the opposite membrane following polymerisation (377,510).

This work has identified that the interaction of TssA proteins with the sheath involves TssA Nt1 domains (Figure 4.20). In the absence of TssA proteins, it has been observed that the formation of sheath structures is either completely lost or much reduced, so TssA proteins are likely involved in the initiation and coordination of tail complex polymerisation (see section 3.6.1) (360,376,377,508). This work also demonstrated that T6SS sheath assembly is dependent on the presence of the cognate TssA Nt1 domain positioned at the periphery of a ring-shaped structure, which can remain functional if the C-terminal region is exchanged (Figure 5.4, 5.5 and 5.6). It is therefore clear that TssA proteins contribute to proper assembly of the tail complex. A model for the contribution of TssA proteins to

the polymerisation of the T6SS has therefore been proposed (see section 5.7.4). This involves the positioning of the TssA C-terminal domain ring at the distal end of the tail complex, with Nt1 domains extending below and docking in grooves on the tip of the sheath complex. It is hypothesised that as new sheath protomers are incorporated at this distal end, repositioning of Nt1 domains allows contacts with the sheath to be maintained.

Following sheath contraction, the ClpV binding site at the N-terminus of TssC is exposed, which allows the recycling of contracted sheath components by the ClpV ATPase (385,391). Interactions have been demonstrated between TssA and ClpV proteins (376,377). It has been suggested that this interaction may be associated with the recycling of the TssA complex, although there is no direct evidence that such a process exists or would even be required for TssA (376). Alternatively, TssA proteins could contribute to the recruitment of ClpV proteins.

6.2.1 Future perspectives: TssA positioning and role

While this work was able to build on the existing data surrounding the interaction of TssA proteins with the tail complex, specifically the interaction with the sheath, the nature and role of interactions with other T6SS components, such as the membrane complex and baseplate complex remain elusive. As outlined above, it has been proposed that TssA may promote the stability and interaction of membrane and baseplate complexes, or alternatively, these interactions may serve purely to recruit TssA to the T6SS. The main questions to answer in the characterisation of these interactions are: How does TssA interact with these components? What is the functional contribution of these interactions to T6SS activity?

Identification and characterisation of TssA interactions with other T6SS components commonly involves biochemical approaches. Interaction partners of TssA proteins have been identified using a variety of approaches, however, a more detailed characterisation of these interactions could offer further insight into functional contributions. This could be gained from an understanding of which domains of TssA participate in these interactions. Such characterisation was attempted in this study, using a BTH approach, but should be supplemented in future with additional techniques including pulldowns. *In silico* methods can build on biochemical data to model interactions, however these rely on structural data which should be expanded upon, for example resolving the structure of the TssA1 Nt1 domain would improve the reliability of a model for the docking to the H1-T6SS sheath structure.

Previous insights into the dynamics and role of TssA interactions have been gained through fluorescence microscopy (360). This approach could further be used to answer questions about the

role of the association between TssA and the membrane and baseplate complexes. For example, the fluorophore tagging of components, i.e. TssM and TssK, could allow the abundance and co-localisation of these complexes to be assessed in the presence and absence of TssA, to validate whether this protein promotes their association or stability. Furthermore, such an approach could help elucidate whether proteins that have been identified to interact, such as TssA and ClpV, can be shown to co-localise during the activity of the T6SS, which could provide clues to a functional role. Within this project, studying the co-localisation of T6SS proteins, such as TssA and TssB, proved challenging (Figure 3.9). It may be that future optimisation can improve this, as *P. aeruginosa* PAO1 has been successfully used for such experiments by other groups (377). However, we have previously had more success in studying co-localisation using the *P. putida* K1-T6SS (508), which may be a more promising model organism for studying the T6SS by fluorescence microscopy.

Characterisation of the interactions of TssA proteins, both at the biochemical and functional level, is key to revealing the full role that this protein plays in the assembly and dynamics of the T6SS. Previous work has enabled us to propose a model of TssA as a crucial component in the polymerisation of the tail complex, but whether TssA also contributes at other stages during T6SS activity remains a key question.

6.2.2 Future perspectives: Validation of TssA-sheath docking hypothesis

This work has identified the specific interaction between TssA Nt1 domains and cognate sheath components, from which a model for the docking of the TssA1 Nt1 domain to the H1-T6SS sheath was proposed (see section 5.7.4). Further work is required to validate whether this model is accurate.

The reliability of the current docking model is affected by using a structural model for the TssA Nt1 domain generated from the only available Nt1 domain structure to date, $TssA^{BC}$ (509). Thus, resolving the structure of the TssA1 Nt1 domain would allow a more accurate docking to be predicted. From a reliable docking model, it is possible to identify residues which are proposed to stabilise such an interaction, whose contribution to the interaction could be tested by mutagenesis. Given the specificity identified for the interactions of the Nt1 domains (Figure 5.9), if the structures of multiple Nt1 domains were available, such as those of TssA2 and TssA3, structural comparisons could help in identifying the determinants of specificity in interactions with cognate sheath components. Given the time-consuming nature of resolving protein structures, an alternative or parallel strategy could be the use of the AlphaFold system to generate structural models, which may be more reliable (605).

A hypothesis suggested in this work was that the ImpA_N region may be responsible for sheath binding. Structural characterisation of Nt1 domains would also allow ImpA_N region structures to be compared. This hypothesis could further be tested by assessing the interaction of ImpA_N regions alone with their respective sheath components.

To date, no high-resolution structure of a full length TssA protein has been resolved, only structures of individual domains or pairs of domains, such as C-terminal and Nt2 domains (see section 1.4.1) (360,376,377,509). The absence of such full-length structures is likely due to the flexibility of the linker regions connecting C-terminal regions to Nt1 domains. Despite this, it is widely accepted that the Nt1 domains are peripherally associated with the C-terminal ring structure (360,376,377,509). The proposed model for TssA-sheath docking involves the C-terminal ring structure positioned above the tip of the distal end of the sheath, with some Nt1 domains extending below to contact the sheath (see section 5.7.4). Data that could further inform this model would be understanding the relative position of Nt1 domains relative to the C-terminal ring structure, both in terms of the relative distance between them and the degree of flexibility. It would be interesting to compare this positioning for long and short TssA proteins, where it has been suggested that the Nt1 domains are positioned at a similar distance from the centre of the ring structure via distinct C-terminal regions (Figure 1.24) (509). In $TssA_S$ proteins, the Nt1 domain is connected to the C-terminal domain ring, while in $TssA_L$ proteins, the Nt1 domain in connected to the Nt2 domain which is already flexibly associated with the C-terminal domain ring (Figure 4.32). The relative position and flexibility of these Nt1 domains may therefore vary, which may affect the relative position of the C-terminal region at the distal end of the sheath.

Based on the available evidence a model has been proposed for the interaction between the TssA Nt1 domains and the cognate sheath. Further work is required to firstly validate this model, and then build on the foundations to unpick how TssA influences sheath assembly at the distal end of this structure.

6.3 TssA proteins remain functional with exchange of C-terminal regions

The functional implications of the variation in TssA proteins are poorly understood. It has been identified that the variation in TssA size corresponds with the presence of accessory proteins that influence sheath stability (see section 3.6.3) and with the dynamics of sheath contraction (see section 3.6.4). However, the details of how these functional differences arise are unclear. Despite variation in size, structure, domain organisation and symmetry, TssA proteins are generally similar in their requirement and positioning in the T6SS (see sections 3.6.1 and 4.7.3). It has been proposed that this similarity arises through distinct mechanisms of positioning the conserved Nt1 domains at the periphery of ring structures (509). Here, chimeric TssA proteins were generated, by the exchange of domains and their functionality assessed in each of the *P. aeruginosa* T6SSs to investigate the activity and specificity of TssA domains.

It was identified that functional chimeric TssA proteins could be generated that contained the cognate Nt1 domain but with exchanged C-terminal regions (Figures 5.4, 5.5 and 5.6). For $TssA_S$ proteins, the exchange of, what would be expected to be very similar C-terminal domains, generated chimeric proteins that were indistinguishable functionally from the wildtype. More surprisingly, introduction of these $TssA_S$ C-terminal domains in place of the $TssA_L$ Nt2 and C-terminal domains generated chimeric TssA proteins that were functional in the H2-T6SS. While the generation of functional chimeric TssA proteins from domain exchange between $TssA_S$ proteins was alone incredibly novel, it was even more interesting to find that exchange of domains between long and short TssA proteins generated functional chimeric proteins.

The functionality of certain chimeric TssA proteins suggests that Nt1 domains are the key determinant of the activity and specificity of TssA proteins, while C-terminal regions are not specifically required for that purpose. Instead, it appears that C-terminal regions are important for oligomerisation into a ring-shaped structure that orientates Nt1 domains.

6.3.1 Future perspectives: Functionality of chimeric TssA proteins

Chimeric TssA proteins involving exchange of the $TssA_S$ C-terminal domains showed complete functionality when compared to the wildtype (Figures 5.4 and 5.5). Our understanding of the structures formed by these C-terminal domains is currently incomplete. While the rings they form appear similar (Figures 5.14 and 5.15), it is not known whether these exchanges introduced altered ring dimensions or symmetries. It would therefore be informative to conclusively determine the dimensions and symmetries of these C-terminal domain rings to understand the extent of variation

that is introduced with this exchange. Additionally, generating further chimeric proteins, for example introducing C-terminal domains from previously studied $TssA_S$ proteins $TssA^{BC}$ and $TssA1^{PP}$, could help define whether there are limits to such an exchange. Similar approaches could also be carried out with the $TssA_L$ proteins of $TssA^{EC}$ and $TssA^{VC}$ to determine whether a chimeric TssA protein formed solely of $TssA_L$ domains would also be indistinguishable from the wildtype. An additional level of complexity when considering $TssA_L$ proteins is the structural variation between different $TssA_L$ C-terminal domains introduced by the presence of a C-terminal extension (see section 1.4.1.3). This C-terminal extension alters the relative position of stacked monomers and therefore the thickness of the C-terminal domain ring (509). Given that chimeric TssA proteins with the TssA2 Nt1 domain and the C-terminal domains of $TssA_S$ proteins were functional in the H2-T6SS, it seems likely that exchange of these distinct types of $TssA_L$ C-terminal domains would also generate a functional chimeric protein, but this should be tested.

Some structural characterisations of chimeric TssA proteins could also be informative, for example in validating their oligomerisation into ring-shaped structures. If chimeric TssA proteins were not able to form these structures, it would explain their lack of function.

Given that C-terminal domains are not specifically required for the activity of their TssA, it could be informative to assess sequence and structural conservation. Highly conserved features have been identified in the C-terminal domains of both long and short TssA proteins, the WEP and EPxxP motifs respectively, which are both suggested to be involved in oligomerisation (see section 1.4.1) (509). As outlined previously, some variation has already been identified in the C-terminal domains of $TssA_L$ proteins in the form of a C-terminal extension, which alters the thickness of the C-terminal domain ring (see section 1.4.1.3). However, the oligomeric state of C-terminal domain rings of $TssA_L$ proteins can vary irrespective of this C-terminal extension, both $TssA^{VC}$ and $TssA^{AH}$ lack the C-terminal extension but have respective six- and five-fold symmetries (377,509). Structural comparison identified that these C-terminal domains were very similar with an RMSD of 1.0 Å, while sequence identity was calculated to be 33 %. The ring structures formed from each of these domains fit the trends associated with $TssA_L$ proteins, but the additional subunit introduced in each layer of the $TssA^{VC}$ C-terminal domain ring, increases the lumen from 25 to 53 Å and the ring diameter from 110 to 153 Å. Attempting to understand the variation in both the sequence and structure of C-terminal domain groups is therefore an interesting avenue for further research.

This work has shed new light on the interaction of TssA proteins with the sheath and identified a previously uncharacterised level of specificity. The TssA C-terminal region may not be specifically

required for T6SS activity but probing the limits of domain exchange in chimeric TssA proteins may shed light on the requirements of these regions, which remain important to TssA activity.

6.4 Conclusion

Overall, this project has provided a comprehensive characterisation of the TssA proteins of *P. aeruginosa* in their contribution to T6SS activity and in the positioning within this machinery. Novel features of TssA proteins have been identified, such as the interaction of Nt1 domains with the sheath, the functionality of chimeric TssA proteins and the requirement of Nt1 domains for TssA activity and specificity. With this work an existing hypothesis for how TssA proteins coordinate the polymerisation of the tail complex has been refreshed with new data, elements of which can now be validated or challenged to further our understanding of how TssA proteins influence the assembly and dynamics of the T6SS.

7. Bibliography

1. Rahme LG, Tan M-W, Le L, Wong SM, Tompkins RG, Calderwood S, et al. Use of model plant hosts to identify *Pseudomonas aeruginosa*. Proc Natl Acad Sci. 1997;94(November):13245–50.

2. Morrison AJJ, Wenzel R*P.* Epidemiology of infections due to *Pseudomonas aeruginosa*. Rev Infect Dis. 1984;6 Suppl 3:S627-42.

3. Tan M-W, Rahme LG, Sternberg JA, Tompkins RG, Ausubel FM. *Pseudomonas aeruginosa* killing of Caenorhabditis elegans used to identify *P. aeruginosa* virulence factors. Proc Natl Acad Sci [Internet]. 1999;96(5):2408–13. Available from: http://www.pnas.org/cgi/doi/10.1073/pnas.96.5.2408

4. He J, Baldini RL, Déziel E, Saucier M, Zhang Q, Liberati NT, et al. The broad host range pathogen *Pseudomonas aeruginosa* strain PA14 carries two pathogenicity islands harboring plant and animal virulence genes. Proc Natl Acad Sci U S A [Internet]. 2004;101(8):2530–5. Available from: http://www.pubmedcentral.nih.gov/articlerender.fcgi?artid=356984&tool=pmcentrez&rendertype=abstract

5. Stover CK, Pham XQ, Erwin a L, Mizoguchi SD, Warrener P, Hickey MJ, et al. Complete genome sequence of *Pseudomonas aeruginosa* PAO1, an opportunistic pathogen. Nature. 2000;406(6799):959–64.

6. Mathee K, Narasimhan G, Valdes C, Qiu X, Matewish JM, Koehrsen M, et al. Dynamics of *Pseudomonas aeruginosa* genome evolution. Proc Natl Acad Sci U S A. 2008 Feb;105(8):3100–5.

7. Holloway BW. Genetic recombination in *Pseudomonas aeruginosa*. J Gen Microbiol. 1955;13(3):572–81.

8. Chandler C, Horspool AM, Hill PJ, Wozniak DJ, Schertzer JW, Rasko DA, et al. Genomic and Phenotypic Diversity among Ten Laboratory Isolates of *Pseudomonas aeruginosa* PAO1. J Bacteriol. 2019;201(5).

9. Klockgether J, Cramer N, Wiehlmann L, Davenport CF, Tümmler B. *Pseudomonas aeruginosa* Genomic Structure and Diversity. Front Microbiol. 2011;2:150.

10. Rosenthal VD, Bat-Erdene I, Gupta D, Belkebir S, Rajhans P, Zand F, et al. International Nosocomial Infection Control Consortium (INICC) report, data summary of 45 countries for 2012-2017: Device-associated module. Am J Infect Control. 2020 Apr;48(4):423–32.

11. Weiner LM, Webb AK, Limbago B, Dudeck MA, Patel J, Kallen AJ, et al. Antimicrobial-Resistant Pathogens Associated With Healthcare-Associated Infections: Summary of Data Reported to the National Healthcare Safety Network at the Centers for Disease Control and Prevention, 2011-2014. Infect Control Hosp Epidemiol. 2016 Nov;37(11):1288–301.

12. Norbury W, Herndon DN, Tanksley J, Jeschke MG, Finnerty CC. Infection in Burns. Surg Infect (Larchmt). 2016 Apr;17(2):250–5.

13. Elgohari S, Wilson J, Saei A, Sheridan EA, Lamagni T. Impact of national policies on the microbial aetiology of surgical site infections in acute NHS hospitals in England: analysis of trends between 2000 and 2013 using multi-centre prospective cohort data. Epidemiol Infect. 2017 Apr;145(5):957–69.

14. Massart N, Mansour A, Ross JT, Piau C, Verhoye J-P, Tattevin P, et al. Mortality due to

hospital-acquired infection after cardiac surgery. J Thorac Cardiovasc Surg. 2022 Jun;163(6):2131-2140.e3.

15. Kitagawa K, Shigemura K, Yamamichi F, Osawa K, Uda A, Koike C, et al. Bacteremia complicating urinary tract infection by *Pseudomonas aeruginosa*: Mortality risk factors. Int J Urol Off J Japanese Urol Assoc. 2019 Mar;26(3):358–62.

16. Parker CM, Kutsogiannis J, Muscedere J, Cook D, Dodek P, Day AG, et al. Ventilator-associated pneumonia caused by multidrug-resistant organisms or *Pseudomonas aeruginosa*: prevalence, incidence, risk factors, and outcomes. J Crit Care. 2008 Mar;23(1):18–26.

17. Heyland DK, Cook DJ, Griffith L, Keenan SP, Brun-Buisson C. The attributable morbidity and mortality of ventilator-associated pneumonia in the critically ill patient. The Canadian Critical Trials Grou*P.* Am J Respir Crit Care Med. 1999 Apr;159(4 Pt 1):1249–56.

18. Kollef MH, Chastre J, Fagon J-Y, François B, Niederman MS, Rello J, et al. Global prospective epidemiologic and surveillance study of ventilator-associated pneumonia due to *Pseudomonas aeruginosa*. Crit Care Med. 2014 Oct;42(10):2178–87.

19. Johnson LE, D'Agata EMC, Paterson DL, Clarke L, Qureshi ZA, Potoski BA, et al. *Pseudomonas aeruginosa* bacteremia over a 10-year period: multidrug resistance and outcomes in transplant recipients. Transpl Infect Dis an Off J Transplant Soc. 2009 Jun;11(3):227–34.

20. Cherif H, Kronvall G, Björkholm M, Kalin M. Bacteraemia in hospitalised patients with malignant blood disorders: a retrospective study of causative agents and their resistance profiles during a 14-year period without antibacterial prophylaxis. Hematol J Off J Eur Haematol Assoc. 2003;4(6):420–6.

21. Carvalho AS, Lagana D, Catford J, Shaw D, Bak N. Bloodstream infections in neutropenic patients with haematological malignancies. Infect Dis Heal. 2020 Feb;25(1):22–9.

22. Stern GA. *Pseudomonas* keratitis and contact lens wear: the lens/eye is at fault. Cornea. 1990;9 Suppl 1:S36-8; discussion S39-40.

23. Burns JL, Gibson RL, McNamara S, Yim D, Emerson J, Rosenfeld M, et al. Longitudinal assessment of *Pseudomonas aeruginosa* in young children with cystic fibrosis. J Infect Dis. 2001 Feb;183(3):444–52.

24. Armstrong DS, Grimwood K, Carlin JB, Carzino R, Olinsky A, Phelan PD. Bronchoalveolar lavage or oropharyngeal cultures to identify lower respiratory pathogens in infants with cystic fibrosis. Pediatr Pulmonol. 1996 May;21(5):267–75.

25. Cystic Fibrosis Foundation. Cystic Fibrosis Foundation Patient Registry 2013 Annual Data Report to the Center Directors. Bethesda, Maryland; 2013.

26. Elborn JS. Cystic fibrosis. Vol. 388, The Lancet. 2016. *P.* 2519–31.

27. Riquelme SA, Ahn D, Prince A. *Pseudomonas aeruginosa* and Klebsiella pneumoniae Adaptation to Innate Immune Clearance Mechanisms in the Lung. J Innate Immun. 2018;10(5–6):442–54.

28. FitzSimmons SC. The changing epidemiology of cystic fibrosis. J Pediatr. 1993 Jan;122(1):1–9.

29. Emerson J, Rosenfeld M, McNamara S, Ramsey B, Gibson RL. *Pseudomonas aeruginosa* and other predictors of mortality and morbidity in young children with cystic fibrosis. Pediatr Pulmonol. 2002 Aug;34(2):91–100.

30. Li Z, Kosorok MR, Farrell PM, Laxova A, West SEH, Green CG, et al. Longitudinal development

of mucoid *Pseudomonas aeruginosa* infection and lung disease progression in children with cystic fibrosis. JAMA. 2005 Feb;293(5):581–8.

31. Saint-Criq V, Gray MA. Role of CFTR in epithelial physiology. Cell Mol Life Sci. 2017 Jan;74(1):93–115.

32. Rogers DF, Alton EWFW, Dewar A, Lethem MI, Barnes PJ. Impaired stimulus-evoked mucus secretion in cystic fibrosis bronchi. Exp Lung Res. 1993;19(1):37–53.

33. Matsui H, Wagner VE, Hill DB, Schwab UE, Rogers TD, Button B, et al. A physical linkage between cystic fibrosis airway surface dehydration and *Pseudomonas aeruginosa* biofilms. Proc Natl Acad Sci U S A. 2006 Nov;103(48):18131–6.

34. Mougous JD, Cuff ME, Raunser S, Shen A, Zhou M, Gifford CA, et al. A Virulence Locus of *Pseudomonas aeruginosa* Encodes a Protein Secretion Apparatus. Science (80-). 2006;312(5779):1526–30.

35. Smith EE, Buckley DG, Wu Z, Saenphimmachak C, Hoffman LR, D'Argenio DA, et al. Genetic adaptation by *Pseudomonas aeruginosa* to the airways of cystic fibrosis patients. Proc Natl Acad Sci U S A. 2006 May;103(22):8487–92.

36. Malhotra S, Hayes DJ, Wozniak DJ. Mucoid *Pseudomonas aeruginosa* and regional inflammation in the cystic fibrosis lung. J Cyst Fibros Off J Eur Cyst Fibros Soc. 2019 Nov;18(6):796–803.

37. Martin DW, Schurr MJ, Mudd MH, Govan JRW, Holloway BW, Deretic V. Mechanism of conversion to mucoidy in *Pseudomonas aeruginosa* infecting cystic fibrosis patients. Proc Natl Acad Sci U S A. 1993;90(18):8377–81.

38. Mahenthiralingam E, Campbell ME, Speert D*P.* Nonmotility and phagocytic resistance of *Pseudomonas aeruginosa* isolates from chronically colonized patients with cystic fibrosis. Infect Immun. 1994 Feb;62(2):596–605.

39. Lee VT, Smith RS, Tümmler B, Lory S. Activities of *Pseudomonas aeruginosa* effectors secreted by the Type III secretion system in vitro and during infection. Infect Immun. 2005 Mar;73(3):1695–705.

40. Marvig RL, Damkiær S, Khademi SMH, Markussen TM, Molin S, Jelsbak L. Within-host evolution of *Pseudomonas aeruginosa* reveals adaptation toward iron acquisition from hemoglobin. MBio. 2014 May;5(3):e00966-14.

41. Liou TG, Adler FR, FitzSimmons SC, Cahill BC, Hibbs JR, Marshall BC. Predictive 5-Year Survivorship Model of Cystic Fibrosis. Am J Epidemiol. 2001;153(4):345–52.

42. Jacques I, Derelle J, Weber M, Vidailhet M. Pulmonary evolution of cystic fibrosis patients colonized by *Pseudomonas aeruginosa* and/or *Burkholderia cepacia*. Eur J Pediatr. 1998 May;157(5):427–31.

43. Lillehoj EP, Kim H, Chun EY, Kim KC. *Pseudomonas aeruginosa* stimulates phosphorylation of the airway epithelial membrane glycoprotein Muc1 and activates MAP kinase. Am J Physiol Lung Cell Mol Physiol. 2004 Oct;287(4):L809-15.

44. Adamo R, Sokol S, Soong G, Gomez MI, Prince A. *Pseudomonas aeruginosa* flagella activate airway epithelial cells through asialoGM1 and toll-like receptor 2 as well as toll-like receptor 5. Am J Respir Cell Mol Biol. 2004 May;30(5):627–34.

45. Bucior I, Pielage JF, Engel JN. *Pseudomonas aeruginosa* pili and flagella mediate distinct binding and signaling events at the apical and basolateral surface of airway epithelium. PLoS

Pathog. 2012;8(4):e1002616.

46. Berube BJ, Rangel SM, Hauser AR. *Pseudomonas aeruginosa*: breaking down barriers. Curr Genet. 2016;62(1):109–13.

47. Irie Y, Starkey M, Edwards AN, Wozniak DJ, Romeo T, Parsek MR. *Pseudomonas aeruginosa* biofilm matrix polysaccharide Psl is regulated transcriptionally by RpoS and post-transcriptionally by RsmA. Mol Microbiol. 2010;78(1):158–72.

48. Brencic A, Lory S. Determination of the regulon and identification of novel mRNA targets of *Pseudomonas aeruginosa* RsmA. Physiol Behav. 2011;176(5):139–48.

49. Goodman AL, Kulasekara B, Rietsch A, Boyd D, Smith RS, Lory S. A signaling network reciprocally regulates genes associated with acute infection and chronic persistence in *Pseudomonas aeruginosa*. Dev Cell. 2004;

50. Valentini M, Gonzalez D, Mavridou DA, Filloux A. Lifestyle transitions and adaptive pathogenesis of *Pseudomonas aeruginosa*. Curr Opin Microbiol [Internet]. 2018;41:15–20. Available from: http://dx.doi.org/10.1016/j.mib.2017.11.006

51. Sauer K, Camper AK, Ehrlich GD, Costerton JW, Davies DG. *Pseudomonas aeruginosa* displays multiple phenotypes during development as a biofilm. J Bacteriol. 2002;184(4):1140–54.

52. Monds RD, O'Toole GA. The developmental model of microbial biofilms: ten years of a paradigm up for review. Trends Microbiol. 2009;17(2):73–87.

53. Siryaporn A, Kuchma SL, O'Toole GA, Gitai Z. Surface attachment induces *Pseudomonas aeruginosa* virulence. Proc Natl Acad Sci U S A. 2014 Nov;111(47):16860–5.

54. Chua SL, Liu Y, Yam JKH, Chen Y, Vejborg RM, Tan BGC, et al. Dispersed cells represent a distinct stage in the transition from bacterial biofilm to planktonic lifestyles. Nat Commun. 2014;5.

55. Damron FH, Oglesby-Sherrouse AG, Wilks A, Barbier M. Dual-seq transcriptomics reveals the battle for iron during *Pseudomonas aeruginosa* acute murine pneumonia. Sci Re*P.* 2016 Dec;6:39172.

56. Schaber JA, Triffo WJ, Suh SJ, Oliver JW, Hastert MC, Griswold JA, et al. *Pseudomonas aeruginosa* forms biofilms in acute infection independent of cell-to-cell signaling. Infect Immun. 2007 Aug;75(8):3715–21.

57. Tacconelli E, Carrara E, Savoldi A, Harbarth S, Mendelson M, Monnet DL, et al. Discovery, research, and development of new antibiotics: the WHO priority list of antibiotic-resistant bacteria and tuberculosis. Lancet Infect Dis. 2018 Mar;18(3):318–27.

58. Boucher HW, Talbot GH, Bradley JS, Edwards JE, Gilbert D, Rice LB, et al. Bad bugs, no drugs: no ESKAPE! An update from the Infectious Diseases Society of America. Clin Infect Dis an Off Publ Infect Dis Soc Am. 2009 Jan;48(1):1–12.

59. Bassetti M, Vena A, Croxatto A, Righi E, Guery B. How to manage *Pseudomonas aeruginosa* infections. Drugs Context. 2018;7:1–18.

60. El Zowalaty ME, Al Thani AA, Webster TJ, El Zowalaty AE, Schweizer HP, Nasrallah GK, et al. *Pseudomonas aeruginosa*: arsenal of resistance mechanisms, decades of changing resistance profiles, and future antimicrobial therapies. Future Microbiol. 2015;10(10):1683–706.

61. Magiorakos A-P, Srinivasan A, Carey RB, Carmeli Y, Falagas ME, Giske CG, et al. Multidrug-resistant, extensively drug-resistant and pandrug-resistant bacteria: an international expert

proposal for interim standard definitions for acquired resistance. Clin Microbiol Infect Off Publ Eur Soc Clin Microbiol Infect Dis. 2012 Mar;18(3):268–81.

62. European Centre for Disease Prevention and Control. Antimicrobial resistance surveillance in Europe 2015. Stockholm; 2017.

63. Hancock REW. Resistance Mechanisms in *Pseudomonas aeruginosa* and Other Nonfermentative Gram-Negative Bacteria. Clin Infect Dis [Internet]. 1998;27(December):S93–9. Available from: http://www.jstor.org/stable/4460556

64. Li H, Luo Y-F, Williams BJ, Blackwell TS, Xie C-M. Structure and function of OprD protein in *Pseudomonas aeruginosa*: from antibiotic resistance to novel therapies. Int J Med Microbiol. 2012 Mar;302(2):63–8.

65. Macfarlane ELA, Kwasnicka A, Ochs MM, Hancock REW. PhoP-PhoQ homologues in *Pseudomonas aeruginosa* regulate expression of the outer-membrane protein OprH and polymyxin B resistance. Mol Microbiol. 1999;34(2):305–16.

66. Young ML, Bains M, Bell A, Hancock RE. Role of *Pseudomonas aeruginosa* outer membrane protein OprH in polymyxin and gentamicin resistance: isolation of an OprH-deficient mutant by gene replacement techniques. Antimicrob Agents Chemother. 1992 Nov;36(11):2566–8.

67. Dreier J, Ruggerone *P.* Interaction of antibacterial compounds with RND efflux pumps in *Pseudomonas aeruginosa*. Front Microbiol. 2015;6:660.

68. Poole K. Multidrug efflux pumps and antimicrobial resistance in *Pseudomonas aeruginosa* and related organisms. J Mol Microbiol Biotechnol. 2001 Apr;3(2):255–64.

69. Masuda N, Sakagawa E, Ohya S, Gotoh N, Tsujimoto H, Nishino T. Contribution of the MexX-MexY-OprM efflux system to intrinsic resistance in *Pseudomonas aeruginosa*. Antimicrob Agents Chemother. 2000;44(9):2242–6.

70. Lister PD, Wolter DJ, Hanson ND. Antibacterial-resistant *Pseudomonas aeruginosa*: clinical impact and complex regulation of chromosomally encoded resistance mechanisms. Clin Microbiol Rev. 2009 Oct;22(4):582–610.

71. Girlich D, Naas T, Nordmann *P.* Biochemical characterization of the naturally occurring oxacillinase OXA-50 of *Pseudomonas aeruginosa*. Antimicrob Agents Chemother. 2004;48(6):2043–8.

72. Fajardo A, Hernando-Amado S, Oliver A, Ball G, Filloux A, Martinez JL. Characterization of a novel Zn^{2+}-dependent intrinsic imipenemase from *Pseudomonas aeruginosa*. J Antimicrob Chemother. 2014 Nov;69(11):2972–8.

73. Weldhagen GF, Prinsloo A. Molecular detection of GES-2 extended spectrum β-lactamase producing *Pseudomonas aeruginosa* in Pretoria, South Africa. Int J Antimicrob Agents. 2004;24(1):35–8.

74. Villegas MV, Lolans K, Correa A, Kattan JN, Lopez JA, Quinn J*P.* First identification of *Pseudomonas aeruginosa* isolates producing a KPC-type carbapenem-hydrolyzing β-lactamase. Antimicrob Agents Chemother. 2007;51(4):1553–5.

75. Poole K. Aminoglycoside Resistance in *Pseudomonas aeruginosa*. Antimicrob Agents Chemother. 2005;49(2):479–87.

76. Doi Y, Arakawa Y. 16S ribosomal RNA methylation: emerging resistance mechanism against aminoglycosides. Clin Infect Dis an Off Publ Infect Dis Soc Am. 2007 Jul;45(1):88–94.

77. Bellido F, Veuthey C, Blaser J, Banernfeind A, Pechére JC. Novel resistance to imipenem associated with an altered PBP-4 in a *Pseudomonas aeruginosa* clinical isolate. J Antimicrob Chemother. 1990;25(1):57–68.

78. Aldred KJ, Kerns RJ, Osheroff N. Mechanism of quinolone action and resistance. Biochemistry. 2014 Mar;53(10):1565–74.

79. McPhee JB, Lewenza S, Hancock REW. Cationic antimicrobial peptides activate a two-component regulatory system, PmrA-PmrB, that regulates resistance to polymyxin B and cationic antimicrobial peptides in *Pseudomonas aeruginosa*. Mol Microbiol. 2003 Oct;50(1):205–17.

80. Shigeta M, Tanaka G, Komatsuzawa H, Sugai M, Suginaka H, Usui T. Permeation of antimicrobial agents through *Pseudomonas aeruginosa* biofilms: a simple method. Chemotherapy. 1997;43(5):340–5.

81. Brown MRW, Allison DG, Gilbert *P.* Resistance of bacterial biofilms to antibiotics: a growth-rate related effect? J Antimicrob Chemother. 1999;22:777–83.

82. Madsen JS, Burmølle M, Hansen LH, Sørensen SJ. The interconnection between biofilm formation and horizontal gene transfer. FEMS Immunol Med Microbiol. 2012;65(2):183–95.

83. Driffield K, Miller K, Bostock JM, O'Neill AJ, Chopra I. Increased mutability of *Pseudomonas aeruginosa* in biofilms. J Antimicrob Chemother. 2008 May;61(5):1053–6.

84. Liu Q, Li X, Li W, Du X, He JQ, Tao C, et al. Influence of carbapenem resistance on mortality of patients with *Pseudomonas aeruginosa* infection: A meta-analysis. Sci Re*P.* 2015;5(March):1–10.

85. Barrasa-Villar JI, Aibar-Remón C, Prieto-Andrés P, Mareca-Doñate R, Moliner-Lahoz J. Impact on Morbidity, Mortality, and Length of Stay of Hospital-Acquired Infections by Resistant Microorganisms. Clin Infect Dis an Off Publ Infect Dis Soc Am. 2017 Aug;65(4):644–52.

86. Riu M, Chiarello P, Terradas R, Sala M, Garcia-Alzorriz E, Castells X, et al. Cost Attributable to Nosocomial Bacteremia. Analysis According to Microorganism and Antimicrobial Sensitivity in a University Hospital in Barcelona. PLoS One. 2016;11(4):e0153076.

87. Henderson JC, Zimmerman SM, Crofts AA, Boll JM, Kuhns LG, Herrera CM, et al. The Power of Asymmetry: Architecture and Assembly of the Gram-Negative Outer Membrane Lipid Bilayer. Annu Rev Microbiol. 2016 Sep;70:255–78.

88. Raetz CRH, Whitfield C. Lipopolysaccharide endotoxins. Annu Rev Biochem. 2002;71:635–700.

89. King JD, Kocíncová D, Westman EL, Lam JS. Lipopolysaccharide biosynthesis in *Pseudomonas aeruginosa*. Innate Immun. 2009 Oct;15(5):261–312.

90. Nikaido H. Molecular basis of bacterial outer membrane permeability revisited. Microbiol Mol Biol Rev. 2003 Dec;67(4):593–656.

91. Chow JC, Young DW, Golenbock DT, Christ WJ, Gusovsky F. Toll-like receptor-4 mediates lipopolysaccharide-induced signal transduction. J Biol Chem. 1999 Apr;274(16):10689–92.

92. Wieland CW, Siegmund B, Senaldi G, Vasil ML, Dinarello CA, Fantuzzi G. Pulmonary inflammation induced by *Pseudomonas aeruginosa* lipopolysaccharide, phospholipase C, and exotoxin A: role of interferon regulatory factor 1. Infect Immun. 2002 Mar;70(3):1352–8.

93. Eutamene H, Theodorou V, Schmidlin F, Tondereau V, Garcia-Villar R, Salvador-Cartier C, et al.

LPS-induced lung inflammation is linked to increased epithelial permeability: role of MLCK. Eur Respir J. 2005 May;25(5):789–96.

94. Alshalchi SA, Anderson GG. Expression of the lipopolysaccharide biosynthesis gene lpxD affects biofilm formation of *Pseudomonas aeruginosa*. Arch Microbiol. 2015 Mar;197(2):135–45.

95. Murphy K, Park AJ, Hao Y, Brewer D, Lam JS, Khursigara CM. Influence of O polysaccharides on biofilm development and outer membrane vesicle biogenesis in *Pseudomonas aeruginosa* PAO1. J Bacteriol. 2014 Apr;196(7):1306–17.

96. Lam MY, McGroarty EJ, Kropinski AM, MacDonald LA, Pedersen SS, Høiby N, et al. Occurrence of a common lipopolysaccharide antigen in standard and clinical strains of *Pseudomonas aeruginosa*. J Clin Microbiol. 1989 May;27(5):962–7.

97. Li W, Yan F, Zhou H, Lin X, Wu Y, Chen C, et al. *P. aeruginosa* lipopolysaccharide-induced MUC5AC and CLCA3 expression is partly through Duox1 in vitro and in vivo. PLoS One. 2013;8(5):e63945.

98. Yan F, Li W, Jono H, Li Q, Zhang S, Li J-D, et al. Reactive oxygen species regulate *Pseudomonas aeruginosa* lipopolysaccharide-induced MUC5AC mucin expression via PKC-NADPH oxidase-ROS-TGF-alpha signaling pathways in human airway epithelial cells. Biochem Biophys Res Commun. 2008 Feb;366(2):513–9.

99. Mann EE, Wozniak DJ. *Pseudomonas* biofilm matrix composition and niche biology. FEMS Microbiol Rev. 2012;36(4).

100. O'Toole GA, Kolter R. Flagellar and twitching motility are necessary for *Pseudomonas aeruginosa* biofilm development. Mol Microbiol. 1998 Oct;30(2):295–304.

101. Ma L, Conover M, Lu H, Parsek MR, Bayles K, Wozniak DJ. Assembly and development of the *Pseudomonas aeruginosa* biofilm matrix. PLoS Pathog. 2009;5(3).

102. Cherny KE, Sauer K. *Pseudomonas aeruginosa* Requires the DNA-Specific Endonuclease EndA To Degrade Extracellular Genomic DNA To Disperse from the Biofilm. J Bacteriol. 2019 Sep;201(18).

103. Baker P, Hill PJ, Snarr BD, Alnabelseya N, Pestrak MJ, Lee MJ, et al. Exopolysaccharide biosynthetic glycoside hydrolases can be utilized to disrupt and prevent *Pseudomonas aeruginosa* biofilms. Sci Adv. 2016 May;2(5):e1501632.

104. Pearson JP, Pesci EC, Iglewski BH. Roles of *Pseudomonas aeruginosa* las and rhl quorum-sensing systems in control of elastase and rhamnolipid biosynthesis genes. J Bacteriol. 1997 Sep;179(18):5756–67.

105. Sakuragi Y, Kolter R. Quorum-sensing regulation of the biofilm matrix genes (pel) of *Pseudomonas aeruginosa*. J Bacteriol. 2007 Jul;189(14):5383–6.

106. Diggle SP, Stacey RE, Dodd C, Cámara M, Williams P, Winzer K. The galactophilic lectin, LecA, contributes to biofilm development in *Pseudomonas aeruginosa*. Environ Microbiol. 2006 Jun;8(6):1095–104.

107. Passos da Silva D, Matwichuk ML, Townsend DO, Reichhardt C, Lamba D, Wozniak DJ, et al. The *Pseudomonas aeruginosa* lectin LecB binds to the exopolysaccharide Psl and stabilizes the biofilm matrix. Nat Commun. 2019 May;10(1):2183.

108. Tielen P, Rosenau F, Wilhelm S, Jaeger K-E, Flemming H-C, Wingender J. Extracellular enzymes affect biofilm formation of mucoid *Pseudomonas aeruginosa*. Microbiology. 2010 Jul;156(Pt

7):2239–52.

109. Valentini M, Filloux A. Biofilms and Cyclic di-GMP (c-di-GMP) signaling: Lessons from *Pseudomonas aeruginosa* and other bacteria. J Biol Chem. 2016;291(24):12547–55.

110. Leifson E. Staining, shape and arrangement of bacterial flagella. J Pathol Bacteriol. 1951;62:25–32.

111. Yeung ATY, Parayno A, Hancock REW. Mucin promotes rapid surface motility in *Pseudomonas aeruginosa*. MBio. 2012;3(3).

112. Chevance FF V, Hughes KT. Coordinating assembly of a bacterial macromolecular machine. Nat Rev Microbiol. 2008 Jun;6(6):455–65.

113. Minamino T, Imada K. The bacterial flagellar motor and its structural diversity. Trends Microbiol. 2015 May;23(5):267–74.

114. Francis NR, Sosinsky GE, Thomas D, DeRosier DJ. Isolation, characterization and structure of bacterial flagellar motors containing the switch complex. J Mol Biol. 1994 Jan;235(4):1261–70.

115. Thomas DR, Francis NR, Xu C, DeRosier DJ. The three-dimensional structure of the flagellar rotor from a clockwise-locked mutant of *Salmonella enterica* serovar Typhimurium. J Bacteriol. 2006 Oct;188(20):7039–48.

116. Suzuki H, Yonekura K, Namba K. Structure of the rotor of the bacterial flagellar motor revealed by electron cryomicroscopy and single-particle image analysis. J Mol Biol. 2004 Mar;337(1):105–13.

117. Morimoto Y V., Minamino T. Structure and function of the bi-directional bacterial flagellar motor. Biomolecules. 2014;4(1):217–34.

118. Kojima S, Blair DF. Conformational change in the stator of the bacterial flagellar motor. Biochemistry. 2001 Oct;40(43):13041–50.

119. Braun TF, Al-Mawsawi LQ, Kojima S, Blair DF. Arrangement of core membrane segments in the MotA/MotB proton-channel complex of *Escherichia coli*. Biochemistry. 2004 Jan;43(1):35–45.

120. Chen S, Beeby M, Murphy GE, Leadbetter JR, Hendrixson DR, Briegel A, et al. Structural diversity of bacterial flagellar motors. EMBO J. 2011;30(14):2972–81.

121. Minamino T, Morimoto Y V., Hara N, Namba K. An energy transduction mechanism used in bacterial flagellar type III protein export. Nat Commun. 2011;2(1).

122. Ferris HU, Furukawa Y, Minamino T, Kroetz MB, Kihara M, Namba K, et al. FlhB regulates ordered export of flagellar components via autocleavage mechanism. J Biol Chem. 2005 Dec;280(50):41236–42.

123. Kinoshita M, Hara N, Imada K, Namba K, Minamino T. Interactions of bacterial flagellar chaperone-substrate complexes with FlhA contribute to co-ordinating assembly of the flagellar filament. Mol Microbiol. 2013 Dec;90(6):1249–61.

124. Ibuki T, Imada K, Minamino T, Kato T, Miyata T, Namba K. Common architecture of the flagellar type III protein export apparatus and F- and V-type ATPases. Nat Struct Mol Biol. 2011;18(3):277–82.

125. Fraser GM, González-Pedrajo B, Tame JRH, Macnab RM. Interactions of FliJ with the

Salmonella type III flagellar export apparatus. J Bacteriol. 2003 Sep;185(18):5546–54.

126. Homma M, Kutsukake K, Hasebe M, Iino T, Macnab RM. FlgB, FlgC, FlgF and FlgG. A family of structurally related proteins in the flagellar basal body of *Salmonella typhimurium*. J Mol Biol. 1990 Jan;211(2):465–77.

127. Samatey FA, Matsunami H, Imada K, Nagashima S, Shaikh TR, Thomas DR, et al. Structure of the bacterial flagellar hook and implication for the molecular universal joint mechanism. Nature. 2004 Oct;431(7012):1062–8.

128. Turner L, Stern AS, Berg HC. Growth of flagellar filaments of *Escherichia coli* is independent of filament length. J Bacteriol. 2012 May;194(10):2437–42.

129. Samatey FA, Imada K, Nagashima S, Vonderviszt F, Kumasaka T, Yamamoto M, et al. Structure of the bacterial flagellar protofilament and implications for a switch for supercoiling. Nature. 2001 Mar;410(6826):331–7.

130. Evans LDB, Poulter S, Terentjev EM, Hughes C, Fraser GM. A chain mechanism for flagellum growth. Nature [Internet]. 2013;504(7479):287–90. Available from: http://dx.doi.org/10.1038/nature12682

131. Yonekura K, Maki S, Morgan DG, Derosier DJ, Vonderviszt F, Imada K. The Bacterial Flagellar Cap as the Rotary Promoter of Flagellin Self-Assembly. Science (80-). 2000;290(December):2148–53.

132. Song WS, Cho SY, Hong HJ, Park SC, Yoon S il. Self-Oligomerizing Structure of the Flagellar Cap Protein FliD and Its Implication in Filament Assembly. J Mol Biol [Internet]. 2017;429(6):847–57. Available from: http://dx.doi.org/10.1016/j.jmb.2017.02.001

133. Macnab RM, Ornston MK. Normal-to-curly flagellar transitions and their role in bacterial tumbling. Stabilization of an alternative quaternary structure by mechanical force. J Mol Biol. 1977;112(1):1–30.

134. Schwarzer C, Fischer H, Machen TE. Chemotaxis and Binding of *Pseudomonas aeruginosa* to Scratch-Wounded Human Cystic Fibrosis Airway Epithelial Cells. PLoS One. 2016;11(3):1–21.

135. Feldman M, Bryan R, Rajan S, Scheffler L, Brunnert S, Tang H, et al. Role of flagella in pathogenesis of *Pseudomonas aeruginosa* pulmonary infection. Infect Immun. 1998;66(1):43–51.

136. De Bentzmann S, Roger P, Dupuit F, Bajolet-Laudtnat O, Fuchey C, Plotkowski MC, et al. Asialo GM1 is a receptor for *Pseudomonas aeruginosa* adherence to regenerating respiratory epithelial cells. Infect Immun. 1996;64(5):1582–8.

137. Saiman L, Prince A. *Pseudomonas aeruginosa* pili bind to asialoGM1 which is increased on the surface of cystic fibrosis epithelial cells. J Clin Invest. 1993 Oct;92(4):1875–80.

138. Landry RM, An D, Hupp JT, Singh PK, Parsek MR. Mucin-*Pseudomonas aeruginosa* interactions promote biofilm formation and antibiotic resistance. Mol Microbiol. 2006 Jan;59(1):142–51.

139. Tart AH, Wolfgang MC, Wozniak DJ. The alternative sigma factor AlgT represses *Pseudomonas aeruginosa* flagellum biosynthesis by inhibiting expression of *fleQ*. J Bacteriol. 2005 Dec;187(23):7955–62.

140. Guttenplan SB, Kearns DB. Regulation of flagellar motility during biofilm formation. FEMS Microbiol Rev. 2013 Nov;37(6):849–71.

141. Wolfgang MC, Jyot J, Goodman AL, Ramphal R, Lory S. *Pseudomonas aeruginosa* regulates

flagellin expression as part of a global response to airway fluid from cystic fibrosis patients. Proc Natl Acad Sci U S A. 2004 Apr;101(17):6664–8.

142. Hayashi F, Smith KD, Ozinsky A, Hawn TR, Yi EC, Goodlett DR, et al. The innate immune response to bacterial flagellin is mediated by Toll-like receptor 5. Nature. 2001 Apr;410(6832):1099–103.

143. Bradley DE. A function of *Pseudomonas aeruginosa* PAO polar pili: twitching motility. Can J Microbiol. 1980 Feb;26(2):146–54.

144. Merz AJ, So M, Sheetz M*P.* Pilus retraction powers bacterial twitching motility. Nature. 2000 Sep;407(6800):98–102.

145. Köhler T, Curty LK, Barja F, van Delden C, Pechère JC. Swarming of *Pseudomonas aeruginosa* is dependent on cell-to-cell signaling and requires flagella and pili. J Bacteriol. 2000 Nov;182(21):5990–6.

146. Skerker JM, Berg HC. Direct observation of extension and retraction of type IV pili. Proc Natl Acad Sci U S A. 2001;98(12):6901–4.

147. Maier B, Potter L, So M, Long CD, Seifert HS, Sheetz M*P.* Single pilus motor forces exceed 100 pN. Proc Natl Acad Sci U S A. 2002 Dec;99(25):16012–7.

148. Giltner CL, Habash M, Burrows LL. *Pseudomonas aeruginosa* minor pilins are incorporated into type IV pili. J Mol Biol. 2010 May;398(3):444–61.

149. Paranchych W, Sastry PA, Frost LS, Carpenter M, Armstrong GD, Watts TH. Biochemical studies on pili isolated from *Pseudomonas aeruginosa* strain PAO. Can J Microbiol. 1979 Oct;25(10):1175–81.

150. Jacobsen T, Bardiaux B, Francetic O, Izadi-Pruneyre N, Nilges M. Structure and function of minor pilins of type IV pili. Med Microbiol Immunol [Internet]. 2020;209(3):301–8. Available from: https://doi.org/10.1007/s00430-019-00642-5

151. Crowther LJ, Anantha RP, Donnenberg MS. The inner membrane subassembly of the enteropathogenic *Escherichia coli* bundle-forming pilus machine. Mol Microbiol. 2004 Apr;52(1):67–79.

152. Lee KK, Sheth HB, Wong WY, Sherburne R, Paranchych W, Hodges RS, et al. The binding of *Pseudomonas aeruginosa* pili to glycosphingolipids is a tip-associated event involving the C-terminal region of the structural pilin subunit. Mol Microbiol. 1994 Feb;11(4):705–13.

153. Argenio DAD, Gallagher LA, Berg CA, Manoil C. Drosophila as a model host for *Pseudomonas aeruginosa* infection. J Bacteriol. 2001;183(4):1466–71.

154. Heiniger RW, Winther-Larsen HC, Pickles RJ, Koomey M, Wolfgang MC. Infection of human mucosal tissue by *Pseudomonas aeruginosa* requires sequential and mutually dependent virulence factors and a novel pilus-associated adhesin. Cell Microbiol. 2010 Aug;12(8):1158–73.

155. Persat A, Inclan YF, Engel JN, Stone HA, Gitai Z. Type IV pili mechanochemically regulate virulence factors in *Pseudomonas aeruginosa*. Proc Natl Acad Sci U S A. 2015;112(24):7563–8.

156. van Schaik EJ, Giltner CL, Audette GF, Keizer DW, Bautista DL, Slupsky CM, et al. DNA binding: a novel function of *Pseudomonas aeruginosa* type IV pili. J Bacteriol. 2005 Feb;187(4):1455–64.

157. Ribbe J, Baker AE, Sebastian E, O'Toole GA, Maier B. Role of Cyclic Di-GMP and

Exopolysaccharide in Type IV Pilus Dynamics. J Bacteriol. 2017;199(8):1–10.

158. Gelimson A, Zhao K, Lee CK, Kranz WT, Wong GCL, Golestanian R. Multicellular Self-Organization of *P. aeruginosa* due to Interactions with Secreted Trails. Phys Rev Lett. 2016 Oct;117(17):178102.

159. Lindestam Arlehamn CS, Evans TJ. *Pseudomonas aeruginosa* pilin activates the inflammasome. Cell Microbiol. 2011;13(3):388–401.

160. Abdel-Mawgoud AM, Lépine F, Déziel E. Rhamnolipids: diversity of structures, microbial origins and roles. Appl Microbiol Biotechnol. 2010 May;86(5):1323–36.

161. Murray TS, Kazmierczak BI. *Pseudomonas aeruginosa* exhibits sliding motility in the absence of type IV pili and flagella. J Bacteriol. 2008 Apr;190(8):2700–8.

162. Tremblay J, Richardson A-P, Lépine F, Déziel E. Self-produced extracellular stimuli modulate the *Pseudomonas aeruginosa* swarming motility behaviour. Environ Microbiol. 2007 Oct;9(10):2622–30.

163. Raya A, Sodagari M, Pinzon NM, He X, Zhang Newby B-M, Ju L-K. Effects of rhamnolipids and shear on initial attachment of *Pseudomonas aeruginosa* PAO1 in glass flow chambers. Environ Sci Pollut Res Int. 2010 Nov;17(9):1529–38.

164. Davey ME, Caiazza NC, O'Toole GA. Rhamnolipid surfactant production affects biofilm architecture in *Pseudomonas aeruginosa* PAO1. J Bacteriol. 2003 Feb;185(3):1027–36.

165. Zulianello L, Canard C, Köhler T, Caille D, Lacroix J-S, Meda *P.* Rhamnolipids are virulence factors that promote early infiltration of primary human airway epithelia by *Pseudomonas aeruginosa*. Infect Immun. 2006 Jun;74(6):3134–47.

166. Dössel J, Meyer-Hoffert U, Schröder J-M, Gerstel U. *Pseudomonas aeruginosa*-derived rhamnolipids subvert the host innate immune response through manipulation of the human beta-defensin-2 expression. Cell Microbiol. 2012 Sep;14(9):1364–75.

167. Watt AP, Courtney J, Moore J, Ennis M, Elborn JS. Neutrophil cell death, activation and bacterial infection in cystic fibrosis. Thorax. 2005;60(8):659–64.

168. Jensen P, Bjarnsholt T, Phipps R, Rasmussen TB, Calum H, Christoffersen L, et al. Rapid necrotic killing of polymorphonuclear leukocytes is caused by quorum-sensing-controlled production of rhamnolipid by *Pseudomonas aeruginosa*. Microbiology. 2007;153(5):1329–38.

169. Gdaniec BG, Bonini F, Prodon F, Braschler T, Köhler T, van Delden C. *Pseudomonas aeruginosa* rhamnolipid micelles deliver toxic metabolites and antibiotics into *Staphylococcus aureus*. iScience. 2022;25(1).

170. Andrews SC, Robinson AK, Rodríguez-Quiñones F. Bacterial iron homeostasis. FEMS Microbiol Rev. 2003;27(2–3):215–37.

171. Meyer JM. Pyoverdines: pigments, siderophores and potential taxonomic markers of fluorescent *Pseudomonas* species. Arch Microbiol. 2000 Sep;174(3):135–42.

172. Meyer J-M, Stintzi A, De Vos D, Cornelis P, Tappe R, Taraz K, et al. Use of siderophores to type pseudomonads: the three *Pseudomonas aeruginosa* pyoverdine systems. Microbiology. 1997 Jan;143 (Pt 1:35–43.

173. Bonneau A, Roche B, Schalk IJ. Iron acquisition in *Pseudomonas aeruginosa* by the siderophore pyoverdine: an intricate interacting network including periplasmic and membrane proteins. Sci Re*P.* 2020 Jan;10(1):120.

174. Ghysels B, Dieu BTM, Beatson SA, Pirnay J-P, Ochsner UA, Vasil ML, et al. FpvB, an alternative type I ferripyoverdine receptor of *Pseudomonas aeruginosa*. Microbiology. 2004 Jun;150(Pt 6):1671–80.

175. Poole K, Neshat S, Krebes K, Heinrichs DE. Cloning and nucleotide sequence analysis of the ferripyoverdine receptor gene fpvA of *Pseudomonas aeruginosa*. J Bacteriol. 1993 Aug;175(15):4597–604.

176. Meyer JM, Neely A, Stintzi A, Georges C, Holder IA. Pyoverdin is essential for virulence of *Pseudomonas aeruginosa*. Infect Immun. 1996 Feb;64(2):518–23.

177. Banin E, Vasil ML, Greenberg E*P.* Iron and *Pseudomonas aeruginosa* biofilm formation. Proc Natl Acad Sci U S A. 2005 Aug;102(31):11076–81.

178. Lamont IL, Beare PA, Ochsner U, Vasil AI, Vasil ML. Siderophore-mediated signaling regulates virulence factor production in *Pseudomonas aeruginosa*. Proc Natl Acad Sci U S A. 2002 May;99(10):7072–7.

179. Cox CD, Rinehart KLJ, Moore ML, Cook JCJ. Pyochelin: novel structure of an iron-chelating growth promoter for *Pseudomonas aeruginosa*. Proc Natl Acad Sci U S A. 1981 Jul;78(7):4256–60.

180. Coffman TJ, Cox CD, Edeker BL, Britigan BE. Possible role of bacterial siderophores in inflammation. Iron bound to the *Pseudomonas* siderophore pyochelin can function as a hydroxyl radical catalyst. J Clin Invest. 1990 Oct;86(4):1030–7.

181. Ghysels B, Ochsner U, Möllman U, Heinisch L, Vasil M, Cornelis P, et al. The *Pseudomonas aeruginosa pirA* gene encodes a second receptor for ferrienterobactin and synthetic catecholate analogues. FEMS Microbiol Lett. 2005 May;246(2):167–74.

182. Ochsner UA, Johnson Z, Vasil ML. Genetics and regulation of two distinct haem-uptake systems, *phu* and *has*, in *Pseudomonas aeruginosa*. Microbiology. 2000 Jan;146 (Pt 1:185–98.

183. Hall S, McDermott C, Anoopkumar-Dukie S, McFarland AJ, Forbes A, Perkins A V, et al. Cellular Effects of Pyocyanin, a Secreted Virulence Factor of *Pseudomonas aeruginosa*. Toxins (Basel). 2016 Aug;8(8).

184. Hassan HM, Fridovich I. Mechanism of the Antibiotic Action of Pyocyanine. J Bacteriol. 1980;141(1):3069–73.

185. Denning GM, Wollenweber LA, Railsback MA, Cox CD, Stoll LL, Britigan BE. *Pseudomonas* pyocyanin increases interleukin-8 expression by human airway epithelial cells. Infect Immun. 1998 Dec;66(12):5777–84.

186. Britigan BE, Roeder TL, Rasmussen GT, Shasby DM, McCormick ML, Cox CD. Interaction of the *Pseudomonas aeruginosa* secretory products pyocyanin and pyochelin generates hydroxyl radical and causes synergistic damage to endothelial cells. Implications for *Pseudomonas*-associated tissue injury. J Clin Invest. 1992 Dec;90(6):2187–96.

187. Gardner PR. Superoxide production by the mycobacterial and pseudomonad quinoid pigments phthiocol and pyocyanine in human lung cells. Arch Biochem Biophys. 1996 Sep;333(1):267–74.

188. Das T, Manefield M. Pyocyanin promotes extracellular DNA release in *Pseudomonas aeruginosa*. PLoS One. 2012;7(10):e46718.

189. Schmitt L, Benabdelhak H, Blight MA, Holland IB, Stubbs MT. Crystal structure of the nucleotide-binding domain of the ABC-transporter haemolysin B: identification of a variable

region within ABC helical domains. J Mol Biol. 2003 Jul;330(2):333–42.

190. Dinh T, Paulsen IT, Saier MHJ. A family of extracytoplasmic proteins that allow transport of large molecules across the outer membranes of gram-negative bacteria. J Bacteriol. 1994 Jul;176(13):3825–31.

191. Koronakis V, Sharff A, Koronakis E, Luisi B, Hughes C. Crystal structure of the bacterial membrane protein TolC central to multidrug efflux and protein export. Nature. 2000 Jun;405(6789):914–9.

192. Costa TRD, Felisberto-Rodrigues C, Meir A, Prevost MS, Redzej A, Trokter M, et al. Secretion systems in Gram-negative bacteria: structural and mechanistic insights. Nat Rev Microbiol. 2015;

193. Higgins CF. ABC transporters: from microorganisms to man. Annu Rev Cell Biol. 1992;8:67–113.

194. Thanabalu T, Koronakis E, Hughes C, Koronakis V. Substrate-induced assembly of a contiguous channel for protein export from E. *coli*: Reversible bridging of an inner-membrane translocase to an outer membrane exit pore. EMBO J. 1998;17(22):6487–96.

195. Eswaran J, Hughes C, Koronakis V. Locking TolC entrance helices to prevent protein translocation by the bacterial type I export apparatus. J Mol Biol. 2003 Mar;327(2):309–15.

196. Andersen C, Koronakis E, Bokma E, Eswaran J, Humphreys D, Hughes C, et al. Transition to the open state of the TolC periplasmic tunnel entrance. Proc Natl Acad Sci U S A. 2002;99(17):11103–8.

197. Balakrishnan L, Hughes C, Koronakis V. Substrate-triggered recruitment of the TolC channel-tunnel during type I export of hemolysin by *Escherichia coli*. J Mol Biol. 2001 Oct;313(3):501–10.

198. Parmely M, Gale A, Clabaugh M, Horvat R, Zhou WW. Proteolytic inactivation of cytokines by *Pseudomonas aeruginosa*. Infect Immun. 1990 Sep;58(9):3009–14.

199. Létoffé S, Nato F, Goldberg ME, Wandersman C. Interactions of HasA, a bacterial haemophore, with haemoglobin and with its outer membrane receptor HasR. Mol Microbiol. 1999;33(3):546–55.

200. Zhao K, Li W, Li J, Ma T, Wang K, Yuan Y, et al. TesG is a type I secretion effector of *Pseudomonas aeruginosa* that suppresses the host immune response during chronic infection. Nat Microbiol. 2019 Mar;4(3):459–69.

201. Duong F, Bonnet E, Géli V, Lazdunski A, Murgier M, Filloux A. The AprX protein of *Pseudomonas aeruginosa*: a new substrate for the Apr type I secretion system. Gene. 2001 Jan;262(1–2):147–53.

202. Hong YQ, Ghebrehiwet B. Effect of *Pseudomonas aeruginosa* elastase and alkaline protease on serum complement and isolated components C1q and C3. Clin Immunol Immunopathol. 1992 Feb;62(2):133–8.

203. Laarman AJ, Bardoel BW, Ruyken M, Fernie J, Milder FJ, van Strijp JAG, et al. *Pseudomonas aeruginosa* Alkaline Protease Blocks Complement Activation via the Classical and Lectin Pathways . J Immunol. 2012;188(1):386–93.

204. Bardoel BW, van der Ent S, Pel MJC, Tommassen J, Pieterse CMJ, van Kessel KPM, et al. *Pseudomonas* evades immune recognition of flagellin in both mammals and plants. PLoS Pathog. 2011 Aug;7(8):e1002206.

205. Jaffar-Bandjee MC, Lazdunski A, Bally M, Carrère J, Chazalette JP, Galabert C. Production of elastase, exotoxin A, and alkaline protease in sputa during pulmonary exacerbation of cystic fibrosis in patients chronically infected by *Pseudomonas aeruginosa*. J Clin Microbiol. 1995 Apr;33(4):924–9.

206. Butterworth MB, Zhang L, Heidrich EM, Myerburg MM, Thibodeau PH. Activation of the epithelial sodium channel (ENaC) by the alkaline protease from *Pseudomonas aeruginosa*. J Biol Chem. 2012 Sep;287(39):32556–65.

207. Py B, Loiseau L, Barras F. An inner membrane platform in the type II secretion machinery of Gram-negative bacteria. EMBO Re*P.* 2001;2(3):244–8.

208. Durand E, Bernadac A, Ball G, Lazdunski A, Sturgis JN, Filloux A. Type II protein secretion in *Pseudomonas aeruginosa*: the pseudopilus is a multifibrillar and adhesive structure. J Bacteriol. 2003 May;185(9):2749–58.

209. Brok R, Van Gelder P, Winterhalter M, Ziese U, Koster AJ, de Cock H, et al. The C-terminal domain of the *Pseudomonas* secretin XcpQ forms oligomeric rings with pore activity. J Mol Biol. 1999 Dec;294(5):1169–79.

210. Korotkov K V, Sandkvist M, Hol WGJ. The type II secretion system: biogenesis, molecular architecture and mechanism. Nat Rev Microbiol. 2012;10(5):359–75.

211. Camberg JL, Sandkvist M. Molecular analysis of the *Vibrio cholerae* type II secretion ATPase EpsE. J Bacteriol. 2005 Jan;187(1):249–56.

212. Korotkov K V, Gray MD, Kreger A, Turley S, Sandkvist M, Hol WGJ. Calcium is essential for the major pseudopilin in the type 2 secretion system. J Biol Chem. 2009 Sep;284(38):25466–70.

213. Korotkov K V, Hol WGJ. Structure of the GspK-GspI-GspJ complex from the enterotoxigenic *Escherichia coli* type 2 secretion system. Nat Struct Mol Biol. 2008 May;15(5):462–8.

214. Korotkov K V, Delarosa JR, Hol WGJ. A dodecameric ring-like structure of the N0 domain of the type II secretin from enterotoxigenic *Escherichia coli*. J Struct Biol. 2013 Sep;183(3):354–62.

215. Reichow SL, Korotkov K V, Hoi WG, Gonen T. Structure of the cholera toxin secretion channel in its closed state. Nat Struct Mol Biol. 2010;17(10).

216. Voulhoux R, Ball G, Ize B, Vasil ML, Lazdunski AÂE, Wu L-F, et al. Involvement of the twin-arginine translocation system in protein secretion via the type II pathway. EMBO J. 2001;20(23):6735–41.

217. Pugsley A*P.* The complete general secretory pathway in gram-negative bacteria. Microbiol Rev. 1993;57(1):50–108.

218. Korotkov K V, Johnson TL, Jobling MG, Pruneda J, Pardon E, Héroux A, et al. Structural and functional studies on the interaction of GspC and GspD in the type II secretion system. PLoS Pathog. 2011 Sep;7(9):e1002228.

219. Douzi B, Ball G, Cambillau C, Tegoni M, Voulhoux R. Deciphering the Xcp *Pseudomonas aeruginosa* type II secretion machinery through multiple interactions with substrates. J Biol Chem. 2011 Nov;286(47):40792–801.

220. Bally M, Filloux A, Akrim M, Ball G, Lazdunski A, Tommassen J. Protein secretion in *Pseudomonas aeruginosa*: characterization of seven xcp genes and processing of secretory apparatus components by prepilin peptidase. Mol Microbiol. 1992 May;6(9):1121–31.

221. Ball G, Durand E, Lazdunski A, Filloux A. A novel type II secretion system in *Pseudomonas aeruginosa*. Mol Microbiol. 2002 Jan;43(2):475–85.

222. Cadoret F, Ball G, Douzi B, Voulhoux R. Txc, a new type II secretion system of *Pseudomonas aeruginosa* strain PA7, is regulated by the TtsS/TtsR two-component system and directs specific secretion of the CbpE chitin-binding protein. J Bacteriol. 2014;196(13):2376–86.

223. Braun P, de Groot A, Bitter W, Tommassen J. Secretion of elastinolytic enzymes and their propeptides by *Pseudomonas aeruginosa*. J Bacteriol. 1998 Jul;180(13):3467–9.

224. Jaeger KE, Ransac S, Dijkstra BW, Colson C, van Heuvel M, Misset O. Bacterial lipases. FEMS Microbiol Rev. 1994 Sep;15(1):29–63.

225. Martínez A, Ostrovsky P, Nunn DN. LipC, a second lipase of *Pseudomonas aeruginosa*, is LipB and Xcp dependent and is transcriptionally regulated by pilus biogenesis components. Mol Microbiol. 1999 Oct;34(2):317–26.

226. Barker AP, Vasil AI, Filloux A, Ball G, Wilderman PJ, Vasil ML. A novel extracellular phospholipase C of *Pseudomonas aeruginosa* is required for phospholipid chemotaxis. Mol Microbiol. 2004 Aug;53(4):1089–98.

227. Filloux A, Bally M, Soscia C, Murgier M, Lazdunski A. Phosphate regulation in *Pseudomonas aeruginosa*: cloning of the alkaline phosphatase gene and identification of phoB- and phoR-like genes. Mol Gen Genet. 1988 Jun;212(3):510–3.

228. Vance RE, Hong S, Gronert K, Serhan CN, Mekalanos JJ. The opportunistic pathogen *Pseudomonas aeruginosa* carries a secretable arachidonate 15-lipoxygenase. Proc Natl Acad Sci U S A. 2004 Feb;101(7):2135–9.

229. Nomura K, Obata K, Keira T, Miyata R, Hirakawa S, Takano K, et al. *Pseudomonas aeruginosa* elastase causes transient disruption of tight junctions and downregulation of PAR-2 in human nasal epithelial cells. Respir Res. 2014 Feb;15(1):21.

230. Kuang Z, Hao Y, Walling BE, Jeffries JL, Ohman DE, Lau GW. *Pseudomonas aeruginosa* elastase provides an escape from phagocytosis by degrading the pulmonary surfactant protein-A. PLoS One. 2011;6(11):e27091.

231. Yang J, Lee K-M, Park S, Cho Y, Lee E, Park J-H, et al. Bacterial Secretant from *Pseudomonas aeruginosa* Dampens Inflammasome Activation in a Quorum Sensing-Dependent Manner. Front Immunol. 2017;8:333.

232. Casilag F, Lorenz A, Krueger J, Klawonn F, Weiss S, Häussler S. The LasB Elastase of *Pseudomonas aeruginosa* Acts in Concert with Alkaline Protease AprA To Prevent Flagellin-Mediated Immune Recognition. Infect Immun. 2016 Jan;84(1):162–71.

233. Liu P V. Extracellular toxins of *Pseudomonas aeruginosa*. J Infect Dis. 1974 Nov;130 Suppl(0):S94-9.

234. Kounnas MZ, Morris RE, Thompson MR, FitzGerald DJ, Strickland DK, Saelinger CB. The alpha 2-macroglobulin receptor/low density lipoprotein receptor-related protein binds and internalizes *Pseudomonas* exotoxin A. J Biol Chem. 1992 Jun;267(18):12420–3.

235. Ogata M, Fryling CM, Pastan I, FitzGerald DJ. Cell-mediated cleavage of *Pseudomonas* exotoxin between Arg279 and Gly280 generates the enzymatically active fragment which translocates to the cytosol. J Biol Chem. 1992 Dec;267(35):25396–401.

236. Jackson ME, Simpson JC, Girod A, Pepperkok R, Roberts LM, Lord JM. The KDEL retrieval system is exploited by *Pseudomonas* exotoxin A, but not by Shiga-like toxin-1, during

retrograde transport from the Golgi complex to the endoplasmic reticulum. J Cell Sci. 1999 Feb;112 (Pt 4:467–75.

237. Iglewski BH, Liu P V, Kabat D. Mechanism of action of *Pseudomonas aeruginosa* exotoxin A: adenosine diphosphate-ribosylation of mammalian elongation factor 2 in vitro and in vivo. Infect Immun. 1977 Jan;15(1):138–44.

238. Chang J-H, Kwon H-Y. Expression of 14-3-3delta, cdc2 and cyclin B proteins related to exotoxin A-induced apoptosis in HeLa S3 cells. Int Immunopharmacol. 2007 Sep;7(9):1185–91.

239. Jenkins CE, Swiatoniowski A, Issekutz AC, Lin T-J. *Pseudomonas aeruginosa* exotoxin A induces human mast cell apoptosis by a caspase-8 and -3-dependent mechanism. J Biol Chem. 2004 Aug;279(35):37201–7.

240. Schultz MJ, Rijneveld AW, Florquin S, Speelman P, Van Deventer SJH, Van Der Poll T. Impairment of host defence by exotoxin A in *Pseudomonas aeruginosa* pneumonia in mice. J Med Microbiol. 2001 Sep;50(9):822–7.

241. Schultz MJ, Speelman P, Zaat SA, Hack CE, van Deventer SJ, van der Poll T. The effect of *Pseudomonas* exotoxin A on cytokine production in whole blood exposed to *Pseudomonas aeruginosa*. FEMS Immunol Med Microbiol. 2000 Nov;29(3):227–32.

242. Rosqvist R, Magnusson KE, Wolf-Watz H. Target cell contact triggers expression and polarized transfer of Yersinia YopE cytotoxin into mammalian cells. EMBO J. 1994;13(4):964–72.

243. Sory MP, Cornelis GR. Translocation of a hybrid YopE-adenylate cyclase from *Yersinia enterocolitica* into HeLa cells. Mol Microbiol. 1994 Nov;14(3):583–94.

244. Yahr TL, Vallis AJ, Hancock MK, Barbieri JT, Frank DW. ExoY, an adenylate cyclase secreted by the *Pseudomonas aeruginosa* type III system. Proc Natl Acad Sci U S A. 1998 Nov;95(23):13899–904.

245. Frank DW. The exoenzyme S regulon of *Pseudomonas aeruginosa*. Mol Microbiol. 1997 Nov;26(4):621–9.

246. Brutinel ED, Vakulskas CA, Brady KM, Yahr TL. Characterization of ExsA and of ExsA-dependent promoters required for expression of the *Pseudomonas aeruginosa* type III secretion system. Mol Microbiol. 2008 May;68(3):657–71.

247. Pastor A, Chabert J, Louwagie M, Garin J, Attree I. PscF is a major component of the *Pseudomonas aeruginosa* type III secretion needle. FEMS Microbiol Lett. 2005 Dec;253(1):95–101.

248. Worrall LJ, Lameignere E, Strynadka NCJ. Structural overview of the bacterial injectisome. Curr Opin Microbiol [Internet]. 2011;14(1):3–8. Available from: http://dx.doi.org/10.1016/j.mib.2010.10.009

249. Kawamoto A, Morimoto Y V, Miyata T, Minamino T, Hughes KT, Kato T, et al. Common and distinct structural features of *Salmonella* injectisome and flagellar basal body. Sci Re*P.* 2013 Nov;3:3369.

250. Milne-Davies B, Wimmi S, Diepold A. Adaptivity and dynamics in type III secretion systems. Mol Microbiol. 2021;115(November 2020):395–411.

251. Lara-Tejero M, Kato J, Wagner S, Liu X, Galán JE. A sorting platform determines the order of protein secretion in bacterial type III systems. Science. 2011 Mar;331(6021):1188–91.

252. Dacheux D, Goure J, Chabert J, Usson Y, Attree I. Pore-forming activity of type III system-secreted proteins leads to oncosis of *Pseudomonas aeruginosa*-infected macrophages. Mol Microbiol. 2001 Apr;40(1):76–85.

253. Schoehn G, Di Guilmi AM, Lemaire D, Attree I, Weissenhorn W, Dessen A. Oligomerization of type III secretion proteins PopB and PopD precedes pore formation in *Pseudomonas*. EMBO J. 2003 Oct;22(19):4957–67.

254. Goure J, Pastor A, Faudry E, Chabert J, Dessen A, Attree I. The V antigen of *Pseudomonas aeruginosa* is required for assembly of the functional PopB/PopD translocation pore in host cell membranes. Infect Immun. 2004 Aug;72(8):4741–50.

255. Sawa T, Yahr TL, Ohara M, Kurahashi K, Gropper MA, Wiener-Kronish JP, et al. Active and passive immunization with the *Pseudomonas* V antigen protects against type III intoxication and lung injury. Nat Med. 1999 Apr;5(4):392–8.

256. Kundracik E, Trichka J, Díaz Aponte J, Roistacher A, Rietsch A. PopB-PcrV Interactions Are Essential for Pore Formation in the *Pseudomonas aeruginosa* Type III Secretion System Translocon. MBio. 2022 Sep;e0238122.

257. Parsot C, Hamiaux C, Page A-L. The various and varying roles of specific chaperones in type III secretion systems. Curr Opin Microbiol. 2003 Feb;6(1):7–14.

258. Sory MP, Boland A, Lambermont I, Cornelis GR. Identification of the YopE and YopH domains required for secretion and internalization into the cytosol of macrophages, using the cyaA gene fusion approach. Proc Natl Acad Sci U S A. 1995 Dec;92(26):11998–2002.

259. Feltman H, Schulert G, Khan S, Jain M, Peterson L, Hauser AR. Prevalence of type III secretion genes in clinical and environmental isolates of *Pseudomonas aeruginosa*. Microbiology. 2001 Oct;147(Pt 10):2659–69.

260. Barbieri JT, Sun J. *Pseudomonas aeruginosa* ExoS and ExoT. Rev Physiol Biochem Pharmacol. 2004;152:79–92.

261. Sato H, Frank DW. ExoU is a potent intracellular phospholipase. Mol Microbiol. 2004 Sep;53(5):1279–90.

262. Cuzick A, Stirling FR, Lindsay SL, Evans TJ. The type III pseudomonal exotoxin U activates the c-Jun NH2-terminal kinase pathway and increases human epithelial interleukin-8 production. Infect Immun. 2006 Jul;74(7):4104–13.

263. McMorran B, Town L, Costelloe E, Palmer J, Engel J, Hume D, et al. Effector ExoU from the type III secretion system is an important modulator of gene expression in lung epithelial cells in response to *Pseudomonas aeruginosa* infection. Infect Immun. 2003 Oct;71(10):6035–44.

264. Cowell BA, Evans DJ, Fleiszig SMJ. Actin cytoskeleton disruption by ExoY and its effects on *Pseudomonas aeruginosa* invasion. FEMS Microbiol Lett. 2005 Sep;250(1):71–6.

265. Sayner SL, Frank DW, King J, Chen H, VandeWaa J, Stevens T. Paradoxical cAMP-induced lung endothelial hyperpermeability revealed by *Pseudomonas aeruginosa* ExoY. Circ Res. 2004 Jul;95(2):196–203.

266. Wolfgang MC, Kulasekara BR, Liang X, Boyd D, Wu K, Yang Q, et al. Conservation of genome content and virulence determinants among clinical and environmental isolates of *Pseudomonas aeruginosa*. Proc Natl Acad Sci U S A. 2003 Jul;100(14):8484–9.

267. Finck-Barbançon V, Goranson J, Zhu L, Sawa T, Wiener-Kronish JP, Fleiszig SM, et al. ExoU expression by *Pseudomonas aeruginosa* correlates with acute cytotoxicity and epithelial

injury. Mol Microbiol. 1997 Aug;25(3):547–57.

268. Burstein D, Satanower S, Simovitch M, Belnik Y, Zehavi M, Yerushalmi G, et al. Novel type III effectors in *Pseudomonas aeruginosa*. MBio. 2015;6(2):2–7.

269. Engel J, Balachandran *P.* Role of *Pseudomonas aeruginosa* type III effectors in disease. Curr Opin Microbiol. 2009 Feb;12(1):61–6.

270. Hauser AR, Cobb E, Bodi M, Mariscal D, Vallés J, Engel JN, et al. Type III protein secretion is associated with poor clinical outcomes in patients with ventilator-associated pneumonia caused by *Pseudomonas aeruginosa*. Crit Care Med. 2002 Mar;30(3):521–8.

271. Zheng Z, Chen G, Joshi S, Brutinel ED, Yahr TL, Chen L. Biochemical characterization of a regulatory cascade controlling transcription of the *Pseudomonas aeruginosa* type III secretion system. J Biol Chem. 2007 Mar;282(9):6136–42.

272. West SEH, Sample AK, Runyen-Janecky LJ. The *vfr* gene product, required for *Pseudomonas aeruginosa* exotoxin A and protease production, belongs to the cyclic AMP receptor protein family. J Bacteriol. 1994;176(24):7532–42.

273. Intile PJ, Diaz MR, Urbanowski ML, Wolfgang MC, Yahr L. The AlgZR Two-Component System Recalibrates the RsmAYZ Posttranscriptional Regulatory System To Inhibit Expression of the *Pseudomonas aeruginosa* Type III Secretion System. J Bacteriol. 2014;196(2):357–66.

274. Alonso A, Rojo F, Martínez JL. Environmental and clinical isolates of *Pseudomonas aeruginosa* show pathogenic and biodegradative properties irrespective of their origin. Environ Microbiol. 1999 Oct;1(5):421–30.

275. Wu W, Badrane H, Arora S, Baker H V, Jin S. MucA-mediated coordination of type III secretion and alginate synthesis in *Pseudomonas aeruginosa*. J Bacteriol. 2004 Nov;186(22):7575–85.

276. Jones AK, Fulcher NB, Balzer GJ, Urbanowski ML, Pritchett CL, Schurr MJ, et al. Activation of the *Pseudomonas aeruginosa* AlgU regulon through *mucA* mutation inhibits cyclic AMP/Vfr signaling. J Bacteriol. 2010;192(21):5709–17.

277. Fan E, Chauhan N, Gupta Udatha DBRK, Leo JC, Linke D. Type V secretion systems in bacteria. Virulence Mech Bact Pathog. 2016;(2):305–35.

278. Mazar J, Cotter PA. New insight into the molecular mechanisms of two-partner secretion. Trends Microbiol. 2007 Nov;15(11):508–15.

279. Wilhelm S, Tommassen J, Jaeger KE. A novel lipolytic enzyme located in the outer membrane of *Pseudomonas aeruginosa*. J Bacteriol. 1999 Nov;181(22):6977–86.

280. Kida Y, Taira J, Yamamoto T, Higashimoto Y, Kuwano K. EprS, an autotransporter protein of *Pseudomonas aeruginosa*, possessing serine protease activity induces inflammatory responses through protease-activated receptors. Cell Microbiol. 2013 Jul;15(7):1168–81.

281. Luckett JCA, Darch O, Watters C, Abuoun M, Wright V, Paredes-Osses E, et al. A novel virulence strategy for *Pseudomonas aeruginosa* mediated by an autotransporter with arginine-specific aminopeptidase activity. PLoS Pathog. 2012;8(8):e1002854.

282. van den Berg B. Crystal structure of a full-length autotransporter. J Mol Biol. 2010 Feb;396(3):627–33.

283. Wilhelm S, Gdynia A, Tielen P, Rosenau F, Jaeger K-E. The autotransporter esterase EstA of *Pseudomonas aeruginosa* is required for rhamnolipid production, cell motility, and biofilm formation. J Bacteriol. 2007 Sep;189(18):6695–703.

284. Paulsson M, Su Y-C, Ringwood T, Uddén F, Riesbeck K. *Pseudomonas aeruginosa* uses multiple receptors for adherence to laminin during infection of the respiratory tract and skin wounds. Sci Re*P.* 2019 Dec;9(1):18168.

285. Salacha R, Kovacić F, Brochier-Armanet C, Wilhelm S, Tommassen J, Filloux A, et al. The *Pseudomonas aeruginosa* patatin-like protein PlpD is the archetype of a novel Type V secretion system. Environ Microbiol. 2010 Jun;12(6):1498–512.

286. Kida Y, Higashimoto Y, Inoue H, Shimizu T, Kuwano K. A novel secreted protease from *Pseudomonas aeruginosa* activates NF-kappaB through protease-activated receptors. Cell Microbiol. 2008 Jul;10(7):1491–504.

287. Borlee BR, Goldman AD, Murakami K, Samudrala R, Wozniak DJ, Parsek MR. *Pseudomonas aeruginosa* uses a cyclic-di-GMP-regulated adhesin to reinforce the biofilm extracellular matrix. Mol Microbiol. 2010 Feb;75(4):827–42.

288. Kajava A V, Cheng N, Cleaver R, Kessel M, Simon MN, Willery E, et al. Beta-helix model for the filamentous haemagglutinin adhesin of *Bordetella pertussis* and related bacterial secretory proteins. Mol Microbiol. 2001 Oct;42(2):279–92.

289. Ruhe ZC, Subramanian P, Song K, Nguyen JY, Stevens TA, Low DA, et al. Programmed Secretion Arrest and Receptor-Triggered Toxin Export during Antibacterial Contact-Dependent Growth Inhibition. Cell. 2018 Nov;175(4):921-933.e14.

290. Ruhe ZC, Nguyen JY, Xiong J, Koskiniemi S, Beck CM, Perkins BR, et al. CdiA Effectors Use Modular Receptor- Binding Domains To Recognize Target Bacteria. MBio. 2017;8(2):1–16.

291. Aoki SK, Webb JS, Braaten BA, Low DA. Contact-dependent growth inhibition causes reversible metabolic downregulation in *Escherichia coli*. J Bacteriol. 2009 Mar;191(6):1777–86.

292. Willett JLE, Gucinski GC, Fatherree JP, Low DA, Hayes CS. Contact-dependent growth inhibition toxins exploit multiple independent cell-entry pathways. Proc Natl Acad Sci U S A. 2015 Sep;112(36):11341–6.

293. Aoki SK, Diner EJ, de Roodenbeke CT, Burgess BR, Poole SJ, Braaten BA, et al. A widespread family of polymorphic contact-dependent toxin delivery systems in bacteria. Nature. 2010 Nov;468(7322):439–42.

294. Morse RP, Nikolakakis KC, Willett JLE, Gerrick E, Low DA, Hayes CS, et al. Structural basis of toxicity and immunity in contact-dependent growth inhibition (CDI) systems. Proc Natl Acad Sci U S A. 2012;109(52):21480–5.

295. Allen JP, Hauser AR. Diversity of Contact-Dependent Growth Inhibition Systems of *Pseudomonas aeruginosa*. J Bacteriol. 2019 Jul;201(14).

296. Mercy C, Ize B, Salcedo SP, de Bentzmann S, Bigot S. Functional characterization of *Pseudomonas* contact dependent growth inhibition (CDI) systems. PLoS One. 2016;11(1):1–21.

297. Allen JP, Ozer EA, Minasov G, Shuvalova L, Kiryukhina O, Satchell KJF, et al. A comparative genomics approach identifies contact-dependent growth inhibition as a virulence determinant. Proc Natl Acad Sci U S A. 2020;117(12):6811–21.

298. Abouhamad WN, Manson MD. The dipeptide permease of *Escherichia coli* closely resembles other bacterial transport systems and shows growth-phase-dependent expression. Mol Microbiol. 1994 Dec;14(5):1077–92.

299. Bayer-Santos E, Cenens W, Matsuyama BY, Oka GU, Di Sessa G, Del Valle Mininel I, et al. The opportunistic pathogen *Stenotrophomonas maltophilia* utilizes a type IV secretion system for interbacterial killing. PLoS Pathog [Internet]. 2019;15(9):1–29. Available from: http://dx.doi.org/10.1371/journal.ppat.1007651

300. Souza DP, Oka GU, Alvarez-Martinez CE, Bisson-Filho AW, Dunger G, Hobeika L, et al. Bacterial killing via a type IV secretion system. Nat Commun. 2015;6:1–9.

301. Vergunst AC, Schrammeijer B, den Dulk-Ras A, de Vlaam CM, Regensburg-Tuïnk TJ, Hooykaas PJ. VirB/D4-dependent protein translocation from *Agrobacterium* into plant cells. Science. 2000 Nov;290(5493):979–82.

302. Hilbi H, Nagai H, Kubori T, Roy CR. Subversion of Host Membrane Dynamics by the *Legionella* Dot/Icm Type IV Secretion System. Curr Top Microbiol Immunol. 2017;413:221–42.

303. Ilangovan A, Connery S, Waksman G. Structural biology of the Gram-negative bacterial conjugation systems. Trends Microbiol. 2015 May;23(5):301–10.

304. Hofreuter D, Odenbreit S, Haas R. Natural transformation competence in *Helicobacter pylori* is mediated by the basic components of a type IV secretion system. Mol Microbiol. 2001 Jul;41(2):379–91.

305. Burts ML, Williams WA, DeBord K, Missiakas DM. EsxA and EsxB are secreted by an ESAT-6-like system that is required for the pathogenesis of *Staphylococcus aureus* infections. Proc Natl Acad Sci U S A. 2005 Jan;102(4):1169–74.

306. Cao Z, Casabona MG, Kneuper H, Chalmers JD, Palmer T. The type VII secretion system of *Staphylococcus aureus* secretes a nuclease toxin that targets competitor bacteria. Nat Microbiol. 2016 Oct;2:16183.

307. Hood RD, Singh P, Hsu F, Güvener T, Carl MA, Trinidad RRS, et al. A Type VI Secretion System of *Pseudomonas aeruginosa* Targets a Toxin to Bacteria. Cell Host Microbe. 2010;7(1):25–37.

308. Trunk K, Peltier J, Liu YC, Dill BD, Walker L, Gow NARR, et al. The type VI secretion system deploys antifungal effectors against microbial competitors. Nat Microbiol [Internet]. 2018;3(8):920–31. Available from: http://dx.doi.org/10.1038/s41564-018-0191-x

309. Pukatzki S, Ma AT, Revel AT, Sturtevant D, Mekalanos JJ. Type VI secretion system translocates a phage tail spike-like protein into target cells where it cross-links actin. Proc Natl Acad Sci [Internet]. 2007;104(39):15508–13. Available from: http://www.pnas.org/cgi/doi/10.1073/pnas.0706532104

310. Han Y, Wang T, Chen G, Pu Q, Liu Q, Zhang Y, et al. A *Pseudomonas aeruginosa* type VI secretion system regulated by CueR facilitates copper acquisition. PLoS Pathog. 2019;15(12):1–25.

311. Lin J, Zhang W, Cheng J, Yang X, Zhu K, Wang Y, et al. A *Pseudomonas* T6SS effector recruits PQS-containing outer membrane vesicles for iron acquisition. Nat Commun. 2017;8(14888).

312. Böck D, Medeiros JM, Tsao H, Penz T, Weiss GL, Aistleitner K, et al. In situ architecture, function, and evolution of a contractile injection system. Science (80-). 2017;357:713–7.

313. Leiman PG, Basler M, Ramagopal UA, Bonanno JB, Sauder JM, Pukatzki S, et al. Type VI secretion apparatus and phage tail-associated protein complexes share a common evolutionary origin. Proc Natl Acad Sci U S A [Internet]. 2009;106(11):4154–9. Available from: http://www.pubmedcentral.nih.gov/articlerender.fcgi?artid=2657435&tool=pmcentrez&rendertype=abstract

314. Nguyen VS, Douzi B, Durand E, Roussel A, Cascales E, Cambillau C. Towards a complete structural deciphering of Type VI secretion system. Curr Opin Struct Biol [Internet]. 2018;49:77–84. Available from: https://doi.org/10.1016/j.sbi.2018.01.007

315. Bingle LEH, Bailey CM, Pallen MJ. Type VI secretion: a beginner's guide. Curr Opin Microbiol. 2008;11:3–8.

316. Pukatzki S, Ma AT, Sturtevant D, Krastins B, Sarracino D, Nelson WC, et al. Identification of a conserved bacterial protein secretion system in *Vibrio cholerae* using the Dictyostelium host model system. Proc Natl Acad Sci. 2006;103(5):1528–33.

317. Russell AB, Wexler AG, Harding BN, Whitney JC, Bohn AJ, Goo YA, et al. A type VI secretion-related pathway in Bacteroidetes mediates interbacterial antagonism. Cell Host Microbe [Internet]. 2014;23(1):1–7. Available from: https://www.ncbi.nlm.nih.gov/pmc/articles/PMC3624763/pdf/nihms412728.pdf

318. Abby SS, Cury J, Guglielmini J, Néron B, Touchon M, Rocha EPC. Identification of protein secretion systems in bacterial genomes. Sci Rep [Internet]. 2016;6(October 2015):1–14. Available from: http://dx.doi.org/10.1038/srep23080

319. Nano FE, Schmerk C. The *Francisella* pathogenicity island. Ann N Y Acad Sci. 2007;1105:122–37.

320. García-Bayona L, Coyne MJ, Comstock LE. Mobile Type VI secretion system loci of the gut Bacteroidales display extensive intra-ecosystem transfer, multi-species spread and geographical clustering. PLoS Genet. 2021;17(4):1–25.

321. Salomon D, Klimko JA, Trudgian DC, Kinch LN, Grishin N V., Mirzaei H, et al. Type VI Secretion System Toxins Horizontally Shared between Marine Bacteria. PLoS Pathog. 2015;11(8):1–20.

322. Tang L, Yue S, Li GY, Li J, Wang XR, Li SF, et al. Expression, secretion and bactericidal activity of type VI secretion system in *Vibrio anguillarum*. Arch Microbiol. 2016;198(8):751–60.

323. Guillemette R, Ushijima B, Jalan M, Häse CC, Azam F. Insight into the resilience and susceptibility of marine bacteria to T6SS attack by *Vibrio cholerae* and *Vibrio coralliilyticus*. PLoS One. 2020;15(1):1–19.

324. Bernal P, Allsopp LP, Filloux A, Llamas MA. The *Pseudomonas putida* T6SS is a plant warden against phytopathogens. ISME J [Internet]. 2017;11:972–87. Available from: http://www.nature.com/doifinder/10.1038/ismej.2016.169

325. Vacheron J, Péchy-Tarr M, Brochet S, Heiman CM, Stojiljkovic M, Maurhofer M, et al. T6SS contributes to gut microbiome invasion and killing of an herbivorous pest insect by plant-beneficial *Pseudomonas protegens*. ISME J [Internet]. 2019;13(5):1318–29. Available from: http://dx.doi.org/10.1038/s41396-019-0353-8

326. Guckes KR, Cecere AG, Wasilko NP, Williams AL, Bultman KM, Mandel MJ, et al. Incompatibility of *Vibrio fischeri* strains during symbiosis establishment depends on two functionally redundant *hcp* genes. J Bacteriol. 2019;201(19).

327. Speare L, Cecere AG, Guckes KR, Smith S, Wollenberg MS, Mandel MJ, et al. Bacterial symbionts use a type VI secretion system to eliminate competitors in their natural host. Proc Natl Acad Sci U S A. 2018;115(36):E8528–37.

328. Storey D, McNally A, Åstrand M, Santos JPG, Rodriguez-Escudero I, Elmore B, et al. *Klebsiella pneumoniae* type VI secretion system-mediated microbial competition is PhoPQ controlled and reactive oxygen species dependent. Vol. 16, PLoS Pathogens. 2020. 1–54 *P.*

329. Carruthers MD, Nicholson PA, Tracy EN, Munson RS. *Acinetobacter baumannii* Utilizes a Type VI Secretion System for Bacterial Competition. PLoS One. 2013;8(3).

330. Soria-Bustos J, Ares MA, Gómez-Aldapa CA, González-y-Merchand JA, Girón JA, De la Cruz MA. Two Type VI Secretion Systems of *Enterobacter cloacae* Are Required for Bacterial Competition, Cell Adherence, and Intestinal Colonization. Front Microbiol. 2020;11(September):1–14.

331. Hare RF, Hueffer K. *Francisella novicida* pathogenicity island encoded proteins were secreted during infection of macrophage-like cells. PLoS One. 2014;9(8).

332. Blondel CJ, Jiménez JC, Contreras I, Santiviago CA. Comparative genomic analysis uncovers 3 novel loci encoding type six secretion systems differentially distributed in *Salmonella* serotypes. BMC Genomics. 2009;10(i).

333. Ma J, Sun M, Bao Y, Pan ZH, Zhang W, Lu C, et al. Genetic diversity and features analysis of type VI secretion systems loci in avian pathogenic *Escherichia coli* by wide genomic scanning. Infect Genet Evol [Internet]. 2013;20:454–64. Available from: http://dx.doi.org/10.1016/j.meegid.2013.09.031

334. Unterweger D, Miyata ST, Bachmann V, Brooks TM, Mullins T, Kostiuk B, et al. The *Vibrio cholerae* type VI secretion system employs diverse effector modules for intraspecific competition. Nat Commun. 2014;5:1–9.

335. Marasini D, Karki AB, Bryant JM, Sheaff RJ, Fakhr MK. Molecular characterization of megaplasmids encoding the type VI secretion system in *Campylobacter jejuni* isolated from chicken livers and gizzards. Sci Rep [Internet]. 2020;10(1):1–10. Available from: https://doi.org/10.1038/s41598-020-69155-z

336. Coyne MJ, Roelofs KG, Comstock LE. Type VI secretion systems of human gut Bacteroidales segregate into three genetic architectures, two of which are contained on mobile genetic elements. BMC Genomics [Internet]. 2016;17(1):1–21. Available from: http://dx.doi.org/10.1186/s12864-016-2377-z

337. Wu HY, Chung PC, Shih HW, Wen SR, Lai EM. Secretome analysis uncovers an Hcp-family protein secreted via a type VI secretion system in *Agrobacterium tumefaciens*. J Bacteriol. 2008;190(8):2841–50.

338. Allsopp LP, Wood TE, Howard SA, Maggiorelli F, Nolan LM, Wettstadt S, et al. RsmA and AmrZ orchestrate the assembly of all three type VI secretion systems in *Pseudomonas aeruginosa*. Proc Natl Acad Sci [Internet]. 2017;114(29):7707–12. Available from: http://www.pnas.org/lookup/doi/10.1073/pnas.1700286114

339. Shalom G, Shaw JG, Thomas MS. In vivo expression technology identifies a type VI secretion system locus in *Burkholderia pseudomallei* that is induced upon invasion of macrophages. Microbiology. 2007;153(8):2689–99.

340. Pissaridou P, Allsopp LP, Wettstadt S, Howard SA, Mavridou DAI. The *Pseudomonas aeruginosa* T6SS-VgrG1b spike is topped by a PAAR protein eliciting DNA damage to bacterial competitors. Proc Natl Acad Sci. 2018;(14):2–7.

341. Ross BD, Verster AJ, Radey MC, Schmidtke DT, Pope CE, Hoffman LR, et al. Human gut bacteria contain acquired interbacterial defence systems. Nature [Internet]. 2019;575(7781):224–8. Available from: http://dx.doi.org/10.1038/s41586-019-1708-z

342. Boyer F, Fichant G, Berthod J, Vandenbrouck Y, Attree I. Dissecting the bacterial type VI secretion system by a genome wide in silico analysis: what can be learned from available

microbial genomic resources? BMC Genomics [Internet]. 2009;10(1):104. Available from: http://www.pubmedcentral.nih.gov/articlerender.fcgi?artid=2660368&tool=pmcentrez&rendertype=abstract%5Cnhttp://www.ncbi.nlm.nih.gov/pubmed/19284603%5Cnhttp://www.pubmedcentral.nih.gov/articlerender.fcgi?artid=PMC2660368%5Cnhttp://bmcgenomics.biomedcentral

343. Barret M, Egan F, Fargier E, Morrissey JP, Gara FO. Genomic analysis of the type VI secretion systems in *Pseudomonas* spp .: novel clusters and putative effectors uncovered. Microbiology. 2019;157:1726–39.

344. Durand E, Zoued A, Spinelli S, Watson PJH, Aschtgen M-S, Journet L, et al. Structural Characterization and Oligomerization of the TssL Protein , a Component Shared by Bacterial Type VI and Type IVb Secretion Systems * □. J Biol Chem. 2012;287(17):14157–68.

345. Aschtgen M-S, Gavioli M, Dessen A, Lloubès R, Cascales E. The SciZ protein anchors the enteroaggregative *Escherichia coli* Type VI secretion system to the cell wall. Mol Microbiol. 2010;75(4):886–99.

346. Aschtgen M-S, Bernard CS, De Bentzmann S, Lloubès R, Cascales E. SciN is an outer membrane lipoprotein required for type VI secretion in enteroaggregative *Escherichia coli*. J Bacteriol. 2008;190(22):7523–31.

347. Durand E, Nguyen VS, Zoued A, Logger L, Pehau-Arnaudet G, Aschtgen M-S, et al. Biogenesis and structure of a type VI secretion membrane core complex. Nature [Internet]. 2015 Jul 30;523(7562):555–60. Available from: http://dx.doi.org/10.1038/nature14667

348. Felisberto-Rodrigues C, Durand E, Aschtgen MS, Blangy S, Ortiz-Lombardia M, Douzi B, et al. Towards a structural comprehension of bacterial type vi secretion systems: Characterization of the TssJ-TssM complex of an *Escherichia coli* pathovar. PLoS Pathog. 2011;7(11):1–11.

349. Ma LS, Lin JS, Lai EM. An IcmF family protein, ImpLM, is an integral inner membrane protein interacting with ImpKL, and its Walker a motif is required for type VI secretion system-mediated Hcp secretion in *Agrobacterium tumefaciens*. J Bacteriol. 2009;

350. Zheng J, Leung KY. Dissection of a type VI secretion system in *Edwardsiella tarda*. Mol Microbiol. 2007;66(5):1192–206.

351. Logger L, Aschtgen M-S, Guérin M, Cascales E, Durand E. Molecular Dissection of the Interface between the Type VI Secretion TssM Cytoplasmic Domain and the TssG Baseplate Component. J Mol Biol [Internet]. 2016;428(22):4424–37. Available from: http://dx.doi.org/10.1016/j.jmb.2016.08.032

352. Ma L-S, Narberhaus F, Lai EM. IcmF family protein TssM exhibits ATPase activity and energizes type VI secretion. J Biol Chem. 2012;287(19):15610–21.

353. Ma L-S, Lin J-SS, Lai E-MM. An IcmF Family Protein, ImpL M, Is an Integral Inner Membrane Protein Interacting with ImpK L, and Its Walker A Motif Is Required for Type VI Secretion System-Mediated Hcp Secretion in *Agrobacterium tumefaciens*. J Bacteriol. 2009;191(13):4316–29.

354. Zoued A, Cassaro CJ, Durand E, Douzi B, España AP, Cambillau C, et al. Structure–Function Analysis of the TssL Cytoplasmic Domain Reveals a New Interaction between the Type VI Secretion Baseplate and Membrane Complexes. J Mol Biol. 2016;22(428):4413-4423

355. Aschtgen M-S, Thomas MS, Cascales E. Anchoring the type VI secretion system to the peptidoglycan: TssL, TagL, Tag*P*... what else? Virulence [Internet]. 2010;1(6):535–40. Available from: http://www.tandfonline.com/doi/abs/10.4161/viru.1.6.13732

356. Rapisarda C, Cherrak Y, Kooger R, Schmidt V, Pellarin R, Logger L, et al. In situ and high-resolution cryo-EM structure of a bacterial type VI secretion system membrane complex. EMBO J. 2019;38:1–18.

357. Chang Y, Rettberg LA, Ortega DR, Jensen GJ. *In vivo* structures of an intact type VI secretion system revealed by electron cryotomography. EMBO Re*P.* 2017;18(7):1090–9.

358. Weber BS, Hennon SW, Wright MS, Scott NE, Berardinis V De, Foster LJ, et al. Genetic Dissection of the Type VI Secretion System in Acinetobacter and Identification of a Novel Peptidoglycan Hydrolase, TagX, Required for Its Biogenesis. Am Soc Microbiol. 2016;7(5):1–17.

359. Santin YG, Cascales E. Domestication of a housekeeping transglycosylase for assembly of a Type VI secretion system. EMBO Rep*.* 2017;18(1):138–49.

360. Zoued A, Durand E, Brunet YR, Spinelli S, Douzi B, Guzzo M, et al. Priming and polymerization of a bacterial contractile tail structure. Nature [Internet]. 2016;531(7592):59–63. Available from: http://dx.doi.org/10.1038/nature17182

361. Zoued A, Durand E, Santin YG, Journet L, Roussel A, Cambillau C, et al. TssA: The cap protein of the Type VI secretion system tail. Vol. 39, BioEssays. 2017. *P.* 1–9.

362. Yin M, Yan Z, Li X. Architecture of type VI secretion system membrane core complex. Cell Res. 2019;29(3):251–3.

363. Kikuchi Y, King J. Genetic Control of Bacteriophage T4 Baseplate Morphogenesis I. Sequential Assembly of the Major Precursor, in vivo and in vitro. J Mol Biol. 1975;99(4):645–72.

364. Nazarov S, Schneider JP, Brackmann M, Goldie KN, Stahlberg H, Basler M. Cryo-EM reconstruction of Type VI secretion system baseplate and sheath distal end. EMBO J [Internet]. 2017;37:e201797103. Available from: http://emboj.embopress.org/lookup/doi/10.15252/embj.201797103

365. Cherrak Y, Rapisarda C, Pellarin R, Bouvier G, Bardiaux B, Allain F, et al. Biogenesis and structure of a type VI secretion baseplate. Nat Microbiol [Internet]. 2018;3(December). Available from: http://dx.doi.org/10.1038/s41564-018-0260-1

366. Spínola-Amilibia M, Davó-Siguero I, Ruiz FM, Santillana E, Medrano FJ, Romero A. The structure of VgrG1 from *Pseudomonas aeruginosa*, the needle tip of the bacterial type VI secretion system. Acta Crystallogr Sect D Struct Biol. 2016;72(1):22–33.

367. Hachani A, Allsopp LP, Oduko Y, Filloux A. The VgrG proteins are “a la carte” delivery systems for bacterial type VI effectors. J Biol Chem. 2014;289(25):17872–84.

368. Wettstadt S, Wood TE, Fecht S, Filloux A. Delivery of the *Pseudomonas aeruginosa* Phospholipase Effectors PldA and PldB in a VgrG- and H2-T6SS-Dependent Manner. Front Microbiol. 2019;10(July):1–18.

369. Park Y, Lacourse KD, Veesler D, Dimaio F, Mougous JD. Structure of the type VI secretion system TssK–TssF–TssG baseplate subcomplex revealed by cryo-electron microscopy. Nat Commun [Internet]. 2018;9(5385):1–11. Available from: http://dx.doi.org/10.1038/s41467-018-07796-5

370. Brunet YR, Zoued A, Boyer F, Douzi B, Cascales E. The Type VI Secretion TssEFGK-VgrG Phage-Like Baseplate Is Recruited to the TssJLM Membrane Complex via Multiple Contacts and Serves As Assembly Platform for Tail Tube/Sheath Polymerization. PLoS Genet. 2015;11(10):1–21.

371. Zoued A, Durand E, Bebeacua C, Brunet YR, Douzi B, Cambillau C, et al. TssK is a trimeric cytoplasmic protein interacting with components of both phage-like and membrane anchoring complexes of the Type VI secretion system. J Biol Chem. 2013;288:27031–27041.

372. Nguyen VS, Logger L, Spinelli S, Legrand P, Huyen Pham TT, Nhung Trinh TT, et al. Type VI secretion TssK baseplate protein exhibits structural similarity with phage receptor-binding proteins and evolved to bind the membrane complex. Nat Microbiol [Internet]. 2017;2(June):1–9. Available from: http://dx.doi.org/10.1038/nmicrobiol.2017.103

373. Renault MG, Beas JZ, Douzi B, Chabalier M, Zoued A, Brunet YR, et al. The gp27-like Hub of VgrG Serves as Adaptor to Promote Hcp Tube Assembly. J Mol Biol [Internet]. 2018;430(18):3143–56. Available from: https://doi.org/10.1016/j.jmb.2018.07.018

374. Leiman PG, Shneider MM. Contractile tail machines of bacteriophages. Adv Exp Med Biol. 2012;726:93–114.

375. Lossi NS, Dajani R, Freemont PS, Filloux A. Structure – function analysis of HsiF, a gp25-like component of the type VI secretion system, in *Pseudomonas aeruginosa*. Microbiology. 2011;157:3292–305.

376. Planamente S, Salih O, Manoli E, Albesa-Jové D, Freemont PS, Filloux A. TssA forms a gp6-like ring attached to the type VI secretion sheath. EMBO J [Internet]. 2016;35(15):e201694024. Available from: http://emboj.embopress.org/lookup/doi/10.15252/embj.201694024%5Cnhttp://www.ncbi.nlm.nih.gov/pubmed/27288401

377. Schneider JP, Nazarov S, Adaixo R, Liuzzo M, David P, Stahlberg H, et al. Diverse roles of TssA-like proteins in the assembly of bacterial type VI secretion systems. EMBO J. 2019;38(18):1–17.

378. Ballister ER, Lai AH, Zuckermann RN, Cheng Y, Mougous JD. In vitro self-assembly of tailorable nanotubes from a simple protein building block. Proc Natl Acad Sci [Internet]. 2008;105(10):3733–8. Available from: http://www.pnas.org/cgi/doi/10.1073/pnas.0712247105

379. Brunet YR, Henin J, Herve C, Cascales E, Hénin J, Celia H, et al. Type VI secretion and bacteriophage tail tubes share a common assembly pathway. EMBO Re*P.* 2014;15(3):315–21.

380. Silverman JM, Agnello D, Zheng H, Andrews B, Li M, Catalano C, et al. Haemolysin Co-regulated Protein is an Exported Receptor and Chaperone of Type VI Secretion Substrates. Cell. 2013;51(5):1089–98.

381. Bröms JE, Ishikawa T, Wai SN, Sjöstedt A. A functional VipA-VipB interaction is required for the type VI secretion system activity of *Vibrio cholerae* O1 strain A1552. BMC Microbiol. 2013;13(1).

382. Zhang XY, Brunet YR, Logger L, Douzi B, Cambillau C, Journet L, et al. Dissection of the TssB-TssC interface during type VI secretion sheath complex formation. PLoS One. 2013;8(11):1–8.

383. Kube S, Kapitein N, Zimniak T, Herzog F, Mogk A, Wendler *P.* Structure of the VipA / B Type VI Secretion Complex Suggests a Contraction-State-Specific Recycling Mechanism. Cell Rep [Internet]. 2014;8(1):20–30. Available from: http://dx.doi.org/10.1016/j.celre*P.*2014.05.034

384. Brackmann M, Nazarov S, Wang J. Using Force to Punch Holes: Mechanics of Contractile Nanomachines. Trends Cell Biol [Internet]. 2017;27(9):623–32. Available from: http://dx.doi.org/10.1016/j.tcb.2017.05.003

385. Kudryashev M, Wang RY, Brackmann M, Scherer S, Maier T, Baker D, et al. Structure of the Type VI secretion system contractile sheath. Cell. 2016;160(5):952–62.

386. Wang J, Brackmann M, Castaño-díez D, Kudryashev M, Goldie KN, Maier T, et al. Cryo-EM structure of the extended type VI secretion system sheath – tube complex. Nat Microbiol [Internet]. 2017;2(November). Available from: http://dx.doi.org/10.1038/s41564-017-0020-7

387. Vettiger A, Winter J, Lin L, Basler M. The type VI secretion system sheath assembles at the end distal from the membrane anchor. Nat Commun [Internet]. 2017;8(May):1–9. Available from: http://dx.doi.org/10.1038/ncomms16088

388. Abuladze NK, Gingery M, Tsai J, Eiserling FA. Tail length determination in bacteriophage T4. Virology [Internet]. 1994 Mar;199(2):301—310. Available from: https://doi.org/10.1006/viro.1994.1128

389. Basler M, Pilhofer M, Henderson GP, Jensen GJ, Mekalanos JJ. Type VI secretion requires a dynamic contractile phage tail-like structure. Nature [Internet]. 2012;483(7388):182–6. Available from: http://www.nature.com/doifinder/10.1038/nature10846

390. Pietrosiuk A, Lenherr ED, Falk S, Bönemann G, Kopp J, Zentgraf H, et al. Molecular basis for the unique role of the AAA + chaperone ClpV in type VI protein secretion. J Biol Chem. 2011;286(34):30010–21.

391. Basler M, Mekalanos JJ. Type 6 secretion dynamics within and between bacterial cells. Science (80-). 2012;337(6069).

392. Kapitein N, Bönemann G, Pietrosiuk A, Seyffer F, Hausser I, Locker JK, et al. ClpV recycles VipA/VipB tubules and prevents non-productive tubule formation to ensure efficient type VI protein secretion. Mol Microbiol. 2013;87(5):1013–28.

393. Bönemann G, Pietrosiuk A, Diemand A, Zentgraf H, Mogk A. Remodelling of VipA/VipB tubules by ClpV-mediated threading is crucial for type VI protein secretion. EMBO J [Internet]. 2009;28(4):315–25. Available from: http://emboj.embopress.org/cgi/doi/10.1038/emboj.2008.269

394. Zheng J, Ho BT, Mekalanos JJ. Genetic Analysis of Anti-Amoebae and Anti-Bacterial Activities of the Type VI Secretion System in *Vibrio cholerae*. PLoS One. 2011;6(8).

395. Basler M. Type VI secretion system: Secretion by a contractile nanomachine. Philos Trans R Soc B Biol Sci. 2015;370(1679).

396. Vettiger A, Basler M. Type VI Secretion System Substrates Are Transferred and Reused among Sister Cells. Cell [Internet]. 2016;167(1):99-110.e12. Available from: http://dx.doi.org/10.1016/j.cell.2016.08.023

397. Ge P, Scholl D, Leiman PG, Yi X, Miller JF, Zhou ZH, et al. Atomic structures of a bactericidal contractile nanotube in its pre- and postcontraction states. Nat Struct Mol Biol. 2015;22(5):377–83.

398. Heymann JB, Bartho JD, Rybakova D, Venugopal HP, Winkler DC, Sen A, et al. Three-dimensional structure of the toxin-delivery particle antifeeding prophage of *Serratia entomophila*. J Biol Chem. 2013;288(35):25276–84.

399. Uratani Y, Hoshino T. Pyocin R1 Inhibits Active Transport in *Pseudomonas aeruginosa* and Depolarizes Membrane Potential. J Bacteriol. 1984;157:632–6.

400. Yang G, Dowling AJ, Gerike U, Ffrench-Constant RH, Waterfield NR. *Photorhabdus* virulence cassettes confer injectable insecticidal activity against the wax moth. J Bacteriol.

2006;188(6):2254–61.

401. Shikuma NJ, Pilhofer M, Weiss GL, Hadfield MG, Jensen GJ, Newman DK. Marine tubeworm metamorphosis induced by arrays of bacterial phage tail-like structures. Science (80-). 2014;343(6170):529–33.

402. Filloux A, Freemont *P.* Structural biology: Baseplates in contractile machines. Nat Microbiol. 2016;1(7).

403. Thomassen E, Gielen G, Schütz M, Schoehn G, Abrahams JP, Miller S, et al. The structure of the receptor-binding domain of the bacteriophage T4 short tail fibre reveals a knitted trimeric metal-binding fold. J Mol Biol. 2003;331(2):361–73.

404. Buth SA, Shneider MM, Scholl D, Leiman PG. Structure and analysis of R1 and R2 pyocin receptor-binding fibers. Viruses. 2018;10(8).

405. Leiman PG, Chipman PR, Kostyuchenko VA, Mesyanzhinov V V., Rossmann MG. Three-dimensional rearrangement of proteins in the tail of bacteriophage T4 on infection of its host. Cell. 2004;118(4):419–29.

406. Taylor NMI, Prokhorov NS, Guerrero-Ferreira RC, Shneider MM, Browning C, Goldie KN, et al. Structure of the T4 baseplate and its function in triggering sheath contraction. Nature [Internet]. 2016;533(7603):346–52. Available from: http://dx.doi.org/10.1038/nature17971

407. Kanamaru S, Leiman PG, Kostyuchenko VA. Structure of the cell-puncturing device of bacteriophage T4. Nature. 2002;2428(2001):553–7.

408. Pell LG, Kanelis V, Donaldson LW, Howell PL, Davidson AR. The phage λ major tail protein structure reveals a common evolution for long-tailed phages and the type VI bacterial secretion system. Proc Natl Acad Sci U S A. 2009;106(11):4160–5.

409. Aksyuk AA, Leiman PG, Kurochkina LP, Shneider MM, Kostyuchenko VA, Mesyanzhinov V V., et al. The tail sheath structure of bacteriophage T4: A molecular machine for infecting bacteria. EMBO J [Internet]. 2009;28(7):821–9. Available from: http://dx.doi.org/10.1038/emboj.2009.36

410. Rybakova D, Schramm P, Mitra AK, Hurst MRH. Afp14 is involved in regulating the length of Anti-feeding prophage (Afp). Mol Microbiol. 2015;96(4):815–26.

411. Kostyuchenko VA, Chipman PR, Leiman PG, Arisaka F, Mesyanzhinov V V., Rossmann MG. The tail structure of bacteriophage T4 and its mechanism of contraction. Nat Struct Mol Biol. 2005;12(9):810–3.

412. Howard SA, Furniss RCD, Bonini D, Amin H, Paracuellos P, Zlotkin D, et al. The breadth and molecular basis of Hcp-driven type VI secretion system effector delivery. MBio. 2021;12(3):1–19.

413. Flaugnatti N, Hang Le TT, Canaan S, Aschtgen M-S, Nguyen VS, Blangy S, et al. A phospholipase A 1 antibacterial Type VI secretion effector interacts directly with the C-terminal domain of the VgrG spike protein for delivery. Mol Microbiol. 2016;99(February):1099–118.

414. Burkinshaw BJ, Liang X, Wong M, Le ANH, Lam L, Dong TG. A type VI secretion system effector delivery mechanism dependent on PAAR and a chaperone–co-chaperone complex. Nat Microbiol [Internet]. 2018;3(May). Available from: http://dx.doi.org/10.1038/s41564-018-0144-4

415. Quentin D, Ahmad S, Shanthamoorthy P, Mougous JD, Whitney JC, Rausner S. Mechanism of

loading and translocation of type VI secretion system effector Tse6. Physiol Behav. 2017;176(3):139–48.

416. Ma J, Pan Z, Huang J, Sun M, Lu C, Yao H. The Hcp proteins fused with diverse extended-toxin domains represent a novel pattern of antibacterial effectors in type VI secretion systems. Virulence [Internet]. 2017;8(7):1189–202. Available from: https://doi.org/10.1080/21505594.2017.1279374

417. Whitney JC, Quentin D, Sawai S, Leroux M, Harding BN, Ledvina HE, et al. An Interbacterial NAD(P)+ Glycohydrolase Toxin Requires Elongation Factor Tu for Delivery to Target Cells. Cell. 2015;163(3):607–19.

418. Pei TT, Li H, Liang X, Wang ZH, Liu G, Wu LL, et al. Intramolecular chaperone-mediated secretion of an Rhs effector toxin by a type VI secretion system. Nat Commun. 2020;11(1).

419. Song L, Pan J, Yang Y, Zhang Z, Cui R, Jia S, et al. Contact-independent killing mediated by a T6SS effector with intrinsic cell-entry properties. Nat Commun [Internet]. 2021;12(1). Available from: http://dx.doi.org/10.1038/s41467-020-20726-8

420. Cianfanelli FR, Monlezun L, Coulthurst SJ. Aim, Load, Fire: The Type VI Secretion System, a Bacterial Nanoweapon [Internet]. Vol. 24, Trends in Microbiology. Elsevier Ltd; 2016. *P.* 51–62. Available from: http://dx.doi.org/10.1016/j.tim.2015.10.005

421. Wood TE, Howard SA, Wettstadt S, Filloux A. PAAR proteins act as the 'sorting hat' of the type VI secretion system. Microbiology. 2019;165:1203–18.

422. Lacourse KD, Peterson SB, Kulasekara HD, Radey MC, Kim J, Mougous JD. Conditional toxicity and synergy drive diversity among antibacterial effectors. Nat Microbiol [Internet]. 2018;3(April). Available from: http://dx.doi.org/10.1038/s41564-018-0113-y

423. Arnold R, Brandmaier S, Kleine F, Tischler P, Heinz E, Behrens S, et al. Sequence-based prediction of type III secreted proteins. PLoS Pathog. 2009 Apr;5(4):e1000376.

424. Salomon D, Kinch LN, Trudgian DC, Guo X, Klimko JA, Grishin N V, et al. Marker for type VI secretion system effectors. Proc Natl Acad Sci. 2014;111(25).

425. Jana B, Fridman CM, Bosis E, Salomon D. A modular effector with a DNase domain and a marker for T6SS substrates. Nat Commun [Internet]. (2019). Available from: http://dx.doi.org/10.1038/s41467-019-11546-6

426. Li L, Zhang W, Liu Q, Gao Y, Gao Y, Wang Y, et al. Structural insights on the bacteriolytic and self-protection mechanism of muramidase effector Tse3 in *Pseudomonas aeruginosa*. J Biol Chem. 2013;288(42):30607–13.

427. Ting S, Bosch DE, Mangiameli SM, Radey MC, Huang S, Young-Jun P, et al. Bifunctional Immunity Proteins Protect Bacteria against FtsZ-Targeting ADP-Ribosylating Toxins. Cell [Internet]. 2018;175(5):1380-1392.e14. Available from: https://doi.org/10.1016/j.cell.2018.09.037

428. Russell AB, Hood RD, Bui NK, Leroux M, Vollmer W, Mougous JD. Type VI secretion delivers bacteriolytic effectors to target cells. Nature. 2011;1.

429. Troselj V, Treuner-Lange A, Søgaard-Andersen L, Wall D. Physiological heterogeneity triggers sibling conflict mediated by the type VI secretion system in an aggregative multicellular bacterium. MBio. 2018;9(1).

430. Russell AB, Singh P, Brittnacher M, Bui NK, Hood, Rachel D, Carl MA, et al. A widespread bacterial type VI secretion effector superfamily identified using a heuristic approach. Cell

Host Microbe. 2012;11(5):538–49.

431. Whitney JC, Chou S, Russell AB, Biboy J, Gardiner TE, Ferrin MA, et al. Identification , Structure , and Function of a Novel Type VI Secretion Peptidoglycan Glycoside Hydrolase. J Biol Chem. 2013;288(37):26616–24.

432. Brooks TM, Unterweger D, Bachmann V, Kostiuk B, Pukatzki S. Lytic Activity of the *Vibrio cholerae* Type VI Secretion Toxin VgrG-3 Is Inhibited by the Antitoxin TsaB *. J Biol Chem. 2013;288(11):7618–25.

433. Miyata ST, Unterweger D, Rudko SP, Pukatzki S. Dual Expression Profile of Type VI Secretion System Immunity Genes Protects Pandemic *Vibrio cholerae*. PLoS Pathog. 2013;9(12).

434. Bondage DD, Lin JS, Ma L-S, Kuo CH, Lai EM. VgrG C terminus confers the type VI effector transport specificity and is required for binding with PAAR and adaptor-effector complex. Proc Natl Acad Sci U S A. 2016;113(27):E3931–40.

435. Ahmad S, Wang B, Walker MD, Tran HR, Stogios PJ, Savchenko A, et al. An interbacterial toxin inhibits target cell growth by synthesizing (p) ppApp. Nature [Internet]. 2019;575(May). Available from: http://dx.doi.org/10.1038/s41586-019-1735-9

436. Nolan LM, Cain AK, Clamens T, Furniss RCD, Manoli E, Sainz-Polo MA, et al. Identification of Tse8 as a Type VI secretion system toxin from *Pseudomonas aeruginosa* that targets the bacterial transamidosome to inhibit protein synthesis in prey cells. Nat Microbiol [Internet]. 2021;6(9):1199–210. Available from: http://dx.doi.org/10.1038/s41564-021-00950-8

437. Ma L-S, Hachani A, Lin J-S, Filloux A, Lai E-M. *Agrobacterium tumefaciens* deploys a superfamily of type VI secretion DNase effectors as weapons for interbacterial competition in planta. Cell Host Microbe [Internet]. 2014;16(1):94–104. Available from: http://dx.doi.org/10.1016/j.chom.2014.06.002

438. Ringel PD, Hu D, Basler M. The Role of Type VI Secretion System Effectors in Target Cell Lysis and Subsequent Horizontal Gene Transfer. Cell Re*P.* 2017;21(13):3927–40.

439. Liang X, Kamal F, Pei TT, Xu P, Mekalanos JJ, Dong TG. An onboard checking mechanism ensures effector delivery of the type VI secretion system in *Vibrio cholerae*. Proc Natl Acad Sci U S A. 2019;116(46):23292–8.

440. Wu C, Lien Y, Bondage D, Lin J, Pilhofer M, Shih Y, et al. Effector loading onto the VgrG carrier activates type VI secretion system assembly . EMBO Re*P.* 2020;21(1):1–12.

441. Suarez G, Sierra JC, Erova TE, Sha J, Horneman AJ, Chopra AK. A Type VI Secretion System Effector Protein, VgrG1 , from *Aeromonas hydrophila* That Induces Host Cell Toxicity by ADP Ribosylation of Actin. J Bacteriol. 2010;192(1):155–68.

442. Sana TG, Baumann C, Merdes A, Soscia C, Rattei T, Hachani A, et al. Internalization of *Pseudomonas aeruginosa* Strain PAO1 into Epithelial Cells Is Promoted by Interaction of a T6SS Effector with the. MBio. 2015;6(3):1–11.

443. Toesca IJ, French CT, Miller JF. The Type VI Secretion System Spike Protein VgrG5 Mediates Membrane Fusion during Intercellular Spread by Pseudomallei Group *Burkholderia* Species. Infect Immun. 2014;82(4):1436–44.

444. Chen H, Yang D, Han F, Tan J, Zhang L, Xiao J, et al. The Bacterial T6SS Effector EvpP Prevents NLRP3 Inflammasome Activation by Inhibiting the Ca 2 + - Dependent MAPK-Jnk Pathway Article The Bacterial T6SS Effector EvpP Prevents NLRP3 Inflammasome Activation by Inhibiting. Cell Host Microbe [Internet]. 2017;21(1):47–58. Available from:

http://dx.doi.org/10.1016/j.chom.2016.12.004

445. Wood TE, Howard SA, Förster A, Nolan LM, Manoli E, Bullen NP, et al. The *Pseudomonas aeruginosa* T6SS Delivers a Periplasmic Toxin that Disrupts Bacterial Cell Morphology. Cell Rep. 2019;29(1):187-201.e7.

446. Si M, Zhao C, Burkinshaw B, Zhang B, Wei D, Wang Y, et al. Manganese scavenging and oxidative stress response mediated by type VI secretion system in *Burkholderia thailandensis*. Proc Natl Acad Sci. 2017;10:2233–42.

447. Si M, Wang Y, Zhang B, Si M, Wang Y, Zhang B, et al. The Type VI Secretion System Engages a Redox- Regulated Dual-Functional Heme Transporter for Zinc Acquisition. CellReports [Internet]. 2017;20(4):949–59. Available from: http://dx.doi.org/10.1016/j.celre*P.*2017.06.081

448. Li C, Zhu L, Wang D, Wei Z, Hao X, Wang Z, et al. T6SS secretes an LPS-binding effector to recruit OMVs for exploitative competition and horizontal gene transfer. ISME J. 2022;16(2):500–10.

449. Le N, Peters K, Espaillat A, Sheldon JR, Gray J, Venanzio G Di, et al. Peptidoglycan editing provides immunity to *Acinetobacter baumannii* during bacterial warfare. Sci Adv. 2020;6:1–8.

450. Hersch SJ, Watanabe N, Stietz MS, Manera K, Kamal F, Burkinshaw B, et al. Envelope stress responses defend against type six secretion system attacks independently of immunity proteins. Nat Microbiol [Internet]. 2020;10. Available from: http://dx.doi.org/10.1038/s41564-020-0672-6

451. Kamal F, Liang X, Manera K, Pei TT, Kim H, Lam LG, et al. Differential Cellular Response to Translocated Toxic Effectors and Physical Penetration by the Type VI Secretion System. Cell Rep [Internet]. 2020;31(11):107766. Available from: https://doi.org/10.1016/j.celre*P.*2020.107766

452. Haapalainen M, Mosorin H, Dorati F, Wu RF, Roine E, Taira S, et al. Hcp2, a secreted protein of the phytopathogen *Pseudomonas syringae* pv. tomato DC3000, is required for fitness for competition against bacteria and yeasts. J Bacteriol. 2012;194(18):4810–22.

453. Sana TG, Flaugnatti N, Lugo KA, Lam LH, Jacobson A, Baylot V, et al. *Salmonella* Typhimurium utilizes a T6SS-mediated antibacterial weapon to establish in the host gut. Proc Natl Acad Sci [Internet]. 2016;113(34):E5044–51. Available from: http://www.pnas.org/lookup/doi/10.1073/pnas.1608858113

454. Anderson MC, Vonaesch P, Saffarian A, Marteyn BS, Sansonetti PJ. *Shigella sonnei* Encodes a Functional T6SS Used for Interbacterial Competition and Niche Occupancy. Cell Host Microbe [Internet]. 2017;21(6):769-776.e3. Available from: http://dx.doi.org/10.1016/j.chom.2017.05.004

455. Logan SL, Thomas J, Yan J, Baker RP, Shields DS, Xavier JB, et al. The *Vibrio cholerae* type VI secretion system can modulate host intestinal mechanics to displace gut bacterial symbionts. Proc Natl Acad Sci U S A. 2018;115(16):E3779–87.

456. Fast D, Kostiuk B, Foley E, Pukatzki S. Commensal pathogen competition impacts host viability. Proc Natl Acad Sci U S A. 2018;115(27):7099–104.

457. Zhao W, Caro F, Robins W, Mekalanos JJ. Antagonism toward the intestinal microbiota and its effect on *Vibrio cholerae* virulence. Science (80-). 2018;359(6372):210–3.

458. Hecht AL, Casterline BW, Earley ZM, Goo YA, Goodlett DR, Bubeck Wardenburg J. Strain

competition restricts colonization of an enteric pathogen and prevents *coli*tis. EMBO Re*P.* 2016;17(9):1281–91.

459. Decoin V, Barbey C, Bergeau D, Latour X, Feuilloley MGJ, Orange N, et al. A type VI secretion system is involved in *Pseudomonas fluorescens* bacterial competition. PLoS One. 2014;9(2).

460. Smith WPJ, Vettiger A, Winter J, Ryser T, Comstock LE, Basler M, et al. The evolution of the type VI secretion system as a disintegration weapon. PLoS Biol [Internet]. 2020;18(5):1–26. Available from: http://dx.doi.org/10.1371/journal.pbio.3000720

461. Borgeaud S, Metzger LC, Scrignari T, Blokesch M. The type VI secretion system of *Vibrio cholerae* fosters horizontal gene transfer. Science (80-). 2015;347(6217):63–8.

462. Thomas J, Watve SS, Ratcliff WC, Hammer BK. Horizontal gene transfer of functional type VI killing genes by natural transformation. MBio. 2017;8(4).

463. Kirchberger PC, Unterweger D, Provenzano D, Pukatzki S, Boucher Y. Sequential displacement of Type VI Secretion System effector genes leads to evolution of diverse immunity gene arrays in *Vibrio cholerae*. Sci Re*P.* 2017;7(February):1–12.

464. Corbitt J, Yeo JS, Davis CI, Leroux M, Wiggins PA. Type VI Secretion System Dynamics Reveals a Novel Secretion Mechanism in *Pseudomonas aeruginosa*. J Bacteriol. 2018;200(11):1–13.

465. Ventre I, Goodman AL, Vallet-gely I, Vasseur P, Soscia C, Molin S, et al. Multiple sensors control reciprocal expression of *Pseudomonas aeruginosa* regulatory RNA and virulence genes. Pnas. 2006;103(1):171–6.

466. Goodman AL, Merighi M, Hyodo M, Ventre I, Filloux A, Lory S. Direct interaction between sensor kinase proteins mediates acute and chronic disease phenotypes in a bacterial pathogen. Genes Dev. 2009;23(2):249–59.

467. Chambonnier G, Roux L, Redelberger D, Fadel F, Filloux A, Sivaneson M, et al. The Hybrid Histidine Kinase LadS Forms a Multicomponent Signal Transduction System with the GacS/GacA Two-Component System in *Pseudomonas aeruginosa*. PLoS Genet. 2016;12(5):1–30.

468. Kong W, Chen L, Zhao J, Shen T, Surette MG, Shen L, et al. Hybrid sensor kinase PA1611 in *Pseudomonas aeruginosa* regulates transitions between acute and chronic infection through direct interaction with RetS. Mol Microbiol. 2013 May;88(4):784–97.

469. Bhagirath AY, Pydi SP, Li Y, Lin C, Kong W, Chelikani P, et al. Characterization of the Direct Interaction between Hybrid Sensor Kinases PA1611 and RetS That Controls Biofilm Formation and the Type III Secretion System in *Pseudomonas aeruginosa*. ACS Infect Dis. 2017 Feb;3(2):162–75.

470. Wang BX, Wheeler KM, Cady KC, Lehoux S, Cummings RD, Laub MT, et al. Mucin Glycans Signal through the Sensor Kinase RetS to Inhibit Virulence-Associated Traits in *Pseudomonas aeruginosa*. Curr Biol. 2021 Jan;31(1):90-102.e7.

471. Mulcahy H, Lewenza S. Magnesium limitation is an environmental trigger of the *Pseudomonas aeruginosa* biofilm lifestyle. PLoS One. 2011;6(8):e23307.

472. Broder UN, Jaeger T, Jenal U. LadS is a calcium-responsive kinase that induces acute-to-chronic virulence switch in *Pseudomonas aeruginosa*. Nat Microbiol. 2016 Oct;2:16184.

473. Ali-Ahmad A, Fadel F, Sebban-Kreuzer C, Ba M, Pélissier GD, Bornet O, et al. Structural and functional insights into the periplasmic detector domain of the GacS histidine kinase controlling biofilm formation in *Pseudomonas aeruginosa*. Sci Re*P.* 2017;7(1):1–13.

474. Kay E, Humair B, Dénervaud V, Riedel K, Spahr S, Eberl L, et al. Two GacA-dependent small RNAs modulate the quorum-sensing response in *Pseudomonas aeruginosa*. J Bacteriol. 2006;188(16):6026–33.

475. Mougous JD, Gifford CA, Ramsdell TL, Mekalanos JJ. Threonine phosphorylation post-translationally regulates protein secretion in *Pseudomonas aeruginosa*. Nat Cell Biol [Internet]. 2007;9(7):797–803. Available from: http://www.nature.com/doifinder/10.1038/ncb1605

476. Hsu F, Schwarz S, Mougous JD. TagR Promotes PpkA-Catalyzed Type VI Secretion Activation in *Pseudomonas aeruginosa*. Mol Microbiol. 2009;72(5):1111–25.

477. Casabona MG, Silverman JM, Sall KM, Boyer F, Couté Y, Poirel J, et al. An ABC transporter and an outer membrane lipoprotein participate in posttranslational activation of type VI secretion in *Pseudomonas aeruginosa*. Environ Microbiol. 2013;15(2):471–86.

478. Liebl D, Robert-Genthon M, Job V, Cogoni V, Attrée I. Baseplate Component TssK and Spatio-Temporal Assembly of T6SS in *Pseudomonas aeruginosa*. Front Microbiol. 2019;10(JULY):1–15.

479. Basler M, Ho BT, Mekalanos JJ. Tit-for-tat: Type VI secretion system counterattack during bacterial cell-cell interactions. Cell [Internet]. 2013;152(4):884–94. Available from: http://dx.doi.org/10.1016/j.cell.2013.01.042

480. Ostrowski A, Cianfanelli FR, Porter M, Mariano G, Peltier J, Wong JJ, et al. Killing with proficiency: Integrated post-translational regulation of an offensive Type VI secretion system. PLoS Pathog. 2018;14(7):1–25.

481. Lin JS, Pissaridou P, Wu HH, Tsai MD, Filloux A, Lai EM. TagF-mediated repression of bacterial type VI secretion systems involves a direct interaction with the cytoplasmic protein Fha. J Biol Chem. 2018;293(23):8829–42.

482. Smith WPJ, Brodmann M, Unterweger D, Davit Y, Comstock LE, Basler M, et al. The evolution of tit-for-tat in bacteria via the type VI secretion system. Nat Commun [Internet]. 2020;11(1). Available from: http://dx.doi.org/10.1038/s41467-020-19017-z

483. Ho B, Basler M, Mekalanos JJ. Type VI secretion system-mediated Immunity to Type IV secretion system-mediated Horizontal Gene Transfer. Science (80-). 2013;342(6155):250–3.

484. Stolle A, Thomas B, Toska J, Mekalanos JJ. Endogenous membrane stress induces T6SS activity in *Pseudomonas aeruginosa*. Proc Natl Acad Sci. 2021;1–12.

485. Wilton M, Wong MJQ, Tang L, Liang X, Moore R, Parkins MD, et al. Chelation of membrane-bound cations by extracellular DNA activates the type VI secretion system in *Pseudomonas aeruginosa*. Infect Immun. 2016;84(8):2355–61.

486. Passador L, Cook JM, Gambello MJ, Rust L, Iglewski BH. Expression of *Pseudomonas aeruginosa* virulence genes requires cell-to-cell communication. Science (80-). 1993;260(5111):1127–30.

487. Nealson KH, Hastings JW. Bacterial bioluminescence: Its control and ecological significance. Microbiol Rev. 1979;43(4):496–518.

488. Davies DG, Parsek MR, Pearson JP, Iglewski BH, Costerton JW, Greenberg E*P.* The involvement of cell-to-cell signals in the development of a bacterial biofilm. Science (80-). 1998;280(5361):295–8.

489. Schuster M, Greenberg EP*.* Early activation of quorum sensing in *Pseudomonas aeruginosa*

reveals the architecture of a complex regulon. BMC Genomics. 2007;8:1–11.

490. Cao H, Krishnan G, Goumnerov B, Tsongalis J, Tompkins R, Rahme LG. A quorum sensing-associated virulence gene of *Pseudomonas aeruginosa* encodes a LysR-like transcription regulator with a unique self-regulatory mechanism. Proc Natl Acad Sci U S A. 2001;98(25):14613–8.

491. Lee J, Wu J, Deng Y, Wang J, Wang C, Wang J, et al. A cell-cell communication signal integrates quorum sensing and stress response. Nat Chem Biol. 2013;9(5):339–43.

492. Pessi G, Williams F, Hindle Z, Heurlier K, Holden MTG, Cámara M, et al. The global posttranscriptional regulator RsmA modulates production of virulence determinants and N-acylhomoserine lactones in *Pseudomonas aeruginosa*. J Bacteriol. 2001;183(22):6676–83.

493. Kulkarni PR, Jia T, Kuehne SA, Kerkering TM, Morris ER, Searle MS, et al. A sequence-based approach for prediction of CsrA/RsmA targets in bacteria with experimental validation in *Pseudomonas aeruginosa*. Nucleic Acids Res. 2014;42(11):6811–25.

494. Lesic B, Starkey M, He J, Hazan R, Rahme LG. Quorum sensing differentially regulates *Pseudomonas aeruginosa* type VI secretion locus I and homologous loci II and III, which are required for pathogenesis. Microbiology. 2009;

495. Sana TG, Soscia C, Tonglet CM, Garvis S, Bleves S. Divergent Control of Two Type VI Secretion Systems by RpoN in *Pseudomonas aeruginosa*. PLoS One. 2013;8(10):1–10.

496. Buck M, Cannon W. Specific binding of the transcription factor sigma-54 to promoter DNA. Nature. 1992;358(July):19–21.

497. Barrios H, Valderrama B, Morett E. Compilation and analysis of σ54-dependent promoter sequences. Nucleic Acids Res. 1999;27(22):4305–13.

498. Morrett E, Segovia L. The sigma54 Bacterial Enhancer-Binding Protein Family: Mechanism of Action and Phylogenetic Relationship of Their Functional Domains. J Bacteriol. 1993;175(19).

499. Francke C, Groot Kormelink T, Hagemeijer Y, Overmars L, Sluijter V, Moezelaar R, et al. Comparative analyses imply that the enigmatic sigma factor 54 is a central controller of the bacterial exterior. BMC Genomics [Internet]. 2011;12(1):385. Available from: http://www.biomedcentral.com/1471-2164/12/385

500. Shao X, Zhang X, Zhang Y, Zhu M, Yang P, Yuan J, et al. RpoN-Dependent Direct Regulation of Quorum Sensing and the Type VI Secretion System in *Pseudomonas aeruginosa* PAO1. J Bacteriol. 2018;200(16):1–17.

501. Allsopp LP, Collins ACZ, Hawkins E, Wood TE, Filloux A. RpoN/Sfa2-dependent activation of the *Pseudomonas aeruginosa* H2-T6SS and its cognate arsenal of antibacterial toxins. Nucleic Acids Res. 2022;50(1):227–43.

502. Termine E, Michel GPF. Transcriptome and secretome analyses of the adaptive response of *Pseudomonas aeruginosa* to suboptimal growth temperature. Int Microbiol. 2009;12(1):7–12.

503. Hachani A, Lossi NS, Filloux A. A visual assay to monitor T6SS-mediated bacterial competition. J Vis Exp [Internet]. 2013;(73):e50103. Available from: http://www.pubmedcentral.nih.gov/articlerender.fcgi?artid=3639552&tool=pmcentrez&rendertype=abstract%5Cnhttp://www.ncbi.nlm.nih.gov/pubmed/23542679

504. Sana TG, Hachani A, Bucior I, Soscia C, Garvis S, Termine E, et al. The second type VI secretion system of *Pseudomonas aeruginosa* strain PAO1 is regulated by quorum sensing and fur and modulates internalization in epithelial cells. J Biol Chem. 2012;287(32):27095–105.

505. Bains M, Fernández L, Hancock REW. Phosphate starvation promotes swarming motility and cytotoxicity of *Pseudomonas aeruginosa*. Appl Environ Microbiol. 2012;78(18):6762–8.

506. Reen FJ, Flynn S, Woods DF, Dunphy N, Chróinín MN, Mullane D, et al. Bile signalling promotes chronic respiratory infections and antibiotic tolerance. Sci Rep [Internet]. 2016;6(March):1–14. Available from: http://dx.doi.org/10.1038/srep29768

507. Reen FJ, Woods DF, Mooij MJ, Adams C, O'Gara F. Respiratory Pathogens Adopt a Chronic Lifestyle in Response to Bile. PLoS One. 2012;7(9).

508. Bernal P, Furniss RCD, Fecht S, Leung RCY, Spiga L, Mavridou DAI, et al. A novel stabilization mechanism for the type VI secretion system sheath. Proc Natl Acad Sci. 2021;118(7):1–9.

509. Dix SR, Owen HJ, Sun R, Ahmad A, Shastri S, Spiewak HL, et al. Structural insights into the function of type VI secretion system TssA subunits. Nat Commun [Internet]. 2018;9(1):1–16. Available from: http://www.nature.com/articles/s41467-018-07247-1

510. Santin YG, Doan T, Lebrun R, Espinosa L, Journet L, Cascales E. In vivo TssA proximity labelling during type VI secretion biogenesis reveals TagA as a protein that stops and holds the sheath. Nat Microbiol [Internet]. 2018;3:1304–13. Available from: http://www.nature.com/articles/s41564-018-0234-3

511. Shrivastava S, Mande SS. Identification and functional characterization of gene components of type VI secretion system in bacterial genomes. PLoS One. 2008;3(8).

512. Stietz MS, Liang X, Li H, Zhang X, Dong TG. TssA-TssM-TagA interaction modulates type VI secretion system sheath-tube assembly in *Vibrio cholerae*. Nat Commun [Internet]. 2020;11(5065):1–11. Available from: http://dx.doi.org/10.1038/s41467-020-18807-9

513. Lin L, Capozzoli R, Ferrand A, Plum M, Vettiger A, Basler M. Subcellular localization of Type VI secretion system assembly in response to cell–cell contact. EMBO J. 2022;41(13):1–18.

514. Lossi NS, Manoli E, Simpson P, Jones C, Hui K, Dajani R, et al. The archetype *Pseudomonas aeruginosa* proteins TssB and TagJ form a novel subcomplex in the bacterial type VI secretion system. Mol Microbiol. 2012;86(2):437–56.

515. Förster A, Planamente S, Manoli E, Lossi NS, Freemont PS, Filloux A. Coevolution of the ATPase ClpV, the sheath proteins TssB and TssC, and the accessory protein TagJ/HsiE1 distinguishes type VI secretion classes. J Biol Chem. 2014;289(47):33032–43.

516. Karimova G, Pidoux J, Ullmann A, Ladant D. A bacterial two-hybrid system based on a reconstituted signal transduction pathway. Proc Natl Acad Sci [Internet]. 1998;95(10):5752–6. Available from: http://www.pnas.org/cgi/doi/10.1073/pnas.95.10.5752

517. Herrero M, de Lorenzo V, Timmis KN. Transposon vectors containing non-antibiotic resistance selection markers for cloning and stable chromosomal insertion of foreign genes in gram-negative bacteria. J Bacteriol. 1990 Nov;172(11):6557–67.

518. Figurski DH, Helinski DR. Replication of an origin-containing derivative of plasmid RK2 dependent on a plasmid function provided in trans. Proc Natl Acad Sci U S A. 1979 Apr;76(4):1648–52.

519. Kaniga K, Delor I, Cornelis GR. A wide-host-range suicide vector for improving reverse genetics in gram-negative bacteria: inactivation of the *blaA* gene of Yersinia enterocolitica. Gene. 1991 Dec;109(1):137–41.

520. Kovach ME, Elzer PH, Hill DS, Robertson GT, Farris MA, Roop RM, et al. Four new derivatives of the broad-host-range cloning vector pBBR1MCS, carrying different antibiotic-resistance

cassettes. Gene [Internet]. 1995;166(1):175–6. Available from: http://www-ab.informatik.uni-tuebingen.de/toolbox/index.php?view=domainpred

521. Fürste JP, Pansegrau W, Frank R, Blöcker H, Scholz P, Bagdasarian M, et al. Molecular cloning of the plasmid RP4 primase region in a multi-host-range tacP expression vector. Gene. 1986;48(1):119–31.

522. Heeb S, Blumer C, Haas D. Regulatory RNA as mediator in GacA/RsmA-dependent global control of exoproduct formation in *Pseudomonas fluorescens* CHA0. J Bacteriol. 2002;184(4):1046–56.

523. Hachani A, Lossi NS, Hamilton A, Jones C, Bleves S, Albesa-Jové D, et al. Type VI secretion system in *Pseudomonas aeruginosa*: secretion and multimerisation of VgrG proteins. J Biol Chem. 2011;286:12317–27.

524. Jones C, Hachani A, Manoli E, Filloux A. An rhs gene linked to the second type VI secretion cluster is a feature of the *Pseudomonas aeruginosa* strain PA14. J Bacteriol. 2014;196(4):800–10.

525. Cox J, Mann M. MaxQuant enables high peptide identification rates, individualized p.p.b.-range mass accuracies and proteome-wide protein quantification. Nat Biotechnol. 2008 Dec;26(12):1367–72.

526. Tyanova S, Temu T, Sinitcyn P, Carlson A, Hein MY, Geiger T, et al. The Perseus computational platform for comprehensive analysis of (prote)omics data. Nat Methods. 2016;13(9):731–40.

527. Winsor GL, Griffiths EJ, Lo R, Dhillon BK, Shay JA, Brinkman FSL. Enhanced annotations and features for comparing thousands of *Pseudomonas*genomes in the *Pseudomonas* genome database. Nucleic Acids Res. 2016;44(D1):D646–53.

528. Needleman SB, Wunsch CD. A general method applicable to the search for similarities in the amino acid sequence of two proteins. J Mol Biol. 1970;48(3):443–53.

529. Sievers F, Wilm A, Dineen D, Gibson TJ, Karplus K, Li W, et al. Fast, scalable generation of high-quality protein multiple sequence alignments using Clustal Omega. Mol Syst Biol. 2011;7(539).

530. Krogh A, Larsson B, Von Heijne G, Sonnhammer ELL. Predicting transmembrane protein topology with a hidden Markov model: Application to complete genomes. J Mol Biol. 2001;305(3):567–80.

531. Schindelin J, Arganda-Carreras I, Frise E, Kaynig V, Longair M, Pietzsch T, et al. Fiji: An open-source platform for biological-image analysis. Nat Methods. 2012;9(7):676–82.

532. Song Y, DiMaio F, Wang RY-R, Kim D, Miles C, Brunette T, et al. High-resolution comparative modeling with RosettaCM. Structure. 2013 Oct;21(10):1735–42.

533. Waterhouse A, Bertoni M, Bienert S, Studer G, Tauriello G, Gumienny R, et al. SWISS-MODEL: homology modelling of protein structures and complexes. Nucleic Acids Res. 2018 Jul;46(W1):W296–303.

534. Fraczkiewicz R, Braun W. Exact and efficient analytical calculation of the accessible surface areas and their gradients for macromolecules. J Comput Chem. 1998;19(3):319–33.

535. Pierce BG, Wiehe K, Hwang H, Kim B-H, Vreven T, Weng Z. ZDOCK server: interactive docking prediction of protein-protein complexes and symmetric multimers. Bioinformatics. 2014 Jun;30(12):1771–3.

536. Holm L. Using Dali for Protein Structure Comparison. Methods Mol Biol. 2020;2112:29–42.

537. Szwedziak P, Pilhofer M. Bidirectional contraction of a type six secretion system. Nat Commun [Internet]. 2019;10(1565). Available from: http://dx.doi.org/10.1038/s41467-019-09603-1

538. Lin L, Lezan E, Schmidt A. Abundance of bacterial Type VI secretion system components measured by targeted proteomics. Nat Commun [Internet]. 2019;10. Available from: http://dx.doi.org/10.1038/s41467-019-10466-9

539. Romero M, Silistre H, Lovelock L, Wright VJ, Chan K, Hong K, et al. Genome-wide mapping of the RNA targets of the *Pseudomonas aeruginosa* riboregulatory protein RsmN. Nucleic Acids Res. 2018;46(13):25–8.

540. Chihara K, Barquist L, Takasugi K, Noda N, Tsuneda S. Global identification of RsmA/N binding sites in *Pseudomonas aeruginosa* by in vivo UV CLIP-seq. RNA Biol [Internet]. 2021;18(12):2401–16. Available from: https://doi.org/10.1080/15476286.2021.1917184

541. Marden JN, Diaz MR, Walton WG, Gode CJ, Betts L, Urbanowski ML, et al. An unusual CsrA family member operates in series with RsmA to amplify posttranscriptional responses in *Pseudomonas aeruginosa*. Proc Natl Acad Sci. 2013;110(37):15055–60.

542. Schulmeyer KH, Diaz MR, Bair TB, Sanders W, Gode CJ, Laederach A, et al. Primary and secondary sequence structure requirements for recognition and discrimination of target RNAs by *Pseudomonas aeruginosa* RsmA and RsmF. J Bacteriol. 2016;198(18):2458–69.

543. Smith S, Salvato F, Garikipati A, Kleiner M, Septer AN. Activation of the type VI secretion system in the squid symbiont *Vibrio fischeri* requires the transcriptional regulator TasR and the structural proteins TssM and TssA. J Bacteriol. 2021;203(21).

544. Jiang F, Waterfield NR, Yang J, Yang G, Jin Q. A *Pseudomonas aeruginosa* Type VI Secretion Phospholipase D Effector Targets Both Prokaryotic and Eukaryotic Cells. Cell Host Microbe [Internet]. 2014;15(5):600–10. Available from: http://dx.doi.org/10.1016/j.chom.2014.04.010

545. Aubert DF, Xu H, Yang J, Chen S, Valvano MA, Shao F, et al. A Burkholderia Type VI Effector Deamidates Rho GTPases to Activate the Pyrin Inflammasome and Trigger Inflammation. Cell Host Microbe [Internet]. 2016;19(5):664–74. Available from: http://dx.doi.org/10.1016/j.chom.2016.04.004

546. Chen W-J, Kuo T-Y, Hsieh F-C, Chen P-Y, Wang C-S, Shih Y-L, et al. Involvement of type VI secretion system in secretion of iron chelator pyoverdine in *Pseudomonas taiwanensis*. Sci Rep. 2016;

547. Allsopp LP, Bernal P, Nolan LM, Filloux A. Causalities of war: The connection between type VI secretion system and microbiota. Cell Microbiol. 2019;22(3):1–9.

548. Schell MA, Ulrich RL, Ribot WJ, Brueggemann EE, Hines HB, Chen D, et al. Type VI secretion is a major virulence determinant in *Burkholderia mallei*. Mol Microbiol. 2007 Jun;64(6):1466–85.

549. Moscoso JA, Mikkelsen H, Heeb S, Williams P, Filloux A. The *Pseudomonas aeruginosa* sensor RetS switches type III and type VI secretion via c-di-GMP signalling. Environ Microbiol. 2011 Dec;13(12):3128–38.

550. Brencic A, McFarland KA, McManus HR, Castang S, Mogno I, Dove SL, et al. The GacS/GacA signal transduction system of *Pseudomonas aeruginosa* acts exclusively through its control over the transcription of the RsmY and RsmZ regulatory small RNAs. Mol Microbiol.

2009;73:434–45.

551. Morris ER, Hall G, Li C, Heeb S, Kulkarni R V., Lovelock L, et al. Structural rearrangement in an RsmA/CsrA Ortholog of *Pseudomonas aeruginosa* creates a dimeric RNA-binding protein, RsmN. Structure. 2013;21(9):1659–71.

552. Reimmann C, Valverde C, Kay E, Haas D. Posttranscriptional repression of GacS/GacA-controlled genes by the RNA-binding protein RsmE acting together with RsmA in the biocontrol strain *Pseudomonas fluorescens* CHA0. J Bacteriol. 2005;187(1):276–85.

553. Pusic P, Sonnleitner E, Bläsi U. Specific and global RNA regulators in *Pseudomonas aeruginosa*. Int J Mol Sci. 2021;22(16).

554. O'Callaghan J, Reen FJ, Adams C, O'Gara F. Low oxygen induces the type III secretion system in *Pseudomonas aeruginosa* via modulation of the small RNAs rsmZ and rsmY. Microbiology. 2011;157(12):3417–28.

555. Chakravarty S, Melton CN, Bailin A, Yahr TL, Anderson GG. *Pseudomonas aeruginosa* magnesium transporter MgtE inhibits type III secretion system gene expression by stimulating rsmYZ transcription. J Bacteriol. 2017;199(23):1–11.

556. Sonnleitner E, Schuster M, Sorger-Domenigg T, Greenberg EP, Bläsi U. Hfq-dependent alterations of the transcriptome profile and effects on quorum sensing in *Pseudomonas aeruginosa*. Mol Microbiol. 2006 Mar;59(5):1542–58.

557. Petrova OE, Sauer K. The novel two-component regulatory system BfiSR regulates biofilm development by controlling the small RNA rsmZ through CafA. J Bacteriol. 2010;192(20):5275–88.

558. Miller CL, Romero M, Karna SLR, Chen T, Heeb S, Leung KP. RsmW, *Pseudomonas aeruginosa* small non-coding RsmA-binding RNA upregulated in biofilm versus planktonic growth conditions. BMC Microbiol [Internet]. 2016;16(1):1–16. Available from: http://dx.doi.org/10.1186/s12866-016-0771-y

559. Janssen KH, Diaz MR, Gode CJ, Wolfgang MC, Yahr TL. RsmV, a Small Noncoding Regulatory RNA in *Pseudomonas aeruginosa* That Sequesters RsmA and RsmF from Target mRNAs. J Bacteriol. 2018;200(16):1–13.

560. Janssen KH, Diaz MR, Golden M, Graham JW, Sanders W, Wolfgang MC, et al. Functional analyses of the RsmY and RsmZ small noncoding regulatory RNAs in *Pseudomonas aeruginosa*. J Bacteriol. 2018;200(11):1–15.

561. Schubert M, Lapouge K, Duss O, Oberstrass FC, Jelesarov I, Haas D, et al. Molecular basis of messenger RNA recognition by the specific bacterial repressing clamp RsmA/CsrA. Nat Struct Mol Biol. 2007;14(9):807–13.

562. Rife C, Schwarzenbacher R, McMullan D, Abdubek P, Ambing E, Axelrod H, et al. Crystal structure of the global regulatory protein CsrA from *Pseudomonas putida* at 2.05 Å resolution reveals a new fold. Proteins Struct Funct Genet. 2005;61(2):449–53.

563. Gutiérrez P, Li Y, Osborne MJ, Pomerantseva E, Liu Q, Gehring K. Solution structure of the carbon storage regulator protein CsrA from *Escherichia coli*. J Bacteriol. 2005;187(10):3496–501.

564. Heeb S, Kuehne SA, Bycroft M, Crivii S, Allen MD, Haas D, et al. Functional analysis of the post-transcriptional regulator RsmA reveals a novel RNA-binding site. J Mol Biol. 2006;355(5):1026–36.

565. Dubey AK, Baker CS, Romeo T, Babitzke P. RNA sequence and secondary structure participate in high-affinity CsrA-RNA interaction. RNA. 2005;11(10):1579–87.

566. Lapouge K, Perozzo R, Iwaszkiewicz J, Bertelli C, Zoete V, Michielin O, et al. RNA pentaloop structures as effective targets of regulators belonging to the RsmA/CsrA protein family. RNA Biol. 2013;10(6):1030–41.

567. Valverde C, Lindell M, Wagner EGH, Haas D. A repeated GGA motif is critical for the activity and stability of the riboregulator RsmY of *Pseudomonas fluorescens*. J Biol Chem [Internet]. 2004;279(24):25066–74. Available from: http://dx.doi.org/10.1074/jbc.M401870200

568. Dubey AK, Baker CS, Suzuki K, Jones AD, Pandit P, Romeo T, et al. CsrA regulates translation of the *Escherichia coli* carbon starvation gene, cstA, by blocking ribosome access to the cstA transcript. J Bacteriol. 2003;185(15):4450–60.

569. Yakhnin H, Baker CS, Berezin I, Evangelista MA, Rassin A, Romeo T, et al. CsrA Represses Translation of *sdiA*, Which Encodes the N-acylhomoserine-L-lactone receptor of *Escherichia coli,* by Binding exclusively within the coding region of *sdiA* mRNA. J Bacteriol. 2011;193(22):6162–70.

570. Basler M, Pilhofer M, Henderson GP, Jensen GJ, Mekalanos JJ. Type VI secretion requires a dynamic contractile phage tail-like structure. Nature. 2012;7388(483):182-186.

571. Ullmann A, Danchin A. Role of cyclic AMP in regulatory mechanisms in bacteria. Trends Biochem Sci. 1980;5(4):95–6.

572. Hanson PI, Whiteheart SW. AAA+ proteins: Have engine, will work. Nat Rev Mol Cell Biol. 2005;6(7):519–29.

573. Schaefer J, Jovanovic G, Kotta-Loizou I, Buck M. Single-step method for beta-galactosidase assays in *Escherichia coli* using a 96-well microplate reader. Anal Biochem. 2016 Jun;503:56–7.

574. Noreen Z, Jobichen C, Abbasi R, Seetharaman J, Sivaraman J, Bokhari H. Structural basis for the pathogenesis of *Campylobacter jejuni* Hcp1, a structural and effector protein of the Type VI Secretion System. FEBS J. 2018;285(21):4060–70.

575. Osipuik J, Xu X, Hong C, Savchenko A, Edwards A, Joachimiak A. Crystal structure of secretory protein Hcp3 from *Pseudomonas aeruginosa*. J Struct Fucntional Genomics. 2011;12(1):759–85.

576. Jobichen C, Chakraborty S, Li M, Zheng J, Joseph L, Mok YK, et al. Structural basis for the secretion of *evpC*: A key type vi secretion system protein from *Edwardsiella tarda*. PLoS One. 2010;5(9):1–10.

577. Lim YT, Jobichen C, Wong J, Limmathurotsakul D, Li S, Chen Y, et al. Extended loop region of Hcp1 is critical for the assembly and function of type VI secretion system in *Burkholderia pseudomallei*. Sci Rep. 2015;5:1–10.

578. Ruiz FM, Santillana E, Spínola-Amilibia M, Torreira E, Culebras E, Romero A. Crystal structure of Hcp from *Acinetobacter baumannii*: A component of the type VI secretion system. PLoS One. 2015;10(6):1–16.

579. Salih O, He S, Planamente S, Stach L, MacDonald JT, Manoli E, et al. Atomic Structure of Type VI Contractile Sheath from *Pseudomonas aeruginosa*. Structure [Internet]. 2018;26(2):329-336.e3. Available from: https://doi.org/10.1016/j.str.2017.12.005

580. Clemens DL, Ge P, Lee B, Horwitz MA, Hong Z. Atomic Structure and Mutagenesis of T6SS

Reveals Interlaced Array Essential to Function. Cell. 2015;160(5):940–51.

581. Goodsell DS, Olson AJ. Structural symmetry and protein function. Annu Rev Biophys Biomol Struct. 2000;29:105–53.

582. Hendrix RW. Symmetry mismatch and DNA packaging in large bacteriophages. Biochemistry. 1978;75(10):4779–83.

583. Johnson JE, Chiu W. DNA packaging and delivery machines in tailed bacteriophages. Curr Opin Struct Biol. 2007;17(2):237–43.

584. Simpson AA, Tao Y, Leiman PG. Structure of the bacteriophage φ29 DNA packaging motor. Nature. 2000;408(December):745–50.

585. Durie CL, Sheedlo MJ, Chung JM, Byrne BG, Su M, Knight T, et al. Structural analysis of the *Legionella pneumophila* Dot/Icm type IV secretion system core complex. Elife. 2020;9:1–23.

586. Amin H, Ilangovan A, Costa TRD. Architecture of the outer-membrane core complex from a conjugative type IV secretion system. Nat Commun. 2021;12(1):1–12.

587. Cho SY, Song WS, Yoon S il. Crystal structure of the flagellar cap protein FliD from *Bdellovibrio bacteriovorus*. Biochem Biophys Res Commun [Internet]. 2019;519(3):652–8. Available from: https://doi.org/10.1016/j.bbrc.2019.09.024

588. Cho SY, Song WS, Hong HJ, Lee GS, Kang SG, Ko HJ, et al. Tetrameric structure of the flagellar cap protein FliD from *Serratia marcescens*. Biochem Biophys Res Commun [Internet]. 2017;489(1):63–9. Available from: http://dx.doi.org/10.1016/j.bbrc.2017.05.093

589. Postel S, Deredge D, Bonsor DA, Yu X, Diederichs K, Helmsing S, et al. Bacterial flagellar capping proteins adopt diverse oligomeric states. Elife. 2016;5:1–20.

590. Ikeda T, Asakura S, Kamiya R. “Cap” on the tip of *Salmonella* flagella. J Mol Biol [Internet]. 1985;184:735–7. Available from: http://www.sciencedirect.com/science/article/pii/0022283685903171

591. Ikeda T, Yamaguchi S, Hotani H. Flagellar growth in a filament-less *Salmonella fliD* mutant supplemented with purified hook-associated protein 2. J Biochem. 1993;114(1):39–44.

592. Yonekura K, Maki-Yonekura S, Namba K. Complete atomic model of the bacterial flagellar filament by electron cryomicroscopy. Nature. 2003;424(6949):643–50.

593. Inaba S, Hashimoto M, Jyot J, Aizawa SI. Exchangeability of the flagellin (FliC) and the cap protein (FliD) among different species in flagellar assembly. Biopolymers. 2013;99(1):63–72.

594. Aksyuk AA, Leiman PG, Shneider MM, Mesyanzhinov V V., Rossmann MG. The Structure of Gene Product 6 the Hinge-Pin of the Baseplate. Struct Des [Internet]. 2009;17(6):800–8. Available from: http://dx.doi.org/10.1016/j.str.2009.04.005

595. Madeira F, Pearce M, Tivey ARN, Basutkar P, Lee J, Edbali O, et al. Search and sequence analysis tools services from EMBL-EBI in 2022. Nucleic Acids Res [Internet]. 2022 Apr;gkac240. Available from: https://doi.org/10.1093/nar/gkac240

596. Salih O, He S, Planamente S, Stach L, MacDonald JT, Manoli E, et al. Atomic Structure of Type VI Contractile Sheath from *Pseudomonas aeruginosa*. Structure. 2018 Feb;26(2):329-336.e3.

597. Al-Otaibi NS, Taylor AJ, Farrell DP, Tzokov SB, DiMaio F, Kelly DJ, et al. The cryo-EM structure of the bacterial flagellum cap complex suggests a molecular mechanism for filament elongation. Nat Commun. 2020;11(1):1-11.

598. Leiman PG, Arisaka F, Raaij MJ Van, Kostyuchenko VA, Aksyuk AA, Kanamaru S, et al. Morphogenesis of the T4 tail and tail fibers. Virol J. 2010;7(355):1–28.

599. Brodmann M, Dreier RF, Broz P, Basler M. Francisella requires dynamic type VI secretion system and ClpB to deliver effectors for phagosomal escape. Nat Commun [Internet]. 2017;8(May):1–12. Available from: http://dx.doi.org/10.1038/ncomms15853

600. Schwarz S, Singh P, Robertson JD, LeRoux M, Skerrett SJ, Goodlett DR, et al. VgrG-5 is a Burkholderia type VI secretion system-exported protein required for multinucleated giant cell formation and virulence. Infect Immun. 2014 Apr;82(4):1445–52.

601. Shneider MM, Buth SA, Ho BT, Basler M, Mekalanos JJ, Leiman PG. PAAR-repeat proteins sharpen and diversify the type VI secretion system spike. Nature. 2013;500:350–3.

602. Liang X, Moore R, Wilton M, Wong MJQ, Lam L, Dong TG. Identification of divergent type VI secretion effectors using a conserved chaperone domain. Proc Natl Acad Sci U S A. 2015;112(29):9106–11.

603. Unterweger D, Kostiuk B, Ötjengerdes R, Wilton A, Diaz-Satizabal L, Pukatzki S. Chimeric adaptor proteins translocate diverse type VI secretion system effectors in Vibrio cholerae. EMBO J. 2015;34(16):2198–210.

604. Kostyuchenko VA, Leiman PG, Chipman PR, Kanamaru S, Van Raaij MJ, Arisaka F, et al. Three-dimensional structure of bacteriophage T4 baseplate. Nat Struct Biol. 2003;10(9):688–93.

605. Jumper J, Evans R, Pritzel A, Green T, Figurnov M, Ronneberger O, et al. Highly accurate protein structure prediction with AlphaFold. Nature [Internet]. 2021;596(7873):583–9. Available from: http://dx.doi.org/10.1038/s41586-021-03819-2

8. Appendices

Appendix I: Pulldown data

Data from pulldown experiments using the following bait proteins: TssA2, TssA3 and PA2373. Two pulldown experiments were carried out for each bait using different conditions for sample growth, either growth in liquid culture at 37 °C or growth on solid media at either 25 °C for TssA2 or 30 °C for TssA3 or PA2372. Hits are ordered by the fold change between the FLAG-tagged protein of interest and the untagged protein of interest. Significance is -log(p-value), where a value greater than 1.3 equals a p-value of < 0.05. Description is based on the Pseudomonas genome database description for each protein. Data presented are those with a fold change above 1.5 and a significance of above 1.3.

Table 8.1 TssA2 pulldown 1: 37 °C liquid culture

Gene	Gene ID	Fold change	Significance	Description
purU1	PA4314	5.97	4.55	formyltetrahydrofolate deformylase
tssA2	PA1656	4.85	3.21	TssA2
fabF1	PA2965	3.96	1.64	beta-ketoacyl-acyl carrier protein synthase II
glpE	PA0589	3.63	2.26	Conserved hypothetical protein
	PA5250	3.59	3.37	Conserved hypothetical protein
pheT	PA2739	3.48	1.51	phenylalanyl-tRNA synthetase, beta subunit
nfuA	PA1847	3.42	2.65	Fe/S biogenesis protein NfuA
pilR	PA4547	3.29	1.45	two-component response regulator PilR
fadD1	PA3299	3.27	3.93	Long-chain-fatty-acid--CoA ligase
atoB	PA2001	3.09	1.63	acetyl-CoS acetyletransferase
yvaG	PA1344	3.06	1.95	probable short-chain dehydrogenase
oxyR	PA5344	2.65	2.70	OxyR
dctD	PA5166	2.63	2.58	DctD
pauD2	PA1742	2.60	1.33	glutamine amidotransferase class I
hcpABC	PA1512 PA0263 PA5267	2.53	1.80	Hcp2
hxrA	PA5210	2.46	1.80	probable secretion pathway ATPase
ydfG	PA4907	2.33	1.82	probable short-chain dehydrogenase
hslV	PA5053	2.31	1.40	heat shock protein HslV
	PA0284	2.28	1.34	hypothetical protein
	PA3727	2.26	1.61	hypothetical protein
phzM	PA4209	2.17	1.42	probable phenazine-specific methyltransferase
	PA4338	2.17	1.42	hypothetical protein

	PA1203	2.14	3.03	hypothetical protein
tssB2	PA1657	2.09	1.89	TssB2
	PA0126	2.04	1.63	hypothetical protein
tagQ1	PA0070	2.04	1.40	TagQ1
gntK	PA2321	2.03	1.78	GntK
tssC2	PA1658	1.96	4.68	TssC2
prpB	PA0796	1.88	2.49	carboxyphosphoenolpyruvate phoshponomutase
lpd	PA1587	1.85	2.19	dihydrolipoamide dehydrogenase Lpd
pqsD	PA0999	1.82	2.49	3-oxoacyl-[acyl-carrier-protein] synthase III

Table 8.2 TssA2 pulldown 2: 25 °C solid media

Gene	Gene ID	Fold change	Significance	Description
tolB	PA0972	6.54	4.48	TolB
fhp	PA2664	4.95	4.38	flavohemoprotein
dnaK	PA4761	1.93	4.09	DnaK
tssA2	PA1656	6.36	3.89	TssA2
tpx	PA2532	1.83	3.05	Thiol peroxidase
algR	PA5261	3.10	2.49	alginate biosynthesis regulatory protein AlgR
soxA	PA5418	1.70	2.14	sarcosine oxidase alpha subunit
ftsA	PA4408	1.67	1.99	cell division protein FtsA
	PA3440	1.81	1.89	conserved hypothetical protein
	PA1036	2.80	1.78	hypothetical protein
rpoD	PA0576	1.73	1.50	sigma factor RpoD
	PA2915	1.88	1.48	hypothetical protein
uup	PA3019	3.53	1.47	probable ATP-binding component of ABC transporter
hcpABC	PA1512, PA0263, PA5267	2.44	1.42	Hcp2 (HcpA/B/C)
nfuA	PA1847	2.35	1.37	NfuA
obg	PA4566	2.18	1.34	GTP-binding protein Obg
folP	PA4750	3.08	1.31	dihydropteroate synthase

Table 8.3 TssA3 pulldown 1: 37 °C liquid culture

Gene	Gene ID	Fold change	Significance	Description
tssA3	PA2360	8.87	2.44	TssA3
	PA3716	5.61	2.87	hypothetical protein
	PA3262	5.38	3.36	probable peptidyl-prolyl cis-trans isomerase FkbP-type
atpF	PA5588	4.68	1.88	ATP synthase B chain

	PA0126	4.23	4.04	hypothetical protein
dadA	PA5304	4.21	1.52	D-amino acid dehydrogenase, small subunit
tagQ1	PA0070	4.20	2.96	TagQ1
clpV2	PA1662	3.75	2.61	ClpV2
	PA3800	3.63	3.15	conserved hypothetical protein
	PA2823	3.22	5.04	conserved hypothetical protein
grpE	PA4762	3.22	4.73	heat shock protein GrpE
fad1	PA3299	3.22	1.39	long-chain-fatty-acid--CoS ligase
ppiD	PA1805	3.18	1.79	peptidyl-prolyl cis-trans isomerase D
psfA	PA0473	2.99	2.12	probable glutathione S-transferase
dnaK	PA4761	2.99	5.01	DnaK
	PA4636	2.94	3.70	hypothetical protein
mqoA	PA3452	2.87	2.23	malate:quinone oxidoreductase
	PA1011	2.85	2.64	hypothetical protein
clpV1	PA0090	2.84	2.52	ClpV1
	PA3710	2.79	2.42	probable GMC-type oxidoreductase
lsfA	PA3450	2.77	1.34	1-Cys peroxiredoxin LsfA
mltA	PA1222	2.66	2.54	probable membrane-bound lytic murein transglycosylase
asrA	PA0779	2.66	4.11	AsrA
	PA1324	2.64	1.55	hypothetical protein
	PA5113	2.55	1.88	hypothetical protein
ibpA	PA3126	2.48	1.91	heat-shock protein ibpA
oprI	PA2853	2.44	2.12	outer membrane lipoprotein OprI precursor
dnaJ	PA4760	2.27	4.47	DnaJ
	PA2793	2.19	3.49	hypothetical protein
	PA3804	2.19	2.18	hypothetical protein
	PA1064	2.10	2.69	hypothetical protein
magD	PA4489	2.10	2.80	MagD
	PA3691	2.08	2.93	hypothetical protein
	PA5414	2.05	3.18	hypothetical protein
htpG	PA1596	2.01	3.68	Heat shock protein HtpG
triB	PA0157	1.99	2.75	Resistance-Nodulation-Cell Division (RND) triclosan efflux membrane fusion protein, TriB
yfgM	PA3801	1.78	1.35	conserved hypothetical protein
	PA4131	1.76	2.19	probable iron-sulfur protein
mrp	PA3481	1.75	2.21	conserved hypothetical protein
clpB	PA4542	1.73	2.50	ClpB
pgk	PA0552	1.69	1.53	phosphoglycerate kinase
	PA5502	1.63	1.32	hypothetical protein
	PA4441	1.62	3.31	hypothetical protein

	PA3729	1.60	1.88	conserved hypothetical protein
tolB	PA0972	1.54	1.71	TolB

Table 8.4 TssA3 pulldown 2: 30 °C solid media

Gene	Gene ID	Fold change	Significance	Description
tssA3	PA2360	15.93	3.04	TssA3
	PA5441	5.28	1.64	hypothetical protein
	PA3262	3.21	1.73	probable peptidyl-prolyl cis-trans isomerase, FkbP-type
	PA2953	3.10	2.83	electron transfer flavoprotein-ubiquinone oxidoreductase
	PA3674	3.03	1.34	hypothetical protein
	PA2920	2.83	1.75	probable chemotaxis transducer
	PA4441	2.62	2.32	hypothetical protein
ppiD	PA1805	2.61	1.71	peptidyl-prolyl cis-trans isomerase D
icmP	PA4370	2.34	2.33	Insulin-cleaving metalloproteinase outer membrane protein precursor
	PA0126	2.33	1.46	hypothetical protein
oprI	PA2853	2.29	3.46	Outer membrane lipoprotein OprI precursor
mexA	PA0425	2.22	1.62	Resistance-Nodulation-Cell Division (RND) multidrug efflux membrane fusion protein MexA precursor
dadA	PA5304	2.19	2.39	D-amino acid dehydrogenase, small subunit
	PA3710	2.17	2.99	probable GMC-type oxidoreductase
clpV2	PA1662	2.08	2.00	ClpV2
gcp	PA0580	2.03	1.38	O-sialoglycoprotein endopeptidase
mexX	PA2019	2.01	1.96	Resistance-Nodulation-Cell Division (RND) multidrug efflux membrane fusion protein MexX precursor
synonym: yqjD	PA3040	1.94	1.69	conserved hypothetical protein
nuoD	PA2639	1.88	3.71	NADH dehydrogenase I chain C,D
atpF	PA5558	1.82	2.07	ATP synthase B chain
	PA3691	1.78	1.64	hypothetical protein
	PA3031	1.74	1.32	hypothetical protein
recA	PA3617	1.68	3.91	RecA
tagQ1	PA0070	1.65	1.60	TagQ1
dnaK	PA4761	1.61	3.13	DnaK
yraM	PA4423	1.55	2.37	conserved hypothetical protein
phoU	PA5365	1.52	1.36	phosphate uptake regulatory protein PhoU
	PA2725	1.52	1.46	probable chaperone

Table 8.5 PA2372 pull down 1: 37 °C liquid culture

Gene	Gene ID	Fold change	Significance	Description
	PA2372	10.59	2.07	hypothetical protein
glyA3	PA4602	9.60	4.33	serine hydroxymethyltransferase
	PA0739	7.96	4.24	probable transcriptional regulator
lis/lipA	PA3996	7.87	3.65	lipoate synthase
thiC	PA4973	6.57	3.88	thiamin biosynthesis protein ThiC
	PA0178	5.42	3.59	probable two-component sensor
	PA0290	5.39	3.34	putative diguanylate cyclase
algQ	PA5255	5.05	2.37	alginate regulatory protein, AlgQ
glmS	PA5549	4.80	3.80	glucosamine--fructose-6-phosphatase aminotransferase
cgrC	PA2126	4.66	2.56	cupA gene regulator C, cgrC
phnA	PA1001	4.46	1.50	anthranilate synthase component I
tsi7	PA0100	4.25	3.48	hypothetical protein
	PA3243	4.24	3.44	cell division inhibitor MinC
clpV2	PA1662	4.06	2.70	ClpV2
pqsA	PA0996	3.92	2.63	PqsA
fruI	PA3562	3.91	5.40	phosphotransferase system transporter enzyme I, FruI
bkdA2	PA2248	3.85	2.26	2-oxoisovalerate dehydrogense (beta subunit)
	PA4803	3.85	3.70	hypothetical protein
glpE	PA0589	3.83	1.36	conserved hypothetical protein
nuoB	PA2638	3.81	2.65	NADH dehydrogenase I chain B
	PA5294	3.33	3.12	putative multidrug efflux pump
	PA2823	3.30	3.15	conserved hypothetical protein
hisH2	PA3152	3.18	3.71	glutamine amidotransferase
ibpA	PA3126	3.17	2.54	heat-shock protein IbpA
nuoD	PA2639	2.97	1.60	NADH dehydrogenase I chain C,D
yhbL	PA5245	2.97	2.36	conserved hypothetical protein
vgrG2b	PA0262	2.93	1.53	VgrG2b
fdnH	PA4811	2.91	2.93	nitrate-inducible formate dehydrogenase, beta subunit

wbpD	PA3156	2.91	2.83	UDP-2-acetoamido3-amino-2,3-dideoxy-d-glucuronic acid N-acetyltransferase, WbpD
ylaK	PA3919	2.80	2.22	conserved hypothetical protein
ahpB	PA0848	2.75	1.59	alkyl hydroperoxide reducatse, AhpB
lytB	PA4557	2.73	2.56	LytB protein
gltR	PA3192	2.65	1.46	two-component response regulator GltR
kynA	PA2579	2.62	1.84	L-tryptophan:oxygen 2,3-oxidoreducatse (decyclizing) KynA
purF	PA3108	2.55	1.79	amidophosphoribosyltransferase
pyrG	PA3637	2.51	2.67	CTP synthase
nfuA	PA1847	2.45	1.37	NfuA
	PA1880	2.45	1.42	probable oxidoreductase
truB	PA4742	2.38	1.41	tRNA pseudouridine 55 synthase
dnaB	PA4931	2.37	1.48	replicative DNA helicase
yegQ	PA5440	2.33	1.35	probable peptidase
glmM	PA4749	2.29	1.57	phosphoglucosamine mutase
yqjM	PA3723	2.27	3.97	probable FMN oxidoreductase
def	PA0019	2.26	2.87	polypeptide deformylase
nrdJa	PA5497	2.22	2.36	class II (cobalamin-dependent) ribonucleotide-diphosphate reducatse subunit, NrdJa
	PA1752	2.20	2.96	hypothetical protein
nrdJb	PA5496	2.17	1.88	class II (cobalamin-dependent) ribonucleotide-diphosphate reducatse subunit, NrdJb
	PA1372	2.15	4.81	hypothetical protein
hisF	PA5140	2.11	2.18	imidazoleglycerol-phosphate synthase, cyclase subunit
hsiB3	PA2365	2.08	1.58	TssB3
murA	PA4450	2.07	2.97	UDP-N-acetylglucosamine 1-carboxyvinyltransferase
	PA3091	2.07	2.12	hypothetical protein
trmU	PA2626	2.07	1.51	tRNA methyltransferase
hemN	PA1546	1.98	2.94	oxygen-independentco-proporphyrinogen III oxidase
	PA3613	1.94	2.61	hypothetical protein
phzM	PA4209	1.91	1.98	probable phenazine-specific methyltransferase
pprB	PA4296	1.85	3.23	two-component response regulator, PprB
yadR	PA0665	1.85	1.88	conserved hypothetical protein
lasR	PA1430	1.83	2.23	transcriptional regulator LasR
iscS	PA3814	1.82	2.42	L-cysterin desulfurase (pyridoxal phosphate-dependent)
pchF	PA4225	1.79	2.89	pyochelin synthetase

nuoG	PA2642	1.78	1.68	NADH dehydrogenase I chain G
rhlB	PA3478	1.76	1.70	rhamnosyltransferase chain B
	PA2111	1.72	1.46	hypothetical protein
	PA4130	1.64	3.42	probable sulfite or nitrite reductase
pqsB	PA0997	1.64	3.09	PqsB
tsaA	PA3529	1.62	2.81	alkylhydorperoxide reductase C
ambE	PA2302	1.60	1.89	AmbE
dnaN	PA0002	1.58	1.61	DNA polyermase III, beta chain
minE	PA3245	1.50	2.00	cell division topological specificity factor MinE

Table 8.6 PA2372 pulldown 2: 30 °C solid media

Gene	Gene ID	Fold change	Significance	Description
	PA2373	15.86	4.80	hypothetical protein
glyA3	PA4602	10.95	4.48	serine hydroxymethyltransferase
vgrG2b	PA0262	2.58	3.96	VgrG2b
tsaA	PA3529	1.54	3.72	alkylhydroperoxide reductase C
wrbA	PA0949	1.69	3.23	Trp repressor binding protein WrbA
	PA2823	2.99	3.15	conserved hyothetical protein
atoB	PA2001	1.59	3.14	acetyl-CoA acetyltransferase
metK	PA0546	1.52	3.00	methionine adenosyltransferase
fruI	PA3562	2.61	3.00	phosphotransferase system transporter enzyme I, FruI
	PA0739	8.38	2.99	probable transcriptional regulator
lis	PA3996	4.16	2.76	lipoate synthase
dapB	PA4759	1.94	2.45	dihydrodipicolinate reductase
bkdA2	PA2248	3.71	2.29	2-oxoisovalerate dehydrogenase (beta subunit)
dspI	PA0745	1.59	2.16	DspI
ibpA	PA3126	2.32	1.87	IbpA
sodB	PA4366	2.11	1.78	superoxide dismutase
	PA3417	1.72	1.72	probable pyruvate dehydrogenase E1 component, alpha subunit
ubiG	PA3171	1.61	1.54	3-demethylubiquinone-9 3-methyltransferase
	PA5220	1.67	1.54	hypothetical protein
amiE	PA3366	1.71	1.46	aliphatic amidase
glmS	PA5549	1.63	1.36	glucosamine--fructose-6-phosphate aminotransferase

antC	PA2514	1.96	1.33	anthranilate dioxygenase reductase
metE	PA1927	1.60	1.33	5-methyltetrahydropteroyltriglutamate-homocysteine S-methyltransferase

Appendix II: Published works associated with this thesis

Bernal P, Furniss RCD, Fecht S, Leung RCY, Spiga L, Mavridou DAI, et al. A novel stabilization mechanism for the type VI secretion system sheath. Proc Natl Acad Sci. 2021;118(7):1–9.

8.1 Image Permissions

SPRINGER NATURE LICENSE
TERMS AND CONDITIONS

Aug 03, 2022

This Agreement between Miss. Selina Fecht ("You") and Springer Nature ("Springer Nature") consists of your license details and the terms and conditions provided by Springer Nature and Copyright Clearance Center.

License Number	5361360724596
License date	Aug 03, 2022
Licensed Content Publisher	Springer Nature
Licensed Content Publication	Nature
Licensed Content Title	Priming and polymerization of a bacterial contractile tail structure
Licensed Content Author	Abdelrahim Zoued et al
Licensed Content Date	Feb 24, 2016
Type of Use	Thesis/Dissertation
Requestor type	academic/university or research institute
Format	print and electronic
Portion	figures/tables/illustrations
Number of figures/tables/illustrations	1
High-res required	no
Will you be translating?	no
Circulation/distribution	1 - 29
Author of this Springer Nature content	no
Title	Characterising the role of TssA proteins in the assembly and dynamics of the type VI secretion system

Institution name	Imperial College London
Expected presentation date	Oct 2022
Order reference number	1
Portions	Extended Data Figure 8
Requestor Location	Miss. Selina Fecht Flowers Building Imperial College London London, SW7 2AZ United Kingdom Attn: Miss. Selina Fecht
Total	0.00 GBP

SPRINGER NATURE LICENSE
TERMS AND CONDITIONS

Oct 17, 2022

This Agreement between Miss. Selina Fecht ("You") and Springer Nature ("Springer Nature") consists of your license details and the terms and conditions provided by Springer Nature and Copyright Clearance Center.

License Number	5411411134960
License date	Oct 17, 2022
Licensed Content Publisher	Springer Nature
Licensed Content Publication	Nature Reviews Microbiology
Licensed Content Title	Coordinating assembly of a bacterial macromolecular machine
Licensed Content Author	Fabienne F. V. Chevance et al
Licensed Content Date	Dec 31, 1969
Type of Use	Thesis/Dissertation
Requestor type	academic/university or research institute
Format	print and electronic
Portion	figures/tables/illustrations
Number of figures/tables/illustrations	1
Will you be translating?	no
Circulation/distribution	1 - 29
Author of this Springer Nature content	no
Title	Characterising the role of TssA proteins in the assembly and dynamics of the type VI secretion system
Institution name	Imperial College London
Expected presentation date	Oct 2022

Order reference number	Flagellum
Portions	Figure 2
Requestor Location	Miss. Selina Fecht Flowers Building Imperial College London London, SW7 2AZ United Kingdom Attn: Miss. Selina Fecht
Total	0.00 GBP

SPRINGER NATURE LICENSE
TERMS AND CONDITIONS

Aug 09, 2022

This Agreement between Miss. Selina Fecht ("You") and Springer Nature ("Springer Nature") consists of your license details and the terms and conditions provided by Springer Nature and Copyright Clearance Center.

License Number	5364811049766
License date	Aug 09, 2022
Licensed Content Publisher	Springer Nature
Licensed Content Publication	Nature Microbiology
Licensed Content Title	Structural biology: Baseplates in contractile machines
Licensed Content Author	Alain Filloux et al
Licensed Content Date	Jun 24, 2016
Type of Use	Thesis/Dissertation
Requestor type	academic/university or research institute
Format	print and electronic
Portion	figures/tables/illustrations
Number of figures/tables/illustrations	1
High-res required	no
Will you be translating?	no
Circulation/distribution	1 - 29
Author of this Springer Nature content	no
Title	Characterising the role of TssA proteins in the assembly and dynamics of the type VI secretion system
Institution name	Imperial College London

Expected presentation date	Oct 2022
Order reference number	6
Portions	Figure 1
Requestor Location	Miss. Selina Fecht Flowers Building Imperial College London London, SW7 2AZ United Kingdom Attn: Miss. Selina Fecht
Total	0.00 GBP

ELSEVIER LICENSE
TERMS AND CONDITIONS

Aug 29, 2022

This Agreement between Miss. Selina Fecht ("You") and Elsevier ("Elsevier") consists of your license details and the terms and conditions provided by Elsevier and Copyright Clearance Center.

License Number	5378141203074
License date	Aug 29, 2022
Licensed Content Publisher	Elsevier
Licensed Content Publication	Current Opinion in Microbiology
Licensed Content Title	Lifestyle transitions and adaptive pathogenesis of Pseudomonas aeruginosa
Licensed Content Author	Martina Valentini,Diego Gonzalez,Despoina AI Mavridou,Alain Filloux
Licensed Content Date	Feb 1, 2018
Licensed Content Volume	41
Licensed Content Issue	n/a
Licensed Content Pages	6
Start Page	15
End Page	20
Type of Use	reuse in a thesis/dissertation
Portion	figures/tables/illustrations
Number of figures/tables/illustrations	1
Format	both print and electronic
Are you the author of this Elsevier article?	No
Will you be translating?	No

Title	Characterising the role of TssA proteins in the assembly and dynamics of the type VI secretion system
Institution name	Imperial College London
Expected presentation date	Oct 2022
Order reference number	5
Portions	Figure 1
Requestor Location	Miss. Selina Fecht Flowers Building Imperial College London London, SW7 2AZ United Kingdom Attn: Miss. Selina Fecht
Publisher Tax ID	GB 494 6272 12
Total	0.00 GBP

SPRINGER NATURE LICENSE
TERMS AND CONDITIONS

Aug 05, 2022

This Agreement between Miss. Selina Fecht ("You") and Springer Nature ("Springer Nature") consists of your license details and the terms and conditions provided by Springer Nature and Copyright Clearance Center.

License Number	5362521080133
License date	Aug 05, 2022
Licensed Content Publisher	Springer Nature
Licensed Content Publication	Nature Microbiology
Licensed Content Title	Biogenesis and structure of a type VI secretion baseplate
Licensed Content Author	Yassine Cherrak et al
Licensed Content Date	Oct 15, 2018
Type of Use	Thesis/Dissertation
Requestor type	academic/university or research institute
Format	print and electronic
Portion	figures/tables/illustrations
Number of figures/tables/illustrations	1
High-res required	no
Will you be translating?	no
Circulation/distribution	1 - 29
Author of this Springer Nature content	no
Title	Characterising the role of TssA proteins in the assembly and dynamics of the type VI secretion system
Institution name	Imperial College London

Expected presentation date	Oct 2022
Order reference number	2
Portions	Figure 3
Requestor Location	Miss. Selina Fecht Flowers Building Imperial College London London, SW7 2AZ United Kingdom Attn: Miss. Selina Fecht
Total	0.00 GBP

ELSEVIER LICENSE
TERMS AND CONDITIONS

Aug 09, 2022

This Agreement between Miss. Selina Fecht ("You") and Elsevier ("Elsevier") consists of your license details and the terms and conditions provided by Elsevier and Copyright Clearance Center.

License Number	5364820636772
License date	Aug 09, 2022
Licensed Content Publisher	Elsevier
Licensed Content Publication	Trends in Cell Biology
Licensed Content Title	Using Force to Punch Holes: Mechanics of Contractile Nanomachines
Licensed Content Author	Maximilian Brackmann,Sergey Nazarov,Jing Wang,Marek Basler
Licensed Content Date	Sep 1, 2017
Licensed Content Volume	27
Licensed Content Issue	9
Licensed Content Pages	10
Start Page	623
End Page	632
Type of Use	reuse in a thesis/dissertation
Portion	figures/tables/illustrations
Number of figures/tables/illustrations	2
Format	both print and electronic
Are you the author of this Elsevier article?	No
Will you be translating?	No

Title	Characterising the role of TssA proteins in the assembly and dynamics of the type VI secretion system
Institution name	Imperial College London
Expected presentation date	Oct 2022
Order reference number	7
Portions	Figure 2 and Figure 3
Requestor Location	Miss. Selina Fecht Flowers Building Imperial College London London, SW7 2AZ United Kingdom Attn: Miss. Selina Fecht
Publisher Tax ID	GB 494 6272 12
Total	0.00 GBP

This is a License Agreement between Miss Selina Fecht ("User") and Copyright Clearance Center, Inc. ("CCC") on behalf of the Rightsholder identified in the order details below. The license consists of the order details, the Marketplace Order General Terms and Conditions below, and any Rightsholder Terms and Conditions which are included below.

All payments must be made in full to CCC in accordance with the Marketplace Order General Terms and Conditions below.

Order Date

08-Aug-2022

Order License ID

1255588-1

ISSN

1545-3251

Type of Use

Republish in a thesis/dissertation

Publisher

ANNUAL REVIEWS

Portion

Chart/graph/table/figure

LICENSED CONTENT

Publication Title

Annual review of microbiology

Date

01/01/1947

Language

English

Country

United States of America

Rightsholder

Annual Reviews, Inc.

Publication Type

e-Journal

URL

http://arjournals.annualreviews.org/loi/micro

REQUEST DETAILS

Portion Type

Chart/graph/table/figure

Number of charts / graphs / tables / figures requested

1

Format (select all that apply)

Print, Electronic

Who will republish the content?

Academic institution

Duration of Use

Life of current edition

Lifetime Unit Quantity

Up to 499

Rights Requested

Main product

Distribution

Worldwide

Translation

Original language of publication

Copies for the disabled?

No

Minor editing privileges?

No

Incidental promotional use?

No

Currency

GBP

NEW WORK DETAILS

Title

Miss

Instructor name

Selina Fecht

Institution name

Imperial College London

Expected presentation date

2022-10-20

ADDITIONAL DETAILS

Order reference number

5

The requesting person / organization to appear on the license

Miss Selina Fecht

REUSE CONTENT DETAILS

Title, description or numeric reference of the portion(s)

Figure 4

Editor of portion(s)

N/A

Volume of serial or monograph

N/A

Page or page range of portion

628

Title of the article/chapter the portion is from

2.3. Tube-Sheath Complex

Author of portion(s)

N/A

Issue, if republishing an article from a serial

N/A

Publication date of portion

2019-06-21

This is a License Agreement between Miss Selina Fecht ("User") and Copyright Clearance Center, Inc. ("CCC") on behalf of the Rightsholder identified in the order details below. The license consists of the order details, the Marketplace Order General Terms and Conditions below, and any Rightsholder Terms and Conditions which are included below.

All payments must be made in full to CCC in accordance with the Marketplace Order General Terms and Conditions below.

Order Date

05-Aug-2022

Order License ID

1255110-1

ISSN

1545-3251

Type of Use

Republish in a thesis/dissertation

Publisher

ANNUAL REVIEWS

Portion

Chart/graph/table/figure

LICENSED CONTENT

Publication Title

Annual review of microbiology

Date

01/01/1947

Language

English

Country

United States of America

Rightsholder

Annual Reviews, Inc.

Publication Type

e-Journal

URL

http://arjournals.annualreviews.org/loi/micro

REQUEST DETAILS

Portion Type

Chart/graph/table/figure

Number of charts / graphs / tables / figures requested

1

Format (select all that apply)

Print, Electronic

Who will republish the content?

Academic institution

Duration of Use

Life of current edition

Lifetime Unit Quantity

Up to 499

Rights Requested

Main product

Distribution

Worldwide

Translation

Original language of publication

Copies for the disabled?

No

Minor editing privileges?

No

Incidental promotional use?

No

Currency

GBP

NEW WORK DETAILS

Title

Miss

Instructor name

Selina Fecht

Institution name

Imperial College London

Expected presentation date

2022-10-20

ADDITIONAL DETAILS

Order reference number

4

The requesting person / organization to appear on the license

Miss Selina Fecht

REUSE CONTENT DETAILS

Title, description or numeric reference of the portion(s)

Figure 3

Editor of portion(s)

N/A

Volume of serial or monograph

N/A

Page or page range of portion

626

Title of the article/chapter the portion is from

2.2. Baseplate structure

Author of portion(s)

N/A

Issue, if republishing an article from a serial

N/A

Publication date of portion

2019-06-21